Towards Rapid and Precise Parallel Kinematic Machines

Samah Aref Shayya

Collège Doctoral du Languedoc-Roussillon

THÈSE

Pour obtenir le grade de

Docteur

Délivré par **UNIVERSITE DE MONTPELLIER**

Préparée au sein de l'école doctorale **Information, Structures et Systèmes**

Et de l'unité de recherche **Laboratoire d'Informatique de Robotique et de Microélectronique de Montpellier**

Spécialité : **Génie Informatique, Automatique et Traitement du Signal**

Présentée par **Samah Aref SHAYYA**

Vers des Robots et Machines Parallèles Rapides et Précis

(Towards Rapid and Precise Parallel Kinematic Machines)

Soutenue le 19/02/2015 devant le jury composé de

M. Andreas MÜLLER, Professeur, Johannes Kepler Universität, Linz, Autriche	Rapporteur (Président du Jury)
M. Stéphane CARO, Chargé de recherche CNRS, IRCCyN, Nantes, France	Rapporteur
M. Pascal RAY, Professeur, Institut Mines-Télécom, Saint Etienne, France	Examinateur
M. Franck JOURDAN, Professeur UM, LMGC, Montpellier, France	Examinateur
M. Cédric BARADAT, Dr., Directeur technologique, Tecnalia France, Montpellier, France	Examinateur
M. Sébastien KRUT, Chargé de recherche CNRS, LIRMM, Montpellier, France	Co-Encadrant de Thèse
M. Olivier COMPANY, Maître de Conférences UM, LIRMM, Montpellier, France	Co-Encadrant de Thèse
M. François PIERROT, Directeur de recherche CNRS, LIRMM, Montpellier, France	Directeur de Thèse

UNIVERSITÉ DE MONTPELLIER

Foreword

This doctoral thesis would not have been possible without the support, provision, and wise guidance of my supervisors: Dr. Sébastien KRUT, Dr. Olivier COMPANY, Dr. Cédric BARADAT (industrial supervisor), and Dr. François PIERROT. Their plentiful knowledge and experiences have been very essential in paving my research path and sculpting my research skills. They never hesitated to inspire me with their brilliant ideas and in-depth scrutiny, while keeping the necessary balance between their recommendations and my independent ideas. For them, I would like to express my sincere gratitude and acknowledgement for all what they have done! Thank you all!

I further thank Dr. KRUT for his tremendous efforts and close contact regarding my work and advancement. Perhaps, he worked as much as I have or even more in this project, especially in the scope of control implementation. His kind help has been indispensable for the success of this research and for which I owe him many thanks!

I would like also to thank the engineering team at Symétrie, the company that executed the prototype, for their efforts and creativity. Their work made the project a reality. Thank you!

Furthermore, I would like to thank all the jury members, Pr. Andreas MÜLLER, Dr. (HDR) Stephane CARO, Pr. Pascal RAY, and Pr. Franck JOURDAN, for accepting the evaluation and examination of my thesis, and for their rigorous scrutiny and comments. Having them assess my work is a great honor. For them, I express my genuine respect, gratefulness, and appreciation!

In addition, I would like to thank Tecnalia France for funding my thesis and providing me with all the needed support. I address many thanks to Dr. Valerie AUFFRAY and Dr. Frederick VAN MEER, the current and former directors of Tecnalia France, for welcoming me in the company. Additionally, I owe many thanks for my colleagues at Tecnalia: Dr. Micaël MICHELIN, Dr. Lotfi CHIKH, Dr. Jean-Baptiste IZARD, Dr. Hai YANG, and Dr. Vincent NABAT, for their enriching discussions and encouragement. Thank you Micaël and Hai for the precious help in the control aspects. I learned a lot from you! Thank you Lotfi for all the experience you have shared with me, especially regarding calibration. Thanks to Ms. Justin ANCEL and Ms. Emmanuelle BOUGEROL, the former and current executive assistants at Tecnalia France, for all their help in the administrative issues.

Special thanks go to Dr. Rany RIZK for recommending me as candidate for this doctoral thesis, and for the trust he has invested in me. Other special thanks I would like to address to Pr. Etienne DOMRE, Dr. Ahmed CHEMORI, and Dr. Marc GOUTTEFARDE, for the enlightening discussions and heartfelt encouragement at many occasions.

At LIRMM, many people have kindly aided me in different aspects and at various occasions, namely: Pr. Pascal NOUET (the responsible of specialty and representative of the Ecole Doctorale), Mr. Michel BENOIT (for his precious help in the experimentation with the LIRMM rapid prototypes), Mr. Olivier TEMPIER (for his technical support), Mr. Pierre-Elie HERVE, Mrs. Cécile LUKASIK, Mr. Nicolas SERRURIER (for all his help in administrative issues at LIRMM), Ms.

Laurie LAVERNHE, Mrs. Nicole GLEIZES, Mr. Olivier FLOUCAT, Mrs. Isabelle GOUAT, Mrs. Elisabeth GREVERIE, and Mrs. Genevieve CARRIERE. For all of them, I express my sincere gratitude and appreciation. Thank you all!

During these three years, I have shared many enjoyable discussions with many colleagues, some of which have already graduated and others who are still working on their dissertations. I would like to thank them for all these good memories. In names, I mention: Alain HASSOUN, Divine MAALOUF, Abdulrahman ALBAKRI, Dinh Quan NGUYEN, Andrea COLLO, Florent VEYE, Fabien DESPINOY, Mariam ABDALLAH, Rida KHEIRALLAH, Mohamad NAJEM, Julien PRADES, Moussab BENNEHAR, Mohamed BOUSHAKI, Jing GUO, Ederson DORILEO, Gamal ELGHAZALY, Ayad AL-DUJAILI, and Irina GAVRILOVICH.

Finally, I owe my success to my ever-supporting parents and brothers. Whatever I say and whatever I do, I cannot fulfill the least of their rights, especially my mother (Mona) and father (Aref). A thank you is nothing in front of your sacrifices, perseverance, and unlimited giving. You have been and will always be my source of inspiration and my motive to do the best. You are the main contributors for my success and if this presented work deserves any sort of appreciation, you are the ones who should be praised, for you being the source. For you my dear parents and brothers (Farid, Wissam, and Samer), I give my deepest thanks and appreciation, and for you I dedicate this dissertation!

At last, thanks for God, the creator of everything and my source of strength, hope, and enthusiasm. Thank you God for all the blessings you have endowed me!

Samah Aref SHAYYA

Abstract

Parallel manipulators (PMs) have been there for more than half a century and they have been subject of intensive research. In comparison with their serial counterparts, PMs consist of several kinematic chains that connect the fixed base to the moving platform. The interest in such architectures is due to the several advantages they offer, among which we mention: high rigidity and payload-to-weight ratio, elevated dynamical capabilities due to reduced moving masses (especially when the actuators are at or near the base), better precision, higher proper frequencies, etc. Nevertheless, despite of the aforementioned merits, their exploitation as machine tools is still timid and limited, in which they most often do not exceed the research and prototyping stages at university laboratories and machine tool manufacturers. The main drawbacks that hinder the widespread of parallel kinematic machines (PKMs) are the following: limited operational workspace and tilting capacity, presence of singular configurations, design complexities, calibration difficulties, collision-related problems, sophistication of control (especially in the case of actuation redundancy), etc. Besides, though PMs have met a great success in pick-and-place applications, thanks to their rapidity (acceleration capacity), still their precision is less than what has been initially anticipated. On the other hand, extremely precise PMs exist, but unfortunately with poor dynamic performance. Starting from the aforementioned problematics, the current thesis focuses on obtaining PKMs with a good compromise between rapidity and precision. We begin by providing a survey of the available literature regarding PKMs and the major advancements in this field, while emphasizing the shortcomings on the level of design as well as performance. Moreover, an overview on the state of the art regarding performance evaluation is presented, and the inadequacies of classical measures, when dealing with redundancy and heterogeneity predicaments, are highlighted. In fact, if finding the proper architectures is one of the prominent issues hindering PKMs' widespread, the performance evaluation and the criteria upon which these PKMs are dimensionally synthesized are of an equal importance. Therefore, novel performance indices are proposed to assess precision, kinetostatic, and dynamic capabilities of general manipulators, while overcoming the aforementioned dilemmas. Subsequently, several novel architectures with 3T-2R and 3T-1R degrees of freedom (T and R signify translational and rotational degrees of freedom), namely MachLin5, ARROW V1, and ARROW V2 with its mutated versions ARROW V2 M1/M2, are presented. Furthermore, the dimensional synthesis of the executed PKM, namely ARROW V2 M2, is discussed with its preliminary performances and possible future enhancements, particularly regarding precision amelioration.

Key words:

Parallel kinematic machines (PKMs), rapidity, precision, large operational workspace, large tilting capacity, actuation redundancy, kinematic redundancy, performance indices, 3T-2R and 3T-1R PKMs, MachLin5 PKM, ARROW V1 PKM, ARROW V2 PKM, ARROW V2 M1/M2 PKMs

Résumé

Les machines parallèles (MPs) existent depuis plus d'un demi-siècle et ils ont fait l'objet d'études intensives. Par opposition avec leurs homologues de structure série, ces mécanismes sont constitués de plusieurs chaînes cinématiques qui relient la base fixe à la plateforme mobile. L'intérêt de ces architectures s'explique par les nombreux avantages qu'elles offrent, parmi lesquels: une rigidité élevée, un rapport important charge/poids global, des capacités dynamiques élevées en raison des masses en mouvement réduites (en particulier lorsque les actionneurs sont sur ou près de la base), une meilleure précision, des fréquences propres plus élevées, etc. Néanmoins, leur exploitation comme machines-outils reste timide et limitée, et le plus souvent elles ne dépassent pas le stade d'étude et de prototype de laboratoires universitaires ou de fabricants de machines-outils. Les principaux inconvénients qui entravent la généralisation des MPs dans l'industrie sont les suivants: un espace de travail limité, des débattements angulaires réduits, la présence de configurations singulières, la complexité de conception, les difficultés d'étalonnage, les problèmes causés par les collisions, la complexité du contrôle/commande (en particulier dans le cas de redondance à actionnement), etc. De plus, si les MPs ont rencontré un grand succès dans les applications de pick-and-place grâce à leur rapidité (capacité d'accélération), leur précision reste inférieure à ce qui a été prévu initialement. Par ailleurs, on trouve également des MPs de très précision, mais malheureusement avec de faibles performances dynamiques. En partant du constat précédant, cette thèse se concentre sur l'obtention de MPs avec un bon compromis entre rapidité et précision. Nous commençons par donner un aperçu de la bibliographie disponible concernant MPs et les avancées majeures dans ce domaine, tout en soulignant les limites de performance des MPs, ainsi que les limites des outils de conception classique. En outre, nous insistons sur les outils d'évaluation des performances, et montrons leurs limites dès qu'il s'agit de traiter le cas de la redondance ou l'hétérogénéité des degrés de liberté (ddl). En effet, si la synthèse architecturale est un point dur de la conception de MPs, la synthèse dimensionnelle reposant sur des indices de performances réellement significatifs l'est également. Par conséquent, de nouveaux indices de performance sont proposés pour évaluer la précision, les capacités cinétostatiques et dynamiques des manipulateurs de manière générale qui apportent des solutions aux difficultés évoquées ci-dessus. Par la suite, plusieurs nouvelles architectures 3T-2R et 3T-1R (T: signifie ddl en translation et R signifie un ddl de rotation) sont présentées, à savoir MachLin5, ARROW V1, et ARROW V2 et ses versions dérivées ARROW V2 M1 et M2. En outre, la synthèse dimensionnelle d'ARROW V2 M2 est réalisée, et les performances de la machine sont évaluées. Finalement, des améliorations futures concernant la précision sont proposées au regard de premiers résultats obtenus sur le prototype.

Mots clés:

Machines parallèles (MPs), rapidité, précision, grand espace de travail opérationnel, grande capacité d'inclinaison, redondance à actionnement, redondance cinématique, indices de performance, 3T-2R et 3T-1R MPs, MachLin5 MP, ARROW V1 MP, ARROW V2 MP, ARROW V2 M1/M2 MPs

Contents

List of Figures

List of Tables

General Introduction

In these few pages, we provide a general overview on the thesis context within the inclusive ARROW project, clarifying the motivations and major contributions.

The ARROW project is a French project financed by the French National Research Agency (ANR) under the number ANR 2011 BS3 006 01. Its main objectives can be summarized as the design of **A**ccurate and **R**apid **R**obots with large **O**perational **W**orkspace, from which the acronym "**ARROW**" has been derived. The project embraces three partners:

1. IRCCyN (Institut de Recherche en Communication et Cybernétique de Nantes);
2. LIRMM (Laboratoire d'Informatique, de Robotique et de Microélectronique de Montpellier);
3. And Tecnalia France.

The current PhD thesis falls within the Industrial Conventions for Research Training CIFRE (**C**onventions **I**ndustrielles de **F**ormation par la **Re**cherche in French), and it has been financed by Tecnalia France, and in a part by the ANR.

Context

The recent decades have witnessed an increased industrial interest in parallel manipulators (PMs). Undeniably, this increase has been due to the great success of the Delta robot introduced by (CLAVEL, 1991), and which opened a new era of lightweight robots (or so-called Delta-like robots). Unfortunately, despite of that, the major implementation of PMs in industry has been limited to pick-and-place applications, with rather few and shy exploitations in other industrial operations, such as machining processes.

In fact, the rapidity and highly decreased cycle times achievable by PMs, allowed them to be highly competitive compared with serial counterparts in the field of pick-and-place operations, especially where the precision demand is not that high.

However, in applications demanding both rapidity and elevated precision, the available PMs fall short of supplying these requirements. In fact, we have been able to design ultra-rapid robots with mediocre or poor precision on one hand, and high-precision robots but with almost quasi-static performance on the other hand. As exemplification on the former robots, we mention: Adept Quattro (PIERROT, et al., 2008) (the fastest pick-and-place industrial robot with up to $15\,\mathrm{g}$ acceleration[1]), Par2 (BARADAT, et al., 2008) (with acceleration that reaches $43\,\mathrm{g}$),

[1] "g": corresponds to gravitational acceleration ($1\,\mathrm{g} = 10\,\mathrm{m/s^2}$).

and the exceptional R4 (CORBEL, et al., 2010) with its incredible $100\,g$ acceleration capability (CHEMORI, et al., 2013). As for high-precision robots, we mention the hexapods of PI company that are designed for micro-positioning purposes (refer to http://www.physikinstrumente.com/en/products/prdetail.php?sortnr=1000770).

Based on this argument, the ARROW project has been initiated in the year 2011, with the aim of achieving rapid and precise parallel kinematic machines (PKMs). For this ultimate goal, two different scenarios have been proposed:

1. The first scenario has considered the development of robots with large acceleration capacity, small cycle time, and elevated precision only at the end-points of a given trajectory. The intended application of such robots is the assembly of electronic components and the alike. This scenario has been approached by IRCCyN.
2. The second scenario has been concerned with the development of robots with high acceleration capability and elevated precision following any trajectory within a desired workspace. Such robots can be implemented in industrial applications as laser or water-jet cutting, welding, rapid prototyping, etc. This scenario has been dealt with by LIRMM and Tecnalia.

This latter objective constitutes the main subject of the current PhD thesis that details the major achievements and contributions in this aspect.

Motivations

As it has been mentioned above, we have targeted the establishment of a PKM with high dynamic capability and precision. The numerical set goals have been achieving up to $20\,g$ regarding linear acceleration and less than $20\,\mu m$ absolute accuracy. As for the PKM's operational degrees of freedom (dofs), they are supposed to be five dofs (3T-2R)[2], as they are sufficient for most industrial applications.

However, although acceleration and precision are the main targets, they are not the sole ones. Actually, the PKM must be characterized by large singularity-free workspace and tilting capacity. This is not to mention the design simplicity that is essential, not just for having simple models, but also to facilitate the manufacturing of this PKM.

Based on all the above, several mechanisms have been synthesized and studied after the establishment of suitable performance measures, which constitute one of the major contributions of this research in addition to the PKM itself. These contributions will be detailed in the upcoming section.

[2] "T" and "R" stand for translational and rotational dofs respectively.

Contributions

In the scope of the work to accomplish the preset objectives, the following contributions have been made:

1. Establishment of original performance measures: These can be used for the assessment and dimensional synthesis of a general robot based on precision, kinetostatic, and/or dynamic performances. They overcome two major issues as compared with the classical available ones, namely redundancy (whether of actuation or kinematic type) and heterogeneity relative to operational dofs or actuator types (i.e. having rotational and prismatic actuators at the same time). The generality of the approach embraces: serial, parallel, and hybrid robots. Furthermore, the approach is applicable on not only rigid manipulators, but also cable-driven ones.
2. Synthesis of several novel parallel architectures: Among these, we mention the MachLin5, ARROW V1, and ARROW V2 with its mutated versions, ARROW V2 M1/M2. MachLin5 is a five-dof (3T-2R) manipulator; whereas the rest are four-dof (3T-1R) redundantly actuated PKMs.

Finally, in what follows, we describe the general outline of the dissertation:

1. The first chapter will provide some generalities and basic definitions regarding PMs. Then, an exposition of the state of art regarding PMs and implemented PKMs will be presented, emphasizing the merits and demerits of some particular designs. After that, the issue of performance evaluation and the corresponding available literature will be discussed while highlighting the major encountered limitations, especially when dealing with redundant or heterogeneous-dof robots.
2. The second chapter will be dedicated to the presentation of the newly established approach for the performance assessment and optimization of general manipulators, relative to precision, kinetostatics, and/or dynamics. Besides, two case studies will be provided to demonstrate the methodology. The first analysis will be done on DUAL V (WIJK, et al., 2013), a redundantly actuated rigid robot with planar motion (three dofs, 2T-1R). As for the second study, it will be carried on a fully constrained cable-driven parallel robot (CDPR), with planar motion (three dofs, 2T-1R) and four active cables.
3. The third chapter will be devoted for the presentation of several novel mechanisms. This presentation will include geometric models, Jacobians, and singularity analysis. Also, the manufacturing procedure and the necessarily modifications done on the chosen robot for execution, will be discussed. Moreover, the dimensional synthesis of the implemented PKM and another architecture will be provided.
4. The fourth chapter will emphasize some points regarding the control of the ARROW PKM and the possible error compensations that can be made in the future.
5. Ultimately, the dissertation ends with general conclusions and perspectives regarding possible future research directions.

Notations

In this thesis, the equations are numbered in order of appearance and depending on the chapter number. Moreover, the following notations are adopted:

- Scalar variables are italicized and numbers are written in a regular font, for example: i, j, 1, 2, etc.
- Vectors and matrices are italicized in bold, for example: $\boldsymbol{v}$, $\boldsymbol{M}$, etc.
- $\mathbf{1}_{n\times n}$ denotes the $n\times n$ identity matrix.
- $\mathbf{0}_{m\times n}$ denotes the $m\times n$ zero matrix.
- $\boldsymbol{M}^{-1}$ and $\boldsymbol{M}^{\mathrm{T}}$ correspond to the inverse and transpose of matrix $\boldsymbol{M}$, respectively.
- $\boldsymbol{M}^{*}$ denotes the pseudo-inverse of matrix $\boldsymbol{M}$.
- $\mathrm{diag}\left(\lambda_i\right)$ designates the $n\times n$ diagonal matrix whose diagonal terms are λ_i, with $i=1...n$.
- $\mathrm{eigs}\left(\boldsymbol{Matrix}\right)$ denotes the list of eigenvalues of the square matrix $\boldsymbol{Matrix}$.
- $\mathrm{sing}\left(\boldsymbol{Matrix}\right)$ denotes the list of singular values of the matrix $\boldsymbol{Matrix}$.
- $\underline{\underline{val}}$ and $\overline{\overline{val}}$ correspond to lower and upper bounds of the term val.
- $\dot{f}$ and $\dot{\boldsymbol{q}}$ represent the time derivative of the function, f, and the vector, $\boldsymbol{q}$, respectively. Similarly, $\ddot{f}$ and $\ddot{\boldsymbol{q}}$ represent the second time derivatives of the aforementioned terms.
- $\boldsymbol{e}_x$, $\boldsymbol{e}_y$, and $\boldsymbol{e}_z$ are the unit vectors along the x, y, and z axes of the base frame.
- $\mathrm{Rot}_x\left(\theta_x\right)=\begin{bmatrix}1 & 0 & 0\\ 0 & \cos\left(\theta_x\right) & -\sin\left(\theta_x\right)\\ 0 & \sin\left(\theta_x\right) & \cos\left(\theta_x\right)\end{bmatrix}$: is the rotation matrix in the case of a rotation of θ_x about the x-axis.
- $\mathrm{Rot}_y\left(\theta_y\right)=\begin{bmatrix}\cos\left(\theta_y\right) & 0 & \sin\left(\theta_y\right)\\ 0 & 1 & 0\\ -\sin\left(\theta_y\right) & 0 & \cos\left(\theta_y\right)\end{bmatrix}$: is the rotation matrix in the case of a rotation of θ_y about the y-axis.
- $\mathrm{Rot}_z\left(\theta_z\right)=\begin{bmatrix}\cos\left(\theta_z\right) & -\sin\left(\theta_z\right) & 0\\ \sin\left(\theta_z\right) & \cos\left(\theta_z\right) & 0\\ 0 & 0 & 1\end{bmatrix}$: is the rotation matrix in the case of a rotation of θ_z about the z-axis.

- $\mathrm{Rot}(\boldsymbol{u},\theta)=\begin{bmatrix} u_x^2\,(1-c_\theta)+c_\theta & u_x\,u_y\,(1-c_\theta)-u_z\,s_\theta & u_x\,u_z\,(1-c_\theta)+u_y\,s_\theta \\ u_x\,u_y\,(1-c_\theta)+u_z\,s_\theta & u_y^2\,(1-c_\theta)+c_\theta & u_y\,u_z\,(1-c_\theta)-u_x\,s_\theta \\ u_x\,u_z\,(1-c_\theta)-u_y\,s_\theta & u_y\,u_z\,(1-c_\theta)+u_x\,s_\theta & u_z^2\,(1-c_\theta)+c_\theta \end{bmatrix}$: is the rotation matrix in the case of θ rotation about an axis of direction $\boldsymbol{u}=\begin{pmatrix} u_x & u_y & u_z \end{pmatrix}^{\mathrm{T}}$.
- $\hat{\boldsymbol{a}}=\begin{bmatrix} 0 & -a_z & a_y \\ a_z & 0 & -a_x \\ -a_y & a_x & 0 \end{bmatrix}$: is the pre-cross product matrix of vector $\boldsymbol{a}=\begin{pmatrix} a_x & a_y & a_z \end{pmatrix}^{\mathrm{T}}$, meaning $\boldsymbol{a}\times\boldsymbol{b}=\hat{\boldsymbol{a}}\,\boldsymbol{b}$ where $\boldsymbol{b}=\begin{pmatrix} b_x & b_y & b_z \end{pmatrix}^{\mathrm{T}}$.

Also, graph diagrams are used to depict mechanism topologies. For this purpose, the following notations are adopted:

- $\mathbf{R}$, $\mathbf{U}$, $\mathbf{S}$, $\mathbf{C}$, $\mathbf{H}$, and $\mathbf{P}$ stand for revolute, universal, spherical, cylindrical, helical, and prismatic joints, respectively.
- $\boxed{\boldsymbol{X}}$ and $\boxed{\boldsymbol{X}}$ represent passive and actuated joints, respectively.
- $\underline{\mathbf{X}}$ means that the joint $\mathbf{X}$ is equipped with a position sensor.

Finally, several acronyms are frequently used in the report. These are supplied here to serve as a quick reference for the reader:

- AR, KR, and TR: stand for actuation, kinematic, and task redundancies, respectively.
- NRM, RAM, KRM, and MRM: stand for non-redundant, redundantly actuated, kinematically redundant, and mixed-redundancy manipulators or machines, respectively.
- IBAR and BAR: stand for in-branch and branch actuation redundancies, respectively.
- IGM and DGM: stand for inverse and direct geometric models.
- IKM and DKM: stand for inverse and direct kinematic models.
- DM (SDM): corresponds to dynamic model (respectively simplified dynamic model).
- IDM and DDM: stand for inverse and direct dynamic models.
- DWS: means desired workspace.
- TPAF and OPAF: correspond to translational and orientation amplification factors, respectively.
- $\mathrm{WTPAF}_{\mathrm{DWS}}$: is the worst value of TPAF over DWS, i.e. the maximum value.
- ILA and PLA: are respectively the isotropic and peak linear accelerations starting from rest, and in the absence of any external non-gravitational wrench.
- $\mathrm{WILA}_{\mathrm{DWS}}$: is the worst value of ILA over DWS, i.e. the minimum value.

Chapter 1: State of the Art

In this chapter:

Available literature is rich with parallel manipulators (PMs), and some have found their way into industrial applications. However, the number of parallel kinematic machines (PKMs) that has been implemented so far is still very low. This poor exploitation is due to several reasons. In this chapter, an overview on the state of art of PMs and available industrial PKMs will be exposed, highlighting the problematics that hinder their widespread. In addition, the available literature on performance evaluation of manipulators will be discussed, emphasizing the major limitations encountered in the case of robots with heterogeneous degrees of freedom (dofs) and/or with redundancy (whether of actuation or kinematic type). This latter problematic is crucial as the synthesis of both, the architecture and its geometrical dimensions, are supposed to be based on solid criteria well interpretable and that fit machine tool basic requirements. Starting from the aforementioned points, the thesis problematics will be clarified by the end of the chapter and the approach to overcome them will be outlined.

1.1- Generalities and Definitions

1.1.1- A Brief History on the First Parallel Robots and Parallel Kinematic Machine Tools

In most articles, it has been reported that the first PMs were the tyre-testing machine of (GOUGH & WHITEHALL, 1962) (see **Fig. 1-1**) and the flight simulator of (STEWART, 1965). However, according to (BONEV, 2003), the first PM perhaps dates back to 1931 (GWINNETT, 1931) and it has been proposed as an amusement device; but it is not known whether the aforementioned architecture has been built or not. Nevertheless, it is undeniable that Gough-Stewart platforms have played an essential role in popularizing PMs and inspiring new ones.

Actually, parallel robots at their earlier beginnings, were of full mobility[1] and mainly based on the Gough-Stewart architectures. As for the trend towards lower mobility[2] parallel mechanisms, it can be traced back, according to (ANGELES, 2004), to the work of (HUNT, 1983) and after which planar, spherical, and later spatial mechanisms have been synthesized.

Moreover, another remarkable milestone in the world of parallel mechanisms is perhaps the Delta robot introduced by (CLAVEL, 1991) (see **Fig. 1-2**). This robot not only has been vastly industrialized, but also it inspired many new ones with similar features.

According to (KRUT, 2003), one can speak of two generations of parallel mechanisms: the first being described by Gough-Stewart platforms and based upon architectures, while the second being embodied by Delta-like or lightweight structures. In fact, thanks to the features

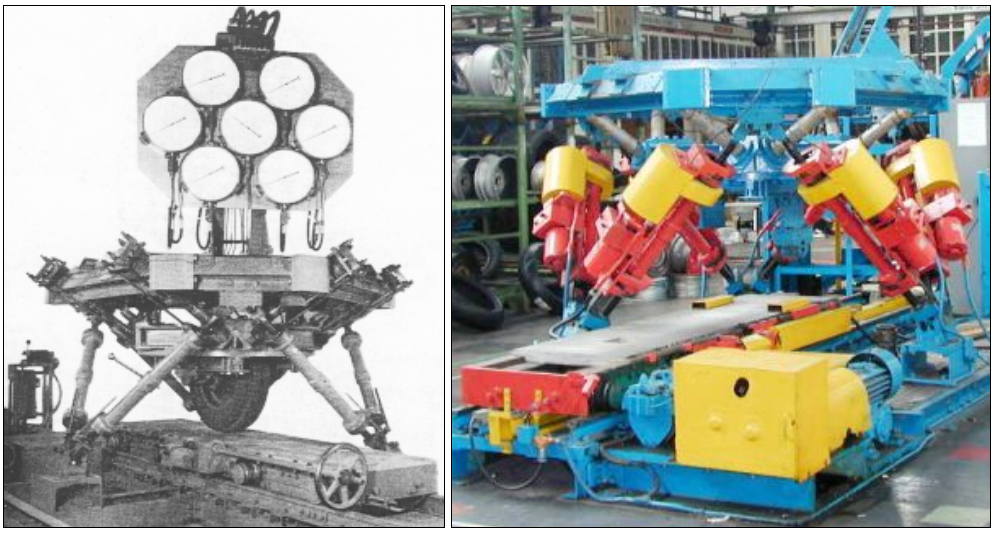

Fig. 1-1: Original Gough platform and shortly before its transfer into the British National Museum of Science and Industry in 2000 (Dunlop Tyres).

[1] With six dofs

[2] With the number of dofs less than six

present in the latter manipulators, such as fixed actuators at the base and lightweight components and parallelograms, exceptional performances with up to $10\,\mathrm{m/s}$ in speed and $15\,\mathrm{g}$ in acceleration can be reached, even more!

This was a very short briefing regarding parallel robots. Concerning machine tools, the first one based on parallel kinematics, as contrasted to the conventional or serial counterparts, was the Variax[3] of Giddings & Lewis (see **Fig. 1-3**). It has been presented publically in 1994 within the International Machine Tool Show held at Chicago. It was based on the Gough-Stewart idea and intended for milling applications.

Afterwards, many industries started researching and developing parallel kinematic machine

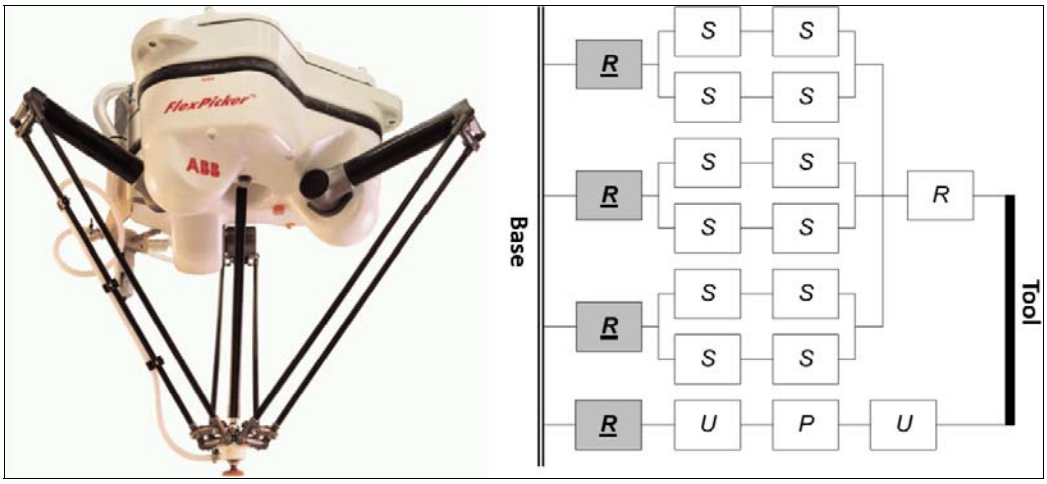

Fig. 1-2: FlexPicker (ABB Robotics) industrial robot: photo and graph diagram.

Fig. 1-3: Variax parallel kinematics machine tool (Giddings & Lewis).

[3] A video regarding this machine is available at: https://www.youtube.com/watch?v=7TowJZQi-qY .

tools (PKMs) in parallel with university laboratories. Among these PKMs, we mention: H0H600 (Ingersoll), 6X Hexapod (Mikromat), G500 and G1000 (Geodetics), Cosmo Center PM-600 (Okuma), Tornado 2000 (Hexel), HEXACT (developed by INA and IFW), Hexapode 300 (CMW), Triaglide (Mikron), Quickstep (Krause & Mauser), UraneSX (Renault Automation/Comau), Georg V of IFW (University of Hanover), Eclipse (Seoul National University), etc. In (COMPANY, 2000) and (WECK & STAIMER, 2002), a more elaborate information is presented regarding the history and state of the art of machine tools in general, and PKMs in particular. Later in this chapter, we will expose only a sample of these machines that exhibit some interesting features.

However, despite the increased interest in PKMs, their spread in industrial and machining applications is rather shy, and still conventional or serial kinematic machines (SKMs) are the highly dominant, with PKMs not exceeding research stages. In fact, comparing the number of theoretically synthesized architectures to that of the implemented ones, clearly shows the huge gap between theory and industrial needs. While the higher motion coupling and insufficiency of the processors' capabilities were a major hinder for PKMs spread before 1994, the present status, where large advancement in electronics yielded highly performant controllers, shows that other constraints have come into the light presenting new challenges and obstacles to overcome. This will become clear by the end of the chapter.

Nevertheless, before going any further in the world of parallel mechanisms, it is indispensable to provide some definitions to clarify their notion and particularities as compared to serial ones, emphasizing the merits and drawbacks of each. These are discussed in the following sections.

1.1.2- Serial Robots

The most industrial robots built until now are serial manipulators (SMs). An SM is an open chain formed by a series of links interconnected one to another by an actuated joint. An example of such manipulators is shown in **Fig. 1-4**.

While SMs are characterized by large workspaces and being rather simple to deal with regarding control, they suffer from the following drawbacks:

- High moving masses which limit their dynamic capability;
- Poor rigidity as a result of the series configuration and which leads to cumulative errors regarding the end-effector pose;
- Wear of the power and sensor connections (cables, flexible tubes) and which might lead to hazardous consequences;

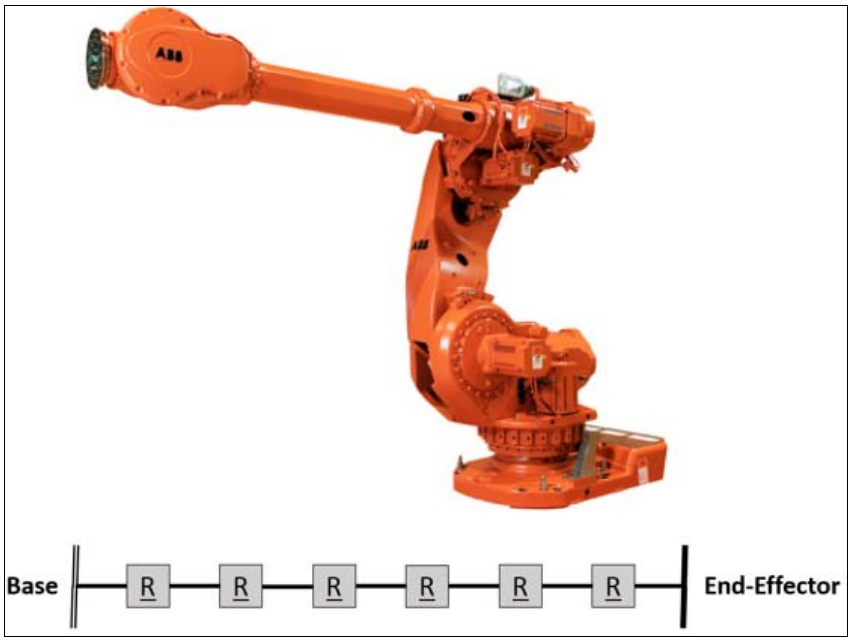

Fig. 1-4: Robot IRB 7600-150 (ABB Robotics): photo and graph diagram.

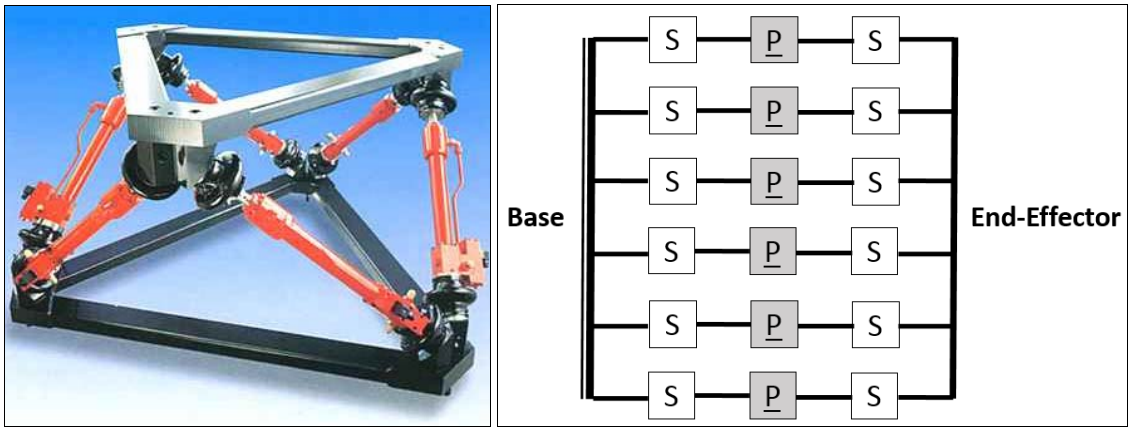

Fig. 1-5: Hexamove system (OHE Hagenbuch AG): photo and graph diagram.

1.1.3- Parallel Robots

A parallel manipulator (PM) is defined, according to (MERLET, 2006), as a closed-loop kinematic chain mechanism whose end-effector is linked to the base by several independent kinematic chains. Examples on such manipulators are those in **Fig. 1-1**, **Fig. 1-2**, **Fig. 1-3**, and **Fig. 1-5**.

Such mechanisms have their interesting features that made them suitable candidates to overcome the limitations of SMs. Unfortunately, they are not without their own demerits. In the upcoming subsections, we expose these virtues and hindrances.

A- Advantages

In general, PMs are characterized by the following advantages:

- High payload-to-weight ratio;
- High stiffness due to the parallel structure;
- High dynamic capabilities due to small moving masses, especially when the actuators are placed at or near the base;
- Improved accuracy due to the parallel structure and in which unlike SMs, the end-effector pose errors are non-cumulative;
- Higher proper frequency due to elevated rigidity and therefore, lessened repeatability errors due to the uncontrolled structural oscillations;
- Moreover, the possibility of placing the actuators at the base allows for the following additional benefits:
  - Higher flexibility regarding the choice of motors and/or gearboxes, as their masses do not highly influence the eventual inertia of the robot (particularly the moving inertia);
  - Reduction of the problems arising from cable connections between the motors, sensors, and controller.
  - Enhanced cooling of the actuators resulting in reduced errors due to thermal expansions;
  - Easier isolation of the motors from the possible detrimental environmental conditions that might be present in the workspace (e.g. applications that might require heavy water rinsing).

It is worth emphasizing that the above-mentioned features might not necessarily be present in all PMs. In fact, the première designs experienced problems of precision and rigidity (KRUT, 2003).

B- Inconveniences

Despite the interesting features described above, PMs suffer usually from the following inconveniences:

- Reduced workspace and tilting capacity: This results from the parallel structure itself, as the end-effector workspace is the intersection of the regions permissible by the individual kinematic chains. Another cause of this reduction is the possibility of inter-collisions. Additionally, we mention the usually rather complex shapes of the feasible workspaces, especially when internal singularities (i.e. inside the geometrically accessible workspace) exist.
- Singularities: Unlike SMs, PMs present, in addition to serial-type singularities, other singularity types with more subtleties regarding their identification and classification. These singularities are critical and can lead to uncontrollable motion of the platform (end-effector) or the deterioration of the mechanical system. The avoidance of such singularities constitutes an essential challenge in the design of a PM. This will be discussed in the subsequent part.
- The difficulty of having closed-form solution for the direct geometric model (DGM): This is nowadays less severe as numerical solutions can be implemented without influencing computation time. This is due to the advanced performance of modern controllers.
- Calibration difficulties whether relative to geometry, elasticity, and/or dynamics: This is due to the high coupling between the different chains and the large number of parameters involved as compared with SMs.

- High motion coupling and control complexity: Currently, with the advancement in electronics and development of highly performant processing units, these have become less critical.

C- Singularities of PMs

Singularities of PMs and their study constitute one of the prominent fields of research in robotics. In fact, the first attempt to set a general framework regarding singularity analysis of PMs can be traced back to (GOSSELIN & ANGELES, 1990). It has been based on the differentiation of the constraint equations, $\mathbf{F}(\boldsymbol{q}, \boldsymbol{x}) = \mathbf{0}$, relating the joint positions, $\boldsymbol{q}$, to the end-effector pose, $\boldsymbol{x}$. This leads to the following relation between the joint velocities, $\dot{\boldsymbol{q}}$, and the operational twist[4], $\boldsymbol{t}_{red}$ (the reduced n-dimensional twist for an n-dof robot):

$$\boldsymbol{J}_q \, \dot{\boldsymbol{q}} = \boldsymbol{J}_x \, \boldsymbol{t}_{red} \tag{1.1}$$

According to (GOSSELIN & ANGELES, 1990), three types of singularities exist depending on the rank deficiency of $\boldsymbol{J}_q$ and/or $\boldsymbol{J}_x$. These are described as follows:

a) Type-1 singularity (aka[5] inverse kinematic or serial singularity): It occurs when $\boldsymbol{J}_q$ is rank deficient. In such a case, the actuators can move while the platform is fixed.
b) Type-2 singularity (aka direct kinematic or parallel singularity): It corresponds to the case where $\boldsymbol{J}_x$ is rank deficient; meaning that the platform can move even when the actuators are fixed (at least one of the dofs is uncontrollable). We mention that type-2 singularity can be also termed as force singularity according to (MULLER, 2013), since certain operational wrenches cannot be supported by the manipulator in such a situation.
c) Type-3 singularity: It is the case where both matrices, $\boldsymbol{J}_q$ and $\boldsymbol{J}_x$, are simultaneously singular. The two phenomena described in types 1 and 2 can be noticed.

However, the above study does not embrace all possible singularities. An example on that is the well-known 3-UPU translational PM of Seoul National University (SNU). The mechanism was suggested by (TSAI, 1996) as a three-dof translational robot with actuated P joints. But the developed PM revealed peculiar motion for the case of equal limbs and fixed actuators. This was despite the absence of parallel singularities. The phenomenon was investigated by several researchers ((BONEV & ZLATANOV, 2001), (GREGORIO & PARENTI-CASTELLI, 2002), (JOSHI & TSAI, 2002), (WOLF, et al., 2002)) and became a popular example to demonstrate the insufficiency of considering only input-output kinematic relation in singularity analysis. Its singularity is what (BONEV & ZLATANOV, 2001) referred to as a constraint singularity.

---

[4] In the general case, we have $\boldsymbol{t}_{red} = \begin{pmatrix} \boldsymbol{v}^{\mathrm{T}} & \boldsymbol{\omega}^{\mathrm{T}} \end{pmatrix}^{\mathrm{T}}$ for a six-dof robot, with $\boldsymbol{v}$ and $\boldsymbol{\omega}$ being the linear and angular velocities, respectively. The twist $\boldsymbol{t}_{red}$ of a translational three-dof robot is $\boldsymbol{t}_{red} = \boldsymbol{v} = \begin{pmatrix} v_x & v_y & v_z \end{pmatrix}^{\mathrm{T}}$.

[5] "aka": also known as

A more generalized study was proposed by ((ZLATANOV, et al., 1995), (ZLATANOV, et al., 1998)). Unlike (GOSSELIN & ANGELES, 1990), the study of (ZLATANOV, et al., 1995) includes the passive joint velocities in the play. Accordingly, six types of singularities have been defined based on the solvability of the instantaneous forward and inverse kinematic problems: (IFKP) and (IIKP), respectively. Actually, the IFKP starts from given actuated joint velocities to establish both, the end-effector twist and the passive joint velocities. The failure of deriving a definite solution for any of the latter two quantities corresponds to a singularity. Similarly, starting from the end-effector twist, the IIKP seeks the establishment of definite actuated and passive joint velocities. Having any of the latter quantities indefinite implies a singularity as well. Therefore, a non-singular configuration of the mechanism is a one that does not present either type of singularities. Based on the above, the six singularity types are: redundant input (RI), redundant output (RO), redundant passive motion (RPM), impossible input (II), impossible output (IO), and increased instantaneous mobility (IIM). Moreover, n-order singularity types have been investigated by (WOHLHART, 1999) and (LIU, et al., 2003); however, they are rather difficult to put into practical use. In addition, another taxonomy of singularities has been suggested recently by (CONCONI & CARRICATO, 2009). For more information on singularities and their theory, the reader may refer to (MERLET, 2006) and (DONELAN, 2007).

In this section, we present the recommended singularity study following the general approach of (ZLATANOV, et al., 1998), but considering the full end-effector twist[6], $\boldsymbol{t} = \begin{pmatrix} \boldsymbol{v}^{\mathrm{T}} & \boldsymbol{\omega}^{\mathrm{T}} \end{pmatrix}^{\mathrm{T}}$ (instead of the full-cycle[7] or n-dimensional one in the general case of an n-dof robot). Denote by $\dot{\boldsymbol{\psi}}$ and $\dot{\boldsymbol{q}}$ the passive and actuated joint velocities, respectively. Also, consider the decomposition of $\boldsymbol{t}$ into: $\boldsymbol{t}_{red}$ and $\boldsymbol{t}_{comp}$. The term $\boldsymbol{t}_{red}$ denotes the n-dimensional twist for a mechanism whose full-cycle mobility is n (HUNT, 1978). As for $\boldsymbol{t}_{comp}$, it is the complementary twist[8] of $\boldsymbol{t}_{red}$ or in other words, the constrained part of $\boldsymbol{t}$.

Then, the differential equation relating $\dot{\boldsymbol{q}}$, $\boldsymbol{t}$, and $\dot{\boldsymbol{\psi}}$ is of the form:

$$\boldsymbol{L}_q \, \dot{\boldsymbol{q}} + \boldsymbol{L}_p \, \dot{\boldsymbol{\psi}} + \boldsymbol{L}_t \, \boldsymbol{t} = \boldsymbol{0} \tag{1.2}$$

Relation (1.2) can also be written simply as below:

$$\boldsymbol{L} \begin{pmatrix} \dot{\boldsymbol{q}}^{\mathrm{T}} & \dot{\boldsymbol{\psi}}^{\mathrm{T}} & \boldsymbol{t}^{\mathrm{T}} \end{pmatrix}^{\mathrm{T}} = \boldsymbol{0} \tag{1.3}$$

---

[6] $\boldsymbol{t} = \begin{pmatrix} \boldsymbol{v}^{\mathrm{T}} & \boldsymbol{\omega}^{\mathrm{T}} \end{pmatrix}^{\mathrm{T}}$, where $\boldsymbol{v}$ and $\boldsymbol{\omega}$ are respectively the linear and angular velocities in the three-dimensional space.

[7] Full-cycle mobility is the minimum instantaneous mobility of the platform for all the possible configurations (HUNT, 1978).

[8] For instance, the complementary twist of a three-dof translational robot is $\boldsymbol{t}_{comp} = \boldsymbol{\omega} = \begin{pmatrix} \omega_x & \omega_y & \omega_z \end{pmatrix}^{\mathrm{T}}$, i.e. the angular velocity. If at the considered configuration there is no instantaneous increase of mobility, we should have $\boldsymbol{t}_{comp} = \boldsymbol{\omega} = \boldsymbol{0}$ for the aforementioned robot.

Therefore, we categorize three singularity types, which are:

a) Redundant input singularity (RI): In this case, there exists $\dot{\boldsymbol{q}} \neq \mathbf{0}$ for which $\boldsymbol{t} = \mathbf{0}$. This is identical to type-1 singularity of (GOSSELIN & ANGELES, 1990) and indicates that the IIKP is not solvable.

b) Redundant output singularity (RO): In this case, for $\dot{\boldsymbol{q}} = \mathbf{0}$, a non-zero twist, $\boldsymbol{t} \neq \mathbf{0}$, is possible. In fact, RO embraces the type-2 singularity of (GOSSELIN & ANGELES, 1990), but the converse is not necessarily true. In particular, RO corresponds to type-2 only if $\boldsymbol{t}_{red} \neq \mathbf{0}$. However, if $\boldsymbol{t}_{comp} \neq \mathbf{0}$ and $\boldsymbol{t}_{red} = \mathbf{0}$, it is an RO singularity that cannot be detected utilizing the classical input-output kinematic relation. Such a case is referred to as constraint singularity ((BONEV & ZLATANOV, 2001) and (ZLATANOV, et al., 2001)). Moreover, it is possible to distinguish a particular type of constraint singularities, namely the architectural ones. These occur when the motion of the travelling platform is finite and in this case, the robot is coined as self-motion robot (e.g. (KARGER, 2003)).

c) Redundant passive motion singularity (RPM): Despite having the actuators and the platform fixed (i.e. $\dot{\boldsymbol{q}} = \mathbf{0}$ and $\boldsymbol{t} = \mathbf{0}$), the passive joint velocities are not necessarily zero ($\dot{\boldsymbol{\psi}} \neq \mathbf{0}$). Such singularity has been referred to as an actuator singularity in the work of (HAN, et al., 2002). An easy example would be having an arm between two passive spherical (S) joints. Then, although the extremities are fixed, the arm can rotate freely about the axis joining the centers of these two S-joints. Theoretically speaking, such a singularity would not produce a motion of the end-effector, but practically it must be rather circumvented due to the unavoidable imperfections in the joints (MERLET, 2006).

With the above, a non-exhaustive but sufficient overview on the PMs' singularities has been given. Also, the general approach based on (ZLATANOV, et al., 1998) has been clarified. The essence to be kept in mind is what follows. To assure the absence of singularities of any type at a certain configuration, it is sufficient to show the following three points:

a) $\boldsymbol{t}_{comp} = \mathbf{0}$: meaning that the undesired motion of the platform is always constrained and therefore, the end-effector twist is always the n-dimensional one associated with the full-cycle mobility, n;

b) For each $\boldsymbol{t}_{red}$, there exist unique definite $\dot{\boldsymbol{q}}$ and $\dot{\boldsymbol{\psi}}$;

c) And finally for each $\dot{\boldsymbol{q}}$, there exist unique definite $\boldsymbol{t}_{red}$ and $\dot{\boldsymbol{\psi}}$, with $\boldsymbol{t}_{comp} = \mathbf{0}$ necessarily.

It is worth mentioning that different tools can be used to verify the aforementioned ideas, whether linear algebra that we are going to use later in the analysis of our mechanisms, or Grassmann geometry (e.g. (MERLET, 2006), (BEN-HORIN & SHOHAM, 2009), (MBAREK, et al., 2007)).

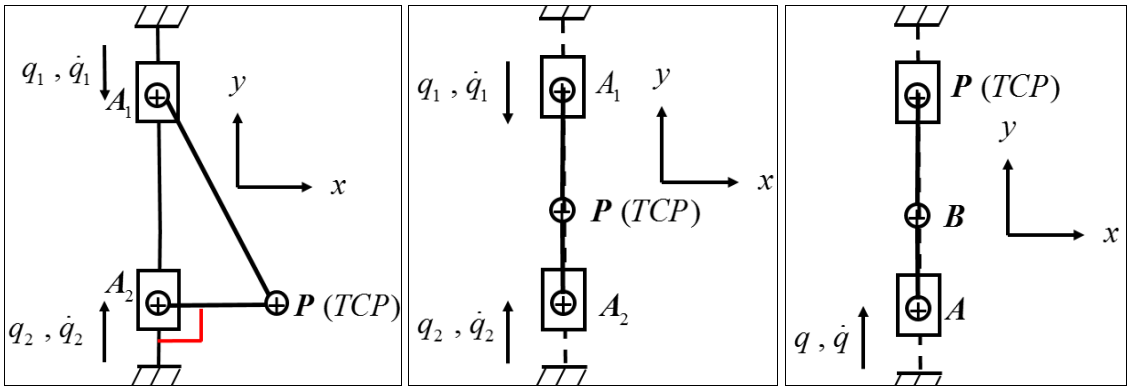

Fig. 1-6: Singularities: series singularity (or RI singularity) (left), parallel singularity (or RO singularity) (middle), and internal singularity (or RPM singularity) (right).

Furthermore, it is important to emphasize that in most of the studies of singularities done at LIRMM, the nomenclature as adopted by (KRUT, 2003) is usually used. This nomenclature categorizes singularities into: series singularities or under-mobilities, parallel singularities or over-mobilities, and the rest being called internal singularities. Note that the "internal" adjective used in this context refers to the internal structure of the mechanism and its internal mobilities, and not in the sense of having the singularity inside the accessible workspace.

The different three types of singularities are illustrated in **Fig. 1-6**. In the left drawing, the second slider can perform an infinitesimal motion while the TCP[9] is fixed, which indicates series singularity. In the middle diagram, the TCP can do an infinitesimal motion along the x-axis while the actuators are fixed indicating a parallel-type singularity. In the right hand side of the same figure, we can fix both, the actuator and the TCP, but still the point B can do an infinitesimal motion along x (indicating an infinitesimal rotation of the passive revolute at B); this is an internal/RPM singularity.

1.2- State of the Art of PMs: Between Theoretical Synthesis and Industrial Implementation

1.2.1- Type Synthesis of Parallel Mechanisms

Before exploring the available PMs, it is important to talk first on their type synthesis. In fact, the existing approaches can be classified into three main classes ((MERLET, 2006), (SICILLIANO & KHATIB, 2008)):

a) Approaches based on graph theory (e.g. (EARL & ROONEY, 1983)): For a given number of dofs, these methods assume a set of finite number of possible kinematic pairs, and then enumerate all the possible architectures that can be obtained by the different combinations of these pairs. Such methods utilize classical mobility formulae, e.g.

[9] Tool Center Point

Chebychev–Grübler–Kutzbach formula, to establish a relation between the structural parameters (number of joints, joint constraints, number of links) and the end-effector dofs. Nonetheless, as these formulae do not account for the geometrical constraints, they might not correctly predict the actual number of dofs (refer to (GOGU, 2005a)). Therefore, synthesis based strictly on graph theory can yield limited results and has been largely outdated.

b) Approaches based on group theory (e.g. (HERVE, 1995), (SPARACINO & HERVE, 1993), (ANGELES, 2004), (LI, et al., 2004)): These methods make use of the fact that rigid body displacements can be described by the structure of a group, referred to as displacement group. Within it, we have different subgroups, such as the spatial translations and the Schönflies (3T-1R) motion. However, not all body displacements form a subgroup, such as the 3T-2R motion. Therefore, 3T-2R mechanisms, for instance, cannot be synthesized using this method. The methodology of synthesis, based on this approach, is done in the following manner:
   i. First, the subgroup S that describes the desired end-effector motion is determined.
   ii. Then, all the possible subgroups whose intersection is S are established.
   iii. Eventually, all the motion generators of these subgroups are considered. These will constitute the kinematic chains of the PM.

c) Approaches based on screw theory (e.g.: (FRISOLI, et al., 2000), (KONG & GOSSELIN, 2001), (KONG & GOSSELIN, 2004a), (FANG & TSAI, 2002), (HUANG & LI, 2002), (CARRICATO, 2005)): In these approaches, the wrench system S that is reciprocal to the desired end-effector twist T is determined in a first step. Then, the wrenches of the kinematic chains of the PM whose union spans S are enumerated. These latter wrenches will be used to determine all the possible structures of the kinematic chains constituting the PM. Nevertheless, as these wrenches and twists are instantaneous, it is mandatory to verify that the platform mobility is the full-cycle mobility and not only the instantaneous one (for more details, refer to (KONG & GOSSELIN, 2007)).

We may add here a fourth approach, which is that based on the theory of linear transformations adopted primarily in the synthesis of the mechanisms described by ((GOGU, 2004a), (GOGU, 2007), (GOGU, 2009)) and several books for the same author. In these works, the new mobility and spatiality formulae, which have been established in (GOGU, 2005b), are used to overcome the limitations of the classical mobility formulations.

Based on the above methods, thousands of mechanisms are and can be synthesized, and it is rather impossible to keep track of even the fewer interesting ones emphasized in literature. In this aspect, it is sufficient, for instance, to look on the gathered lists of articles and patents on the webpages[10] of Dr. BONEV and Dr. MERLET to know the massiveness of these contributions,

[10] See the following webpages: http://www.parallemic.org/ and http://www-sop.inria.fr/members/Jean-Pierre.Merlet/merlet_eng.html.

reflecting both the interest and hopes held on such parallel structured architectures; also, they sadly highlight the gap between theory and industry.

Among the synthesized mechanisms, it is worth stopping at some intriguing architectures based on more recent trend towards maximally regular[11], fully isotropic[12], uncoupled[13], or decoupled[14] motions. Such mechanisms, especially the first three types, are interesting in the sense of their simplicity regarding control and energy saving (GOGU, 2007). This is due to that in the case of a unidirectional motion along one axis, only one motor is working while the others are locked. Nevertheless, such mechanisms are not fully virtuous and have their drawbacks, which we are going to emphasize at the end of the section. First, let us present some samples of such architectures, mainly with 3T, 3T-1R, and 3T-2R motions.

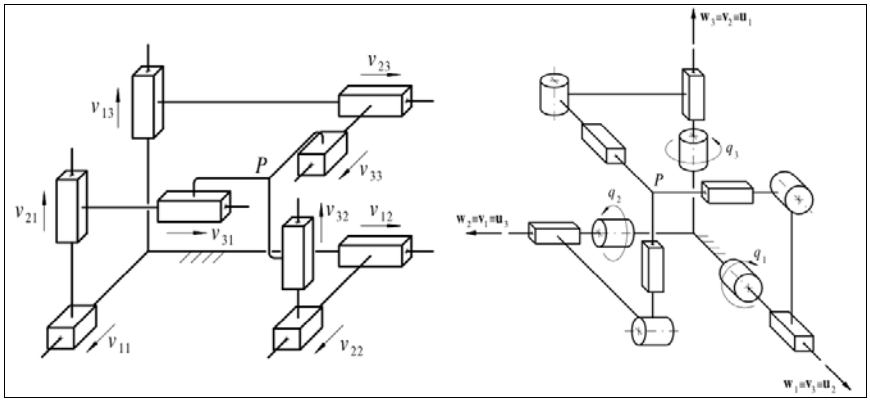

Fig. 1-7: Two fully isotopic translational PMs: the left is one of the T_3 family (it is more precisely maximally regular), whereas on the right is a type II of T_4 family (CARRICATO & PARENTI-CASTELLI, 2002).

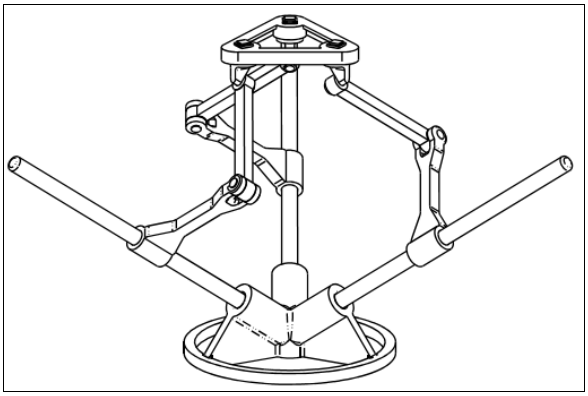

Fig. 1-8: The isotropic 3-CRR translational PM (KONG & GOSSELIN, 2002).

[11] Meaning with identity Jacobian matrix throughout the workspace.

[12] Meaning with diagonal Jacobian matrix such that the diagonal entries are the same throughout the workspace.

[13] Meaning with diagonal Jacobian matrix such that the diagonal entries are not necessarily equal throughout the workspace.

[14] In this case, the Jacobian is a triangular matrix throughout the workspace.

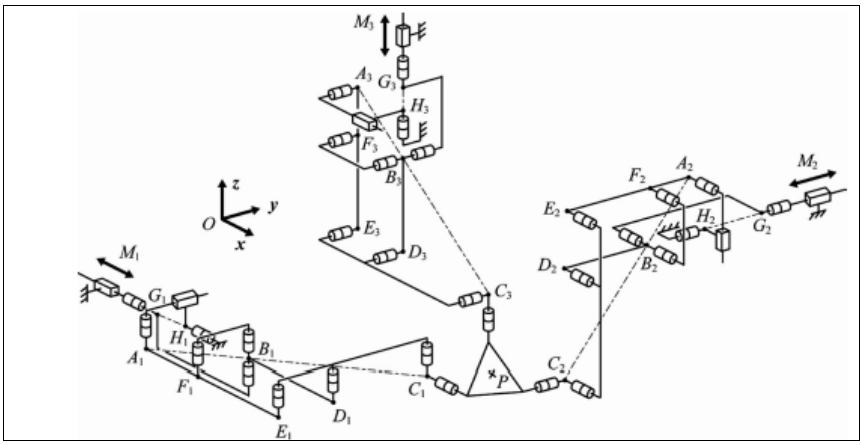

Fig. 1-9: Schematics of the Pantopteron (fully isotropic translational PM) (BRIOT & BONEV, 2009).

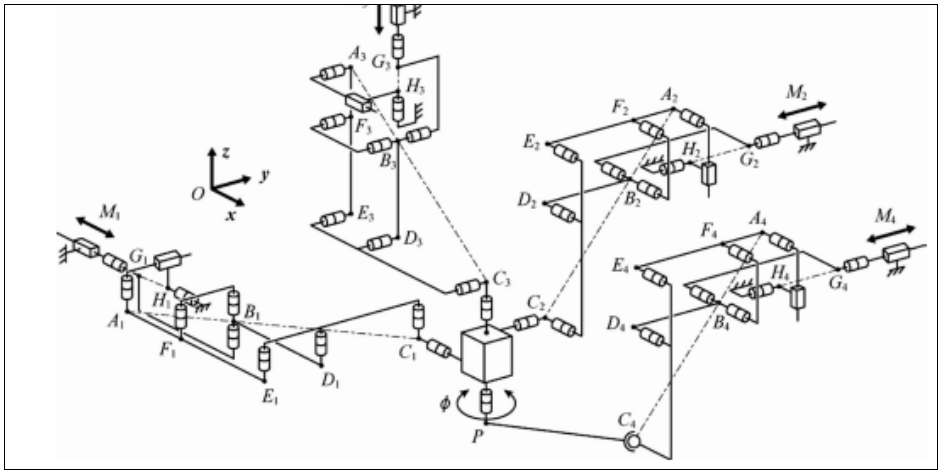

Fig. 1-10: Pantopteron with four-dof (3T-1R) uncoupled PM (BRIOT & BONEV, 2009).

Regarding translational mechanisms, (CARRICATO & PARENTI-CASTELLI, 2002) presented a topological synthesis for fully isotropic symmetric PMs with 3T motion. Their approach has been based on constraint and direct singularity investigation, in the purpose of their elimination. Two examples of such PMs are depicted in **Fig. 1-7**. Among other works, we mention, for instance, the fully isotropic version of the 3-CRR of (KONG & GOSSELIN, 2002) (**Fig. 1-8**), the fully isotropic 3-PRRR manipulator of (KIM & TSAI, 2002), the fully decoupled (more precisely fully isotropic) Pantopteron of (BRIOT & BONEV, 2009), and the synthesized fully isotropic translational PMs of (GOGU, 2004c). In **Fig. 1-9**, an illustration of the Pantopteron is given. This manipulator has been synthesized for pick-and-place applications and is characterized by the use of pantograph linkages to amplify the actuators' displacements. Also, a four-dof (3T-1R) version with uncoupled motions has been presented in (BRIOT & BONEV, 2009) as well and is depicted in **Fig. 1-10**.

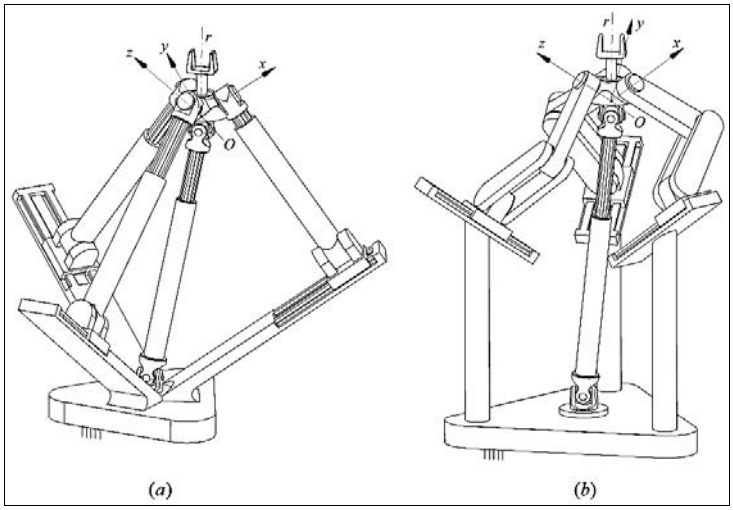

Fig. 1-11: Models of two fully isotropic mechanisms for Schoenflies motion (CARRICATO, 2005).

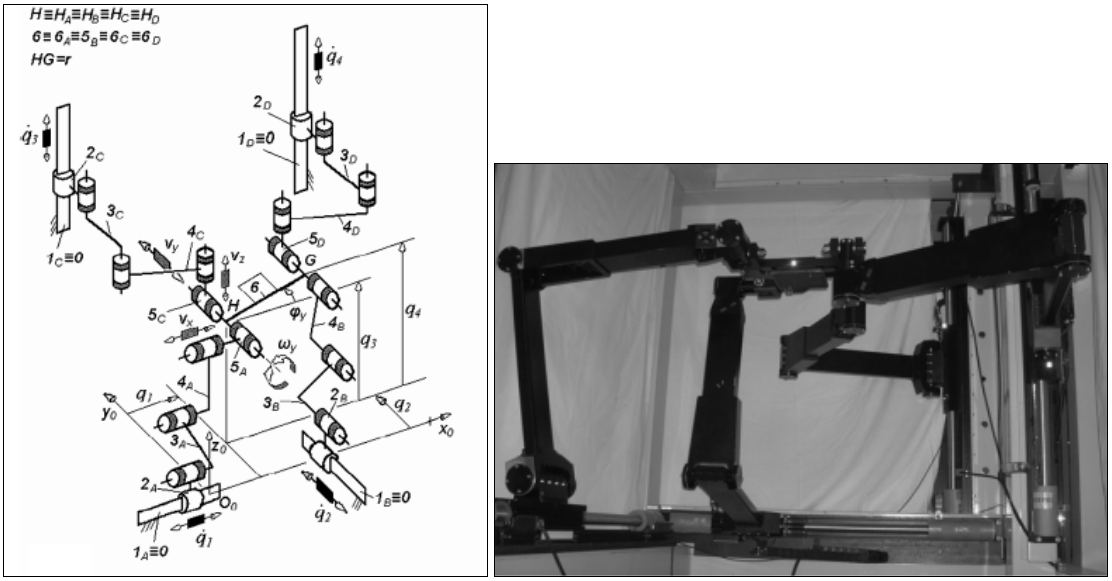

Fig. 1-12: Example of basic kinematics structure of PM with decoupled Schönflies motions: Isoglide4-T3R1-A5 schematic and its constructed prototype at the French Institute of Advanced Mechanics (GOGU, 2007).

As for fully isotropic parallel manipulators with Schönflies motion, they have been proposed in ((GOGU, 2004b), (GOGU, 2005c), (CARRICATO, 2005), (GOGU, 2007)) for the first time. Also, other uncoupled and decoupled PMs with 3T-1R motions have been suggested in (GOGU, 2007). In **Fig. 1-11**, two examples of the PMs suggested by (CARRICATO, 2005) are depicted, while in **Fig. 1-12**, **Fig. 1-13**, and **Fig. 1-14**, examples on decoupled, uncoupled and fully isotropic PMs among those synthesized in (GOGU, 2007) are given.

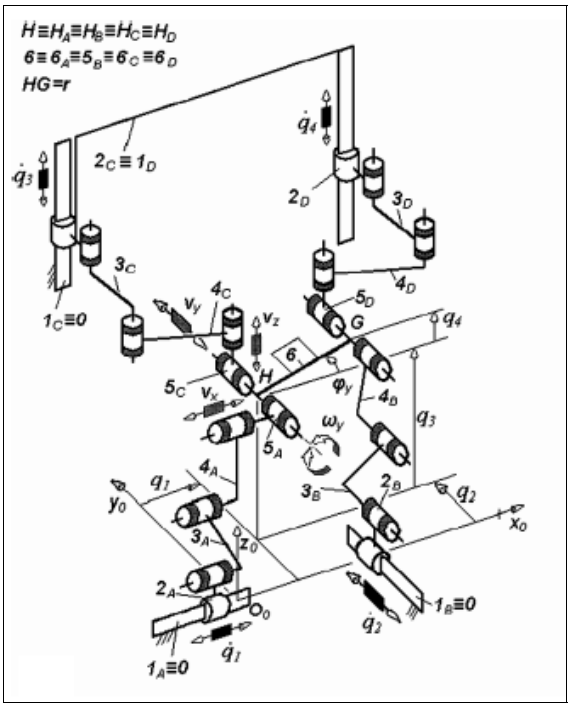

Fig. 1-13: Uncoupled (PMs) with Schönflies motion: Isoglide4-T3R1-B5 (GOGU, 2007). Note that this (PM) is similar to Isoglide4-T3R1-A5 in Fig. 1-12, except that $2_C \equiv 1_D$.

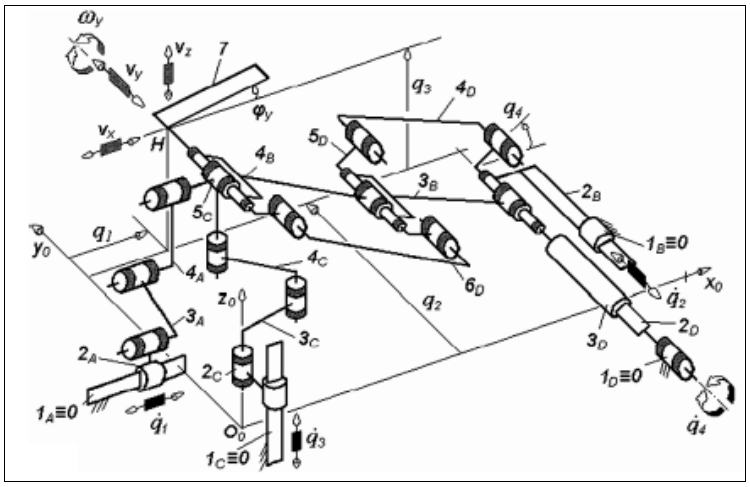

Fig. 1-14: Example of kinematic structure of fully isotropic PM with Schönflies motions: Isoglide4-T3R1-C5-2 (GOGU, 2007).

This was regarding 3T and 3T-1R PMs. In what concerns five-dof (3T-2R) PMs, the synthesized architectures are rather few in comparison with others (e.g. (FANG & TSAI, 2002), (GAO, et al., 2002), (HUANG & LI, 2002)) and are mostly coupled. In fact, the synthesis of the first maximally regular non-redundant or redundantly actuated PMs of 3T-2R motion can be tracked back to the recent work of ((GOGU, 2006a), (GOGU, 2006b), (GOGU, 2006c), and (GOGU, 2009)). In (GOGU, 2009), some decoupled and uncoupled five-dof (3T-2R) PMs, in addition to the maximally regular ones, have been synthesized as well. In **Fig. 1-15**, several examples of such PMs are presented.

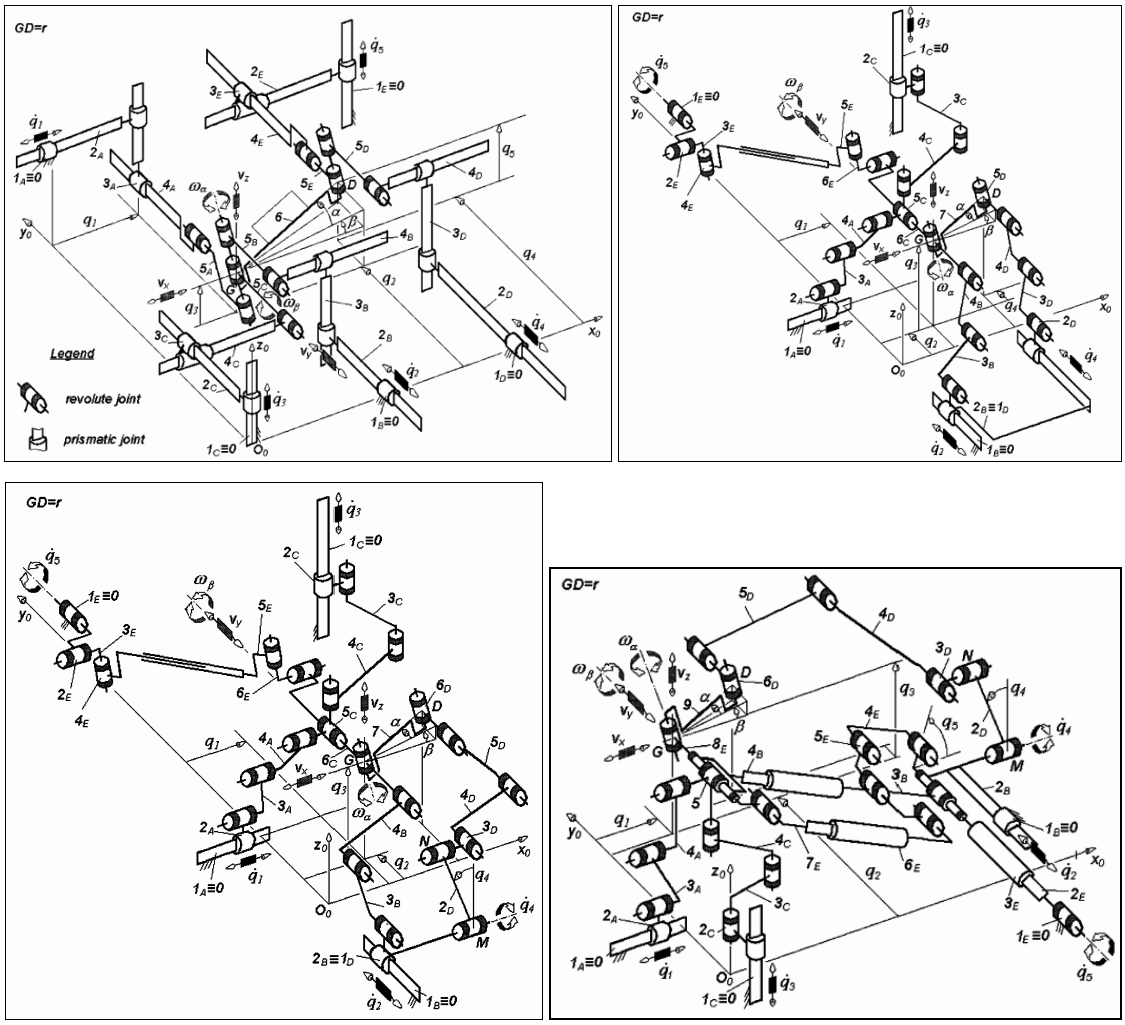

Fig. 1-15: From left to right and top to bottom: Isoglide5-T3R2-A1 (5-PPPRR-type) (decoupled), Isoglide5-T3R2-B1 (uncoupled), Isoglide5-T3R2-C1 (maximally regular), and Isoglide5-T3R2-C3 (maximally regular) (GOGU, 2009).

As we have given an overview on particular types of synthesized mechanisms, with decoupled and uncoupled motions, it important to make some points in this aspect. In fact, despite the interesting features that uncoupled mechanisms provide, they suffer from the following limitations:

- Most of these mechanisms are characterized by large number of passive joints and links. This is discouraged from industrial perspective. The reasons behind that are the added complexity, increased masses, reduced stiffness, and reduced precision, especially when there are joint clearances.
- Most of these designs have limited workspaces due in one part to chain complexities and possible collisions, and in another part to the use of prismatic joints with non-parallel axes and/or use of rotational actuators.

In brief, this section has provided a summary on the type synthesis of PMs and highlighted some recent trends in this domain. In fact, while the innovative approaches of synthesis of the

last decades have led to thousands of architectures, yet those that have been implemented and adopted for industrial applications are extremely few and countable. This clearly highlights the huge gap between theory and application.

In the next section, we will present some of the parallel robots and parallel kinematic machine tools that have been so far implemented. In addition, we will talk about some contributions that have been made in this scope.

1.2.2- Some Parallel Robots and Parallel Kinematic Machine Tools

In this part, we are going to expose several industrial machine tools based on parallel kinematics, as well as some other implemented prototypes or industrial parallel robots. The exposition is done based on the number of dofs. The list presented is a non-exhaustive one. Here, we focus on four-dof (3T-1R), five-dof (3T-2R), and six-dof (3T-3R) designs only.

In fact, most industrial applications do not require more than five dofs of 3T-2R nature. In others, fewer might be even sufficient. However, these five dofs can be achieved via different means:

- Six-dof (3T-3R) design: In this case, one of the rotational dofs, particularly that whose axis is parallel to that of the spindle, is disregarded. The result is task redundancy, which helps in enlarging the workspace. Such machines have been firstly designed, yet not all made proper use of the aforementioned redundancy.
- Five-dof (3T-2R) structure: In this case, the design is intended for the real need of five axis machining or other industrial applications.

Note that within each of the above two categories, hybrid structure, whether in the form of series-parallel or right-hand left-hand paradigm (branched structure), can be used. Our presentation starts with six dofs down to four dofs, which constitute the scope of the current thesis.

A- Six DoFs (3T-3R)

In addition, to the Gough-Stewart (aka hexapod) based designs (e.g. **Fig. 1-1**, **Fig. 1-3**, **Fig. 1-5**), some others with slight or major modifications have been implemented in recent decades. Here, we are going to focus only on those that have some interesting features.

Hexa, HexaM, Hexaglide, Dynamil, and Lambda Kinematics

In fact, after the introduction of Delta robot and the great success it achieved, many researchers investigated the possibility of extending this idea to the synthesis of other types of PMs. In ((PIERROT, 1991), (PIERROT, et al., 1991a), (PIERROT, et al., 1991b)), the design of a six dof (3T-3R) robot, assimilating the features of Delta regarding rapidity and lightness, has been investigated and led to Hexa robot, which is depicted in **Fig. 1-16**. Later, the aforementioned robot has been industrialized by Toyoda Machine Works Ltd. under the name of HexaM

(PIERROT & SHIBUKAWA, 1999), and it was intended for milling applications. The graph diagram and CAD drawing of HexaM are shown in **Fig. 1-17**. Compared with Hexa, the rotary actuators have been replaced by prismatic ones to avoid the high bending on the actuated arms. Thanks to having the actuators at the base and the light structure, HexaM is very similar in performance to Delta robot. It is worth mentioning here that HexaM, as compared with classical hexapods, has the placement of the prismatic and first universal joints interchanged in each kinematic chain (we have 6-PUS instead of 6-UPS).

Another interesting six-dof PKM is Hexaglide (WIEGAND, et al., 1996), a concept developed at the Institute of Machine Tools of the Swiss Federal Institute of Technology Zurich, for milling

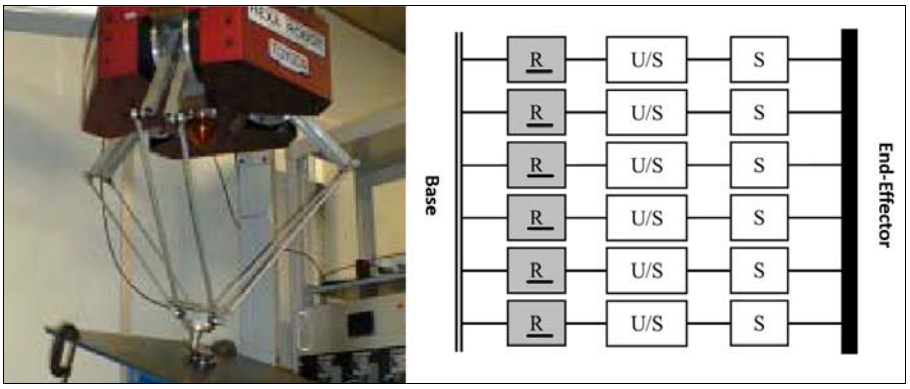

Fig. 1-16: HEXA Robot: prototype and graph diagram.

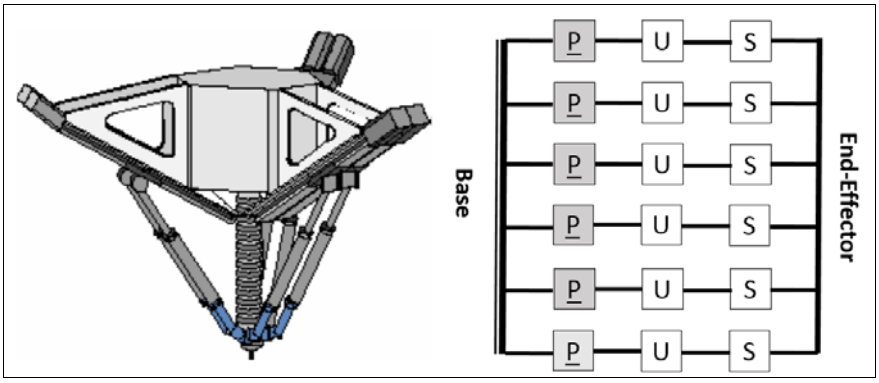

Fig. 1-17: HexaM Machine Tool (Toyoda): CAD drawing, graph diagram and photo.

applications as well. The machine is similar to HexaM. The difference is in having all the linear actuators along one direction and hence, allowing independent motion along this axis. The schematic of the PKM is illustrated in **Fig. 1-18**.

Similar machines to the aforementioned ones exist. These have same graph diagram, but different geometric configurations (e.g.: Paralix PKM of IFW at Stuttgart and Dynamil PKM of ISW at Aachen, which is depicted in **Fig. 1-19**).

The Lambda Kinematics PKM, introduced in the Mach21[15] project, is a slight variant of the aforementioned concepts. Instead of connecting the arms directly from the base into the platform, the arms are considered in pairs. In each pair, one of the arms is connected into the other that is then articulated to the platform. This limits the risk of internal collisions (see **Fig. 1-20**).

Unfortunately, still such machines suffer from workspace limitations and/or reduced tilting capacity, as it is the case with the classical hexapods.

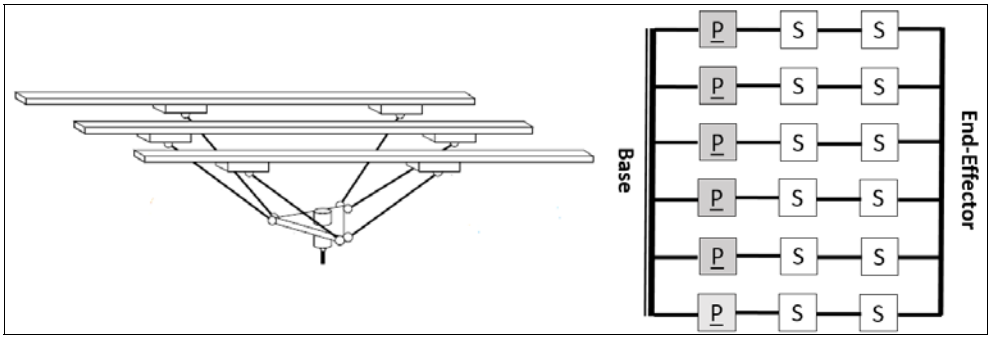

Fig. 1-18: Hexaglide: schematic (from (HONEGGER, et al., 1997)) and graph diagram.

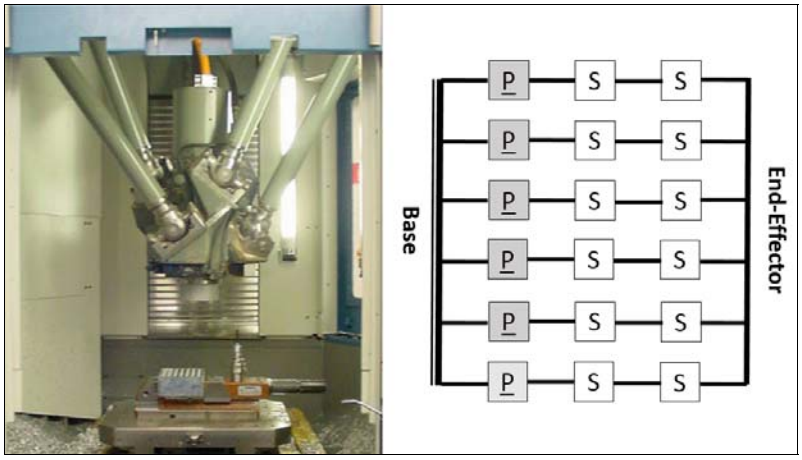

Fig. 1-19: Dynamil PKM (ISW): photo and graph diagram.

[15] Mach21 (Multipurpose and cross-sectorial modernization of manufacturing processes through parallel kinematics) is a European research program that involved 12 partners: Fatronik (currently Tecnalia), WZL, INA, IWU, Karl Mayer, LIRMM, Anayak, Gamesa, ISW, Comau, Arjal, and Lernsttat. It began in January 2000 and ended in January 2003.

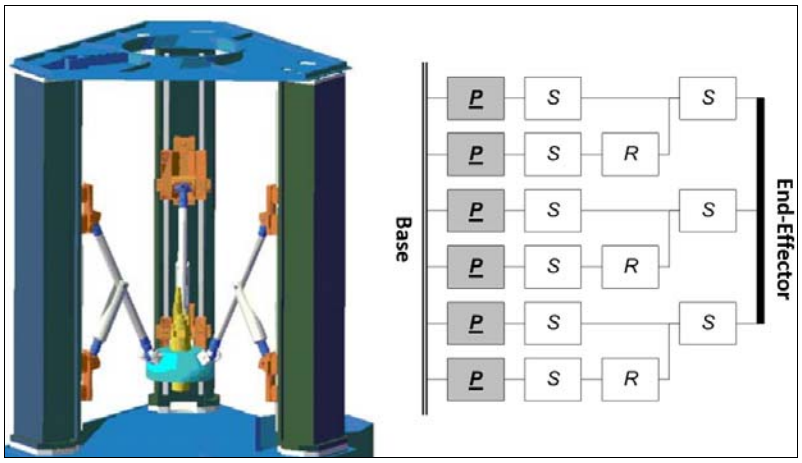

Fig. 1-20: Lambda Kinematics machine tool: CAD drawing and graph diagram.

Fig. 1-21: Fanuc M-3iA robot (http://www.fanucrobotics.fr/fr/countries/frfr/news/m3ia).

Fanuc M-3iA Robot

A different six-dof variant from the above and explicitly implementing the Delta structure exists. It is the Fanuc industrial robot with up to six dofs (3T dofs and up to 3R dofs). Actually, it is a Delta robot equipped with a wrist and it has been developed as high-speed and assembly robot (see **Fig. 1-21**). The actuators of the wrist are placed on the parallelograms, next to the actuated arms, as to have them as closer to the base as possible and hence, reducing their impact regarding dynamics. It is characterized by a cycle time of $0.3\,\mathrm{s}$ for $0.1\,\mathrm{kg}$ load and a pick-and-place path of $25\,\mathrm{mm}\times 200\,\mathrm{mm}\times 25\,\mathrm{mm}$. Note that this robot is a complex parallel structure and not a hybrid one. This is because the actuation of the wrist dofs is not done in place, but by means of transmission chains from the actuators on the parallelograms.

Hexapteron

Finally, we end the panorama on six-dof 3T-3R category by highlighting an interesting recently introduced design, the Hexapteron of (SEWARD & BONEV, 2014). It is characterized by a simple direct geometric model and can be used for machining or rapid prototyping applications. The prototype for 3D printing application is under construction. First simulations show a tilting capacity of $45°$ about any direction. The manipulator is depicted in **Fig. 1-22**.

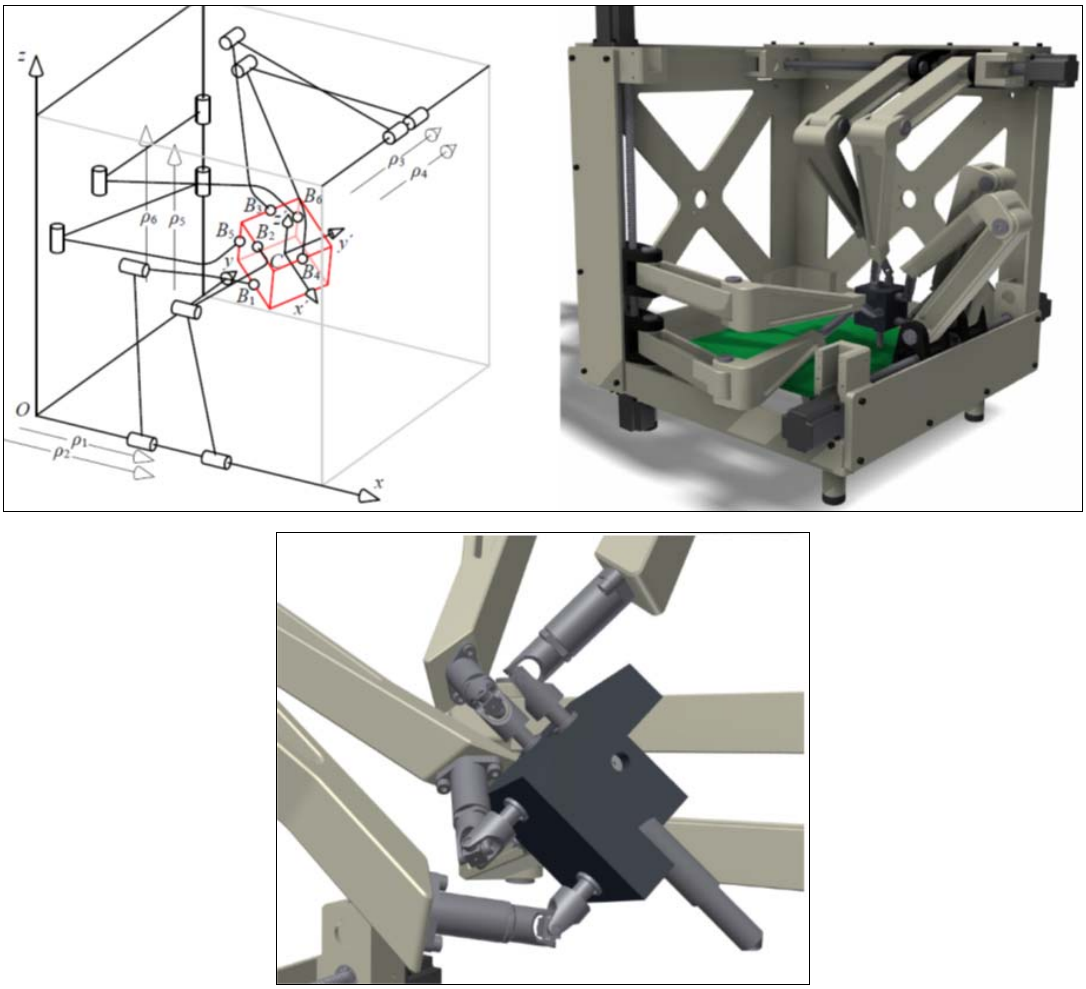

Fig. 1-22: Hexapteron: schematic drawing, the under-construction mechanical design, and the close-up view of the mobile platform at an extreme orientation (SEWARD & BONEV, 2014).

Such a machine might suffer from inter-collisions and therefore, a considerable attention for parts design must be paid. Furthermore, the different directions of actuators and the limits imposed by singularities highly constrict the workspace.

B- Five DoFs (3T-2R)

Seyanka

Seyanka is a five-axis milling machine designed by Tekniker, as a prototype to demonstrate the suitability of PKMs for high-speed milling applications (HERRERO, et al., 2000). The machine was publically presented in the Machine Tool Show of Bilbao in 2000 (BIEMH 2000). In this design, the usually unused rotation of the platform (i.e. that about the same axis of the spindle) has been removed, thanks to the passive chain (see **Fig. 1-23**). Also, compared to other machines with similar structure, the configuration of the actuators in the initial position is done with $90°$ symmetry instead of $120°$. This is more suitable for the intended application, since it allows the working volume to be almost prismatic-shaped. According to (HERRERO, et al.,

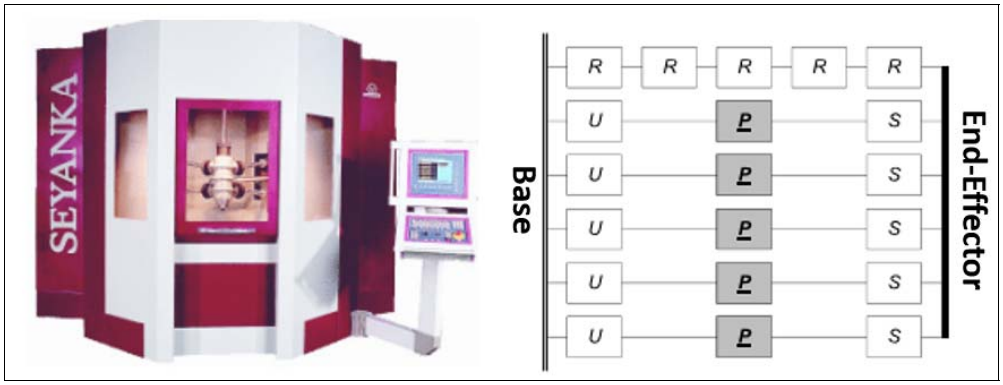

Fig. 1-23: Seyanka (Tekniker): photo and graph diagram.

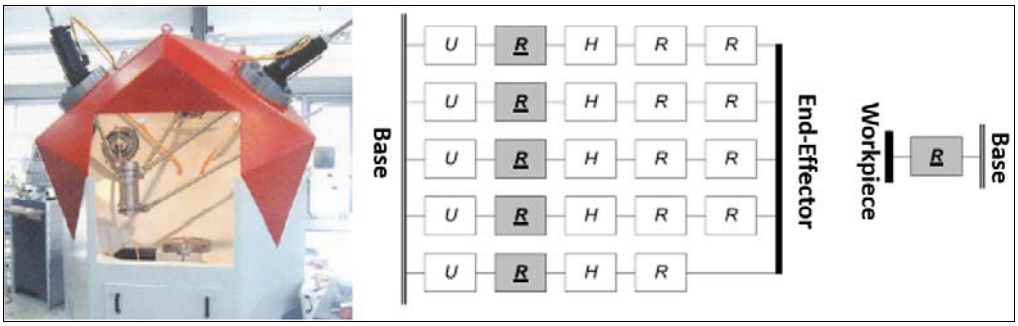

Fig. 1-24: P 800 (Metrom): photo and graph diagram.

2000), the machine is characterized by a speed of $60\,\mathrm{m/min}$ and an acceleration of $10\,\mathrm{m/s^2}$ (i.e. $1\,\mathrm{g}$).

P 800

In **Fig. 1-24**, we depict the P 800 (Metrom) machine. It obeys the right-hand left-hand paradigm, where a five-axis (3T-2R) parallel module is incorporated with a one-dof (1R) turntable. This machine is characterized by elevated tilting capacity, but the workspace is highly irregular, mainly due to arm inter-collisions. Actually, this was the reason behind equipping the machine with a turntable. The mechanism is kinematically redundant and perhaps, the only one so far that intentionally makes use of such redundancy to enhance the angular motion capability.

Tricept and Exechon

Among the successful five-axis machines based on parallel kinematics is the Tricept (Neos Robotics AB), which is depicted in **Fig. 1-25**. It is a typical hybrid machine with parallel structure followed by a series wrist, which therefore, allows large rotational motion. The machine, like the Seyanka, utilizes a passive kinematic chain (the U-P chain) to constrain the platform of the parallel structure. Among the characteristics of the machine, we mention the following: $\pm 50\,\mu\mathrm{m}$ accuracy, $\pm 10\,\mu\mathrm{m}$ repeatability, $90\,\mathrm{m/min}$ maximum feed rate, and $2\,\mathrm{g}$ maximum

acceleration[16]. The applications of this PKM range from light machining (e.g. cutting aluminum, plastic, wood, composites) to applications where the required path accuracy and/or high process force cannot be handled by conventional robots (e.g. friction welding) (DONG, 2002).

Nevertheless, Tricept is not stiff enough for some high-precision manufacturing tasks, such as aircraft assembly (NEUMANN, 2006). To overcome this limitation, another machine tool, called Exechon (see **Fig. 1-26**), has been developed by Exechon AB. It is also formed of a parallel module followed by a series wrist. Exechon has shown better performance as compared to Tricept (JIN, et al., 2012).

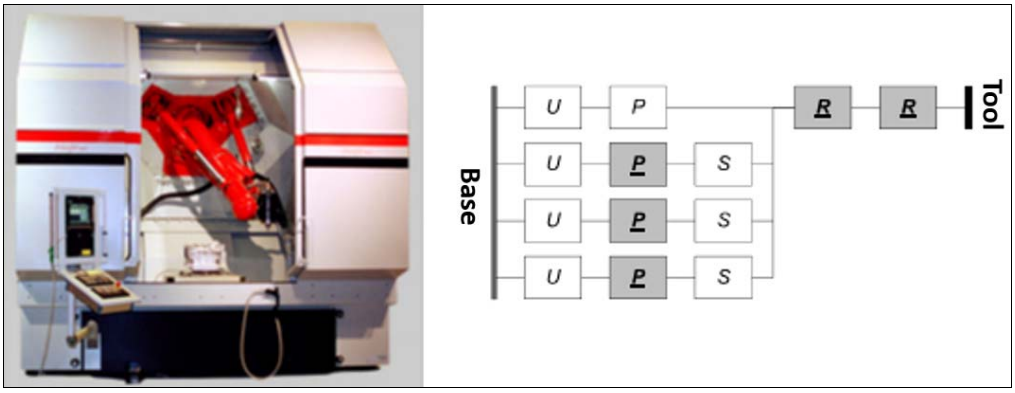

Fig. 1-25: Tricept 845 (Neos Robotics AB): photo and graph diagram.

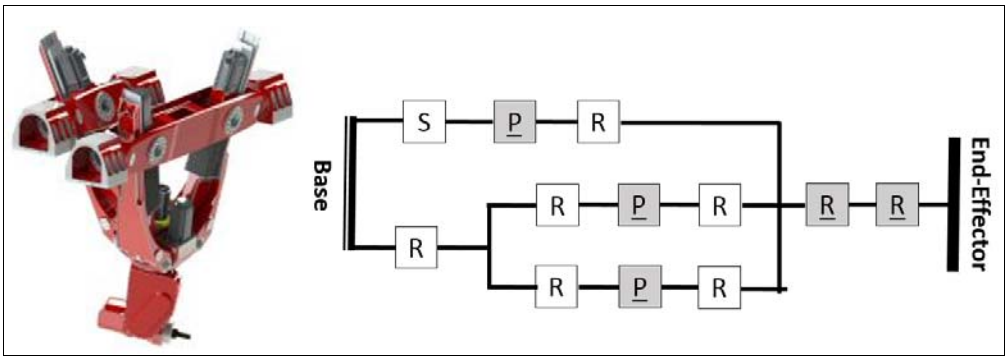

Fig. 1-26: Exechon (Exechon AB): photo and graph diagram.

Sprint Z3 and Hermes

Another hybrid PKM, the Sprint Z3 (DS Technology), is depicted in **Fig. 1-27**. The PKM has been developed for aeronautical industrial applications. It consists of series–structured carrier providing the xy-motion. On this carrier, a parallel module is fixed. The latter provides the wrist motions (two rotations) and the translational motion along the z-axis (the direction of the prismatic actuators). The design is quite simple, and it has met a real commercial success. Concerning its capabilities, it can achieve $50\,\mathrm{m/min}$ speed, $1\,\mathrm{g}$ acceleration along each axis,

[16]See: http://www.pkm-news.de/deu/tricepttmc845.html .

$\pm 40°$ orientation (A/B)[17], $80°/s$ maximum rotational speed (A/B), and $685°/s^2$ rotational acceleration (A/B). It is worth mentioning here that the Z3 head belongs to the group of so-called 3-[PP]-S[18] parallel mechanisms, defined as those whose three spherical joints move in vertical planes intersecting at a common line (LIU & BONEV, 2008). Such architectures are referred to as zero-torsion[19] mechanisms, and they are characterized by simple kinematic models (see (BONEV, 2002)).

Inspired by Sprint Z3, another similar PKM has emerged, which is Hermes (Fatronik, now Tecnalia). The PKM and its graph diagrams are shown in **Fig. 1-28**. As it can be clearly noticed, the only difference is using $(U\text{-}S)_2$ instead of R-S chains.

Dumbo

It is another hybrid machine (one dof carrier + parallel module + series wrist) developed at IFW of University of Hannover (Germany). It is presented in **Fig. 1-29**. Such a machine though has the advantages of large workspace and tilting capacity, it falls in the trap of a serial structure and the pyramidal effect regarding moving masses, thus influencing dynamics.

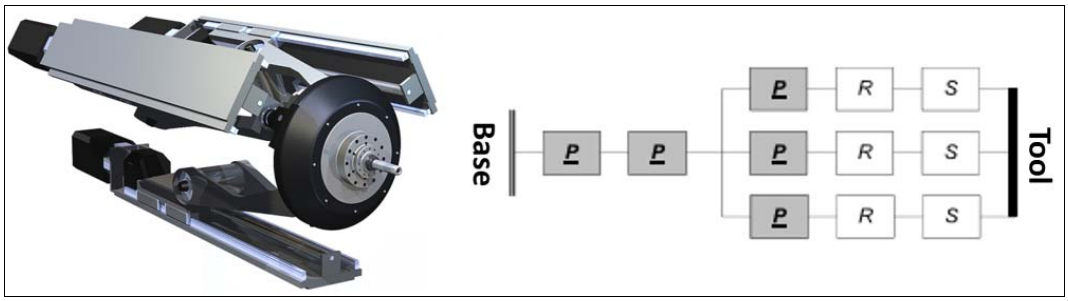

Fig. 1-27: Sprint Z3 (DS Technology): photo of the wrist and graph diagram.

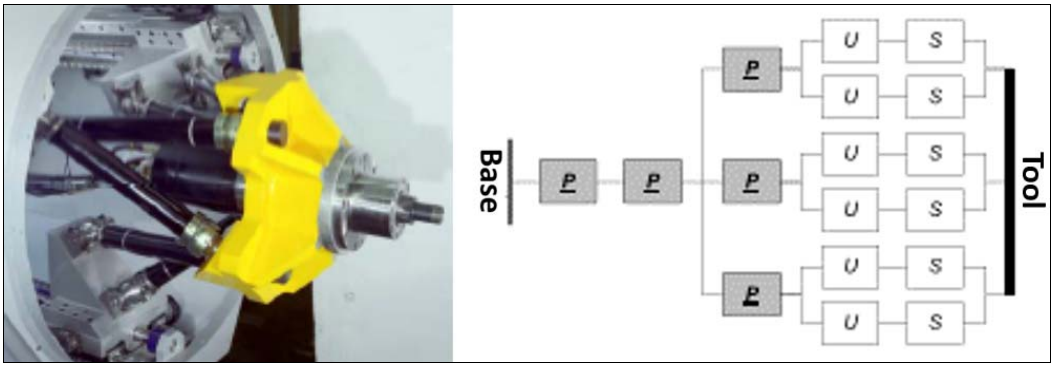

Fig. 1-28: Hermes (Fatronik, now Tecnalia): photo and graph diagram.

[17] "A" and "B" are the designation of rotations about x and y axes respectively (nomenclature adopted in machine tools)

[18] [PP] denotes any combination of joints that allows two-dof planar motion (adapted from (BONEV, 2008)).

[19] Tilt-and-Torsion (T&T) is an orientation representation, like Euler angles, but that allows better interpretation and simpler presentation. For details, refer to (BONEV, 2002, pp. 75-97).

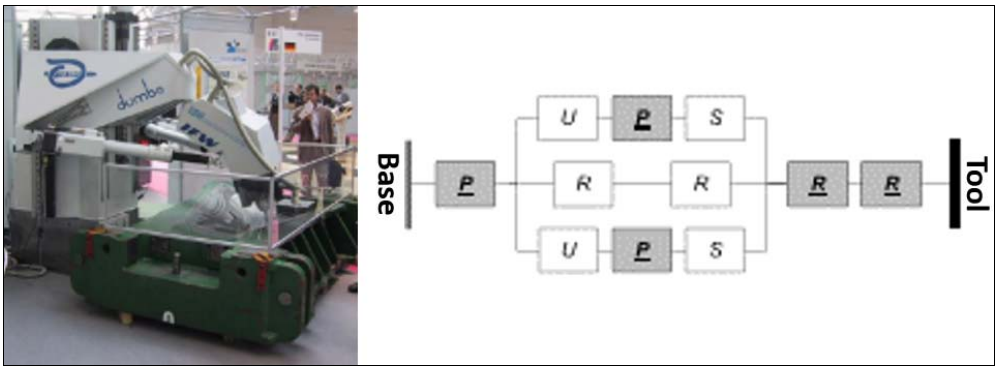

Fig. 1-29: Dumbo (IFW): photo and graph diagram.

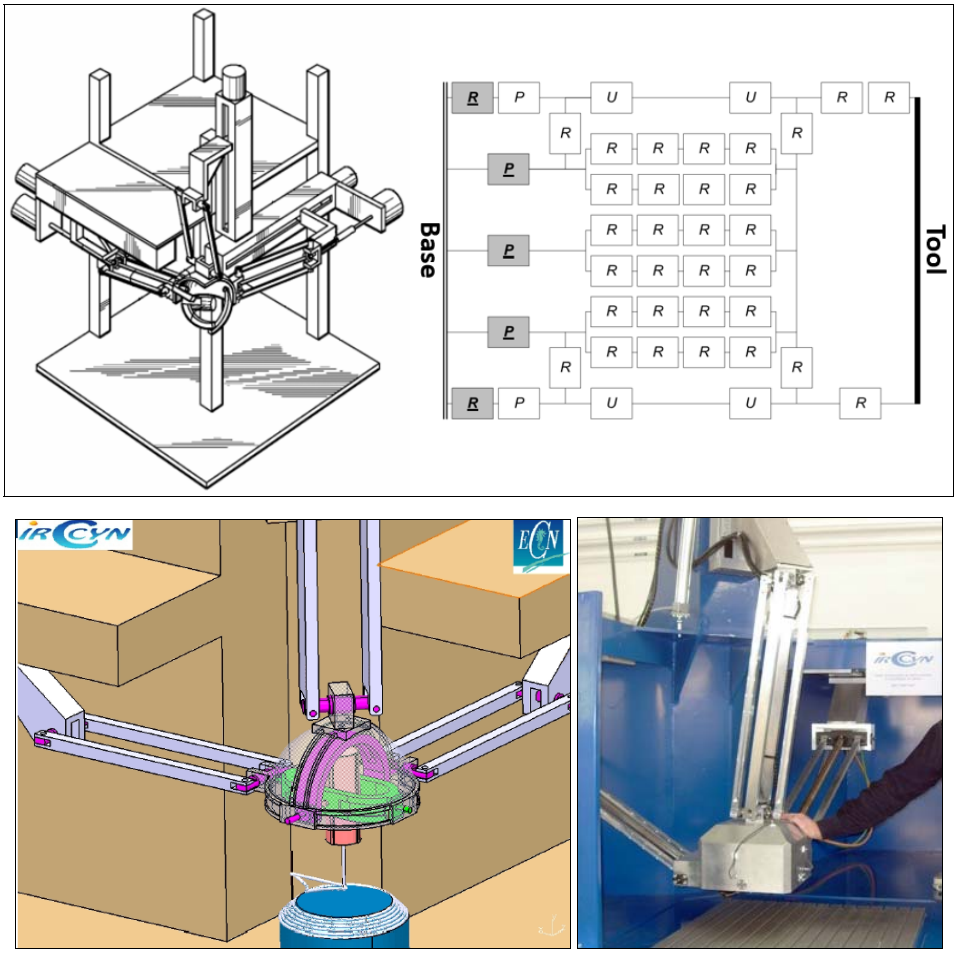

Fig. 1-30: Orthoglide five-axis version (IRCCyN): schematic, graph diagram, simplified CAD drawing, and prototype photo.

Orthoglide Five-Axis Version

An interesting five-dof (3T-2R) prototype, namely the Orthoglide five-axis version [20] (CHABLAT & WENGER, 2003), has been implemented at IRCCyN. The design combines the

[20] See videos available at: http://www.irccyn.ec-nantes.fr/fr/plateformes/orthoglide .

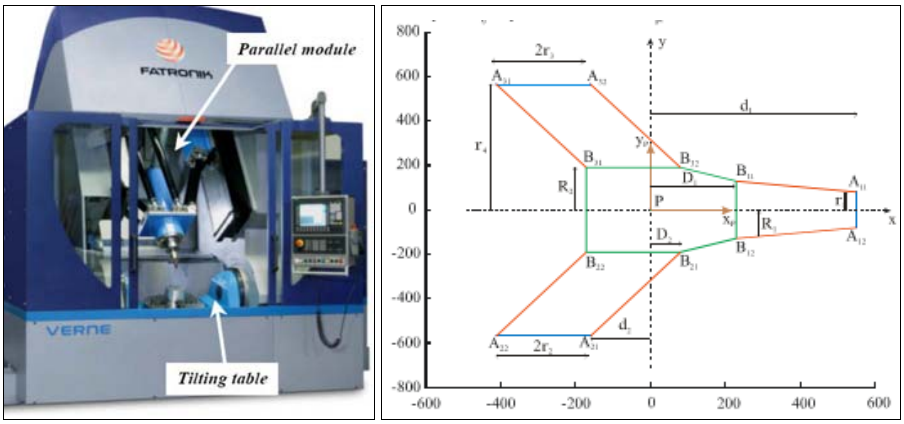

Fig. 1-31: VERNE machine (Fatronik, now Tecnalia): a photo and a schematic depicting the top view of the parallel module along its direction (from (KANAAN, et al., 2009)).

Orthoglide three-axis version ((WENGER & CHABLAT, 2000), (CHABLAT & WENGER, 2003)) and the two-dof (2R) Agile Eye (GOSSELIN, et al., 1996), with the former being a translational parallel mechanism and the latter a parallel spherical wrist. The Orthoglide represents a complex parallel architecture, and not a hybrid one (similar to the Fanuc robot in **Fig. 1-21**). This becomes clear by inspecting its graph diagram. In fact, if the actuation of the wrist were done in place, we would had a hybrid structure. Here, it is not the case. Instead, two transmission chains are used to transfer the motion from the rotary motors at the base to the wrist (see **Fig. 1-30**).

VERNE

VERNE is a hybrid branched-structure machine developed by Fatronik (now Tecnalia). It consists of three-dof parallel module and two-dof (2R) turntable (see **Fig. 1-31**). For the first glance, the parallel module seems to be a Delta structure, but a closer look reveals that this is partially true. In fact, unlike Delta where all the three arms are parallelograms, VERNE is characterized by having one arm being a trapezium and the others being classical parallelograms. Also, the trapezium individual rods are shorter than the other ones. This asymmetric structure of VERNE results in a coupled rotation of the tool about one of the axes with its translational motion (KANAAN, et al., 2009).

Hita-STT

The Hita-STT hybrid machine introduced by (CLAVEL, 2002) falls also within the category of left-hand right-hand structures. It is composed of four-dof (3T-1R) PM (see **Fig. 1-32**) and a one-dof (1R) turntable. An interesting feature of this PM is having parallel sliders and thus, allowing independent motion along their direction. This PM is capable of $\pm 60^{\circ}$ rotation and its stiffness is ensured in any position. Despite of that, it is not able to handle large parts due to the vertical axis of the rotary table (ANCUTA, 2008). Another disadvantage is the complicated mechanism in the architecture that provides rotation. Possible applications can be light finishing operations, such as polishing or deburring.

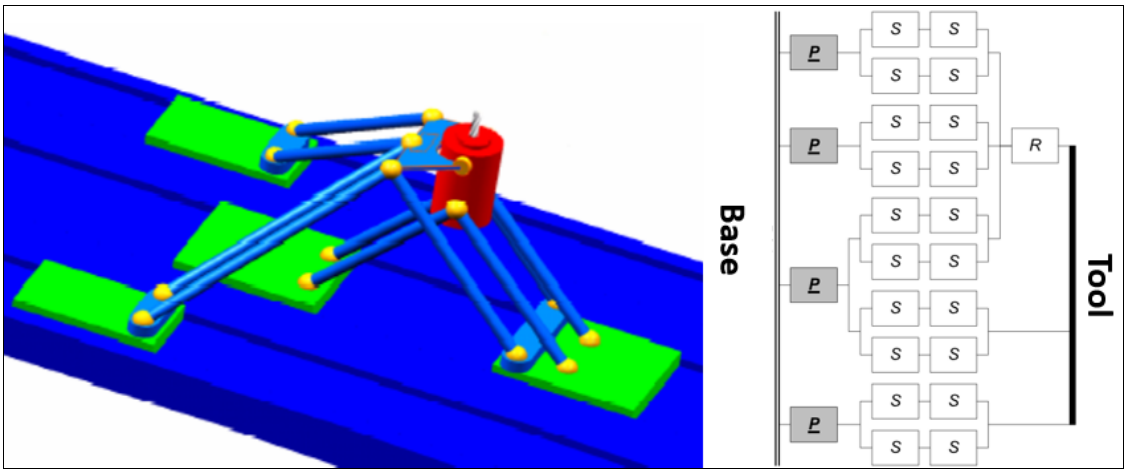

Fig. 1-32: Hita-STT (parallel module): CAD drawing and graph diagram.

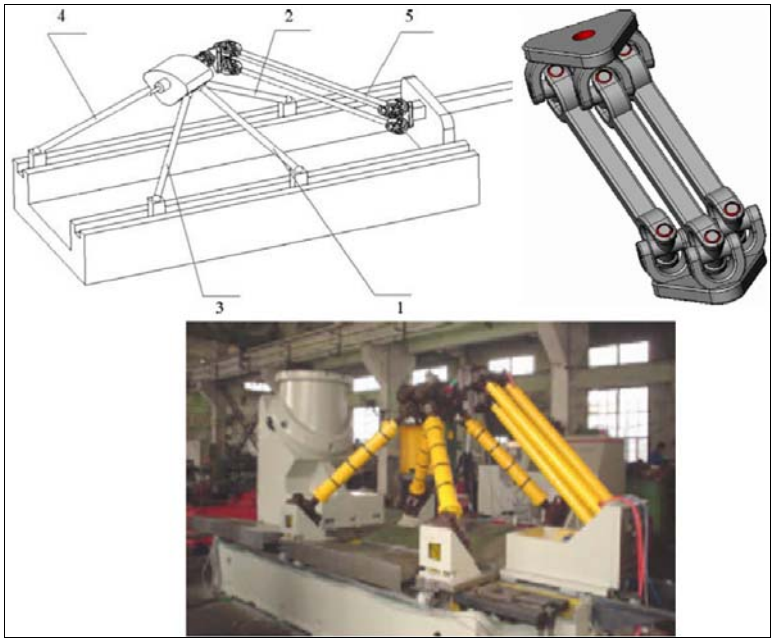

Fig. 1-33: A five-dof (3T-2R) PKM: global schematic, fifth limb illustration, and machine photo (GAO, et al., 2006).

Other Interesting Machines

Among other interesting five-dof (3T-2R) machines, we mention that of (GAO, et al., 2006) (see **Fig. 1-33**). It is composed of five limbs: four of them are of PSU type and the remaining fifth limb is a complex one denoted by PU*U. In all the limbs, the P-joint is actuated. The fifth limb can be described precisely as P-$(U\text{-}U)_3$-U, where $(U\text{-}U)_3$ corresponds to U* between the slider and the U joint. This fifth chain is the constraining one, which allows having the five dofs (3T-2R).

We terminate the section with the Reconfigurable Gantry-Tau PKM (ABB Robotics) and the ROBOTEX/Spider4 machine tool recently developed at LIRMM. The actuators in the former (**Fig. 1-34**) are: three fixed parallel electrically driven linear ball screws for positioning and two piston type electrically driven ball screws for tool orientation. The main reason for the industrial interest in this structure is that high machining performance can be obtained without needing the very heavy, expensive and difficult to install serial gantry robots used today. Moreover, its accessible workspace is larger than that based on serial kinematics (for more information, refer to (HUNT, 2007)). In fact, having the three positioning linear actuators along one direction, allows for independent motion along this direction, only limited by the available stroke. As for ROBOTEX/Sipder4, it consists of three-dof (3T) redundantly actuated parallel structure and two-dof (2R) series wrist. The former structure is inherited from R4 robot (CORBEL, et al., 2010) that has been also developed at LIRMM and that achieved incredible acceleration of $100\,\mathrm{g}$ (CHEMORI, et al., 2013). The actuation redundancy helps in eliminating singularities as well as

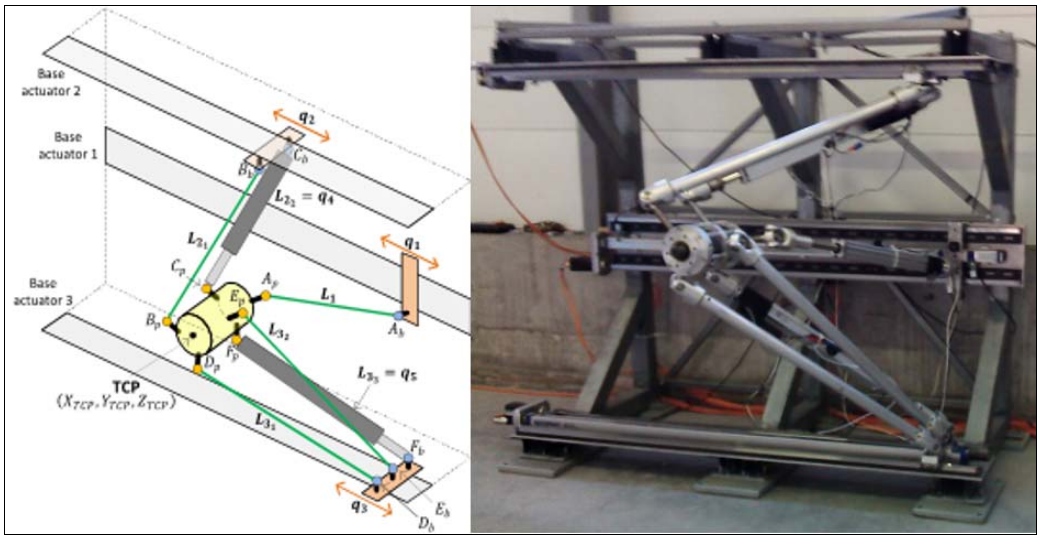

Fig. 1-34: The five-dof Gantry-Tau PKM (ABB Robotics): schematic and photo (from (TYAPIN & HOVLAND, 2013)).

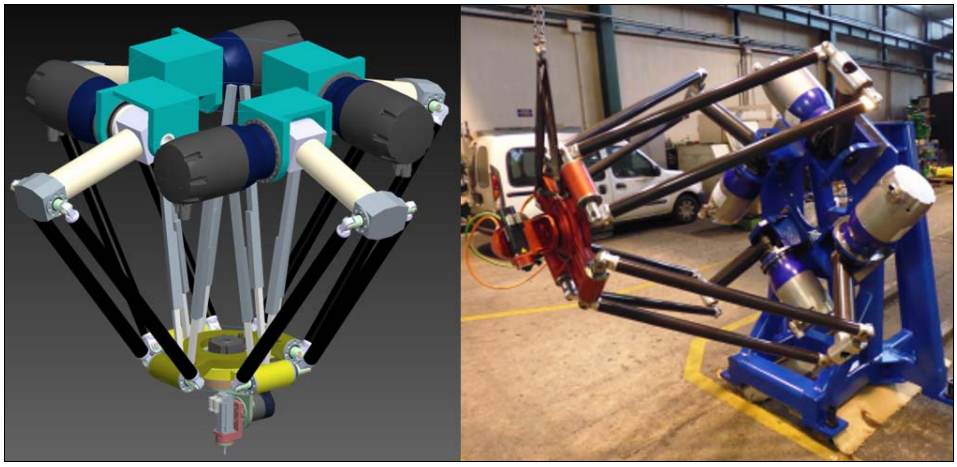

Fig. 1-35: ROBOTEX machine (LIRMM): CAD drawing and photo.

homogenizing and elevating dynamic performance over the workspace. In numbers, it is expected to achieve an acceleration of about $4-5\,g$, but still real performance is to be evaluated. The machine is depicted in **Fig. 1-35**. As it can be noticed, it is equipped with measuring struts to better measure the pose of the robot and hence, promote its precision characteristics. Finally, we mention that at LIRMM, two other designs that incorporate five dofs (3T-2R) in one non-hybrid structure and exploit both, actuation redundancy and parallel linear actuators at the base, have been suggested by (KRUT, et al., 2003) and (ANCUTA, 2008)(see **Fig. 1-36** and **Fig. 1-37**). The former is interesting regarding its workspace, performance homogeneity, and large tilting capacity, but the main limitation is in the use of gear or tendon based mechanism that may influence accuracy. Regarding the second, the collision related aspect and its impact on tilting capacity could be a drawback, though it has the advantage of large spatial workspace and performance homogeneity. A more recent design by (SHAYYA, et al., 2014a) has been also proposed. It utilizes an articulated platform and parallel linear actuators, but this time with only five motors. This will be discussed later in **Chapter 3**.

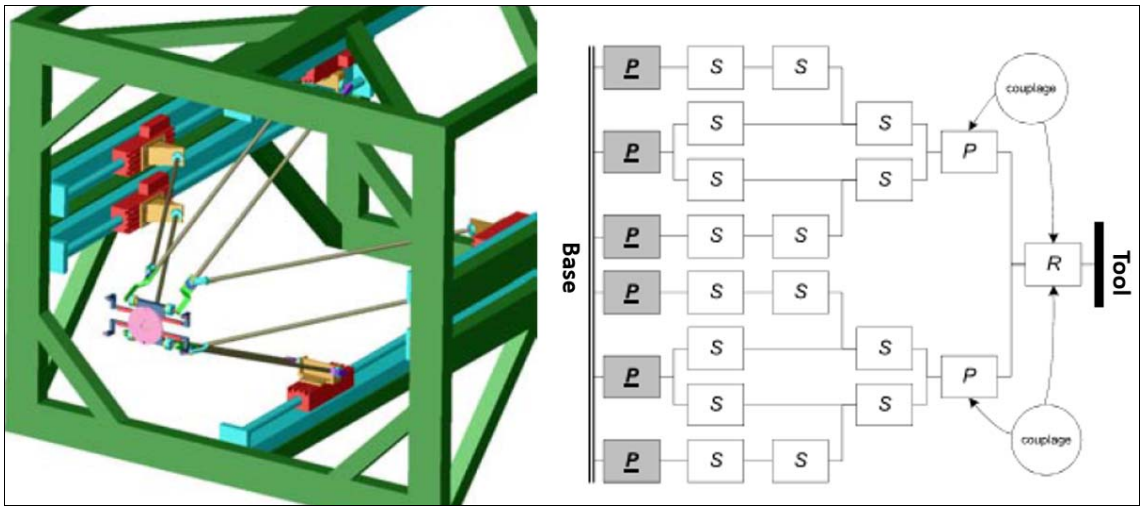

Fig. 1-36: Eureka (KRUT, et al., 2003): CAD design and graph diagram.

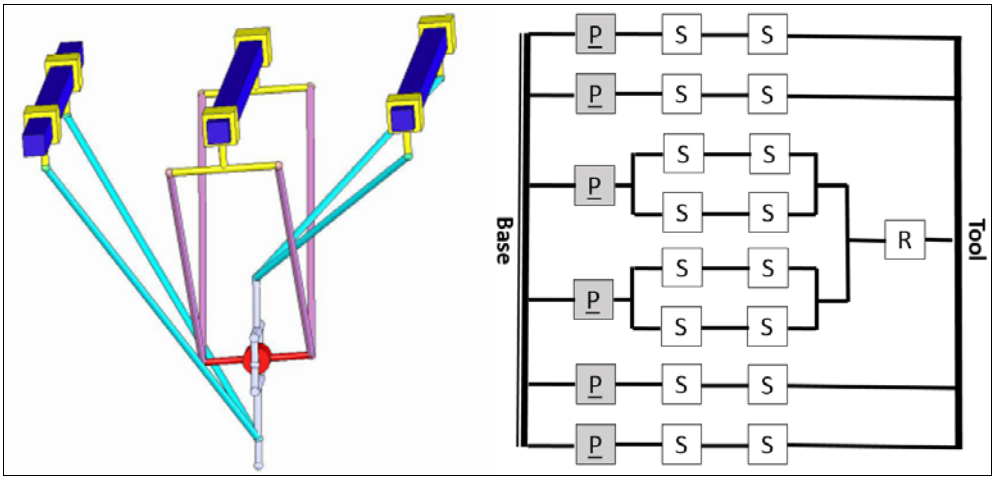

Fig. 1-37: Five-dof (3T-2R) manipulator (ANCUTA, 2008): schematic and graph diagram.

C- Four DoFs (3T-1R)

Perhaps, it is classical to start with the well-known and industrialized Delta robot with RUPU chain of (CLAVEL, 1991) (see **Fig. 1-2**). As early mentioned, thanks to the fixed actuators, lightweight components and use of parallelograms with simple technology, such robot is characterized by an exceptional performance ($10\ \mathrm{m/s}$ speed and $15\ \mathrm{g}$ for $1\ \mathrm{kg}$ charge[21]). As for positional repeatability, it is about $0.1\ \mathrm{mm}$ [21]. Moreover, the robot is characterized by large workspace, especially if linear Delta is considered (i.e. using linear actuators instead of rotary ones for the parallelograms). Nonetheless, this workspace remains restricted by the RUPU chain and particularly the available stroke for its corresponding prismatic joint. Also, the rotational stiffness can be impaired due to the use of universal joints; this is not to mention the vibration issues. These latter shortcomings have motivated some researchers in the quest for even better designs.

In the work of (ROLLAND, 1999), two robots, called Manta and Kanuk, have been introduced for industrial handling purposes. These are depicted in **Fig. 1-38** and **Fig. 1-39**, respectively. In both designs, the two undesired rotational motions are constrained, thanks to the pair of parallelograms that does not permit except one rotational motion (specifically that about the common axis). Their interesting features are the parallel linear actuators that help enlarge the

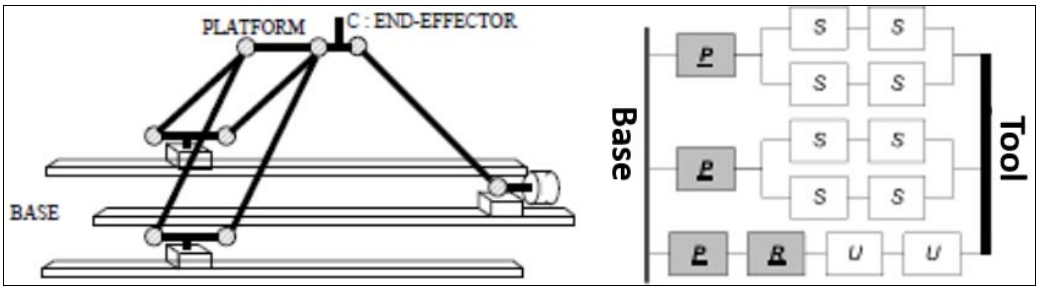

Fig. 1-38: Manta (ROLLAND, 1999): schematic and graph diagram.

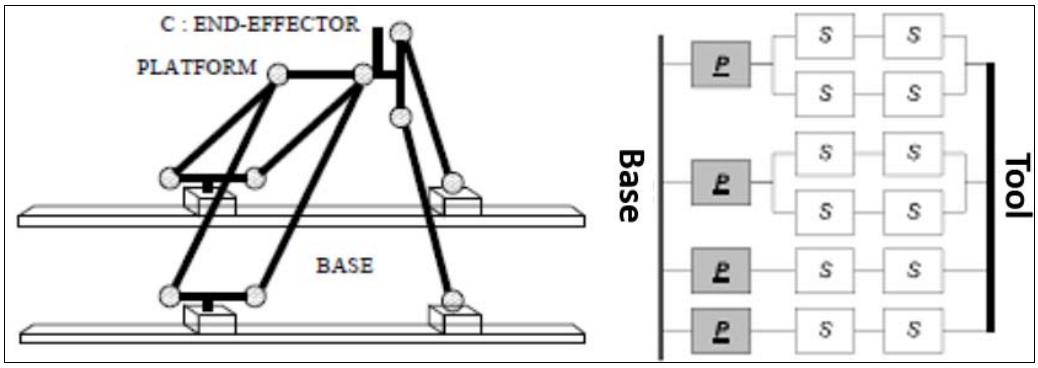

Fig. 1-39: Kanuk (ROLLAND, 1999): schematic and graph diagram.

[21] See for example:
http://www05.abb.com/global/scot/scot241.nsf/veritydisplay/c1b594e2b0a6f035c1257403005371b2/$file/Fiche%20IRB%20360%20FR%20rev1.pdf .

workspace along their direction on one hand, and having the sliders in the same plane on the other hand, which contributes to design simplicity. Moreover, the first robot, which has been implemented, has its rotation provided by a rotary actuator placed on the linear one and transmitted by a UU chain. Hence, its rotational capacity is unlimited and does not restrict the workspace, as compared with what we had in the case of Delta. Yet, it suffers from the possible impact on stiffness, in addition to the vibration issue. As for the Kanuk, the structure is fully parallel and replaces the PRUU chain by two PSS chains. This robot may be better than Manta for two reasons: the first is getting rid of the UU chain and the second is reducing the number of slider guides yielding an even simpler design, with fewer parameters. The latter point is particularly interesting, especially when dealing with calibration-related issues. Nevertheless, the Kanuk, as compared with Manta, is characterized by a limited rotational capacity.

In the same scope and in the attempt to eliminate the use of RUPU chain in Delta robot, several works have been done at LIRMM embodied in the doctoral theses of (COMPANY, 2000), (KRUT, 2003), (NABAT, 2007), and (ANCUTA, 2008). In fact, among the interesting contributions of (COMPANY, 2000), is the idea of articulated platforms and that led to the H4 family of symmetric and asymmetric robots. Later then, H4 concept evolved within the work of (KRUT, 2003) to the I4 version and afterwards, the concept of Par4 emerged with the work of (NABAT, 2007). This latter version has been industrialized under the name of Adept Quattro and is the world's fastest-pick-and-place industrial robot. In (ANCUTA, 2008), an extension of those works has been done, and architectures with Schönflies motion and rigid platform have been proposed. In what follows, we emphasize some points regarding the aforementioned works.

Concerning the H4 robot, it consists of four parallelogram arms connected to three-part articulated platform. The H4 prototype is depicted in **Fig. 1-40**. The rotary actuators can be replaced with prismatic ones, and the platform can be substituted by another one including a gear sub-mechanism to amplify the rotational capability (see **Fig. 1-41**). Furthermore, in the latter case, a redundant sensor to measure the rotational angle can be added; this version is depicted in **Fig. 1-42**. Nonetheless, H4 has the following limitations:

- The conditioning of the Jacobian matrix may vary considerably with tool orientation and hence, implying a change in machine behavior (KRUT, et al., 2003).
- Depending on the practical design, internal collisions might occur.
- Also, as discussed in (PIERROT & COMPANY, 1999), the relative positions of the four "spatial parallelograms" must be properly selected to avoid singularities (particularly internal ones). Specifically, placing them at $90°$ from each other is not recommended, though it would be interesting to have a symmetrical design with respect to the vertical axis for practicality reasons.

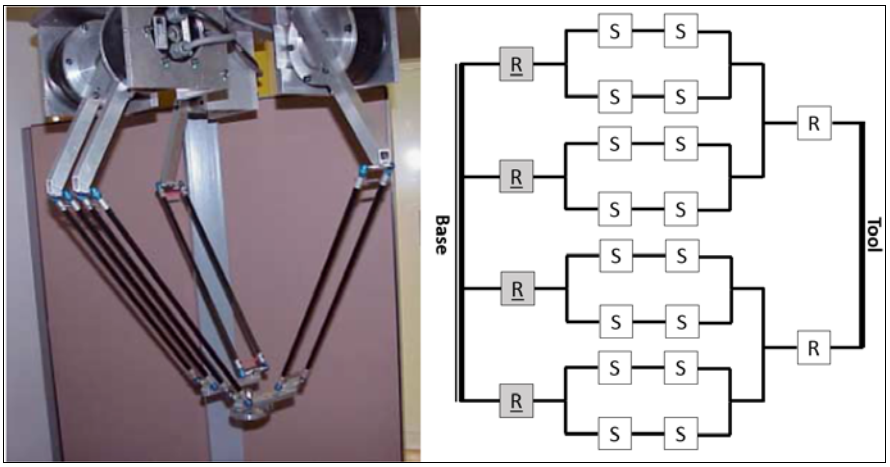

Fig. 1-40: H4 robot (COMPANY, 2000): photo and graph diagram.

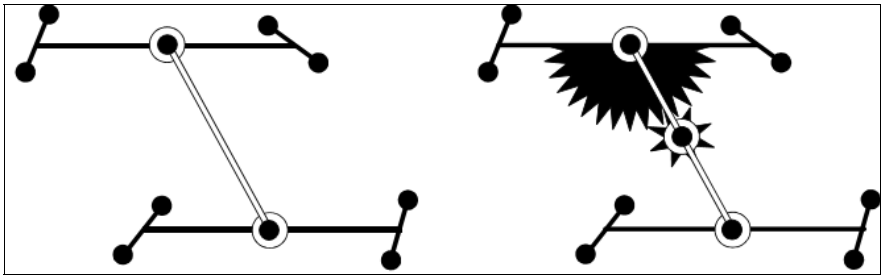

Fig. 1-41: H4 articulated platform: basic platform (left) and modified platform including amplification gear assembly (right) (image from (KRUT, 2003)).

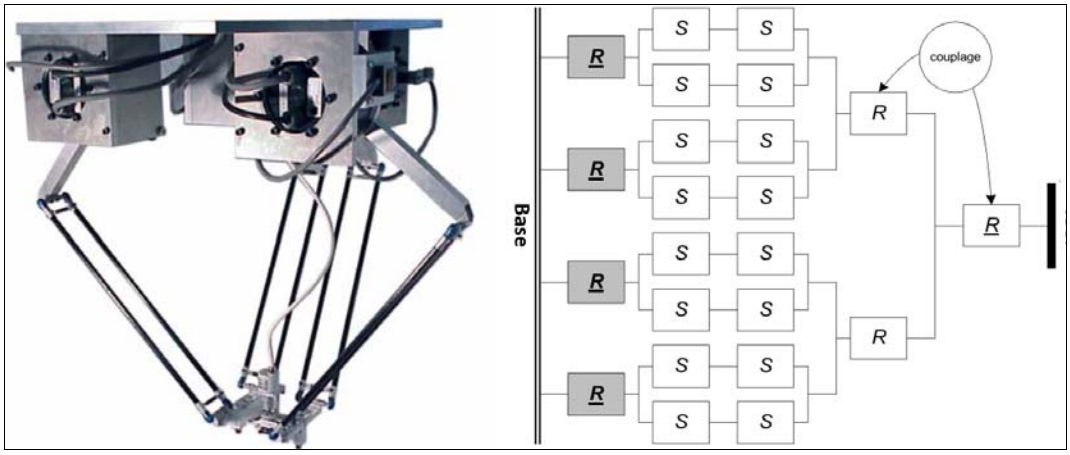

Fig. 1-42: H4 modified version (KRUT, 2003): photo and graph diagram.

Starting from the aforementioned issues, the I4 family has been suggested by (KRUT, et al., 2003). The basic idea behind I4, as compared with H4, is the replacement of pivot joints by prismatic ones and gears by rack-and-pinion assembly. In **Fig. 1-43**, I4L ("L" meaning with linear actuators) is shown with its graph diagram. However, for high-speed applications, the use of prismatic joints in the mobile platform is less recommended due to short-life service. Based on this, Par4 has been developed later by (NABAT, et al., 2005) utilizing only revolute joints in the

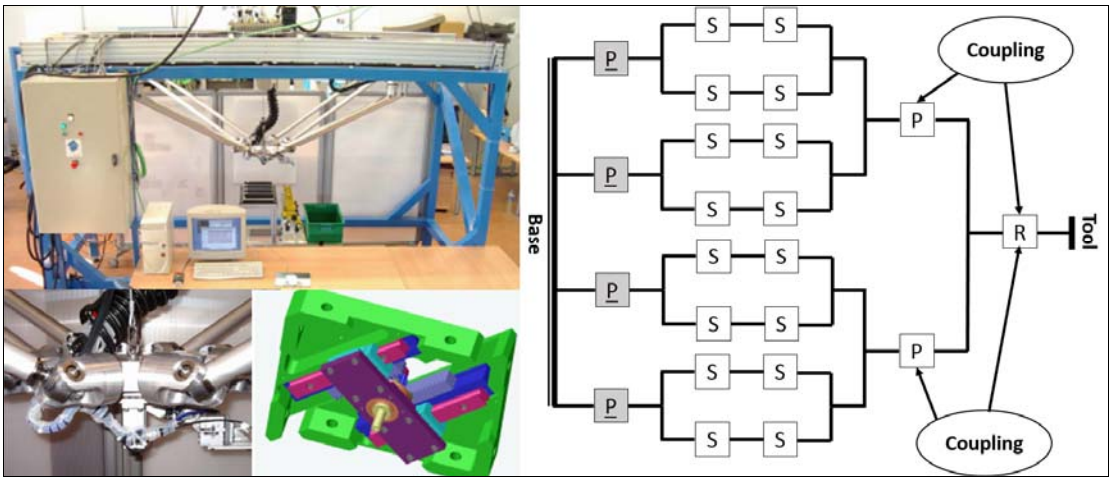

Fig. 1-43: I4L prototype (KRUT, 2003): photo, platform close-up view, CAD drawing, and graph diagram.

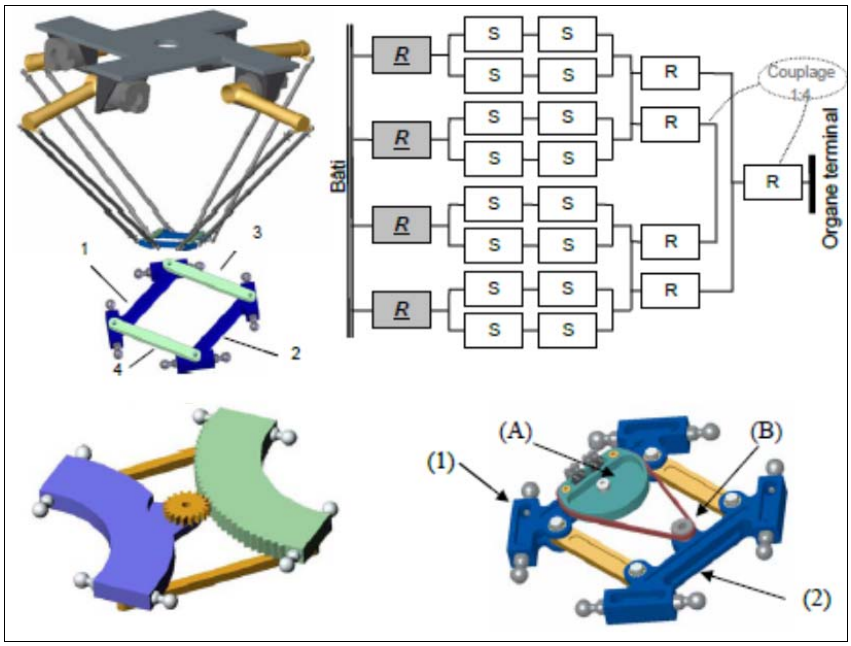

Fig. 1-44: Par4 (NABAT, 2007): CAD drawing, graph diagram and the two platforms with gear and cable-pulley amplification mechanisms.

articulated platform. Also, two amplification systems for rotation have been proposed: the first utilizes a gear assembly and the other exploits pulleys and cables. The generic CAD drawing and graph diagrams are depicted in **Fig. 1-44**, and the industrialized version is shown in **Fig. 1-45**. Another robot, also proposed by (NABAT, 2007), is the Héli4. The idea of this latter robot is to achieve the four dofs (3T-1R) by a compact simple platform. This has been accomplished by means of two-part platform joined by screw-nut system. The Héli4 prototype and its graph

Fig. 1-45: Industrialized version of Par4 (Adept Quattro).

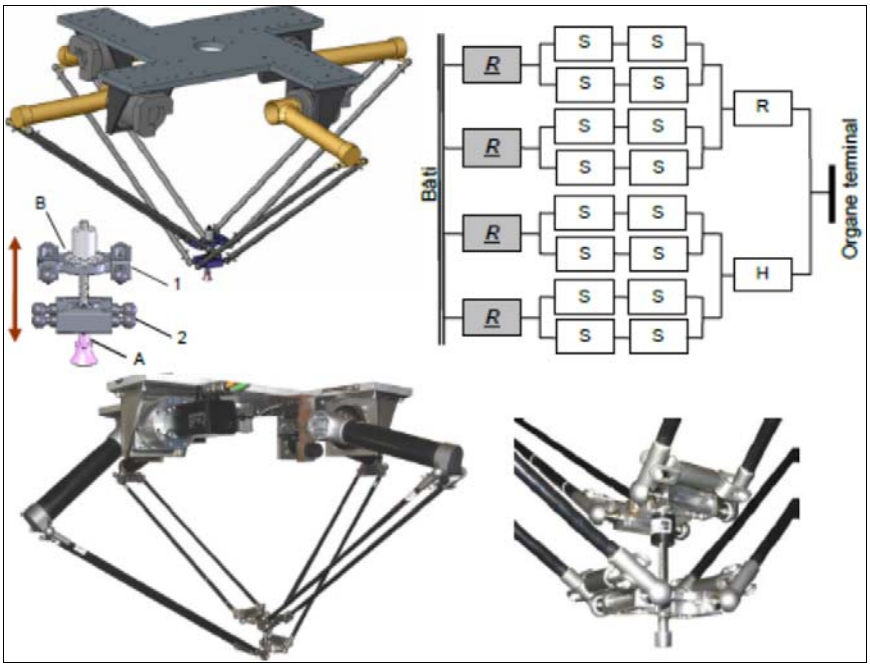

Fig. 1-46: Héli4 (NABAT, 2007): CAD drawing, graph diagram, prototype photo, and close-up view of the platform.

diagram are depicted in **Fig. 1-46**. The robot has been later industrialized by Penta Robotics under the name of Veloce[22] (see **Fig. 1-47**). The robot has rotational capacity of up to $180°$. Its cycle time is $0.32\,\mathrm{s}$, for a $0.2\,\mathrm{kg}$ load and a pick-and-place path described by

[22] See : http://pentarobotics.com/products/. Notice also that the slight difference between Veloce and Héli4 is the presence of prismatic guides in the former connecting the two parts of the platform.

Fig. 1-47: Veloce (Penta Robotics): photo and platforms (on the left corresponds to the case of three dofs (3T), and on the right corresponds to the case of four dofs (3T-1R)).

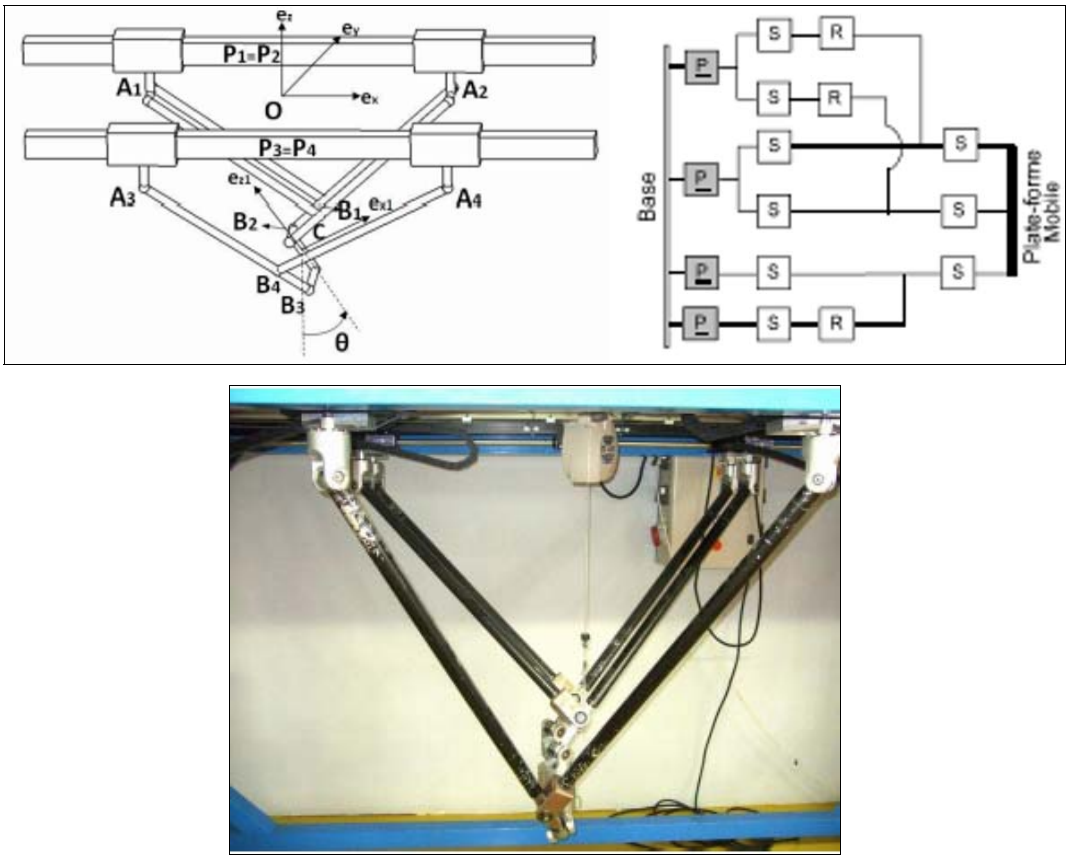

Fig. 1-48: λ-Quadriglide-V1 (ANCUTA, 2008): schematic, graph diagram and prototype photo.

$25\ \text{mm} \times 305\ \text{mm} \times 25\ \text{mm}$. Positional repeatability of Veloce is about $0.1\ \text{mm}$ (according to the technical specifications provided by Penta Robotics[22]). We end the overview on the LIRMM robots by presenting the λ-Quadriglide-V1 of (ANCUTA, 2008). In (ANCUTA, 2008), the demerits of articulated platforms, such as reduced stiffness and accuracy, were the motive behind seeking a rigid-platform-based manipulator while maintaining large workspace and design

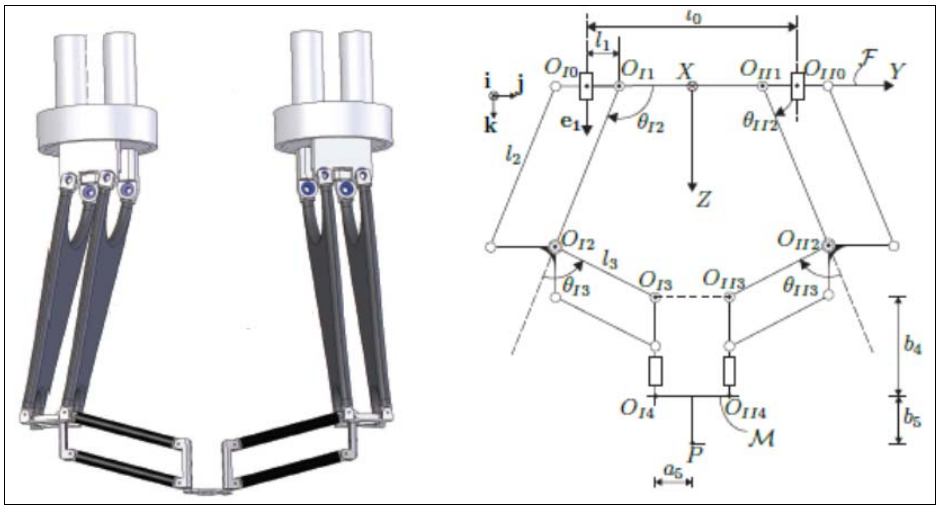

Fig. 1-49: The SMG of McGill University (ANGELES, et al., 2006): CAD drawing and clarifying schematic.

simplicity. The result of this work was the λ-Quadriglide-V1 consisting of parallel linear actuators and crank-like platform (see **Fig. 1-48**). In this design, two parallelogram arms are used to constrain undesired rotations with the other chains being of simple type. An interesting point in this mechanism is the pairing of arms, which is done in λ-shaped scheme, rendering it more feasible from manufacturability point of view. In this case, the use of spherical joints based on ball-socket and spring technology is eliminated together with their undesirable effects. The angular motion limits are in the vicinity of $\pm 45°$.

We end the panorama of four-dof (3T-1R) robots by the Schönflies Motion Generator (SMG) (ANGELES, et al., 2006) developed at McGill University, and the robot introduced by (KIM, et al., 2009). The SMG (see **Fig. 1-49**) consists of two R∏∏R chains with the ∏ indicating a parallelogram linkage playing the role of a kinematic pair, termed ∏-joint. In each chain, the revolute and the first ∏ (one revolute of ∏) are active. The robot has been designed with the target of achieving a pick-and-place cycle within at most $500\ \text{ms}$ for the path described by $25\ \text{mm} \times 300\ \text{mm} \times 25\ \text{mm}$, with a concomitant $180°$ turn. However, such design may suffer from poor rigidity and vibration. As for the robot of (KIM, et al., 2009) (see **Fig. 1-50**), it utilizes similar but non-identical kinematic chains. Each is composed of a simple actuated arm in series with a parallelogram one. The parallelogram is connected to the platform with a revolute joint parallel to the axis of rotation of the platform, as depicted in **Fig. 1-50**. However, having identical chains results in an architectural singularity, which occurs at the center of the workspace. Thus, to get rid of such singularity, an asymmetric design must be considered (similar to what we have in H4). Consequently, this would result in a highly inhomogeneous performance.

Finally, we mention that a more recent four-dof (3T-1R) PKM with actuation redundancy has been introduced and studied by ((SHAYYA, et al., 2013a), (SHAYYA, et al., 2013b), (SHAYYA, et al., 2014c) and (SHAYYA, et al., 2014b)). This PKM and its different modifications will be discussed later in **Chapter 3**.

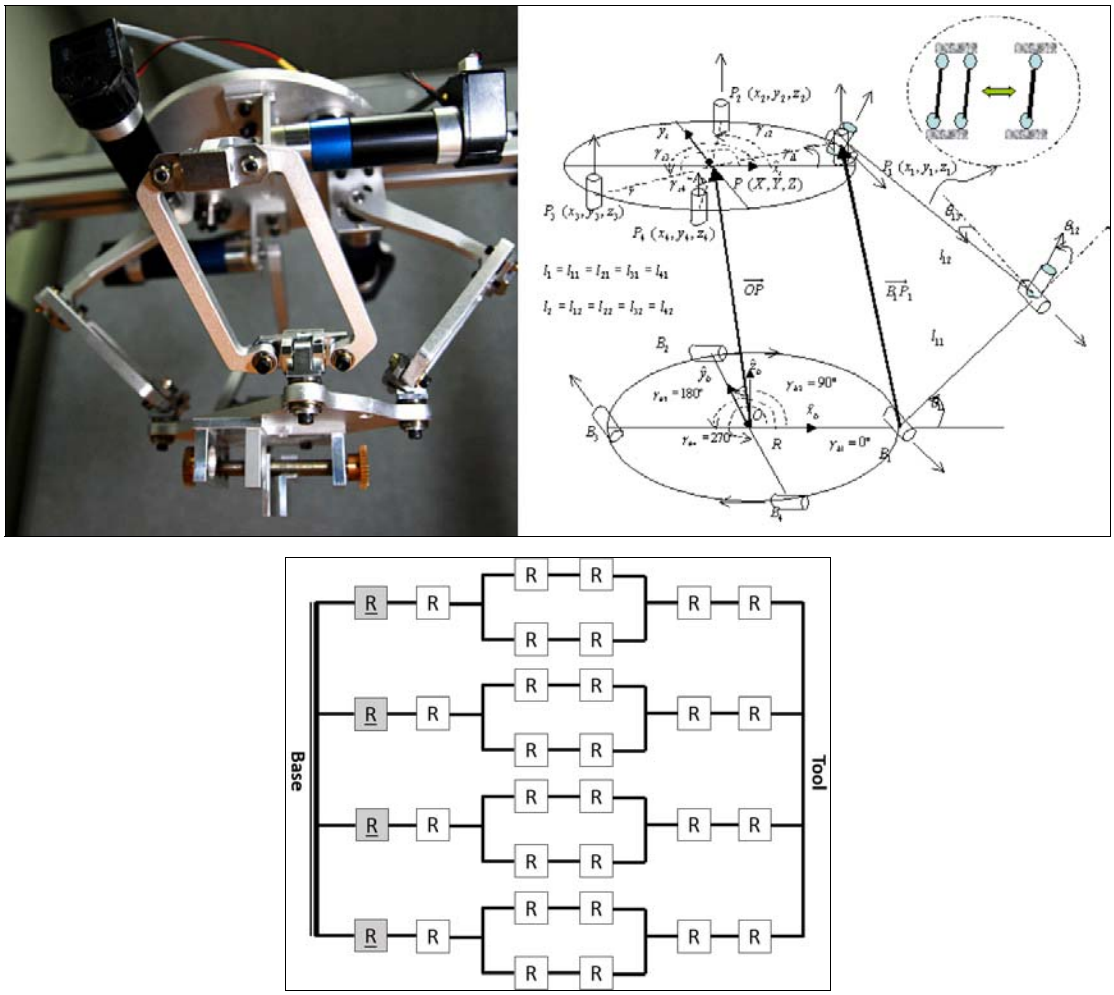

Fig. 1-50: Four-dof (3T-1R) parallel manipulator (KIM, et al., 2009): photo of exemplary device, clarifying schematic, and graph diagram.

With this, we end the overview on PKMs. In the next part, the performance evaluation regarding the precision of LIRMM rapid prototypes will be discussed.

1.3- Precision-Related Performances of Some Prototypes

In order to have insights on the precision-related performances of the most rapid parallel manipulators, a precision evaluation of several prototypes and industrial robots has been done at LIRMM. This assessment considered accuracy[23] and repeatability[24], not only for static poses but also in dynamics, i.e. as the robot follows a pre-specified trajectory. Moreover, multi-

[23] It is the distance between the mean of the attained poses and the commanded one. The closer it is to zero, the better.

[24] It is the radius of the smallest sphere centered at the mean pose and circumscribing all the attained ones.

directional variation of accuracy[25], in the case of statics, has been investigated as well. The norm adopted for all the aforementioned tests is **[ISO 9283; 1998 (F)]**.

The study considered the following robots: Quattro, Par2, DUAL V, and Veloce (the prototype). However, regarding dynamic performance (path following), not all robots were possible to evaluate due to technical issues and constraints.

In this section, we are not interested in detailing the results but rather synthesizing the main points, and emphasizing the major aspects and conclusions. For more details and clarifications, refer to **Appendix A.**

Briefly, in the light of the aforementioned static and dynamic precision evaluation, we have concluded that the positional accuracies and repeatabilities are in the order of millimeters and tenths of millimeters. As for orientation errors, the accuracies and repeatabilities are mainly degraded for the controlled rotation. Regarding the constrained orientations, their accuracies and repeatabilities are usually very small and due to assembly errors. Furthermore, the static repeatability results of Par2 and DUAL V, being between $10\,\mu m$ and $25\,\mu m$, are quite interesting[26], though their accuracies do not differ much from the other robots. In particular, the good overall performance of DUAL V has been of great impact and provided many insights. It accentuated that actuation redundancy is not problematic, especially when well treated on the control level. Based on the results of Quattro with rigid platform, such a conclusion is not possible to make. In addition, the use of revolute joints, in comparison with the joint technology used for parallelogram spherical joints in Quattro and Veloce, has been an essential factor in promoting DUAL V precision[27], and particularly its repeatability. We add to this, the use of direct actuation that eliminates backlash problems, which are usually inherent with the use of gear trains. Furthermore, the results of Veloce and Quattro (in its articulated version) emphasize the limitations of articulated platforms.

Based on the above, it becomes obvious that though the aforementioned robots are characterized by high rapidity, their precision is not sufficient for high-speed and high-precision applications. Thus, reaching a good compromise between rapidity and precision, the target of the ARROW project, should be planned along three directions:

1. The first direction is synthesizing the ideal mechanical structure and design of the PKM, while considering large workspace requirements and design simplicity.
2. The second direction is the proper choice of the optimization criteria for the dimensional synthesis of the geometric parameters of the PKM. This is essential and presents some

[25] It is the largest distance between the means of attained poses along different directions.

[26] Note that the repeatability of the measurement device is about $10\,\mu m$. Note also that accuracy results, especially for DUAL V, are not very reliable due to several technical issues (refer to **Appendix A)**.

[27] Precision, as referred to in several places in literature, is more related to repeatability than accuracy. Here, we will use the words “precision” and “precise” to refer globally to all terms, such as accuracy, repeatability and resolution (operational resolution), which we will discuss later in **Chapter 2**.

barriers to overcome. We expose this issue, highlighting the state of the art in this matter, in the upcoming section.

3. The final point is the proper control strategy, in which different advanced control laws are to be investigated. This point is not within the scope of the current thesis.

1.4- Performance Criteria and Parallel Kinematic Machine Tools

Thus far, we have exposed a non-exhaustive overview on parallel mechanisms and some of their precision evaluation. The main conflict that can be concluded regarding their poor exploitation in industry is the lack of architectures that have large singularity-free workspace, large tilting capacity, high stiffness, and design simplicity. Besides, so far we cannot find a PM that is both rapid and acceptably precise for handling high-speed and high-precision applications, such as laser cutting, welding, etc. Nevertheless, if finding the proper architectures is one of the prominent issues hindering PKMs' wide-spread, the performance evaluation and the criteria upon which these PKMs are dimensionally synthesized are of an equal importance. As (WECK & STAIMER, 2002) mentioned, "A poor topology but optimally designed may perform better than a mechanism with appropriate topology, but poor design." Moreover, if classically established performance measures have been more or less suitable for the synthesis of non-redundant robots with homogeneous dofs and same nature of actuators, still they are most often inadequate and debatable for robots characterized by redundancy or heterogeneous dofs. Actually, performance evaluation, despite of its importance and the rich research done in this scope, remains an open issue.

In this section, we discuss a non-extensive list of the available measures and their suitability for design and dimensional synthesis.

In general, these measures deal with singularity, precision, kinetostatics, dynamics, stiffness, natural frequencies, etc. In this thesis, we will be focusing on the first four domains, in which our contribution mostly falls.

Among the precision and kinetostatic measures, we mention for exemplification: the condition number κ (SALISBURY & CRAIG, 1982), the manipulability index μ (YOSHIKAWA, 1985b), the global conditioning index GCI (GOSSELIN & ANGELES, 1991), the motion/force transmissibility indices ((XIE, et al., 2011), (CHEN & ANGELES, 2007), (WANG, et al., 2010)), the minimum singular value (STOUGHTON & KOKKINIS, 1987), the use of semi-axes lengths of largest inscribed ellipsoid and pseudo-condition numbers ((KRUT, et al., 2004b) (KRUT, et al., 2002), (KRUT, et al., 2004a)), etc. It is worth mentioning that the aforementioned indices hold also some singularity significance, particularly concerning singularities related to the Jacobian matrix. Even some of them (e.g. condition number, manipulability, etc.) have been established primarily with the target of measuring the quality of the pose and its farness from singularity,

all while embracing some physical significance. Nevertheless, as other types of singularities[28] are not detectable by these measures, we prefer listing them under the aforementioned category, at least in what concerns PMs.

In fact, most of these works ((SALISBURY & CRAIG, 1982), (YOSHIKAWA, 1985b), (GOSSELIN & ANGELES, 1991), (STOUGHTON & KOKKINIS, 1987), (KRUT, et al., 2002), (KRUT, et al., 2004a), (KRUT, et al., 2004b)) have been based on quantifying the isotropy of kinetostatic performance (variation of force, velocity and accuracy[29] capabilities with direction), but from two different perspectives that only become distinguishable upon studying redundant robots. For example, in ((SALISBURY & CRAIG, 1982), (YOSHIKAWA, 1985b), (GOSSELIN & ANGELES, 1991), (STOUGHTON & KOKKINIS, 1987)), the indices provide a measure of the variation of transmission values with direction, while in ((KRUT, et al., 2002), (KRUT, et al., 2004a), (KRUT, et al., 2004b)), the target has been quantifying the maximal output performance with direction, i.e. an isotropy measure of output performance based on zonotope approximation by largest inscribed ellipsoid (mathematically referred to as John's Ellipsoid[30] (BALL, 1992)). In non-redundant robots, however, both concepts coexist naturally[31]. So while singular values and based upon indices serve well regarding singularity, precision, and kinetostatic performances in non-redundant robots, their kinetostatic significance, as described in ((KRUT, et al., 2002), (KRUT, et al., 2004a), (KRUT, et al., 2004b)), is lost in redundant ones. This is because the minimum and maximum output performances are not necessarily along the directions of the minimum and maximum transmission values. Not far from that, (MERLET, 2006) has revisited the concept of condition number and manipulability in the case of PMs, in which some important remarks regarding accuracy and the norms to be used have been pointed out. More precisely, the assumption that joint errors are described by unit-radius sphere has been criticized being non-realistic and therefore, its substitution by a unit-half-side cube has been favored. In addition, a comparison and a discussion on the suitability of the condition number and manipulability indices have been made. In (KLEIN & BLAHO, 1987), a survey of the various local kinematic dexterity measures is provided and definitions for positional, orientation, and spatial isotropies are given in (KLEIN & MIKLOS, 1991). In (PARK & KIM, 1998), the choice of the Riemannian metric to establish the manipulabity of closed kinematic chains, including those with redundancy, has been discussed. To end the scrutiny on the above-cited works, we emphasize that motion/force transmissibility indices as compared with others, always serve as

[28] Such as constraint singularities in parallel manipulators.

[29] Note that accuracy and velocity are similarly treated as they are both related by the Jacobian matrix. In fact, they are antagonist. Improving velocity leads to deteriorating accuracy, as it means error transmission value is increased.

[30] It is important to mention that John's Ellipsoid is unique for any convex compact region. This uniqueness is important feature added to the methodology of using the largest inscribed ellipsoid semi-axis lengths and the pseudo-condition numbers, as they are unique as well.

[31] Because the largest inscribed ellipsoid in the operational zonotope (whether velocity or force) is the image of the unit-radius sphere in the joint zonotope.

a measure to qualify good or bad transmission, but not indicative regarding the extreme output performances.

In a recent work (GUAY, et al., 2013), an index called "minimum degree of constraint satisfaction," has been introduced and applied on cable-driven parallel robots (CDPRs) to assess the capability of producing a specified set of wrenches. It can be applied on rigid robots equally well. It considers the minimum distance between the specified set to the zonotope boundary. However, to deal with the case of heterogeneous-dof robots, an arbitrary homogenization has been adopted and hence, falling as most other indices in the debate that accompanies such procedure.

Actually, in addition to redundancy that has been particularly treated for example by the works of (KRUT, et al., 2004b) (KRUT, et al., 2002), (KRUT, et al., 2004a) and (XIE, et al., 2011), the heterogeneity problem (case of robots with heterogeneous dofs or actuators) has constituted another dilemma that attracted numerous researchers as well. For instance, among the homogenization techniques, we mention the use of some sort of weighting/normalizing matrix or characteristic length, as in ((MA & ANGELES, 1991), (ANGELES, 1992), (STOCCO, et al., 1998)). In other works, such as ((GOSSELIN, 1992), (KIM & RYU, 2003), (KIM & RYU, 2004), (POND & CARRETERO, 2006)), the homogenization of the Jacobian has been achieved by considering the velocities (or forces) of two or three points situated on the end-effector, after relating them to the actuated joint velocities (or torques). Such methods are characterized by arbitrariness and lack of direct interpretable kinetostatic significance. Particularly, such homogenization would not affect highly the singularity assessment, though numerical value varies with the arbitrary homogenization. This is since if we are using, for instance, singular values to assess singularity, then theoretically and regardless of the homogenization technique[32], the singular configurations remain invariant and occur for zero or infinite singular value. As for kinetostatics, the indication of the homogenized vector is not easy to interpret or relate to the end-effector twist (or wrench). In more recent works ((MANSOURI & OUALI, 2009), (MANSOURI & OUALI, 2011)), the issue has been addressed based on the apparent power concept to achieve homogeneous formulation of the problem. The methodology introduces some weighting factors K_L and K_R, the ratio of which is important. Then, a minimization of some quantity is carried out to get a unique value of $\beta = K_L / K_R$, upon which the final power manipulabity depends. However, the relation of the established measures to the operational twist and wrench is rather vague. This is not to mention the associated complexity.

In fact, the arbitrariness involved in dealing with heterogeneity conflict is inevitable consequence of the absence of a natural metric for the geometry of $SE(3)$ as stated by (PARK & KIM, 1998), although in the work of (PARK, 1995) some insight on homogenization technique has been provided. Actually, (PARK, 1995) has discussed left and right invariant distance metrics, and proved the non-existence of a bi-invariant one. Furthermore, a discussion on the

[32] As long as the homogenized matrix and the initial one are equivalent regarding their rank.

invariance issue of manipulability indices can be found in (STAFFETTI, et al., 2002). Therefore, an intuitive approach to get rid of such predicament would be to study translational and rotational performances separately. This has been suggested by (YOSHIKAWA, 1991) through the translational and rotational manipulabilities, defined in the weak and strong senses. In a more recent work, Direction-Selective Indices (DSIs) have been proposed by (BOSCHETTI, et al., 2011). In this approach, the manipulabilities of the individual translational dofs are studied independently. Such method can be used equally with rotational and heterogeneous-dof robots. However, the individual study of translational and rotational performances resembles the redundancy situation; therefore, classical indices become less significant in this sense. In another work, the Force-Velocity Isotropy Index and the treatment of heterogeneous-dof robots by proper separation of translation and rotation have been discussed by (SHAYYA, et al., 2014d). This will be detailed later in **Chapter 2**. In the scope of precision, a similar approach can be considered. For example, the kinematic-sensitivity indices that separate orientation and position errors have been suggested by (CARDOU, et al., 2010). In this work, for bounded p-norm of joint errors, the maximal p-norm of orientation and positional errors are considered as to overcome the heterogeneity issue. This means if we consider, say infinity norm for joint errors, we end with same norm regarding orientation and positional ones. Therefore, the orientation (or positional) errors are geometrically interpreted as rectangular parallelepiped. Likewise, in the case of using Euclidean norm on joint errors, we end with an ellipsoid representing orientation (or positional) errors. In either cases (Euclidean norm or infinity norm), only the realistic aspect of one of the two errors, either joint or operational errors, is considered properly. More precisely, the infinity norm is the reasonable to use for joint errors, being generally independent[33]. However, it is not consistent for those of the operational space. As the translation (similarly rotation) is a coupled motion, the Euclidean norm is the more consistent to use, as the spatial accuracy is the more interesting and not the axial one. This idea is what we are going to present and discuss in **Chapter 2**. An additional point to make is that while the proper separation of translation and rotation for precision evaluation is always justifiable, it is not the case regarding kinetostatics for only one exception. This is the case where the robot performs the two motions (or supports force and moment) in separate phases. Apart from that, such decomposition is not indicative. That is why a relevant approach to co-assess simultaneous performance in translation and rotation has been investigated in this thesis (see **Chapter 2**).

While most of the works were concentrated on investigating input-output performance, (BRIOT, et al., 2013) suggested the study of reactional forces in the passive joints. This is indispensable in the design of any manipulator. Nevertheless, it remains an intermediate step that influences dynamics. Knowing the magnitudes of these forces, proper sizing of the joints and components to sustain stiffness and prevent failure can be done. The impact would be

[33] The independency of joint errors is true only for non-redundant robots. When the robot is redundantly actuated, some dependency relations exist and therefore, its accuracy analysis must account for this particularity.

embodied then in the inertia whose effect can be inferred via dynamic measures. Therefore, considering these forces by themselves as an objective is less favored.

Moreover, in (VOGLEWEDE & EBERT-UPHOFF, 2005), the authors investigated different indices in the attempt to identify the most suitable ones that can detect singularities (the classical ones), while providing both: a sort of distance measure to singularity on one hand, and interesting relevant physical significance on the other. They concluded that while power and input torque measures are not sufficient to detect all singularities, the natural frequency does and more importantly merges stiffness and mass inertia together.

Stiffness, whether the control-related one or that of the physical structure itself, is undeniably essential and especially for machine tools. The same applies for natural frequency. However, such criteria can be fulfilled at the design stage of the parts through both: their proper dimensioning (for structural stiffness and natural frequency), and tuning of the controller (for control-related stiffness). Based on this, such indices are not that critical to consider as main objectives.

It remains finally to discuss the literature in what concerns dynamics. Among the available indices, we exemplify: the dynamic manipulability (YOSHIKAWA, 1985a), the dynamic conditioning index ((MA & ANGELES, 1990), (MA & ANGELES, 1993)), the generalized inertia ellipsoid as means of evaluation of the capability of changing end-effector velocity in different directions for the given kinetic energy ((ASADA, 1983), (ASADA, 1984)), the maximum singular value of the generalized inertia matrix or its row vector matrix ((LI, et al., 2005), (HUANG, et al., 2005)), the acceleration radius (GRAETTINGER & KROGH, 1988), the acceleration hyper-parallelepiped (KHATIB & BURDICK, 1987), the Dynamic Load Carrying Capacity (DLCC) ((WANG & RAVANI, 1988a), (WANG & RAVANI, 1988b)), the Acceleration Set Theory (KIM & DESA, 1993), the motion isotropy hypersurface (BOWLING & KHATIB, 1998), the actuation efficiency measure (BOWLING & KHATIB, 2000), the actuator-selection criteria based on dynamic performance discussed by (BOWLING & KHATIB, 2003), the maximum-required-torque-based indices of (ZHAO & GAO, 2009), etc.

Unfortunately, each of these measures, in addition to its features, has its own drawbacks. For example, in ((YOSHIKAWA, 1985a), (MA & ANGELES, 1990), (MA & ANGELES, 1993), (ASADA, 1983), (ASADA, 1984), (LI, et al., 2005), (HUANG, et al., 2005)), the velocity and gravity terms are not considered. This makes them less suited for high-speed manipulators or heavy ones used for applications with large load requirements. Also, the arbitrary homogenization needed in ((YOSHIKAWA, 1985a), (MA & ANGELES, 1990), (MA & ANGELES, 1993), (ASADA, 1983), (ASADA, 1984), (LI, et al., 2005), (HUANG, et al., 2005), (GRAETTINGER & KROGH, 1988), (KHATIB & BURDICK, 1987)) to deal with heterogeneous-dof robots renders these measures less significant. The Acceleration Set Theory (KIM & DESA, 1993) does not address the heterogeneity problem. As for DLCC ((WANG & RAVANI, 1988a), (WANG & RAVANI, 1988b)), it is not influenced by heterogeneity conflict, but it is trajectory-based measure. It considers performance required to move in one direction along a particular path and therefore, it is more suitable for pick-and-place applications than machine tools. As for (ZHAO & GAO, 2009), an

implicit homogenization, in the case of heterogeneous-dof robots, is considered via the assumption of $\|\boldsymbol{\chi}\|_2^2 = 1$ (where $\boldsymbol{\chi}$ is six-dimensional velocity or acceleration vector). Furthermore, the computation of the maximum torques is done assuming sole translation along or rotation about one of the coordinate axes with unitary value (in velocity or acceleration), as implied by the use of infinite-matrix norm. Hence, the suggested indices of (ZHAO & GAO, 2009) suffer from the same limitations and arguments accompanying arbitrary homogenization.

In the work of (BOWLING & KHATIB, 1998), the approach of overcoming arbitrary homogenization by decomposing each of the acceleration and twist into their composing translational and rotational parts is remarkable. However, the isotropy hypersurface itself is not that easy to use. For this purpose, the same authors introduced the actuation efficiency measure and discussed actuator-selection criteria in (BOWLING & KHATIB, 2000) and (BOWLING & KHATIB, 2003), respectively.

The actuation efficiency in (BOWLING & KHATIB, 2000), as its name indicates, is more suitable to assess actuation but cannot give an insight on the isotropic accelerations themselves. This is not to mention the complexity, as volume integration is required for the calculation of the aforementioned measure. The approach discussed in (BOWLING & KHATIB, 2003) allows the user to inspect whether the pre-specified performance at a configuration is attainable or not (depending on having α_i or α_{ij} superior or inferior to one). An additional feature is including external forces and moments in the play, which is quite interesting. Among the cited works, (BOWLING & KHATIB, 2003) is the closer to our proposed methodology in **Chapter 2**. However, unlike (BOWLING & KHATIB, 2003), our indices tell not only whether certain dynamic performances are applicable simultaneously in all directions, but also the extreme that can be reached in each aspect while fulfilling the others. Thus, more interesting options and features are available, permitting better design optimization. Besides, the approach is not restricted to rigid manipulators, and its extension to deal with CDPRs is formulated as well.

With this, we end the overview on performance evaluation and the available literature. It remains to state the general outline of the thesis, the subject of the next section.

1.5- Thesis Outline

Having exposed the state of art of PMs and the literature concerning performance measures, the following chapters detail the different steps taken towards the achievement of the preset goals. The rest of the thesis is planned as follows:

- **Chapter 2** details the establishment of adequate precision, kinetostatic, and dynamic measures that consider machine tool requirements. In addition, their formulation to treat CDPRs is provided as well.
- Afterwards, **Chapter 3** presents several interesting novel architectures that have been synthesized during the course of the thesis. Additionally, the dimensional syntheses

concerning two of them are provided, among which is that of the final implemented ARROW PKM.

- **Chapter 4** exposes the geometric sensitivity of the eventual PKM and suggests some possible methodologies of compensation for geometric and elastic errors. This would be a second step to go for further amelioration of precision performance.
- Ultimately, a separate part concludes the major accomplishments and discusses the possible future research directions.

Chapter 2: Performance Evaluation of General Manipulators

In this chapter:

This chapter introduces a relevant novel methodology to tackle the performance evaluation of general manipulators and machine tools, regardless of being based on serial, parallel or hybrid kinematics. The presented measures fall within precision, kinetostatic, and dynamic performance fields. They overcome two main quandaries that have been highlighted in the previous chapter, namely: heterogeneity problem (heterogeneous dofs or actuators) and redundancy. Regarding the latter issue, only manipulators with either pure actuation or kinematic redundancy are discussed. Therefore, robots that exhibit both types of redundancy are beyond the scope of the current chapter. However, the methodology is not restricted to rigid manipulators, but extensible to cable-driven ones equally well. The mathematical formulation for both cases are elaborated and supported by case studies.

2.1- Introduction

Before introducing our approach, we need to talk first of some generalities regarding manipulator kinetostatic relations. While such relations are straightforward for non-redundant manipulators, few particularities are worth emphasizing in what concerns redundancy. Moreover, it is equally important to discuss the latter's major benefits and types. This is the subject of the current section.

While actuation redundancy (AR) is only applicable to PMs, kinematic redundancy (KR) is applicable to both serial and parallel structured mechanisms (SMs and PMs). A common point between the two is having at least one extra actuator as compared with the end-effector dofs. Thus, if we assume m and n the respective numbers of actuators and operational dofs[1], then in the case of redundancy, we have $m > n$. We emphasize here that redundancy and its definition can be slightly misleading as highlighted in (CONKUR & BUCKINGHAM, 1997). In particular, kinematic and task redundancies might be messed up. In what follows, we attempt to make all these terms as clear as possible.

2.1.1- Kinematic Redundancy (KR)

According to (CONKUR & BUCKINGHAM, 1997), a kinematically redundant manipulator (KRM) is a one whose joint-space dimension is greater than that of the end-effector. The joint space meant here is the consistent one, with consistency being related to the kinematic constraints. While in SMs the consistent joint space is always of dimension m, it is not the case with PMs (case of AR for instance).

This means that in the case of a KRM, for each end-effector pose, $\boldsymbol{x}$, there corresponds infinite possible values of actuated-joint configurations, $\boldsymbol{q}$. The same can be translated regarding kinematics by considering the end-effector twist, $\boldsymbol{t}$, and the actuated-joint velocities, $\dot{\boldsymbol{q}}$.

This type of redundancy helps reducing or even eliminating serial-type singularities, enlarging the workspace, and elevating speed capacity. Yet, it adds additional moving masses that impairs dynamics. Moreover, while $\dot{\boldsymbol{q}}$ are freely chosen, the actuators torques, $\boldsymbol{\tau}$, are subject to $(m-n)$ dependency relations. This indicates that load capability cannot directly be optimized in this sense. Nevertheless, the possibility of having different joint configurations for the same pose can be used as an alternative to change the torque distributions in the actuators.

An example of PMs with KR is the three-dof (3T) robot, called Speed-R-Man (depicted in **Fig. 2-1**), of (REBOULET, et al., 1992). The robot is characterized by an important working volume and speed capacity. It utilizes six prismatic actuators and therefore, the aforementioned

[1] Meaning that of the end-effector.

advantages come with the drawbacks embodied by the additional costs (three extra actuators) and the added complexity at the control level.

To end this part, we highlight another type of redundancy that might be confused with KR, and which is task redundancy (TR). If only r dofs (with $r < n$) of the end-effector are used for particular application, the redundancy is referred to as TR. This redundancy enhances the task accomplishment and improves accessibility. However, it has nothing to do with the mechanical structure itself or its intrinsic properties, but with the intended task. Such redundancy has been already highlighted in the previous chapter in the use of six-dof PKMs for five-axis machining. In the scope of this report, we will not be dealing with it.

2.1.2- Actuation Redundancy (AR)

A redundantly actuated manipulator (RAM) is one that has greater number of actuators than its end-effector dofs (i.e. $m > n$), and in which there exists infinite possible values of actuated joint torques, $\boldsymbol{\tau}$, to counteract an external wrench, $\boldsymbol{w}$, on the end-effector (FIRMANI, et al., 2008).

More precisely, in the case of an AR, we have $m > n$ with $(m-n)$ dependency relations imposed on $\dot{\boldsymbol{q}}$. These latter conditions are usually referred to as synchronization relations. Therefore, commanding an RAM to move without respecting the aforementioned constraints would lead to system damage.

Furthermore, two main subtypes of AR can be distinguished, namely: in-branch actuation redundancy (IBAR) and branch actuation redundancy (BAR) (FIRMANI, et al., 2008). In the former (i.e. IBAR), one or more passive joints in the initially non-redundant PM are actuated. While this preserves the initial workspace, it adds more moving masses and as a result, can be less desirable. As for the latter case (i.e. BAR), additional chains with actuated joints are added

Fig. 2-1: Speed-R-Man (from http://www.onera.fr/fr/dcsd/robots-paralleles?page=2).

to the structure. Though their added influence regarding moving masses may be less severe (not necessarily always), it restricts more the workspace.

Many examples on AR exist and we already mentioned several of them in the first chapter (see for instance **Fig. 1-35**, **Fig. 1-36**, and **Fig. 1-37)**.

The major benefits of AR are reducing or eliminating parallel-type singularities, homogenizing performances, and improving wrench capabilities as well as dynamics. Moreover, it can be utilized to reduce the influence of passive joint clearances and backlashes, thanks to the possibility of applying pre-stress on the structure (MULLER, 2005).

2.1.3- Mixed-Redundancy Manipulators (MRMs)

An MRM is a one that exhibits both kinematic and actuation redundancies. To most of our knowledge, MRMs are not being researched as they combine the demerits of both types of redundancy rather than their virtues. But to make their idea clear, perhaps an example can be enough for this purpose. In **Fig. 2-2**, a simple example, yet sufficient to demonstrate the complexity, is shown.

The kinematic relation for the mechanism is expressed by:

$$\dot{q}_1 + \dot{q}_2 = \dot{q}_3 = \dot{x} \tag{2.1}$$

Thus, infinite solutions are possible for the inverse kinematics. These are obtained by choosing any value for $\dot{q}_1$ (or $\dot{q}_2$) and adapting the other $\dot{q}_2$ (or $\dot{q}_1$) to satisfy (2.1). This explains the KR in the exemplified mechanism. However, not every combination of joint velocities is permissible. In particular, choosing $\dot{q}_3 \neq \dot{q}_1 + \dot{q}_2$ leads to system damage and implies the presence of AR as well. More clearly, we can explain AR by considering the force relationships. If we have a force f acting on the platform, then the forces of the actuators should satisfy the following:

$$\begin{cases} \tau_1 = \tau_2 \\ \tau_2 + \tau_3 = f \end{cases} \tag{2.2}$$

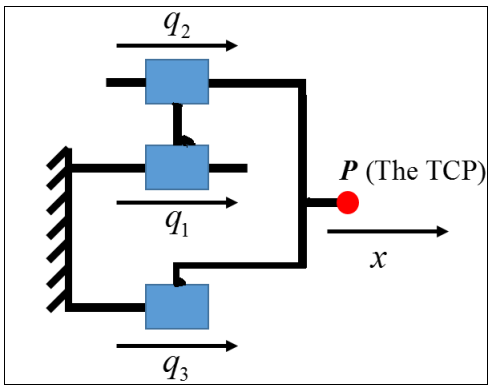

Fig. 2-2: A simple example on mixed redundant manipulators: two series prismatic joints in parallel with another prismatic joint (one dof and three actuators).

From (2.2), it is clear that infinite possible distributions of forces among the actuators exist to counteract the same external force. These distributions consist of arbitrary choosing $\tau_1 = \tau_2$ or τ_3, while satisfying the 2nd relation of (2.2). Hence, at the control level, we must deal with two problems, specifically the optimal choice of joint velocities, and that of actuation forces. Thus with this, we have clarified the concept of mixed redundancy and its inherent intricacy.

It is worth mentioning that another type of redundancy called metrological or measurement redundancy exists. This type of redundancy is characterized by having extra number of sensors than needed. For instance, if we have five sensors in a four-dof robot, then the robot is said to be metrologically redundant. Despite that such redundancy can help improve pose calculation (via simplifying direct geometric model), the way the measurements are exploited in control constitutes a non-trivial issue. A final word in this aspect is that in the case of RAMs, where all actuated joints are equipped with feedback sensors, we have also measurement redundancy.

These were the major points to emphasize regarding redundancy. The rest of the chapter is outlined as follows. First, rigid manipulators are considered and their precision, kinetostatic, and dynamic performances are addressed. Afterwards, cable-driven parallel robots (CDPRs) are considered and the extension of the proposed kinetostatic and dynamic measures is done. Alongside, case studies are provided to make better sense of the concepts and their implementations. Also, few remarks are made, and recommendations concerning design optimization are discussed. The chapter is eventually concluded by highlighting some essential points.

2.2- General Rigid Manipulators

2.2.1- Generalities on the Kinetostatics of Redundant and Non-Redundant Manipulators

Consider any rigid manipulator with the following system of constraint equations describing its kinematic structure:

$$\begin{cases} \mathbf{F}(\boldsymbol{q}, \boldsymbol{x}) = \mathbf{0}, \text{ with:} \\ \dim(\boldsymbol{q}) = m, \ \dim(\boldsymbol{x}) = n, \\ \dim\left(\mathbf{F}(\boldsymbol{q}, \boldsymbol{x})\right) = n_c, \ n \le n_c \le m \end{cases} \tag{2.3}$$

The differentiation of (2.3) with respect to time yields the following well-known kinematic relation:

$$\begin{cases} \boldsymbol{J}_q \, \dot{\boldsymbol{q}} = \boldsymbol{J}_x \, \boldsymbol{t}, \text{ with:} \\ \dim\left(\boldsymbol{J}_q\right) = n_c \times m, \ \dim\left(\boldsymbol{J}_x\right) = n_c \times n \end{cases} \tag{2.4}$$

In the case of non-redundant manipulator (NRM), both $\boldsymbol{J}_q$ and $\boldsymbol{J}_x$ are square matrices (i.e. $n_c = n = m$). Nonetheless, in the situation of redundancy (KR or AR), we have $m > n$ and at least

one of the aforementioned matrices is rectangular. In specific, if $\boldsymbol{J}_q$ is only rectangular, then pure KR exists. On the other hand, having $\boldsymbol{J}_x$ solely non-square corresponds to pure AR. Having both matrices rectangular (i.e. $n < n_c < m$) results in mixed redundancy (KR and AR), and in which we are not concerned.

In what follows, we give the generally known kinetostatic relations for NRM, KRM, and RAM. Starting with NRMs, we always have (at regular non-singular pose[2]):

$$\begin{cases} \dot{\boldsymbol{q}} = \boldsymbol{J}_{\boldsymbol{m}}\ \boldsymbol{t} \text{ or } \boldsymbol{t} = \boldsymbol{J}\ \dot{\boldsymbol{q}}, \text{ with:} \\ \boldsymbol{J}_{\boldsymbol{m}} = \boldsymbol{J}_{\boldsymbol{q}}^{-1}\ \boldsymbol{J}_{\boldsymbol{x}} \text{ and } \boldsymbol{J} = \boldsymbol{J}_{\boldsymbol{x}}^{-1}\ \boldsymbol{J}_{\boldsymbol{q}} \end{cases} \tag{2.5}$$

and[3]

$$\boldsymbol{w} = \boldsymbol{J}_{\boldsymbol{m}}^{\mathrm{T}}\ \boldsymbol{\tau} \text{ or } \boldsymbol{\tau} = \boldsymbol{J}^{\mathrm{T}}\ \boldsymbol{w} \tag{2.6}.$$

The terms $\boldsymbol{J}_{\boldsymbol{m}}$ and $\boldsymbol{J}$ are respectively the inverse and direct/forward Jacobian matrices. While both, $\boldsymbol{J}_{\boldsymbol{m}}$ and $\boldsymbol{J}$, are naturally available[4] in NRMs, this is not the case with KRMs and RAMs where only one of the two is available –the other requiring pseudo-inversion operation based on some assumptions.

In the case of a KRM, we naturally have $\boldsymbol{J}$ as the forward kinematic problem is unique, unlike the inverse one. Therefore, only the forms of the kinetostatic relations ((2.5) and (2.6)) that are based on $\boldsymbol{J}$ are directly applicable. As for the inverse kinematic and forward static problems, they are expressed as follows:

$$\dot{\boldsymbol{q}} = \boldsymbol{J}^{*}\ \boldsymbol{t} + \left[\mathrm{null}\left(\boldsymbol{J}\right)\right]\boldsymbol{\lambda},\ \text{with}\ \boldsymbol{\lambda} \in \mathbb{R}^{m-n}\ (\text{arbitrary}) \tag{2.7}$$

and

$$\boldsymbol{w} = \boldsymbol{J}^{*\mathrm{T}}\ \boldsymbol{\tau},\ \text{with}\ \boldsymbol{\tau}^{\mathrm{T}}\left[\mathrm{null}\left(\boldsymbol{J}\right)\right] = \boldsymbol{0}_{1\times(m-n)} \tag{2.8}.$$

The term $\left[\mathrm{null}\left(\boldsymbol{J}\right)\right]$ corresponds to a null space basis vector of $\boldsymbol{J}$. Note that as we are always considering regular non-singular pose, $\mathrm{null}\left(\boldsymbol{J}\right)$ is of exactly $\left(m-n\right)$ dimension.

On the other hand, in the case of RAMs, only the forms of the kinetostatic relations ((2.5) and (2.6)) that are based on $\boldsymbol{J}_{\boldsymbol{m}}$ are directly applicable, in contrast with what we had for KRMs. Additionally, the forward kinematic and inverse static solutions are given respectively by:

---

[2] Which is the always-assumed case throughout the chapter.

[3] Note that under the form of (2.6), we are describing how the actuators torques are transmitted into the operational space and vice-versa. In this sense, $\boldsymbol{w}$ is the opposite of the real applied wrench. This form is considered here for convenience. However, later in cable-driven robots, the equilibrium form will be used instead, i.e.: $\boldsymbol{w} + \boldsymbol{J}_{\boldsymbol{m}}^{\mathrm{T}}\ \boldsymbol{\tau} = \boldsymbol{0}$ (platform equilibrium) or $\boldsymbol{\tau} + \boldsymbol{J}^{\mathrm{T}}\ \boldsymbol{w} = \boldsymbol{0}$ (actuators equilibrium).

[4] Meaning they are computable with no assumptions, by means of matrix inversion operations (no pseudo-inverse procedure).

$$\boldsymbol{t} = \boldsymbol{J}_{\boldsymbol{m}}^{*}\,\dot{\boldsymbol{q}},\ \text{with}\ \dot{\boldsymbol{q}}^{\mathrm{T}}\left[\operatorname{null}\left(\boldsymbol{J}_{\boldsymbol{m}}^{\mathrm{T}}\right)\right] = \boldsymbol{0}_{1\times(m-n)} \tag{2.9}$$

and

$$\boldsymbol{\tau} = \boldsymbol{J}_{\boldsymbol{m}}^{*\mathrm{T}}\,\boldsymbol{w} + \left[\operatorname{null}\left(\boldsymbol{J}_{\boldsymbol{m}}^{\mathrm{T}}\right)\right]\boldsymbol{\lambda},\ \text{with}\ \boldsymbol{\lambda}\in\mathbb{R}^{m-n}\ \text{(arbitrary)} \tag{2.10}.$$

The relations (2.7) and (2.10) show that when dealing with KR and AR, one should get rid of the arbitrariness of $\boldsymbol{\lambda}$. One way to do that is considering the solutions of $\dot{\boldsymbol{q}}$ and $\boldsymbol{\tau}$ that do not have any component along the null spaces of $\boldsymbol{J}$ and $\boldsymbol{J}_{\boldsymbol{m}}^{\mathrm{T}}$ respectively; this means setting $\boldsymbol{\lambda}=\boldsymbol{0}$. These are mathematically referred to as minimum norm solutions. Note that choosing $\boldsymbol{\lambda}\neq\boldsymbol{0}$ results in antagonist forces that can deform the robot structure; these forces are referred to as internal preloads and can be used to eliminate the influence of clearances and to control stiffness (MULLER, 2006).

The particular solutions with $\boldsymbol{\lambda}=\boldsymbol{0}$ will be assumed in the kinetostatic analysis, and they can be practically achieved by control means (refer to **§4.2** in **Chapter 4** for more information on the methodology). Therefore, for rigid manipulators, regardless of being redundant or not, both forms of the relations ((2.5) and (2.6)) are applicable with the following assumption:

$$\begin{cases}\boldsymbol{J}_{\boldsymbol{m}} = \boldsymbol{J}^{*},\ \text{if KRM}\\ \boldsymbol{J} = \boldsymbol{J}_{\boldsymbol{m}}^{*},\ \text{if RAM}\end{cases} \tag{2.11}.$$

Nonetheless, in what concerns precision evaluation, the particularities of redundancy must be considered, as we are going to see in the following part. As for dynamics, a similar approach to deal with redundancy is adopted as well. This will be made clear later in place. It remains just to emphasize that we will consider the following decompositions of $\boldsymbol{J}_{\boldsymbol{m}}$ and $\boldsymbol{J}$:

$$\begin{cases}\boldsymbol{J}_{\boldsymbol{m}} = \begin{bmatrix}\boldsymbol{J}_{\boldsymbol{mp}} & \boldsymbol{J}_{\boldsymbol{mo}}\end{bmatrix}\\ \boldsymbol{J} = \begin{bmatrix}\boldsymbol{J}_{\boldsymbol{p}}\\ \boldsymbol{J}_{\boldsymbol{o}}\end{bmatrix}\end{cases} \tag{2.12}.$$

The subscripts “p” and “o” in (2.12) are used to denote the respective translational/positional and orientation/rotational parts of $\boldsymbol{J}_{\boldsymbol{m}}$ and $\boldsymbol{J}$.

2.2.2- Precision-Related Performance Measures

When dealing with machine tool design, among the most important aspects to consider is precision. This precision embraces several terms, such as accuracy, repeatability, and operational resolution. The first two have been previously discussed and explained in **Chapter 1**, with further information being provided in **Appendix A**. It remains to shed the lights on the operational resolution of a robot or machine.

In fact, one is more familiar with measurement resolution of some measuring device, such as a scale. For instance, consider a ruler with $1\,\mathrm{mm}$ graduations. Then, we cannot measure any length inferior to this resolution. In fact, every measurement of a length L using the

aforementioned device is done with roughly $\pm 1\,\mathrm{mm}$ error and thus, the resolution stands also for the measurement uncertainty (CORBEL, 2008).

If we consider the same notion applied to an actuator, the latter's resolution is the smallest step that it can perform. According to (CORBEL, 2008), the resolution of a motor can be seen in several ways. The most common is to consider it equal to that of the associated encoder. However and according to the same reference, this value adopted for resolution is not necessarily equal to the physical one of the motor, but it may be lower or higher. (CORBEL, 2008) supports this idea by considering the results of the work of (BRETHE & LEFEBVRE, 2007), in which the granular space structure of some industrial robots has been discussed. Our opinion in this matter is quite different. From our point of view, the actuator resolution is not only the smallest step that can be done, but also detected. The necessity of detection makes resolution a characteristic of the actuator-encoder system rather than the actuator itself. As a result, it should be a multiple of the encoder resolution.

Regarding the robot, its operational resolution is the smallest detectable step that the end-effector can do in the operational space. In conventional machines where each axis of motion is activated by a sole actuator, we may speak of axial resolution, i.e. the smallest step that can be done along each Cartesian axis. Nonetheless, in machines based on parallel kinematics, though resolutions along particular directions can be defined, they are less indicative. This is due to the coupled nature of the end-effector motion. Consequently, it is preferable to speak of operational translational and orientation resolutions instead.

In the following, we define theoretical resolutions as well as accuracies and repeatabilities for all robots (NRMs, KRMs, and RAMs). But what we will be interested in later, is replacing those three measures by a single one, though this is possible only for the particular situation of having the same type of actuators.

A- Theoretical Accuracy, Repeatability, and Resolution

In this section, we assume that the actuators' resolutions, accuracies, and repeatabilities are all sufficiently small to have the following assumption valid:

$$\boldsymbol{\delta q} = \boldsymbol{J}_{\boldsymbol{m}}\ \boldsymbol{\delta x} \text{ or } \boldsymbol{\delta x} = \boldsymbol{J}\ \boldsymbol{\delta q} \qquad (2.13).$$

Relation (2.13) means that for very small errors (which is usually the case for machine tools), the relation in the vicinity of the considered pose is linear. In this case, the actuated-joint displacement zonotope[5] is transformed into an operational one. However, attention must be paid regarding RAMs and the synchronization imposed on their joint-displacements.

To calculate the theoretical operational resolutions at non-singular pose for given actuators' resolutions, denoted by R_{qi} ($\forall i = 1...m$), we define the following joint zonotope $\mathcal{Z}_q$:

[5] It is a rectangular parallelepiped in the case of NRMs and KMRs only. In the case of RAMs and due to synchronization constraints, it is part of a rectangular parallelepiped.

$$\mathcal{Z}_{\boldsymbol{q}} = \begin{cases} \left\{ \begin{array}{l} \boldsymbol{\delta q} \in \mathbb{R}^m;\ \left|\delta q_i\right| \le Res_{qi},\ \forall i = 1...m, \\ \text{and } \left[\text{null}\left(\boldsymbol{J}_{\boldsymbol{m}}^{\mathrm{T}}\right)\right]^{\mathrm{T}} \boldsymbol{\delta q} = \boldsymbol{0} \end{array} \right\},\ \text{if RAM} \\ \text{or:} \\ \left\{ \boldsymbol{\delta q} \in \mathbb{R}^m;\ \left|\delta q_i\right| \le Res_{qi},\ \forall i = 1...m \right\},\ \text{if NRM or KRM} \end{cases} \tag{2.14}.$$

Then, the theoretical translational (orientation) resolution is the smallest translational (orientation) step detectable in the operational space. In other words, it is the radius of the smallest sphere that circumscribes the translational (orientation) zonotope, the image of $\mathcal{Z}_{\boldsymbol{q}}$ under the mapping described by $\boldsymbol{J}_{\boldsymbol{p}}$ (correspondingly $\boldsymbol{J}_{\boldsymbol{o}}$). Denoting translational and orientation resolutions by Res_p and Res_o respectively, we get:

$$\begin{cases} Res_p = \max\limits_{\boldsymbol{\delta q} \in \mathcal{Z}_{\boldsymbol{q}}} \left(\left\| \boldsymbol{J}_{\boldsymbol{p}}\ \boldsymbol{\delta q} \right\| \right) \\ Res_o = \max\limits_{\boldsymbol{\delta q} \in \mathcal{Z}_{\boldsymbol{q}}} \left(\left\| \boldsymbol{J}_{\boldsymbol{o}}\ \boldsymbol{\delta q} \right\| \right) \end{cases} \tag{2.15}.$$

Based on the above, Res_p (Res_o) is the maximal Euclidean distance from the origin of the translational (orientation) zonotope to the corresponding vertices (the image of those of $\mathcal{Z}_{\boldsymbol{q}}$).

Denoting the N vertices of $\mathcal{Z}_{\boldsymbol{q}}$ by $\boldsymbol{V}_i$ ($\forall i = 1...N$), we can rewrite (2.15) as:

$$\begin{cases} Res_p = \max\limits_{i=1...N} \left(\left\| \boldsymbol{J}_{\boldsymbol{p}}\ \boldsymbol{V}_i \right\| \right) \\ Res_o = \max\limits_{i=1...N} \left(\left\| \boldsymbol{J}_{\boldsymbol{o}}\ \boldsymbol{V}_i \right\| \right) \end{cases} \tag{2.16}.$$

A similar approach can be used to estimate the theoretical translational or orientation accuracies and repeatabilities. This is done by replacing Res_{qi} by E_{qi} (i-th joint accuracy) to get the translational (orientation) accuracy E_p (respectively E_o). On the other hand, replacing Res_{qi} by Rep_{qi} (i-th joint repeatability), we get the estimated translational and orientation repeatabilities, denoted by Rep_p and Rep_o respectively. It is worth mentioning here that regarding accuracy and repeatability, another statistical approach exists. This is done by assuming a certain statistical distribution for joint errors with a specific mean and standard deviation, then establishing the mean and standard deviation of the operational error based on (2.13) (e.g. (BRETHE & LEFEBVRE, 2007)). However, it can be rather complex, especially that in the case of RAMs, the joint errors are dependent. Also in this scope, we mention the work of (MERLET & DANEY, 2005), in which interval analysis has been used in the design of a robot with a specified accuracy over a given workspace. This has been done while taking into account not only the actuated-joint errors, but also the tolerances on the geometric parameters. Despite that theoretically such approach is the most relevant, putting it into practice is undeniably difficult and presents computational complexities. This is not to mention being time-expensive. Besides, in the design of machine tools, the geometric errors are supposedly small, and they are later compensated by means of calibration.

So far, we have presented the methodology in the general case, yet our focus will be on the particular situation where all actuators are of same nature, meaning either linear or rotational.

In such a case, we set $Res_q = \max_{\boldsymbol{x}\in DWS}\left(\max_{i=1...m}\left(Res_{qi}\right)\right)$, being the worst resolution among the actuators and over the whole desired workspace, DWS. The following step is to replace the above definition of $\mathcal{Z}_{\boldsymbol{q}}$ by:

$$\mathcal{Z}_{\boldsymbol{q}} = \begin{cases} \left\{ \begin{array}{l} \boldsymbol{\delta q} \in \mathbb{R}^m;\ \left|\delta q_i\right| \le R_q,\ \forall i = 1...m, \\ \text{and } \left[\text{null}\left(\boldsymbol{J}_{\boldsymbol{m}}^{\mathrm{T}}\right)\right]^{\mathrm{T}} \boldsymbol{\delta q} = \boldsymbol{0} \end{array} \right\}, \text{ if RAM} \\ \text{or:} \\ \left\{\boldsymbol{\delta q} \in \mathbb{R}^m;\ \left|\delta q_i\right| \le R_q,\ \forall i = 1...m\right\}, \text{ if NRM or KRM} \end{cases} \tag{2.17}$$

Then, we can calculate the operational resolutions, accuracies, and repeatabilities[6] via the same equation (2.16), and where $E_q = \max_{\boldsymbol{x}\in DWS}\left(\max_{i=1...m}\left(E_{qi}\right)\right)$ and $Rep_q = \max_{\boldsymbol{x}\in DWS}\left(\max_{i=1...m}\left(Rep_{qi}\right)\right)$. Hence, we define what we may call precision amplification factors in translation and orientation, denoted by $TPAF$ and $OPAF$ correspondingly:

$$\begin{cases} TPAF = \dfrac{Res_p}{Res_q} = \dfrac{E_p}{E_q} = \dfrac{Rep_p}{Rep_q} \\ OPAF = \dfrac{Res_o}{Res_q} = \dfrac{E_o}{E_q} = \dfrac{Rep_o}{Rep_q} \end{cases} \tag{2.18}$$

Note that the calculation of $TPAF$ and $OPAF$ does not necessitate the knowledge of Res_q, E_q, or Rep_q. This is very interesting, especially at the design level where we might have these terms still unknown. Optimizing any design in the sense of minimizing $\max_{\boldsymbol{x}\in DWS}\left(TPAF\right)$ and $\max_{\boldsymbol{x}\in DWS}\left(OPAF\right)$ results in a precise robot. This is what we are going to employ later in the dimensional synthesis of ARROW PKM in **Chapter 3**.

B- Precision and Peak Operational Speeds

Perhaps, it is worth emphasizing the relation between peak operational speeds on one side, and precision measures on the other side, though this relation can be intuitively noticed.

To demonstrate the case, the simplest way is to consider a robot with identical actuators of maximal speed being $\dot{q}_{\max}$. Then, one can easily show that the peak linear v_{peak} and angular ω_{peak} speeds are related to precision measures as follows:

[6] Regarding accuracy and repeatability, replace Res_q by E_q and Rep_q respectively.

$$\begin{cases} \dfrac{v_{peak}}{\dot{q}_{\max}} = TPAF \\ \dfrac{\omega_{peak}}{\dot{q}_{\max}} = OPAF \end{cases}, \text{ all actuators being identical} \qquad (2.19).$$

Hence, improving precision (i.e. reducing $TPAF$ and $OPAF$) is accompanied by decreasing peak speed capacities. While the relation is straightforward in the case of identical actuators, it becomes less direct in the general situation, being more or less coupled. For machine tools, the peak speeds are not the interesting ones to maximize, but rather the isotropic ones (those that can be attained in all directions). The antagonism between the latter speeds and precision factors is more intriguing and to be compromised in the optimization of a robotic design, in which rapidity and precision are among the sought goals.

As the main points in what concerns precision have been clarified, it remains to present a case study, the subject of the upcoming section.

C- Case Study: DUAL V

In **Fig. 2-3**, DUAL V is depicted with simplified schematic and CAD drawings. It is a redundantly actuated PM with three dofs (2T-1R), and four identical actuators. Its complete description with its models can be found in (WIJK, et al., 2013).

Its inverse Jacobian matrix $\boldsymbol{J_m}$ is given by:

$$\boldsymbol{J_m} = \boldsymbol{J_q}^{-1}\,\boldsymbol{J_x} \qquad (2.20),$$

with:

$$\boldsymbol{J_q} = \mathbf{diag}\left(\boldsymbol{B_i C_i^T}\left(\boldsymbol{e_z} \times \boldsymbol{A_i B_i}\right)\right),\ \dim\left(\boldsymbol{J_q}\right) = 4\times 4 \qquad (2.21)$$

and

$$\boldsymbol{J_x} = \begin{bmatrix} \boldsymbol{B_1 C_1^T}\,\boldsymbol{e_x} & \boldsymbol{B_1 C_1^T}\,\boldsymbol{e_y} & -\boldsymbol{B_1 C_1^T}\left(\boldsymbol{P C_1} \times \boldsymbol{e_z}\right) \\ \vdots & \vdots & \vdots \\ \boldsymbol{B_4 C_4^T}\,\boldsymbol{e_x} & \boldsymbol{B_4 C_4^T}\,\boldsymbol{e_y} & -\boldsymbol{B_4 C_4^T}\left(\boldsymbol{P C_4} \times \boldsymbol{e_z}\right) \end{bmatrix},\ \dim\left(\boldsymbol{J_x}\right) = 4\times 3 \qquad (2.22).$$

The $TPAF$ and $OPAF$ for DUAL V have been calculated for the case of $\theta = 0°$. The results are depicted in **Fig. 2-4**. The actuators are of type ETEL RTMB0140-100. According to the data sheet, the accuracy and repeatability are about $25\,\text{arcsec}$ and $5\,\text{arcsec}$, respectively. This means that the expected worst translational accuracy and repeatability are about $54\,\mu\text{m}$ and $11\,\mu\text{m}$ respectively (considering $\max\left(TPAF\right) \approx 0.45$). However, these values do not account for control errors and only serve as rough estimate. In **Table Ap-12** of **Appendix A.2**, we can only consider repeatability, as accuracy is not that reliable due to the technical difficulties explained therein. Aside from pose P_1, the results are somehow in close agreement. We should keep in mind the existence of other factors, such as the measurement device repeatability,

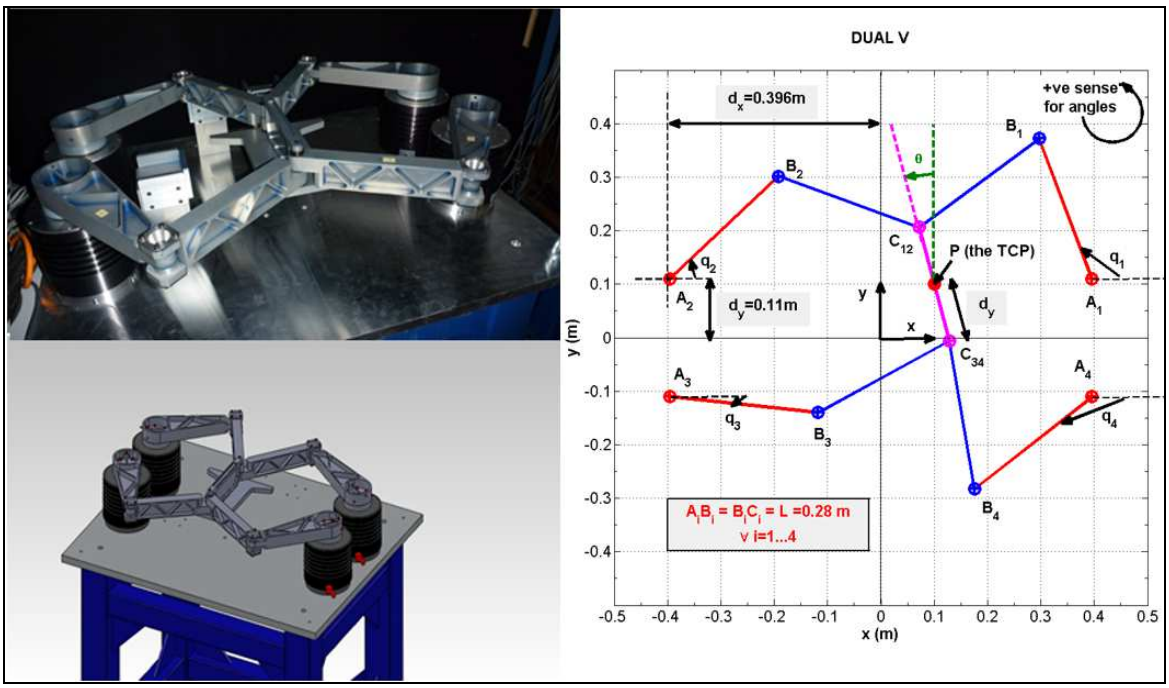

Fig. 2-3: DUAL V: prototype, CAD drawing and simplified schematic diagram showing the principal geometric parameters.

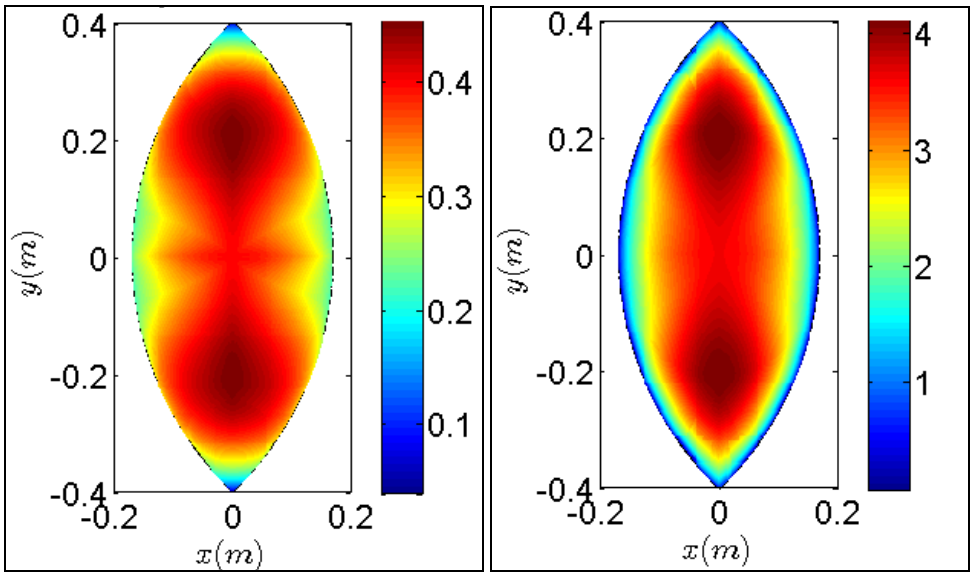

Fig. 2-4: DUAL V: translational and orientation precision amplification factors TPAF (left) and OPAF (right), for the case of zero rotation.

experimentation imperfections, etc. Also, we should know that the datasheet values are given for certain environmental conditions that can slightly differ from those at experimentation time.

By this case study, we end up the discussion on precision assessment measures. It remains to discuss kinetostatic measures regarding twists and static wrenches, before moving into dynamics.

2.2.3- Kinetostatic Performance Evaluation

In the design of machine tools, the most important points to investigate are the twist and static wrench capabilities. But as these are direction-dependent, possibly a relevant approach would be only to consider the isotropic capacities; i.e. the maximal values that can be achieved by the manipulator irrespective of direction. This part concentrates on these aspects. We start by considering a robot with homogeneous dofs and end with the most generic case of robots with heterogeneous dofs.

A- Kinetostatic Measures: Case of Robots with Homogeneous DoFs

Let us consider a manipulator with homogeneous dofs, say a translational one. Then, depending on the intended task, a certain minimal value of speed and static force are usually required to be achieved in all directions. So why do not we consider isotropic speed, v_{iso}, and force, f_{iso}, as kinetostatic measures?!

In fact, the first step we have done to deal with homogeneous-dof robots was considering the aforementioned values in one composite measure, the Force-Velocity Isotropy index (FVI) and that includes also the minimal requirements in speed and static force, denoted by v_{req} and f_{req} respectively. It is given as follows:

$$FVI = \min\left(\frac{v_{iso}}{v_{req}}, \frac{f_{iso}}{f_{req}}\right) \tag{2.23}$$

As for v_{iso} (f_{iso}), it is nothing other than the maximum value that can be achieved regardless of velocity (respectively force) direction. Geometrically, v_{iso} (f_{iso}) is the radius of the largest sphere inscribed in the operational velocity (respectively force) zonotope. Mathematically, v_{iso} and f_{iso} are calculated as follows[7]:

$$v_{iso} = \min_{i=1\ldots m}\left(\frac{\dot{q}_i^{\max}}{\left\|\boldsymbol{j}_{\boldsymbol{mr}_i}\right\|}\right) \tag{2.24}$$

and

$$f_{iso} = \min_{i=1\ldots m}\left(\frac{\tau_i^{\max}}{\left\|\boldsymbol{j}_{\boldsymbol{c}_i}\right\|}\right) \tag{2.25}$$

with $\boldsymbol{j}_{\boldsymbol{mr}_i}$ and $\boldsymbol{j}_{\boldsymbol{c}_i}$ being the i-th row and column vectors of $\boldsymbol{J}_{\boldsymbol{m}}$ and $\boldsymbol{J}$ respectively, and where $\dot{q}_i^{\max}$ and $\tau_i^{\max}$ are the corresponding maximal speed and torque capacities of the i-th actuator (i.e. $\left|\dot{q}_i\right| \le \dot{q}_i^{\max}$ and $\left|\tau_i\right| \le \tau_i^{\max}$). Note that regarding redundant manipulators, the calculation is based on the assumption (2.11). It can be easily shown that if the general solution with

[7] The derivation is very simple and trivial. However, one can find it in **2.2.3.C** as a special case.

arbitrary $\boldsymbol{\lambda}$ is considered ((2.7) and (2.10)) in the case of KRMs and RAMs, then the isotropic speed will be larger than or equal to that of (2.24) for a KRM, and the isotropic static force will be greater than or equal to that of (2.25) for an RAM. This is since the minimum norm solution set (i.e. the case in which $\boldsymbol{\lambda}=\mathbf{0}$) is a subset of the general one. Thus, with (2.24) and (2.25) the guaranteed minimum isotropic values are computed. Yet, later and after dealing with CDPRs, one will become capable of computing the isotropic values for the general solution with arbitrary $\boldsymbol{\lambda}$, although we do not recommend it for rigid manipulators.

Finally, it remains to highlight that when $v_{iso}\to 0$ (or $f_{iso}\to 0$), we are close to series-type singularity (correspondingly parallel-type singularity). Thus, the higher FVI is, the better the robot is regarding isotropic kinetostatic capabilities, and the farther the pose is from classical singularities. In particular, when $FVI\geq 1$, it means that all the requirements have been fulfilled. In this sense, v_{req} and f_{req} serve as numerical tolerance to indicate singularity, in the same way one puts a tolerance on singular values. Nevertheless, unlike what we had in the case of singular values and especially with redundant robots, v_{req} and f_{req} are clear and physically significant.

Despite the ease of their computation, these isotropic values necessitate arbitrary homogenization for heterogeneous-dof robots, and as the debate of **Chapter 1** concluded, the result is lack of direct physical significance.

Therefore, to overcome this issue, one suggestion is to consider translation and rotation separately. This is justifiable as long as translation and rotation occur in two separate phases (e.g. pick-and-place applications[8]). This is the subject of the upcoming section.

B- Kinetostatic Performance Evaluation by Separation of Translation and Rotation

Let us consider now a heterogeneous-dof robot regardless of being redundant or not. Then, to use the above-defined FVI index, a prior homogenization is needed. However, unlike classical indices, such as those based on singular values, the homogenization required is only regarding the operational dofs; meaning no particular treatment is demanded in the case of having actuators of different nature.

Nevertheless, the FVI index based on homogenization, called FVI_h, maintains only the significance regarding classical series and parallel type singularities. Regarding kinetostatics, the physical interpretation is no more concrete and is rather difficult to interpret. That is why studying translational and rotational performances separately, but in proper manner, is favored.

For instance, one can define **pure isotropic linear speed,** v_{iso}^{p}, for the case where angular velocity is assumed null (i.e. $\boldsymbol{\omega}=\mathbf{0}$). Also, we may define the **pure static isotropic force,** f_{iso}^{p},

[8] Where pure rotation occurs at the end-points and pure translation in between.

that can be supported by the manipulator in the case where no external moment is acting on the end-effector (i.e. $\boldsymbol{m} = \boldsymbol{0}$). Likewise, we define **pure isotropic angular speed,** ω_{iso}^{p} , and **pure isotropic static moment,** m_{iso}^{p}. The aforementioned terms can be easily derived to get as a result:

$$v_{iso}^{p} = \min_{i=1\ldots m}\left(\frac{\dot{q}_i^{\max}}{\left\|\boldsymbol{j}_{\boldsymbol{mpr}_i}\right\|}\right) \tag{2.26},$$

$$\omega_{iso}^{p} = \min_{i=1\ldots m}\left(\frac{\dot{q}_i^{\max}}{\left\|\boldsymbol{j}_{\boldsymbol{mor}_i}\right\|}\right) \tag{2.27},$$

$$f_{iso}^{p} = \min_{i=1\ldots m}\left(\frac{\tau_i^{\max}}{\left\|\boldsymbol{j}_{\boldsymbol{pc}_i}\right\|}\right) \tag{2.28}$$

and

$$m_{iso}^{p} = \min_{i=1\ldots m}\left(\frac{\tau_i^{\max}}{\left\|\boldsymbol{j}_{\boldsymbol{oc}_i}\right\|}\right) \tag{2.29}.$$

The terms $\boldsymbol{j}_{\boldsymbol{mpr}_i}$ ($\boldsymbol{j}_{\boldsymbol{mor}_i}$) and $\boldsymbol{j}_{\boldsymbol{pc}_i}$ ($\boldsymbol{j}_{\boldsymbol{oc}_i}$) correspond to the i-th row and column vectors of $\boldsymbol{J}_{\boldsymbol{mp}}$ ($\boldsymbol{J}_{\boldsymbol{mo}}$) and $\boldsymbol{J}_{\boldsymbol{p}}$ ($\boldsymbol{J}_{\boldsymbol{o}}$) respectively.

Thus, based on the requirements, one can define different FVI indices. For example, we can define translational and orientation indices, denoted by FVI_p and FVI_o respectively. These are expressed as follows:

$$FVI_p = \min\left(\frac{v_{iso}^{p}}{v_{req}^{p}}, \frac{f_{iso}^{p}}{f_{req}^{p}}\right) \tag{2.30}$$

and

$$FVI_o = \min\left(\frac{\omega_{iso}^{p}}{\omega_{req}^{p}}, \frac{m_{iso}^{p}}{m_{req}^{p}}\right) \tag{2.31}.$$

The terms v_{req}^{p} and ω_{req}^{p} are the minimum required pure isotropic linear and angular speeds. Similarly, f_{req}^{p} and m_{req}^{p} are the minimal required pure static isotropic force and moment to be supported by the robot.

Note that other combinations of pure isotropic values can be used depending on what the user needs. However, indices built on the aforementioned values do not necessarily exhibit a singularity significance, but solely a kinetostatic one. To be more clear, having one of the

isotropic values zero, say $v_{iso}^{p} = 0$, implies a series-type singularity[9]. Nonetheless, having $v_{iso}^{p} \neq 0$ is not sufficient to prove the non-existence of series-type singularity. Similar note can be made regarding f_{iso}^{p} and parallel-type singularity.

The exploitation of pure isotropic values is justifiable only when translation and rotation motions are done separately and/or when only pure force or moment is being counteracted at a time. As for the other cases where simultaneous motion is to be done or a mixed-type wrench[10] is to be supported, another alternative must be investigated. The subsequent section is dedicated for discussing this second alternative, which is founded on the simultaneous isotropic kinetostatic performance evaluation.

C- Kinetostatic Isotropic Performance Co-Assessment: A Novel Approach that Overwhelms Heterogeneity Predicament and Fits Adequately Machine Tools

The kinetostatic performance measures that we are to introduce here, not only respond directly to the requirements to be satisfied when designing a machine tool, but also overcome the dilemma embodied in both: heterogeneity and redundancy. Actually, a machine tool is designed to perform a coupled heterogeneous motion (simultaneous translation and rotation) on one hand, and to support an external mixed-type wrench (force and moment) on the other hand. Thus, based on the type of application or machining task, one can set minimum requirements for isotropic linear and angular speeds, static force, and static moment that must be achievable by the manipulator simultaneously and regardless of direction. Denote these in respective order by: v_{req}, ω_{req}, f_{req} and m_{req}.

Starting from the aforementioned requirements and to assess simultaneous mixed kinetostatic performances in translation and rotation, a novel concept has been introduced. It is the notion of specific isotropic values. These values will be discussed in the ensuing subsection.

Description and Mathematical Formulation

In what follows, we define isotropic values and derive their formulae. For instance, the **specific isotropic linear speed,** v_{iso}^{sp}, is the maximal linear speed attainable in all directions while allowing the angular velocity, $\boldsymbol{\omega}$, to reach ω_{req} in all directions. Analogous definitions can be made for **specific isotropic angular speed,** ω_{iso}^{sp}, **specific isotropic static force,** f_{iso}^{sp}, and **specific isotropic static moment,** m_{iso}^{sp}. These terms not only hold a physical kinetostatic interpretation, but also a singularity one as it will become clear by the end of the section.

[9] In this case, the origin of the operational twist zonotope belongs to its boundary, i.e. the twist zonotope is collapsed, and which corresponds to series-type singularity.

[10] We mean by mixed-type wrench the one with non-zero force and non-zero moment.

To calculate v_{iso}^{sp}, we consider the condition $\left|\dot{q}_i\right| \le \dot{q}_i^{\max}, \ \forall i = 1...m$ and which can be rewritten as:

$$-\dot{q}_i^{\max} \le \dot{q}_i = \boldsymbol{j}_{\boldsymbol{mpr}_i}^{\mathrm{T}} \boldsymbol{v} + \boldsymbol{j}_{\boldsymbol{mor}_i}^{\mathrm{T}} \boldsymbol{\omega} \le \dot{q}_i^{\max}, \ \ \forall i = 1...m \tag{2.32}$$

Let us consider the right-hand side of the double inequality (2.32). It can be written as:

$$\boldsymbol{j}_{\boldsymbol{mpr}_i}^{\mathrm{T}} \boldsymbol{v} \le \dot{q}_i^{\max} - \boldsymbol{j}_{\boldsymbol{mor}_i}^{\mathrm{T}} \boldsymbol{\omega}, \ \ \forall i = 1...m \tag{2.33}$$

Then, to calculate v_{iso}^{sp}, we need to consider the worst case of (2.33) in terms of $\boldsymbol{v}$ and $\boldsymbol{\omega}$, such that $\left\|\boldsymbol{\omega}\right\| \le \omega_{req}$. This corresponds to having $\dot{q}_i^{\max} - \boldsymbol{j}_{\boldsymbol{mor}_i}^{\mathrm{T}} \boldsymbol{\omega}$ minimal and $\boldsymbol{j}_{\boldsymbol{mpr}_i}^{\mathrm{T}} \boldsymbol{v}$ maximal and which obviously occurs for:

$$\begin{cases} \boldsymbol{\omega} = \omega_{req} \dfrac{\boldsymbol{j}_{\boldsymbol{mor}_i}}{\left\|\boldsymbol{j}_{\boldsymbol{mor}_i}\right\|}, \ \text{if} \ \left\|\boldsymbol{j}_{\boldsymbol{mor}_i}\right\| \ne 0 \\ \text{indifferent of } \boldsymbol{\omega}, \ \text{if} \ \left\|\boldsymbol{j}_{\boldsymbol{mor}_i}\right\| = 0 \end{cases} \tag{2.34}$$

and

$$\begin{cases} \boldsymbol{v} = v \dfrac{\boldsymbol{j}_{\boldsymbol{mpr}_i}}{\left\|\boldsymbol{j}_{\boldsymbol{mpr}_i}\right\|} \ \text{with} \ v = \left\|\boldsymbol{v}\right\| \ge 0, \ \text{if} \ \left\|\boldsymbol{j}_{\boldsymbol{mpr}_i}\right\| \ne 0 \\ \text{indifferent of } \boldsymbol{v}, \ \text{if} \ \left\|\boldsymbol{j}_{\boldsymbol{mpr}_i}\right\| = 0 \end{cases} \tag{2.35}$$

Hence, substituting (2.34) and (2.35) in (2.33) yields:

$$\left\|\boldsymbol{j}_{\boldsymbol{mpr}_i}\right\| v \le \dot{q}_i^{\max} - \left\|\boldsymbol{j}_{\boldsymbol{mor}_i}\right\| \omega_{req}, \ \ \forall i = 1...m \tag{2.36}$$

As $\left\|\boldsymbol{j}_{\boldsymbol{mpr}_i}\right\| v \ge 0$, it is mandatory to have $\dot{q}_i^{\max} - \left\|\boldsymbol{j}_{\boldsymbol{mor}_i}\right\| \omega_{req} \ge 0$. Otherwise, it means that the robot cannot initially fulfill the rotational motion requirement in the absence of translation. In this latter case, v_{iso}^{sp} does not really exist and it is set to zero by convention. Aside from that, we get:

$$\begin{cases} v \le A_i^+, \ \text{with:} \\ A_i^+ = \begin{cases} 0 \ , \ \text{if} \ \ a_i^+ < 0 \\ \dfrac{a_i^+}{\left\|\boldsymbol{j}_{\boldsymbol{mpr}_i}\right\|}, \ \text{if} \ \left\|\boldsymbol{j}_{\boldsymbol{mpr}_i}\right\| \ne 0 \ \text{and} \ a_i^+ \ge 0, \ \forall i = 1...m \\ \infty \ , \ \ \text{otherwise} \end{cases} \\ a_i^+ = \dot{q}_i^{\max} - \left\|\boldsymbol{j}_{\boldsymbol{mor}_i}\right\| \omega_{req}, \ \forall i = 1...m \end{cases} \tag{2.37}$$

Proceeding in the same manner with left-hand inequality of (2.32), we obtain:

$$v \le A_i^-, \ \text{with} \ A_i^- = A_i^+ \tag{2.38}$$

or simply we can say (based on (2.37) and (2.38)), we have:

$$\begin{cases} v \le A_i, \text{ with:} \\ A_i = \begin{cases} 0 \text{ , if } \quad a_i < 0 \\ \dfrac{a_i}{\left\| \boldsymbol{j}_{\boldsymbol{mpr}_i} \right\|}, \text{ if } \quad \left\| \boldsymbol{j}_{\boldsymbol{mpr}_i} \right\| \neq 0 \text{ and } a_i \ge 0, \ \forall i = 1...m \\ \infty \text{ , otherwise} \end{cases} \\ a_i = \dot{q}_i^{\max} - \left\| \boldsymbol{j}_{\boldsymbol{mor}_i} \right\| \omega_{req}, \ \forall i = 1...m \end{cases} \quad (2.39).$$

As v_{iso}^{sp} is the largest attainable isotropic linear speed while allowing angular speed to reach ω_{req} in all directions, v_{iso}^{sp} is then:

$$\begin{cases} v_{iso}^{sp} = \min_{i=1...m} \left(A_i \right), \text{ with:} \\ A_i = \begin{cases} 0 \text{ , if } \quad a_i < 0 \\ \dfrac{a_i}{\left\| \boldsymbol{j}_{\boldsymbol{mpr}_i} \right\|}, \text{ if } \quad \left\| \boldsymbol{j}_{\boldsymbol{mpr}_i} \right\| \neq 0 \text{ and } a_i \ge 0, \ \forall i = 1...m \\ \infty \text{ , otherwise} \end{cases} \\ a_i = \dot{q}_i^{\max} - \left\| \boldsymbol{j}_{\boldsymbol{mor}_i} \right\| \omega_{req}, \ \forall i = 1...m \end{cases} \quad (2.40).$$

Following the same lead, the mathematical expressions of the other specific isotropic terms are as follows:

$$\begin{cases} \omega_{iso}^{sp} = \min_{i=1...m} \left(B_i \right), \text{ with:} \\ B_i = \begin{cases} 0 \text{ , if } \ b_i < 0 \\ \dfrac{b_i}{\left\| \boldsymbol{j}_{\boldsymbol{mor}_i} \right\|}, \text{ if } \quad \left\| \boldsymbol{j}_{\boldsymbol{mor}_i} \right\| \neq 0 \text{ and } b_i \ge 0, \ \forall i = 1...m \\ \infty \text{ , otherwise} \end{cases} \\ b_i = \dot{q}_i^{\max} - \left\| \boldsymbol{j}_{\boldsymbol{mpr}_i} \right\| v_{req}, \ \forall i = 1...m \end{cases} \quad (2.41),$$

$$\begin{cases} f_{iso}^{sp} = \min_{i=1...m} \left(C_i \right), \text{ with:} \\ C_i = \begin{cases} 0 \text{ , if } c_i < 0 \\ \dfrac{c_i}{\left\| \boldsymbol{j}_{\boldsymbol{pc}_i} \right\|}, \text{ if } \quad \left\| \boldsymbol{j}_{\boldsymbol{pc}_i} \right\| \neq 0 \text{ and } c_i \ge 0, \ \forall i = 1...m \\ \infty \text{ , otherwise} \end{cases} \\ c_i = \tau_i^{\max} - \left\| \boldsymbol{j}_{\boldsymbol{oc}_i} \right\| m_{req}, \ \forall i = 1...m \end{cases} \quad (2.42)$$

and

$$\begin{cases} m_{iso}^{sp} = \min\limits_{i=1...m}\left(D_i\right), \text{ with:} \\ D_i = \begin{cases} 0 \text{ , if } d_i < 0 \\ \dfrac{d_i}{\left\|\boldsymbol{j}_{\boldsymbol{oc}_i}\right\|}, \text{ if } \left\|\boldsymbol{j}_{\boldsymbol{oc}_i}\right\| \neq 0 \text{ and } d_i \geq 0, \ \forall i = 1...m \\ \infty \text{ , otherwise} \end{cases} \\ d_i = \tau_i^{\max} - \left\|\boldsymbol{j}_{\boldsymbol{pc}_i}\right\| f_{req}, \ \forall i = 1...m \end{cases} \quad (2.43).$$

To better understand the above values and have some insight on their geometrical interpretation, illustrations for the cases of two-dof (1T-1R) and three-dof (2T-1R) robots are provided in **Fig. 2-5** and **Fig. 2-6**, respectively.

In these figures, the operational twist zonotopes as well as the geometrical interpretation of v_{iso}^{sp} and ω_{iso}^{sp} are illustrated. Note that the interpretation of v_{iso}^{sp} and ω_{iso}^{sp} that appears as rectangular regions in the case of (1T-1R) must be carefully understood, as it can be misleading. That is why, the second example of (2T-1R) robot has been provided in the hope of eliminating any ambiguity. Perhaps, an even better example would be to consider the case of at least (2T-2R) manipulator, but unfortunately, such a case is graphically impossible to represent or comprehend. Nonetheless, with **Fig. 2-6**, a deeper insight on the true nature of the regions described by:

$$\begin{cases} \boldsymbol{\Omega} = \left\{\boldsymbol{t} \in \mathbb{R}^n; \ \left\|\boldsymbol{\omega}\right\| \leq \omega_{req} \text{ and } \left\|\boldsymbol{v}\right\| \leq v_{req}\right\} \\ \boldsymbol{\mathcal{R}}_1 = \left\{\boldsymbol{t} \in \mathbb{R}^n; \ \left\|\boldsymbol{\omega}\right\| \leq \omega_{req} \text{ and } \left\|\boldsymbol{v}\right\| \leq v_{iso}^{sp}\right\} \\ \boldsymbol{\mathcal{R}}_2 = \left\{\boldsymbol{t} \in \mathbb{R}^n; \ \left\|\boldsymbol{v}\right\| \leq v_{req} \text{ and } \left\|\boldsymbol{\omega}\right\| \leq \omega_{iso}^{sp}\right\} \end{cases} \quad (2.44)$$

can be achieved.

The Interesting Features of Specific Isotropic Values

It remains to discuss some interesting features of specific isotropic values. First, we emphasize that it is enough to consider one specific isotropic speed (v_{iso}^{sp} or ω_{iso}^{sp}) to verify that both translational and rotational speed requirements are fulfilled simultaneously. This is done by checking if its value is greater or equal to the corresponding requirement. Likewise, it is sufficient to know one of the specific isotropic static loads (i.e. f_{iso}^{sp} or m_{iso}^{sp}) to verify whether the mixed external wrench capacity requirements are satisfied or not. In fact, we can easily prove that specific isotropic values satisfy the following properties[11]:

1. $v_{iso}^{sp} \geq v_{req} \Leftrightarrow \omega_{iso}^{sp} \geq \omega_{req}$.

[11] The proof is as follows. For instance, let us consider the first property. As $v_{iso}^{sp} \geq v_{req}$, then we can guarantee that we can simultaneously and isotropically achieve at least ω_{req} and v_{req} (see definition of v_{iso}^{sp}). Then, based on the definition of ω_{iso}^{sp}, this latter is necessarily greater or equal to ω_{req}; otherwise, we have contradiction. For better understanding, the reader may refer to **Fig. 2-5**.

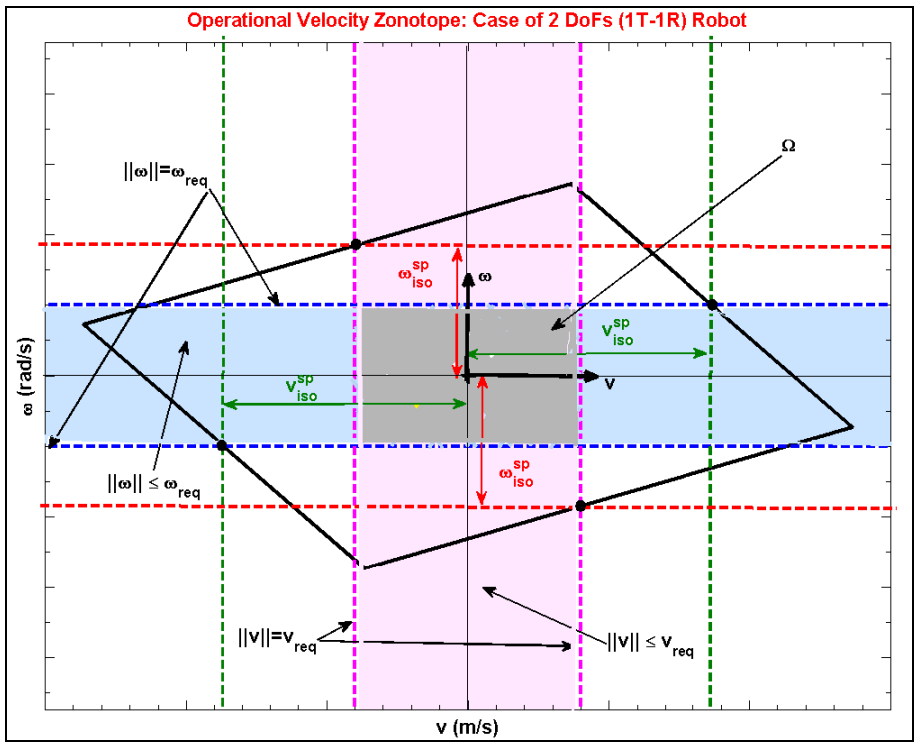

Fig. 2-5: Geometrical interpretation of specific isotropic values in the case of two-dof (1T-1R) robot.

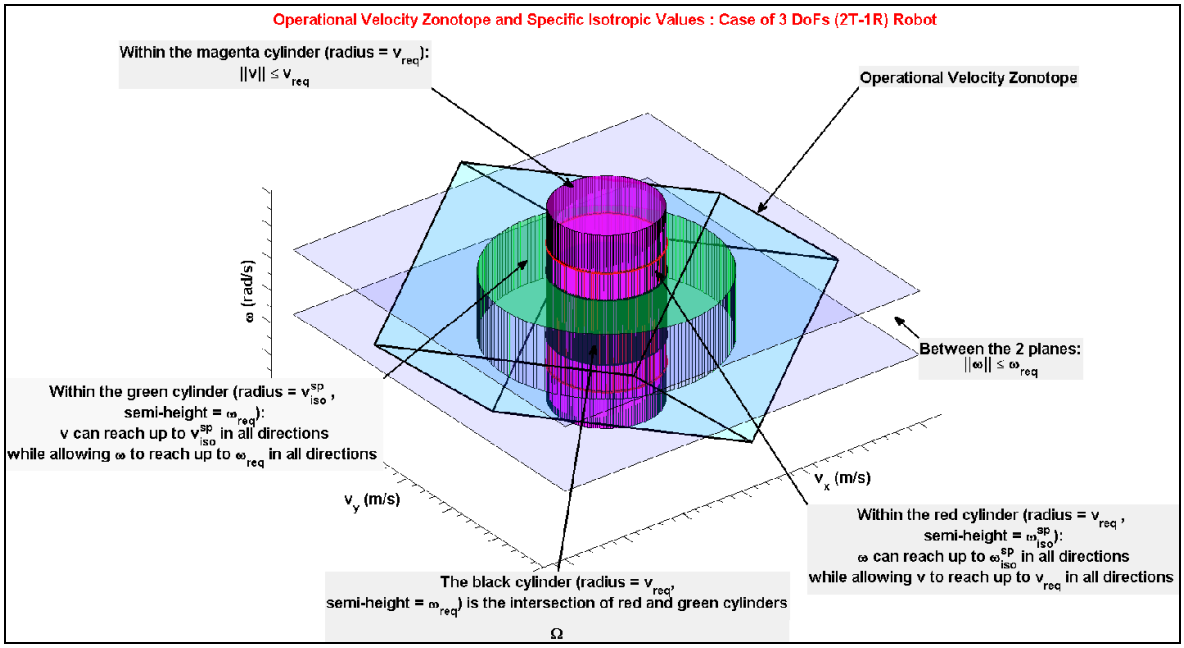

Fig. 2-6: Geometrical interpretation of specific isotropic values in the case of three-dof (2T-1R) robot.

2. $f_{iso}^{sp} \geq f_{req} \Leftrightarrow m_{iso}^{sp} \geq m_{req}$.
3. $v_{iso}^{sp} \leq v_{iso}^{p}$, $\omega_{iso}^{sp} \leq \omega_{iso}^{p}$, $f_{iso}^{sp} \leq f_{iso}^{p}$, and $m_{iso}^{sp} \leq m_{iso}^{p}$ with the terms having "p" superscript and "iso" subscript indicating the same meaning and definition as introduced in **§2.2.3.B**. It is clear that v_{iso}^{p}, ω_{iso}^{p}, f_{iso}^{p}, and m_{iso}^{p} are special cases of the specific isotropic values. They

correspond to the case where $\omega_{req}=0$, $v_{req}=0$, $m_{req}=0$, and $f_{req}=0$, respectively. This can be directly noticed from equations (2.40) through (2.43).

4. $v_{iso}^{sp}\geq v_{req}$ (or $\omega_{iso}^{sp}\geq\omega_{req}$) implies that all speed requirements are fulfilled and the pose is sufficiently far from series-type singularity. Similarly, $f_{iso}^{sp}\geq f_{req}$ (or $m_{iso}^{sp}\geq m_{req}$) indicates satisfaction of mixed wrench requirements and that the pose is adequately far from classical parallel-type singularity.

It is worth emphasizing that v_{req} and ω_{req} serve as some sort of numerical tolerances for series-type singularity. To clarify this further, consider the set $\mathcal{Q}$ .Then, to assure that the pose is sufficiently distant from series-type singularity, the aforementioned region should be included in the operational-twist zonotope. The region $\mathcal{Q}$ is the grey rectangle and the black cylinder in **Fig. 2-5** and **Fig. 2-6**, respectively. Similar argument can be considered regarding static wrench capacities and parallel-type singularity.

Ultimately, to be able to co-assess simultaneous mixed motion, mixed static wrench capacities, and assure farness from classical series and parallel type singularities, we need to build an index using at least one specific isotropic speed (v_{iso}^{sp} or ω_{iso}^{sp})[12] and one specific isotropic static load (f_{iso}^{sp} or m_{iso}^{sp})[13]. In fact, the choice depends on what the roboticist needs or favors. For example, if he/she is interested in obtaining the utmost of robot capability in linear speed and static moment capacity, then it is recommended to use v_{iso}^{sp} and m_{iso}^{sp}. In this case, optimizing for v_{iso}^{sp} and m_{iso}^{sp}, by maximizing the composite index $CI=\min\left(v_{iso}^{sp}/v_{req}, m_{iso}^{sp}/m_{req}\right)$ for instance, will elevate v_{iso}^{sp} and m_{iso}^{sp} without caring for maximizing ω_{iso}^{sp} and f_{iso}^{sp}. But surely, these latter two cannot drop below ω_{req} and f_{req}, respectively. This is due to the mutuality described by the first and second properties above. Of course, if one would like to elevate all, then he/she should combine them all in a composite index, and this does not lead to any computational expenses, as all are very simple to get. Note also that to globally assess or optimize a robot over a desired workspace, DWS, it is sufficient to consider the worst values of the aforementioned local measures over DWS.

Hence, it is obvious that with these novel measures, we can assess and optimize heterogeneous-dof manipulators with confidence regarding classical singularity and kinetostatic aspects. Using this approach, one knows well what he/she is optimizing or assessing a robot for, as compared to the available techniques based on arbitrary homogenization.

Case Study: DUAL V

Now, as the mathematical formulation of the new kinetostatic measures has been made, we proceed by performing a case study on DUAL V to concretize the concepts. The actuator

[12] To assess the twist capacity and the farness from series-type singularity.

[13] To assess the wrench capability and the farness from parallel-type singularity.

Table 2-1: DUAL V actuators' characteristics and the desired kinetostatic requirements.*

Symbol	Quantity	Value
$\dot{q}^{\max}$	Actuator's Maximum Speed	$550 \text{ rpm} = 57 \text{ rad/s}$
$\tau^{\max}$	Actuator's Maximum Torque	127 N m
v_{req}	Required Linear Speed	$0.2\ \dot{q}^{\max}\ L = 3.2 \text{ m/s}$
ω_{req}	Required Angular Speed	$0.2\ \dot{q}^{\max} = 110 \text{ rpm} = 11.5 \text{ rad/s}$
f_{req}	Required Static Force Capacity	$0.2\ \tau^{\max}/L = 90.6 \text{ N}$
m_{req}	Required Static Moment Capacity	$0.2\ \tau^{\max} = 25.4 \text{ N m}$

***All actuators are identical of type ETEL RTMB-0140-100.**

characteristics and the desired minimum requirements in translation and rotation are given in **Table 2-1**.

The specific isotropic values and the satisfactory regions are presented in **Fig. 2-7**, in terms of $\dot{q}^{\max}$ and $\tau^{\max}$. In this analysis, the rotation is fixed to $\theta = 0°$ to allow visualization. Note that the regions where $v_{iso}^{sp} \geq v_{req}$ and $\omega_{iso}^{sp} \geq \omega_{req}$ are the same. Similar observation can be mentioned regarding the regions where $f_{iso}^{sp} \geq f_{req}$ and $m_{iso}^{sp} \geq m_{req}$. These concurrences are expected as discussed previously (first and second properties).

At the end of the kinetostatic evaluation section, we mention that the introduced measures can be sufficient as sole performance criteria only in the case where the manipulator under study works in quasi-static conditions. An example would be a machining application where we have two phases: a transient phase and a machining one. In the transient phase, the end-effector is supposed to move fast, usually at constant speed, from the current position to nearby the piece. Afterwards, the machining stage starts in which the tool moves at low speeds but counteracts considerable external wrenches due to material removal. Thus, considering only kinetostatic measures in such situations is valid. Nevertheless, in the case where the application involves considerable acceleration, speed, and external wrenches at the same time, a dynamic assessment is inevitable to evaluate the expected capabilities of the manipulator. This will be dealt with in the next part.

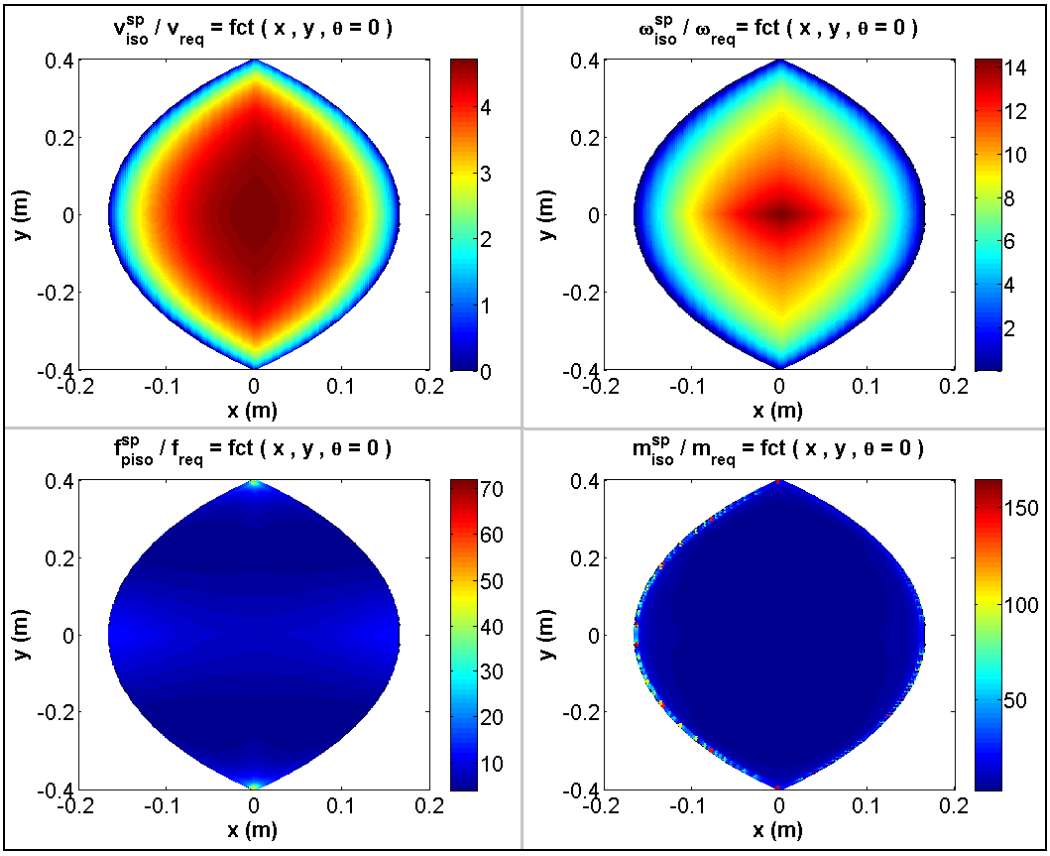

(a)

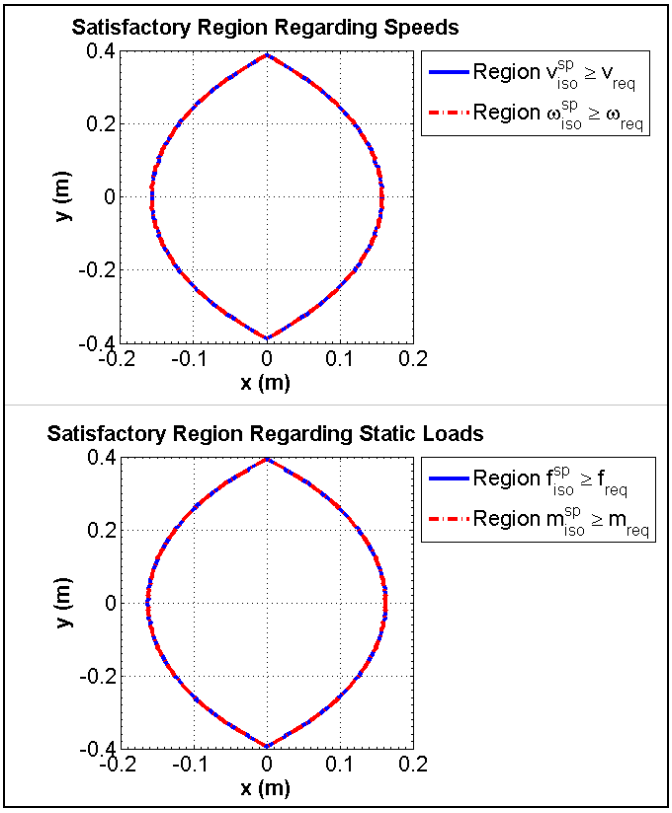

(b)

Fig. 2-7: DUAL V kinetostatic performance evaluation: the specific isotropic values (a) and the satisfactory regions (b).

2.2.4- Dynamic Performance Evaluation: A Novel Approach Based on Multi-Assessment of Isotropic Dynamic Capabilities

When the intended task of the manipulator or machine tool cannot be assumed quasi-static, it is then mandatory to put the dynamics of the whole system into the play. Considering the dynamic model (DM), an estimation of the isotropic simultaneous dynamic performances can be established. This establishment follows a similar methodology to that adopted for kinetostatics.

The complexity of the method is rather that of obtaining the DM itself. In fact, once the DM in the required form is obtained, the dynamic measures can be computed or estimated effortlessly via analytical formulae. Only in the case of heterogeneous-dof manipulators, where the effects of linear and angular velocities are coupled in the DM, the computation of the exact values necessitates a numerical optimization. Nevertheless, this numerical optimization can be done relatively at ease or can be replaced by analytical lower bounds, as a safe approximation. Although this latter point can be considered as a drawback, it is not that severe considering the various benefits the method provides. This will become clear by the end of the section.

In what follows, we will establish the analytical lower bounds of the dynamic specific isotropic values in the most general case of heterogeneous-dof robots. These lower bounds become the exact values in the situation of homogeneous dofs or uncoupled velocity effects.

A- Generalities and Assumptions

As a starting point, we assume that the DM of the robot has been obtained as a function of the operational variables and actuated-joint torques only. In this aspect, several methods exist and are classified into four main categories (ZHAO & GAO, 2009): Newton-Euler method (e.g., (KHALIL & GUEGAN, 2002), (HARIB & SRINIVASAN, 2003)), Lagrangian method (e.g., (PANG & SHAHINPOOR, 1994), (LEE & LEE, 2003)), Kane's method (e.g. (BEN-HORIN, et al., 1998), (LIU, et al., 2000)), and virtual work principle based method (e.g. (WANG & GOSSELIN, 1998), (SOKOLOV & XIROUCHAKIS, 2007)). We further mention that in the case of redundant manipulators, a pseudo-inversion would be needed to acquire the DM in the aforementioned form. This can be done by assuming the solution with zero components along the null space of the considered matrix.

Anyway, we should have the DM as follows:

$$\boldsymbol{M}(\boldsymbol{x})\,\boldsymbol{\rho}+\boldsymbol{C}(\boldsymbol{x},\boldsymbol{t})\,\boldsymbol{t}+\boldsymbol{\tau}_{g}(\boldsymbol{x})+\boldsymbol{D}(\boldsymbol{x})\,\boldsymbol{w}_{e}=\boldsymbol{\tau} \tag{2.45}$$

The terms $\boldsymbol{\rho}=\left(\boldsymbol{a}^{\mathrm{T}} \quad \boldsymbol{\alpha}^{\mathrm{T}}\right)^{\mathrm{T}}$, $\boldsymbol{\tau}_{g}(\boldsymbol{x})$, and $\boldsymbol{w}_{e}=\left(\boldsymbol{f}_{e}^{\mathrm{T}} \quad \boldsymbol{m}_{e}^{\mathrm{T}}\right)^{\mathrm{T}}$ correspond orderly to the operational accelerations ($\boldsymbol{a}=\dot{\boldsymbol{v}}$ and $\boldsymbol{\alpha}=\dot{\boldsymbol{\omega}}$), the torques due to gravitational forces, and the non-gravitational external wrench[14] acting on the end-effector (external force, $\boldsymbol{f}_{e}$, and external

[14] This is the wrench due to machining, for instance.

moment, $\boldsymbol{m}_e$). $\boldsymbol{M}(\boldsymbol{x})$ is the generalized $m \times n$ inertia matrix, whereas $\boldsymbol{c}(\boldsymbol{x},\boldsymbol{t}) = \boldsymbol{C}(\boldsymbol{x},\boldsymbol{t})\,\boldsymbol{t}$ represents the generalized Coriolis and centrifugal effects, with $\boldsymbol{C}(\boldsymbol{x},\boldsymbol{t})$ being of $m \times n$ dimension. As for $\boldsymbol{D}(\boldsymbol{x})$, it is an $m \times n$ matrix as well. The rest of symbols hold exactly the same meanings as before. Notice that in (2.45), friction is not considered. This has been done to simplify the analysis, as we are interested in evaluating the preliminary expected performances. Yet, the effect of friction can be included if it can be written under a similar form as any of the aforementioned terms.

Note that $\boldsymbol{c}(\boldsymbol{x},\boldsymbol{t})$ can be written under the following form:

$$\boldsymbol{c}(\boldsymbol{x},\boldsymbol{t}) = \begin{pmatrix} \boldsymbol{t}^{\mathrm{T}}\,\boldsymbol{H}_1\,\boldsymbol{t} & \cdots & \boldsymbol{t}^{\mathrm{T}}\,\boldsymbol{H}_m\,\boldsymbol{t} \end{pmatrix}^{\mathrm{T}} = \boldsymbol{h}^{v}(\boldsymbol{x},\boldsymbol{t}) + \boldsymbol{h}^{\omega}(\boldsymbol{x},\boldsymbol{t}) + \boldsymbol{h}^{v\omega}(\boldsymbol{x},\boldsymbol{t}) \tag{2.46},$$

with:

$$\boldsymbol{h}^{v}(\boldsymbol{x},\boldsymbol{v}) = \begin{pmatrix} \boldsymbol{v}^{\mathrm{T}}\,\boldsymbol{H}_1^{v}\,\boldsymbol{v} & \cdots & \boldsymbol{v}^{\mathrm{T}}\,\boldsymbol{H}_m^{v}\,\boldsymbol{v} \end{pmatrix}^{\mathrm{T}} \tag{2.47},$$

$$\boldsymbol{h}^{\omega}(\boldsymbol{x},\boldsymbol{\omega}) = \begin{pmatrix} \boldsymbol{\omega}^{\mathrm{T}}\,\boldsymbol{H}_1^{\omega}\,\boldsymbol{\omega} & \cdots & \boldsymbol{\omega}^{\mathrm{T}}\,\boldsymbol{H}_m^{\omega}\,\boldsymbol{\omega} \end{pmatrix}^{\mathrm{T}} \tag{2.48}$$

and

$$\boldsymbol{h}^{v\omega}(\boldsymbol{x},\boldsymbol{t}) = \begin{pmatrix} 2\,\boldsymbol{v}^{\mathrm{T}}\,\boldsymbol{H}_1^{v\omega}\,\boldsymbol{\omega} & \cdots & 2\,\boldsymbol{v}^{\mathrm{T}}\,\boldsymbol{H}_m^{v\omega}\,\boldsymbol{\omega} \end{pmatrix}^{\mathrm{T}} \tag{2.49}.$$

The terms $\boldsymbol{H}_i$, $\boldsymbol{H}_i^{v}$, $\boldsymbol{H}_i^{\omega}$, and $\boldsymbol{H}_i^{v\omega}$ are pose-dependent[15] matrices of respective dimensions: $n \times n$, $\dim(\boldsymbol{v}) \times \dim(\boldsymbol{v})$, $\dim(\boldsymbol{\omega}) \times \dim(\boldsymbol{\omega})$, and $\dim(\boldsymbol{v}) \times \dim(\boldsymbol{\omega})$.

As a result, (2.45) can be written as:

$$\boldsymbol{K}\,\dot{\boldsymbol{\xi}} + \boldsymbol{h}^{v} + \boldsymbol{h}^{\omega} + \boldsymbol{h}^{v\omega} + \boldsymbol{\tau}_g = \boldsymbol{\tau} \tag{2.50},$$

where $\boldsymbol{K} = \boldsymbol{K}(\boldsymbol{x}) = \begin{bmatrix} \boldsymbol{M}(\boldsymbol{x}) & \boldsymbol{D}(\boldsymbol{x}) \end{bmatrix}$ and $\dot{\boldsymbol{\xi}} = \begin{pmatrix} \boldsymbol{\rho}^{\mathrm{T}} & \boldsymbol{w}_e^{\mathrm{T}} \end{pmatrix}^{\mathrm{T}}$. This is the favorable form for our analysis. Henceforth, we are going to drop the $(\boldsymbol{x})$ and $(\boldsymbol{x},\boldsymbol{t})$ notations in $\boldsymbol{K}$, $\boldsymbol{h}^{v}$, etc. for readability purpose.

Concerning the constraints on actuators' capabilities, we only account for the following speed and torque limits:

$$\begin{cases} |\dot{q}_i| \le \dot{q}_i^{\max} \\ |\tau_i| \le \tau_i^{\max} \end{cases}, \ \forall i = 1 \ldots m \tag{2.51}.$$

Based on these hypotheses, the subsequent section describes briefly the approach to analyze the dynamic performance.

---

[15] Function of pose, $\boldsymbol{x}$, only.

B- Brief Description and Mathematical Formulation

Suppose that based on the intended application, the machine tool must be able to achieve simultaneously certain minimal isotropic requirements in: $\boldsymbol{a}$, $\boldsymbol{\alpha}$, $\boldsymbol{v}$, $\boldsymbol{\omega}$, $\boldsymbol{f_e}$, and $\boldsymbol{m_e}$. Denote them in corresponding order by: ${}^{d}a_{req}$, ${}^{d}\alpha_{req}$, ${}^{d}v_{req}$, ${}^{d}\omega_{req}$, ${}^{d}f_{ereq}$, and ${}^{d}m_{ereq}$ [16], all of which being positive scalars.

Then, we may define the specific dynamic isotropic values as means of dynamic assessment. For instance, the **specific isotropic linear acceleration**, ${}^{d}a_{iso}^{sp}$, is defined as the maximal value of linear acceleration attainable by the robot regardless of direction, while allowing $\boldsymbol{\alpha}$, $\boldsymbol{v}$, $\boldsymbol{\omega}$, $\boldsymbol{f_e}$, and $\boldsymbol{m_e}$ to reach their corresponding requirements in all directions. Similarly, we define the **specific isotropic angular acceleration,** ${}^{d}\alpha_{iso}^{sp}$, the **specific isotropic linear speed,** ${}^{d}v_{iso}^{sp}$, the **specific isotropic angular speed,** ${}^{d}\omega_{iso}^{sp}$, the **specific isotropic force,** ${}^{d}f_{eiso}^{sp}$, and the **specific isotropic moment,** ${}^{d}m_{eiso}^{sp}$ [16].

As mentioned earlier, in the general case of heterogeneous-dof robots, we can consider some particular lower bounds for the specific isotropic values. These are denoted by: $\underline{\underline{{}^{d}a_{iso}^{sp}}}$, $\underline{\underline{{}^{d}\alpha_{iso}^{sp}}}$, $\underline{\underline{{}^{d}v_{iso}^{sp}}}$, $\underline{\underline{{}^{d}\omega_{iso}^{sp}}}$, $\underline{\underline{{}^{d}f_{eiso}^{sp}}}$, and $\underline{\underline{{}^{d}m_{eiso}^{sp}}}$**.** The computation of all these terms is done starting from definition and considering the following system of relations:

$$\begin{cases} \boldsymbol{K}\ \boldsymbol{\xi} + \boldsymbol{h}^{v} + \boldsymbol{h}^{\omega} + \boldsymbol{h}^{v\omega} + \boldsymbol{\tau}_{g} = \boldsymbol{\tau} \\ \dot{\boldsymbol{q}} = \boldsymbol{J}_{\boldsymbol{m}}\ \boldsymbol{t} \\ \left|\dot{q}_i\right| \le \dot{q}_i^{\max},\ \forall i = 1...m \\ \left|\tau_i\right| \le \tau_i^{\max},\ \forall i = 1...m \end{cases} \tag{2.52}$$

Based on (2.52) and following the procedure detailed in **Appendix B.1** and **Appendix B.2**, we get the following compact forms for the different specific isotropic values (note that $val = a, \alpha, f_e, m_e$ and $vel = v, \omega$):

[16] The superscript "d" is used to indicate the case of dynamics as distinguished from kinetostatics, particularly for: linear and angular speeds, external force, and external moment.

$$
\begin{cases}
{}^{d}val_{iso}^{sp} \geq \underline{\underline{{}^{d}a_{iso}^{sp}}} = \min\limits_{i=1\ldots m}\left(K_C, \underline{\underline{{}^{val}E_i^-}}, \underline{\underline{{}^{val}E_i^+}}\right), \text{ with:} \\
K_C = \begin{cases} 0, \text{ if } {}^{k}v_{iso}^{sp} < {}^{d}v_{req} \text{ (or } {}^{k}\omega_{iso}^{sp} < {}^{d}\omega_{req}) \\ \infty, \text{ otherwise} \end{cases} \\
\underline{\underline{{}^{val}E_i^-}} = \begin{cases} 0, \text{ if } \overline{\overline{{}^{val}e_i^-}} > 0 \\ -\dfrac{\overline{\overline{{}^{val}e_i^-}}}{\left\|\boldsymbol{k}_{\boldsymbol{r}_i}^{\boldsymbol{val}}\right\|}, \text{ if } \overline{\overline{{}^{val}e_i^-}} \leq 0 \text{ and } \left\|\boldsymbol{k}_{\boldsymbol{r}_i}^{\boldsymbol{val}}\right\| \neq 0 \\ \infty, \text{ otherwise} \end{cases}, \underline{\underline{{}^{val}E_i^+}} = \begin{cases} 0, \text{ if } \underline{\underline{{}^{val}e_i^+}} < 0 \\ \dfrac{\underline{\underline{{}^{val}e_i^+}}}{\left\|\boldsymbol{k}_{\boldsymbol{r}_i}^{\boldsymbol{val}}\right\|}, \text{ if } \underline{\underline{{}^{\boldsymbol{val}}e_i^+}} \geq 0 \text{ and } \left\|\boldsymbol{k}_{\boldsymbol{r}_i}^{\boldsymbol{val}}\right\| \neq 0 \\ \infty, \text{ otherwise} \end{cases} \quad (2.53), \\
\overline{\overline{{}^{val}e_i^-}} = -\tau_i^{\max} + sum_{val} - \zeta_{\min_i}^{v}\left({}^{d}v_{req}\right)^2 - \zeta_{\min_i}^{\omega}\left({}^{d}\omega_{req}\right)^2 + 2\,\sigma_{\max_i}^{v\omega}\,{}^{d}v_{req}\,{}^{d}\omega_{req} - \tau_{g_i} \\
\underline{\underline{{}^{val}e_i^+}} = +\tau_i^{\max} - sum_{val} - \zeta_{\max_i}^{v}\left({}^{d}v_{req}\right)^2 - \zeta_{\max_i}^{\omega}\left({}^{d}\omega_{req}\right)^2 - 2\,\sigma_{\max_i}^{v\omega}\,{}^{d}v_{req}\,{}^{d}\omega_{req} - \tau_{g_i} \\
\forall i = 1\ldots m
\end{cases}
$$

and

$$
\begin{cases}
{}^{d}vel_{iso}^{sp} \geq \underline{\underline{{}^{d}vel_{iso}^{sp}}} = \min\limits_{i=1\ldots m}\left({}^{k}vel_{iso}^{sp}, \underline{\underline{{}^{vel}E_i^-}}, \underline{\underline{{}^{vel}E_i^+}}\right), \text{ with:} \\
\underline{\underline{{}^{vel}E_i^-}} = \begin{cases} vel_{oi1}^-, \text{ if } \overline{\overline{{}^{vel}e_i^-}} \leq 0,\ val_1 \neq 0, \text{ and } \zeta_{\min_i}^{vel} = 0 \\ vel_{oi2}^-, \text{ if } \overline{\overline{{}^{vel}e_i^-}} \leq 0,\ \zeta_{\min_i}^{vel} \neq 0, \text{ and } vel_{oi2}^- \geq 0 \\ \infty, \text{ if } \overline{\overline{{}^{vel}e_i^-}} \leq 0,\ val_1 = 0, \text{ and } \zeta_{\min_i}^{vel} = 0 \\ 0, \text{ otherwise} \end{cases} \\
\underline{\underline{{}^{vel}E_i^+}} = \begin{cases} vel_{oi1}^+, \text{ if } \underline{\underline{{}^{vel}e_i^+}} \geq 0,\ val_1 \neq 0, \text{ and } \zeta_{\max_i}^{vel} = 0 \\ vel_{oi2}^+, \text{ if } \underline{\underline{{}^{vel}e_i^+}} \geq 0,\ \zeta_{\max_i}^{vel} \neq 0, \text{ and } vel_{oi2}^+ \geq 0 \\ \infty, \text{ if } \underline{\underline{{}^{vel}e_i^+}} \geq 0,\ val_1 = 0, \text{ and } \zeta_{\max_i}^{vel} = 0 \\ 0, \text{ otherwise} \end{cases} \\
vel_{oi1}^- = \dfrac{-\overline{\overline{{}^{vel}e_i^-}}}{2\,val_1},\ vel_{oi2}^- = \dfrac{val_1 - \sqrt{\left(val_1\right)^2 + \zeta_{\min_i}^{vel}\,\overline{\overline{{}^{vel}e_i^-}}}}{\zeta_{\min_i}^{vel}} \\
\overline{\overline{{}^{vel}e_i^-}} = -\tau_i^{\max} + \left\|\boldsymbol{k}_{\boldsymbol{r}_i}^{\boldsymbol{a}}\right\|{}^{d}a_{req} + \left\|\boldsymbol{k}_{\boldsymbol{r}_i}^{\boldsymbol{\alpha}}\right\|{}^{d}\alpha_{req} + \left\|\boldsymbol{k}_{\boldsymbol{r}_i}^{\boldsymbol{f_e}}\right\|{}^{d}f_{ereq} + \left\|\boldsymbol{k}_{\boldsymbol{r}_i}^{\boldsymbol{m_e}}\right\|{}^{d}m_{ereq} - val_2 - \tau_{g_i} \\
vel_{oi1}^+ = \dfrac{\underline{\underline{{}^{vel}e_i^+}}}{2\,val_1},\ vel_{oi2}^+ = \dfrac{-val_1 + \sqrt{\left(val_1\right)^2 + \zeta_{\max_i}^{vel}\,\underline{\underline{{}^{vel}e_i^+}}}}{\zeta_{\max_i}^{vel}} \quad (2.54), \\
\underline{\underline{{}^{vel}e_i^+}} = \tau_i^{\max} - \left\|\boldsymbol{k}_{\boldsymbol{r}_i}^{\boldsymbol{a}}\right\|{}^{d}a_{req} - \left\|\boldsymbol{k}_{\boldsymbol{r}_i}^{\boldsymbol{\alpha}}\right\|{}^{d}\alpha_{req} - \left\|\boldsymbol{k}_{\boldsymbol{r}_i}^{\boldsymbol{f_e}}\right\|{}^{d}f_{ereq} - \left\|\boldsymbol{k}_{\boldsymbol{r}_i}^{\boldsymbol{m_e}}\right\|{}^{d}m_{ereq} - val_3 - \tau_{g_i} \\
\forall i = 1\ldots m
\end{cases}
$$

Table 2-2: The significance of the general terms used in relations (2.53) and (2.54).

Definition of the terms appearing in relation (2.53)			
val	sum_{val}		
a	$\left\|\boldsymbol{k}_{\boldsymbol{r}_i}^{\boldsymbol{a}}\right\| {}^{d}\alpha_{req} + \left\|\boldsymbol{k}_{\boldsymbol{r}_i}^{\boldsymbol{f_e}}\right\| {}^{d}f_{ereq} + \left\|\boldsymbol{k}_{\boldsymbol{r}_i}^{\boldsymbol{m_e}}\right\| {}^{d}m_{ereq}$		
α	$\left\|\boldsymbol{k}_{\boldsymbol{r}_i}^{\boldsymbol{a}}\right\| {}^{d}a_{req} + \left\|\boldsymbol{k}_{\boldsymbol{r}_i}^{\boldsymbol{f_e}}\right\| {}^{d}f_{ereq} + \left\|\boldsymbol{k}_{\boldsymbol{r}_i}^{\boldsymbol{m_e}}\right\| {}^{d}m_{ereq}$		
f_e	$\left\|\boldsymbol{k}_{\boldsymbol{r}_i}^{\boldsymbol{a}}\right\| {}^{d}a_{req} + \left\|\boldsymbol{k}_{\boldsymbol{r}_i}^{\boldsymbol{\alpha}}\right\| {}^{d}\alpha_{req} + \left\|\boldsymbol{k}_{\boldsymbol{r}_i}^{\boldsymbol{m_e}}\right\| {}^{d}m_{ereq}$		
m_e	$\left\|\boldsymbol{k}_{\boldsymbol{r}_i}^{\boldsymbol{a}}\right\| {}^{d}a_{req} + \left\|\boldsymbol{k}_{\boldsymbol{r}_i}^{\boldsymbol{\alpha}}\right\| {}^{d}\alpha_{req} + \left\|\boldsymbol{k}_{\boldsymbol{r}_i}^{\boldsymbol{f_e}}\right\| {}^{d}f_{ereq}$		
Definition of the terms in relation (2.54)			
vel	val_1	val_2	val_3
v	$\sigma_{\max_i}^{v\omega}\ {}^{d}\omega_{req}$	$\zeta_{\min_i}^{\omega}\left({}^{d}\omega_{req}\right)^2$	$\zeta_{\max_i}^{\omega}\left({}^{d}\omega_{req}\right)^2$
ω	$\sigma_{\max_i}^{v\omega}\ {}^{d}v_{req}$	$\zeta_{\min_i}^{v}\left({}^{d}v_{req}\right)^2$	$\zeta_{\max_i}^{v}\left({}^{d}v_{req}\right)^2$

with:

$$\begin{cases} {}^{k}v_{iso}^{sp} = \min\limits_{i=1...m}\left(A_i\right), \text{ such that:} \\ A_i = \begin{cases} 0\ , \text{ if } \ a_i < 0 \\ \dfrac{a_i}{\left\|\boldsymbol{j}_{\boldsymbol{mpr}_i}\right\|}, \text{ if } \ \left\|\boldsymbol{j}_{\boldsymbol{mpr}_i}\right\| \neq 0 \text{ and } a_i \geq 0 \\ \infty\ , \text{ otherwise} \end{cases}, \\ a_i = \dot{q}_i^{\max} - \left\|\boldsymbol{j}_{\boldsymbol{mor}_i}\right\| {}^{d}\omega_{req} \\ \forall i = 1...m \end{cases} \tag{2.55}$$

$$\begin{cases} {}^{k}\omega_{iso}^{sp} = \min\limits_{i=1...m}\left(B_i\right), \text{ such that:} \\ B_i = \begin{cases} 0\ , \text{ if } \ b_i < 0 \\ \dfrac{b_i}{\left\|\boldsymbol{j}_{\boldsymbol{mor}_i}\right\|}, \text{ if } \ \left\|\boldsymbol{j}_{\boldsymbol{mor}_i}\right\| \neq 0 \text{ and } b_i \geq 0 \\ \infty\ , \text{ otherwise} \end{cases} \\ b_i = \dot{q}_i^{\max} - \left\|\boldsymbol{j}_{\boldsymbol{mpr}_i}\right\| {}^{d}v_{req} \\ \forall i = 1...m \end{cases} \tag{2.56}$$

and[17]

$$\begin{cases} \zeta^{v}_{\min_i} = \min\left(\text{eigs}\left(\boldsymbol{H}_i^{v}\right),0\right),\ \zeta^{v}_{\max_i} = \max\left(\text{eigs}\left(\boldsymbol{H}_i^{v}\right),0\right), \\ \zeta^{\omega}_{\min_i} = \min\left(\text{eigs}\left(\boldsymbol{H}_i^{\omega}\right),0\right),\ \zeta^{\omega}_{\max_i} = \max\left(\text{eigs}\left(\boldsymbol{H}_i^{\omega}\right),0\right),\ \forall i = 1...m \\ \text{and } \sigma^{v\omega}_{\max_i} = \max\left(\text{sing}\left(\boldsymbol{H}_i^{v\omega}\right)\right) \end{cases} \quad (2.57).$$

As for the significance of the terms val, sum_{val}, vel, val_1, val_2, and val_3 in (2.53) and (2.54), refer to **Table 2-2**. Also, for explicit formulae of specific isotropic values, they are given in **Appendix B.1**.

Hence, we have established some particular lower bounds for the specific isotropic values in dynamics. These lower bounds become the exact values in the following cases:

1. Homogeneous-dof manipulators;
2. Heterogeneous-dof manipulators with $\boldsymbol{h}^{v\omega} = \boldsymbol{0}$ (uncoupled effect of $\boldsymbol{v}$ and $\boldsymbol{\omega}$);
3. And heterogeneous-dof manipulators with ${}^{d}v_{req} = 0$ or ${}^{d}\omega_{req} = 0$.

We emphasize that knowing one of the specific isotropic values in dynamics is sufficient to test for the fulfillment of all dynamic requirements. The same applies regarding the computed lower bounds. For instance, we have:

$$\underline{\underline{{}^{d}a^{sp}_{iso}}} \geq {}^{d}a_{req} \Leftrightarrow \begin{cases} \underline{\underline{{}^{d}\alpha^{sp}_{iso}}} \geq {}^{d}\alpha_{req}\ ,\ \underline{\underline{{}^{d}v^{sp}_{iso}}} \geq {}^{d}v_{req}\ ,\ \underline{\underline{{}^{d}\omega^{sp}_{iso}}} \geq {}^{d}\omega_{req} \\ \underline{\underline{{}^{d}f^{sp}_{eiso}}} \geq {}^{d}f_{ereq}\ ,\ \text{and}\ \underline{\underline{{}^{d}m^{sp}_{eiso}}} \geq {}^{d}m_{ereq} \end{cases} \quad (2.58).$$

Regarding design optimization or assessment, the roboticist can choose one or more of the specific isotropic values, depending on his/her interest. Finally, a case study on DUAL V is presented in **Appendix B.3**.

2.3- Cable-Driven Parallel Robots (CDPRs)

2.3.1- Few Words on CDPRs

CDPRs have been extensively investigated in the last decades, due to several merits as compared to classical rigid PMs. Perhaps, the most intriguing of these features are large workspace volume with respect to global machine size, design simplicity, low cost, high payload to weight ratio, flexibility, and ease of reconfiguration. Also, having low moving inertia[18] allows high dynamical performances to be achievable (e.g. the FALCON robot with a peak linear speed

[17] Recall that $\text{eigs}(\boldsymbol{Mat})$ and $\text{sing}(\boldsymbol{Mat})$ denote the lists of eigenvalues and singular values of the matrix $\boldsymbol{Mat}$, respectively.

[18] Due to having only cables connecting the platform with the actuators instead of rigid limbs.

of $13\,\mathrm{m/s}$ and peak linear acceleration of $43\,\mathrm{g}$ (KAWAMURA, et al., 1995)). Besides, most often the wires can be considered massless and inextensible, which simplifies their modeling.

Yet, CDPRs are not without their own limitations. In particular, when cables become lengthy, their mass cannot be any more ignored. Also, when high tension forces exist, the hypothesis of inextensibility is no more justifiable. All these complicate the modeling of CDPRs, as sagging and deformations are to be necessarily considered. Furthermore, as cables can only pull and not push, the feasibility of a pose is not only dependable on length admissibility of the wires and collision avoidance, but also on the possibility of having static equilibrium. Actually, the problem of tension distribution in CDPRs is a non-trivial issue and one of the key research topics in this field. This is not to mention the challenges that CDPRs present on the control level. Additionally, CDPRs are usually characterized by poor precision and stiffness as compared to rigid robots. The major sources of precision errors are the incomplete modeling, deformations, and sagging of wires. These errors become higher with the increase of payload. For more information regarding CDPRs, their state-of-art, applications, and advancements, the reader may refer to (LAMAURY, 2013), (TANG, 2014), the articles cited here and therein.

This was a brief overview on CDPRs. It remains to talk a little about their classification. Generally, we may distinguish three groups of CDPRs, namely the partially constrained, the fully constrained, and the underactuated ones.

In the case of partially constrained CDPRs (e.g. (ALBUS, et al., 1993)), their functioning depends on an external action such as gravity, which helps put all cables under tension. In fully constrained CDPRs (e.g. (LAFOURCADE & LLIBRE, 2002), (KAWAMURA, et al., 2000)), additional active cables are added to fully constrain the moving platform. As for underactuated ones, these are characterized by having fewer active cables than the number of dofs of the end effector, such as the Winch-Bot presented in (CUNNINGHAM & H. H. ASADA, 2009). These latter CDPRs are beyond our scope. In fact, we only consider in the current report CDPRs having m active cables and n controllable dofs such that $m \geq n$.

In what follows, we only deal with the kinetostatic and dynamic analysis of CDPRs following the same paradigm used for rigid manipulators, but after doing the necessarily mathematical reformulations. As for precision, though the methodology used for rigid robots can be adopted here, it is unreasonable as control errors are not the primary source of pose inaccuracy. In fact, regarding this latter issue, the other sources of error, such as elasticity and sagging, are more worth to focus on.

2.3.2- Generalities on the Kinetostatics of CDPRs

Consider a CDPR with m active cables and n controllable dofs for the end-effector, such that $m \geq n$. Then, the kinetostatic relations at a feasible pose and that are always available for CDPRs are:

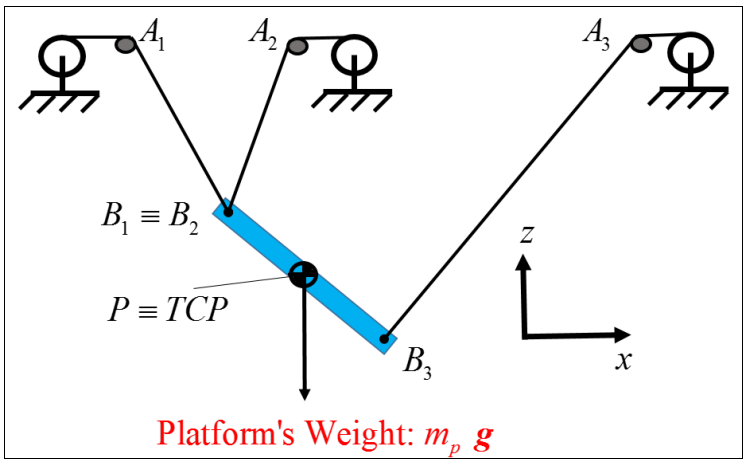

Fig. 2-8: A partially constrained CDPR with three dofs (2T-1R) in the vertical plane: x, z and Θ (rotation about y-axis) motion.

$$\dot{\boldsymbol{q}} = \boldsymbol{J}_{\boldsymbol{m}}\ \boldsymbol{t} \tag{2.59}$$

and

$$\boldsymbol{w} + \boldsymbol{J}_{\boldsymbol{m}}^{\mathrm{T}}\ \boldsymbol{\tau} = \boldsymbol{0} \tag{2.60},$$

with all symbols carrying the same meaning as before.

As for the direct Jacobian, $\boldsymbol{J}$, it is usually not available except in the case where we have $m = n$, as in the case of the partially constrained CDPR depicted in **Fig. 2-8**. Such CDPR can perform a planar motion (2T-1R) in the vertical plane and have the additional two equations at a feasible pose:

$$\boldsymbol{t} = \boldsymbol{J}\ \dot{\boldsymbol{q}} \tag{2.61}$$

and

$$\boldsymbol{\tau} + \boldsymbol{J}^{\mathrm{T}}\ \boldsymbol{w} = \boldsymbol{0} \tag{2.62},$$

with $\boldsymbol{J} = \boldsymbol{J}_{\boldsymbol{m}}^{-1}$.

Other CDPRs with $m > n$ have their forward kinematic and inverse static models given by:

$$\boldsymbol{t} = \boldsymbol{J}_{\boldsymbol{m}}^{*}\ \dot{\boldsymbol{q}},\ \text{with}\ \dot{\boldsymbol{q}}^{\mathrm{T}}\left[\mathrm{null}\left(\boldsymbol{J}_{\boldsymbol{m}}^{\mathrm{T}}\right)\right] = \boldsymbol{0}_{1\times(m-n)} \tag{2.63}$$

and

$$\boldsymbol{\tau} = -\boldsymbol{J}_{\boldsymbol{m}}^{*\mathrm{T}}\ \boldsymbol{w} + \left[\mathrm{null}\left(\boldsymbol{J}_{\boldsymbol{m}}^{\mathrm{T}}\right)\right]\boldsymbol{\lambda},\ \boldsymbol{\lambda} \in \mathbb{R}^{m-n}\,(\text{quasi-arbitrary}) \tag{2.64}.$$

This case resembles redundantly actuated rigid manipulators. Yet, it is not quite the same. As the cables can only pull, $\boldsymbol{\lambda}$ is not fully but quasi arbitrary. This is due to the fact that $\boldsymbol{\lambda}$ must be chosen in such a way to have positive cable tensions, $\boldsymbol{f}_{\boldsymbol{c}} = \begin{pmatrix} f_{c_1} & \cdots & f_{c_m} \end{pmatrix}^{\mathrm{T}}$. Thus, choosing $\boldsymbol{\lambda} = \boldsymbol{0}$ as in rigid robots is not justifiable anymore.

In the case of statics, the positiveness condition of cable tensions:

$$0 \leq f_{c_i}^{\min} \leq f_{c_i} \leq f_{c_i}^{\max},\ \forall i = 1...m \tag{2.65},$$

can be written in terms of actuators' torques as below:

$$0 \leq \tau_i^{\min} \leq \tau_i \leq \tau_i^{\max},\ \forall i = 1...m \tag{2.66}.$$

This is since in statics, the cable tensions and actuators' torques are related by $\boldsymbol{\Psi}$, a diagonal matrix of positive entries[19], i.e.:

$$\boldsymbol{\tau} = \boldsymbol{\Psi}\ \boldsymbol{f_c} \tag{2.67}.$$

As for the bounds $\tau_i^{\min}$ and $\tau_i^{\max}$ in (2.66), they depend on $f_{c_i}^{\min}$, $f_{c_i}^{\max}$, and the maximal torque capacity of the i-th actuator for $i = 1...m$.

Thus, with this basic knowledge, we can proceed with the formulation of the kinetostatic analysis in terms of the operational twist and wrench.

2.3.3- Kinetostatic Performance Evaluation of CDPRs: An Extension of the Approach Applied on Rigid Manipulators

In this section, we seek to extend the notion of kinetostatic isotropic values defined for rigid manipulators into the realm of CDPRs. Regarding specific isotropic speeds, v_{iso}^{sp} and ω_{iso}^{sp}, they can be computed exactly as in the case of rigid manipulators, since they depend on (2.59) and the maximal speeds of the actuators, $\dot{q}_i^{\max}$ (with $i = 1...m$). This is valid provided the pose is feasible. The formulae for these speeds are found in (2.40) and (2.41).

Therefore, it only remains to establish the mathematical formulation of specific isotropic force and moment. For this purpose, we consider the two generic cases. The first case (A) is having CDPRs with $m = n$, whereas the second one (B) is having CDPRs with $m > n$.

For both cases, we need first to decompose the external wrench, $\boldsymbol{w}$, into two parts: the gravitational $\boldsymbol{w_g} = \left(\boldsymbol{f_g}^{\mathrm{T}} \quad \boldsymbol{m_g}^{\mathrm{T}} \right)^{\mathrm{T}}$ and non-gravitational $\boldsymbol{w_e} = \left(\boldsymbol{f_e}^{\mathrm{T}} \quad \boldsymbol{m_e}^{\mathrm{T}} \right)^{\mathrm{T}}$ external wrenches. In the case of suspended partially constrained CDPRs, the presence of $\boldsymbol{w_g}$ is indispensable for the functioning of the robot, whereas it is not the case for fully constrained ones. Thus, the study is now transformed from $\boldsymbol{w}$-space into the $\boldsymbol{w_e}$-space.

In all what follows, we assume that the demanded simultaneous minimum external force and moment requirements are: $f_{ereq} > 0$ and $m_{ereq} > 0$, respectively. So, how to calculate the specific isotropic force f_{eiso}^{sp} and moment m_{eiso}^{sp} ?

[19] Note that to have $\boldsymbol{\Psi}$ with positive diagonal terms, we should choose the positive sense of actuator torque as to generate tension in the corresponding cable.

A- Specific Isotropic Force and Moment for CDPRs with Square Inverse Jacobian Matrices

In this situation, the calculation is straightforward and almost the same as what we have done for rigid robots, except that we need to account for $\boldsymbol{w_g}$ and the modified torque limits described in (2.66).

Considering the static model in (2.62) and replacing $\boldsymbol{w}$ by $\boldsymbol{w_g} + \boldsymbol{w_e}$, we get:

$$\boldsymbol{\tau} = -\boldsymbol{J}^{\mathrm{T}}\ \boldsymbol{w_e} + \boldsymbol{\tau_g} \tag{2.68},$$

with $\boldsymbol{\tau_g} = -\boldsymbol{J}^{\mathrm{T}}\ \boldsymbol{w_g}$. Then, the inequalities of (2.66) can be reformed as below:

$$\tau_i^{\min} \le -\boldsymbol{j}_{\boldsymbol{pc}_i}^{\mathrm{T}}\ \boldsymbol{f_e} - \boldsymbol{j}_{\boldsymbol{oc}_i}^{\mathrm{T}}\ \boldsymbol{m_e} + \tau_{g_i} \le \tau_i^{\max},\ \ \forall i = 1...m \tag{2.69},$$

where τ_{g_i} is the i-th component of $\boldsymbol{\tau_g}$. Then, to calculate f_{eiso}^{sp} when the static moment can reach m_{ereq} in all directions, we need to rewrite (2.69) isolating the term containing $\boldsymbol{f_e}$ as follows:

$$\tau_i^{\min} + \boldsymbol{j}_{\boldsymbol{oc}_i}^{\mathrm{T}}\ \boldsymbol{m_e} - \tau_{g_i} \le -\boldsymbol{j}_{\boldsymbol{pc}_i}^{\mathrm{T}}\ \boldsymbol{f_e} \le \tau_i^{\max} + \boldsymbol{j}_{\boldsymbol{oc}_i}^{\mathrm{T}}\ \boldsymbol{m_e} - \tau_{g_i},\ \forall i = 1...m \tag{2.70}.$$

Hence, considering each side of the double inequality of (2.70) in the worst case, we get certain upper bounds on $f_e = \|\boldsymbol{f_e}\|$ over the region described by $m_e = \|\boldsymbol{m_e}\| \le m_{ereq}$. As this step is analogous to the already detailed one in the case of rigid manipulators, we directly provide the result, which is:

$$\begin{cases} f_{eiso}^{sp} = \min\limits_{i=1...(m=n)} \left(E_i^+, E_i^-\right), \ \text{with:} \\ E_i^+ = \begin{cases} 0, \ \text{if } e_i^+ < 0 \\ \dfrac{e_i^+}{\left\|\boldsymbol{j}_{\boldsymbol{pc}_i}\right\|}, \ \text{if } \left\|\boldsymbol{j}_{\boldsymbol{pc}_i}\right\| \ne 0 \text{ and } e_i^+ \ge 0 \\ \infty, \text{otherwise} \end{cases}, \ E_i^- = \begin{cases} 0, \ \text{if } e_i^- < 0 \\ \dfrac{e_i^-}{\left\|\boldsymbol{j}_{\boldsymbol{pc}_i}\right\|}, \ \text{if } \left\|\boldsymbol{j}_{\boldsymbol{pc}_i}\right\| \ne 0 \text{ and } e_i^- \ge 0 \\ \infty, \text{otherwise} \end{cases} \\ e_i^+ = \tau_i^{\max} - \left\|\boldsymbol{j}_{\boldsymbol{oc}_i}\right\| m_{ereq} - \tau_{g_i}, \ \ e_i^- = -\tau_i^{\min} - \left\|\boldsymbol{j}_{\boldsymbol{oc}_i}\right\| m_{ereq} + \tau_{g_i} \\ \forall i = 1...(m = n) \end{cases} \tag{2.71}.$$

Similarly, we get the value of m_{eiso}^{sp} to be:

$$\begin{cases} m_{eiso}^{sp} = \min\limits_{i=1\ldots(m=n)} \left(H_i^+, H_i^-\right), \text{ with:} \\ H_i^+ = \begin{cases} 0, \text{ if } h_i^+ < 0 \\ \dfrac{h_i^+}{\left\| \boldsymbol{j}_{\boldsymbol{oc}_i} \right\|}, \text{ if } \left\| \boldsymbol{j}_{\boldsymbol{oc}_i} \right\| \neq 0 \text{ and } h_i^+ \geq 0 \\ \infty, \text{ otherwise} \end{cases}, H_i^- = \begin{cases} 0, \text{ if } h_i^- < 0 \\ \dfrac{h_i^-}{\left\| \boldsymbol{j}_{\boldsymbol{oc}_i} \right\|}, \text{ if } \left\| \boldsymbol{j}_{\boldsymbol{oc}_i} \right\| \neq 0 \text{ and } h_i^- \geq 0 \\ \infty, \text{ otherwise} \end{cases} \\ h_i^+ = \tau_i^{\max} - \left\| \boldsymbol{j}_{\boldsymbol{pc}_i} \right\| f_{ereq} - \tau_{g_i}, \; h_i^- = -\tau_i^{\min} - \left\| \boldsymbol{j}_{\boldsymbol{pc}_i} \right\| f_{ereq} + \tau_{g_i} \\ \forall i = 1\ldots(m=n) \end{cases} \quad (2.72).$$

Note that in (2.71) and (2.72), the terms $\boldsymbol{j}_{\boldsymbol{pc}_i}$ and $\boldsymbol{j}_{\boldsymbol{oc}_i}$ hold the same significance as before[20].

As it can be noticed, only slight dissimilarities exist in comparison with the formulae of (2.42) and (2.43). Now, it is time to deal with the more generic case, which is having $m > n$.

B- Specific Isotropic Force and Moment for CDPRs with Non-Square Inverse Jacobian Matrices

For this case, we need to consider (2.59) after substituting $\boldsymbol{w} = \boldsymbol{w}_{\boldsymbol{g}} + \boldsymbol{w}_{\boldsymbol{e}}$ to have:

$$\boldsymbol{w} = \boldsymbol{w}_{\boldsymbol{e}} + \boldsymbol{w}_{\boldsymbol{g}} = -\boldsymbol{J}_{\boldsymbol{m}}^{\mathrm{T}} \, \boldsymbol{\tau} \quad (2.73).$$

Then, to be able to calculate f_{eiso}^{sp} and m_{eiso}^{sp}, it is compulsory to get the operational wrench zonotope boundaries based on (2.66) and (2.73). For this purpose, we implement the quite efficient and quick method suggested by (BOUCHARD, et al., 2008). This procedure is described in **Appendix C**. It yields the following system of inequalities describing the operational wrench zonotope:

$$\boldsymbol{\eta}_k^{\mathrm{T}} \, \boldsymbol{w} \leq \boldsymbol{\eta}_k^{\mathrm{T}} \, \boldsymbol{w}_{0k}, \; \forall k = 1\ldots 2\, n_p \quad (2.74),$$

with $\boldsymbol{\eta}_k$ being the unit outward normal of the k-th hyperplane, $\boldsymbol{w}_{0k}$ a point on this plane, and $2\, n_p$ the total number of boundary planes.

The system of inequalities (2.74) can be rewritten under the following form:

$$\boldsymbol{\eta}_{\boldsymbol{p}_k}^{\mathrm{T}} \; \boldsymbol{f}_{\boldsymbol{e}} + \boldsymbol{\eta}_{\boldsymbol{o}_k}^{\mathrm{T}} \, \boldsymbol{m}_{\boldsymbol{e}} + \boldsymbol{\eta}_k^{\mathrm{T}} \, \boldsymbol{w}_{\boldsymbol{g}} \leq \boldsymbol{\eta}_k^{\mathrm{T}} \, \boldsymbol{w}_{0k}, \; \forall k = 1\ldots.2\, n_p \quad (2.75),$$

with $\boldsymbol{\eta}_k$ being expressed as $\boldsymbol{\eta}_k = \left(\boldsymbol{\eta}_{\boldsymbol{p}_k}^{\mathrm{T}} \quad \boldsymbol{\eta}_{\boldsymbol{o}_k}^{\mathrm{T}}\right)^{\mathrm{T}}$ for $k = 1\ldots 2\, n_p$. Based on (2.75), the terms f_{eiso}^{sp} and m_{eiso}^{sp} are derived in a similar fashion as before to get the following formulae:

[20] That is the i-th column vectors of $\boldsymbol{J}_{\boldsymbol{p}}$ (translational/positional part of $\boldsymbol{J}$) and $\boldsymbol{J}_{\boldsymbol{o}}$ (rotational/ orientation part of $\boldsymbol{J}$), respectively.

$$\begin{cases} f_{eiso}^{sp} = \min\limits_{i=1...2\,n_p} \left(\Phi_i\right), \text{ with:} \\ \Phi_i = \begin{cases} 0, \text{ if } \varphi_i < 0 \\ \dfrac{\varphi_i}{\left\|\boldsymbol{\eta}_{\boldsymbol{p}_i}\right\|}, \text{ if } \left\|\boldsymbol{\eta}_{\boldsymbol{p}_i}\right\| \neq 0 \text{ and } \varphi_i \geq 0, \forall i = 1...2\,n_p \\ \infty, \text{otherwise} \end{cases} \\ \varphi_i = \boldsymbol{\eta}_i^{\mathrm{T}}\, \boldsymbol{w}_{0i} - \left\|\boldsymbol{\eta}_{\boldsymbol{o}_i}\right\| m_{ereq} - \boldsymbol{\eta}_i^{\mathrm{T}}\, \boldsymbol{w}_{\boldsymbol{g}}, \ \forall i = 1...2\,n_p \end{cases} \tag{2.76}$$

and

$$\begin{cases} m_{eiso}^{sp} = \min\limits_{i=1...2\,n_p} \left(\Psi_i\right), \text{ with:} \\ \Psi_i = \begin{cases} 0, \text{ if } \psi_i < 0 \\ \dfrac{\psi_i}{\left\|\boldsymbol{\eta}_{\boldsymbol{o}_i}\right\|}, \text{ if } \left\|\boldsymbol{\eta}_{\boldsymbol{o}_i}\right\| \neq 0 \text{ and } \psi_i \geq 0, \forall i = 1...2\,n_p \\ \infty, \text{otherwise} \end{cases} \\ \psi_i = \boldsymbol{\eta}_i^{\mathrm{T}}\, \boldsymbol{w}_{0i} - \left\|\boldsymbol{\eta}_{\boldsymbol{p}_i}\right\| f_{ereq} - \boldsymbol{\eta}_i^{\mathrm{T}}\, \boldsymbol{w}_{\boldsymbol{g}}, \ \forall i = 1...2\,n_p \end{cases} \tag{2.77}.$$

With this, we terminate the mathematical formulation of the kinetostatic performance measures in the case of CDPRs. We emphasize that these measures admit the same properties discussed in **§2.2.3.C**. As a summary, this extension of specific isotropic values, though have necessitated some additional steps, still it is rather simple and computationally efficient. We also highlight that although we have treated case (A) separately, still it can be approached as in case (B) without any problem. This means that one can use the approach in (B) to evaluate all CDPRs having $m \geq n$, with relatively no noticeable computational impact. In the following section, we provide a case study on a fully constrained CDPR to further clarify the methodology.

C- Case Study: A Fully Constrained CDPR

In **Fig. 2-9**, we depict the fully constrained CDPR that will be analyzed in this part. It can perform a planar motion (2T-1R) in the horizontal plane and consists of four active cables connected to the mobile platform. Straight-line models of the tensioned cables are assumed, while neglecting the deformation due to tension (so in this case, it is similar to a rigid robot except that the cables must be under tension).

Here, the gravitational wrench is not included in the study, as it has no effect (i.e. $\boldsymbol{w}_{\boldsymbol{g}} = \begin{pmatrix} f_{gx} & f_{gy} & m_{gz} \end{pmatrix}^{\mathrm{T}} = \boldsymbol{0}$). The cables are wound on reels of equal radii of value $r_e = 0.1\,\mathrm{m}$, and the actuated-joint variables are defined as follows:

$$q_i = \frac{L_i^{ref} - \left\|\boldsymbol{A}_i\boldsymbol{B}_i\right\|}{r_e}, \ \forall i = 1...4 \tag{2.78},$$

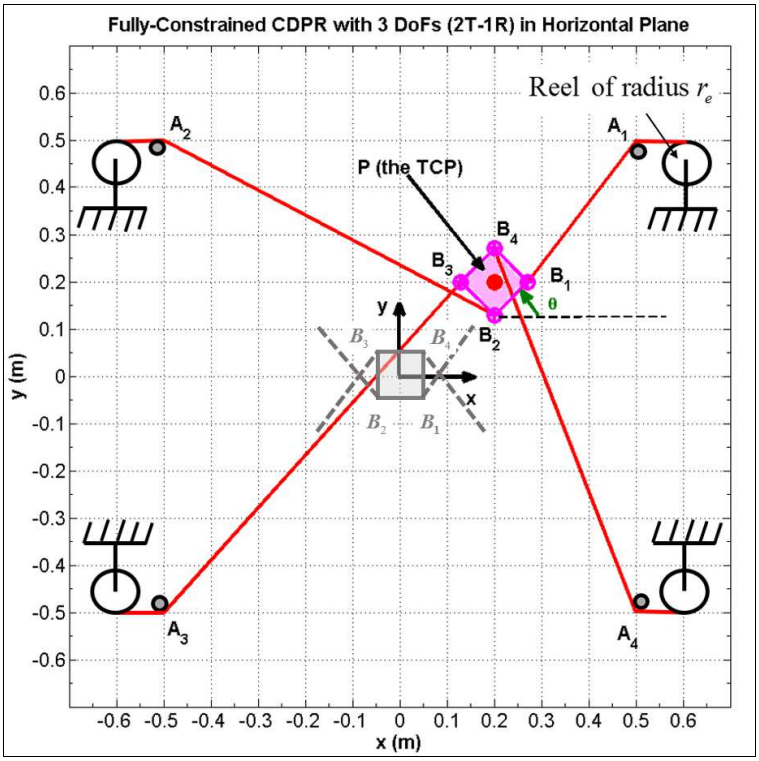

Fig. 2-9: A fully constrained CDPR with horizontal planar motion (2T-1R) (grey configuration corresponds to zero rotation).

with $L_i^{ref} = 0.71\,\mathrm{m}$ for $i = 1...4$ (i.e. positive rotation of the actuator winds the cable), $x_{A1,4} = -x_{A2,3} = 0.5\,\mathrm{m}$, $y_{A1,2} = -y_{A3,4} = 0.5\,\mathrm{m}$, and $B_1B_2B_3B_4$ a square of side $\|\boldsymbol{B_1B_2}\| = 0.05\,\mathrm{m}$ and center $P \equiv TCP$ (see **Fig. 2-9**).

The inverse Jacobian matrix is given by:

$$\boldsymbol{J_m} = \boldsymbol{J_q}^{-1}\,\boldsymbol{J_x} \tag{2.79}$$

with[21]:

$$\boldsymbol{J_q} = -\mathrm{diag}\left(r_e,...,r_e\right),\ \dim\left(\boldsymbol{J_q}\right) = 4\times 4 \tag{2.80}$$

$$\boldsymbol{J_x} = \begin{bmatrix} \boldsymbol{n}_1^{\mathrm{T}} & -\boldsymbol{n}_1^{\mathrm{T}}\left(\boldsymbol{PB}_1\times\boldsymbol{e}_z\right) \\ \vdots & \vdots \\ \boldsymbol{n}_4^{\mathrm{T}} & -\boldsymbol{n}_4^{\mathrm{T}}\left(\boldsymbol{PB}_4\times\boldsymbol{e}_z\right) \end{bmatrix},\ \dim\left(\boldsymbol{J_x}\right) = 4\times 3 \tag{2.81}$$

and $\boldsymbol{n}_i$ the unit vector along $\boldsymbol{A_iB_i}$ for $i = 1...4$.

[21] To derive $\boldsymbol{J_q}$, $\boldsymbol{J_x}$, and $\boldsymbol{J_m}$, we assume that when $\dot{q}_i > 0$, the cable is being wound on the pulley and thus, the velocity of point A_i is in the opposite sense to $\boldsymbol{n}_i$ for $i = 1...4$. This means $\boldsymbol{n}_i^{\mathrm{T}}\,\boldsymbol{v}_{A_i} = -r_e\,\dot{q}_i = \boldsymbol{n}_i^{\mathrm{T}}\,\boldsymbol{v}_{B_i} = \boldsymbol{n}_i^{\mathrm{T}}\left(\boldsymbol{v} - \left(\boldsymbol{PB}_i\times\boldsymbol{e}_z\right)\dot{\theta}_z\right)$ for $i = 1...4$ and as a result, relations (2.80) and (2.81) follow.

Table 2-3: The speed and static load requirements for the CDPR in Fig. 2-9*

Symbol	Significance	Value
$\dot{q}^{\max}$	Maximum Actuator's Speed	$550\ \text{rpm} = 57\ \text{rad/s}$
$\tau^{\max}$	Maximum Actuator's Torque	$127\ \text{N m}$
$\tau^{\min}$	Positive Minimum Allowed Torque	$0.1\,\tau^{\max}$
v_{req}	Required Linear Speed	$0.65\,\dot{q}^{\max}\ r_e$
ω_{req}	Required Angular Speed	$0.45\,\dot{q}^{\max}$
f_{ereq}	Required Static Force Capacity	$0.5\,\tau^{\max}/r_e$
m_{ereq}	Required Static Moment Capacity	$0.5\,\tau^{\max}$

***All actuators are identical. The positive sense of the actuator torque is that of the positive sense of rotation that leads to shortening of the cable.**

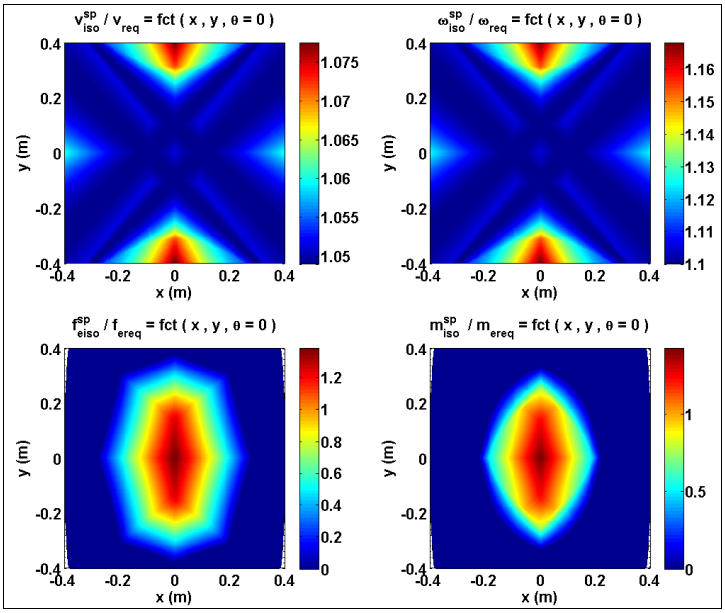

Fig. 2-10: Ratios of specific isotropic values to corresponding requirements for the CDPR in Fig. 2-9.

For this study, we have considered the requirements regarding speeds and static force and moment as given in **Table 2-3**. The plots depicting the specific isotropic values are shown in **Fig. 2-10**, as ratios relative to their corresponding requirements for the ease of comprehension. Notice that the study has been done as a function of x and y, while maintaining $\theta = 0°$. Moreover, the satisfactory regions regarding kinetostatic requirements are shown in **Fig. 2-11**.

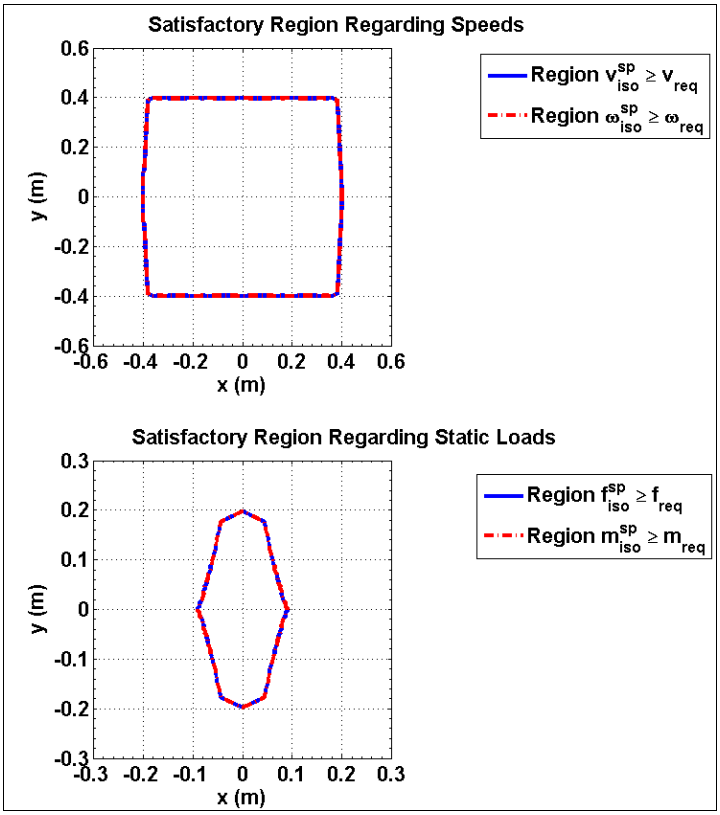

Fig. 2-11: Satisfactory regions in terms of kinetostatic performances based on specific isotropic values for the CDPR in Fig. 2-9.

It is worth emphasizing that the variation of performances of the CDPR along x and y directions, for $\theta = 0°$, are not the same (see **Fig. 2-10** and **Fig. 2-11**). This is due to the asymmetry in the cable connections at the platform level (see the grey configuration in **Fig. 2-9**). Also, it can be noticed clearly from **Fig. 2-11** that the region in which the CDPR fulfills both kinetostatic requirements in terms of twist and external wrench coincides with the wrench satisfactory one (i.e. the region in the second graph of **Fig. 2-11**).

With this case study, we end the kinetostatic performance assessment of CDPRs. This evaluation is sufficient as long as the intended application falls within the quasi-static field. Aside from that, it is not enough and a dynamic analysis is necessary. This is the objective of the upcoming section.

2.3.4- Dynamic Performance Analysis of CDPRs: An Extension of the Approach Applied on Rigid Manipulators

In this section, we provide the reformulation of the dynamic measures introduced in **§2.2.4** in order to deal with CDPRs. For this purpose, the DM should be written under the following compact form[22] (notice that friction is neglected here as in **§2.2.4**):

[22] This is applicable to all CDPRs with $m \geq n$.

$$\begin{cases} \boldsymbol{K}\,\boldsymbol{\xi}+\boldsymbol{h}^{v}+\boldsymbol{h}^{v\omega}+\boldsymbol{h}^{\omega}-\boldsymbol{w}_{g}=\boldsymbol{\Phi}\,\boldsymbol{\gamma}, \text{ with:} \\ \boldsymbol{K}=\begin{bmatrix} \boldsymbol{M}' & -\boldsymbol{1}_{n\times n} \\ \boldsymbol{I}_{a}\,\boldsymbol{J}_{m} & \boldsymbol{0}_{m\times n} \end{bmatrix},\ \boldsymbol{\xi}=\begin{pmatrix} \boldsymbol{\rho} \\ \boldsymbol{w}_{e} \end{pmatrix},\ \boldsymbol{w}_{g}=\begin{pmatrix} \boldsymbol{w}_{geq} \\ \boldsymbol{w}_{ga} \end{pmatrix},\ \boldsymbol{\Phi}=\begin{bmatrix} \boldsymbol{J}_{m}^{\mathrm{T}} & \boldsymbol{0}_{n\times m} \\ \boldsymbol{1}_{m\times m} & -\boldsymbol{\Psi} \end{bmatrix},\ \boldsymbol{\gamma}=\begin{pmatrix} \boldsymbol{\tau} \\ \boldsymbol{f}_{c} \end{pmatrix} \\ \boldsymbol{h}=\boldsymbol{h}^{v}+\boldsymbol{h}^{v\omega}+\boldsymbol{h}^{\omega}=\begin{bmatrix} \boldsymbol{C}' \\ \boldsymbol{I}_{a}\,\dot{\boldsymbol{J}}_{m} \end{bmatrix}\boldsymbol{t}=\begin{pmatrix} \boldsymbol{t}^{\mathrm{T}}\,\boldsymbol{H}_{1}\,\boldsymbol{t} \\ \vdots \\ \boldsymbol{t}^{\mathrm{T}}\,\boldsymbol{H}_{n+m}\,\boldsymbol{t} \end{pmatrix}, \\ \boldsymbol{H}_{i}=\boldsymbol{H}_{i}\left(\boldsymbol{x}\right)=\begin{bmatrix} \boldsymbol{H}_{i}^{v}\left(\boldsymbol{x}\right) & \boldsymbol{H}_{i}^{vw}\left(\boldsymbol{x}\right) \\ \left(\boldsymbol{H}_{i}^{vw}\left(\boldsymbol{x}\right)\right)^{\mathrm{T}} & \boldsymbol{H}_{i}^{\omega}\left(\boldsymbol{x}\right) \end{bmatrix}\ \forall i=1...\left(n+m\right) \\ \boldsymbol{h}^{v}=\boldsymbol{h}^{v}\left(\boldsymbol{x},\boldsymbol{v}\right)=\left(\boldsymbol{v}^{\mathrm{T}}\,\boldsymbol{H}_{1}^{v}\,\boldsymbol{v}\quad\cdots\quad\boldsymbol{v}^{\mathrm{T}}\,\boldsymbol{H}_{n+m}^{v}\,\boldsymbol{v}\right)^{\mathrm{T}} \\ \boldsymbol{h}^{\omega}=\boldsymbol{h}^{\omega}\left(\boldsymbol{x},\boldsymbol{\omega}\right)=\left(\boldsymbol{\omega}^{\mathrm{T}}\,\boldsymbol{H}_{1}^{\omega}\,\boldsymbol{\omega}\quad\cdots\quad\boldsymbol{\omega}^{\mathrm{T}}\,\boldsymbol{H}_{n+m}^{\omega}\,\boldsymbol{\omega}\right)^{\mathrm{T}} \\ \boldsymbol{h}^{v\omega}=\boldsymbol{h}^{v\omega}\left(\boldsymbol{x},\boldsymbol{t}\right)=\left(2\,\boldsymbol{v}^{\mathrm{T}}\,\boldsymbol{H}_{1}^{v\omega}\,\boldsymbol{\omega}\quad\cdots\quad2\,\boldsymbol{v}^{\mathrm{T}}\boldsymbol{H}_{n+m}^{v\omega}\,\boldsymbol{\omega}\right)^{\mathrm{T}} \end{cases} \tag{2.82}.$$

In (2.82), $\boldsymbol{M}'=\boldsymbol{M}'\left(\boldsymbol{x}\right)$, $\boldsymbol{C}'=\boldsymbol{C}'\left(\boldsymbol{x},\boldsymbol{t}\right)$, $\boldsymbol{w}_{geq}=\boldsymbol{w}_{geq}\left(\boldsymbol{x}\right)$, and $\boldsymbol{w}_{e}=\left(\boldsymbol{f}_{e}^{\mathrm{T}}\quad\boldsymbol{m}_{e}^{\mathrm{T}}\right)^{\mathrm{T}}$ correspond to the generalized inertia matrix, generalized Coriolis and centrifugal effects matrix, the total gravitational wrench as seen from the platform, and the external non-gravitational wrench acting on the platform, respectively. On the other hand, $\boldsymbol{I}_{a}=\boldsymbol{I}_{a}\left(\boldsymbol{x}\right)$ and $\boldsymbol{w}_{ga}=\boldsymbol{w}_{ga}\left(\boldsymbol{x}\right)$ represent the $m\times m$ diagonal inertia matrix of the actuators and the corresponding gravitational wrenches acting on them due to their proper weight. The dimension of $\boldsymbol{w}_{ga}$ is $m\times1$. Regarding $\boldsymbol{\Psi}=\boldsymbol{\Psi}\left(\boldsymbol{x}\right)$, it is the $m\times m$ diagonal matrix that relates $\boldsymbol{\tau}$, $\ddot{\boldsymbol{q}}$, and $\boldsymbol{f}_{c}$. As for the other symbols, they hold the same meanings as defined earlier[23]. For more details on the establishment of (2.82), refer to **Appendix D.1**. It is worth emphasizing that (2.82) is similar to (2.50) except for the term $\boldsymbol{\Phi}\,\boldsymbol{\gamma}$, where $\boldsymbol{\Phi}$ is an $\left(n+m\right)\times2\,m$ matrix. This difference necessitates a slight modification that resembles what have been done in the case of kinetostatics (**§2.3.3.B**).

Regarding the imposed constraints, we have:

$$\left|\dot{q}_{i}\right|\leq\dot{q}_{i}^{\max},\ \forall i=1...m \tag{2.83},$$

and

[23] Meaning: $\boldsymbol{\rho}=\left(\boldsymbol{a}^{\mathrm{T}}\quad\boldsymbol{\alpha}^{\mathrm{T}}\right)^{\mathrm{T}}=\left(\dot{\boldsymbol{v}}^{\mathrm{T}}\quad\dot{\boldsymbol{\omega}}^{\mathrm{T}}\right)^{\mathrm{T}}$ (operational linear and angular accelerations), and $\boldsymbol{t}=\left(\boldsymbol{v}^{\mathrm{T}}\quad\boldsymbol{\omega}^{\mathrm{T}}\right)^{\mathrm{T}}$ (operational twist).

$$\begin{cases} \gamma_i^{\min} \le \gamma_i \le \gamma_i^{\max}, \ \forall i = 1...2\,m \\ \text{with:} \\ \gamma_i^{\min} = \begin{cases} -\tau_i^{\max}, \ \text{if } i \le m \\ f_{c_{i-m}}^{\min}, \ \text{otherwise} \end{cases}, \ \gamma_i^{\max} = \begin{cases} \tau_i^{\max}, \ \text{if } i \le m \\ f_{c_{i-m}}^{\max}, \ \text{otherwise} \end{cases} \\ \forall i = 1...2\,m \end{cases} \quad (2.84).$$

To be able to acquire the specific isotropic values, or more precisely their lower bounds in the most generic case, we need to determine the zonotope described by:

$$\boldsymbol{f_d} = \boldsymbol{\Phi}\,\boldsymbol{\gamma} \quad (2.85),$$

and for the limits provided in (2.84). This can be easily done following the same method suggested by (BOUCHARD, et al., 2008) and which is summarized in **Appendix C**. As a result, we get the $\boldsymbol{f_d}$-zonotope expressed as:

$$\boldsymbol{\mu}_i^{\mathrm{T}}\ \boldsymbol{f_d} \le \boldsymbol{\mu}_i^{\mathrm{T}}\ \boldsymbol{f_{d0i}}, \ \forall i = 1...n_d \quad (2.86),$$

with $\boldsymbol{\mu}_i$ and $\boldsymbol{f_{d0i}}$ being the unit outward normal and a point belonging to the i-th hyperplane. As for n_d, it is the total number of hyperplanes that constitute the aforementioned zonotope.

Substituting $\boldsymbol{f_d} = \boldsymbol{K}\,\boldsymbol{\xi} + \boldsymbol{h}^{v} + \boldsymbol{h}^{v\omega} + \boldsymbol{h}^{\omega} - \boldsymbol{w_g}$ in (2.86), we get:

$$\begin{cases} \forall i = 1...n_d : \\ \left(\boldsymbol{\beta}_i^{a}\right)^{\mathrm{T}}\,\boldsymbol{a} + \left(\boldsymbol{\beta}_i^{\alpha}\right)^{\mathrm{T}}\,\boldsymbol{\alpha} + \left(\boldsymbol{\beta}_i^{f_e}\right)^{\mathrm{T}}\ \boldsymbol{f_e} + \left(\boldsymbol{\beta}_i^{m_e}\right)^{\mathrm{T}}\,\boldsymbol{m_e} + \boldsymbol{v}^{\mathrm{T}}\,\boldsymbol{\Pi}_i^{v}\,\boldsymbol{v} \\ \qquad\qquad + \boldsymbol{\omega}^{\mathrm{T}}\,\boldsymbol{\Pi}_i^{\omega}\,\boldsymbol{\omega} + 2\,\boldsymbol{v}^{\mathrm{T}}\,\boldsymbol{\Pi}_i^{v\omega}\,\boldsymbol{\omega} \le c_i - \beta_i^{g} \end{cases} \quad (2.87),$$

with:

$$\begin{cases} \boldsymbol{\beta}_i = \left(\boldsymbol{\mu_i}^{\mathrm{T}}\ \boldsymbol{K}\right)^{\mathrm{T}}, \ \beta_i^{v} = \boldsymbol{\mu_i}^{\mathrm{T}}\ \boldsymbol{h}^{v} = \boldsymbol{v}^{\mathrm{T}}\ \boldsymbol{\Pi}_i^{v}\ \boldsymbol{v}, \ \beta_i^{\omega} = \boldsymbol{\mu_i}^{\mathrm{T}}\ \boldsymbol{h}^{\omega} = \boldsymbol{\omega}^{\mathrm{T}}\ \boldsymbol{\Pi}_i^{\omega}\ \boldsymbol{\omega} \\ \beta_i^{v\omega} = \boldsymbol{\mu_i}^{\mathrm{T}}\ \boldsymbol{h}^{v\omega} = 2\,\boldsymbol{v}^{\mathrm{T}}\ \boldsymbol{\Pi}_i^{v\omega}\ \boldsymbol{\omega}, \ \beta_i^{g} = -\boldsymbol{\mu_i}^{\mathrm{T}}\ \boldsymbol{w_g}, \ c_i = \boldsymbol{\mu_i}^{\mathrm{T}}\ \boldsymbol{f_{d0i}} \\ \boldsymbol{\Pi}_i^{v} = \sum_{j=1...(n+m)} \mu_{ij}\ \boldsymbol{H}_j^{v}, \ \boldsymbol{\Pi}_i^{\omega} = \sum_{j=1...(n+m)} \mu_{ij}\ \boldsymbol{H}_j^{\omega}, \ \boldsymbol{\Pi}_i^{v\omega} = \sum_{j=1...(n+m)} \mu_{ij}\ \boldsymbol{H}_j^{v\omega} \\ \mu_{ij} : \text{j-th component of } \boldsymbol{\mu}_i \end{cases}, \ \forall i = 1...n_d \quad (2.88).$$

Based on the relations (2.59), (2.83), and (2.87), it is possible to assess the dynamic capabilities. The derivation is similar to what has been described in **Appendix B.1**.

In brief, suppose that the dynamic simultaneous requirements are given by ${}^{d}a_{req}$, ${}^{d}\alpha_{req}$, ${}^{d}v_{req}$, ${}^{d}\omega_{req}$, ${}^{d}f_{ereq}$, and ${}^{d}m_{ereq}$, with all symbols baring the same significance as before. Then, we get the following compact formulation of the specific isotropic values, or their lower bounds in the most generic case (note that $val = a, \alpha, f_e, m_e$ and $vel = v, \omega$):

$$\begin{cases} {}^{d}val_{iso}^{sp} \geq \underline{\underline{{}^{d}val_{iso}^{sp}}} = \min\limits_{i=1...n_d}\left(K_C, \underline{\underline{{}^{val}E_i}}\right), \text{ with } (\forall i = 1...n_d): \\ K_C = \begin{cases} 0, \text{ if } {}^{k}v_{iso}^{sp} < {}^{d}v_{req} \ (\text{or } {}^{k}\omega_{iso}^{sp} < {}^{d}\omega_{req}) \\ \infty, \text{ otherwise} \end{cases}, \ \underline{\underline{{}^{val}E_i}} = \begin{cases} 0, \text{ if } \underline{\underline{{}^{val}e_i}} < 0 \\ \dfrac{\underline{\underline{{}^{val}e_i}}}{\left\|\boldsymbol{\beta}_i^{\boldsymbol{val}}\right\|}, \text{ if } \underline{\underline{{}^{val}e_i}} \geq 0 \text{ and } \left\|\boldsymbol{\beta}_i^{\boldsymbol{val}}\right\| \neq 0 \\ \infty, \text{ otherwise} \end{cases} \\ \underline{\underline{{}^{val}e_i}} = c_i - \beta_i^g - sum_{val} - \zeta_{\max_i}^{v}\left({}^{d}v_{req}\right)^2 - \zeta_{\max_i}^{\omega}\left({}^{d}\omega_{req}\right)^2 - 2\,\sigma_{\max_i}^{v\omega}\,{}^{d}v_{req}\,{}^{d}\omega_{req} \end{cases} \quad (2.89),$$

and

$$\begin{cases} {}^{d}vel_{iso}^{sp} \geq \underline{\underline{{}^{d}vel_{iso}^{sp}}} = \min\limits_{i=1...n_d}\left({}^{k}vel_{iso}^{sp}, \underline{\underline{{}^{vel}E_i}}\right), \text{ with } (\forall i = 1...n_d): \\ \underline{\underline{{}^{vel}E_i}} = \begin{cases} vel_{oi1}, \text{ if } \underline{\underline{{}^{vel}e_i}} \geq 0, \ val_1 \neq 0, \text{ and } \zeta_{\max_i}^{vel} = 0 \\ vel_{oi2}, \text{ if } \underline{\underline{{}^{vel}e_i}} \geq 0, \ \zeta_{\max_i}^{vel} \neq 0, \text{ and } vel_{oi2} \geq 0 \\ \infty, \text{ if } \underline{\underline{{}^{vel}e_i}} \geq 0, \ val_1 = 0, \text{ and } \zeta_{\max_i}^{vel} = 0 \\ 0, \text{ otherwise} \end{cases} \\ vel_{oi1} = \dfrac{\underline{\underline{{}^{vel}e_i}}}{2\,val_1}, \ vel_{oi2} = \dfrac{-val_1 + \sqrt{\left(val_1\right)^2 + \zeta_{\max_i}^{vel}\ \underline{\underline{{}^{vel}e_i}}}}{\zeta_{\max_i}^{vel}} \\ \underline{\underline{{}^{vel}e_i}} = c_i - \beta_i^g - \left\|\boldsymbol{\beta}_i^{\boldsymbol{a}}\right\|{}^{d}a_{req} - \left\|\boldsymbol{\beta}_i^{\boldsymbol{\alpha}}\right\|{}^{d}\alpha_{req} - \left\|\boldsymbol{\beta}_i^{\boldsymbol{f_e}}\right\|{}^{d}f_{ereq} - \left\|\boldsymbol{\beta}_i^{\boldsymbol{m_e}}\right\|{}^{d}m_{ereq} - val_2 \end{cases} \quad (2.90),$$

with:

$$\begin{cases} \zeta_{\max_i}^{v} = \max\left(\text{eigs}\left(\boldsymbol{\Pi}_i^{v}\right), 0\right) \\ \zeta_{\max_i}^{\omega} = \max\left(\text{eigs}\left(\boldsymbol{\Pi}_i^{\omega}\right), 0\right), \ \forall i = 1...n_d \\ \sigma_{\max_i}^{v\omega} = \max\left(\text{sing}\left(\boldsymbol{\Pi}_i^{v\omega}\right)\right) \end{cases} \quad (2.91).$$

As for ${}^{k}v_{iso}^{sp}$ and ${}^{k}\omega_{iso}^{sp}$, they have the same expressions as given in (2.55) and (2.56), respectively. Regarding the significance of the terms val, sum_{val}, vel, val_1, and val_2, refer to **Table 2-4**.

Hence, the dynamic measures have been established for CDPRs. Despite the fact that a new reformulation has been required to deal with their particularities, these dynamic measures are still possible to compute or estimate analytically. Finally, to demonstrate the methodology, a case study on a fully constrained CDPR is provided in **Appendix D**.

Table 2-4: The significance of the general terms used in relations (2.89) and (2.90).

Definition of the terms appearing in relation (2.89)		
val	sum_{val}	
a	$\left\|\boldsymbol{\beta}_i^{\boldsymbol{a}}\right\| {}^{d}\alpha_{req} + \left\|\boldsymbol{\beta}_i^{\boldsymbol{f_e}}\right\| {}^{d}f_{ereq} + \left\|\boldsymbol{\beta}_i^{\boldsymbol{m_e}}\right\| {}^{d}m_{ereq}$	
α	$\left\|\boldsymbol{\beta}_i^{\boldsymbol{a}}\right\| {}^{d}a_{req} + \left\|\boldsymbol{\beta}_i^{\boldsymbol{f_e}}\right\| {}^{d}f_{ereq} + \left\|\boldsymbol{\beta}_i^{\boldsymbol{m_e}}\right\| {}^{d}m_{ereq}$	
f_e	$\left\|\boldsymbol{\beta}_i^{\boldsymbol{a}}\right\| {}^{d}a_{req} + \left\|\boldsymbol{\beta}_i^{\boldsymbol{\alpha}}\right\| {}^{d}\alpha_{req} + \left\|\boldsymbol{\beta}_i^{\boldsymbol{m_e}}\right\| {}^{d}m_{ereq}$	
m_e	$\left\|\boldsymbol{\beta}_i^{\boldsymbol{a}}\right\| {}^{d}a_{req} + \left\|\boldsymbol{\beta}_i^{\boldsymbol{\alpha}}\right\| {}^{d}\alpha_{req} + \left\|\boldsymbol{\beta}_i^{\boldsymbol{f_e}}\right\| {}^{d}f_{ereq}$	
Definition of the terms in relation (2.90)		
vel	val_1	val_2
v	$\sigma_{\max_i}^{v\omega}\ {}^{d}\omega_{req}$	$\zeta_{\max_i}^{\omega}\left({}^{d}\omega_{req}\right)^2$
ω	$\sigma_{\max_i}^{v\omega}\ {}^{d}v_{req}$	$\zeta_{\max_i}^{v}\left({}^{d}v_{req}\right)^2$

2.4- Few Remarks

In all the kinetostatic and dynamic measures based on the notion of specific isotropic values, we have these latter values always positive. This positiveness is imposed by definition. More precisely, a specific isotropic value is the maximum attainable norm of a vectorial quantity in all directions, while allowing other vectorial quantities to reach their minimum required norms irrespective of their directions. Nevertheless, for the purpose of optimization, we can ignore the test on positiveness. For instance, v_{iso}^{sp} in kinetostatics can be computed as follows:

$$\begin{cases} v_{iso}^{sp} = \min\limits_{i=1\ldots m}\left(A_i\right), \text{ with:} \\ A_i = \begin{cases} \dfrac{a_i}{\left\|\boldsymbol{j}_{\boldsymbol{mpr}_i}\right\|}, \text{ if } \left\|\boldsymbol{j}_{\boldsymbol{mpr}_i}\right\| \neq 0 \\ -\infty \text{ , if } \left\|\boldsymbol{j}_{\boldsymbol{mpr}_i}\right\| = 0 \text{ and } a_i < 0 \\ +\infty, \text{ otherwise} \end{cases}, \ \forall i = 1\ldots m \\ a_i = \dot{q}_i^{\max} - \left\|\boldsymbol{j}_{\boldsymbol{mor}_i}\right\| \omega_{req}, \ \forall i = 1\ldots m \end{cases} \quad (2.92),$$

regardless of having a_i positive or negative. With the form given in (2.92), the optimization problem defined by:

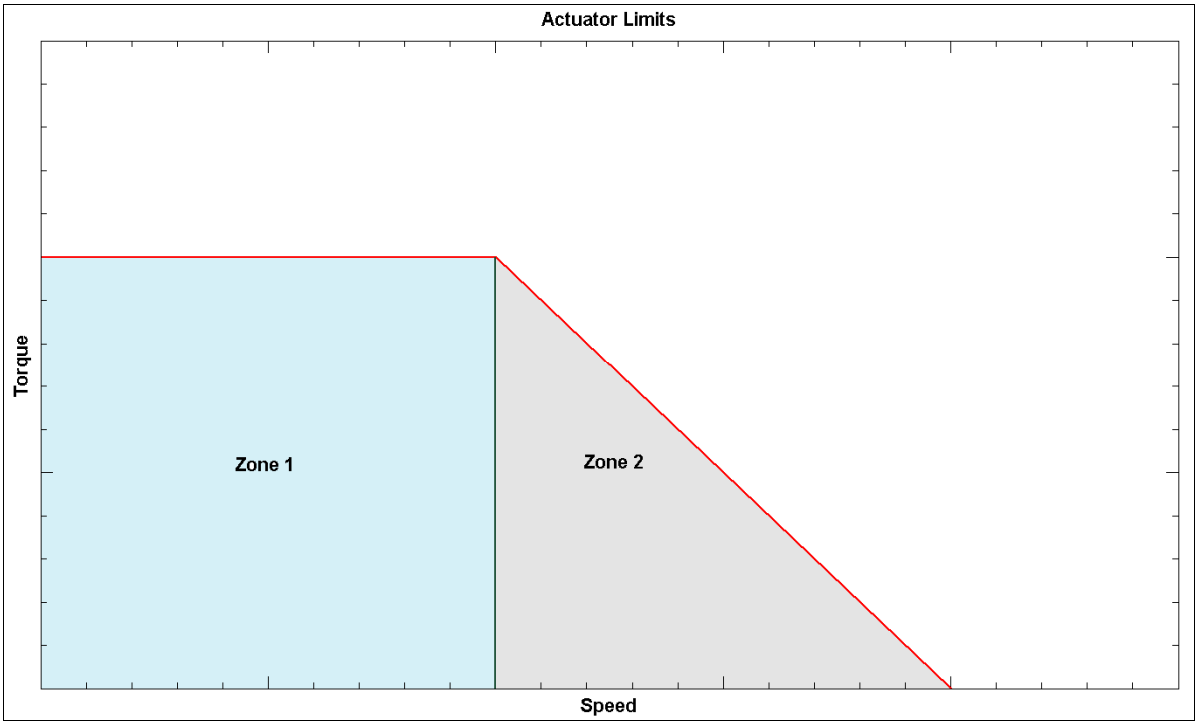

Fig. 2-12: Actuator limits illustration.

$$\begin{cases} \max\limits_{\xi_g}\left(\min\limits_{x\in DWS}\left(v_{iso}^{sp}\left(\boldsymbol{x},\boldsymbol{\xi_g}\right)\right)\right), \text{ with:} \\ v_{iso}^{sp}\left(\boldsymbol{x},\boldsymbol{\xi_g}\right): \ v_{iso}^{sp} \text{ at pose } \boldsymbol{x} \text{ and geometric parameters } \boldsymbol{\xi_g} \end{cases} \tag{2.93}$$

is easier to do in comparison with initial definition given in (2.40).

Additionally, in all the presented dynamic evaluations, we have considered the actuators' speeds and torques to be independent. This is implied by using:

$$\begin{cases} \left|\dot{q}_i\right| \le \dot{q}_i^{\max} \\ \left|\tau_i\right| \le \tau_i^{\max} \end{cases}, \ \forall i = 1...m \tag{2.94}.$$

Such region corresponds to "zone 1" in **Fig. 2-12**. However, the more general case is to have the actuator limits bounded by several segments, like the case of considering the union of zones 1 and 2 for instance (see **Fig. 2-12**). This latter case can be generalized as follows (for m actuators):

$$\boldsymbol{\delta}_{ij}^{\mathrm{T}}\begin{pmatrix}\dot{q}_i \\ \tau_i\end{pmatrix} \le \boldsymbol{\delta}_{ij}^{\mathrm{T}}\,\varsigma_{0ij}, \ \forall i = 1...m, \ \forall j = 1...n_{ab_i} \tag{2.95},$$

with $\boldsymbol{\delta}_{ij}$ representing the unit-outward normal of the j-th limiting segment, ς_{0ij} being a point on this segment, and n_{ab_i} corresponding to the number of limiting segments for the i-th actuator.

These general limits in (2.95) can be easily accounted for in the dynamic study. Yet, we do not recommend it, especially if the region where the speed and torque are independent constitutes a large proportion of the global available one.

Another worthy point to mention is concerning the acceleration limits imposed on the actuators. So far, we presumed there are no restrictions in this matter. Nonetheless, it might not always be the case. Actually, if limits exist, they can be directly utilized or after some simplification. In particular, if the limits are constants or pose-dependent, then their incorporation is a straightforward problem. It is done through considering $\ddot{\boldsymbol{q}} = \boldsymbol{J}_{\boldsymbol{m}}\ \boldsymbol{\rho} + \dot{\boldsymbol{J}}_{\boldsymbol{m}}\ \boldsymbol{t}$, and the inequalities $\left|\ddot{q}_i\right| \leq \ddot{q}_i^{\max}$ for $i = 1...m$. Aside from that, it might be more complex and/or time demanding.

2.5- General Guidelines and Recommendations for the Design Optimization of Machine Tools

Thus far, we have presented several performance indices related to precision, kinetostatics, and dynamics. But how to optimize a given design based on one or more of the aforementioned criteria?

In fact, while the approach is straightforward for single criterion optimization, it is more debatable in the case of multi-objective one. In this latter case, several methodologies exist in literature. These can be classified into two main categories (UNAL, et al., 2008): scalarization and Pareto methods.

Scalarization addresses the multi-criteria optimization problem in an indirect manner, through altering it into a single or a series of single objective problems. As instantiation on this, we mention the hierarchical optimization approach (HAYWARD, et al., 1994), the sequential optimization technique ((ALICI & SHIRINZADEH, 2004), (RISOLI, et al., 1999)), the probabilistic weighting strategy (MCGHEE, et al., 1994), the use of composite index (LEE, et al., 2001), etc. Nonetheless, such methods possess the inherent detriment of requiring preferences or weights to be determined apriori; i.e. before the results of the optimization process are actually known. Since assigning proper weights or prioritizing different criteria is a problem-dependent and a non-trivial task, these techniques fall short of providing a general framework to the design process.

Therefore, we do not recommend such approaches. Instead, we suggest the Pareto-based methods. These incorporate all performance criteria within the optimization process and address them simultaneously to find a set of non-dominated solutions in the objective space (UNAL, et al., 2008). Once the hypersurface resolving the design trade-offs is obtained, an appropriate solution can then be selected. Such techniques are transparent, highly efficient, and do not require high expertise. As examples on this approach, we mention the works of ((KREFFT & HESSELBACH, 2005), (COURTEILLE, et al., 2009), (UR-REHMAN, et al., 2010)), and the recent dimensional synthesis we have done on ARROW V1 (SHAYYA, et al., 2014b), which will

be discussed later in **Chapter 3**. Finally, we point out that in the case where the number of objectives is greater than three, there are some tools that can help visualize the solution sets, such as the use of parallel coordinates for instance (INSELBERG & DIMSDALE, 1990). Nevertheless, it is always favored to keep the number of the criteria as low as possible.

2.6- Conclusion

In this chapter, the performance evaluation of general manipulators has been addressed from non-classical perspective. It has been founded on newly suggested precision, kinetostatic, and dynamic measures that overcome two main predicaments: redundancy and heterogeneity.

Among the prominent features of the approach, we recall the following: applicability to different types of robots (whether of rigid or cable-driven nature), embracing physical significance, computational simplicity, and direct relation with the needs of roboticist, engineer, or end-user.

Furthermore, some refinements concerning these measures have been emphasized, and general recommendations on the design optimization have been made.

In the next chapter, we present some synthesized parallel architectures, the dimensional synthesis of two of them, and the manufactured ARROW prototype.

Chapter 3: The Novel Synthesized Architectures and ARROW PKM

In this chapter:

In this chapter, few novel architectures, among the synthesized PMs, are discussed. These include mechanisms with five and four dofs of respective 3T-2R and 3T-1R nature. Their exposition embraces: geometric and kinematic models, singularity analysis, and workspace evaluation. Moreover, the dynamic models of two of them are detailed, and their dimensional syntheses are presented. In particular, only one of the suggested architectures is considered for implementation. The practical execution procedure and its required modifications are detailed, and the eventual ARROW PKM is exposed.

3.1- Introduction

In the quest for rapid and precise PKMs, several essential points must be considered, starting from the architecture itself, passing through the manufacturing procedure, and ending with the control approach. These three points are not completely separable and one can influence the other, especially the first two. This will become clear when we discuss the prototyped PKM.

Concerning the architecture, certain requirements are to be met. These are derived from the targets of the ARROW project that can be summarized as follows: large singularity-free workspace, high tilting capacity, performance homogeneity over the workspace, design simplicity, and rigidity.

As for manufacturing procedure, the execution of each joint, especially the complex ones (e.g. universal and spherical joints), must be carefully thought of. This consideration should assure maintaining high stiffness and minimizing clearances, as they are indispensable for having a precise machine. Furthermore, the quality control of the manufacturing as well as the assembly of the different components is necessary. It not only aids in having a machine with good initial performances, but also permits future enhancements or refinements, via geometric calibration for instance.

Regarding control, it is indisputably of great prominence. In fact, having a good architecture but with poor control will eventually lead to a poor-performance PKM. As a result, control can be the weakest or the strongest point in any machine tool. Nevertheless, this point is beyond the scope of the current thesis.

For our intended PKM, it should be capable of performing any machining task, although the main target applications have been the contactless ones, such as laser cutting and the alike. These latter applications are among the potential candidates that usually demand or benefit from rapidity, in addition to precision. Nevertheless, all these applications do not require more than five dofs of 3T-2R nature. These dofs can be achieved by various means, for instance: one parallel structure (complex or fully parallel), left-hand right-hand paradigm (i.e. branched structure), or series-parallel hybrid design.

In our case, we have focused mainly on implementing left-hand right-hand paradigm, in which a four-dof (3T-1R) PM is equipped with a one-dof (1R) turntable. However, this does not mean we did not consider five-dof (3T-2R) solutions. In fact, we have synthesized some five-dof mechanisms, among which is MachLin5 described in (SHAYYA, et al., 2014a).

In this chapter, we do not intend detailing all the synthesized mechanisms, but rather discussing the most prominent ones for the sake of compactness.

Finally, the current chapter is organized as follows. First, the five-dof (3T-2R) mechanism, namely MachLin5, is presented. Then, the study of two simple four-dof (3T-1R) PKMs, called ARROW V1 and ARROW V2, follows and some of the mutated versions of ARROW V2 are described. In particular, the mutated version ARROW V2 M2 is ultimately implemented after

some detailed analysis and verifications. Eventually, the chapter is concluded by re-emphasizing the substantial aspects.

3.2- MachLin5: A 5-DoF (3T-2R) Parallel Mechanism with Articulated Platform

Having a PKM with all its desired dofs embedded in one parallel structure has its rewards, as compared with the generally referred to hybrid machines, those implementing series-parallel design or left-hand right-hand paradigm (branched structures). In fact, series-parallel architectures (e.g. Tricept in **Fig. 1-25**, Exechon in **Fig. 1-26**, Sprint Z3 in **Fig. 1-27**, Hermes in **Fig. 1-28**, Dumbo in **Fig. 1-29**, etc.) are not a recommendable choice, as they often possess increased moving masses due to having additional actuators on the platform. Thus, not only their dynamic performance is impaired, but also their global precision and stiffness.

On the other hand, branched-structure mechanisms (e.g. P 800 in **Fig. 1-24**, VERNE in **Fig. 1-31**, HITA-STT whose parallel module is shown in **Fig. 1-32**, etc.) are more favored than series parallel designs since they overcome the latter's aforementioned downsides. But depending on the design itself, it might be less flexible. This is due to the possibility of introducing challenges regarding control and motion planning. This is not to mention the calibration-related issues.

Based on the above, we have been motivated to investigate PMs with five dofs (3T-2R) in a first step. Knowing the inconveniences of similar PMs reported in literature (see **Chapter 1**), we attempted to synthesize new ones that overcome the former limitations. The result has been few novel architectures, among which we are going to present the most intriguing one, called MachLin5. A simplified CAD of this PM and a close-up view of its articulated platform are given in **Fig. 3-1** and **Fig. 3-2**, respectively. The graph diagram is provided in **Fig. 3-3**.

3.2.1- Description

The PM consists of five linear actuators along the same direction (x-axis). Thus, the motion along x is independent of the other dofs and only restricted by the available stroke length for the actuators. Regarding the platform, it is an articulated one and consists of two parts, which are coupled by means of translation-to-rotation transformation system.

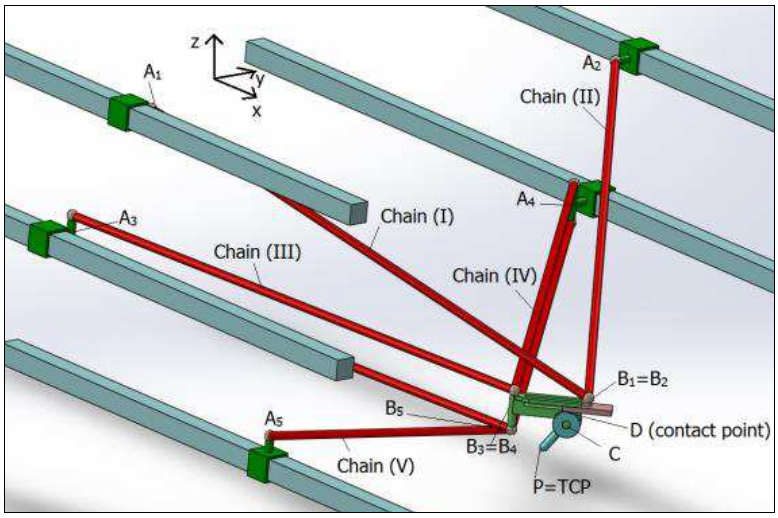

Fig. 3-1: MachLin5: simplified CAD drawing.

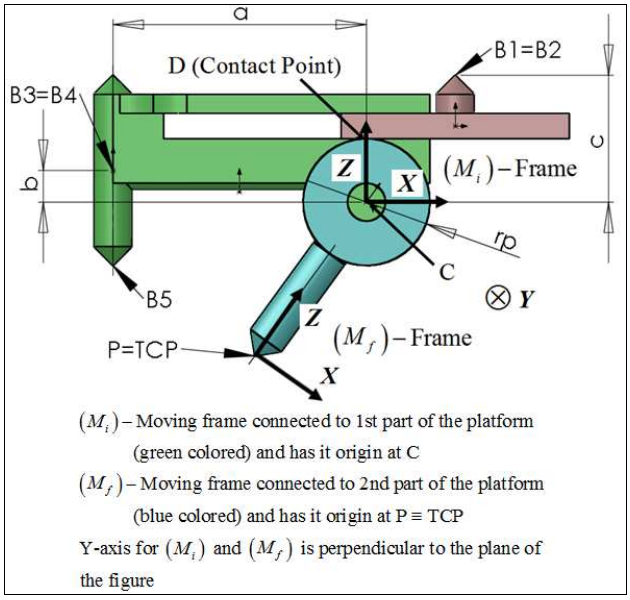

Fig. 3-2: MachLin5: the articulated platform.

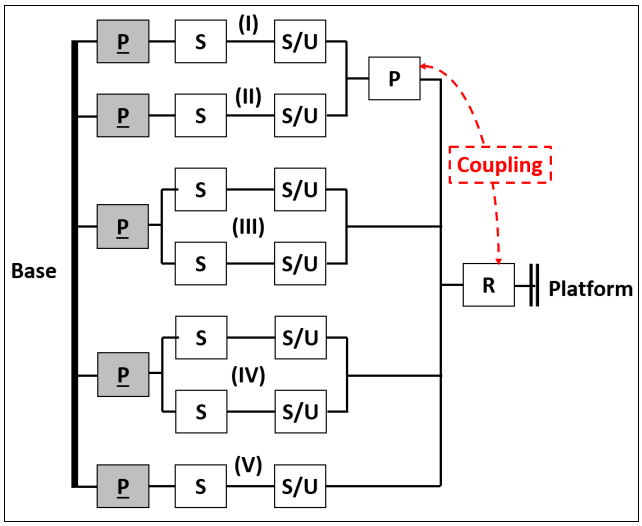

Fig. 3-3: MachLin5: graph diagram.

The functioning of the mechanism is straightforward. Chains (III) through (V) cooperate to position the segment B_4B_5, which remains always vertical thanks to the constraining parallelograms. Then, chains (I) and (II), together, control the two rotational dofs: θ_z about the z-axis of the base frame, and θ_y about the y-axis of the tool frame $\left(M_f\right)$. This is done thanks to the rack-pinion mechanism shown in **Fig. 3-2**, which by fixing the distance from $B_1 \equiv B_2$ to B_4B_5 and rotating it, controls the first rotation θ_z. As for θ_y, it is controlled by moving the rack, which then turns the pinion an angle proportional to the latter's displacement. Hence, the TCP position and the tool orientation are controlled.

It is worth mentioning that we have used a rack-pinion assembly here to simplify the analysis. In general, it can be replaced by any rigid linear-to-rotational motion transformation system. In such a case, the transformation device should not admit any singularities within the required range of rotation for θ_y, which is $\pm 45°$.

Thus, we have a PM characterized by a large workspace and a tilting capacity that can reach $\pm 90°$ for θ_z, and $\pm 45°$ for θ_y. These rotational capacities are usually sufficient to perform five face machining and similar tasks.

This has been a general description of the MachLin5 functioning. In what follows, we emphasize the following essential technical remarks:

1. The S (spherical) joints can be achieved by using three concurrent revolute joints. This helps in overcoming the limited rotational capacity in the case of commercial counterparts.
2. The three S-joints at B_5 can be vertically spaced instead of having them coincident, which is difficult to implement. Thus, we can consider a common S-joint for the lower rods of the parallelograms, and another one for the fifth kinematic chain.

It then remains to give the general geometric designations used in the modeling process. Some of these symbols, particularly a, b, c, r_p, and t_p, are depicted in **Fig. 3-2**. The rest are defined hereafter:

- L_i: the length of the i-th chain for $i = 1...5$, with $L_1 = L_2$ and $L_3 = L_4$;
- $\boldsymbol{A}_i = \begin{pmatrix} x_i & y_i & z_i \end{pmatrix}^{\mathrm{T}} = \begin{pmatrix} q_i & y_i & z_i \end{pmatrix}^{\mathrm{T}}$, $\forall i = 1...5$ with: $-y_1 = y_2 = L_{y1}$, $-y_3 = y_4 = L_{y2}$, $y_5 = 0$, $z_1 = z_2 = L_{z1}$, $z_3 = z_4 = 0$, $z_5 = -L_{z2}$ and where $\boldsymbol{A}_3$ and $\boldsymbol{A}_4$ correspond to the coordinates of points A_3 and A_4 situated on the imaginary mid-axes of the parallelograms (III) and (IV), respectively;
- $\boldsymbol{B}_i = \begin{pmatrix} x_{bi} & y_{bi} & z_{bi} \end{pmatrix}^{\mathrm{T}}$, $\forall i = 1...5$ and where $\boldsymbol{B}_3$ and $\boldsymbol{B}_4$ correspond to the coordinates of the points B_3 and B_4 situated on the imaginary mid-axes of the parallelograms (III) and (IV), respectively;

- $\boldsymbol{P}=\begin{pmatrix} x & y & z \end{pmatrix}^{\mathrm{T}}$, $\boldsymbol{\theta}=\begin{pmatrix} \theta_z & \theta_y \end{pmatrix}^{\mathrm{T}}$, and $\boldsymbol{x}=\begin{pmatrix} \boldsymbol{P}^{\mathrm{T}} & \boldsymbol{\theta}^{\mathrm{T}} \end{pmatrix}^{\mathrm{T}}$: the TCP position, the orientation vector, and the robot pose, respectively;
- $\boldsymbol{e_h}=\begin{pmatrix} \cos(\theta_z) & \sin(\theta_z) & 0 \end{pmatrix}^{\mathrm{T}}$: the unit vector along the x-axis of the frame (M_i);
- $\boldsymbol{e_f}=\begin{pmatrix} -\sin(\theta_z) & \cos(\theta_z) & 0 \end{pmatrix}^{\mathrm{T}}$: the unit vector along the common y-axis of the frames (M_i) and (M_f);
- $\boldsymbol{\Omega}_1=\begin{bmatrix} \boldsymbol{e_z} & \boldsymbol{0}_{3\times1} \end{bmatrix}$ and $\boldsymbol{\Omega}=\begin{bmatrix} \boldsymbol{e_z} & \boldsymbol{e_f} \end{bmatrix}$;
- $\boldsymbol{R_z}=\mathrm{Rot}_{\mathrm{z}}(\theta_z)$, $\boldsymbol{R_y}=\mathrm{Rot}_{\mathrm{y}}(\theta_y)$, and $\boldsymbol{R}=\boldsymbol{R_z}\,\boldsymbol{R_y}$, with $\boldsymbol{R}$ representing the rotation matrix of the frame (M_f) with respect to the base;
- $\boldsymbol{N}=\begin{pmatrix} x_N & y_N & z_N \end{pmatrix}^{\mathrm{T}}$ and $\boldsymbol{N^m}=\begin{pmatrix} x_N^m & y_N^m & z_N^m \end{pmatrix}^{\mathrm{T}}$: the coordinates of some point N in the base frame, and in the frame $m=M_i$, M_f, respectively;
- $\boldsymbol{v}=\dot{\boldsymbol{P}}$: the linear velocity of $P\equiv TCP$;
- $\boldsymbol{\omega}_1=\boldsymbol{\Omega}_1\,\dot{\boldsymbol{\theta}}$ and $\boldsymbol{\omega}=\boldsymbol{\Omega}\,\dot{\boldsymbol{\theta}}$: the angular velocities of the first and second parts of the platform (i.e. frames (M_i) and (M_f)) with respect to the base frame, respectively.

Finally, to simplify the analysis, we assume that the points $B_3\equiv B_4$ and B_5 are confounded (i.e. $B_3\equiv B_4\equiv B_5$). As for the real vertical offset $\|\boldsymbol{B}_4\boldsymbol{B}_5\|_{real}$, it can be accounted for by the proper adjustment of the z-component of point A_5.

Having clarified the principle of functioning of the current PM and the different symbols that will be used in modeling, the next sections are dedicated for the establishment of the diverse geometric and kinematic models. These are then followed by singularity analysis, and workspace and kinetostatic performance evaluations.

3.2.2- Inverse Geometric Model (IGM)

Obtaining the IGM is quite simple in the case of PMs, and this mechanism does not form an exception. Knowing the end-effector pose, $\boldsymbol{x}$, the coordinates of C and D, the contact point between the rack and pinion, are obtained via:

$$\boldsymbol{C}=\boldsymbol{P}+\boldsymbol{R}\,\boldsymbol{C}^{M_f} \tag{3.1}$$

and

$$\boldsymbol{D}=\boldsymbol{C}+r_p\,\boldsymbol{e_z} \tag{3.2},$$

where $\boldsymbol{C}^{M_f}$ and r_p are given (refer to **Fig. 3-2**).

As $\boldsymbol{C}$, $\boldsymbol{D}$, θ_z, and θ_y are all now available, then the coordinates $\boldsymbol{B}_j$ $(\forall j=1...5)$ can be easily derived as follows:

$$\boldsymbol{B}_1\equiv\boldsymbol{B}_2=\boldsymbol{D}+r_p\,\theta_y\,\boldsymbol{e_h}+(c-r_p)\,\boldsymbol{e_z} \tag{3.3}$$

and

$$\boldsymbol{B}_3 \equiv \boldsymbol{B}_4 \equiv \boldsymbol{B}_5 = \boldsymbol{C} + \boldsymbol{R}_z\ \boldsymbol{B}_3^{M_i} \tag{3.4},$$

where $\boldsymbol{B}_3^{M_i} \equiv \boldsymbol{B}_4^{M_i} \equiv \boldsymbol{B}_5^{M_i}$ are all known.

Then, it remains to get the x-component of the points $A_i\ (\forall i = 1...5)$. This can be done utilizing the following relation:

$$\boldsymbol{A}_i\boldsymbol{B}_i^2 = L_i^2,\ \forall i = 1...5 \tag{3.5},$$

which after development yields:

$$q_i = x_i = x_{bi} \pm \sqrt{L_i^2 - (y_{bi} - y_i)^2 - (z_{bi} - z_i)^2}, \forall i = 1...5 \tag{3.6}.$$

Only one solution of (3.6) is acceptable depending on the assembly mode. In our case, we consider the assembly mode described by the following condition:

$$q_i = x_i \le \mathrm{x}_{bi},\ \forall i = 1...5 \tag{3.7}.$$

Consequently, the solution is:

$$q_i = x_i = x_{bi} - \sqrt{L_i^2 - (y_{bi} - y_i)^2 - (z_{bi} - z_i)^2}, \forall i = 1...5 \tag{3.8},$$

and hence, the IGM of the mechanism has been derived.

3.2.3- Direct Geometric Model (DGM)

While the IGM is always computable for PMs, DGM is most often difficult to establish. Fortunately, here we can derive the DGM analytically with ease.

Knowing the joint positions, $\boldsymbol{q}$, the coordinates $\boldsymbol{A}_j\ (\forall j = 1...5)$ are available. The first step is then to compute $\boldsymbol{B}_j\ (\forall j = 1...5)$. For this purpose, we need to consider the following system of equations:

$$\begin{cases} \boldsymbol{A}_3\boldsymbol{B}_3^2 = L_3^2 \\ \boldsymbol{A}_4\boldsymbol{B}_4^2 = L_4^2,\ \text{with: } \boldsymbol{B}_3 \equiv \boldsymbol{B}_4 \equiv \boldsymbol{B}_5 \\ \boldsymbol{A}_5\boldsymbol{B}_5^2 = L_5^2 \end{cases} \tag{3.9}.$$

The system (3.9) can be translated geometrically as the intersection of the three spheres centered at A_3, A_4, and A_5, and with respective radii L_3, L_4, and L_5. This is a classical mathematical problem, which can be easily solved. Therefore, we omit the details. In general, we get two possible solutions, say: $\boldsymbol{B}_3^{s1}$ and $\boldsymbol{B}_3^{s2}$.

As $\boldsymbol{B}_3$ is known, then the z-component of point $B_1 \equiv B_2$ can be determined by:

$$z_{b1} \equiv z_{b2} = z_{b3} + (c - b) \tag{3.10}.$$

Hence, two solutions exist in correspondence to $\boldsymbol{B}_3^{s1}$ and $\boldsymbol{B}_3^{s2}$. Let us denote them by: z_{b1}^{s1} and z_{b1}^{s2}. Then, obtaining the remaining components of $B_1 \equiv B_2$, namely $x_{b1} \equiv x_{b2}$ and $y_{b1} \equiv y_{b2}$, is done by considering the following system of equations:

$$\begin{cases} \boldsymbol{A}_1\boldsymbol{B}_1^2 = L_1^2 \\ \boldsymbol{A}_2\boldsymbol{B}_2^2 = L_2^2 \end{cases}, \text{ where } \boldsymbol{B}_1 \equiv \boldsymbol{B}_2 \tag{3.11}.$$

The solution of (3.11) is geometrically described as the intersection of two circles in the horizontal plane defined by $z = z_{b1}$. For each solution of z_{b1}, we obtain two possible solutions for the coordinates $\boldsymbol{B}_1 \equiv \boldsymbol{B}_2$. For $z_{b1} = z_{b1}^{s1}$, we get $\boldsymbol{B}_1^{s11}$ and $\boldsymbol{B}_1^{s12}$. Similarly for $z_{b1} = z_{b1}^{s2}$, we have $\boldsymbol{B}_1^{s21}$ and $\boldsymbol{B}_1^{s22}$.

Hence, there are four possible solutions described by the set $\mathbb{S} = \{\boldsymbol{S}_1, \boldsymbol{S}_2, \boldsymbol{S}_3, \boldsymbol{S}_4\}$, with: $\boldsymbol{S}_1 = \langle \boldsymbol{B}_3^{s1}, \boldsymbol{B}_1^{s11} \rangle$, $\boldsymbol{S}_2 = \langle \boldsymbol{B}_3^{s1}, \boldsymbol{B}_1^{s12} \rangle$, $\boldsymbol{S}_3 = \langle \boldsymbol{B}_3^{s2}, \boldsymbol{B}_1^{s21} \rangle$, and $\boldsymbol{S}_4 = \langle \boldsymbol{B}_3^{s2}, \boldsymbol{B}_1^{s22} \rangle$. Among these solutions, only one satisfies the assembly mode condition described by (3.7). Thus, we obtain $\boldsymbol{B}_1 \equiv \boldsymbol{B}_2$ and $\boldsymbol{B}_3 \equiv \boldsymbol{B}_4 \equiv \boldsymbol{B}_5$. It remains to compute $\boldsymbol{P}$ and θ.

Defining $\boldsymbol{\eta} = \begin{pmatrix} \eta_x & \eta_y & 0 \end{pmatrix}^{\mathrm{T}} = \boldsymbol{B}_3\boldsymbol{B}_1 - \left(\boldsymbol{B}_3\boldsymbol{B}_1^{\mathrm{T}}\, \boldsymbol{e_z}\right)\boldsymbol{e_z}$, the value of θ_z is obtained by:

$$\theta_z = \operatorname{atan2}\left(\eta_y, \eta_x\right) \in \left]-\pi; +\pi\right] \tag{3.12}.$$

Knowing $\boldsymbol{R_z} = \mathrm{Rot}_z\left(\theta_z\right)$, we get:

$$\boldsymbol{C} = \boldsymbol{B}_3 + \boldsymbol{R}_z\, \boldsymbol{B}_3\boldsymbol{C}^{M_i} \tag{3.13}$$

and

$$\boldsymbol{D} = \boldsymbol{C} + r_p\, \boldsymbol{e_z} \tag{3.14}.$$

Consequently, θ_y and $\boldsymbol{P}$ are computed by means of the following relations:

$$\theta_y = \frac{\left(\boldsymbol{D}\boldsymbol{B}_1 - \left(c - r_p\right)\boldsymbol{e_z}\right)^{\mathrm{T}}\, \boldsymbol{e_h}}{r_p} \tag{3.15}$$

and

$$\boldsymbol{P} = \begin{pmatrix} x & y & z \end{pmatrix}^{\mathrm{T}} = \boldsymbol{C} - \boldsymbol{R}\, \boldsymbol{C}^{M_f} \tag{3.16}.$$

Hence, the pose $\boldsymbol{x} = \begin{pmatrix} x & y & z & \theta_z & \theta_y \end{pmatrix}^{\mathrm{T}}$ is obtained, and the DGM is analytically established.

3.2.4- Kinematic Model

This section is dedicated for the derivation of the kinematic model of the current robot, i.e. the relation between $\dot{\boldsymbol{q}}$ and $\dot{\boldsymbol{x}}$. This can be easily done by following the classical approach.

The first step is to obtain the velocities of all points B_i $(\forall i = 1...5)$ in terms of $\dot{\boldsymbol{x}}$. These are given below as:

$$\begin{cases} \forall i = 1,2: \\ \boldsymbol{v}_{B_i} = \boldsymbol{v}_D + \boldsymbol{\omega}_1 \times \boldsymbol{DB}_i = \boldsymbol{v} + \boldsymbol{\omega} \times \boldsymbol{PD} + \boldsymbol{\omega}_1 \times \boldsymbol{DB}_i \\ \quad = \boldsymbol{v} - \widehat{\boldsymbol{PD}}\ \boldsymbol{\Omega}\ \dot{\boldsymbol{\theta}} - \widehat{\boldsymbol{DB}_i}\ \boldsymbol{\Omega}_1\ \dot{\theta}_i = \left[\mathbf{1}_{3\times 3} \quad -\left(\widehat{\boldsymbol{PD}}\ \boldsymbol{\Omega} + \widehat{\boldsymbol{DB}_i}\ \boldsymbol{\Omega}_1 \right) \right] \dot{\boldsymbol{x}} \end{cases} \tag{3.17}$$

and

$$\begin{cases} \forall i = 3,4,5: \\ \boldsymbol{v}_{B_i} = \boldsymbol{v}_C + \boldsymbol{\omega}_1 \times \boldsymbol{CB}_i = \boldsymbol{v} + \boldsymbol{\omega} \times \boldsymbol{PC} + \boldsymbol{\omega}_1 \times \boldsymbol{CB}_i = \left[\mathbf{1}_{3\times 3} \quad -\left(\widehat{\boldsymbol{PC}}\ \boldsymbol{\Omega} + \widehat{\boldsymbol{CB}_i}\ \boldsymbol{\Omega}_1 \right) \right] \dot{\boldsymbol{x}} \end{cases} \tag{3.18}.$$

Then, as A_iB_i is a rigid body, the projections of the velocities $\boldsymbol{v}_{A_i}$ of point A_i and $\boldsymbol{v}_{B_i}$ of point B_i along $\boldsymbol{A_iB_i}$ are equal, for all $i = 1...5$. This can be written as:

$$\boldsymbol{A_iB_i}^{\mathrm{T}}\ \boldsymbol{v}_{A_i} = \boldsymbol{A_iB_i}^{\mathrm{T}}\ \boldsymbol{v}_{B_i},\ \forall i = 1...5 \tag{3.19},$$

with $\boldsymbol{v}_{A_i} = \dot{q}_i\ \boldsymbol{e}_x\ \ (\forall i = 1...5)$.

The development of (3.19) after substituting (3.17) and (3.18) gives the following relation:

$$\boldsymbol{J}_q\ \dot{\boldsymbol{q}} = \boldsymbol{J}_x\ \dot{\boldsymbol{x}} \tag{3.20},$$

with:

$$\begin{cases} \boldsymbol{J}_q = \mathrm{diag}\left(\boldsymbol{n}_1^{\mathrm{T}}\ \boldsymbol{e}_x, ..., \boldsymbol{n}_5^{\mathrm{T}}\ \boldsymbol{e}_x \right) \\ \boldsymbol{J}_x = \begin{bmatrix} \boldsymbol{n}_1^{\mathrm{T}} & -\boldsymbol{n}_1^{\mathrm{T}} \left(\widehat{\boldsymbol{PD}}\ \boldsymbol{\Omega} + \widehat{\boldsymbol{DB}_1}\ \boldsymbol{\Omega}_1 \right) \\ \boldsymbol{n}_2^{\mathrm{T}} & -\boldsymbol{n}_2^{\mathrm{T}} \left(\widehat{\boldsymbol{PD}}\ \boldsymbol{\Omega} + \widehat{\boldsymbol{DB}_2}\ \boldsymbol{\Omega}_1 \right) \\ \boldsymbol{n}_3^{\mathrm{T}} & -\boldsymbol{n}_3^{\mathrm{T}} \left(\widehat{\boldsymbol{PC}}\ \boldsymbol{\Omega} + \widehat{\boldsymbol{CB}_3}\ \boldsymbol{\Omega}_1 \right) \\ \boldsymbol{n}_4^{\mathrm{T}} & -\boldsymbol{n}_4^{\mathrm{T}} \left(\widehat{\boldsymbol{PC}}\ \boldsymbol{\Omega} + \widehat{\boldsymbol{CB}_4}\ \boldsymbol{\Omega}_1 \right) \\ \boldsymbol{n}_5^{\mathrm{T}} & -\boldsymbol{n}_5^{\mathrm{T}} \left(\widehat{\boldsymbol{PC}}\ \boldsymbol{\Omega} + \widehat{\boldsymbol{CB}_5}\ \boldsymbol{\Omega}_1 \right) \end{bmatrix} \\ \boldsymbol{n}_i = \boldsymbol{A_iB_i},\ \forall i = 1...5 \end{cases} \tag{3.21}.$$

Based on the relation (3.20), we have the following inverse and direct kinematic models, denoted by IKM and DKM respectively:

$$\mathrm{IKM}: \dot{\boldsymbol{q}} = \boldsymbol{J}_m\ \dot{\boldsymbol{x}},\ \text{with}\ \boldsymbol{J}_m = \boldsymbol{J}_q^{-1}\ \boldsymbol{J}_x \tag{3.22}$$

and

$$\mathrm{DKM}: \dot{\boldsymbol{x}} = \boldsymbol{J}\ \dot{\boldsymbol{q}},\ \text{with}: \boldsymbol{J} = \boldsymbol{J}_m^{-1} = \boldsymbol{J}_x^{-1}\ \boldsymbol{J}_q \tag{3.23}.$$

The relations (3.22) and (3.23) are valid provided that $\boldsymbol{J}_q$ and $\boldsymbol{J}_x$ are non-singular matrices.

Having established the kinematic models, we can proceed by investigating the singularity status of MachLin5 machine.

3.2.5- Singularity Analysis

In the case of PMs, there are various singularities to investigate and usually it is not sufficient to consider the input-output kinematic relation, as previously discussed in **Chapter 1**. Fortunately, this mechanism and due to its particular features, it is possible to carry its singularity study in two simple independent steps.

The first step is characterized by the study of constraint singularities, whereas the second is concerned with the classical ones, i.e. those based on the kinematic relation expressed by (3.20).

A- Constraint Singularities

In **§3.2.1**, we have discussed the principle of functioning of the mechanism. Particularly, we have explained that its functionality is held on the premise that the pair of parallelograms fulfills its intended role; i.e. as long as the chains (III) and (IV) constrain the two undesired rotations of the first part of the platform. Hence, a constraint singularity exists when this latter condition is not satisfied.

Actually, this singularity occurs only in the case where the two parallelograms are collinear. Due to the assembly mode condition (3.7), it dictates having $\boldsymbol{A}_3\boldsymbol{B}_3 // \boldsymbol{A}_4\boldsymbol{B}_4 // \boldsymbol{e}_y$. Consequently, we should have:

$$2\,L_{y2} = L_3 + L_4 \tag{3.24}$$

This singularity can then be coined as an architectural one, since it exists for a particular set of geometric parameters (those satisfying (3.24)).

Nevertheless, this singularity is prevented by construction, as we have $L_3 + L_4 > 2\,L_{y2}$. In fact, having $2\,L_{y2} = L_3 + L_4$ renders the robot useless, as the y and z components of $B_3 \equiv B_4$ remain fixed.

In brief, the PM does not admit any constraint singularity provided that $L_3 + L_4 > 2\,L_{y2}$, which is satisfied by construction. Therefore, there is no possibility for an instantaneous increase of mobility.

B- Series-Type Singularities

These occur in the case where $\boldsymbol{J}_{\boldsymbol{q}}$ (in (3.20)) is rank deficient, i.e. $\det\left(\boldsymbol{J}_{\boldsymbol{q}}\right) = 0$. As $\boldsymbol{J}_{\boldsymbol{q}}$ is a diagonal matrix, then this singularity occurs if:

$$\det\left(\boldsymbol{J}_{\boldsymbol{q}}\right) = 0 \Leftrightarrow \exists i_o \in \{1,\ldots,5\};\ \boldsymbol{n}_{i_o}^{\mathrm{T}}\,\boldsymbol{e}_{\boldsymbol{x}} = 0 \Leftrightarrow \boldsymbol{n}_{i_o} \perp \boldsymbol{e}_{\boldsymbol{x}} \tag{3.25}$$

Based on (3.25), series-type singularity occurs when one or more of the arms are completely stretched in the *yz* plane. This occurs, therefore, on the boundary of the geometrically accessible workspace and forms no problem.

C- Parallel-Type Singularities

These occur when $\boldsymbol{J}_x$ (in (3.20)) is rank deficient, i.e. $\det(\boldsymbol{J}_x)=0$. To derive the singular configurations, we proceed by performing some linear operations on $\boldsymbol{J}_x$.

Adding $\begin{pmatrix}\boldsymbol{n}_1^{\mathrm{T}}(\boldsymbol{PC}\times\boldsymbol{e}_z) & \cdots & \boldsymbol{n}_5^{\mathrm{T}}(\boldsymbol{PC}\times\boldsymbol{e}_z)\end{pmatrix}^{\mathrm{T}}$ (linear combination of the first three columns of $\boldsymbol{J}_x$) and $\begin{pmatrix}\boldsymbol{n}_1^{\mathrm{T}}(\boldsymbol{PC}\times\boldsymbol{e}_f) & \cdots & \boldsymbol{n}_5^{\mathrm{T}}(\boldsymbol{PC}\times\boldsymbol{e}_f)\end{pmatrix}^{\mathrm{T}}$ to the fourth and fifth columns of $\boldsymbol{J}_x$ respectively, we obtain the matrix $\boldsymbol{T}_1$ of same rank as $\boldsymbol{J}_x$. $\boldsymbol{T}_1$ is given by:

$$\boldsymbol{T}_1=\begin{bmatrix}\boldsymbol{n}_1^{\mathrm{T}} & -\boldsymbol{n}_1^{\mathrm{T}}\left(\widehat{\boldsymbol{CD}}\,\boldsymbol{\Omega}+\widehat{\boldsymbol{DB}}_1\,\boldsymbol{\Omega}_1\right)\\ \boldsymbol{n}_2^{\mathrm{T}} & -\boldsymbol{n}_2^{\mathrm{T}}\left(\widehat{\boldsymbol{CD}}\,\boldsymbol{\Omega}+\widehat{\boldsymbol{DB}}_2\,\boldsymbol{\Omega}_1\right)\\ \boldsymbol{n}_3^{\mathrm{T}} & -\boldsymbol{n}_3^{\mathrm{T}}\left(\widehat{\boldsymbol{CB}}_3\,\boldsymbol{\Omega}_1\right)\\ \boldsymbol{n}_4^{\mathrm{T}} & -\boldsymbol{n}_4^{\mathrm{T}}\left(\widehat{\boldsymbol{CB}}_4\,\boldsymbol{\Omega}_1\right)\\ \boldsymbol{n}_5^{\mathrm{T}} & -\boldsymbol{n}_5^{\mathrm{T}}\left(\widehat{\boldsymbol{CB}}_5\,\boldsymbol{\Omega}_1\right)\end{bmatrix}=\begin{bmatrix}\boldsymbol{n}_1^{\mathrm{T}} & r_p\,\theta_y\,\boldsymbol{n}_1^{\mathrm{T}}\,\boldsymbol{e}_f & r_p\,\boldsymbol{n}_1^{\mathrm{T}}\,\boldsymbol{e}_h\\ \boldsymbol{n}_2^{\mathrm{T}} & r_p\,\theta_y\,\boldsymbol{n}_2^{\mathrm{T}}\,\boldsymbol{e}_f & r_p\,\boldsymbol{n}_2^{\mathrm{T}}\,\boldsymbol{e}_h\\ \boldsymbol{n}_3^{\mathrm{T}} & -a\,\boldsymbol{n}_3^{\mathrm{T}}\,\boldsymbol{e}_f & 0\\ \boldsymbol{n}_4^{\mathrm{T}} & -a\,\boldsymbol{n}_4^{\mathrm{T}}\,\boldsymbol{e}_f & 0\\ \boldsymbol{n}_5^{\mathrm{T}} & -a\,\boldsymbol{n}_5^{\mathrm{T}}\,\boldsymbol{e}_f & 0\end{bmatrix} \tag{3.26}$$

Again, adding $\begin{pmatrix}a\,\boldsymbol{n}_1^{\mathrm{T}}\,\boldsymbol{e}_f & \cdots & a\,\boldsymbol{n}_5^{\mathrm{T}}\,\boldsymbol{e}_f\end{pmatrix}^{\mathrm{T}}$ to the fourth column of $\boldsymbol{T}_1$ simplifies the latter into $\boldsymbol{T}_2$ that admits the same rank as $\boldsymbol{T}_1$ and $\boldsymbol{J}_x$. It is given by:

$$\boldsymbol{T}_2=\begin{bmatrix}\boldsymbol{n}_1^{\mathrm{T}} & \left(a+r_p\,\theta_y\right)\boldsymbol{n}_1^{\mathrm{T}}\,\boldsymbol{e}_f & r_p\,\boldsymbol{n}_1^{\mathrm{T}}\,\boldsymbol{e}_h\\ \boldsymbol{n}_2^{\mathrm{T}} & \left(a+r_p\,\theta_y\right)\boldsymbol{n}_2^{\mathrm{T}}\,\boldsymbol{e}_f & r_p\,\boldsymbol{n}_2^{\mathrm{T}}\,\boldsymbol{e}_h\\ \boldsymbol{n}_3^{\mathrm{T}} & 0 & 0\\ \boldsymbol{n}_4^{\mathrm{T}} & 0 & 0\\ \boldsymbol{n}_5^{\mathrm{T}} & 0 & 0\end{bmatrix} \tag{3.27}$$

The study of rank deficiency of $\boldsymbol{J}_x$ can then be partitioned into investigating the singularity of two simpler matrices: $\boldsymbol{TS}_1$ and $\boldsymbol{TS}_2$. These are defined hereafter:

$$\boldsymbol{TS}_1=\begin{bmatrix}\boldsymbol{n}_3 & \boldsymbol{n}_4 & \boldsymbol{n}_5\end{bmatrix}^{\mathrm{T}},\ \dim(\boldsymbol{TS}_1)=3\times3 \tag{3.28}$$

and

$$\boldsymbol{TS}_2=\begin{bmatrix}\left(a+r_p\,\theta_y\right)\boldsymbol{n}_1^{\mathrm{T}}\,\boldsymbol{e}_f & r_p\,\boldsymbol{n}_1^{\mathrm{T}}\,\boldsymbol{e}_h\\ \left(a+r_p\,\theta_y\right)\boldsymbol{n}_2^{\mathrm{T}}\,\boldsymbol{e}_f & r_p\,\boldsymbol{n}_2^{\mathrm{T}}\,\boldsymbol{e}_h\end{bmatrix},\ \dim(\boldsymbol{TS}_2)=2\times2 \tag{3.29}$$

$\boldsymbol{J}_x$ is rank deficient when $\boldsymbol{TS}_1$ or $\boldsymbol{TS}_2$ is singular. Starting with $\boldsymbol{TS}_1$, its singularity mandates having the three vectors $\boldsymbol{n}_3$, $\boldsymbol{n}_4$,and $\boldsymbol{n}_5$ coplanar. Due to the assembly condition (3.7), this

cannot happen unless the aforementioned vectors are in the *yz* plane and hence, being confounded with series-type singularity as well. Therefore, it is only possible to occur on the boundary of the geometrically accessible workspace and does not form a problem.

As for $\boldsymbol{TS}_2$, developing its determinant yields:

$$\begin{aligned}\det\left(\boldsymbol{TS}_2\right) &= \left(a + r_p\ \theta_y\right)\left(n_{1x}\ n_{2y} - n_{1y}\ n_{2x}\right)\left(e_{f_x}\ e_{h_y} - e_{f_y}\ e_{h_x}\right) \\ &= -\left(a + r_p\ \theta_y\right)\left(n_{1x}\ n_{2y} - n_{1y}\ n_{2x}\right)\end{aligned} \quad (3.30),$$

where $vect_x$ and $vect_y$ designate the x and y components of vector $\boldsymbol{vect}$, respectively. Since a and r_p can be chosen in such a way to have $\left|a + r_p\ \theta_y\right| > 0$ for $\theta_y \in \left[-\pi/4\,;+\pi/4\right]$, then it remains to investigate the expression $expr = \left(n_{1x}\ n_{2y} - n_{1y}\ n_{2x}\right)$. The term $expr$ is null when the projections of $\boldsymbol{n}_1$ and $\boldsymbol{n}_2$ in the *xy* plane are collinear. But due to condition (3.7), this is not possible unless $\boldsymbol{n}_1$ and $\boldsymbol{n}_2$ are in the *yz* plane, which implies coincidence with series-type singularity. Therefore, such singularity is only possible on the boundary of the workspace and consequently non-problematic.

In conclusion, we have seen that parallel singularities can exist, but confounded with series type ones, which are restricted to the boundary of the geometrically accessible workspace.

D- Results' Briefing

Based on the above analyses, MachLin5 is free of singularities of all types over the accessible region excluding its boundary. This highly prominent feature makes the current mechanism stand out, as compared with those available in literature.

3.2.6- Workspace and Kinetostatic Performance

As the essential steps of modeling and singularity investigation have been done, the current section presents the workspace analysis for some values of the geometric parameters. These values are provided in **Table 3-1** and do not represent an optimal solution with respect to any criterion.

Since the x-motion is independent of the remaining dofs, only the workspace region in terms of y and z will be investigated, for $\theta_z = \theta_y = 0°$ on one hand, and for $\left|\theta_z\right| \le 90°$ and $\left|\theta_y\right| \le 45°$ on the other.

As for the performance indices, we consider the following measures:

Table 3-1: Geometric parameters of MachLin5.*

Geometric Parameter	Value[(1)]	Geometric Parameter	Value[(1)]
$L_i,\ i=1...5$	1	$L_{y1}=L_{y2}$	0.5
L_{z1}	0.3	L_{z2}	0.5
a	0.1	b	0.0875
c	0.125	r_p	0.025
t_p	0.075	t_c	0.0175
t_l	0.2	[(1)]**All values are expressed in meters (m).**	

***The parameters t_c and t_l correspond to the minimum offsets from the sliders' planes in case of zero rotation (i.e. $\theta_z=\theta_y=0°$) and full range of rotations (i.e. $|\theta_z|\le 90°$ and $|\theta_y|\le 45°$), respectively.**

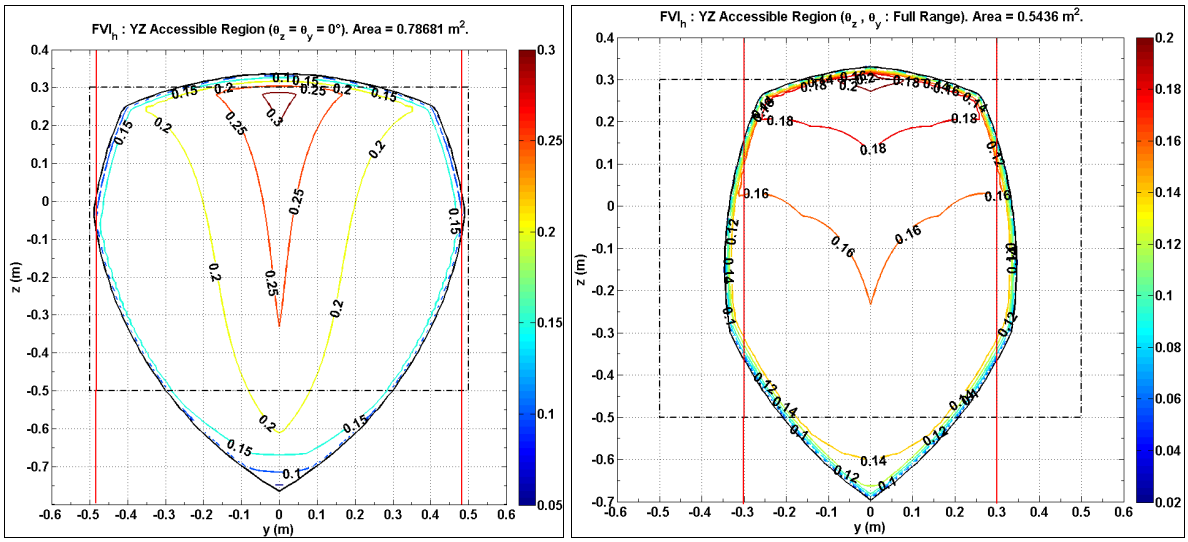

Fig. 3-4: MachLin5 - FVI_h performance: case of zero rotation (left) and case of rotation (i.e. $|\theta_z|\le 90°$ and $|\theta_y|\le 45°$) (right).

- FVI_h: We compute FVI_h at each pose, after homogenizing $\boldsymbol{J_m}$ and $\boldsymbol{J}$ using the matrix $\boldsymbol{W}=\mathrm{diag}(1,1,1,a,t_p)$. The aim is just to have some insight on singularity performance only. We recall that no kinetostatic significance is being sought from this study. We have set $v_{req}^h=\dot{q}_{\max}$ and $f_{req}^h=\tau_{\max}$, where v_{req}^h and f_{req}^h are the required minimal homogenized linear speed and static force.

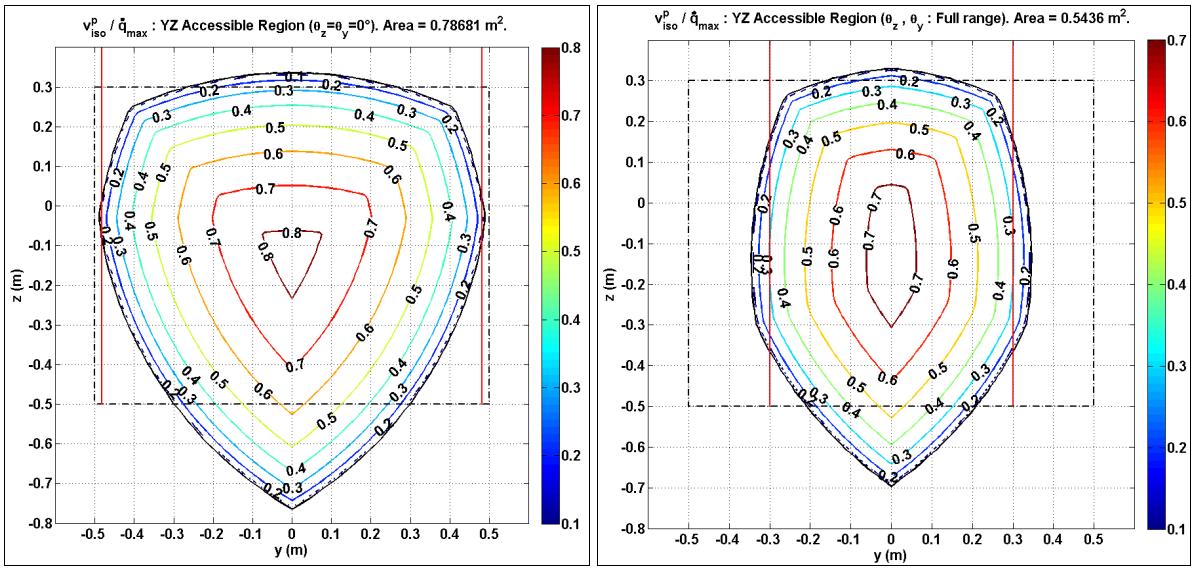

Fig. 3-5: MachLin5 - v^p_{iso} performance: case of zero rotation (left) and full-range rotation (right).

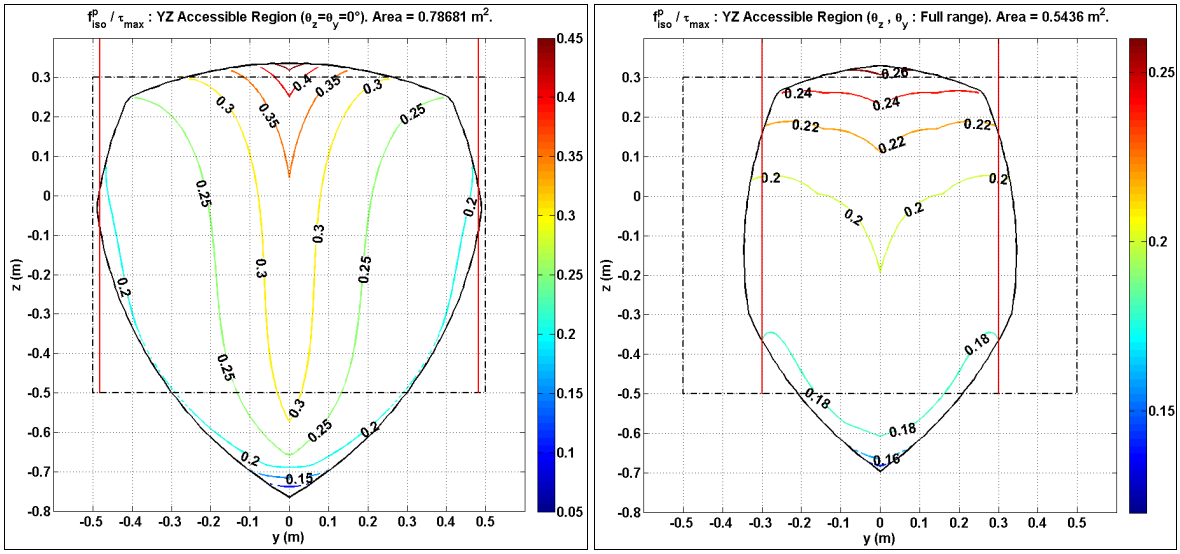

Fig. 3-6: MachLin5 - f^p_{iso} performance: case of zero rotation (left) and full-range rotation (right).

- v^p_{iso} and f^p_{iso}: Here, we are more interested in quantifying pure translational motion and pure static force capacities, as we usually have the requirements regarding rotational motion and static moment less demanding. That is why we limit the kinetostatic study to v^p_{iso} and f^p_{iso}. For this study, we have set the following requirements: $v^p_{req} = \dot{q}_{\max}$ and $f^p_{req} = \tau_{\max}$.

The analysis based on FVI_h is summarized in **Fig. 3-4**. As for v^p_{iso} and f^p_{iso}, the results of their analyses are plotted in **Fig. 3-5** and **Fig. 3-6**, respectively. In all these figures, we clarify the following points:

- The black-dotted box represents the yz projection of the robot's physical limits (i.e. vertical walls, floor, and ceiling).
- The vertical solid red lines represent the limits that should not be exceeded by the TCP to avoid collision with the sliders' planes.
- Finally, in the graphs with rotation, the plotted values are obtained as follows. For each (y,z) position, several values of θ_z and θ_y are assumed and the value of the indices FVI_h, v_{iso}^p and f_{iso}^p are calculated. Then, the worst value (minimal one) is associated with the corresponding (y,z) position. The angles tested are: $\theta_z = \pm(90°, 60°, 45°, 30°, 0°)$ and $\theta_y = \pm(45°, 30°, 0°)$.

Analyzing the results of **Fig. 3-4**, we can clearly notice the performance degradation (low value of FVI_h) near the boundary. We can also notice that while FVI_h smoothly varies within the geometrically accessible regions, it steeply goes down just in the very narrow vicinity of the boundary. This is due to the presence of series or parallel-series type singularities, as discussed in **§3.2.5**. On the other hand, we can notice, based on **Fig. 3-5**, an interesting isotropic linear speed capacity that surpasses $50\,\%$ of $\dot{q}_{\max}$ over a large proportion of the workspace. Regarding $f_{iso}^p / \tau_{\max}$, though not as high as what we had in the case of $v_{iso}^p / \dot{q}_{\max}$, still it is rather fairly well surpassing $18\,\%$ in vast proportion of the workspace. Here, the reader must keep in mind that the geometrical parameters are not optimized and the values being discussed are of isotropic nature.

3.2.7- Synopsis

In this part (**§3.2**), we have studied a novel five-dof (3T-2R) PM, in which we have derived all of its geometric and kinematic models, investigated its singularities, and analyzed its workspace. The results have revealed that this mechanism has the following interesting features:

1. The design is quite simple and easy to model. In particular, it admits an analytical DGM, which can be helpful regarding control. Also, several options are available that can simplify it further, particularly in what concerns the spherical joints and their execution.
2. It admits vast workspace with interesting tilting capacity, and independent x-motion. Also, the design is characterized by the absence of singularities of all types within the geometrically accessible region excluding its boundary.
3. Its singularity and kinetostatic performances over the workspace are interesting. They are subject for further improvement upon the optimization of its geometric parameters.
4. Having all the arms under tension/compression forces means reduced deformation and consequently, better accuracy.
5. The design, being non-redundant, does not compel any special treatment on the control level.

6. The possibility of replacing the rack-pinion assembly by a more rigid linear-to-rotation transformation mechanism helps improving the structural rigidity. This also benefits precision.

Nonetheless, having five sliders with independent guides situated in two planes and along a line is not favored. This is because it will necessitate more severe quality control, such as assuring the surface parallelism and orthogonality on one hand, and the parallelism of the linear guides on the other. Moreover, having an articulated platform is another weak point in the current mechanism. In fact, it has been a discouraging factor, especially after our observation regarding the precision of Veloce prototype and Quattro, with their articulated platform versions.

Therefore, as it seemed rather difficult to have a five-dof architecture embedding all the yearned for characteristics, among which is platform rigidity, we have diverted our attention towards four-dof PMs. Among these PMs, we focus in what follows on two main designs, called ARROW V1 and ARROW V2. In particular, ARROW V2 can be considered as an advancement of ARROW V1. This will become clear as we go through.

3.3- ARROW V1: A Redundantly Actuated Four-DoF (3T-1R) Parallel Manipulator

This section is devoted for discussing the four-dof (3T-1R) PKM, namely ARROW V1 (an acronym for **A**ccurate and **R**apid **R**obot with large **O**perational **W**orkspace **V**ersion 1), which has been the subject of ((SHAYYA, et al., 2013a), (SHAYYA, et al., 2013b), (SHAYYA, et al., 2014b) and (SHAYYA, et al., 2014c)). The CAD of the PKM and its graph diagram are provided in **Fig. 3-7**. Also, the frontal and close-up side views of the PKM and its platform are depicted in **Fig. 3-8**.

In the upcoming subsection, a brief description of ARROW V1 and its principle of functioning are provided.

3.3.1- Description

ARROW V1 is a redundantly actuated PKM consisting of six linear actuators for four dofs of 3T-1R type. The actuators are aligned along the same direction (x-axis) and partitioned into two sets. Each set consists of three actuators, equidistant one from another, and laying in the same vertical plane. The PKM is structurally symmetric, which is highly favorable from industrial and manufacturing perspectives. Besides, the parallelism of its actuators contributes to the independent motion along the x-axis and therefore, having a vast workspace. Moreover, it is capable of performing $\pm 90^\circ$ about the z - axis, which constitutes one of the significant merits of the design.

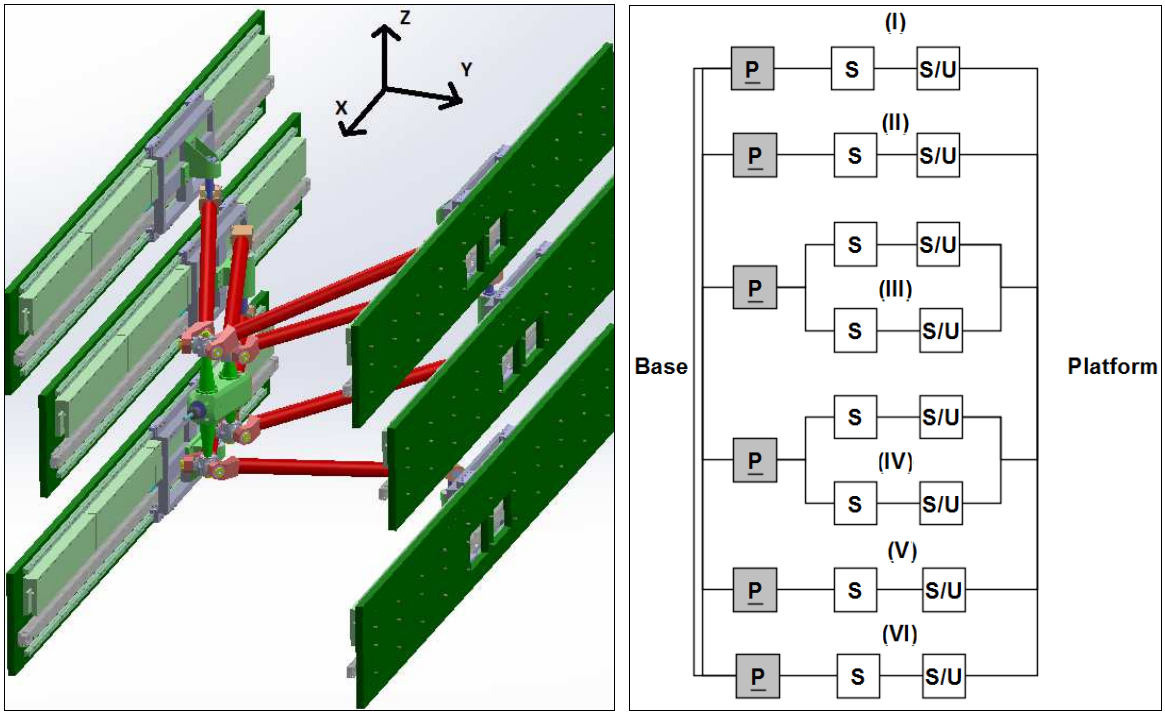

Fig. 3-7: ARROW V1 PKM: CAD drawing and graph diagram.

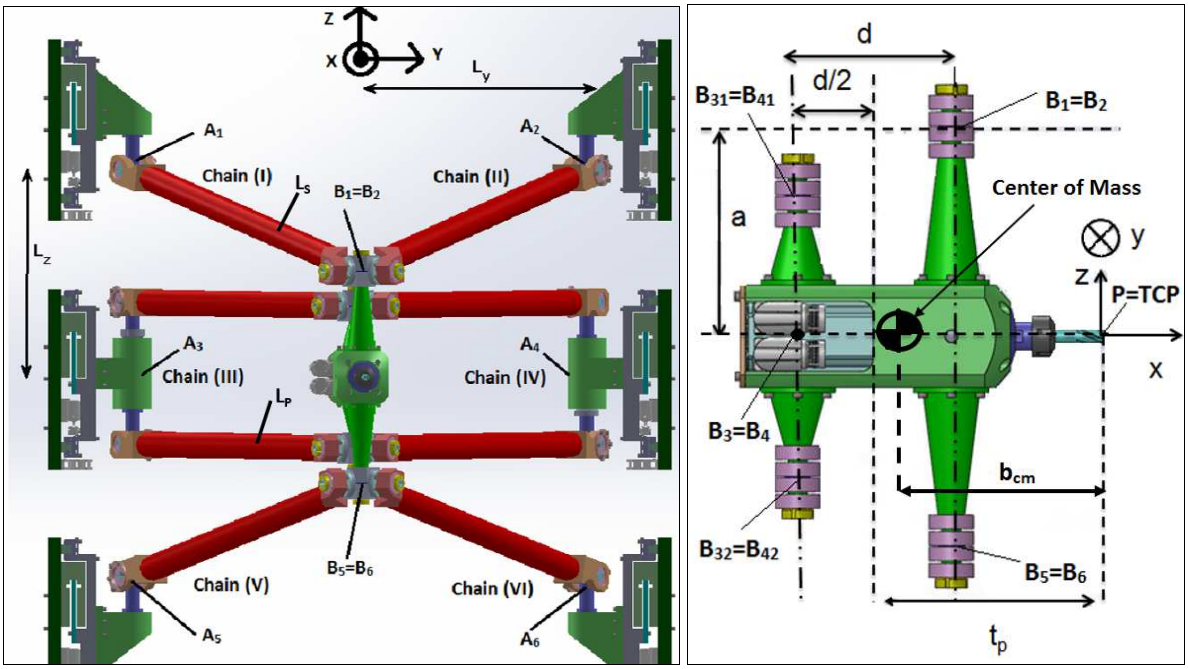

Fig. 3-8: Frontal view of ARROW V1 PKM and close-up side view of its platform.

The principle of functioning of the mechanism is quite simple. The pair of parallelograms (i.e. chains (III) and (IV)) constrains all rotations except that about the z-axis of the base frame. Then, all the chains cooperate to position the TCP and control the tool orientation. But for the mechanism to function properly, it is mandatory to have $L_z \neq a$ (see **Fig. 3-8**). In practice, L_z is chosen to be larger than a. This condition and its importance will be clarified later.

Finally and before presenting the modeling of ARROW V1, we mention that the symbols that we are going to use are clarified in **Fig. 3-8**. Also, notice that L_i designates the i-th arm length for all $i=1...6$, such that $L_1=L_2=L_5=L_6=L_s$, and $L_3=L_4=L_p$.

3.3.2- Inverse Geometric Model (IGM)

As the design is simple and its modeling is similar to that of MachLin5, we are going to omit redundant details. Given the end-effector pose $\boldsymbol{x}=\begin{pmatrix} x & y & z & \theta_z \end{pmatrix}^{\mathrm{T}}$, then the coordinates $\boldsymbol{P}=\begin{pmatrix} x & y & z \end{pmatrix}^{\mathrm{T}}$ of P (the TCP) and the rotation matrix $\boldsymbol{R}=\mathrm{Rot}_{\mathrm{z}}\left(\theta_z\right)$ of the platform are all known. Thus, the coordinates $\boldsymbol{B}_i$ of points B_i $\left(\forall i=1...6\right)$ are computable via:

$$\boldsymbol{B}_i=\begin{pmatrix} x_{bi} & y_{bi} & z_{bi} \end{pmatrix}^{\mathrm{T}}=\boldsymbol{P}+\boldsymbol{R}\,\boldsymbol{B}_i^{plat},\ \forall i=1...6 \tag{3.31},$$

where $\boldsymbol{B}_i^{plat}$ corresponds to the known coordinates of B_i in the frame connected to the moving platform. Then, substituting (3.31) in the following relation:

$$\begin{cases} \boldsymbol{A}_i\boldsymbol{B}_i^2=L_i^2,\ \forall i=1...6,\ \text{with:} \\ \boldsymbol{A}_i=\begin{pmatrix} x_i & y_i & z_i \end{pmatrix}^{\mathrm{T}}=\begin{pmatrix} q_i & y_i & z_i \end{pmatrix}^{\mathrm{T}},\ y_i=(-1)^i\,L_y \\ z_i=\begin{cases} L_z,\ \text{if } i=1,2 \\ 0,\ \text{if } i=3,4 \\ -L_z,\ \text{if } i=5,6 \end{cases} \end{cases} \tag{3.32}$$

and considering the assembly mode condition described by:

$$q_i=x_i\le x_{bi},\ \forall i=1...6 \tag{3.33},$$

we get the solution of the IGM as below:

$$\begin{cases} q_i=x_i=x_{bi}-\sqrt{L_i^2-\left(y_i-y_{bi}\right)^2-\left(z_i-z_{bi}\right)^2},\ \forall i=1...6 \\ \text{with:} \\ L_i=\begin{cases} L_s,\ \text{if } i=1,2,5,6 \\ L_p,\ \text{otherwise} \end{cases} \end{cases} \tag{3.34}.$$

3.3.3- Direct Geometric Model (DGM)

Unlike most PKMs, ARROW V1 admits an analytical DGM. In fact, due to actuation redundancy there exists no unique way to establish it. In what follows, we describe one of the possible methods.

Assuming that the joint positions vector $\boldsymbol{q}$ is known, then the coordinates $\boldsymbol{A}_i$ are available as well, for all $i=1...6$.

Let us consider the following system of equations:

$$\begin{cases} \boldsymbol{A}_1\boldsymbol{B}_1^2 = L_1^2 \\ \boldsymbol{A}_2\boldsymbol{B}_2^2 = L_2^2 \\ \boldsymbol{A}_5\boldsymbol{B}_5^2 = L_5^2 \end{cases} \tag{3.35}$$

But as $\boldsymbol{B}_1 \equiv \boldsymbol{B}_2$ and $\boldsymbol{B}_1\boldsymbol{B}_5 = -2\,a\,\boldsymbol{e}_z$, the system (3.35) is transformable into the following form:

$$\begin{cases} \boldsymbol{A}_1\boldsymbol{B}_1^2 = L_1^2 \\ \boldsymbol{A}_2\boldsymbol{B}_1^2 = L_2^2, \text{ with: } \boldsymbol{A}_5' = \boldsymbol{A}_5 + 2\,a\,\boldsymbol{e}_z \\ \boldsymbol{A}_5'\boldsymbol{B}_1^2 = L_5^2 \end{cases} \tag{3.36}$$

System (3.36) represents a classical mathematical problem, which corresponds geometrically to the intersection of the three spheres of centers A_1, A_2, and A_5' (of coordinates $\boldsymbol{A}_5'$), and with radii L_1, L_2, and L_5, respectively. Omitting details, we get in general two possible solutions for $\boldsymbol{B}_1$. Let us denote them by $\boldsymbol{B}_1^{s1}$ and $\boldsymbol{B}_1^{s2}$. Then, we still need to get $\boldsymbol{B}_3 \equiv \boldsymbol{B}_4$. For this purpose, we consider the following relations:

$$\begin{cases} \boldsymbol{A}_3\boldsymbol{B}_3^2 = L_3^2 \\ \boldsymbol{A}_4\boldsymbol{B}_4^2 = L_4^2 \end{cases}, \text{ with: } \boldsymbol{B}_3 \equiv \boldsymbol{B}_4 \tag{3.37}$$

But we know that $z_{b3} \equiv z_{b4} = z_{b1} - a$, then (3.37) can be rewritten after incorporating the aforementioned relation as:

$$\begin{cases} \boldsymbol{A}_3\boldsymbol{B}_3^2 = L_3^2 \\ \boldsymbol{A}_4\boldsymbol{B}_3^2 = L_4^2 \\ z_{b3} = z_{b1} - a \end{cases} \tag{3.38}$$

The problem expressed by (3.38) is described geometrically as the intersection of two circles in the horizontal plane of equation $z = z_{b3} = z_{b1} - a$. It can be easily solved for each possible solution of z_{b1}. For $z_{b1} = z_{b1}^{s1}$ (corresponding to the z-component of $\boldsymbol{B}_1^{s1}$), we get generally two possible solutions for $\boldsymbol{B}_3$, denoted by $\boldsymbol{B}_3^{s11}$ and $\boldsymbol{B}_3^{s12}$. Likewise, for $z_{b1} = z_{b1}^{s2}$ (corresponding to the z-component of $\boldsymbol{B}_1^{s2}$), we get another two possible solutions, say: $\boldsymbol{B}_3^{s21}$ and $\boldsymbol{B}_3^{s22}$.

In brief, we generally obtain a set of four possible solutions, denoted by $\mathbb{S} = \{\boldsymbol{S}_1, \boldsymbol{S}_2, \boldsymbol{S}_3, \boldsymbol{S}_4\}$, with $\boldsymbol{S}_1 = \langle \boldsymbol{B}_1^{s1}, \boldsymbol{B}_3^{s11} \rangle$, $\boldsymbol{S}_2 = \langle \boldsymbol{B}_1^{s1}, \boldsymbol{B}_3^{s12} \rangle$, $\boldsymbol{S}_3 = \langle \boldsymbol{B}_1^{s2}, \boldsymbol{B}_3^{s21} \rangle$,and $\boldsymbol{S}_4 = \langle \boldsymbol{B}_1^{s2}, \boldsymbol{B}_3^{s22} \rangle$. Among these four solutions, there is only one $\boldsymbol{S} \in \mathbb{S}$ that satisfies the assembly mode condition described by (3.33). Hence, we have determined uniquely $\boldsymbol{B}_1$ through $\boldsymbol{B}_6$. It remains to calculate $\boldsymbol{P}$ and θ_z.

Defining $\boldsymbol{\eta} = \begin{pmatrix} \eta_x & \eta_y & 0 \end{pmatrix}^{\mathrm{T}} = \boldsymbol{B}_3\boldsymbol{B}_1 - \left(\boldsymbol{B}_3\boldsymbol{B}_1^{\mathrm{T}}\,\boldsymbol{e}_z\right)\boldsymbol{e}_z$, the rotation θ_z is calculated, thanks to the equation below:

$$\theta_z = \operatorname{atan2}\left(\eta_y, \eta_x\right) \tag{3.39}$$

As for $\boldsymbol{P}$, it is given by:

$$\boldsymbol{P} = \begin{pmatrix} x & y & z \end{pmatrix}^{\mathrm{T}} = \boldsymbol{B}_1 - \boldsymbol{R}\,\boldsymbol{B}_1^{plat}, \text{ with } \boldsymbol{R} = \mathrm{Rot}_{\mathrm{z}}\left(\theta_z\right) \tag{3.40}$$

As a result, the end-effector pose $\boldsymbol{x} = \begin{pmatrix} x & y & z & \theta_z \end{pmatrix}^{\mathrm{T}}$ is computed and the DGM is established.

3.3.4- Kinematic Model

Let us now derive the relation between $\dot{\boldsymbol{q}}$ and $\dot{\boldsymbol{x}}$. For this purpose, we proceed in the very same manner as in **§3.2.4**. First, we get the velocities $\boldsymbol{v}_{B_i}$ and $\boldsymbol{v}_{A_i}$ in terms of $\dot{\boldsymbol{x}}$ and $\dot{\boldsymbol{q}}$, respectively. This is described via the equations:

$$\begin{cases} \boldsymbol{v}_{B_i} = \boldsymbol{v} + \boldsymbol{\omega} \times \boldsymbol{PB}_i = \boldsymbol{v} - \dot{\theta}_z\,(\boldsymbol{PB}_i \times \boldsymbol{e}_z) = \begin{bmatrix} \mathbf{1}_{3\times 3} & -(\boldsymbol{PB}_i \times \boldsymbol{e}_z) \end{bmatrix} \dot{\boldsymbol{x}} \\ \text{with:} \\ \boldsymbol{v} = \dot{\boldsymbol{P}} \text{ and } \boldsymbol{\omega} = \dot{\theta}_z\,\boldsymbol{e}_z \\ \forall i = 1...6 \end{cases} \tag{3.41}$$

and

$$\boldsymbol{v}_{A_i} = \dot{q}_i\,\boldsymbol{e}_x, \ \forall i = 1...6 \tag{3.42}$$

As A_iB_i is a rigid body for all $i = 1...6$, then we have:

$$\boldsymbol{A}_i\boldsymbol{B}_i^{\mathrm{T}}\,\boldsymbol{v}_{A_i} = \boldsymbol{A}_i\boldsymbol{B}_i^{\mathrm{T}}\,\boldsymbol{v}_{B_i}, \ \forall i = 1...6 \tag{3.43}$$

Based on (3.43), and substituting (3.41) and (3.42), we get the following kinematic relation:

$$\begin{cases} \boldsymbol{J}_q\,\dot{\boldsymbol{q}} = \boldsymbol{J}_x\,\dot{\boldsymbol{x}}, \text{ with:} \\ \boldsymbol{J}_q = \mathrm{diag}\left(\boldsymbol{n}_1^{\mathrm{T}}\,\boldsymbol{e}_x, ..., \boldsymbol{n}_6^{\mathrm{T}}\,\boldsymbol{e}_x\right) \\ \boldsymbol{J}_x = \begin{bmatrix} \boldsymbol{n}_1^{\mathrm{T}} & -\boldsymbol{n}_1^{\mathrm{T}}\left(\boldsymbol{PB}_1 \times \boldsymbol{e}_z\right) \\ \vdots & \vdots \\ \boldsymbol{n}_6^{\mathrm{T}} & -\boldsymbol{n}_6^{\mathrm{T}}\left(\boldsymbol{PB}_6 \times \boldsymbol{e}_z\right) \end{bmatrix} \\ \boldsymbol{n}_i = \dfrac{\boldsymbol{A}_i\boldsymbol{B}_i}{\left\|\boldsymbol{A}_i\boldsymbol{B}_i\right\|}, \ \forall i = 1...6 \end{cases} \tag{3.44}$$

Notice that $\boldsymbol{J}_q$ is a 6×6 square matrix as compared with $\boldsymbol{J}_x$, which is rectangular of 6×4 dimension. This is due to actuation redundancy. Thus, we can get naturally the inverse kinematic model (IKM), based on the inverse Jacobian, $\boldsymbol{J}_m$. This is given by:

$$\text{IKM: } \dot{\boldsymbol{q}} = \boldsymbol{J}_m\,\dot{\boldsymbol{x}}, \text{ with } \boldsymbol{J}_m = \boldsymbol{J}_q^{-1}\,\boldsymbol{J}_x \tag{3.45}$$

As for the direct kinematic model (DKM), it requires a pseudo-inversion procedure and it can be expressed as follows:

$$\text{DKM: } \dot{\boldsymbol{x}} = \boldsymbol{J}\,\dot{\boldsymbol{q}} = \boldsymbol{J}_m^{*}\,\dot{\boldsymbol{q}}, \text{ provided that } \dot{\boldsymbol{q}}^{\mathrm{T}}\left[\mathrm{null}\left(\boldsymbol{J}_m^{\mathrm{T}}\right)\right] = \mathbf{0}_{1\times2} \tag{3.46}$$

The relations (3.45) and (3.46) are valid as long as $\boldsymbol{J}_q$ and $\boldsymbol{J}_x$ are non-singular.

3.3.5- Singularity Analysis

Similarly to MachLin5, the singularity analysis of ARROW V1 can be partitioned into separate steps. The first step is concerned with the constraint singularities and mainly focuses on the pair of parallelograms. As for the second step, it deals with the classical singularities based on (3.44).

A- Constraint Singularities

Following the same reasoning as in **§3.2.5.A**, there is no constraint singularity since it is avoided by construction. Actually, it would occur if and only if the parallelograms are collinear. Due to the assembly condition (3.33), this cannot happen unless:

$$2\,L_y = L_3 + L_4 \tag{3.47}$$

is satisfied. As this singularity occurs for a specific set of geometric parameters, those satisfying (3.47), then it is of architectural nature.

Nevertheless, (3.47) is avoided by having $L_3 + L_4 > 2\,L_y$. In fact, having (3.47) fulfilled, the PKM is rendered useless ($\boldsymbol{B}_3 \equiv \boldsymbol{B}_4$ maintains always fixed y and z components).

It remains then to consider (3.44) and its related singularities. These will be discussed in what follows.

B- Series-Type Singularities

These occur when $\det\left(\boldsymbol{J}_q\right) = 0$, which can be mathematically described as:

$$\det\left(\boldsymbol{J}_q\right) = 0 \Leftrightarrow \exists i_o \in \{1,...,6\};\ \boldsymbol{n}_{i_o}^{\mathrm{T}}\,\boldsymbol{e}_x = 0 \Leftrightarrow \boldsymbol{n}_{i_o} \perp \boldsymbol{e}_x \tag{3.48}.$$

From (3.48), this occurs when one or more arms are completely stretched and laid in the yz plane. This cannot happen except on the boundary of the geometric workspace, provided the pose is accessible.

C- Parallel-Type Singularities

Such singularities occur when $\boldsymbol{J}_x$ becomes rank deficient. To study these singularities, some linear operations are performed on $\boldsymbol{J}_x$ to arrive at a simpler matrix $\boldsymbol{T}_1$, possessing the same rank as $\boldsymbol{J}_x$. Adding $\left(\boldsymbol{n}_1^{\mathrm{T}}\,(\boldsymbol{PB}_1 \times \boldsymbol{e}_z) \quad \cdots \quad \boldsymbol{n}_6^{\mathrm{T}}\,(\boldsymbol{PB}_1 \times \boldsymbol{e}_z)\right)^{\mathrm{T}}$ to the fourth column of $\boldsymbol{J}_x$ yields $\boldsymbol{T}_1$, defined by:

$$\boldsymbol{T}_1 = \begin{bmatrix} \boldsymbol{n}_1^{\mathrm{T}} & 0 \\ \boldsymbol{n}_2^{\mathrm{T}} & 0 \\ \boldsymbol{n}_3^{\mathrm{T}} & -\boldsymbol{n}_3^{\mathrm{T}}\left(\boldsymbol{r}\times\boldsymbol{e}_z\right) \\ \boldsymbol{n}_4^{\mathrm{T}} & -\boldsymbol{n}_4^{\mathrm{T}}\left(\boldsymbol{r}\times\boldsymbol{e}_z\right) \\ \boldsymbol{n}_5^{\mathrm{T}} & 0 \\ \boldsymbol{n}_6^{\mathrm{T}} & 0 \end{bmatrix}, \text{ with } \boldsymbol{r} = \boldsymbol{B}_1\boldsymbol{B}_3 \equiv \boldsymbol{B}_1\boldsymbol{B}_4 \qquad (3.49).$$

Then, we can guarantee that $\boldsymbol{T}_1$ (equivalently $\boldsymbol{J}_x$) is of full rank if the following two submatrices:

$$\boldsymbol{TS}_1 = \begin{bmatrix} \boldsymbol{n}_1 & \boldsymbol{n}_2 & \boldsymbol{n}_5 & \boldsymbol{n}_6 \end{bmatrix}^{\mathrm{T}} \qquad (3.50)$$

and

$$\boldsymbol{TS}_2 = \begin{bmatrix} -\boldsymbol{n}_3^{\mathrm{T}}\left(\boldsymbol{r}\times\boldsymbol{e}_z\right) \\ -\boldsymbol{n}_4^{\mathrm{T}}\left(\boldsymbol{r}\times\boldsymbol{e}_z\right) \end{bmatrix} \qquad (3.51)$$

are non-singular.

$\boldsymbol{TS}_1$ becomes singular when the four vectors $\boldsymbol{n}_1$, $\boldsymbol{n}_2$, $\boldsymbol{n}_5$, and $\boldsymbol{n}_6$ are coplanar. Due to (3.33) and as we have chosen $L_z \neq a$ (particularly $L_z > a$), the only possibility of coplanarity is having all the concerned arms in the *yz* plane. Hence, the configuration is also confounded with series-type singularity. Therefore, this situation if to occur, it will be on the boundary of the geometric workspace and not inside it.

On the other hand, $\boldsymbol{TS}_2$ becomes rank deficient in the case where:

$$\boldsymbol{n}_3^{\mathrm{T}}\left(\boldsymbol{r}\times\boldsymbol{e}_z\right) = \boldsymbol{n}_4^{\mathrm{T}}\left(\boldsymbol{r}\times\boldsymbol{e}_z\right) = 0 \qquad (3.52).$$

The condition (3.52) implies that we should have $\boldsymbol{n}_3$, $\boldsymbol{r}$, and $\boldsymbol{e}_z$ coplanar on one side, and we should have $\boldsymbol{n}_4$, $\boldsymbol{r}$, and $\boldsymbol{e}_z$ coplanar on the other. But $\boldsymbol{r}$, $\boldsymbol{e}_z$, and $\boldsymbol{r}\times\boldsymbol{e}_z$ are always non-zero. So based on this latter idea and the assembly condition (3.33), the aforementioned coplanarity is possible if and only if $\boldsymbol{n}_3$, $\boldsymbol{n}_4$, and $\boldsymbol{r}$ reside in the *yz* plane. This means being confounded with series-type singularity that cannot occur except on the boundary of the geometric workspace.

Therefore, we deduce that if parallel-type singularities are to exist, then they are restricted to the boundary of the workspace and form no problem.

D- Results' Briefing

Based on the above analyses, we brief the results as follows. ARROW V1 does not admit any type of singularities within the geometrically accessible workspace excluding its boundary. This is provided that $L_z \neq a$ and $L_3 + L_4 \neq 2\,L_y$. These latter two conditions are always satisfied by construction since having them otherwise renders the PKM functionless in the first place.

3.3.6- Simplified Dynamic Model (SDM)

In this section, we present the SDM of ARROW V1. The simplification done here is embodied by the following hypotheses:

1. The frictional forces of all types, whether dry or viscous, are neglected.
2. The arms are considered massless and their influence is compensated by partitioning their real masses into two halves. The first half-mass of each arm is added on the corresponding linear actuator, whereas the second half is placed on the platform at the articulation point. This is actually justifiable due to the small mass of the arms in comparison with the other components.

Applying the law of motion on the actuators, we get:

$$\begin{cases} \boldsymbol{M_a}\ \ddot{\boldsymbol{q}} = \boldsymbol{\tau} + \boldsymbol{J_q}^{\mathrm{T}}\ (-\boldsymbol{f}\,) \\ \boldsymbol{M_a} = \mathrm{diag}\left(m_{as}, m_{as}, m_{ap}, m_{ap}, m_{as}, m_{as}\right) \\ \boldsymbol{\tau} = \left(\tau_1 \quad \cdots \quad \tau_6\right)^{\mathrm{T}} \\ \boldsymbol{f} = \left(f_1 \quad \cdots \quad f_6\right)^{\mathrm{T}} \end{cases} \tag{3.53},$$

with

- m_{as} : the mass of the actuator, moving cart, and the half-mass of the simple arm (chain (I), (II), (V) or (VI));
- m_{ap} : the mass of the actuator, moving cart, and the half-mass of the parallelogram arm (chain (III) or (IV));
- τ_i : the actuation force of the i-th actuator, for all $i = 1...6$;
- and f_i : the force due to the acceleration and the gravitational force acting on the platform. The force f_i is applied on the arm at point A_i, for all $i = 1...6$.

On the other hand, applying Newton-Euler method on the platform, we get:

$$\boldsymbol{M_p}\ \ddot{\boldsymbol{x}} + \boldsymbol{\Lambda_c}\ \dot{\boldsymbol{x}} = \boldsymbol{J_x}^{\mathrm{T}}\ \boldsymbol{f} + m_p\ \boldsymbol{g} \tag{3.54},$$

with:

- $\boldsymbol{M_p} = \begin{bmatrix} m_p & 0 & 0 & -b\ m_p\ \sin(\theta_z) \\ 0 & m_p & 0 & b\ m_p\ \cos(\theta_z) \\ 0 & 0 & m_p & 0 \\ -b\ m_p\ \sin(\theta_z) & b\ m_p\ \cos(\theta_z) & 0 & I_{pzz} \end{bmatrix}$: the inertia matrix of the platform;
- $\boldsymbol{\Lambda_c} = \begin{bmatrix} 0 & 0 & 0 & -b\ m_p\ \cos(\theta_z) \\ 0 & 0 & 0 & -b\ m_p\ \sin(\theta_z) \\ 0 & 0 & 0 & 0 \\ 0 & 0 & 0 & 0 \end{bmatrix}$: the matrix of Coriolis and centrifugal effects;
- m_p : the total mass of the platform including the half-masses from the different arms;

- b: the x-component of the center of mass of the assembly formed by the platform, and the point masses placed at B_i, for $i=1...6$ (the point mass at B_i being equal to the half-mass of the corresponding arm);
- I_{pzz}: the total moment of inertia about the z-axis passing through the TCP of the assembly formed by the platform and the point masses at B_i, for $i=1...6$;
- $\boldsymbol{g}=\begin{pmatrix}0 & 0 & -G & 0\end{pmatrix}^{\mathrm{T}}$: the gravity wrench acting on the platform per kg mass, where $G=10\ \mathrm{N/kg}=10\ \mathrm{m/s^2}$.

Then, merging (3.53) and (3.54) after substituting[1]:

$$\dot{\boldsymbol{q}}=\boldsymbol{J}_m\ \ddot{\boldsymbol{x}}+\dot{\boldsymbol{J}}_m\ \dot{\boldsymbol{x}} \tag{3.55},$$

we get:

$$\begin{cases}\ddot{\boldsymbol{x}}=\boldsymbol{H}\ \boldsymbol{\tau}-\boldsymbol{\Lambda}\ \dot{\boldsymbol{x}}+\boldsymbol{a}_g^{\boldsymbol{offset}}\\ \boldsymbol{H}=\left(\boldsymbol{M}_p+\boldsymbol{J}_m^{\mathrm{T}}\ \boldsymbol{M}_a\ \boldsymbol{J}_m\right)^{-1}\boldsymbol{J}_m^{\mathrm{T}}\\ \boldsymbol{\Lambda}=\boldsymbol{H}\ \boldsymbol{M}_a\ \dot{\boldsymbol{J}}_m+\left(\boldsymbol{M}_p+\boldsymbol{J}_m^{\mathrm{T}}\ \boldsymbol{M}_a\ \boldsymbol{J}_m\right)^{-1}\boldsymbol{\Lambda}_c\\ \boldsymbol{a}_g^{\boldsymbol{offset}}=\left(\boldsymbol{M}_p+\boldsymbol{J}_m^{\mathrm{T}}\ \boldsymbol{M}_a\ \boldsymbol{J}_m\right)^{-1}m_p\ \boldsymbol{g},\\ \dim\left(\boldsymbol{H}\right)=4\times 6,\ \ \dim\left(\boldsymbol{a}_g^{\boldsymbol{offset}}\right)=4\times 1\\ \dim\left(\boldsymbol{\Lambda}\right)=4\times 4\end{cases} \tag{3.56}.$$

The relation (3.56) represents the direct dynamic model (DDM), which is unique. However, the inverse dynamic model (IDM) is not unique and is generally given by:

$$\begin{cases}\boldsymbol{\tau}=\boldsymbol{C}\left(\ddot{\boldsymbol{x}}+\boldsymbol{\Lambda}\ \dot{\boldsymbol{x}}-\boldsymbol{a}_g^{\boldsymbol{offset}}\right)+\left[\mathrm{null}\left(\boldsymbol{H}\right)\right]\boldsymbol{\lambda},\ \text{with:}\\ \boldsymbol{C}=\boldsymbol{H}^{*}:\ \text{pseudo-inverse of}\ \boldsymbol{H}\\ \boldsymbol{\lambda}\in\mathbb{R}^2\ \text{(arbitrary)}\end{cases} \tag{3.57}.$$

Yet, in our case, we consider the particular solution of the IDM with zero components along the null space of $\boldsymbol{H}$ (which corresponds also to the null space of $\boldsymbol{J}_m^{\mathrm{T}}$)[2], meaning $\boldsymbol{\lambda}=\boldsymbol{0}$.This is mathematically referred to as the minimum norm solution and can be achieved by control means (see **§4.2** in **Chapter 4**). Hence, the IDM is reduced to:

$$\boldsymbol{\tau}=\boldsymbol{C}\left(\ddot{\boldsymbol{x}}+\boldsymbol{\Lambda}\ \dot{\boldsymbol{x}}-\boldsymbol{a}_g^{\boldsymbol{offset}}\right) \tag{3.58}.$$

[1] The matrix $\dot{\boldsymbol{J}}_m$ can be easily derived from $\boldsymbol{J}_m$. Its expression is not given here being lengthy. Yet, it can be easily obtained using the symbolic MATLAB toolbox.

[2] Since $\boldsymbol{H}=\boldsymbol{S}^{-1}\boldsymbol{J}_m^{\mathrm{T}}$ where $\boldsymbol{S}=\left(\boldsymbol{M}_p+\boldsymbol{J}_m^{\mathrm{T}}\ \boldsymbol{M}_a\ \boldsymbol{J}_m\right)$ is supposedly non-singular square matrix; if $\boldsymbol{S}$ is singular, $\boldsymbol{S}^{-1}$ does not exist in the first place.

As a result, the simplified direct and inverse dynamic models have been easily derived. In the upcoming section, we present the dimensional synthesis based on two primary criteria. One of these criteria is related to the dynamic performance. The evaluation of this performance requires only the knowledge of IDM, which is expressed by (3.58).

3.3.7- Dimensional Synthesis Based on Dual Criteria: Precision and Dynamics

Dimensional synthesis is undeniably one of the most prominent steps in the design of any PKM. Therefore, it is essential to choose properly the optimization criteria as to fit the intended application, and its direct requirements. Moreover, we should be very careful about how we perform this optimization, especially if it is of multi-objective nature. In **§2.5**, we have made some suggestions in this matter, in which we recommended the use of Pareto-based methods. Here, we abide by the aforementioned guidelines and exploit our knowledge of the mechanism to the extreme to facilitate the optimization further.

In the case of ARROW V1, the targets have been clearly stated since the early beginning. These are precision and rapidity. This is in addition to being capable of supporting large external wrenches. Under these global goals, we can notice the involvement of several masked sub-criteria, such as singularity-related performance, accuracy, repeatability, resolution, rigidity, twist, wrench, and acceleration capacities. Nonetheless, as the rotational performances are less interesting and expected to be well, we concentrate, therefore, on the translational aspects of the above-mentioned requirements. Still, if we consider all these requirements as they are, we would end up with an optimization based on a huge number of criteria. As a result, it would become difficult not only to visualize the problem based on Pareto method[3], but also to properly make a decision. That is why, in what follows, we approach the problem by first simplifying the targets.

In fact, the rigidity of the PKM can be worked on via the proper dimensioning of the components (cross section of the arms, etc.), and its resulting errors can be even compensated by means of elasto-geometric calibration[4], if needed. Thus, rigidity can be omitted. Regarding precision terms, having the actuators of same nature, then all translational precision requirements can be considered simultaneously through $TPAF$ (the translational precision amplification factor defined in **§2.2.2**). Regarding singularity, we have studied it explicitly, and verified that no singular poses within the geometric accessible workspace excluding the boundary. Also, an investigation based on FVI_h, for some samples of geometric parameters, has demonstrated that the quality of singularity performance is acceptable. Therefore, singularity aspect can be omitted as well. As for the kinetostatic translational performance, we

[3] In general, when the number of criteria exceeds three, it becomes difficult to have a good visualization of the problem, even with the use of the parallel coordinates' concept.

[4] If elasto-geometric calibration is needed, it will not be more complex than the geometric one. This is since it will be sufficient to consider the deformation due to pure tension/compression forces in the arms.

have investigated it via FVI_p, defined in **§2.2.3.B**, for several different sets of geometric parameters. We have found that it is most often satisfactory for the requirements being $v_{req}^{p} = 0.25\,\dot{q}_{\max}$, and $f_{ereq}^{p} = 0.25\,\tau_{\max}$. Hence, we can omit FVI_p as primary criterion, provided we verify it later in a secondary step. In what concerns acceleration capabilities, we consider the isotropic linear acceleration starting from rest in the absence of any external non-gravitational wrench. This can give us a sufficient idea about the PKM acceleration capability. In particular, considering acceleration capacity in the absence of an external non-gravitational wrench is completely justifiable for contactless applications (e.g. laser cutting). This is since it complies with reality. In what concerns other contact machining applications, external wrench is important only in the machining phase. This latter phase is, however, characterized by being rather quasi-static than dynamic. In fact, in a contact application, the interest in elevated acceleration exists in the transient phase[5], which is characterized by the absence of any external non-gravitational wrench.

So in brief, the dimensional synthesis that we are going to present here is based on the dual criteria of precision and dynamics. The precision criterion is the worst $TPAF$, denoted by $WTPAF$, over the desired workspace, DWS. As for the dynamic criterion, it is the worst isotropic linear acceleration, denoted by $WILA$, over DWS. Yet, a verification on the secondary criterion FVI_p will be done on the chosen set of geometric parameters.

The following subsection (**§3.3.7.A**) discusses the optimization process and its results. Afterwards, **§3.3.7.B** presents the workspace analysis, and the detailed performance evaluation.

A- Synthesis Procedure and Its Results

Based on the spindle to be assembled on the platform, the latter's parameters (shown in **Fig. 3-8**) are set to the values given in **Table 3-2**. In this same table, the actuator characteristics are given as well. Regarding the inertia parameters, they are provided in **Table 3-3**.

Concerning DWS, it is defined as follows:

$$DWS: \begin{cases} -0.15\ \mathrm{m} \le y \le +0.15\ \mathrm{m} \\ -0.15\ \mathrm{m} \le z \le +0.15\ \mathrm{m} \\ -45^\circ \le \theta_z \le +45^\circ \end{cases} \qquad (3.59).$$

Notice that the workspace requirement regarding x-motion is not specified in (3.59), as it can be fulfilled by choosing the appropriate stroke length for the linear actuators.

Regarding the parameters to optimize, they are L_y, L_z, and $L_s = L_p$. These parameters must remain within the following ranges:

[5] It is the phase where no machining is done, but the TCP is moved rapidly from the current location to nearby the working piece.

Table 3-2: Platform and actuator characteristics.

Platform Parameters			
Symbol	**Value**	**Symbol**	**Value**
a	0.164 m	b_{cm}	–0.16 m
d	0.12 m	t_p	0.18 m

Actuator Maximal Capacities*			
Symbol	**Value**	**Symbol**	**Value**
$\tau_{\max}$	2500 N	$\dot{q}_{\max}$	5 to 7 m/s
***All actuators are identical. Their type is Ironless ETEL ILM12-060.**			

Table 3-3: ARROW V1: inertia parameters.

Item	Value	Item	Value
Individual Simple Slider Cart's Mass (chains I,II, V and VI)	≈ 8.513 kg	**Individual Parallelogram Slider Cart's Mass (chains III, and IV)**	≈ 8.939 kg
Platform's Mass	≈ 10.542 kg	**Platform's Inertia about its z-axis**	≈ 0.357 kg m^2
Simple Arm Linear Mass (after removing $L_o = 0.155$ m *)	≈ 0.645 kg/m	**Parallelogram Arm Linear Mass (after removing $L_o = 0.155$ m)**	≈ 1.290 kg/m
***Note that $L_o = 0.155$ m is the length of joint interfaces. We emphasize here that the mass of the joints on the side of the platform are added with their moment of inertia to the platform. On the other hand, the mass of the joints on the side of the sliders are added to their corresponding sliders directly.**			

$$\begin{cases} 0.35 \text{ m} \le L_y \le 0.5 \text{ m} \\ 0.314 \text{ m} \le L_z \le 0.5 \text{ m} \\ 0.69 \text{ m} \le L_s = L_p \le 1 \text{ m} \end{cases} \quad (3.60).$$

The lower bounds in (3.60) are to assure accessibility to DWS, defined in (3.59). As for the upper bounds in (3.60), they are based on the consideration of stiffness and compactness of ARROW V1. We mention also that imposing $L_s = L_p$ is done for the benefit of manufacturing.

The Pareto distribution is constructed by taking five equally spaced values for each interval of parameters, then evaluating the different compromises between the two major criteria: $WTPAF = \max_{\boldsymbol{x} \in DWS} \left(\text{TPAF}(\boldsymbol{x}) \right)$ and $WILA = \min_{\boldsymbol{x} \in DWS} \left(\text{ILA}(\boldsymbol{x}) \right)$, where:

- $\text{TPAF}(\boldsymbol{x})$ is the value of $TPAF$ for a pose $\boldsymbol{x}$, defined as in **§2.2.2**;
- $\text{ILA}(\boldsymbol{x})$ is a special case of the specific isotropic linear acceleration, ${}^d a_{iso}^{sp}$, defined in **§2.2.4**, in which we set: ${}^d v_{req} = 0$, ${}^d \omega_{req} = 0$, ${}^d \alpha_{req} = 0$, ${}^d f_{ereq} = 0$, and ${}^d m_{ereq} = 0$.

Note that the expression of $\text{ILA}(\boldsymbol{x})$ is reduced to what follows:

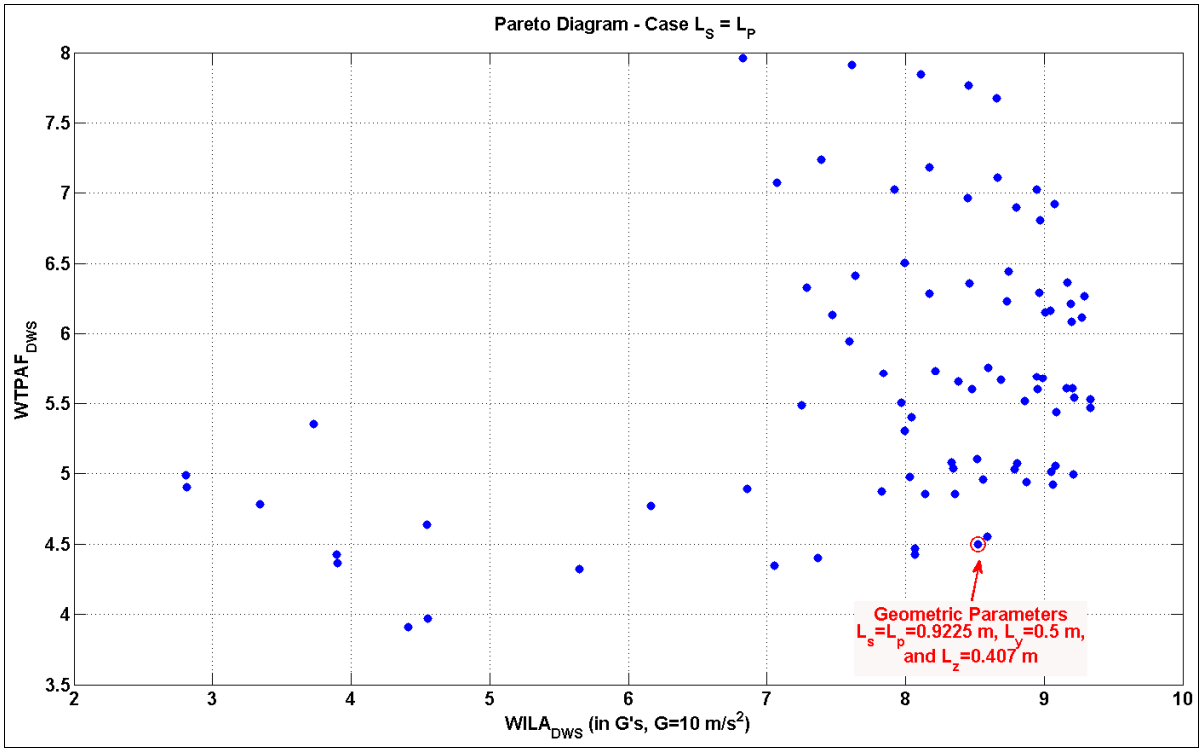

Fig. 3-9: Pareto diagram of ARROW V1 and the chosen geometric parameters.

$$\begin{cases} \mathrm{ILA}(\boldsymbol{x}) = \min_{i=1\ldots6}(\varepsilon_i), \text{ with:} \\ \varepsilon_i = \begin{cases} 0, \text{ if } \left(-\tau_{\max} + t_i^{off}\right) > 0 \text{ or } \left(\tau_{\max} + t_i^{off}\right) < 0 \\ \dfrac{\min\left(\left|-\tau_{\max} + t_i^{off}\right|, \left|\tau_{\max} + t_i^{off}\right|\right)}{\left\|\boldsymbol{c}_{\boldsymbol{pr}_i}\right\|}, \text{ if } \begin{pmatrix} \left(-\tau_{\max} + t_i^{off}\right) < 0 \text{ , } \left(\tau_{\max} + t_i^{off}\right) > 0 \\ \text{and } \left\|\boldsymbol{c}_{\boldsymbol{pr}_i}\right\| \neq 0 \end{pmatrix} \\ \infty, \text{ otherwise} \end{cases} \\ t_i^{off} : \text{ i-th component of } \boldsymbol{t}^{\boldsymbol{off}} = \boldsymbol{C}\, \boldsymbol{a}_{\boldsymbol{g}}^{\boldsymbol{off}} \\ \boldsymbol{c}_{\boldsymbol{pr}_i} : \text{ i-th row vector of } \boldsymbol{C}_{\boldsymbol{p}}, \text{ the translational part of } \boldsymbol{C} \\ \forall i = 1\ldots6 \end{cases} \quad (3.61).$$

The Pareto diagram is provided in **Fig. 3-9**. As it can be noticed from the figure, we did not only plot the Pareto-Front (limiting curve), but all the compromises. This allows us to visualize all possible options, in case we needed to reconsider our choice after verifying the secondary criterion. Based on the shown dual performances, we have decided to set the limits of acceptable solutions, or more precisely the trade-off in performances, to having $WTPAF \leq 4.5$, and $WILA \geq 8\ \mathrm{g}$. This trade-off is satisfied by three candidates, all of which have almost the same value of $WTPAF \approx 4.5$. So, we choose the one with the higher $WILA$, being equal to $8.5\ \mathrm{g}$ (it is encircled in red in **Fig. 3-9**). The investigation of the secondary criterion FVI_p, for $v_{req}^{p} = 0.25\,\dot{q}_{\max}$ and $f_{ereq}^{p} = 0.25\,\tau_{\max}$, shows that $FVI_p > 1.5$ over DWS. Hence, FVI_p is satisfied and therefore, the following geometric parameters are adopted (same as those shown in **Fig. 3-9**, but after some numerical adjustment):

$$\begin{cases} L_s = L_p = 0.93\ \text{m} \\ L_y = 0.5\ \text{m} \\ L_z = 0.41\ \text{m} \end{cases} \quad (3.62).$$

Having synthesized the geometric parameters of ARROW V1 based on Pareto method, the following subsection provides detailed performance evaluation and workspace analysis.

B- Workspace and Performance Evaluation of ARROW V1

We first proceed by presenting the evaluation relative to the dual criteria used in the dimensional synthesis, namely $TPAF$ and ILA. Also, we present the kinetostatic performance relative to v_{iso}^{p} and f_{eiso}^{p}, the pure isotropic linear speed and static force respectively. The plots of v_{iso}^{p} and f_{eiso}^{p} are more expressive than FVI_p, which is defined as $FVI_p = \min\left(v_{iso}^{p}/v_{req}^{p}, f_{eiso}^{p}/f_{ereq}^{p}\right)$ for $v_{req}^{p} = 0.25\,\dot{q}_{\max}$ and $f_{ereq}^{p} = 0.25\,\tau_{\max}$. The presentation is done as function of y and z, for $\theta_z = 0°$ on one hand, and for $\theta_z \in [-45°; +45°]$ on the other. In the presentation with $\theta_z \in [-45°; +45°]$, we highlight what follows. For each (y, z) couple, the performance index is calculated for several values of θ_z, then the worst value of the index is associated with the corresponding (y, z). In all these figures, we consider the legend defined below:

- Dotted black box represents the yz projection of the physical limits of the PKM, i.e. the floor, walls, and ceiling.
- Solid red box represents the limits that the TCP should not exceed in order to avoid collisions.
- Dotted magenta box represents DWS for which the PKM has been optimized.

$TPAF$ and ILA are depicted in **Fig. 3-10** and **Fig. 3-11**, respectively. We recall here that $TPAF$ holds not only a precision significance, but also an indication regarding peak linear speed, v_{peak}. As the actuators are identical, we have $v_{peak}/\dot{q}_{\max} = TPAF$. Based on this, we can say that the theoretical v_{peak} of ARROW V1 is 22.5 to $31.5\ \text{m/s}$. However, this speed occurs only along a particular direction and therefore, it is of least interest from the perspective of machine tools. Regarding ILA, we can notice that on the majority of DWS, the value of ILA is greater than $9\ \text{g}$, and reaches $10\ \text{g}$ for some region in the case of $\theta_z = 0°$. This is intriguing in comparison with the reported acceleration capabilities for some already available PKMs (refer to **Chapter 1**).

In **Fig. 3-12** and **Fig. 3-13**, v_{iso}^{p} and f_{eiso}^{p} of the optimized PKM are mapped into the workspace. The results show that on the majority of DWS, we have $v_{iso}^{p} \geq 0.5\,\dot{q}_{\max} = 2.5$ to $3.5\ \text{m/s}$ and $f_{eiso}^{p} \geq 0.84\,\tau_{\max} = 2100\ \text{N}$. These are quite remarkable, not due to the values in particular but more importantly the associated isotropy significance with them.

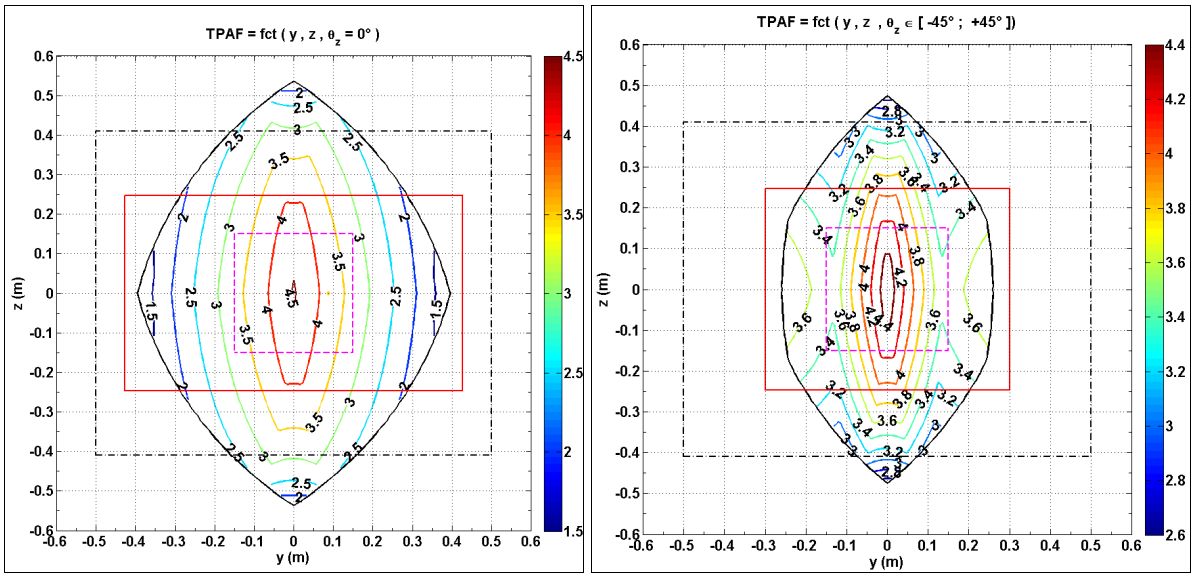

Fig. 3-10: $TPAF$ **of ARROW V1: case of** $\theta_z = 0°$ **(left) and case of** $|\theta_z| \leq 45°$ **(right).**

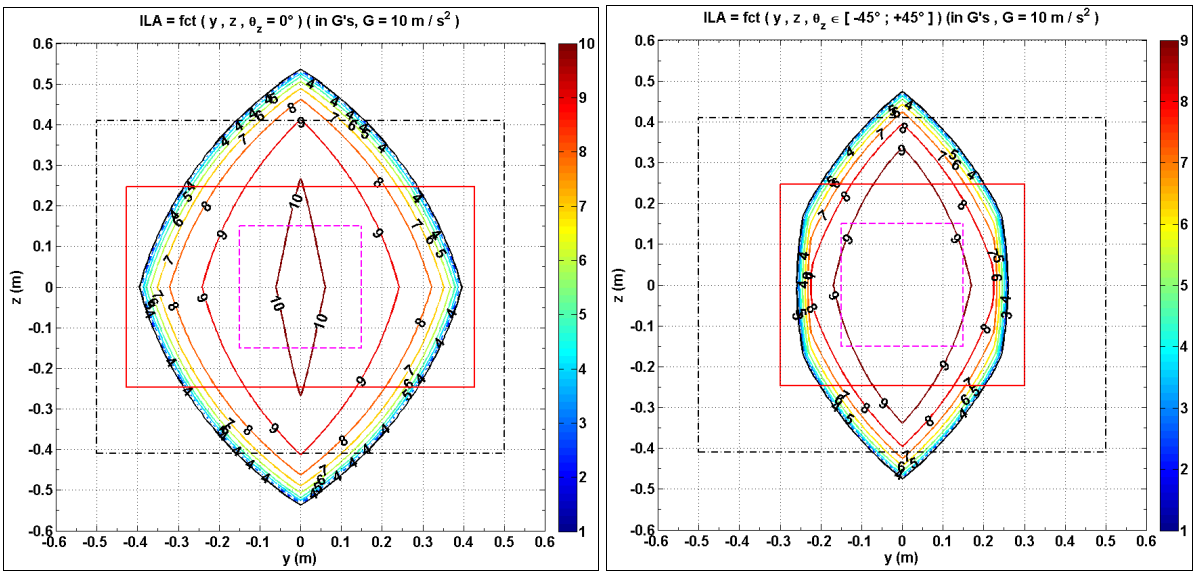

Fig. 3-11: ILA **of ARROW V1: case of** $\theta_z = 0°$ **(left) and case of** $|\theta_z| \leq 45°$ **(right).**

We went further in performance evaluation, in which we have investigated the peak linear acceleration, PLA, starting from rest and in the absence of an external non-gravitational wrench. The mathematical formulation of PLA is given hereafter:

$$\begin{cases} \mathrm{PLA}(\boldsymbol{x}) = \max\limits_{\boldsymbol{\tau} \in \boldsymbol{Z}_{\tau}^{min}} \left(\left\| \boldsymbol{H}_p \, \boldsymbol{\tau} + \boldsymbol{a}_{gp}^{\boldsymbol{offset}} \right\| \right) \\ \boldsymbol{Z}_{\tau}^{min} = \left\{ \boldsymbol{\tau} \in \mathbb{R}^6 ; \; \boldsymbol{\tau}^{\mathrm{T}} \left[\mathrm{null}(\boldsymbol{H}) \right] = \boldsymbol{0}_{1\times 2} \text{ and } |\tau_i| \leq \tau_{\max}, \, \forall i = 1...6 \right\} \\ \boldsymbol{H}_p : \text{ translational part of } \boldsymbol{H} \\ \boldsymbol{a}_{gp}^{\boldsymbol{offset}} = \left(a_{g_1}^{offset} \quad a_{g_2}^{offset} \quad a_{g_3}^{offset} \right)^{\mathrm{T}} : \text{ the first three components of } \boldsymbol{a}_{g}^{\boldsymbol{offset}} \end{cases} \tag{3.63}.$$

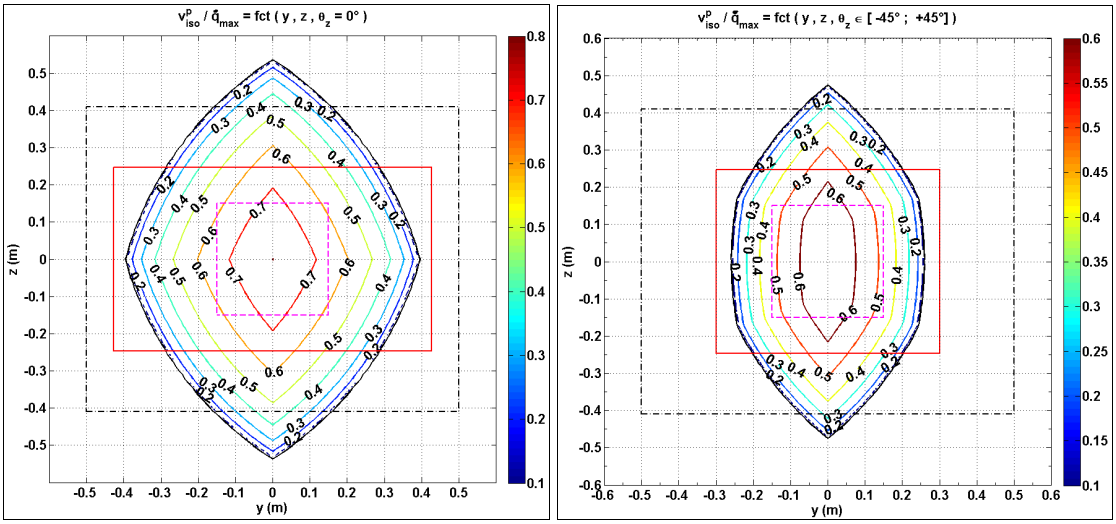

Fig. 3-12: v_{iso}^{p} **of ARROW V1: case of** $\theta_z = 0°$ **(left) and case of** $|\theta_z| \leq 45°$ **(right).**

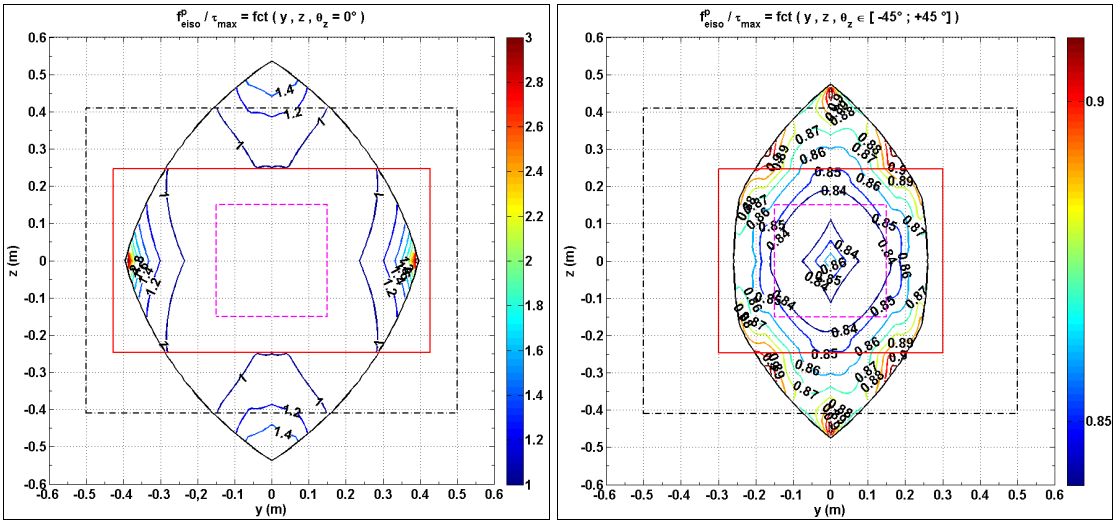

Fig. 3-13: f_{iso}^{p} **of ARROW V1: case of** $\theta_z = 0°$ **(left) and case of** $|\theta_z| \leq 45°$ **(right).**

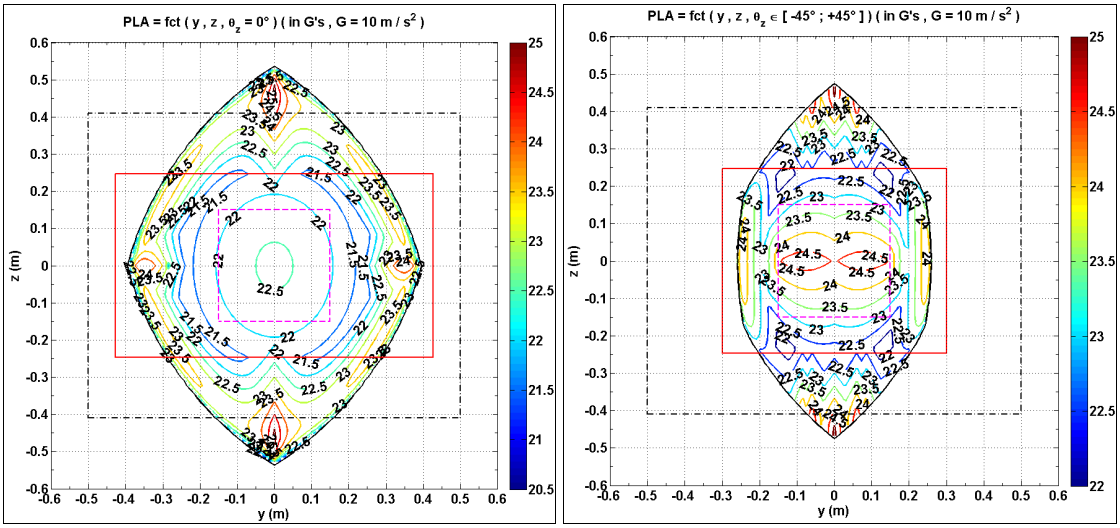

Fig. 3-14: PLA **of ARROW V1: case of** $\theta_z = 0°$ **(left) and case of** $|\theta_z| \leq 45°$ **(right).**

We emphasize that (3.63) can be computed analytically, in the very similar way as we have done for the operational resolutions in **§2.2.2**. The atlases of PLA are represented in **Fig. 3-14**. These show that PLA varies between $22.5\,\mathrm{g}$ and $24.5\,\mathrm{g}$ over DWS, which is interesting. In fact, we have $ILA/PLA \approx 9/22.5 \approx 40\%$ over the majority of DWS; this is noteworthy taking into account the isotropic nature of ILA and the direction-dependency of PLA. It is important to highlight here that the value of PLA associated with (y,z) in the case where $\theta_z \in [-45°;+45°]$ is the largest value of PLA attained for different orientations; i.e. the best value unlike the remaining performance indices where we assumed their worst values.

In addition to what we have mentioned, it is worth highlighting the smooth variations of the different performances over the global workspace. This rather homogenous aspect of performances is attributable to actuation redundancy.

Finally and for the sake of completeness, we provide a sample of the spatial workspaces of ARROW V1 in **Fig. 3-15** and **Fig. 3-16**. These are obtained for the following strokes of linear motors:

$$\begin{cases} \bullet \text{Actuators 1, 2, 5 and 6: Stroke Length} \approx 1.49\ \mathrm{m} \\ \bullet \text{Actuators 3 and 4 : Stroke Length} \approx 1.53\ \mathrm{m} \end{cases} \quad (3.64).$$

These workspaces correspond for the case of having $\theta_z = 0°$ and $\theta_z \in [-45°;+45°]$. Their plots demonstrate that the x-dimensions of the spatial workspaces are relatively acceptable in comparison with the maximum actuator stroke.

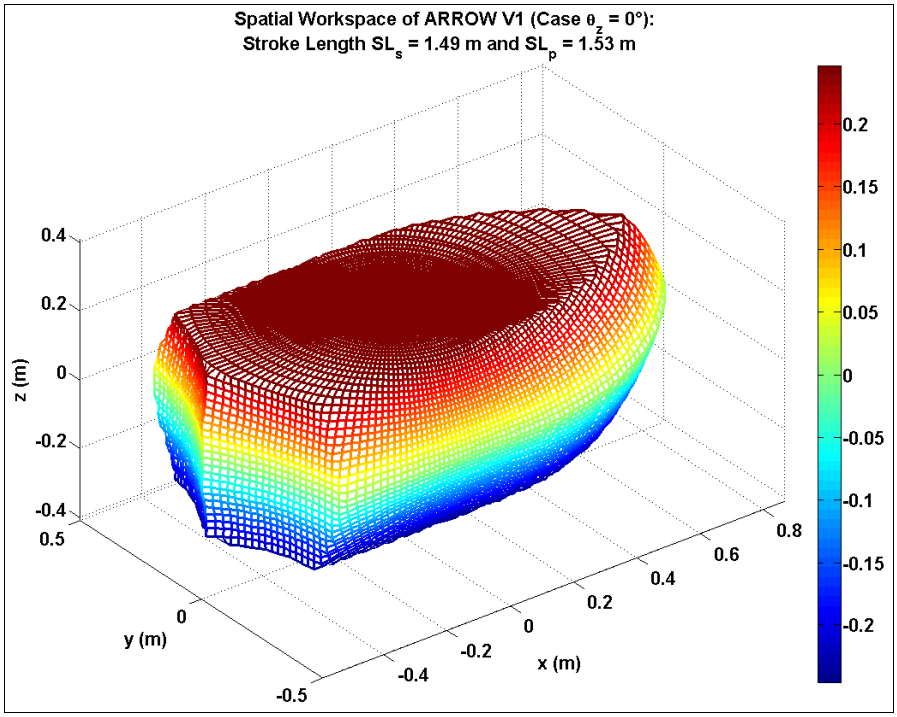

Fig. 3-15: Spatial workspace of ARROW VI in the case $\theta_z = 0°$ and for stroke lengths: $SL_s = 1.49\ \mathrm{m}$ (actuators 1, 2, 5 and 6) and $SL_p = 1.53\ \mathrm{m}$ (actuators 3 and 4).

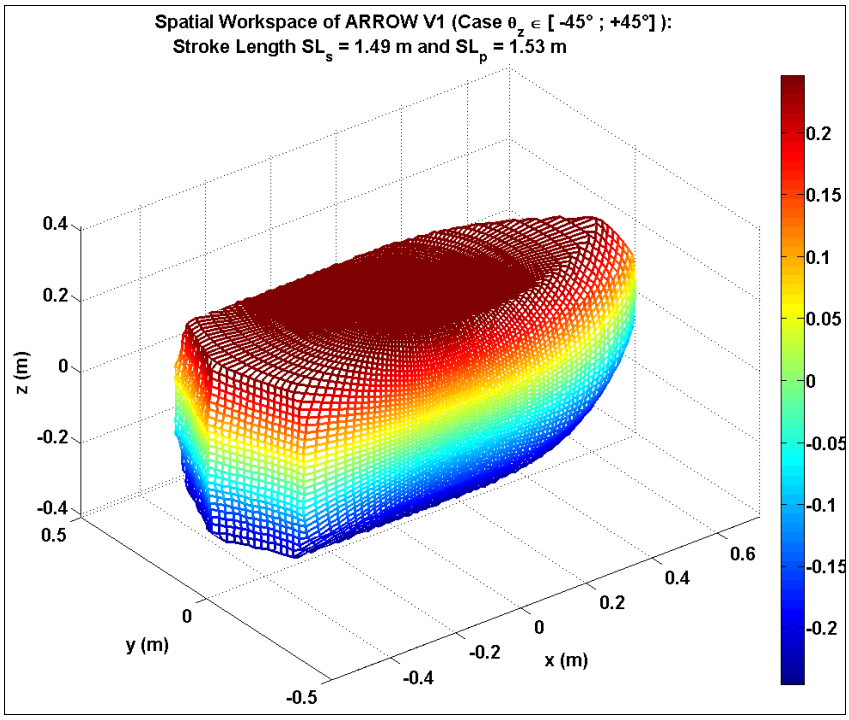

Fig. 3-16: Spatial workspace of ARROW VI in the case $|\theta_z| \leq 45°$ and for stroke lengths: $SL_s = 1.49$ m (actuators 1, 2, 5 and 6) and $SL_p = 1.53$ m (actuators 3 and 4)

3.3.8- Synopsis

In **§3.3**, we have introduced ARROW V1 PKM that is redundantly actuated and capable of four-dof (3T-1R) motion. This PKM is intended to serve as a branch in a left-hand right-hand based machine tool with five dofs (3T-2R). In this latter machine, the second rotational dof is provided by means of a turntable. The detailed analysis of this PKM, starting from its modeling and ending with its performance evaluation, has revealed undeniable characteristics, such as:

1. Large workspace and tilting capacity;
2. Design and modeling simplicities;
3. Absence of singularities within its workspace excluding its boundary;
4. Having arms under tension/compression and therefore, amelioration of precision thanks to the reduced deformation;
5. Performance homogeneity over the workspace;
6. Elevated precision, kinetostatic, and dynamic performances ($WTPAF = 4.5$, $v_{iso}^p \geq 0.5\,\dot{q}_{\max} = 2.5$ to 3.5 m/s , $f_{iso}^p \geq 0.84\,\tau_{\max} = 2100$ N , $WILA = 8.5$ g , and $PLA = 24.5$ g over DWS);
7. The relatively good ratio between the x-dimension of the spatial workspaces and the maximum available stroke length for the actuators.

In comparison with MachLin5 presented in **§3.2**, ARROW V1 has the advantage of having only two parallel walls on which the actuators are placed. This is not to mention the enhanced structural symmetry of the architecture and its simplicity. In this scope, the design can be made

even simpler for implementation by considering the suggestions given in **§3.2.1** regarding the execution of the spherical joints. Nevertheless, the main feature of having independent x-motion is compromised when adding the turntable. In fact, there are two main options for adding the turntable to have the eventual five-dof machine tool. These are described as follows:

1. First option: It consists of adding the turntable with its axis of rotation along the y-axis of the base frame of ARROW V1. This obviously does not make use of the independent x motion of the PKM. Therefore, it is not encouraged.
2. Second option: This consists of adding the turntable along the x-axis of the base frame of ARROW V1. However, this results in inevitable collisions between the turntable and the parallel module. Eventually, this not only reduces the exploitable workspace but also complicates motion planning.

In conclusion, ARROW V1, despite of its features, it is still not adequate to use with a turntable to achieve the five-dof (3T-2R) machine. Nonetheless, with a slight modification, we can arrive at a more feasible architecture. This modification is simply placing all the actuators on one wall and in pairs. The outcome is the ARROW V2 concept, the subject of upcoming part.

3.4- ARROW V2: From Theoretical Concept to Prototype Execution

3.4.1- ARROW V2: An Enhanced Version of ARROW V1

ARROW V2 is an evolution of ARROW V1, aiming at overcoming the latter's drawbacks. The CAD views of the PKM and its platform are shown in **Fig. 3-17** and **Fig. 3-18**, respectively. Regarding the graph diagram, it is the same as that of ARROW V1 (see **Fig. 3-7**). Moreover, regarding the execution of the spherical joints, the suggestions given in **§3.2.1** are applicable here as well.

In **Fig. 3-19**, the five-dof (3T-2R) machine tool based on ARROW V2 is shown. It obeys left-hand right-hand paradigm, in which a turntable is added facing the parallel module. The turntable has its axis aligned along the x-direction of the base frame. With this configuration, several benefits are obtained in comparison with ARROW V1:

1. All the actuators lay in the same plane. Thus, we only need to perfect the planarity of one surface instead of two.
2. Having each pair of actuators share a common track is profitable in three aspects. These are enumerated below:
   a) We only need to control the parallelism of three linear guides instead of six.
   b) The number of geometric parameters is decreased, which facilitates geometric calibration.
   c) The overall costs are reduced.

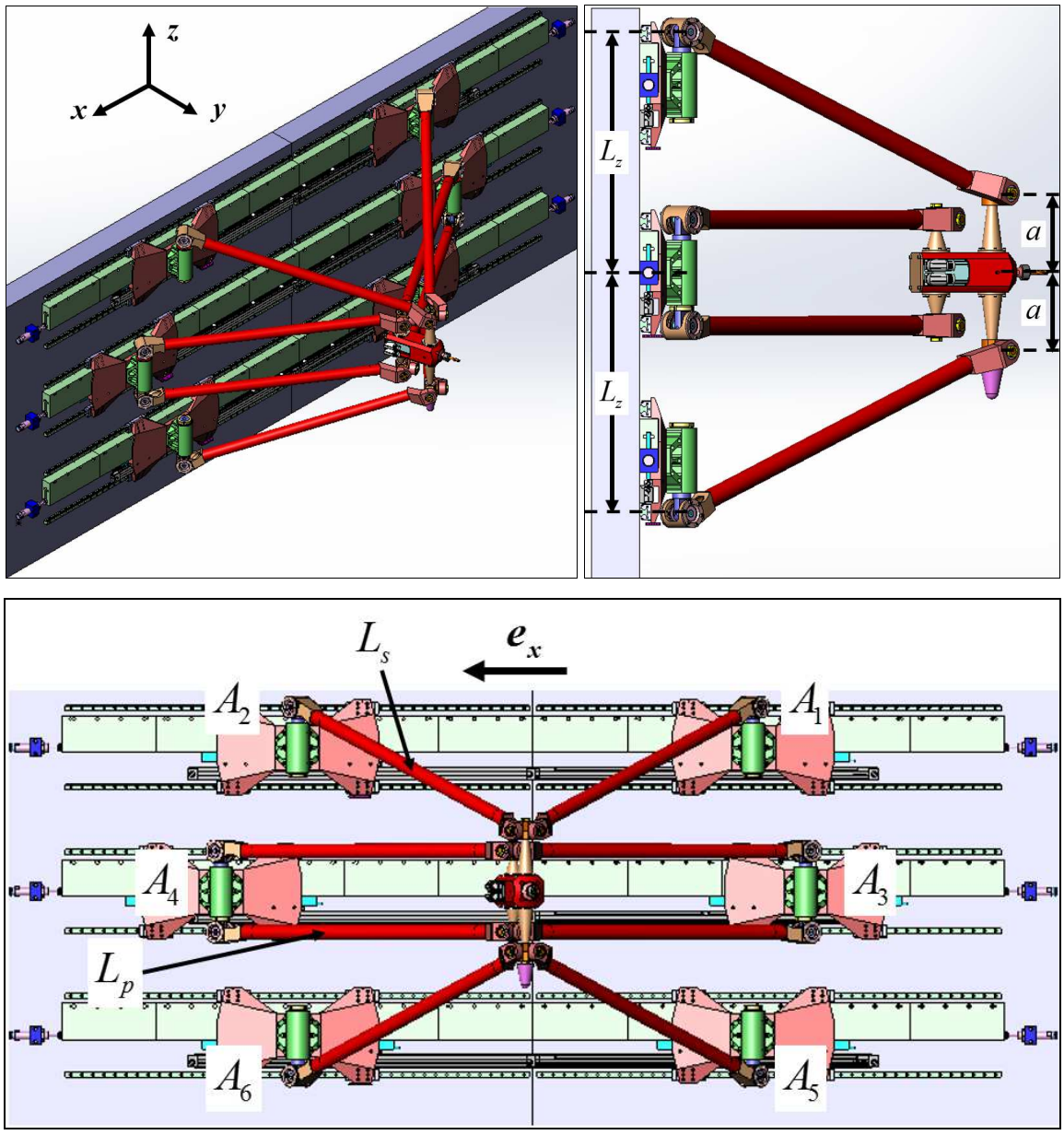

Fig. 3-17: ARROW V2: CAD views and notations.

3. Though there is still a possibility of collision between the turntable and the parallel module, it is not that severe.

As the principle of functioning of ARROW V2 is the same as its precursor and as its models are derivable in the very same manner, we are going to directly give these models in what follows and just concentrate on the singularity analysis. However, it is worth emphasizing that for ARROW V2 to function properly, still the condition of having $L_z \neq a$ must be satisfied. In fact, practicality necessitates having $L_z > a$.

A- Inverse Geometric Model (IGM)

Knowing the pose $\boldsymbol{x} = \begin{pmatrix} x & y & z & \theta_z \end{pmatrix}^{\mathrm{T}}$, the joint positions $\boldsymbol{q} = \begin{pmatrix} q_1 & \cdots & q_6 \end{pmatrix}^{\mathrm{T}}$ are given by:

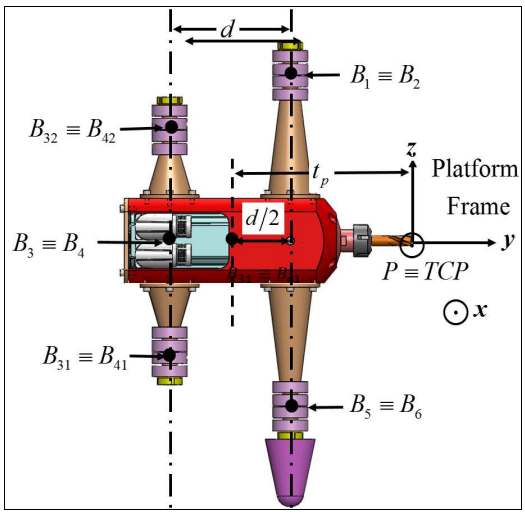

Fig. 3-18: The platform of ARROW V2 and its corresponding notations.

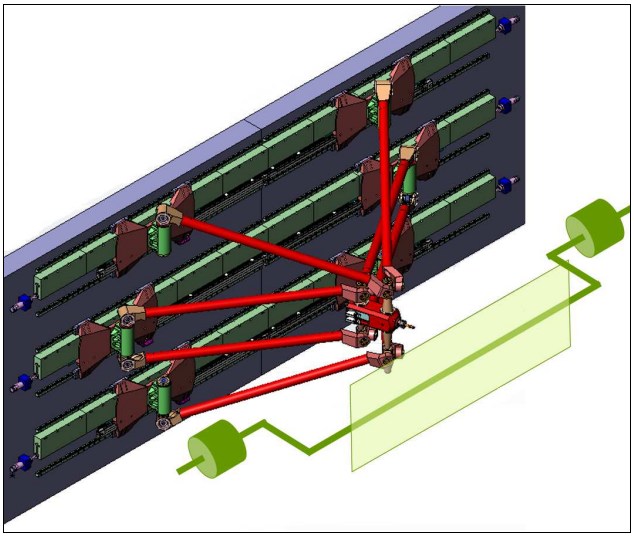

Fig. 3-19: The five-dof (3T-2R) machine tool: ARROW V2 with turntable.

$$q_i = x_i = x_{bi} + (-1)^i \sqrt{L_i^2 - \left(y_{bi} - y_i\right)^2 - \left(z_{bi} - z_i\right)^2} \tag{3.65},$$

with:

$$\begin{cases} \boldsymbol{B}_i = \begin{pmatrix} x_{bi} & y_{bi} & z_{bi} \end{pmatrix} = \boldsymbol{P} + \boldsymbol{R}\,\boldsymbol{B}_i^{plat} \\ \boldsymbol{P} = \begin{pmatrix} x & y & z \end{pmatrix}^{\mathrm{T}},\ \boldsymbol{R} = \mathrm{Rot}_z\left(\theta_z\right) \\ \boldsymbol{A}_i = \begin{pmatrix} x_i & y_i & z_i \end{pmatrix}^{\mathrm{T}} = \begin{pmatrix} q_i & y_i & z_i \end{pmatrix}^{\mathrm{T}},\ y_i = 0 \\ z_i = \begin{cases} L_z, \text{ if } i = 1,2 \\ 0, \text{ if } i = 3,4 \\ -L_z, \text{ otherwise} \end{cases},\ L_i = \left\| \boldsymbol{A}_i \boldsymbol{B}_i \right\| = \begin{cases} L_s, \text{ if } i = 1,2,5,6 \\ L_p, \text{ otherwise} \end{cases} \\ \forall i = 1 \ldots 6 \end{cases} \tag{3.66}$$

and $\boldsymbol{B}_i^{plat}$ $\left(\forall i = 1 \ldots 6\right)$ representing the coordinates of the points B_i in the platform frame of reference.

Note that (3.65) is based on the assembly mode condition described by:

$$x_i \le x_{bi} \equiv x_{b(i+1)} \le x_{i+1},\ \forall i = 1,3,5 \tag{3.67}$$

B- Direct Geometric Model (DGM)

The DGM can be derived exactly as described in **§3.3.3**. However, we are going here to benefit from the structural symmetry ($L_1 = L_2 = L_5 = L_6 = L_s$ and $L_3 = L_4 = L_p$) of ARROW V2 and compute directly the x components of points B_1 through B_6 as follows:

$$\begin{cases} \left(x_{b1} \equiv x_{b2}\right) = \left(x_{b5} \equiv x_{b6}\right) = \dfrac{x_1 + x_2}{2} = \dfrac{x_5 + x_6}{2} \\ x_{b3} \equiv x_{b4} = \dfrac{x_3 + x_4}{2} \end{cases}, \text{ with: } x_i = q_i,\ \forall i = 1...6 \tag{3.68}$$

As result, we can calculate the two possible solutions for $\theta_z \in \left]-\pi;+\pi\right]$, denoted by θ_z^{s1} and θ_z^{s2}, and the unique solution of x via:

$$\theta_z = \begin{cases} \theta_z^{s1} = \operatorname{asin}\left(\dfrac{x_{b3} - x_{b1}}{d}\right) \\ \text{or} \\ \theta_z^{s2} = \begin{cases} \pi - \operatorname{asin}\left(\dfrac{x_{b3} - x_{b1}}{d}\right), \text{ if } \left(x_{b3} - x_{b1}\right) \ge 0 \\ -\pi - \operatorname{asin}\left(\dfrac{x_{b3} - x_{b1}}{d}\right), \text{ otherwise} \end{cases} \end{cases} \tag{3.69}$$

and

$$x = x_1 - \left(t_p - \frac{d}{2}\right)\sin\left(\theta_z\right) = x_1 - \left(t_p - \frac{d}{2}\right)\left(\frac{x_{b3} - x_{b1}}{d}\right) \tag{3.70}$$

To get y and z, we only need to determine the intersection of the two circles (in the vertical plane $x = x_{b1}$) described by:

$$\begin{cases} \boldsymbol{A}_1\boldsymbol{B}_1^2 = L_1^2 = L_s^2 \\ \boldsymbol{A}_5'\boldsymbol{B}_1^2 = L_5^2 = L_s^2 \\ x_{b1} = \dfrac{x_1 + x_2}{2} = \dfrac{q_1 + q_2}{2} \end{cases}, \text{ with: } \boldsymbol{A}_5' = \boldsymbol{A}_5 + 2\,a\,\boldsymbol{e_z} \tag{3.71}$$

From (3.71), two possible solutions exist, say: $\boldsymbol{B}_1^{ss1}$ and $\boldsymbol{B}_1^{ss2}$. The acceptable solution is the one with $y_{b1} \ge 0$. Hence, we get a unique solution for $\boldsymbol{B}_1$. Based on $\boldsymbol{B}_1$, we get:

$$\begin{cases} z = \left(z_{b3} \equiv z_{b4}\right) = z_{b1} - a \\ \left(z_{b5} \equiv z_{b6}\right) = z_{b1} - 2\,a \end{cases} \tag{3.72}$$

Knowing $x_{b3} \equiv x_{b4}$ and $z_{b3} \equiv z_{b4}$, the term $y_{b3} \equiv y_{b4}$ can be computed by using $\boldsymbol{A}_3\boldsymbol{B}_3^2 = L_3^2 = L_s^2$, which yields:

$$y_{b3} \equiv y_{b4} = y_3 \pm \sqrt{L_s^2 - \left(x_{b3} - x_3\right)^2 - \left(z_{b3} - z_3\right)^2} = y_3 \pm \sqrt{L_s^2 - \left(\frac{x_4 - x_3}{2}\right)^2 - \left(z_{b3} - z_3\right)^2} \quad (3.73).$$

But the condition $y_{b3} \equiv y_{b4} \geq y_3 = y_4 = 0$ must be satisfied. Therefore, we only accept the following solution for $y_{b3} \equiv y_{b4}$:

$$y_{b3} \equiv y_{b4} = y_3 + \sqrt{L_s^2 - \left(\frac{x_4 - x_3}{2}\right)^2 - \left(z_{b3} - z_3\right)^2} = \sqrt{L_s^2 - \left(\frac{x_4 - x_3}{2}\right)^2 - \left(z_{b3} - z_3\right)^2} \quad (3.74).$$

Based on the sign of $\left(y_{b1} - y_{b3}\right)$, we can then identify the valid solution for θ_z among $\left\{\theta_z^{s1}, \theta_z^{s1}\right\}$, which is:

$$\theta_z = \begin{cases} \theta_z^{s1}, \text{ if } \left(y_{b1} - y_{b3}\right) \geq 0 \\ \theta_z^{s2}, \text{ otherwise} \end{cases} \quad (3.75).$$

Hence, we easily derived the DGM of ARROW V2 in a slight different fashion, in which we exploited the structural symmetry of the robot.

C- Kinematic Model

Similarly to what have been done in **§3.3.3**, we can effortlessly establish the relation between $\dot{\boldsymbol{q}}$ and $\dot{\boldsymbol{x}}$. This kinematic relation is:

$$\begin{cases} \boldsymbol{J}_{\boldsymbol{q}}\, \dot{\boldsymbol{q}} = \boldsymbol{J}_{\boldsymbol{x}}\, \dot{\boldsymbol{x}}, \text{ with:} \\ \boldsymbol{J}_{\boldsymbol{q}} = \text{diag}\left(\boldsymbol{n}_1^{\mathrm{T}}\, \boldsymbol{e}_{\boldsymbol{x}}, ..., \boldsymbol{n}_6^{\mathrm{T}}\, \boldsymbol{e}_{\boldsymbol{x}}\right), \ \dim\left(\boldsymbol{J}_{\boldsymbol{q}}\right) = 6 \times 6 \\ \boldsymbol{J}_{\boldsymbol{x}} = \begin{bmatrix} \boldsymbol{n}_1^{\mathrm{T}} & -\boldsymbol{n}_1^{\mathrm{T}}\left(\boldsymbol{P}\boldsymbol{B}_1 \times \boldsymbol{e}_{\boldsymbol{z}}\right) \\ \vdots & \vdots \\ \boldsymbol{n}_6^{\mathrm{T}} & -\boldsymbol{n}_6^{\mathrm{T}}\left(\boldsymbol{P}\boldsymbol{B}_6 \times \boldsymbol{e}_{\boldsymbol{z}}\right) \end{bmatrix}, \ \dim\left(\boldsymbol{J}_{\boldsymbol{x}}\right) = 6 \times 4 \\ \boldsymbol{n}_i = \dfrac{\boldsymbol{A}_i\boldsymbol{B}_i}{\left\|\boldsymbol{A}_i\boldsymbol{B}_i\right\|}, \ \forall i = 1...6 \end{cases} \quad (3.76).$$

The inverse kinematic model (IKM) is given based on the inverse Jacobian, $\boldsymbol{J}_{\boldsymbol{m}}$, as below:

$$\text{IKM: } \dot{\boldsymbol{q}} = \boldsymbol{J}_{\boldsymbol{m}}\, \dot{\boldsymbol{x}}, \text{ with: } \boldsymbol{J}_{\boldsymbol{m}} = \boldsymbol{J}_{\boldsymbol{q}}^{-1}\, \boldsymbol{J}_{\boldsymbol{x}} \quad (3.77).$$

On the other hand, the direct kinematic model (DKM) is established by performing a pseudo inversion procedure as follows:

$$\text{DKM: } \dot{\boldsymbol{x}} = \boldsymbol{J}\, \dot{\boldsymbol{q}} = \boldsymbol{J}_{\boldsymbol{m}}^{*}\, \dot{\boldsymbol{q}}, \text{ provided that } \dot{\boldsymbol{q}}^{\mathrm{T}} \left[\text{null}\left(\boldsymbol{J}_{\boldsymbol{m}}^{\mathrm{T}}\right)\right] = \boldsymbol{0}_{1\times 2} \quad (3.78).$$

As we have highlighted in **§3.3.3**, the relations (3.77) and (3.78) hold as long as $\boldsymbol{J}_{\boldsymbol{q}}$ and $\boldsymbol{J}_{\boldsymbol{x}}$ are non-singular.

D- Singularity Analysis

In analogy with ARROW V1, we proceed by analyzing constraint singularities, then the classical ones.

Constraint Singularities

In ARROW V1, the only constraint singularity has been identified as an architectural one. This is since it occurred for a particular set of geometric parameters. Nevertheless, in ARROW V2 it is not any more the case.

The constraint singularity is still related to the capability of the pair of parallelograms to restrict the undesired rotations (those about any axis laying in the xy plane of the base frame). Yet, it can occur for any general set of geometric parameters. In particular, it occurs when the two parallelograms become collinear. This would happen only in two configurations of $\boldsymbol{A}_3\boldsymbol{B}_3$ and $\boldsymbol{A}_4\boldsymbol{B}_4$. These are described below:

1. The first configuration is described by having $\boldsymbol{A}_3\boldsymbol{B}_3$ and $\boldsymbol{A}_4\boldsymbol{B}_4$ in the yz plane. This cannot happen except on the boundary of the geometric workspace. Additionally, it exists necessarily confounded with series-type singularity since it implies $\boldsymbol{n}_3^{\mathrm{T}}\,\boldsymbol{e}_x = \boldsymbol{n}_4^{\mathrm{T}}\,\boldsymbol{e}_x = 0 \Leftrightarrow \det\left(\boldsymbol{J}_q\right) = 0$ (refer to following part). This would not practically occur as inter-collisions between the third and fourth actuators will precede.
2. The second case is when $\boldsymbol{A}_3\boldsymbol{B}_3 // \boldsymbol{A}_4\boldsymbol{B}_4 // \boldsymbol{e}_x$; i.e. the two arms are aligned along the x axis. This also cannot practically befall as collisions antecede that.

Consequently, constraint singularities not only exist on the limits of the geometric workspace, but also cannot practically happen.

Series-Type Singularities

Such singularities exist when the $\boldsymbol{J}_q$ (in (3.76)) is rank deficient, which is equivalent to:

$$\det\left(\boldsymbol{J}_q\right) = 0 \Leftrightarrow \exists i_o \in \{1,\ldots,6\};\ \boldsymbol{n}_{i_o}^{\mathrm{T}}\,\boldsymbol{e}_x = 0 \Leftrightarrow \boldsymbol{n}_{i_o} \perp \boldsymbol{e}_x \qquad (3.79).$$

Fortunately, this not only cannot happen except on the boundary of the geometrically accessibly workspace, but is also preceded by inter-collisions between the actuators on the same linear track. This is since if $(2\,j-1)$-th arm (with $j=1,2,3$) is in the yz plane, the corresponding $(2\,j)$-th limb is necessarily laying in the aforementioned plane as well, and vice versa.

Parallel-Type Singularities

As usual, these happen when $\boldsymbol{J}_x$ becomes rank deficient. Simplifying $\boldsymbol{J}_x$ by linearly operating on it, we arrive at the following matrix $\boldsymbol{T}$ of same rank as $\boldsymbol{J}_x$:

$$\boldsymbol{T}=\begin{bmatrix} \boldsymbol{n}_1^{\mathrm{T}} & 0 \\ \boldsymbol{n}_2^{\mathrm{T}} & 0 \\ \boldsymbol{n}_3^{\mathrm{T}} & -\boldsymbol{n}_3^{\mathrm{T}}\left(\boldsymbol{r}\times\boldsymbol{e}_z\right) \\ \boldsymbol{n}_4^{\mathrm{T}} & -\boldsymbol{n}_4^{\mathrm{T}}\left(\boldsymbol{r}\times\boldsymbol{e}_z\right) \\ \boldsymbol{n}_5^{\mathrm{T}} & 0 \\ \boldsymbol{n}_6^{\mathrm{T}} & 0 \end{bmatrix},\ \text{with } \boldsymbol{r}=\boldsymbol{B}_1\boldsymbol{B}_3\equiv\boldsymbol{B}_1\boldsymbol{B}_4 \qquad (3.80).$$

Based on (3.80), we can assure that $\boldsymbol{T}$ (equivalently $\boldsymbol{J}_x$) is non-singular if the two submatrices, $\boldsymbol{TS}_1$ and $\boldsymbol{TS}_2$, defined by:

$$\boldsymbol{TS}_1=\begin{bmatrix}\boldsymbol{n}_1 & \boldsymbol{n}_2 & \boldsymbol{n}_5 & \boldsymbol{n}_6\end{bmatrix}^{\mathrm{T}} \qquad (3.81)$$

and

$$\boldsymbol{TS}_2=\begin{bmatrix} -\boldsymbol{n}_3^{\mathrm{T}}\left(\boldsymbol{r}\times\boldsymbol{e}_z\right) \\ -\boldsymbol{n}_4^{\mathrm{T}}\left(\boldsymbol{r}\times\boldsymbol{e}_z\right)\end{bmatrix} \qquad (3.82),$$

are of full rank.

$\boldsymbol{TS}_1$ is rank deficient when the four simple arms are coplanar. Since $L_z \neq a$, this would happen only in two configurations:

1. The simple arms are in the *yz* plane (i.e. arms completely stretched). This occurs confoundedly with a series-type singularity, and only on the boundary of the geometrically accessible workspace. In reality, it is not possible as collisions transpire prior to that.
2. The simple arms are in the *xz* plane, which is practically impossible being preceded by collisions as well.

On the other hand, the rank deficiency of $\boldsymbol{TS}_2$ necessitates having the parallelogram arms and $\boldsymbol{r}$ in the same vertical plane, which corresponds to two theoretically possible situations. The first case is having $\boldsymbol{n}_3$, $\boldsymbol{n}_4$, and $\boldsymbol{r}$ in the *xz* plane. Regarding the second situation, it corresponds to having the aforementioned three vectors in the *yz* plane (confounded with series-type singularities). In both cases, we have the same argument as discussed for $\boldsymbol{TS}_1$, summarized as being preceded by collisions.

Therefore, we can assure that ARROW V2 does not admit any parallel type singularity within the feasible workspace.

Results' Briefing

As a conclusion of the above analysis, we can assure that no singularities of any type exist within the feasible workspace. In fact, series singularities not only occur on the boundary of the geometric workspace, but also are practically infeasible due to prior arising of collisions. The same applies for parallel-type singularities. These have the possibility to occur on the boundary

of the geometric workspace, or in the situation where the arms and platform lay in the xz plane. Moreover, we highlight that unlike ARROW V1, the constraint singularities here are not of architectural nature. Nonetheless, their occurrence is limited to having the parallelograms in the yz plane or aligned along the x-axis of the base frame. Both cases are not to be worried about being practically infeasible.

3.4.2- Manufacturability Study of ARROW V2 and Its Mutated Versions

The simplicity of ARROW V2 and its brought in benefits have made it surpass the theoretical study into the implementation stage. In this phase, the manufacturability of each part, as well as the plans of fabrication and assembly, has been deeply investigated. Within the scope of this detailed examination, possible collisions between the arms have been put into attention.

In fact, based on the preliminary CAD presented in **Fig. 3-17** and due to the possibility of having inter-arm collisions for some poses within the workspace, a reconsideration of the design has been made. This reconsideration is particularly at the level of the U-joints that connect the arms to the spindle. To overcome the aforementioned conflict, several suggestions have been made. Among these proposals, only two have been considered and we refer to them by mutations, as they resulted in a topological change of the architecture, though the performances have not been noticeably compromised.

These mutations are described by replacing each of the concerned U-joints by two orthogonal but non-concurrent revolute ones (R-joints). The distance between these R-joints is kept small enough in order not to dramatically alter the global performances of the initial conceptual design. The new common graph diagram for the resulting mutated versions, called ARROW V2 M1/M2[6], is given in **Fig. 3-20**.

In **Fig. 3-21**, we depict the R-joints at the level of the platform in the case of ARROW V2 M1/M2. In the first version, ARROW V2 M1, the R joints are offset one from another while satisfying: $r_p = 0$ and $r \neq 0$ (see their interpretation in **Fig. 3-21**). On the other hand, in ARROW V2 M2, both offset distances, r_p and r, are non-zero. Though ARROW V2 M1 is a special case of ARROW V2 M2, it has been distinguished since its models are simpler to obtain. Nevertheless, the M2 version is better regarding collision avoidance. This can be clearly noticed from **Fig. 3-21**. Therefore, the decision has been made on the implementation of ARROW V2 M2.

However, we should emphasize that this mutation has resulted in some adverse effects. These are detailed as follows:

1. The establishment of the DGM is difficult, if not impossible.

[6] M1 and M2 stand for mutation type 1 and type 2, respectively.

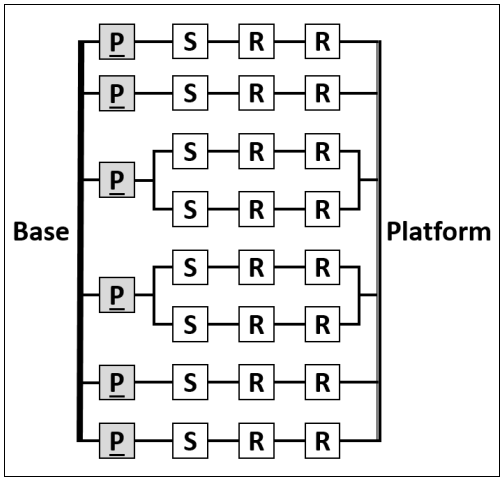

Fig. 3-20: Graph diagram of ARROW V2 M1/M2, the mutated versions of ARROW V2.

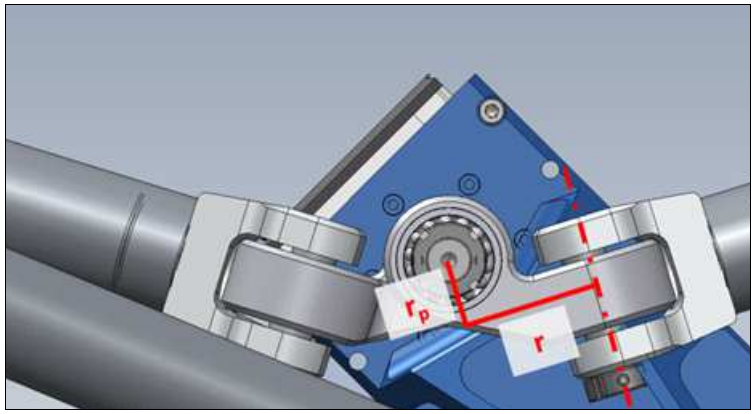

Fig. 3-21: Visualization of the offsets between the revolute joints in ARROW V2 M1/M2 versions (top view): ARROW V2 M1 corresponds to having $r_p = 0$ and $r \neq 0$, whereas ARROW V2 M2 corresponds to the situation where $r_p \neq 0$ and $r \neq 0$.

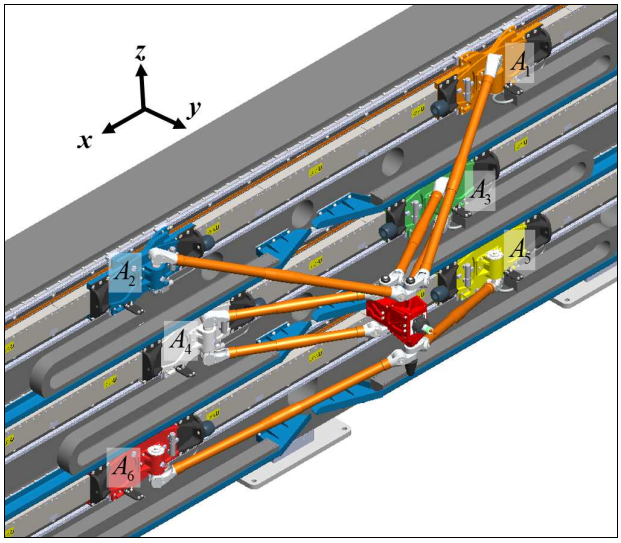

Fig. 3-22: ARROW V2 M2: 3D CAD view.

2. The other models, such as the inverse geometric and kinematic models, are not as straightforward as before.

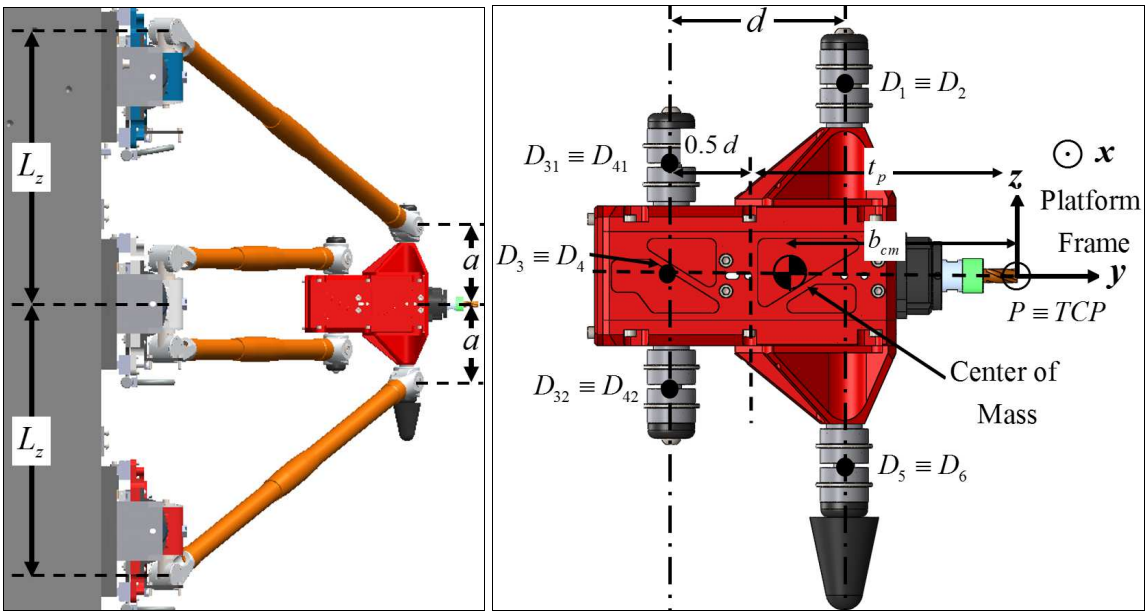

Fig. 3-23: ARROW V2 M2: projective CAD views with notations.

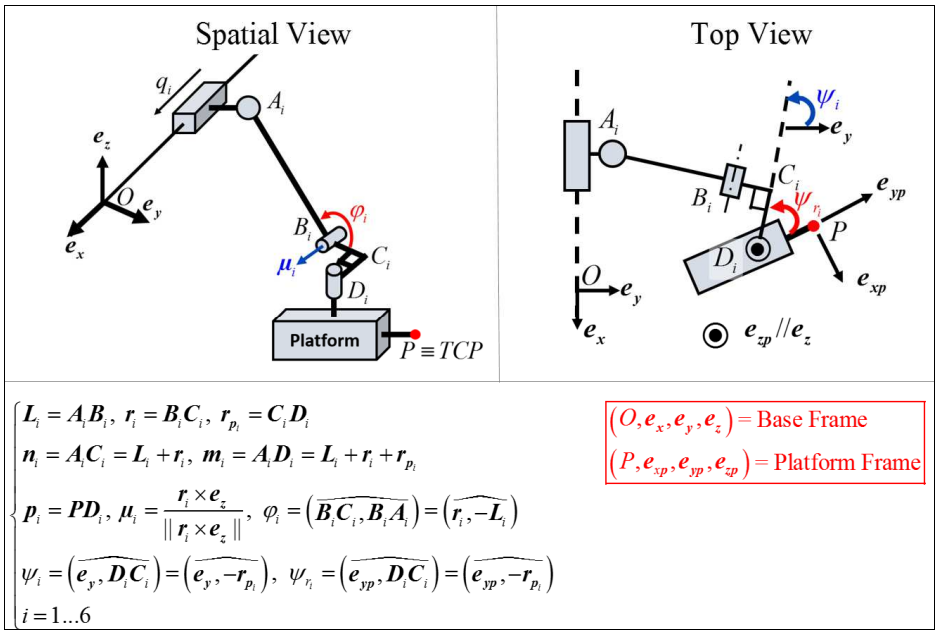

Fig. 3-24: ARROW V2 M2: schematic of a kinematic chain and its different notations.

3. Singularity analysis is more complex to perform.

Thus, it is indispensable to discuss the geometric and kinematic models as well as the singularity analysis of ARROW V2 M2. All these points, in addition to the dynamic model and the dimensional synthesis, will be discussed in the upcoming section.

3.4.3- ARROW V2 M2: The Implemented PKM

The CAD drawings of ARROW V2 M2 with some notations are given in **Fig. 3-22** and **Fig. 3-23**. **Fig. 3-24** presents a schematic of a kinematic chain of this PKM with additional symbols. These will be used later in modeling. Note that in the case of complex chains (i.e. chains (III) and (IV) with P-$(SRR)_2$ structure), the representation in **Fig. 3-24** corresponds to the virtual equivalent

PURR chain in the mediator plane of P-(SRR)$_2$. The lengths L_i $(\forall i=1,2,5,6)$ of the simple arms are equal to L_s. Regarding those of the complex ones (i.e. L_i with $i=3,4$), they are equal to L_p. Having clarified the different symbols and their geometric interpretation, in what follows, we present the models of ARROW V2 M2.

We emphasize that the modeling is based on the idea that the complex limbs maintain the same constraints as a classical pair of parallelograms. The validity of this assumption is proved later by investigating constraint singularities.

A- Inverse Geometric Model (IGM)

We denote the base-frame coordinates of the points A_i, B_i, C_i, and D_i by: $\boldsymbol{A}_i=\begin{pmatrix}x_i & y_i & z_i\end{pmatrix}^{\mathrm{T}}=\begin{pmatrix}q_i & y_i & z_i\end{pmatrix}^{\mathrm{T}}$, $\boldsymbol{B}_i=\begin{pmatrix}x_{bi} & y_{bi} & z_{bi}\end{pmatrix}^{\mathrm{T}}$, $\boldsymbol{C}_i=\begin{pmatrix}x_{ci} & y_{ci} & z_{ci}\end{pmatrix}^{\mathrm{T}}$, and $\boldsymbol{D}_i=\begin{pmatrix}x_{di} & y_{di} & z_{di}\end{pmatrix}^{\mathrm{T}}$, respectively and for all $i=1...6$. To derive the IGM, we use the following properties ($\forall i=1...6$):

1. Points A_i, B_i, and C_i are in the same vertical plane. This means that their projections on the xy plane are collinear.
2. Points B_i, C_i, and D_i lay in the same horizontal plane. Thus, they all have the same z component in the base frame.

Then, knowing the end-effector pose $\boldsymbol{x}=\begin{pmatrix}x & y & z & \theta_z\end{pmatrix}^{\mathrm{T}}$ and $\boldsymbol{p}_i^{plat}=\boldsymbol{P}\boldsymbol{D}_i^{plat}$ (the coordinates of D_i in the platform frame of reference), we get $\boldsymbol{D}_i$ as follows:

$$\begin{cases}\boldsymbol{D}_i=\begin{pmatrix}x_{di} & y_{di} & z_{di}\end{pmatrix}^{\mathrm{T}}=\boldsymbol{P}+\boldsymbol{R}\ \boldsymbol{p}_i^{plat},\ \text{with:}\\ \boldsymbol{P}=\begin{pmatrix}x & y & z\end{pmatrix}^{\mathrm{T}},\ \boldsymbol{R}=\mathrm{Rot}_z\left(\theta_z\right)\ \text{and}\ \boldsymbol{p}_i^{plat}=\boldsymbol{P}\boldsymbol{D}_i^{plat}\\ \forall i=1...6\end{cases} \tag{3.83}$$

Then, we proceed by getting the length L_{xyi} $(\forall i=1...6)$ of the xy projection of $\boldsymbol{L}_i=\boldsymbol{A}_i\boldsymbol{B}_i$, which is:

$$\begin{cases}L_{xyi}=\sqrt{L_i^2-\left(z_i-z_{bi}\right)^2},\ \text{with:}\\ L_i=\begin{cases}L_p,\ \text{if } i=3,4\\ L_s,\ \text{otherwise}\end{cases}\\ z_i=\begin{cases}L_z,\ \text{if } i=1,2\\ 0,\ \text{if } i=3,4\\ -L_z,\ \text{otherwise}\end{cases}\\ z_{bi}=z_{di}\end{cases},\ \forall i=1...6 \tag{3.84}$$

The length n_{xyi} $(\forall i=1...6)$ of the projection of $\boldsymbol{n}_i=\boldsymbol{A}_i\boldsymbol{C}_i$ on the xy plane is therefore computable and given by:

$$\begin{cases} n_{xyi} = L_{xyi} + r_i, \text{ with:} \\ r_i = \|\boldsymbol{r}_i\| = \|\boldsymbol{B}_i\boldsymbol{C}_i\| = r \end{cases}, \ \forall i = 1...6 \tag{3.85}$$

As the projections of A_i, C_i, and D_i on xy plane form a right triangle at C_i (for all $i = 1...6$), we can then compute the xy-projected length m_{xyi} of $\boldsymbol{m}_i = \boldsymbol{A}_i\boldsymbol{D}_i$, thanks to the relation hereafter:

$$\begin{cases} m_{xyi} = \sqrt{n_{xyi}^2 + r_{p_i}^2} = \sqrt{\left(L_{xyi} + r_i\right)^2 + r_{p_i}^2}, \text{ with :} \\ r_{p_i} = \|\boldsymbol{r}_{\boldsymbol{p}_i}\| = \|\boldsymbol{C}_i\boldsymbol{D}_i\| = r_p \end{cases}, \ \forall i = 1...6 \tag{3.86}$$

Based on (3.86), we can easily derive $q_i = x_i \ \left(\forall i = 1...6\right)$ by solving the following equation:

$$m_{xyi} = \sqrt{\left(x_{di} - x_i\right)^2 + \left(y_{di} - y_i\right)^2} = \sqrt{\left(x_{di} - q_i\right)^2 + \left(y_{di} - y_i\right)^2}, \ \forall i = 1...6 \tag{3.87}$$

which yields:

$$q_i = x_i = x_{di} \pm \sqrt{m_{xyi}^2 - \left(y_{di} - y_i\right)^2}, \ \forall i = 1...6 \tag{3.88}$$

But the assembly mode condition, described clearly in **Fig. 3-17**, dictates having:

$$q_i = x_i \le x_{di} \equiv x_{d(\,i+1\,)} \le q_{i+1} = x_{i+1}, \ \forall i = 1,3,5 \tag{3.89}$$

Hence, the IGM of ARROW V2 M2 is expressed by:

$$q_i = x_i = x_{di} + (-1)^i \sqrt{m_{xyi}^2 - \left(y_{di} - y_i\right)^2}, \ \forall i = 1...6 \tag{3.90}$$

B- Kinematic Model

Unlike the previously discussed architectures, the input-output kinematic relation is not as easy to get here, at least not in the usual compact form. Of course, it is still simple to get the inverse kinematic model (IKM) by differentiating the symbolic expression of the IGM. But this does not result in a suitable form for the Jacobians, $\boldsymbol{J}_{\boldsymbol{q}}$ and $\boldsymbol{J}_{\boldsymbol{x}}$, as to facilitate their analyses.

So, to establish the kinematic model in a more compact form, we start by defining the following quantities: $\boldsymbol{v} = \dot{\boldsymbol{P}}$, $\boldsymbol{\omega} = \dot{\theta}_z\,\boldsymbol{e}_z$, $\dot{\boldsymbol{\varphi}} = \begin{pmatrix} \dot{\varphi}_1 & \cdots & \dot{\varphi}_6 \end{pmatrix}^{\mathrm{T}}$, and $\dot{\boldsymbol{\psi}} = \begin{pmatrix} \dot{\psi}_1 & \cdots & \dot{\psi}_6 \end{pmatrix}^{\mathrm{T}}$. For the definition of angles φ_i and ψ_i, refer to **Fig. 3-24**. The absolute angular velocities of parts $B_iC_iD_i$ and A_iB_i are respectively given by:

$$\boldsymbol{\omega}_{\boldsymbol{p}_i} = \dot{\psi}_i\,\boldsymbol{e}_{\boldsymbol{z}}, \ \forall i = 1...6 \tag{3.91}$$

and

$$\boldsymbol{\omega}_{\boldsymbol{a}_i} = \dot{\varphi}_i\,\boldsymbol{\mu}_i + \dot{\psi}_i\,\boldsymbol{e}_{\boldsymbol{z}}, \ \forall i = 1...6 \tag{3.92}$$

Based on the aforementioned, we can then write the respective linear velocities of D_i and B_i as follows:

$$\boldsymbol{v}_{D_i} = \boldsymbol{v} + \boldsymbol{\omega} \times \boldsymbol{p}_i = \boldsymbol{v} - \left(\boldsymbol{p}_i \times \boldsymbol{e}_z\right)\dot{\theta}_z = \left[\mathbf{1}_{3\times 3} \quad -\left(\boldsymbol{p}_i \times \boldsymbol{e}_z\right)\right]\dot{\boldsymbol{x}}, \ \forall i = 1...6 \tag{3.93}$$

and

$$\boldsymbol{v}_{B_i} = \boldsymbol{v}_{D_i} + \boldsymbol{\omega}_{p_i} \times \boldsymbol{D}_i\boldsymbol{B}_i = \left[\mathbf{1}_{3\times 3} \quad -\left(\boldsymbol{p}_i \times \boldsymbol{e}_z\right) \quad \left(\left(\boldsymbol{r}_i + \boldsymbol{r}_{p_i}\right) \times \boldsymbol{e}_z\right)\right]\begin{pmatrix}\dot{\boldsymbol{x}} \\ \dot{\psi}_i\end{pmatrix}, \ \forall i = 1...6 \tag{3.94}.$$

As A_iB_i is supposedly a rigid body, we have:

$$\boldsymbol{L}_i^{\mathrm{T}}\, \boldsymbol{v}_{A_i} = \boldsymbol{L}_i^{\mathrm{T}}\, \boldsymbol{v}_{B_i}, \ \forall i = 1...6 \tag{3.95},$$

with the velocity of A_i being:

$$\boldsymbol{v}_{A_i} = \dot{q}_i\, \boldsymbol{e}_x, \ \forall i = 1...6 \tag{3.96}.$$

Substituting (3.94) and (3.96) in (3.95) yields the following relation:

$$\boldsymbol{L}_i^{\mathrm{T}}\, \boldsymbol{e}_x\, \dot{q}_i = \boldsymbol{L}_i^{\mathrm{T}}\, \boldsymbol{v} - \boldsymbol{L}_i^{\mathrm{T}}\left(\boldsymbol{p}_i \times \boldsymbol{e}_z\right)\dot{\theta}_z + \boldsymbol{L}_i^{\mathrm{T}}\left(\boldsymbol{r}_{p_i} \times \boldsymbol{e}_z\right)\dot{\psi}_i, \ \forall i = 1...6 \tag{3.97}.$$

As it is obvious from (3.97), $\dot{\boldsymbol{q}}$ and $\dot{\boldsymbol{x}}$ are coupled with $\dot{\boldsymbol{\psi}}$. Therefore, we need to find other relations. The aim from getting new relations is not only isolating $\dot{\boldsymbol{q}}$ and $\dot{\boldsymbol{x}}$, but also determining the angular velocities of the passive joints, in particular $\dot{\varphi}_i$ and $\dot{\psi}_i$ for all $i = 1...6$. To do that, we first write $\boldsymbol{v}_{A_i}$ in terms of $\boldsymbol{v}_{B_i}$ and $\boldsymbol{\omega}_{a_i}$ as hereafter:

$$\begin{cases} \boldsymbol{v}_{A_i} = \boldsymbol{v}_{B_i} + \boldsymbol{\omega}_{a_i} \times \left(-\boldsymbol{L}_i\right) \\ \quad = \boldsymbol{v} - \left(\boldsymbol{p}_i \times \boldsymbol{e}_z\right)\dot{\theta}_z + \left(\left(\boldsymbol{r}_i + \boldsymbol{r}_{p_i}\right) \times \boldsymbol{e}_z\right)\dot{\psi}_i + \boldsymbol{L}_i \times \left(\dot{\psi}_i\, \boldsymbol{e}_z + \dot{\varphi}_i\, \boldsymbol{\mu}_i\right) \\ \quad = \left[\mathbf{1}_{3\times 3} \quad -\left(\boldsymbol{p}_i \times \boldsymbol{e}_z\right) \quad \left(\boldsymbol{m}_i \times \boldsymbol{e}_z\right) \quad \left(\boldsymbol{L}_i \times \boldsymbol{\mu}_i\right)\right]\begin{pmatrix}\dot{\boldsymbol{x}} \\ \dot{\psi}_i \\ \dot{\varphi}_i\end{pmatrix} \\ \forall i = 1...6 \end{cases} \tag{3.98}.$$

Then, the projection of (3.98) along $\boldsymbol{e}_z$ and $\boldsymbol{\mu}_i$ respectively leads to:

$$\boldsymbol{e}_z^{\mathrm{T}}\, \boldsymbol{v}_{A_i} = 0 = \boldsymbol{e}_z^{\mathrm{T}}\, \boldsymbol{v} + \boldsymbol{e}_z^{\mathrm{T}}\left(\boldsymbol{L}_i \times \boldsymbol{\mu}_i\right)\dot{\varphi}_i, \ \forall i = 1...6 \tag{3.99}$$

and

$$\boldsymbol{\mu}_i^{\mathrm{T}}\, \boldsymbol{v}_{A_i} = \boldsymbol{\mu}_i^{\mathrm{T}}\, \boldsymbol{e}_x\, \dot{q}_i = \boldsymbol{\mu}_i^{\mathrm{T}}\, \boldsymbol{v} - \boldsymbol{\mu}_i^{\mathrm{T}}\left(\boldsymbol{p}_i \times \boldsymbol{e}_z\right)\dot{\theta}_z + \boldsymbol{\mu}_i^{\mathrm{T}}\left(\boldsymbol{m}_i \times \boldsymbol{e}_z\right)\dot{\psi}_i, \ \forall i = 1...6 \tag{3.100}.$$

From (3.99), we get the following relation:

$$\begin{cases} \boldsymbol{J}_{\varphi}\,\dot{\boldsymbol{\varphi}} = \boldsymbol{J}_{x\varphi}\,\dot{\boldsymbol{x}} \;\Rightarrow\; \dot{\boldsymbol{\varphi}} = \boldsymbol{J}_{\varphi m}\,\dot{\boldsymbol{x}}, \text{ with:} \\ \boldsymbol{J}_{\varphi} = \mathrm{diag}\left(\boldsymbol{e}_z^{\mathrm{T}}\left(\boldsymbol{L}_1\times\boldsymbol{\mu}_1\right),...,\boldsymbol{e}_z^{\mathrm{T}}\left(\boldsymbol{L}_6\times\boldsymbol{\mu}_6\right)\right) \\ \boldsymbol{J}_{x\varphi} = \begin{bmatrix} -\boldsymbol{e}_z^{\mathrm{T}} & 0 \\ \vdots & \vdots \\ -\boldsymbol{e}_z^{\mathrm{T}} & 0 \end{bmatrix},\;\; \boldsymbol{J}_{\varphi m} = \boldsymbol{J}_{\varphi}^{-1}\,\boldsymbol{J}_{x\varphi} \\ \dim\left(\boldsymbol{J}_{\varphi}\right) = 6\times 6,\;\; \dim\left(\boldsymbol{J}_{x\varphi}\right) = \dim\left(\boldsymbol{J}_{\varphi m}\right) = 6\times 4 \end{cases} \tag{3.101}$$

The system of equations of (3.97) and (3.100) can be written under the following matrix form (for each $i = 1...6$):

$$\begin{cases} \boldsymbol{M}_{q\psi_i}\begin{pmatrix}\dot{q}_i \\ \dot{\psi}_i\end{pmatrix} = \boldsymbol{M}_{x_i}\,\dot{\boldsymbol{x}}, \text{ with:} \\ \boldsymbol{M}_{q\psi_i} = \begin{bmatrix} \boldsymbol{L}_i^{\mathrm{T}}\,\boldsymbol{e}_x & -\boldsymbol{L}_i^{\mathrm{T}}\left(\boldsymbol{r}_{p_i}\times\boldsymbol{e}_z\right) \\ \boldsymbol{\mu}_i^{\mathrm{T}}\,\boldsymbol{e}_x & -\boldsymbol{\mu}_i^{\mathrm{T}}\left(\boldsymbol{m}_i\times\boldsymbol{e}_z\right) \end{bmatrix},\;\; \dim\left(\boldsymbol{M}_{q\psi_i}\right) = 2\times 2 \\ \boldsymbol{M}_{x_i} = \begin{bmatrix} \boldsymbol{L}_i^{\mathrm{T}} & -\boldsymbol{L}_i^{\mathrm{T}}\left(\boldsymbol{p}_i\times\boldsymbol{e}_z\right) \\ \boldsymbol{\mu}_i^{\mathrm{T}} & -\boldsymbol{\mu}_i^{\mathrm{T}}\left(\boldsymbol{p}_i\times\boldsymbol{e}_z\right) \end{bmatrix},\;\; \dim\left(\boldsymbol{M}_{x_i}\right) = 2\times 4 \end{cases} \tag{3.102}$$

Resolving (3.102) for $\dot{q}_i$ and $\dot{\psi}_i$, we get:

$$\begin{cases} \begin{pmatrix}\dot{q}_i \\ \dot{\psi}_i\end{pmatrix} = \boldsymbol{M}_{q\psi_i}^{-1}\,\boldsymbol{M}_{x_i}\,\dot{\boldsymbol{x}}, \text{ with:} \\ \boldsymbol{M}_{q\psi_i}^{-1} = \dfrac{1}{\det\left(\boldsymbol{M}_{q\psi_i}\right)}\begin{bmatrix} -\boldsymbol{\mu}_i^{\mathrm{T}}\left(\boldsymbol{m}_i\times\boldsymbol{e}_z\right) & \boldsymbol{L}_i^{\mathrm{T}}\left(\boldsymbol{r}_{p_i}\times\boldsymbol{e}_z\right) \\ -\boldsymbol{\mu}_i^{\mathrm{T}}\,\boldsymbol{e}_x & \boldsymbol{L}_i^{\mathrm{T}}\,\boldsymbol{e}_x \end{bmatrix},\;\; \forall i = 1...6 \\ \det\left(\boldsymbol{M}_{q\psi_i}\right) = \left(\boldsymbol{m}_i^{\mathrm{T}}\,\boldsymbol{e}_x\right)\left(\boldsymbol{e}_z^{\mathrm{T}}\left(\boldsymbol{L}_i\times\boldsymbol{\mu}_i\right)\right) \end{cases} \tag{3.103}$$

which is valid provided that $\det\left(\boldsymbol{M}_{q\psi_i}\right) = \left(\boldsymbol{m}_i^{\mathrm{T}}\,\boldsymbol{e}_x\right)\left(\boldsymbol{e}_z^{\mathrm{T}}\left(\boldsymbol{L}_i\times\boldsymbol{\mu}_i\right)\right) \neq 0$.

Based on (3.103) and some simplifications, we arrive at the uncoupled relations between $\dot{\boldsymbol{q}}$ and $\dot{\boldsymbol{x}}$ on one hand, and between $\dot{\boldsymbol{\psi}}$ and $\dot{\boldsymbol{x}}$ on the other. These are given below as:

$$\begin{cases} \boldsymbol{J}_{\boldsymbol{q}}\,\dot{\boldsymbol{q}} = \boldsymbol{J}_{\boldsymbol{x}}\,\dot{\boldsymbol{x}} \;\Rightarrow\; \dot{\boldsymbol{q}} = \boldsymbol{J}_{\boldsymbol{m}}\,\dot{\boldsymbol{x}} \\ \boldsymbol{J}_{\boldsymbol{q}} = \mathrm{diag}\left(\left(\boldsymbol{m}_1^{\mathrm{T}}\,\boldsymbol{e}_x\right)\left(\boldsymbol{e}_z^{\mathrm{T}}\left(\boldsymbol{L}_1\times\boldsymbol{\mu}_1\right)\right),...,\left(\boldsymbol{m}_6^{\mathrm{T}}\,\boldsymbol{e}_x\right)\left(\boldsymbol{e}_z^{\mathrm{T}}\left(\boldsymbol{L}_6\times\boldsymbol{\mu}_6\right)\right)\right) \\ \boldsymbol{J}_{\boldsymbol{x}}: \begin{cases} \boldsymbol{J}_x(i,1) = \left(\boldsymbol{e}_z^{\mathrm{T}}\left(\boldsymbol{L}_i\times\boldsymbol{\mu}_i\right)\right)\left(\boldsymbol{e}_x^{\mathrm{T}}\,\boldsymbol{m}_i\right),\; \boldsymbol{J}_x(i,2) = \left(\boldsymbol{e}_z^{\mathrm{T}}\left(\boldsymbol{L}_i\times\boldsymbol{\mu}_i\right)\right)\left(\boldsymbol{e}_y^{\mathrm{T}}\,\boldsymbol{m}_i\right) \\ \boldsymbol{J}_x(i,3) = \left(\boldsymbol{e}_z^{\mathrm{T}}\left(\boldsymbol{n}_i\times\boldsymbol{\mu}_i\right)\right)\left(\boldsymbol{e}_z^{\mathrm{T}}\,\boldsymbol{m}_i\right),\; \boldsymbol{J}_x(i,4) = -\left(\boldsymbol{e}_z^{\mathrm{T}}\left(\boldsymbol{L}_i\times\boldsymbol{\mu}_i\right)\right)\left(\boldsymbol{e}_z^{\mathrm{T}}\left(\boldsymbol{m}_i\times\boldsymbol{p}_i\right)\right) \\ \forall i = 1...6 \end{cases} \\ \boldsymbol{J}_{\boldsymbol{m}} = \boldsymbol{J}_{\boldsymbol{q}}^{-1}\,\boldsymbol{J}_{\boldsymbol{x}} \\ \dim\left(\boldsymbol{J}_{\boldsymbol{q}}\right) = 6\times 6,\;\; \dim\left(\boldsymbol{J}_{\boldsymbol{x}}\right) = 6\times 4,\;\; \dim\left(\boldsymbol{J}_{\boldsymbol{m}}\right) = 6\times 4 \end{cases} \tag{3.104}$$

and

$$\begin{cases} \boldsymbol{J}_{\psi}\,\dot{\boldsymbol{\psi}} = \boldsymbol{J}_{x\psi}\,\dot{\boldsymbol{x}} \;\Rightarrow\; \dot{\boldsymbol{\psi}} = \boldsymbol{J}_{\psi m}\,\dot{\boldsymbol{x}} \\ \boldsymbol{J}_{\psi} = \mathrm{diag}\left(\left(\boldsymbol{m}_1^{\mathrm{T}}\,\boldsymbol{e}_x\right)\left(\boldsymbol{e}_z^{\mathrm{T}}\left(\boldsymbol{L}_1\times\boldsymbol{\mu}_1\right)\right),\ldots,\left(\boldsymbol{m}_6^{\mathrm{T}}\,\boldsymbol{e}_x\right)\left(\boldsymbol{e}_z^{\mathrm{T}}\left(\boldsymbol{L}_6\times\boldsymbol{\mu}_6\right)\right)\right) \\ \boldsymbol{J}_{x\psi} = \begin{bmatrix} 0 & \boldsymbol{e}_z^{\mathrm{T}}\left(\boldsymbol{L}_1\times\boldsymbol{\mu}_1\right) & -\left(\boldsymbol{e}_x^{\mathrm{T}}\,\boldsymbol{\mu}_1\right)\left(\boldsymbol{e}_z^{\mathrm{T}}\,\boldsymbol{L}_1\right) & \left(\boldsymbol{e}_x^{\mathrm{T}}\,\boldsymbol{p}_1\right)\left(\boldsymbol{e}_z^{\mathrm{T}}\left(\boldsymbol{L}_1\times\boldsymbol{\mu}_1\right)\right) \\ \vdots & \vdots & \vdots & \vdots \\ 0 & \boldsymbol{e}_z^{\mathrm{T}}\left(\boldsymbol{L}_6\times\boldsymbol{\mu}_6\right) & -\left(\boldsymbol{e}_x^{\mathrm{T}}\,\boldsymbol{\mu}_6\right)\left(\boldsymbol{e}_z^{\mathrm{T}}\,\boldsymbol{L}_6\right) & \left(\boldsymbol{e}_x^{\mathrm{T}}\,\boldsymbol{p}_6\right)\left(\boldsymbol{e}_z^{\mathrm{T}}\left(\boldsymbol{L}_6\times\boldsymbol{\mu}_6\right)\right) \end{bmatrix} \\ \boldsymbol{J}_{\psi m} = \boldsymbol{J}_{\psi}^{-1}\,\boldsymbol{J}_{x\psi} \\ \dim\left(\boldsymbol{J}_{\psi}\right) = 6\times 6,\ \ \dim\left(\boldsymbol{J}_{x\psi}\right) = \dim\left(\boldsymbol{J}_{\psi m}\right) = 6\times 4 \end{cases} \tag{3.105}$$

with $\boldsymbol{J}_x(i,j)$ denoting the element of the i-th row and j-th column of $\boldsymbol{J}_x$.

Hence, we have established all the necessary kinematic relations, not only the input-output one. The IKM is uniquely defined and given by $\dot{\boldsymbol{q}} = \boldsymbol{J}_m\,\dot{\boldsymbol{x}}$, with $\boldsymbol{J}_m$ being defined in (3.104). On the other hand, the direct kinematic model (DKM) is obtainable by means of a pseudo-inversion, as we are used to with redundantly actuated PKMs. We then get:

$$\text{DKM: } \dot{\boldsymbol{x}} = \boldsymbol{J}\,\dot{\boldsymbol{q}} = \boldsymbol{J}_m^{*}\,\dot{\boldsymbol{q}},\ \text{provided that } \dot{\boldsymbol{q}}^{\mathrm{T}}\left[\mathrm{null}\left(\boldsymbol{J}_m^{\mathrm{T}}\right)\right] = \boldsymbol{0}_{1\times 2} \tag{3.106}$$

The upcoming step is to analyze the singularities of the PKM at hand. This is crucial as to assure that the topological mutation has not adversely resulted in unanticipated singular configurations.

C- Singularity Analysis

Constraint Singularities

The main target here is to investigate whether the pair of complex chains, namely (III) and (IV), fulfills its premise in prohibiting undesired rotations of the platform (i.e. imposing $\omega_x = \omega_y = 0$: the x and y components of the angular velocity, $\boldsymbol{\omega}$, of the platform).

For this purpose, we consider the full twist, $\boldsymbol{t} = \left(\boldsymbol{v}^{\mathrm{T}}\quad \boldsymbol{\omega}^{\mathrm{T}}\right)^{\mathrm{T}} = \left(v_x\quad v_y\quad v_z\quad \omega_x\quad \omega_y\quad \omega_z\right)^{\mathrm{T}}$, of the end-effector and ignore all components of the PKM except the two limbs: (III) and (IV). Besides, we modify the point P (the TCP) to be confounded with $D_3 \equiv D_4$ for simplification purposes. In addition to the notation presented in **Fig. 3-24** that corresponds to the virtual equivalent chains of limbs (III) and (IV), we define similar vectorial and scalar quantities with subscripts ij (with $i = 3,4$ and $j = 1,2$) (refer to **Fig. 3-25**).

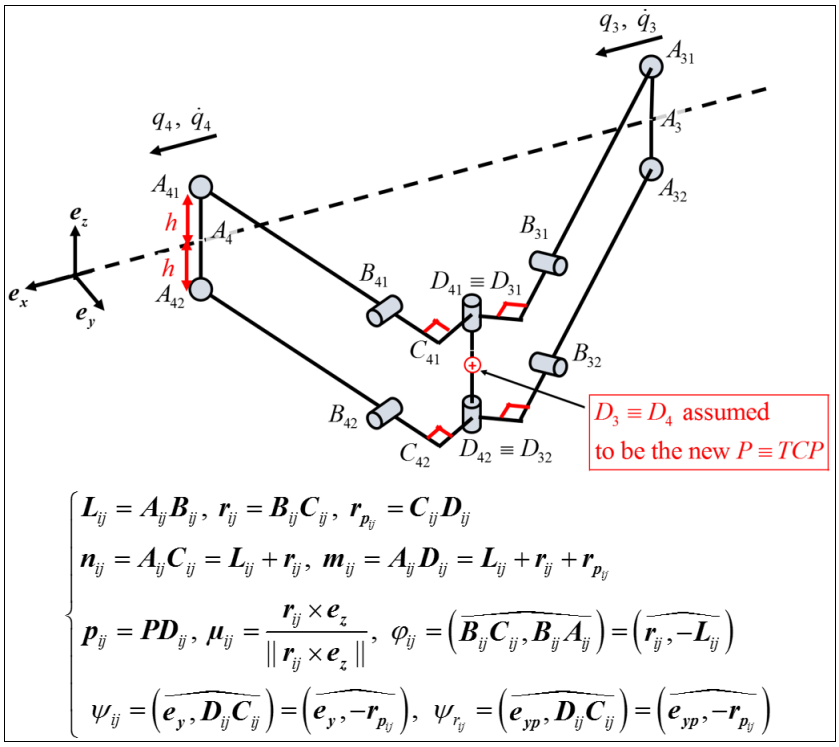

$$\begin{cases} \boldsymbol{L}_{ij} = \boldsymbol{A}_{ij}\boldsymbol{B}_{ij},\ \boldsymbol{r}_{ij} = \boldsymbol{B}_{ij}\boldsymbol{C}_{ij},\ \boldsymbol{r}_{p_{ij}} = \boldsymbol{C}_{ij}\boldsymbol{D}_{ij} \\ \boldsymbol{n}_{ij} = \boldsymbol{A}_{ij}\boldsymbol{C}_{ij} = \boldsymbol{L}_{ij} + \boldsymbol{r}_{ij},\ \boldsymbol{m}_{ij} = \boldsymbol{A}_{ij}\boldsymbol{D}_{ij} = \boldsymbol{L}_{ij} + \boldsymbol{r}_{ij} + \boldsymbol{r}_{p_{ij}} \\ \boldsymbol{p}_{ij} = \boldsymbol{P}\boldsymbol{D}_{ij},\ \boldsymbol{\mu}_{ij} = \dfrac{\boldsymbol{r}_{ij} \times \boldsymbol{e}_z}{\| \boldsymbol{r}_{ij} \times \boldsymbol{e}_z \|},\ \varphi_{ij} = \left(\widehat{\boldsymbol{B}_{ij}\boldsymbol{C}_{ij}, \boldsymbol{B}_{ij}\boldsymbol{A}_{ij}}\right) = \left(\widehat{\boldsymbol{r}_{ij}, -\boldsymbol{L}_{ij}}\right) \\ \psi_{ij} = \left(\widehat{\boldsymbol{e}_y, \boldsymbol{D}_{ij}\boldsymbol{C}_{ij}}\right) = \left(\widehat{\boldsymbol{e}_y, -\boldsymbol{r}_{p_{ij}}}\right),\ \psi_{r_{ij}} = \left(\widehat{\boldsymbol{e}_{yp}, \boldsymbol{D}_{ij}\boldsymbol{C}_{ij}}\right) = \left(\widehat{\boldsymbol{e}_{yp}, -\boldsymbol{r}_{p_{ij}}}\right) \end{cases}$$

Fig. 3-25: The complex chains (III) and (IV) with notations.

In nominal conditions, we have:

$$\begin{cases} \boldsymbol{L}_{i1} = \boldsymbol{L}_{i2} = \boldsymbol{L}_i,\ \boldsymbol{r}_{i1} = \boldsymbol{r}_{i2} = \boldsymbol{r}_i \\ \boldsymbol{r}_{p_{i1}} = \boldsymbol{r}_{p_{i2}} = \boldsymbol{r}_{p_i},\ \boldsymbol{n}_{i1} = \boldsymbol{n}_{i2} = \boldsymbol{n}_i \\ \boldsymbol{m}_{i1} = \boldsymbol{m}_{i2} = \boldsymbol{m}_i,\ \boldsymbol{\mu}_{i1} = \boldsymbol{\mu}_{i2} = \boldsymbol{\mu}_i \\ \boldsymbol{u} = \boldsymbol{e}_z \end{cases},\ \forall i = 3,4 \qquad (3.107),$$

with $\boldsymbol{u}$ representing the unit vector along the direction of the axes of the first revolute joints placed at D_{ij} $(\forall i = 3,4 \text{ and } \forall j = 1,2)$.

Let us denote the absolute angular velocities of the rigid bodies, $B_{ij}C_{ij}D_{ij}$ and $A_{ij}B_{ij}$, by $\boldsymbol{\omega}_{\boldsymbol{p}_{ij}}$ and $\boldsymbol{\omega}_{\boldsymbol{a}_{ij}}$, respectively. Their expressions are given as:

$$\boldsymbol{\omega}_{\boldsymbol{p}_{ij}} = \boldsymbol{\omega} + \dot{\psi}_{ij}\ \boldsymbol{u} = \boldsymbol{\omega} + \dot{\psi}_{ij}\ \boldsymbol{e}_z, \forall i = 3,4\ ;\ \forall j = 1,2 \qquad (3.108)$$

and

$$\boldsymbol{\omega}_{\boldsymbol{a}_{ij}} = \boldsymbol{\omega}_{\boldsymbol{p}_{ij}} + \dot{\varphi}_{ij}\ \boldsymbol{\mu}_{ij} = \boldsymbol{\omega} + \dot{\psi}_{ij}\ \boldsymbol{e}_z + \dot{\varphi}_{ij}\ \boldsymbol{\mu}_{ij}, \forall i = 3,4 \text{ and } \forall j = 1,2 \qquad (3.109).$$

Exploiting (3.108) and (3.109), we derive the respective velocities of D_{ij}, C_{ij}, B_{ij}, and A_{ij} as demonstrated below:

$$\boldsymbol{v}_{D_{ij}} = \boldsymbol{v} - \boldsymbol{p}_{ij} \times \boldsymbol{\omega} = \begin{bmatrix} \boldsymbol{1}_{3\times 3} & -\widehat{\boldsymbol{p}_{ij}} \end{bmatrix} \boldsymbol{t},\ \forall i = 3,4 \text{ and } \forall j = 1,2 \qquad (3.110),$$

$$\begin{cases} \boldsymbol{v}_{\boldsymbol{B}_{ij}} = \boldsymbol{v}_{\boldsymbol{D}_{ij}} + \boldsymbol{\omega}_{\boldsymbol{a}_{ij}} \times \left(-\boldsymbol{r}_{ij} - \boldsymbol{r}_{\boldsymbol{p}_{ij}} \right) \\ \quad = \left[\mathbf{1}_{3\times 3} \quad \left(-\widehat{\boldsymbol{p}_{ij}} + \hat{\boldsymbol{r}}_i + \widehat{\boldsymbol{r}_{\boldsymbol{p}_i}} \right) \quad \left(\boldsymbol{r}_i + \boldsymbol{r}_{\boldsymbol{p}_i} \right) \times \boldsymbol{e}_{\boldsymbol{z}} \right] \begin{pmatrix} \boldsymbol{t} \\ \dot{\boldsymbol{\psi}}_{ij} \end{pmatrix} \\ \forall i = 3,4 \; ; \; \forall j = 1,2 \end{cases} \tag{3.111}$$

and

$$\begin{cases} \boldsymbol{v}_{\boldsymbol{A}_{ij}} = \boldsymbol{v}_{\boldsymbol{A}_i} = \dot{q}_i \; \boldsymbol{e}_{\boldsymbol{x}} = \boldsymbol{v}_{\boldsymbol{B}_{ij}} + \boldsymbol{\omega}_{\boldsymbol{a}_{ij}} \times \left(-\boldsymbol{L}_{ij} \right) \\ \quad = \left[\boldsymbol{I} \quad \left(-\widehat{\boldsymbol{p}_{ij}} + \widehat{\boldsymbol{m}_i} \right) \quad \boldsymbol{m}_i \times \boldsymbol{e}_{\boldsymbol{z}} \quad \boldsymbol{L}_i \times \boldsymbol{\mu}_i \right] \begin{pmatrix} \boldsymbol{t} \\ \dot{\boldsymbol{\psi}}_{ij} \\ \dot{\boldsymbol{\varphi}}_{ij} \end{pmatrix} \\ \forall i = 3,4 \; ; \; \forall j = 1,2 \end{cases} \tag{3.112}.$$

Note that in (3.110) through (3.112), we have $\boldsymbol{p}_{i1} = h \, \boldsymbol{e}_{\boldsymbol{z}}$ and $\boldsymbol{p}_{i2} = -h \, \boldsymbol{e}_{\boldsymbol{z}}$, where h is the semi-height of the complex chain (refer to **Fig. 3-25**).

To inspect constraint singularities, we must analyze (3.112) after regrouping it in the form below:

$$\boldsymbol{C}_{\boldsymbol{E}} \, \dot{\boldsymbol{\Theta}} = \boldsymbol{V}_{\boldsymbol{A}} \;\; ; \; \dim\left(\boldsymbol{C}_{\boldsymbol{E}} \right) = 12 \times 14, \; \dim\left(\dot{\boldsymbol{\Theta}} \right) = 14 \times 1, \text{ and } \dim\left(\boldsymbol{V}_{\boldsymbol{A}} \right) = 12 \times 1 \tag{3.113},$$

with:

$$\dot{\boldsymbol{\Theta}} = \begin{pmatrix} \boldsymbol{t}^{\mathrm{T}} & \dot{\psi}_{31} & \dot{\varphi}_{31} & \dot{\psi}_{32} & \dot{\varphi}_{32} & \dot{\psi}_{41} & \dot{\varphi}_{41} & \dot{\psi}_{42} & \dot{\varphi}_{42} \end{pmatrix}^{\mathrm{T}} \tag{3.114},$$

$$\boldsymbol{V}_{\boldsymbol{A}} = \begin{pmatrix} v_{A_{31x}} & v_{A_{31y}} & v_{A_{31z}} & \cdots & v_{A_{42x}} & v_{A_{42y}} & v_{A_{42z}} \end{pmatrix}^{\mathrm{T}} \tag{3.115}$$

and

$$\boldsymbol{C}_{\boldsymbol{E}} = \begin{bmatrix} \mathbf{1}_{3\times 3} & \left(-\widehat{\boldsymbol{p}_{31}} + \widehat{\boldsymbol{m}_3} \right) & \boldsymbol{m}_3 \times \boldsymbol{e}_{\boldsymbol{z}} & \boldsymbol{L}_3 \times \boldsymbol{\mu}_3 & \mathbf{0}_{3\times 1} & \mathbf{0}_{3\times 1} & \mathbf{0}_{3\times 1} & \mathbf{0}_{3\times 1} & \mathbf{0}_{3\times 1} \\ \mathbf{1}_{3\times 3} & \left(-\widehat{\boldsymbol{p}_{32}} + \widehat{\boldsymbol{m}_3} \right) & \mathbf{0}_{3\times 1} & \mathbf{0}_{3\times 1} & \boldsymbol{m}_3 \times \boldsymbol{e}_{\boldsymbol{z}} & \boldsymbol{L}_3 \times \boldsymbol{\mu}_3 & \mathbf{0}_{3\times 1} & \mathbf{0}_{3\times 1} & \mathbf{0}_{3\times 1} \\ \mathbf{1}_{3\times 3} & \left(-\widehat{\boldsymbol{p}_{41}} + \widehat{\boldsymbol{m}_4} \right) & \mathbf{0}_{3\times 1} & \mathbf{0}_{3\times 1} & \mathbf{0}_{3\times 1} & \mathbf{0}_{3\times 1} & \boldsymbol{m}_4 \times \boldsymbol{e}_{\boldsymbol{z}} & \boldsymbol{L}_4 \times \boldsymbol{\mu}_4 & \mathbf{0}_{3\times 1} \\ \mathbf{1}_{3\times 3} & \left(-\widehat{\boldsymbol{p}_{42}} + \widehat{\boldsymbol{m}_4} \right) & \mathbf{0}_{3\times 1} & \mathbf{0}_{3\times 1} & \mathbf{0}_{3\times 1} & \mathbf{0}_{3\times 1} & \mathbf{0}_{3\times 1} & \boldsymbol{m}_4 \times \boldsymbol{e}_{\boldsymbol{z}} & \boldsymbol{L}_4 \times \boldsymbol{\mu}_4 \end{bmatrix} \tag{3.116}.$$

Note that in (3.115), the terms, v_{Aijx}, v_{Aijy}, and v_{Aijz}, correspond to the x, y, and z components of $\boldsymbol{v}_{\boldsymbol{A}_{ij}}$, with $i = 3,4$ and $j = 1,2$. Also, recall that $\boldsymbol{v}_{\boldsymbol{A}_{i1}} = \boldsymbol{v}_{\boldsymbol{A}_{i2}} = \dot{q}_i \; \boldsymbol{e}_{\boldsymbol{x}}, \; \forall i = 3,4$.

In the absence of any constraint singularity, we should always have $\omega_x = \omega_y = 0$. Utilizing MATLAB R2010a symbolic toolbox, we have determined the following general solution for $\dot{\boldsymbol{\Theta}}$ (in the general case of $\boldsymbol{V}_{\boldsymbol{A}}$, i.e. before substituting $\boldsymbol{v}_{\boldsymbol{A}_{i1}} = \boldsymbol{v}_{\boldsymbol{A}_{i2}} = \dot{q}_i \; \boldsymbol{e}_{\boldsymbol{x}}, \; \forall i = 3,4$):

$$\begin{cases} v_z \text{ (or } \dot{z}) \text{ and } \omega_z \text{: are arbitrary} \\ v_x = \dfrac{\mathrm{f}_1(\boldsymbol{V_A}, v_z, \omega_z)}{2\,h\,(m_{3x}\,m_{4y} - m_{3y}\,m_{4x})(L_{3x}\,\mu_{3y} - L_{3y}\,\mu_{3x})^2\,(L_{4x}\,\mu_{4y} - L_{4y}\,\mu_{4x})^2} \\ v_y = \dfrac{\mathrm{f}_2(\boldsymbol{V_A}, v_z, \omega_z)}{2\,h\,(m_{3x}\,m_{4y} - m_{3y}\,m_{4x})(L_{3x}\,\mu_{3y} - L_{3y}\,\mu_{3x})^2\,(L_{4x}\,\mu_{4y} - L_{4y}\,\mu_{4x})^2} \\ \omega_x = \dfrac{\mathrm{f}_3(\boldsymbol{V_A}, v_z, \omega_z)}{2\,h\,(m_{3x}\,m_{4y} - m_{3y}\,m_{4x})(L_{3x}\,\mu_{3y} - L_{3y}\,\mu_{3x})(L_{4x}\,\mu_{4y} - L_{4y}\,\mu_{4x})} \\ \omega_y = \dfrac{\mathrm{f}_3(\boldsymbol{V_A}, v_z, \omega_z)}{2\,h\,(m_{3x}\,m_{4y} - m_{3y}\,m_{4x})(L_{3x}\,\mu_{3y} - L_{3y}\,\mu_{3x})(L_{4x}\,\mu_{4y} - L_{4y}\,\mu_{4x})} \end{cases} \quad (3.117),$$

$$\begin{cases} \dot{\psi}_{31} = \dfrac{\mathrm{f}_4(\boldsymbol{V_A}, v_z, \omega_z)}{2\,h\,(m_{3x}\,m_{4y} - m_{3y}\,m_{4x})(L_{3x}\,\mu_{3y} - L_{3y}\,\mu_{3x})^2\,(L_{4x}\,\mu_{4y} - L_{4y}\,\mu_{4x})^2} \\ \dot{\psi}_{32} = \dfrac{\mathrm{f}_5(\boldsymbol{V_A}, v_z, \omega_z)}{2\,h\,(m_{3x}\,m_{4y} - m_{3y}\,m_{4x})(L_{3x}\,\mu_{3y} - L_{3y}\,\mu_{3x})^2\,(L_{4x}\,\mu_{4y} - L_{4y}\,\mu_{4x})^2} \\ \dot{\psi}_{41} = \dfrac{\mathrm{f}_6(\boldsymbol{V_A}, v_z, \omega_z)}{2\,h\,(m_{3x}\,m_{4y} - m_{3y}\,m_{4x})(L_{3x}\,\mu_{3y} - L_{3y}\,\mu_{3x})^2\,(L_{4x}\,\mu_{4y} - L_{4y}\,\mu_{4x})^2} \\ \dot{\psi}_{42} = \dfrac{\mathrm{f}_7(\boldsymbol{V_A}, v_z, \omega_z)}{2\,h\,(m_{3x}\,m_{4y} - m_{3y}\,m_{4x})(L_{3x}\,\mu_{3y} - L_{3y}\,\mu_{3x})^2\,(L_{4x}\,\mu_{4y} - L_{4y}\,\mu_{4x})^2} \end{cases} \quad (3.118),$$

and

$$\begin{cases} \dot{\varphi}_{31} = \dfrac{\mathrm{f}_7(\boldsymbol{V_A}, v_z, \omega_z)}{2\,h\,(L_{3x}\,\mu_{3y} - L_{3y}\,\mu_{3x})^2}, \ \dot{\varphi}_{32} = \dfrac{\mathrm{f}_8(\boldsymbol{V_A}, v_z, \omega_z)}{2\,h\,(L_{3x}\,\mu_{3y} - L_{3y}\,\mu_{3x})^2} \\ \dot{\varphi}_{41} = \dfrac{\mathrm{f}_9(\boldsymbol{V_A}, v_z, \omega_z)}{2\,h\,(L_{4x}\,\mu_{4y} - L_{4y}\,\mu_{4x})^2}, \ \dot{\varphi}_{42} = \dfrac{\mathrm{f}_{10}(\boldsymbol{V_A}, v_z, \omega_z)}{2\,h\,(L_{4x}\,\mu_{4y} - L_{4y}\,\mu_{4x})^2} \end{cases} \quad (3.119),$$

with $vect_x$, $vect_y$, and $vect_z$ designating respectively the x, y, and z components of vector $\boldsymbol{vect}$, and with f_1 through f_{10} representing polynomial functions of $\boldsymbol{V_A}$, v_z, and ω_z (these expressions are not given explicitly here being quite lengthy and not necessarily for the study).

Substituting $\boldsymbol{v}_{A_{i1}} = \boldsymbol{v}_{A_{i2}} = \dot{q}_i\,\boldsymbol{e_x}$, $\forall i = 3,4$, we get $\mathrm{f}_3(\boldsymbol{V_A}, v_z, \omega_z) = 0$. So, provided that none of the denominators in (3.117) through (3.119) is null, the chains (III) and (IV) prohibit the undesired rotations by imposing $\omega_x = \omega_y = 0$. Moreover, substituting $\boldsymbol{V_A} = \boldsymbol{0}$ (i.e. locking the actuators in place) yields additionally $\mathrm{f}_1(\boldsymbol{V_A}, v_z, \omega_z) = 0$; meaning $v_x = 0$ and which is intuitively expected.

Therefore, to assure the absence of constraint singularities, we must investigate whether the following condition:

$$h\,(m_{3x}\,m_{4y} - m_{3y}\,m_{4x})(L_{3x}\,\mu_{3y} - L_{3y}\,\mu_{3x})(L_{4x}\,\mu_{4y} - L_{4y}\,\mu_{4x}) \neq 0 \quad (3.120)$$

is satisfied or not.

Then, three main cases lead to the degeneration of (3.117) through (3.119), which are:

1. $h=0$: This is avoided by construction since $h\neq 0$. Such constraint singularity can be coined an architectural one since it occurs for a particular set of geometric parameters.
2. $\left(m_{3x}\,m_{4y}-m_{3y}\,m_{4x}\right)=0$: This means the xy projections of $\boldsymbol{m}_3$ and $\boldsymbol{m}_4$ are collinear.
3. $\left(L_{3x}\,\mu_{3y}-L_{3y}\,\mu_{3x}\right)=0$ or $\left(L_{4x}\,\mu_{4y}-L_{4y}\,\mu_{4x}\right)=0$: This corresponds to having the xy projections of $\boldsymbol{L}_3$ ($\boldsymbol{L}_4$) and $\boldsymbol{\mu}_3$ (correspondingly $\boldsymbol{\mu}_4$) collinear. But due to the structural symmetry of the mechanism, we always have both terms, $\left(L_{3x}\,\mu_{3y}-L_{3y}\,\mu_{3x}\right)$ and $\left(L_{4x}\,\mu_{4y}-L_{4y}\,\mu_{4x}\right)$, simultaneously zero or non-zero.

The case of having $\left(m_{3x}\,m_{4y}-m_{3y}\,m_{4x}\right)=0$ implies that either $m_{3y}=m_{4y}=0$ ($\boldsymbol{m}_3$ and $\boldsymbol{m}_4$ in the xz plane) or $m_{3x}=m_{4x}=0$ ($\boldsymbol{m}_3$ and $\boldsymbol{m}_4$ in the yz plane). Both not only occur on the boundary of the geometric workspace, but also are practically preceded by collisions (collision between platform and sliders' wall in the first case, and between the actuators in the second). Similarly, $\left(L_{3x}\,\mu_{3y}-L_{3y}\,\mu_{3x}\right)=\left(L_{4x}\,\mu_{4y}-L_{4y}\,\mu_{4x}\right)=0$ cannot theoretically happen except in the case where $\boldsymbol{L}_3//\boldsymbol{L}_4//\boldsymbol{e}_z$. In addition to being confounded with classical-type singularity (as we are going to see later), this singularity is circumvented by prior collisions.

Based on the above, we deduce that within the geometric accessible region excluding its boundary, we can guarantee the absence of constraint singularities. In what follows, we discuss the remaining classical singularities.

Classical Singularities

For studying these singularities, we only need to consider (3.101), (3.104), and (3.105). We recall that singularity occurs in two cases:

1. The first case is described as follows: knowing $\dot{\boldsymbol{q}}$, we cannot definitely determine $\dot{\boldsymbol{x}}$, $\dot{\boldsymbol{\varphi}}$ or $\dot{\boldsymbol{\psi}}$. Mathematically, this occurs when $\boldsymbol{J}_{\boldsymbol{x}}$, $\boldsymbol{J}_{\boldsymbol{\varphi}}$, or $\boldsymbol{J}_{\boldsymbol{\psi}}$ is singular.
2. The second case is described as follows: knowing $\dot{\boldsymbol{x}}$, we cannot definitely determine $\dot{\boldsymbol{q}}$, $\dot{\boldsymbol{\varphi}}$, or $\dot{\boldsymbol{\psi}}$. In terms of mathematics, this occurs when $\boldsymbol{J}_{\boldsymbol{q}}$, $\boldsymbol{J}_{\boldsymbol{\varphi}}$, or $\boldsymbol{J}_{\boldsymbol{\psi}}$ is singular.

Let us then inspect the configurations for which one or more of the four matrices, $\boldsymbol{J}_{\boldsymbol{q}}$, $\boldsymbol{J}_{\boldsymbol{x}}$, $\boldsymbol{J}_{\boldsymbol{\varphi}}$, and $\boldsymbol{J}_{\boldsymbol{\psi}}$, become rank deficient.

i- Rank Deficiency of $\boldsymbol{J}_{\boldsymbol{q}}=\boldsymbol{J}_{\boldsymbol{\psi}}$ and $\boldsymbol{J}_{\boldsymbol{\varphi}}$:

We have $\boldsymbol{J}_{\boldsymbol{q}}=\boldsymbol{J}_{\boldsymbol{\psi}}$ singular if and only if:

$$\det\left(\boldsymbol{J}_{\boldsymbol{q}}\right)=\det\left(\boldsymbol{J}_{\boldsymbol{\psi}}\right)=0\Leftrightarrow\exists i_0\in\{1,\ldots,6\};\ \boldsymbol{e}_x^{\mathrm{T}}\,\boldsymbol{m}_{i_0}=0\ \text{or}\ \boldsymbol{e}_z^{\mathrm{T}}\left(\boldsymbol{L}_{i_0}\times\boldsymbol{\mu}_{i_0}\right)=0 \qquad (3.121).$$

As for $\boldsymbol{J}_{\boldsymbol{\varphi}}$, its singularity is equivalent to:

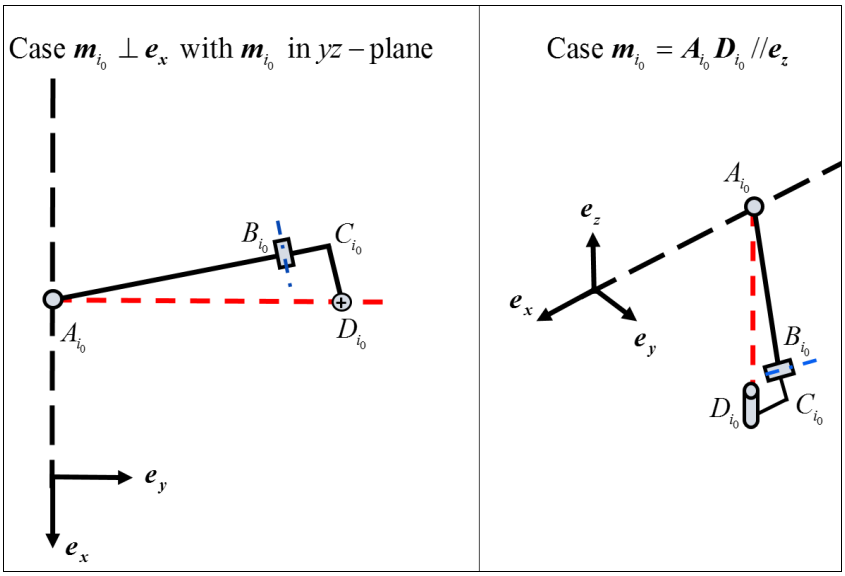

Fig. 3-26: Singularity analysis: case $\boldsymbol{e}_x^{\mathrm{T}}\,\boldsymbol{m}_{i_0} = 0$.

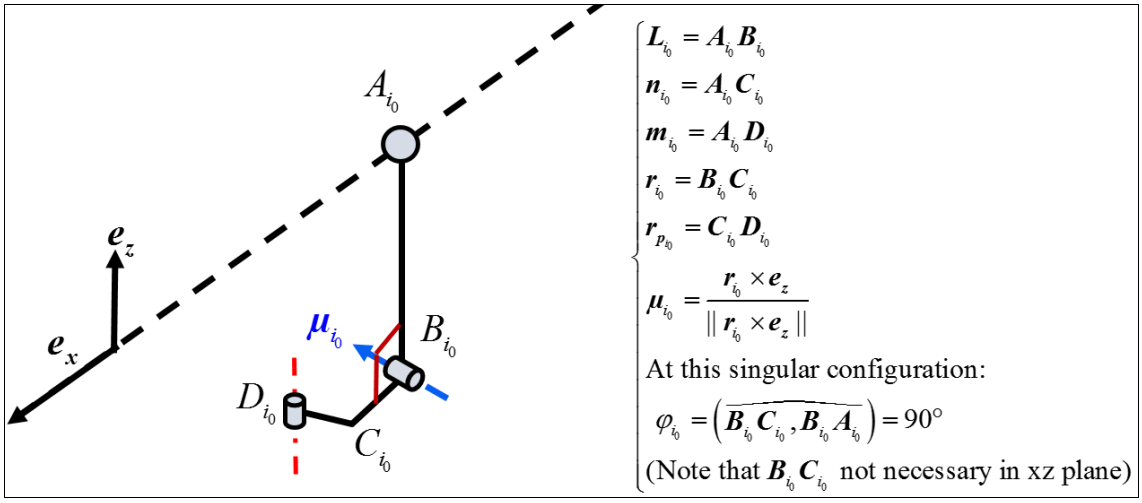

Fig. 3-27: Singularity analysis: case $\boldsymbol{e}_z^{\mathrm{T}}\left(\boldsymbol{L}_{i_0} \times \boldsymbol{\mu}_{i_0}\right) = 0$

$$\det\left(\boldsymbol{J}_{\varphi}\right) = 0 \Leftrightarrow \exists i_0 \in \{1,\ldots,6\};\ \boldsymbol{e}_z^{\mathrm{T}}\left(\boldsymbol{L}_{i_0} \times \boldsymbol{\mu}_{i_0}\right) = 0 \qquad (3.122),$$

which is already embedded in (3.121).

The case $\boldsymbol{e}_x^{\mathrm{T}}\,\boldsymbol{m}_{i_0} = 0$ (see **Fig. 3-26**) corresponds to having $\boldsymbol{m}_{i_0}$ in the yz plane. Again, this not only occurs on the boundary of the geometric workspace, but also provokes prior collisions.

The case where $\boldsymbol{e}_z^{\mathrm{T}}\left(\boldsymbol{L}_{i_0} \times \boldsymbol{\mu}_{i_0}\right) = 0$ is analogous to what have been discussed in the study of constraint singularities. It dictates having $\boldsymbol{L}_{i_0} // \boldsymbol{e}_z$ and leads to prior collisions between the platform and the sliders' plane (refer to **Fig. 3-27**). Notice that in the case where $i_0 \neq 3,4$, the complex chains, namely (III) and (IV), maintain the constraints on the platform. This means that the revolutes at D_i $(\forall i = 1\ldots6)$ sustain their vertical axes and hence, $\varphi_{i_0} = 90°$ is imposed. This latter idea is clarified in the same aforementioned figure.

ii- Rank Deficiency of J_x:

To study the rank of J_x, it is necessary to perform some linear operations to achieve a simpler form. We start by changing the TCP to be confounded with D_1 (note that this corresponds to a linear operation on J_x). As a result, we get the matrix T defined by:

$$\begin{cases} T = \begin{bmatrix} (e_z^T (L_1 \times \mu_1))(e_x^T m_1) & (e_z^T (L_1 \times \mu_1))(e_y^T m_1) & (e_z^T (n_1 \times \mu_1))(e_z^T m_1) & 0 \\ (e_z^T (L_2 \times \mu_2))(e_x^T m_2) & (e_z^T (L_2 \times \mu_2))(e_y^T m_2) & (e_z^T (n_2 \times \mu_2))(e_z^T m_2) & 0 \\ (e_z^T (L_3 \times \mu_3))(e_x^T m_3) & (e_z^T (L_3 \times \mu_3))(e_y^T m_3) & (e_z^T (n_3 \times \mu_3))(e_z^T m_3) & t_{34} \\ (e_z^T (L_4 \times \mu_4))(e_x^T m_4) & (e_z^T (L_4 \times \mu_4))(e_y^T m_4) & (e_z^T (n_4 \times \mu_4))(e_z^T m_4) & t_{44} \\ (e_z^T (L_5 \times \mu_5))(e_x^T m_5) & (e_z^T (L_5 \times \mu_5))(e_y^T m_5) & (e_z^T (n_5 \times \mu_5))(e_z^T m_5) & 0 \\ (e_z^T (L_6 \times \mu_6))(e_x^T m_6) & (e_z^T (L_6 \times \mu_6))(e_y^T m_6) & (e_z^T (n_6 \times \mu_6))(e_z^T m_6) & 0 \end{bmatrix} \\ \text{with:} \\ t_{34} = -(e_z^T (L_3 \times \mu_3))(e_z^T (m_3 \times r_c)),\ t_{44} = -(e_z^T (L_4 \times \mu_4))(e_z^T (m_4 \times r_c)) \\ r_c = D_1 D_3 \equiv D_1 D_4 \end{cases} \quad (3.123).$$

We can assure that T (equivalently J_x) is of full rank if the two matrices, T_1 and T_2, defined by:

$$T_1 = \begin{bmatrix} (e_z^T (L_1 \times \mu_1))(e_x^T m_1) & (e_z^T (L_1 \times \mu_1))(e_y^T m_1) & (e_z^T (n_1 \times \mu_1))(e_z^T m_1) \\ (e_z^T (L_2 \times \mu_2))(e_x^T m_2) & (e_z^T (L_2 \times \mu_2))(e_y^T m_2) & (e_z^T (n_2 \times \mu_2))(e_z^T m_2) \\ (e_z^T (L_5 \times \mu_5))(e_x^T m_5) & (e_z^T (L_5 \times \mu_5))(e_y^T m_5) & (e_z^T (n_5 \times \mu_5))(e_z^T m_5) \\ (e_z^T (L_6 \times \mu_6))(e_x^T m_6) & (e_z^T (L_6 \times \mu_6))(e_y^T m_6) & (e_z^T (n_6 \times \mu_6))(e_z^T m_6) \end{bmatrix} \quad (3.124)$$

and

$$T_2 = \begin{bmatrix} -(e_z^T (L_3 \times \mu_3))(e_z^T (m_3 \times r_c)) \\ -(e_z^T (L_4 \times \mu_4))(e_z^T (m_4 \times r_c)) \end{bmatrix} \quad (3.125),$$

are non-singular.

Starting with the simplest matrix T_2, its singularity necessitates having:

$$(e_z^T (L_3 \times \mu_3))(e_z^T (m_3 \times r_c)) = (e_z^T (L_4 \times \mu_4))(e_z^T (m_4 \times r_c)) = 0 \quad (3.126).$$

Due to the structural symmetry with respect to the mediator plane of segment $[A_3 A_4]$, the relation (3.126) can be reduced to:

$$\begin{cases} \left(\boldsymbol{e}_z^{\mathrm{T}}\left(\boldsymbol{L}_3\times\boldsymbol{\mu}_3\right)\right)=\left(\boldsymbol{e}_z^{\mathrm{T}}\left(\boldsymbol{L}_4\times\boldsymbol{\mu}_4\right)\right)=0 \\ \text{or} \\ \left(\boldsymbol{e}_z^{\mathrm{T}}\left(\boldsymbol{m}_3\times\boldsymbol{r}_c\right)\right)=\left(\boldsymbol{e}_z^{\mathrm{T}}\left(\boldsymbol{m}_4\times\boldsymbol{r}_c\right)\right)=0 \end{cases} \quad (3.127).$$

The first case of (3.127) has been discussed in the previous paragraphs (refer to **Fig. 3-27**). We have proven that it is non-problematic. This is because it is prevented by prior collisions. Regarding the second case (i.e. $\boldsymbol{e}_z^{\mathrm{T}}\left(\boldsymbol{m}_3\times\boldsymbol{r}_c\right)=\boldsymbol{e}_z^{\mathrm{T}}\left(\boldsymbol{m}_4\times\boldsymbol{r}_c\right)=0$), it is geometrically translated to having the four vectors, $\boldsymbol{e}_z$, $\boldsymbol{m}_3$, $\boldsymbol{m}_4$, and $\boldsymbol{r}_c$, in the same plane, which is either the xy or the yz plane. Once more, both situations are practically inapplicable because of collisions between the sliders' plane and the platform, or between the third and fourth actuators. Thus, singularity of $\boldsymbol{T}_2$ is not to be concerned about.

It remains to discuss the singularity of $\boldsymbol{T}_1$. Doing some linear operations on $\boldsymbol{T}_1$ and considering the symmetry of each pair of chains, (I & II) and (V & VI), relative to the mediator planes of the segments $[A_1A_2]$ and $[A_5A_6]$ respectively, we get matrix $\boldsymbol{TS}_1$ of same rank as $\boldsymbol{T}_1$. $\boldsymbol{TS}_1$ is given by:

$$\boldsymbol{TS}_1=\begin{bmatrix} \left(\boldsymbol{e}_z^{\mathrm{T}}\left(\boldsymbol{L}_1\times\boldsymbol{\mu}_1\right)\right)\left(\boldsymbol{m}_1^{\mathrm{T}}\,\boldsymbol{e}_x\right) & 0 & 0 \\ 0 & \left(\boldsymbol{e}_z^{\mathrm{T}}\left(\boldsymbol{L}_1\times\boldsymbol{\mu}_1\right)\right)\left(\boldsymbol{m}_1^{\mathrm{T}}\,\boldsymbol{e}_y\right) & \left(\boldsymbol{e}_z^{\mathrm{T}}\left(\boldsymbol{n}_1\times\boldsymbol{\mu}_1\right)\right)\left(\boldsymbol{L}_1^{\mathrm{T}}\,\boldsymbol{e}_z\right) \\ \left(\boldsymbol{e}_z^{\mathrm{T}}\left(\boldsymbol{L}_5\times\boldsymbol{\mu}_5\right)\right)\left(\boldsymbol{m}_5^{\mathrm{T}}\,\boldsymbol{e}_x\right) & 0 & 0 \\ 0 & \left(\boldsymbol{e}_z^{\mathrm{T}}\left(\boldsymbol{L}_5\times\boldsymbol{\mu}_5\right)\right)\left(\boldsymbol{m}_5^{\mathrm{T}}\,\boldsymbol{e}_y\right) & \left(\boldsymbol{e}_z^{\mathrm{T}}\left(\boldsymbol{n}_5\times\boldsymbol{\mu}_5\right)\right)\left(\boldsymbol{L}_5^{\mathrm{T}}\,\boldsymbol{e}_z\right) \end{bmatrix} \quad (3.128).$$

$\boldsymbol{TS}_1$ (equivalently $\boldsymbol{T}_1$) is of full rank provided that:

$$\begin{cases} \bullet\left(\left(\boldsymbol{e}_z^{\mathrm{T}}\left(\boldsymbol{L}_1\times\boldsymbol{\mu}_1\right)\right)\left(\boldsymbol{m}_1^{\mathrm{T}}\,\boldsymbol{e}_x\right)\neq 0 \text{ or } \left(\boldsymbol{e}_z^{\mathrm{T}}\left(\boldsymbol{L}_5\times\boldsymbol{\mu}_5\right)\right)\left(\boldsymbol{m}_5^{\mathrm{T}}\,\boldsymbol{e}_x\right)\neq 0\right) \\ \text{and} \\ \bullet D_t=\left(\boldsymbol{e}_z^{\mathrm{T}}\left(\boldsymbol{L}_1\times\boldsymbol{\mu}_1\right)\right)\left(\boldsymbol{m}_1^{\mathrm{T}}\,\boldsymbol{e}_y\right)\left(\boldsymbol{e}_z^{\mathrm{T}}\left(\boldsymbol{n}_5\times\boldsymbol{\mu}_5\right)\right)\left(\boldsymbol{L}_5^{\mathrm{T}}\,\boldsymbol{e}_z\right) \\ \qquad -\left(\boldsymbol{e}_z^{\mathrm{T}}\left(\boldsymbol{L}_5\times\boldsymbol{\mu}_5\right)\right)\left(\boldsymbol{m}_5^{\mathrm{T}}\,\boldsymbol{e}_y\right)\left(\boldsymbol{e}_z^{\mathrm{T}}\left(\boldsymbol{n}_1\times\boldsymbol{\mu}_1\right)\right)\left(\boldsymbol{L}_1^{\mathrm{T}}\,\boldsymbol{e}_z\right)\neq 0 \end{cases} \quad (3.129).$$

While the practical inapplicability of $\left(\boldsymbol{e}_z^{\mathrm{T}}\left(\boldsymbol{L}_1\times\boldsymbol{\mu}_1\right)\right)\left(\boldsymbol{m}_1^{\mathrm{T}}\,\boldsymbol{e}_x\right)=\left(\boldsymbol{e}_z^{\mathrm{T}}\left(\boldsymbol{L}_5\times\boldsymbol{\mu}_5\right)\right)\left(\boldsymbol{m}_5^{\mathrm{T}}\,\boldsymbol{e}_x\right)=0$ has been demonstrated in the previous parts, proving that $D_t\neq 0$ over the whole geometric workspace is not an easy task. However, in order to avoid collisions between the platform and the frame's upper and lower limits, the feasible workspace is restricted to the region defined by: $|z|\leq H=L_z-a$, where $L_z>a$. Therefore, it is enough to prove that D_t remains strictly positive over this feasible workspace. For this purpose, we need first to emphasize that $\boldsymbol{m}_1^{\mathrm{T}}\,\boldsymbol{e}_y=\boldsymbol{m}_5^{\mathrm{T}}\,\boldsymbol{e}_y$ because of the structural symmetry. Furthermore, we always have $\boldsymbol{m}_1^{\mathrm{T}}\,\boldsymbol{e}_y=\boldsymbol{m}_5^{\mathrm{T}}\,\boldsymbol{e}_y\neq 0$ except for the practically impossible situation described by having $\boldsymbol{m}_1$ and

$\boldsymbol{m}_5$ in the xz plane. This is physically prevented by prior collisions. This latter idea enables us replacing the study of D_t by another one on D_{tr}, where:

$$D_{tr}=\left(\boldsymbol{e}_{\boldsymbol{z}}^{\mathrm{T}}\left(\boldsymbol{L}_1\times\boldsymbol{\mu}_1\right)\right)\left(\boldsymbol{e}_{\boldsymbol{z}}^{\mathrm{T}}\left(\boldsymbol{n}_5\times\boldsymbol{\mu}_5\right)\right)\left(\boldsymbol{L}_5^{\mathrm{T}}\,\boldsymbol{e}_{\boldsymbol{z}}\right)-\left(\boldsymbol{e}_{\boldsymbol{z}}^{\mathrm{T}}\left(\boldsymbol{L}_5\times\boldsymbol{\mu}_5\right)\right)\left(\boldsymbol{e}_{\boldsymbol{z}}^{\mathrm{T}}\left(\boldsymbol{n}_1\times\boldsymbol{\mu}_1\right)\right)\left(\boldsymbol{L}_1^{\mathrm{T}}\,\boldsymbol{e}_{\boldsymbol{z}}\right) \quad (3.130).$$

In the feasible workspace (i.e. $L_{1z}=m_{1z}\le 0$ and $L_{5z}=m_{5z}\ge 0$), the performed sign analysis on the composing terms of D_{tr} shows that D_{tr} not only is positive, but also equal to the sum of two positive terms. This is clarified below:

$$\begin{cases} D_{tr}=\underbrace{\underbrace{\left(\boldsymbol{e}_{\boldsymbol{z}}^{\mathrm{T}}\left(\boldsymbol{L}_1\times\boldsymbol{\mu}_1\right)\right)}_{\le 0}\underbrace{\left(\boldsymbol{e}_{\boldsymbol{z}}^{\mathrm{T}}\left(\boldsymbol{n}_5\times\boldsymbol{\mu}_5\right)\right)}_{\le 0}\underbrace{\left(\boldsymbol{L}_5^{\mathrm{T}}\,\boldsymbol{e}_{\boldsymbol{z}}\right)}_{\ge 0}}_{t_1\ge 0}-\underbrace{\underbrace{\left(\boldsymbol{e}_{\boldsymbol{z}}^{\mathrm{T}}\left(\boldsymbol{L}_5\times\boldsymbol{\mu}_5\right)\right)}_{\le 0}\underbrace{\left(\boldsymbol{e}_{\boldsymbol{z}}^{\mathrm{T}}\left(\boldsymbol{n}_1\times\boldsymbol{\mu}_1\right)\right)}_{\le 0}\underbrace{\left(\boldsymbol{L}_1^{\mathrm{T}}\,\boldsymbol{e}_{\boldsymbol{z}}\right)}_{\le 0}}_{(-t_2)\le 0} \\ \Rightarrow \mathrm{D}_{tr}=t_1+t_2\ge 0 \end{cases} \quad (3.131).$$

Thus, $D_{tr}=t_1+t_2\ge 0$ with:

$$t_1=\left(\boldsymbol{e}_{\boldsymbol{z}}^{\mathrm{T}}\left(\boldsymbol{L}_1\times\boldsymbol{\mu}_1\right)\right)\left(\boldsymbol{e}_{\boldsymbol{z}}^{\mathrm{T}}\left(\boldsymbol{n}_5\times\boldsymbol{\mu}_5\right)\right)\left(\boldsymbol{L}_5^{\mathrm{T}}\,\boldsymbol{e}_{\boldsymbol{z}}\right)\ge 0 \quad (3.132)$$

and

$$t_2=-\left(\boldsymbol{e}_{\boldsymbol{z}}^{\mathrm{T}}\left(\boldsymbol{L}_5\times\boldsymbol{\mu}_5\right)\right)\left(\boldsymbol{e}_{\boldsymbol{z}}^{\mathrm{T}}\left(\boldsymbol{n}_1\times\boldsymbol{\mu}_1\right)\right)\left(\boldsymbol{L}_1^{\mathrm{T}}\,\boldsymbol{e}_{\boldsymbol{z}}\right)\ge 0 \quad (3.133),$$

over the feasible workspace. Based on (3.132) and (3.133), we can assert that $D_{tr}=0\Leftrightarrow t_1=t_2=0$ and hence, we only need to investigate the case where:

$$\left(\boldsymbol{e}_{\boldsymbol{z}}^{\mathrm{T}}\left(\boldsymbol{L}_1\times\boldsymbol{\mu}_1\right)\right)\left(\boldsymbol{e}_{\boldsymbol{z}}^{\mathrm{T}}\left(\boldsymbol{n}_5\times\boldsymbol{\mu}_5\right)\right)\left(\boldsymbol{L}_5^{\mathrm{T}}\,\boldsymbol{e}_{\boldsymbol{z}}\right)=\left(\boldsymbol{e}_{\boldsymbol{z}}^{\mathrm{T}}\left(\boldsymbol{L}_5\times\boldsymbol{\mu}_5\right)\right)\left(\boldsymbol{e}_{\boldsymbol{z}}^{\mathrm{T}}\left(\boldsymbol{n}_1\times\boldsymbol{\mu}_1\right)\right)\left(\boldsymbol{L}_1^{\mathrm{T}}\,\boldsymbol{e}_{\boldsymbol{z}}\right)=0 \quad (3.134).$$

Relation (3.134) can be put in the following simplified form:

$$\begin{cases} \left[\left(\boldsymbol{e}_{\boldsymbol{z}}^{\mathrm{T}}\left(\boldsymbol{L}_1\times\boldsymbol{\mu}_1\right)\right)=0 \text{ or } \left(\boldsymbol{e}_{\boldsymbol{z}}^{\mathrm{T}}\left(\boldsymbol{n}_5\times\boldsymbol{\mu}_5\right)\right)=0 \text{ or} \left(\boldsymbol{L}_5^{\mathrm{T}}\,\boldsymbol{e}_{\boldsymbol{z}}\right)=0\right] \\ \text{and} \\ \left[\left(\boldsymbol{e}_{\boldsymbol{z}}^{\mathrm{T}}\left(\boldsymbol{L}_5\times\boldsymbol{\mu}_5\right)\right)=0 \text{ or } \left(\boldsymbol{e}_{\boldsymbol{z}}^{\mathrm{T}}\left(\boldsymbol{n}_1\times\boldsymbol{\mu}_1\right)\right)=0 \text{ or } \left(\boldsymbol{L}_1^{\mathrm{T}}\,\boldsymbol{e}_{\boldsymbol{z}}\right)=0\right] \end{cases} \quad (3.135).$$

The practical impossibility of $\boldsymbol{e}_{\boldsymbol{z}}^{\mathrm{T}}\left(\boldsymbol{L}_1\times\boldsymbol{\mu}_1\right)=0$ or $\boldsymbol{e}_{\boldsymbol{z}}^{\mathrm{T}}\left(\boldsymbol{L}_5\times\boldsymbol{\mu}_5\right)=0$ has been discussed earlier. As for the condition $\boldsymbol{e}_{\boldsymbol{z}}^{\mathrm{T}}\left(\boldsymbol{n}_1\times\boldsymbol{\mu}_1\right)=0$ or $\boldsymbol{e}_{\boldsymbol{z}}^{\mathrm{T}}\left(\boldsymbol{n}_5\times\boldsymbol{\mu}_5\right)=0$, it can be translated as having the three concerned vectors in each case laying in the same vertical plane. But as $\boldsymbol{\mu}_i\perp\boldsymbol{n}_i$ and $\mu_{iz}=0$, the only possibility is having $\boldsymbol{n}_1//\boldsymbol{e}_{\boldsymbol{z}}$ or $\boldsymbol{n}_5//\boldsymbol{e}_{\boldsymbol{z}}$, respectively. Nevertheless, this is practically impossible as collisions befall prior to that. Regarding having $\boldsymbol{L}_5^{\mathrm{T}}\,\boldsymbol{e}_{\boldsymbol{z}}=0$ or $\boldsymbol{L}_1^{\mathrm{T}}\,\boldsymbol{e}_{\boldsymbol{z}}=0$, it cannot occur except on the boundary of the feasible workspace. Also, since we have $H=L_z-a\neq 0$, it is not possible to have simultaneously: $\boldsymbol{L}_5^{\mathrm{T}}\,\boldsymbol{e}_{\boldsymbol{z}}=0$ and $\boldsymbol{L}_1^{\mathrm{T}}\,\boldsymbol{e}_{\boldsymbol{z}}=0$.

Therefore, on the feasible workspace, we can guarantee that $\boldsymbol{TS}_1$ (equivalently $\boldsymbol{T}_1$) is of full rank. Besides, as $\boldsymbol{T}_2$ has been proven already to be of full rank over the broader geometrically

accessible workspace, we can then assert that $\boldsymbol{T}$ (equivalently $\boldsymbol{J}_x$) is non-singular over the feasible region.

Results' Briefing

In **§3.4.3.C**, we have detailed the constraint and classical singularity analyses. The results are that within the feasible workspace, we can assure the absence of all types of singularities. Nevertheless, as it can be obviously noticed in comparison with all previous studies, this investigation has not been straightforward but rather complex.

D- Simplified Dynamic Model (SDM)

In brief, to obtain the SDM, we follow the same maneuver and hypotheses described in **§3.3.6**. We get the direct dynamic model (DDM) as below:

$$\begin{cases} \ddot{\boldsymbol{x}} = \boldsymbol{H}\ \boldsymbol{\tau} - \boldsymbol{\Lambda}\ \dot{\boldsymbol{x}} + \boldsymbol{a}_g^{\boldsymbol{offset}} \\ \boldsymbol{H} = \left(\boldsymbol{M}_p + \boldsymbol{J}_m^{\mathrm{T}}\ \boldsymbol{M}_a\ \boldsymbol{J}_m\right)^{-1}\ \boldsymbol{J}_m^{\mathrm{T}} \\ \boldsymbol{\Lambda} = \boldsymbol{H}\ \boldsymbol{M}_a\ \dot{\boldsymbol{J}}_m + \left(\boldsymbol{M}_p + \boldsymbol{J}_m^{\mathrm{T}}\ \boldsymbol{M}_a\ \boldsymbol{J}_m\right)^{-1}\ \boldsymbol{\Lambda}_c \\ \boldsymbol{a}_g^{\boldsymbol{offset}} = \left(\boldsymbol{M}_p + \boldsymbol{J}_m^{\mathrm{T}}\ \boldsymbol{M}_a\ \boldsymbol{J}_m\right)^{-1}\ m_p\ \boldsymbol{g}, \\ \dim\left(\boldsymbol{H}\right) = 4\times 6,\ \ \dim\left(\boldsymbol{a}_g^{\boldsymbol{offset}}\right) = 4\times 1 \\ \dim\left(\boldsymbol{\Lambda}\right) = 4\times 4 \end{cases} \quad (3.136),$$

with all symbols carrying the same significances and definitions as given in **§3.3.6**. Choosing the inverse dynamic model (IDM) based on zero components along the null space of $\boldsymbol{H}$, we get:

$$\begin{cases} \boldsymbol{\tau} = \boldsymbol{C}\left(\ddot{\boldsymbol{x}} + \boldsymbol{\Lambda}\ \dot{\boldsymbol{x}} - \boldsymbol{a}_g^{\boldsymbol{offset}}\right),\ \text{with:} \\ \boldsymbol{C} = \boldsymbol{H}^{*}:\ \text{pseudo-inverse of } \boldsymbol{H} \end{cases} \quad (3.137).$$

Hence, as the IDM has been obtained, we can proceed with the dimensional synthesis of ARROW V2 M2, which will be covered in the upcoming section.

E- Dimensional Synthesis

The dimensional synthesis of ARROW V2 M2 follows the same reasoning and approach described in **§3.3.7**. It is based on the two primary criteria of precision and dynamics, namely $WTPAF$ and $WILA$. Also, it is followed by a secondary verification based on FVI_p, with the values of v_{req}^{p} and f_{req}^{p} being identical to those in **§3.3.7** (i.e. $v_{req}^{p} = 0.25\,\dot{q}_{\max}$ and $f_{req}^{p} = 0.25\,\tau_{\max}$).

Table 3-4: Inertia parameters of ARROW V2 M2 (with some safety margins).

Item	Value	Item	Value
Individual Simple Slider Cart's Mass (chains I,II, V and VI)	≈ 11.100 kg	**Individual Parallelogram Slider Cart's Mass (chains III, and IV)**	≈ 11.340 kg
Platform's Mass	≈ 10.200 kg	**Platform's Inertia about its z-axis**	≈ 0.414 kg m^2
Simple Arm Linear Mass (after removing $L_o = 0.155$ m *)	≈ 1.744 kg/m	**Parallelogram Arm Linear Mass (after removing $L_o = 0.155$ m)**	≈ 3.488 kg/m

***Note that $L_o = 0.155$ m is the length of joint interfaces. We emphasize here that the mass of the joints on the side of the platform are added with their moment of inertia to the platform. On the other hand, the mass of the joints on the side of the sliders are added to their corresponding sliders directly.**

Table 3-5: The fixed geometric parameters and limits of ARROW V2 M2.

Fixed geometric parameters and limits					
Symbol	**Value**	**Symbol**	**Value**	**Symbol**	**Value**
a	0.137 m	b_{cm}	–0.179 m	r	0.048 m
d	0.125 m	t_p	0.1875 m	r_p	0.025 m
L_z	0.480 m	$q_{\min}$	–1.500 m	$q_{\max}$	+1.500 m
d_l	0.600 m	t_l	0.320 m		

$q_{\min}$ and $q_{\max}$: represent the minimum and maximum allowable displacement of each individual linear motor.

d_l: represents the minimum allowed distance between two actuators on the same linear track.

t_l: represents the minimum allowable value of y component of the TCP to avoid collision between the platform and the sliders' wall.

For this synthesis procedure, the actuators' characteristics are exactly those given in **Table 3-2**. As for the inertia and fixed geometric parameters, they are respectively presented in **Table 3-4** and **Table 3-5**.

The target parameters to optimize are the following: L_s, L_p, and y_o, where y_o is the y offset of the center of the desired workspace, DWS, defined by:

$$DWS: \begin{cases} -0.15\text{ m} \le y - y_o \le +0.15\text{ m} \\ -0.15\text{ m} \le z \le +0.15\text{ m} \\ -45^\circ \le \theta_z \le +45^\circ \end{cases} \quad (3.138).$$

As for the x length of DWS, it is desired to be surely the largest possible value obtainable for:

$$q_{\min} = -1.5\text{ m} \le q_i \le q_{\max} = +1.5\text{ m},\ \forall i = 1...6 \quad (3.139),$$

but after fulfilling the primary and secondary criteria. The chosen ranges for L_s, L_p, and y_o are as follows:

$$\begin{cases} 0.84\text{ m} \le L_s \le 1\text{ m} \\ 0.47\text{ m} \le L_p \le 1\text{ m} \\ y_o^{\min} \le y_o \le y_o^{\max} \end{cases} \quad (3.140),$$

with $y_o^{\min}$ and $y_o^{\max}$ representing the lower and upper bounds on y_o that should be respected to allow the accessibility to DWS. These latter terms, $y_o^{\min}$ and $y_o^{\max}$, are dependent on L_s and L_p.

The Pareto diagram is constructed by considering five equally spaced values for each

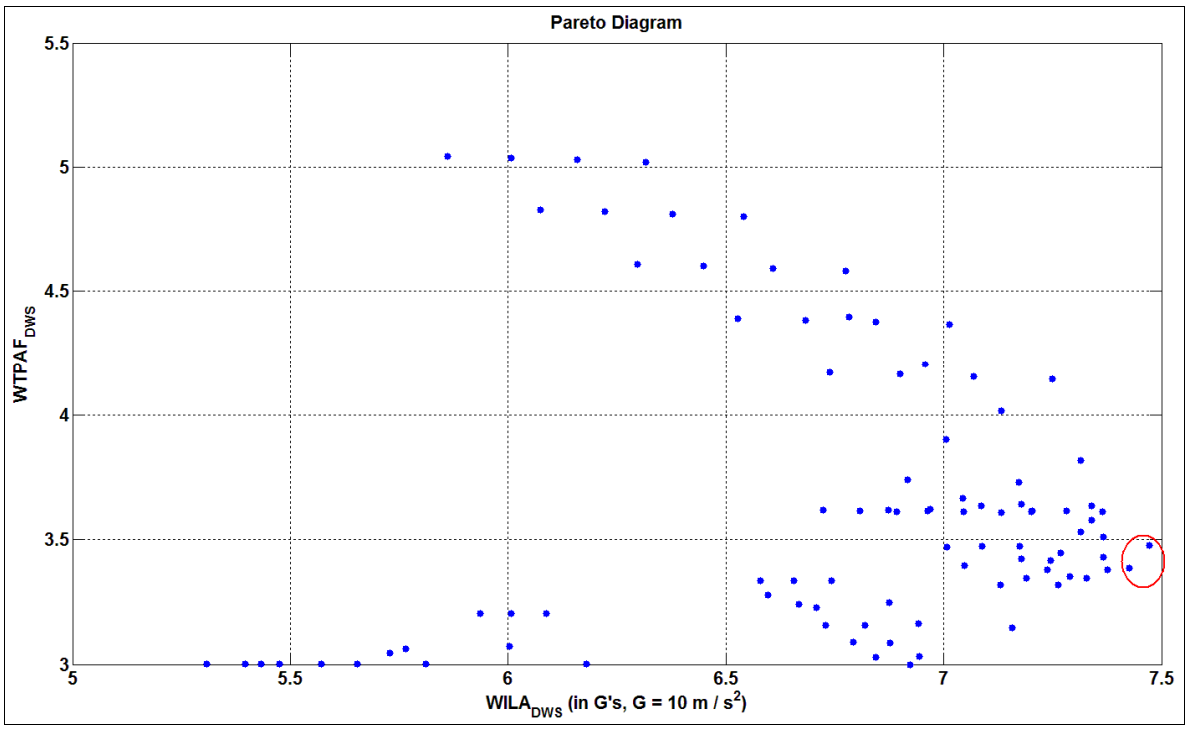

Fig. 3-28: Pareto diagram of ARROW V2 M2 with the two potential candidates encircled in red.

parameter in its valid range, then computing $WTPAF$ and $WILA$ characteristics. The results are depicted in **Fig. 3-28**. Based on the available options, we decided to consider the trade-offs described by having $WTPAF \leq 3.5$ and $WILA \geq 7.4\,\mathrm{g}$, meaning those two solutions encircled in red in **Fig. 3-28**. Among these two sets of geometric parameters, we have selected the one with the largest value of $WILA$. This solution is interesting because although it is has $WTPAF \approx 3.4$, the majority of DWS is characterized by $TPAF \leq 3$. Besides, it admits both: a compact overall structure and a large x-length of DWS, which is about $0.9\,\mathrm{m}$.

The values of the geometric parameters corresponding to this optimal solution are as follows (after slight numerical modifications):

$$\begin{cases} L_s = 0.96\,\mathrm{m} \\ L_p = 0.61\,\mathrm{m} \\ y_o = 0.55\,\mathrm{m} \end{cases} \tag{3.141}$$

For this set of parameters, described in (3.141), we have performed an analysis of FVI_p, the result of which has been satisfactory. In fact, we went further than that and performed an intensive study relative to other performance indices, as well.

In **Fig. 3-29**, **Fig. 3-30**, **Fig. 3-31**, **Fig. 3-32**, and **Fig. 3-33**, we represent the performance atlases of the optimal ARROW V2 M2 PKM with respect to ILA, $TPAF$, v_{iso}^{p}, f_{iso}^{p}, and PLA, respectively. These performances are mapped into the yz workspace of the PKM, for $\theta_z = 0°$ on one side and $\theta_z \in [-45°; +45°]$ on the other.

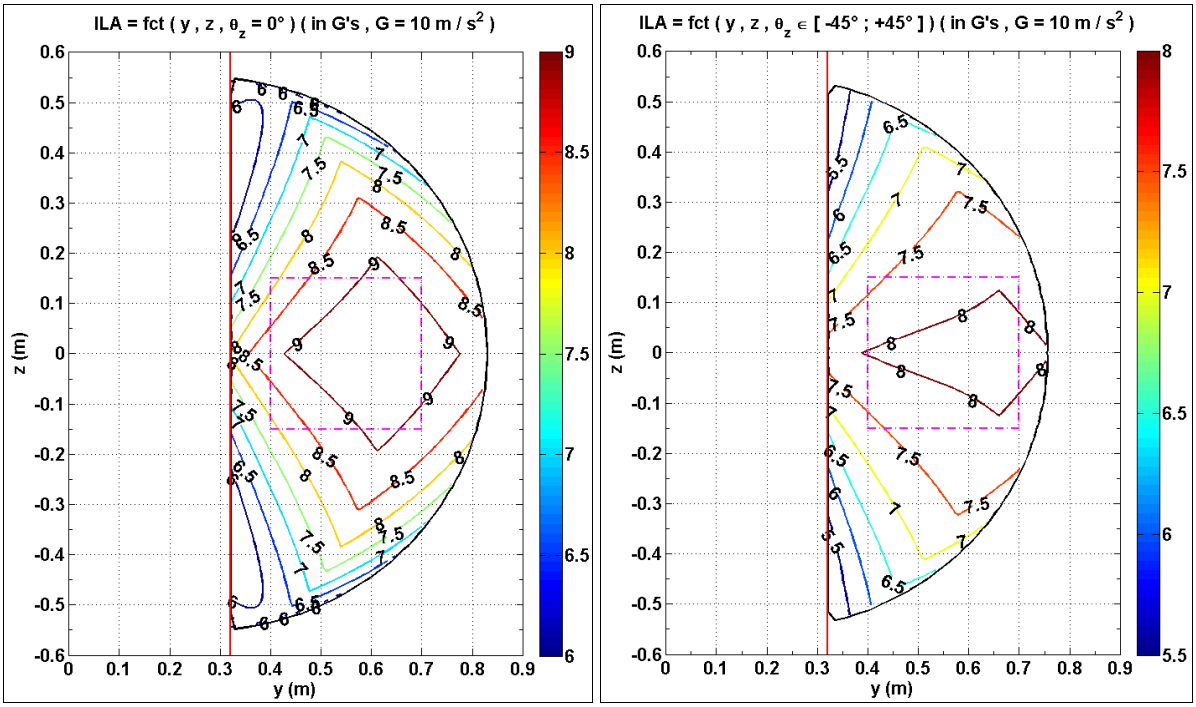

Fig. 3-29: ARROW V2 M2 PKM - ILA capacity: case $\theta_z = 0°$ (left) and case $\theta_z \in [-45°; +45°]$ (right).

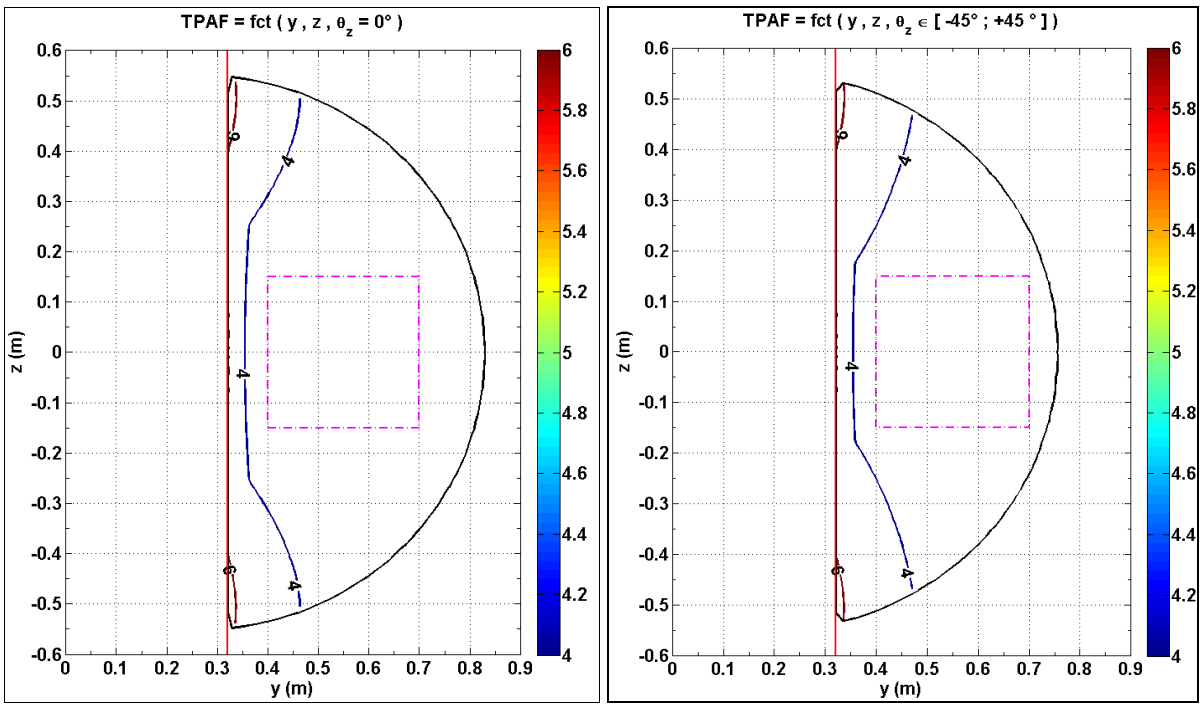

Fig. 3-30: ARROW V2 M2 - $TPAF$ performance: case $\theta_z = 0°$ (left) and case $\theta_z \in [-45°; +45°]$ (right).

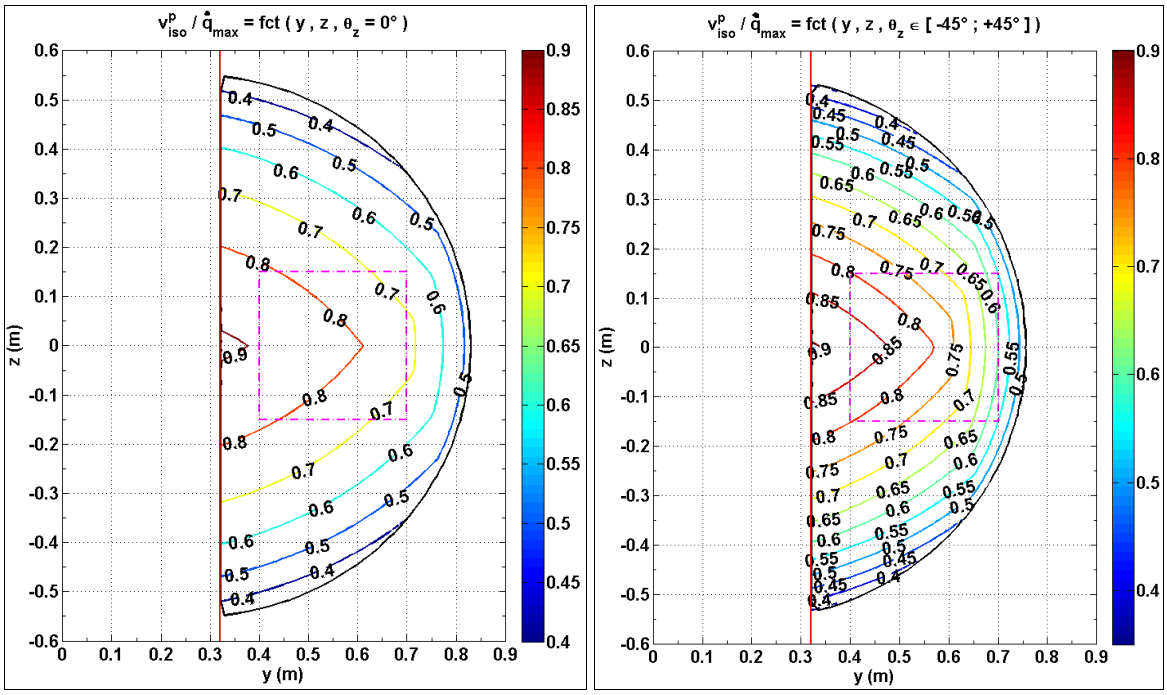

Fig. 3-31: ARROW V2 M2 PKM - v_{iso}^{p} capacity: case $\theta_z = 0°$ (left) and case $\theta_z \in [-45°; +45°]$ (right).

In all the aforementioned figures, the legend (i.e. the significance of the red line and the magenta box) and the methodology of computation for the case of $\theta_z \in [-45°; +45°]$ are the same as clarified in **§3.3.7**.

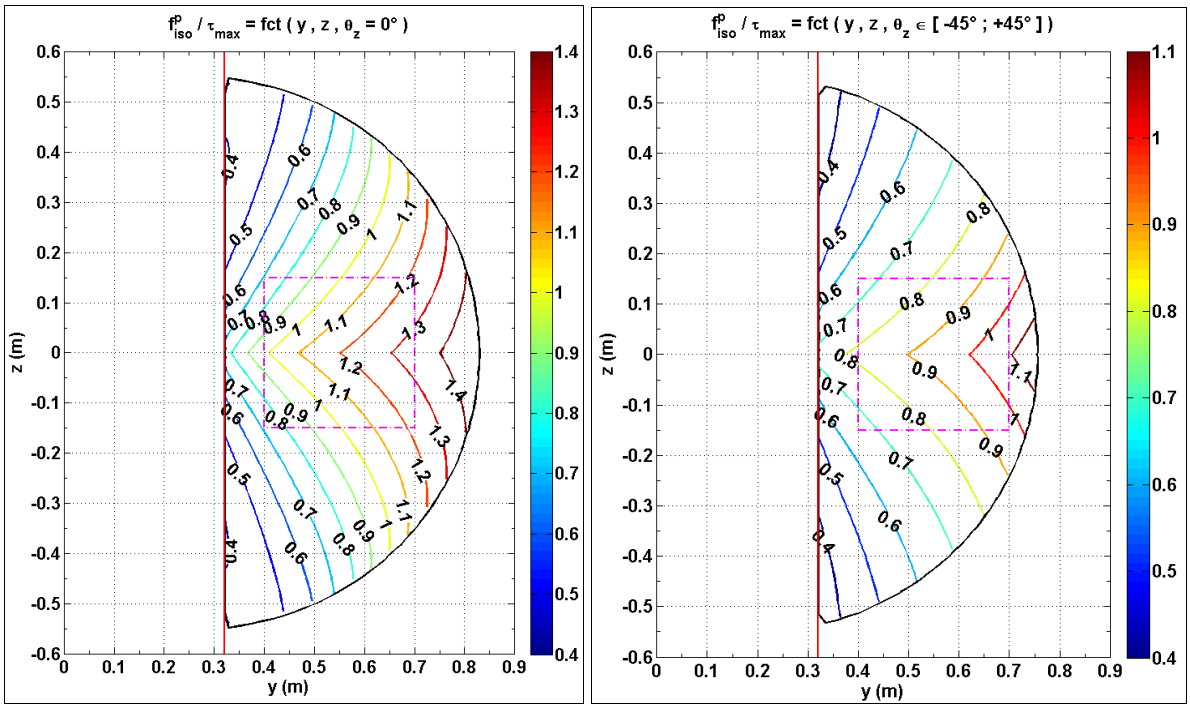

Fig. 3-32: ARROW V2 M2 PKM - f_{iso}^{p} capacity: case $\theta_z = 0°$ (left) and case $\theta_z \in [-45°; +45°]$ (right).

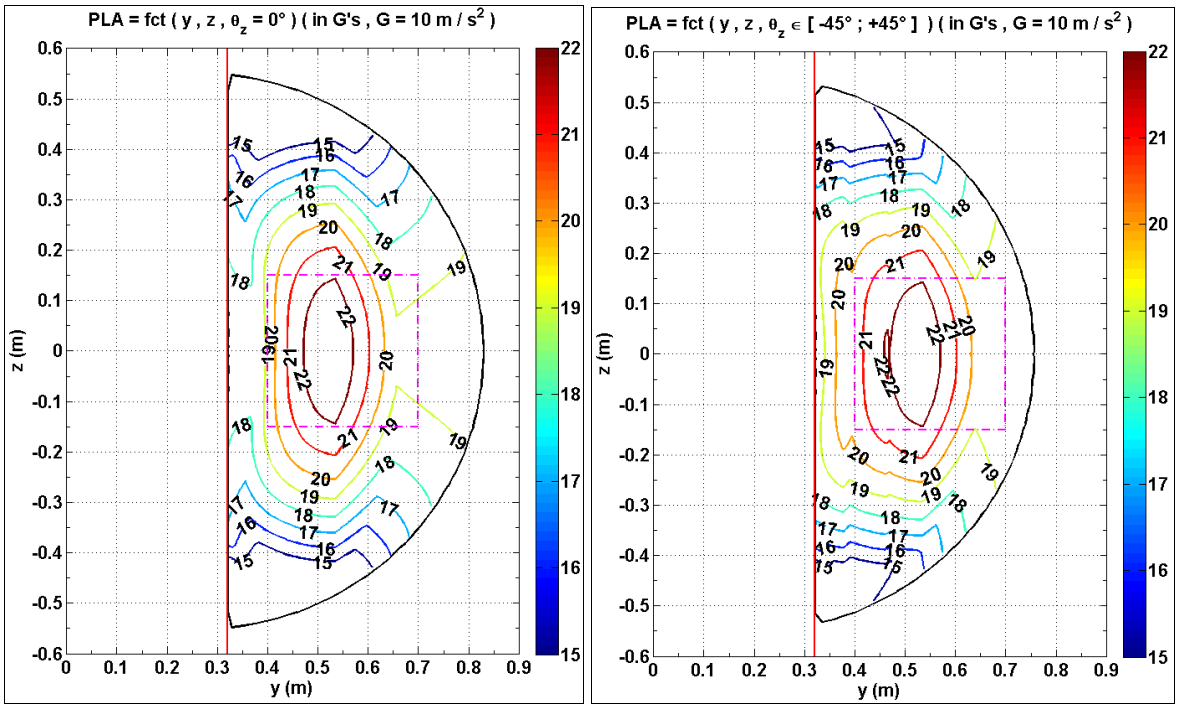

Fig. 3-33: ARROW V2 M2 PKM - PLA capacity: case $\theta_z = 0°$ (left) and case $\theta_z \in [-45°; +45°]$ (right).

Among the interesting results in this analysis, we mention the v_{iso}^{p} capacity that exceeds $0.55\,\dot{q}_{\max}$, and PLA that reaches 22 g, which is absolutely intriguing. This is not to mention the f_{iso}^{p} capacity that exceeds $0.8\,\tau_{\max}$ over DWS.

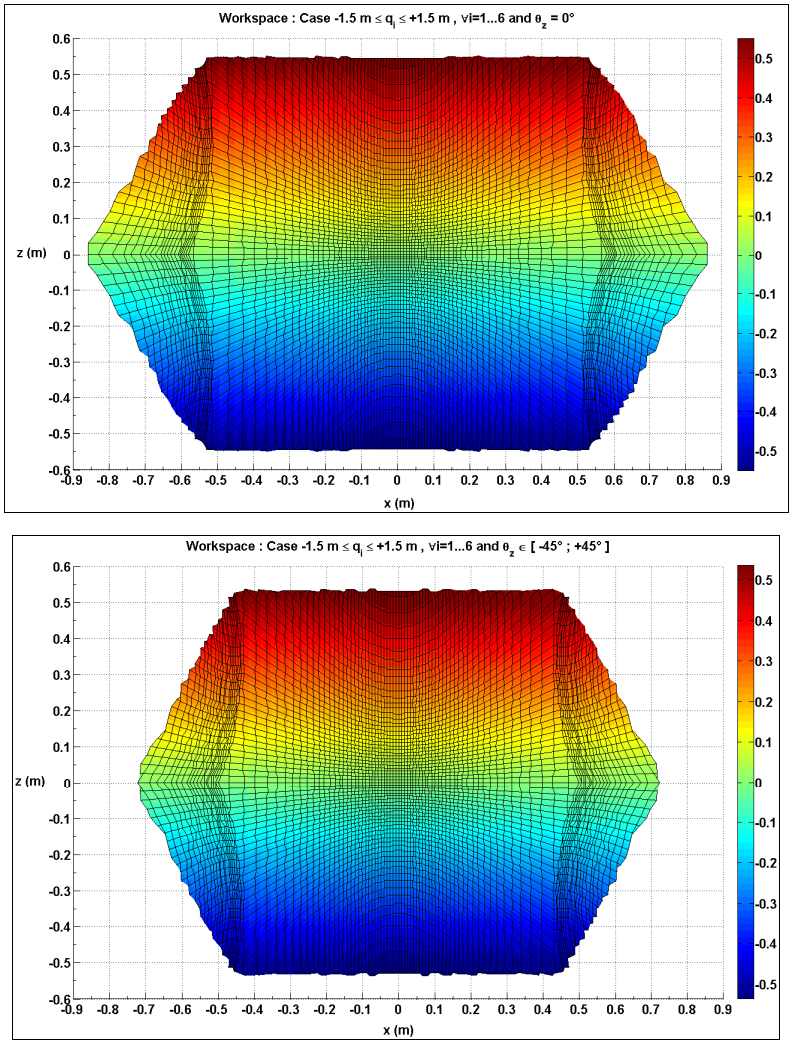

Fig. 3-34: ARROW V2 M2: illustrations of the spatial workspaces in the case of $\theta_z = 0°$ (top) and $\theta_z \in [-45°; +45°]$ (bottom).

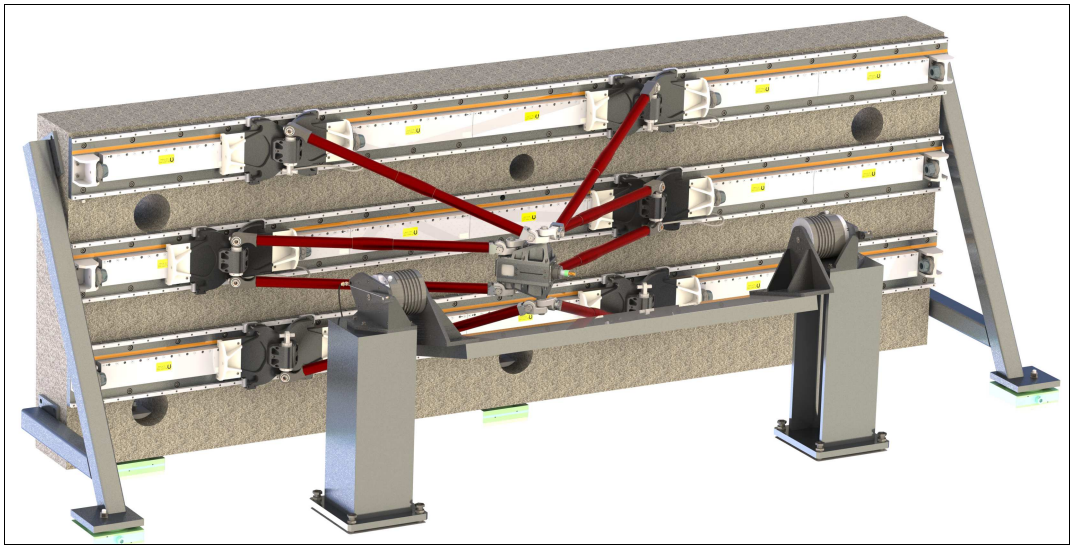

Fig. 3-35: ARROW V2 M2 PKM with turntable (rendered CAD drawing).

Actually, this study reveals not only an outstanding performance, but also a rather

homogeneous one.

To end this section, we provide in **Fig. 3-34** illustrations of the spatial workspaces of ARROW V2 M2 for the stroke lengths given in (3.139). Also, in **Fig. 3-35**, we show the total assembly of ARROW V2 M2 PKM with the turntable. Notice that the turntable has its axis parallel to the x direction and passing through the point P_o of coordinates $\boldsymbol{P_o} = \begin{pmatrix} 0 & y_o & 0 \end{pmatrix}^{\mathrm{T}}$.

3.5- Conclusion

In this chapter, we have discussed some novel architectures and detailed their modeling, singularity analysis, and workspace evaluation. All this has been done while highlighting their merits and drawbacks. Even for some, such as ARROW V1 and ARROW V2, an additional thorough study has been carried out. In particular, ARROW V2 has eventually exceeded the theoretical stage into the scope of practical implementation. Nevertheless, this implementation has put into attention the possibility of inter-arm collisions and necessitated some modifications. With the intention of sustaining the interesting manufacturability features of the initial concept, a slight change in the topology of ARROW V2 has been proposed and validated. The validation has been mainly concerned with assuring that the topological mutation does not result in any type of unexpected singularities. Fortunately, the altered design, namely ARROW V2 M2, has proved to preserve the main characteristics from singularity perspective. However, the mutation has resulted in adverse influence regarding modeling simplicity. An analytical form of the DGM is no more available, and neither the kinematic nor the singularity analysis is a straightforward problem. Ultimately, the dimensional synthesis of ARROW V2 M2 has been presented based on two primary criteria: precision ($WTPAF$) and dynamics ($WILA$). The optimized PKM is characterized by isotropic and peak linear accelerations of about $7.5\,\mathrm{g}$ and $22\,\mathrm{g}$, respectively. As for precision, its translational amplification factor does not exceed $WTPAF = 3.4$ over the desired workspace. Moreover, its isotropic linear speed and static force capacities are respectively more than $0.55\,\dot{q}_{\max} = 2.75$ to $3.85\,\mathrm{m/s}$ and $0.8\,\tau_{\max} = 2000\,\mathrm{N}$. Regarding peak linear speed, it can reach $WTPAF\ \dot{q}_{\max} = 3.4\,\dot{q}_{\max} = 17$ to $23.8\,\mathrm{m/s}$.

Based on the above, ARROW V2 M2 demonstrates to be worth holding its name. It is really an accurate and rapid PKM with a large operational workspace.

It remains to discuss the preliminary performance analysis of the implemented prototype and provide some insights on the possible future amelioration. These constitute the essence of the last chapter of this dissertation.

Chapter 4: ARROW PKM: Preliminary Performances, Geometric Sensitivity, and Possible Error Compensation

In this chapter:

This chapter is dedicated for discussing the preliminary precision evaluation of the ARROW prototype and the possible future enhancements. It starts by giving a general overview on the basic implemented control and the redundancy treatment. Then, the dynamic precision evaluation of the prototype, based on proprioceptive sensors, is presented, and some observations and remarks are accentuated. Afterwards, the general guidelines of geometric calibration and error compensation are provided. In this scope, the main points to deal with the absence of an explicit inverse geometric model, which embraces all the geometric parameters, are detailed. Furthermore, some insights on possible compensation of elastic deformations are discussed, in case a further improvement is needed to attain the anticipated precision.

4.1- Introduction

Within the time allocated for this doctoral thesis and due to the delay in the delivery of the prototype, we could perform neither a detailed performance analysis by exterioceptive means nor a geometric calibration. Nevertheless, we had the opportunity to assess the preliminary performances on the level of precision and dynamics, the results of which are quite promising.

This chapter addresses the aforementioned results and provides an overview on the possible future improvements. These refinements are related to the precision aspects of the PKM, as rapidity and dynamical requirements have been almost fulfilled.

Finally, the current chapter is outlined as follows. First, few words on the current basic control methodology and the treatment of redundancy are discussed. Afterwards, the dynamic precision performance along a sample trajectory is provided. Also, some of the apparent sources of the observed precision errors are accentuated. Based on the presented arguments, a general overview on the geometric calibration and error compensation is presented. Moreover, insights on the compensation of errors due to elastic deformations are exposed. The chapter eventually ends with conclusions.

4.2- ARROW V2 M2 Prototype: The Basic Control Strategy and Treatment of Redundancy

The currently implemented control is depicted in **Fig. 4-1**. Though it is generally based on the classical PID law, perhaps, few points are worth emphasizing, particularly regarding the treatment of redundancy. In fact, the control of RAMs is usually impeded by the possible occurrence of antagonistic control forces that might lead to system deformation, or even damage if not well treated.

This treatment is done by means of adding the regularization matrix, $\boldsymbol{R}_m$, at the entry as well as the output of the PID block (refer to **Fig. 4-1**). This method has been proposed in the confidential Ph.D thesis of (YANG, 2012). A similar approach has been also suggested by (HUFNAGEL & MULLER, 2012) and applied to PD control law. In this latter work, $\boldsymbol{R}_m$ is called antagonism filter (AF). The matrix $\boldsymbol{R}_m$ is defined as follows:

$$\boldsymbol{R}_m = \boldsymbol{J}_m^{\mathrm{T}^*}\,\boldsymbol{J}_m^{\mathrm{T}} \tag{4.1},$$

where $\boldsymbol{J}_m$ is the inverse Jacobian at the reference pose.

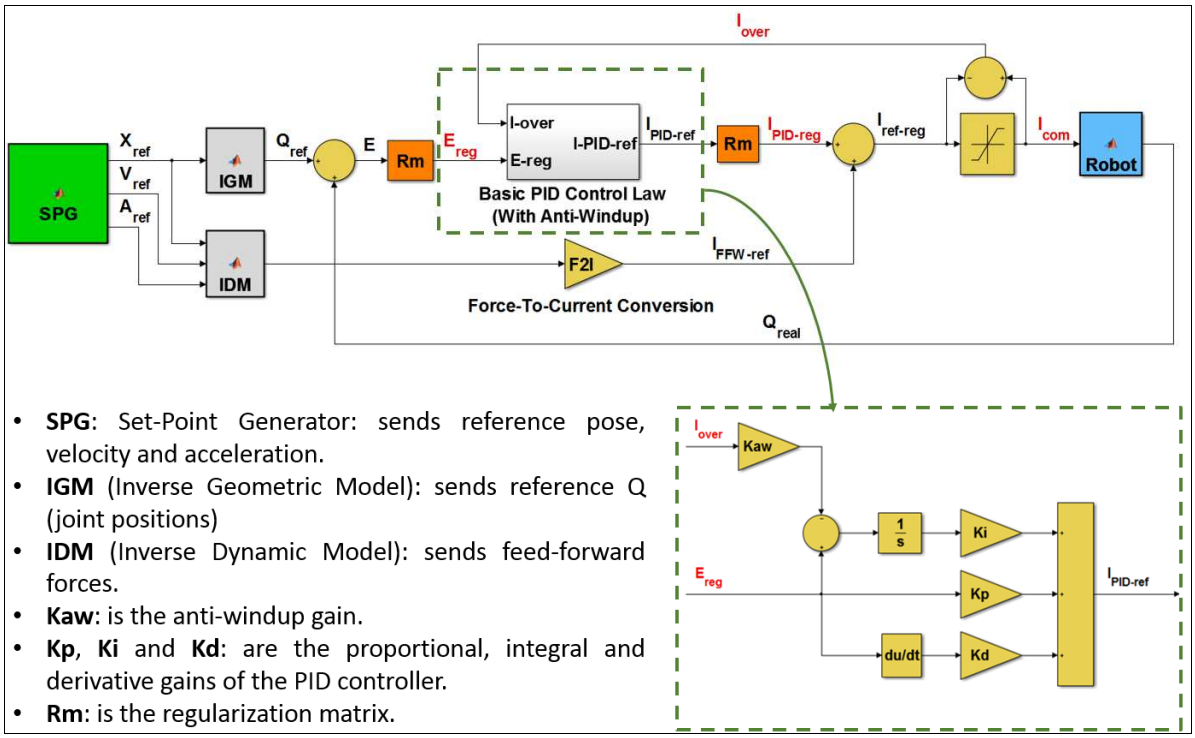

Fig. 4-1: ARROW V2 M2 PKM prototype: basic control model.

In fact, multiplying the joint error vector, $\boldsymbol{\delta q}$, by $\boldsymbol{R}_m$ is to assure that only the consistent part of $\boldsymbol{\delta q}$ is considered by the PID. Then, one might ask: what are the sources of the inconsistent part of $\boldsymbol{\delta q}$? The answer is quite simple. Generally speaking, there are two main sources for having $\boldsymbol{\delta q}^{\mathrm{T}}\left[\mathrm{null}\left(\boldsymbol{J}_m^{\mathrm{T}}\right)\right]\neq\boldsymbol{0}$ (or in other words $\left(\boldsymbol{\delta q}-\boldsymbol{R}_m\,\boldsymbol{\delta q}\right)\neq\boldsymbol{0}$). These are the inaccuracy of the measurement device, and the geometric errors. In our case, as we have very precise encoders with nanometric resolution, the incertitude in measurement has negligible effect. Contrarily to that, geometric errors are most often the primary source of the inconsistent portion of $\boldsymbol{\delta q}$. Actually, as these errors increase, the value $\left\|\boldsymbol{\delta q}-\boldsymbol{R}_m\,\boldsymbol{\delta q}\right\|$ increases as well. That is why the value $\left\|\boldsymbol{\delta q}-\boldsymbol{R}_m\,\boldsymbol{\delta q}\right\|$ can be a good indicator on how well the geometric calibration has been done.

On the other hand, the regularization at the output of the PID block assures that only the actuation-force vector[1], $\boldsymbol{\tau}$, with zero components along the null space of $\boldsymbol{J}_m^{\mathrm{T}}$ (i.e. $\boldsymbol{\tau}^{\mathrm{T}}\left[\mathrm{null}\left(\boldsymbol{J}_m^{\mathrm{T}}\right)\right]=\boldsymbol{0}$), is being considered and commanded for the actuators. This methodology fulfills the assumption we have made in the establishment of the inverse static and dynamic models for this redundantly actuated PKM. Nevertheless, we might have $\boldsymbol{\tau}^{\mathrm{T}}\left[\mathrm{null}\left(\boldsymbol{J}_m^{\mathrm{T}}\right)\right]=\boldsymbol{0}$ violated in one case, which is when electric current saturation occurs.

[1] Note that electric current is directly proportional the force in an electric actuator.

A final remark to make is regarding the anti-windup strategy. The main role of this part is to maintain control stability and avoid oscillatory behavior of the PKM when saturation occurs. In particular, its target is to overcome the problem of integral term accumulation in the mentioned situation. Within the same scope, we highlight that a slighty modified approach to manage integration has been adopted as well, as to avoid numerical overflow. This modified management is that proposed by (YANG, 2012); it is not depicted in **Fig. 4-1** for simplicity.

Having presented briefly the implemented control strategy and clarified the main points concerning redundancy, the following section will present some of the acquired preliminary performances of ARROW V2 M2 PKM.

4.3- Preliminary Precision Evaluation of ARROW V2 M2 PKM

In this section, we provide some dynamic precision analysis of the prototype for a commanded sample trajectory. We highlight here that due to a noticed defect in some of the joints in addition to power supply limitations, we did not exceed $10\,\mathrm{g}$ linear acceleration and $4\,\mathrm{m/s}$ linear speed. Several trajectories have been tested, but we are going to limit our discussion to the most prominent one. This is given in **Fig. 4-2**. We clarify that in this figure, the capitalized notations, X, Y, Z, and B, are the names of the axes of motion of the PKM following the machine tool conventions; they correspond respectively to the notations: x, z, $(-y)$, and θ_z, which are used in modeling and which we adopt throughout this report.

Both the non-regularized and regularized joint tracking errors, namely $\boldsymbol{E} = \boldsymbol{\delta q}$ and $\boldsymbol{E}_{reg} = \boldsymbol{R}_m\ \boldsymbol{\delta q}$ in **Fig. 4-1**, have been registered in realtime and are depicted in **Fig. 4-3**. In **Fig. 4-4**, an estimation of the tracking errors in the operational space have been computed and visualized. Their calculation has been based on the following relation:

$$\boldsymbol{\delta x} = \begin{pmatrix} \delta x & \delta y & \delta z & \delta\theta_z \end{pmatrix}^{\mathrm{T}} = \boldsymbol{J}_{\boldsymbol{m}}^{*}\ \boldsymbol{\delta q} \tag{4.2}$$

Several points can be made based on **Fig. 4-3** and **Fig. 4-4**. These are summarized in the enumerated list below:

1. All tracking errors peak at the same instant (about $t = 64\,\mathrm{s}$) and this is due to the high loading involved on the defected joints, particularly those of the third and fourth complex limbs. Notice that at this instant, we have $10\,\mathrm{g}$ linear acceleration in the vertical direction (refer to the green curve in **Fig. 4-2**). Currently, the design of these joints is being reconsidered. This will probably help overcome the observed phenomenon.

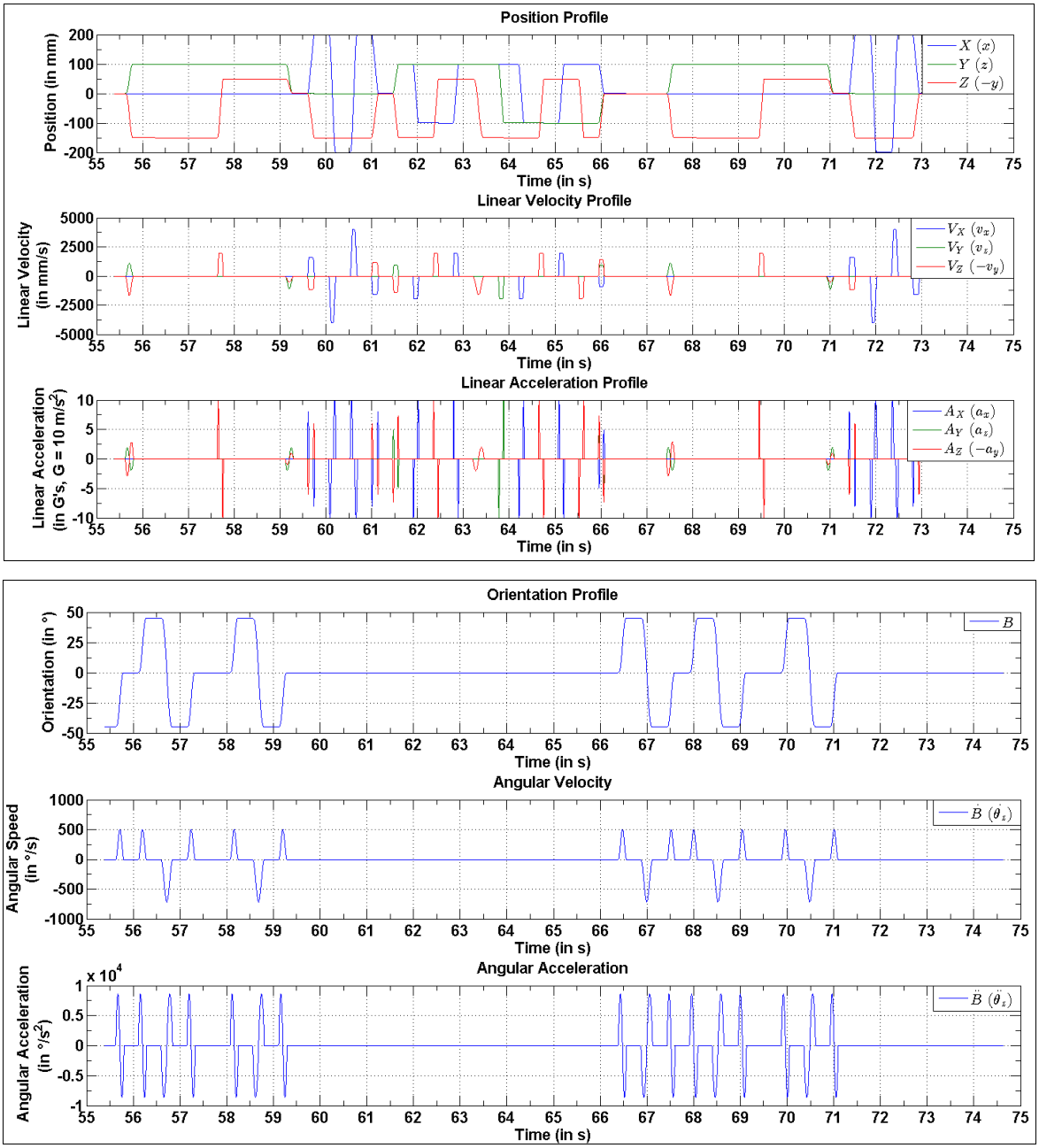

Fig. 4-2: The tested trajectory profile.

2. The translational tracking errors, except for the aforementioned case, seem to be rather interesting, in which they do not exceed $0.1\,\mathrm{mm}$. Moreover, in statics, it has been noticed that such tracking errors go below $20\,\mu\mathrm{m}$, which is quite remarkable.
3. The controlled orientation error is interesting as well. Except for $t \approx 64\,\mathrm{s}$, the estimated error is less than $0.01°$.

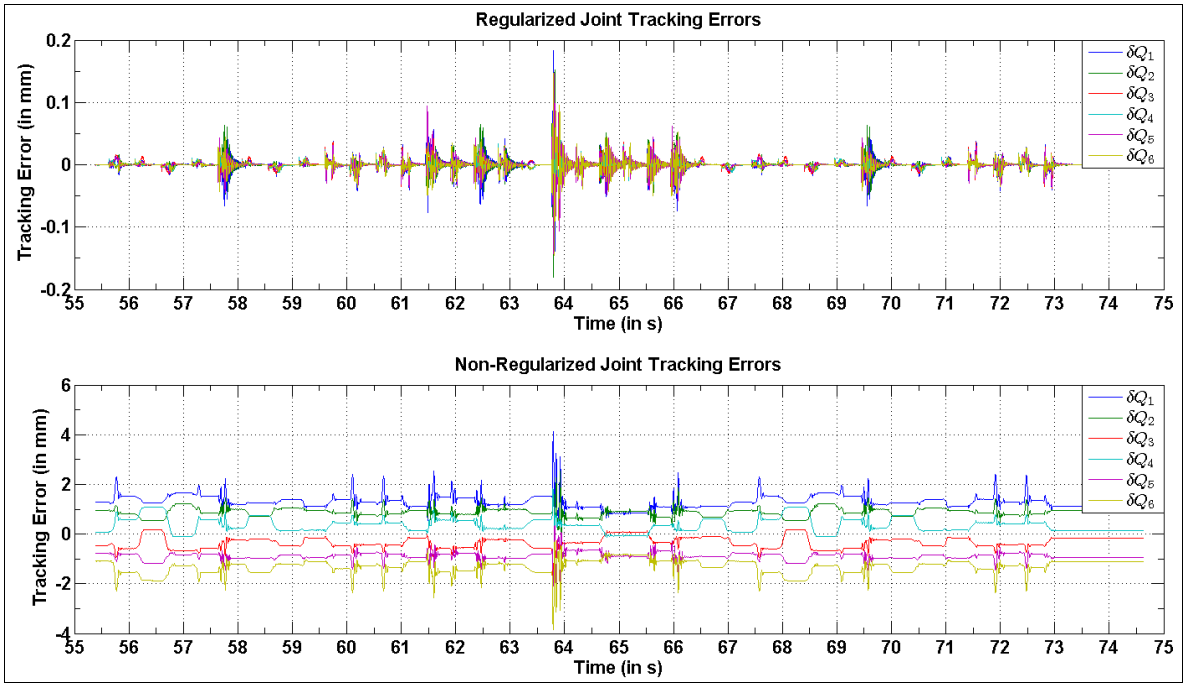

Fig. 4-3: Actuated-joint tracking errors for the trajectory profile in Fig. 4-2.

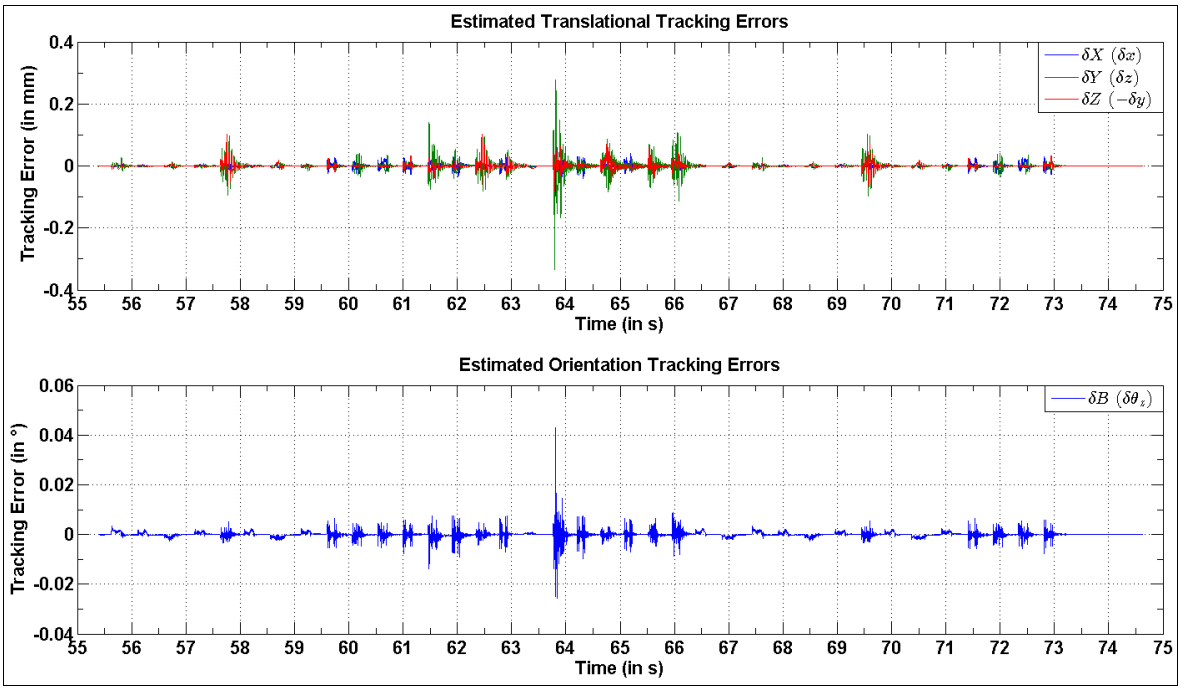

Fig. 4-4: Estimated tracking errors in the operational space.

4. Analyzing **Fig. 4-3** shows that the regularized errors are much less than the non-regularized ones. This indicates the presence of non-negligible geometric errors. This can be supported by observing the non-regularized tracking errors after $t = 73\,\mathrm{s}$ (static phase), in which they settle to about $1\,\mathrm{mm}$. On the other hand, the small-regularized tracking errors show that though the control is of basic nature, it is still rather effective

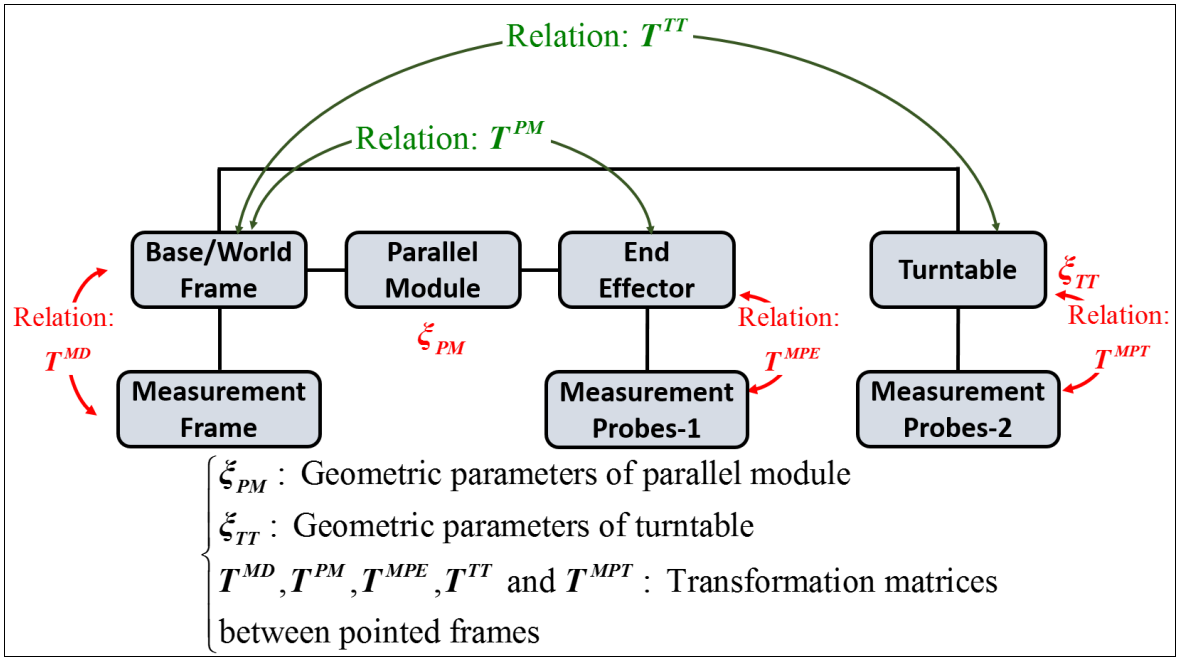

Fig. 4-5: ARROW PKM geometric calibration: the main relations.

and well tuned. Thus, we can expect much better performance based on a more advanced control strategy.

Finally, we highlight that in what concerns geometric errors, we have already some knowledge of these discrepancies. In fact, some of them have been mentioned by the manufacturing company in its quality control report. However, while compensating for some of these errors is a straightforward process (e.g. the simple arm lengths), it is not the case for others (e.g. lengths of the rods in the complex chains, the direction of the revolute joints, etc.).

Therefore, it is indispensable to explore the calibration of ARROW PKM and the possible method of error compensation. These are the essence of the upcoming section.

4.4- Geometric Calibration and Methodology of Error Compensation

While repeatability is attributable to non-deterministic sources, accuracy is of deterministic nature and therefore subject for enhancement. Among the main sources of accuracy degradation are geometric errors. These result at the time of manufacturing of the different components (manufacturing tolerances) or at their assembly. Other causes of inaccuracy are deformations; a machine tool though is usually very stiff, it remains non-infinitely rigid and consequently elastic deformations are inevitable.

This section is dedicated to deal with geometric errors and their compensation, in which we brief the main guidelines. The goal is to present the general approach, as slight modifications exist in comparison to what we are classically used to.

First, we mention that a proper calibration should consider simultaneously: the parallel module, the turntable, the measurement frame on the end-effector, and the proper frame of the measurement device. This is clarified in the schematic given in **Fig. 4-5**. In this figure, the measurement frame corresponds to that of the measurement device, such as the Metris camera, Laser Tracker, etc. Regarding the measurement probes, they correspond to the means by which the end-effector pose is determined, for instance: LEDs, spherical mirrors, etc. Therefore, in practice, we need to identify not only the parallel module and turntable geometric parameters, namely $\boldsymbol{\xi}_{PM}$ and $\boldsymbol{\xi}_{TT}$, but also those that determine the transformation matrices: $\boldsymbol{T}^{MD}$, $\boldsymbol{T}^{MPE}$, and $\boldsymbol{T}^{MPT}$.

However, our aim here is just to give an overview on the calibration approach to deal with the parallel module only. Actually, one of the key issues in this scope is how to account for the influence of the complex chain geometric errors. Obtaining an analytic inverse geometric model (IGM) embracing all the possible geometric parameters, particularly the aforementioned ones, is very difficult, if not impossible. So, how can we overcome this barrier?

Perhaps, the solution is to consider the strategy proposed by (SAVOURE, et al., 2006) for parallelogram-based robots. In the following subsection (**§4.4.1**), we exploit this method to perform a sensitivity analysis on the parallel module of the ARROW machine. Afterwards, **§4.4.2** presents the methodology of error compensation, and **§4.4.3** provides some general remarks.

4.4.1- Geometric Sensitivity of ARROW V2 M2

The geometric parameters that are considered for calibration are clarified in **Fig. 4-6** and **Fig. 4-7**. In these figures, we highlight the following designations:

1. $\boldsymbol{e}_{xp}$ corresponds to the unit vector along the x-direction of the platform frame.
2. $\boldsymbol{vect}^{plat}$ signify the components of vector $\boldsymbol{vect}$ in the platform frame.
3. $\mathrm{proj}_{\mathrm{xy}}(\ldots)$ and $\mathrm{proj}_{\mathrm{xyp}}(\ldots)$ denote the projection of a vector into the xy planes of the base and platform frames, respectively.
4. c_θ and s_θ denote $\cos(\theta)$ and $\sin(\theta)$, respectively.
5. $\boldsymbol{x}_c = \left(\boldsymbol{P}^{\mathrm{T}} \quad \boldsymbol{\theta}^{\mathrm{T}}\right)^{\mathrm{T}} = \left(x \quad y \quad z \quad \theta_x \quad \theta_y \quad \theta_z\right)^{\mathrm{T}}$ is the complete pose of the end-effector, with $\boldsymbol{P}$ being the coordinates of $P \equiv TCP$ and $\boldsymbol{\theta}$ corresponding to the vector composed of Euler angles.
6. $\boldsymbol{e}_k$ corresponds to the direction of the k-th linear track. We have $k=1$ for $i=1,2$, $k=2$ for $i=3,4$ and $k=3$ for $i=5,6$, where i is the number of the kinematic chain.

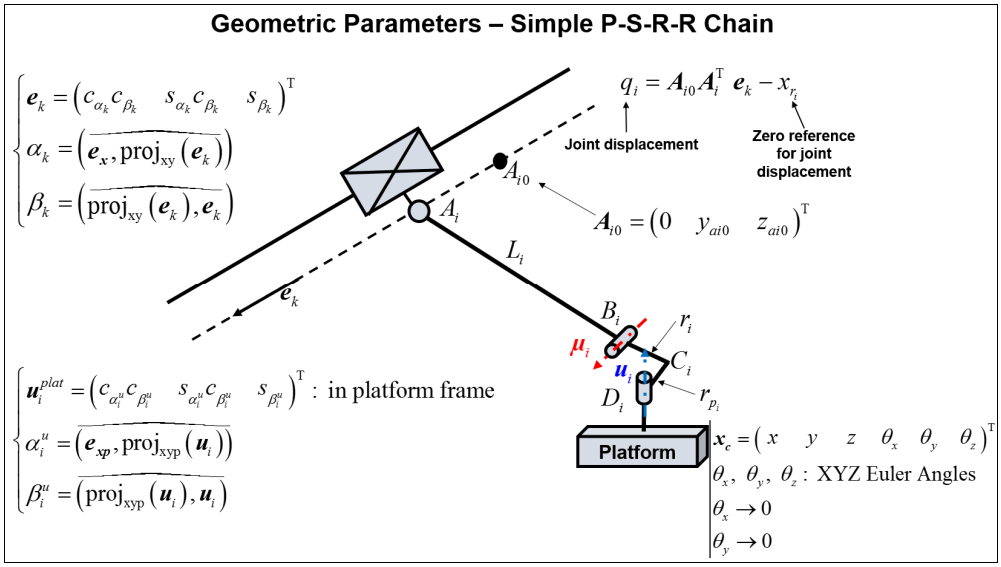

Fig. 4-6: Calibration parameters of the simple PSRR chain.

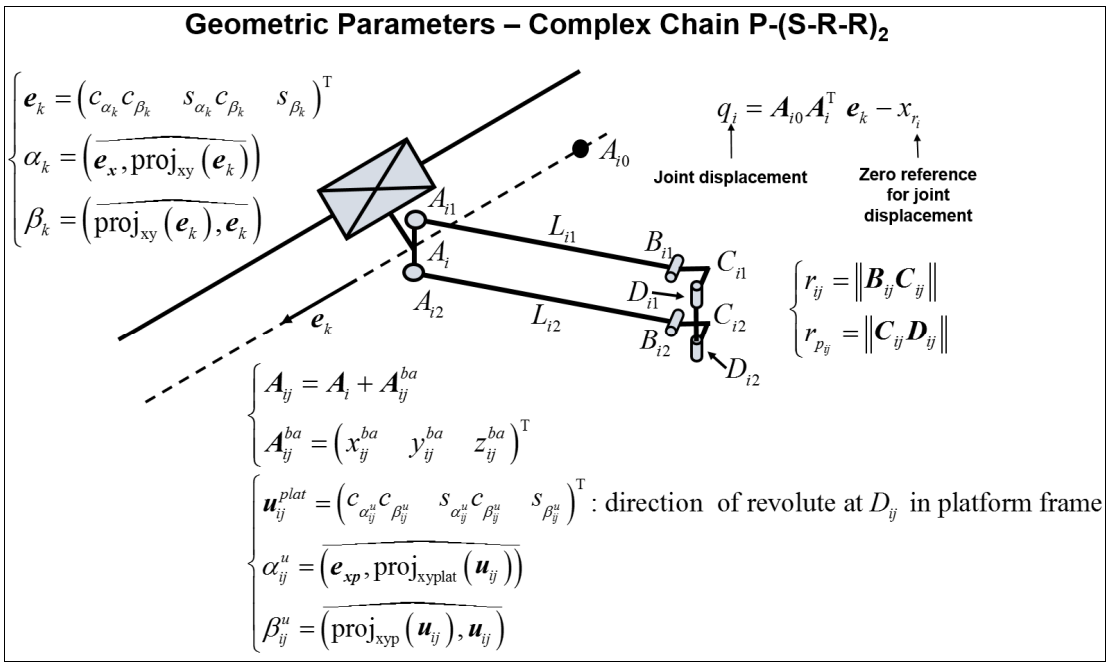

Fig. 4-7: Calibration parameters of the complex P(SRR)$_2$ chain.

7. The points B_i, B_{ij}, D_i, and D_{ij} have the following coordinates in their proper frames: $\boldsymbol{B}_i^{BCD_i} = \begin{pmatrix} x_{bi}^{BCD_i} & y_{bi}^{BCD_i} & z_{bi}^{BCD_i} \end{pmatrix}^{\mathrm{T}}$, $\boldsymbol{B}_{ij}^{BCD_{ij}} = \begin{pmatrix} x_{bij}^{BCD_{ij}} & y_{bij}^{BCD_{ij}} & z_{bij}^{BCD_{ij}} \end{pmatrix}^{\mathrm{T}}$, $\boldsymbol{D}_i^{plat} = \begin{pmatrix} x_{di}^{plat} & y_{di}^{plat} & z_{di}^{plat} \end{pmatrix}^{\mathrm{T}}$, and $\boldsymbol{D}_{ij}^{plat} = \begin{pmatrix} x_{dij}^{plat} & y_{dij}^{plat} & z_{dij}^{plat} \end{pmatrix}^{\mathrm{T}}$, with BCD_i and BCD_{ij} being the proper frames of B_i and B_{ij} of origins D_i and D_{ij}, respectively. Note that BCD_i and BCD_{ij} are shorthands for $B_iC_iD_i$ and $B_{ij}C_{ij}D_{ij}$, respectively.

Then, to establish the relation between the geometric errors of the parallel module, $\boldsymbol{\delta\xi_{PM}}$, and the complete end-effector pose error, $\boldsymbol{\delta x_c} = \begin{pmatrix} \delta x & \delta y & \delta z & \delta\theta_x & \delta\theta_y & \delta\theta_z \end{pmatrix}^{\mathrm{T}}$, a classical approach would be to determine the IGM, then differentiate it with respect to $\boldsymbol{q}$, $\boldsymbol{x_c}$, and $\boldsymbol{\xi_{PM}}$. But as mentioned earlier, such IGM is difficult to establish. Thus, the solution is to consider the basic constraint equations, $\mathbf{F}\left(\boldsymbol{q}, \boldsymbol{x_c}, \boldsymbol{\xi_{PM}}\right) = \mathbf{0}$, as suggested by (SAVOURE, et al., 2006).

Following the lead of (SAVOURE, et al., 2006), we start by considering the following constraints:

$$\boldsymbol{A_i B_i}^2 = L_i^2, \ \forall i = 1,2,5,6 \tag{4.3}$$

and

$$\boldsymbol{A_{ij} B_{ij}}^2 = L_{ij}^2, \ \forall i = 3,4 \text{ and } \forall j = 1,2 \tag{4.4}.$$

Differentiating (4.3) and (4.4), we get:

$$\boldsymbol{A_i B_i}^{\mathrm{T}} \ \boldsymbol{dA_i B_i} = \boldsymbol{A_i B_i}^{\mathrm{T}} \left(\boldsymbol{dB_i} - \boldsymbol{dA_i}\right) = L_i \ dL_i, \ \forall i = 1,2,5,6 \tag{4.5}$$

and

$$\boldsymbol{A_{ij} B_{ij}}^{\mathrm{T}} \ \boldsymbol{dA_{ij} B_{ij}} = \boldsymbol{A_{ij} B_{ij}}^{\mathrm{T}} \left(\boldsymbol{dB_{ij}} - \boldsymbol{dA_{ij}}\right) = L_{ij} \ dL_{ij}, \ \forall i = 3,4 \text{ and } \forall j = 1,2 \tag{4.6}.$$

The idea now is to replace $\boldsymbol{dA_i}$, $\boldsymbol{dB_i}$, $\boldsymbol{dA_{ij}}$, and $\boldsymbol{dB_{ij}}$ in terms of $\boldsymbol{dx_c}$ (the differential of $\boldsymbol{x_c}$), $\boldsymbol{dq}$ (the differential of $\boldsymbol{q}$), and $\boldsymbol{d\xi_{PM}}$ (the differential of $\boldsymbol{\xi_{PM}}$). This is done by considering the following expressions:

$$\boldsymbol{A_i} = \boldsymbol{A_{i0}} + \left(q_i + x_{r_i}\right) \boldsymbol{e_k} \Rightarrow \boldsymbol{dA_i} = \boldsymbol{dA_{i0}} + \left(dq_i + dx_{r_i}\right) \boldsymbol{e_k} + \left(q_i + x_{r_i}\right) \boldsymbol{de_k} \tag{4.7},$$

$$\begin{cases} \boldsymbol{A_{ij}} = \boldsymbol{A_{ij0}} + \left(q_i + x_{r_i}\right) \boldsymbol{e_k} \Rightarrow \boldsymbol{dA_{ij}} = \boldsymbol{dA_{ij0}} + \left(dq_i + dx_{r_i}\right) \boldsymbol{e_k} + \left(q_i + x_{r_i}\right) \boldsymbol{de_k}, \text{ with:} \\ \boldsymbol{A_{ij0}} = \boldsymbol{A_{i0}} + \boldsymbol{A_{ij}^{ba}} \end{cases} \tag{4.8},$$

$$\begin{cases} \boldsymbol{B_i} = \boldsymbol{P} + \boldsymbol{R} \ \boldsymbol{B_i^{plat}} = \boldsymbol{P} + \boldsymbol{R} \left(\boldsymbol{D_i^{plat}} + \boldsymbol{R_{plat}^{BCD_i}} \ \boldsymbol{B_i^{BCD_i}}\right), \text{ which implies:} \\ \boldsymbol{dB_i} = \boldsymbol{dP} + \boldsymbol{dR} \ \boldsymbol{D_i^{plat}} + \boldsymbol{R} \ \boldsymbol{dD_i^{plat}} + \boldsymbol{dR}^{BCD_i} \ \boldsymbol{B_i^{BCD_i}} + \boldsymbol{R}^{BCD_i} \ \boldsymbol{dB_i^{BCD_i}} \end{cases} \tag{4.9},$$

and

$$\begin{cases} \boldsymbol{B_{ij}} = \boldsymbol{P} + \boldsymbol{R} \ \boldsymbol{B_{ij}^{plat}} = \boldsymbol{P} + \boldsymbol{R} \left(\boldsymbol{D_{ij}^{plat}} + \boldsymbol{R_{plat}^{BCD_{ij}}} \ \boldsymbol{B_{ij}^{BCD_{ij}}}\right), \text{ which implies:} \\ \boldsymbol{dB_{ij}} = \boldsymbol{dP} + \boldsymbol{dR} \ \boldsymbol{D_{ij}^{plat}} + \boldsymbol{R} \ \boldsymbol{dD_{ij}^{plat}} + \boldsymbol{dR}^{BCD_{ij}} \ \boldsymbol{B_{ij}^{BCD_{ij}}} + \boldsymbol{R}^{BCD_{ij}} \ \boldsymbol{dB_{ij}^{BCD_{ij}}} \end{cases} \tag{4.10},$$

with:

- $\boldsymbol{R}$: the rotation matrix of the platform with respect to the base frame in terms of Euler angles (θ_x, θ_y, and θ_z);

- $\boldsymbol{N}^{frame}$: the coordinates of a point N ($N = B_i, B_{ij}, D_i, D_{ij}$) expressed in the frame of reference, $frame$ ($frame = plat, BCD_i, BCD_{ij}$);
- $\boldsymbol{R}_{plat}^{BCD_i}$ ($\boldsymbol{R}_{plat}^{BCD_{ij}}$): the rotation matrix of the part BCD_i (correspondingly BCD_{ij}) with respect to the platform;
- and $\boldsymbol{R}^{BCD_i} = \boldsymbol{R}\,\boldsymbol{R}_{plat}^{BCD_i}$ ($\boldsymbol{R}^{BCD_{ij}} = \boldsymbol{R}\,\boldsymbol{R}_{plat}^{BCD_{ij}}$): the rotation matrix of BCD_i (correspondingly BCD_{ij}) with respect to the base frame.

Note that we have $\boldsymbol{R}_{plat}^{BCD_i} = \mathrm{Rot}\left(\boldsymbol{u}_i, \psi_{r_i}\right)$ and $\boldsymbol{R}_{plat}^{BCD_{ij}} = \mathrm{Rot}\left(\boldsymbol{u}_{ij}, \psi_{r_{ij}}\right)$, where ψ_{r_i} and $\psi_{r_{ij}}$ are the rotation angles about $\boldsymbol{u}_i$ and $\boldsymbol{u}_{ij}$, respectively. For nominal conditions of assembly and geometric parameters, we have $\boldsymbol{u}_i = \boldsymbol{u}_{ij} = \boldsymbol{e}_z$ and consequently, ψ_{r_i} and $\psi_{r_{ij}}$ are the same as those clarified in **Fig. 3-24** and **Fig. 3-25**.

In brief, we proceed by developing (4.7) through (4.10) in terms of $\boldsymbol{dq}$, $\boldsymbol{dx_c}$, $\boldsymbol{d\xi_{PM}}$, $d\psi_{r_i}$, and $d\psi_{r_{ij}}$. Then, we substitute the latter results in (4.5) and (4.6) to get the following general relation:

$$\boldsymbol{M_q}\,\boldsymbol{dq} + \boldsymbol{M_{x_c}}\,\boldsymbol{dx_c} + \boldsymbol{M_{\psi_r}}\,\boldsymbol{d\psi_r} + \boldsymbol{M_{\xi_{PM}}}\,\boldsymbol{d\xi_{PM}} = \boldsymbol{0} \tag{4.11},$$

with:

- $\boldsymbol{M_q}$, $\boldsymbol{M_{x_c}}$ and $\boldsymbol{M_{\psi_r}}$: being 8×6 matrices;
- $\boldsymbol{M_{\xi_{PM}}}$: being $8\times\dim\left(\boldsymbol{\xi_{PM}}\right)$ matrix;
- and $\boldsymbol{d\psi_r} = \left(d\psi_{r_1} \quad d\psi_{r_2} \quad d\psi_{r_{31}} \quad d\psi_{r_{32}} \quad d\psi_{r_{41}} \quad d\psi_{r_{42}} \quad d\psi_{r_5} \quad d\psi_{r_6}\right)^{\mathrm{T}}$.

Now, we should get rid of $\boldsymbol{d\psi_r}$ from (4.11). This can be easily done by considering the nominal conditions, in which we can write $\boldsymbol{d\psi_r}$ in terms of $\boldsymbol{dx_c}$ by utilizing (3.105) and knowing that:

$$\begin{cases} d\psi_{r_i} = \dot{\psi}_{r_i}\,dt, \ \forall i = 1,2,5,6 \\ d\psi_{r_{ij}} = \dot{\psi}_{r_{ij}}\,dt, \ \forall i = 3,4 \text{ and } \forall j = 1,2 \\ \dot{\psi}_{r_{i1}} = \dot{\psi}_{r_{i2}} = \dot{\psi}_{r_i}, \ \forall i = 3,4 \\ \dot{\psi}_{r_i} = \dot{\psi}_i - \dot{\theta}_z, \ \forall i = 1\ldots 6 \end{cases} \tag{4.12}.$$

As a result, we get the following general form[2]:

$$\boldsymbol{J_q^F}\,\boldsymbol{dq} + \boldsymbol{J_{x_c}^F}\,\boldsymbol{dx_c} + \boldsymbol{J_{\xi_{PM}}^F}\,\boldsymbol{d\xi_{PM}} = \boldsymbol{0} \tag{4.13},$$

[2] Details are omitted and only general forms are given here. Yet, the explicit expressions can be established symbolically by hand or by using the symbolic toolbox of MATLAB (following the described steps).

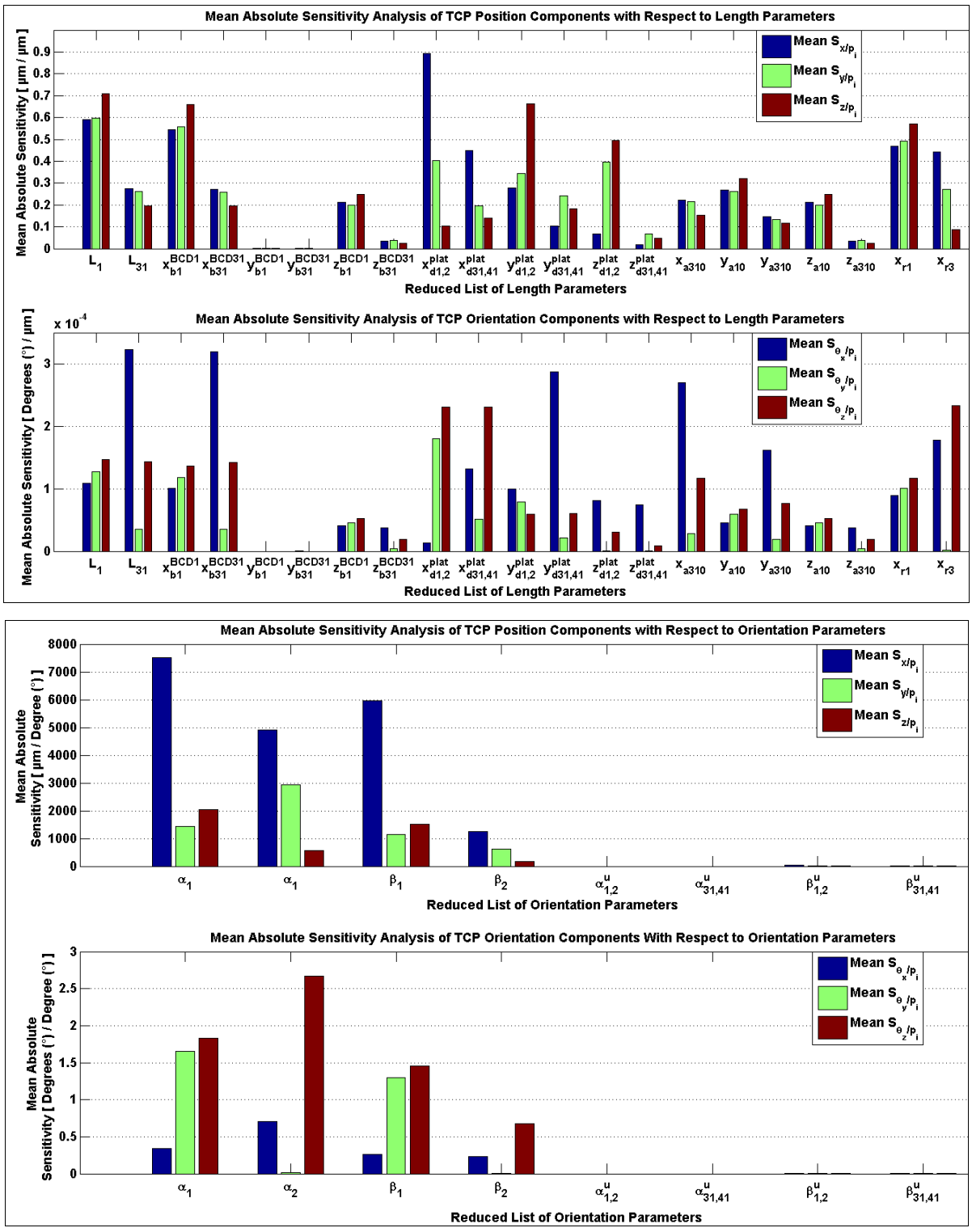

Fig. 4-8: Mean absolute geometric sensitivity of ARROW V2 M2 prototype.

with $\boldsymbol{J}_{\boldsymbol{q}}^{\boldsymbol{F}}$ and $\boldsymbol{J}_{\boldsymbol{x}_c}^{\boldsymbol{F}}$ being 8×6 matrices and $\boldsymbol{J}_{\boldsymbol{\xi}_{PM}}^{\boldsymbol{F}}$ being $8\times\dim\left(\boldsymbol{\xi}_{PM}\right)$ matrix.

As we are only considering geometric errors, we set $\boldsymbol{dq}=\boldsymbol{0}$. This implies:

$$\boldsymbol{dx}_c=\boldsymbol{S}_g\,\boldsymbol{d\xi}_{PM}=-\boldsymbol{J}_{\boldsymbol{x}_c}^{\boldsymbol{F}*}\,\boldsymbol{J}_{\boldsymbol{\xi}_{PM}}^{\boldsymbol{F}}\,\boldsymbol{d\xi}_{PM} \qquad (4.14),$$

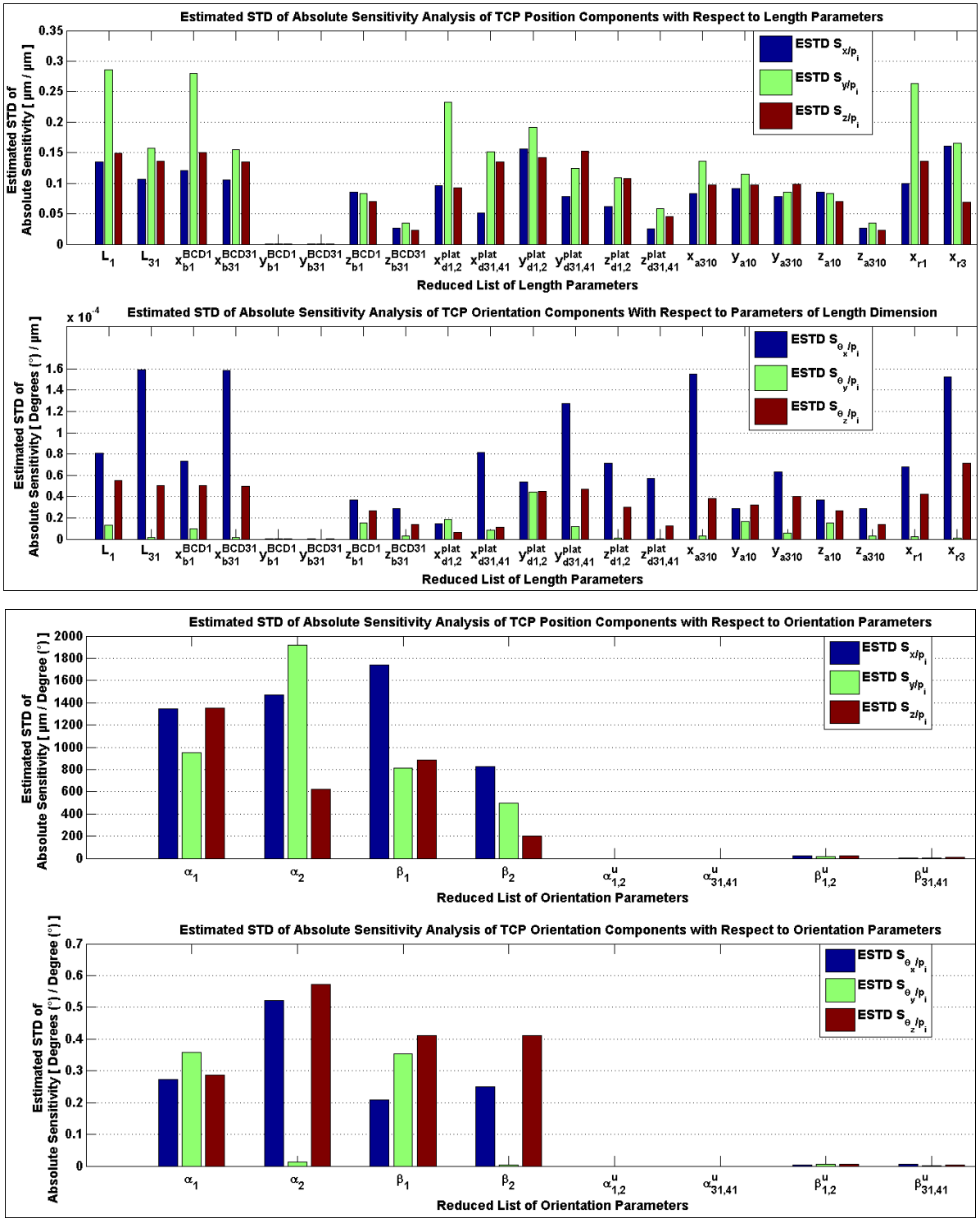

Fig. 4-9: Estimated standard deviation of absolute geometric sensitivity of ARROW V2 M2 prototype.

where $\boldsymbol{S}_g$ is the geometric sensitivity matrix. Hence, for small geometric errors, $\boldsymbol{\delta\xi}_{PM}$, the estimated pose error is:

$$\boldsymbol{\delta x}_c = \boldsymbol{S}_g \, \boldsymbol{\delta\xi}_{PM} \tag{4.15}.$$

As the procedure guidelines have been described, it is essential to discuss the geometric parameters and their proper choice. In fact, we can consider some realistic and practical assumptions to reduce the number of these parameters. These assumptions are: $\boldsymbol{u}_1 \equiv \boldsymbol{u}_2$, $\boldsymbol{u}_{31} \equiv \boldsymbol{u}_{41}$, $\boldsymbol{u}_{32} \equiv \boldsymbol{u}_{42}$, $\boldsymbol{u}_5 \equiv \boldsymbol{u}_6$, $\boldsymbol{D}_1 \equiv \boldsymbol{D}_2$, $\boldsymbol{D}_{31} \equiv \boldsymbol{D}_{41}$, $\boldsymbol{D}_{32} \equiv \boldsymbol{D}_{42}$, and $\boldsymbol{D}_5 \equiv \boldsymbol{D}_6$.

Based on the above, we have 84 geometric parameters (i.e. $\dim(\boldsymbol{\xi}_{\boldsymbol{PM}}) = 84$), namely:

- L_1, L_2, L_{31}, L_{32}, L_{41}, L_{42}, L_5 and L_6 (i.e. 8 parameters);
- $\boldsymbol{e}_k$ $(\forall k = 1,2,3)$ (i.e. α_1, α_2, α_3, β_1, β_2 and β_3: 6 parameters);
- $x_{r1} \dots x_{r6}$ (i.e. 6 parameters);
- $\boldsymbol{A}_{i0} = \begin{pmatrix} 0 & y_{ai0} & z_{ai0} \end{pmatrix}^{\mathrm{T}}$, $\forall i = 1,2,5,6$ (i.e. 8 parameters);
- $\boldsymbol{A}_{ij0} = \begin{pmatrix} x_{aij0} & y_{aij0} & z_{aij0} \end{pmatrix}^{\mathrm{T}}$, $\forall i = 3,4$ and $\forall j = 1,2$ (i.e. 12 parameters)[3];
- $\boldsymbol{u}_i$ $(\forall i = 1,2,5,6)$ and $\boldsymbol{u}_{ij}$ $(\forall i = 3,4 \text{ and } \forall j = 1,2)$ (i.e. $\alpha_1^u \equiv \alpha_2^u$, $\beta_1^u \equiv \beta_2^u$, $\alpha_{31}^u \equiv \alpha_{41}^u$, $\beta_{31}^u \equiv \beta_{41}^u$, $\alpha_{32}^u \equiv \alpha_{42}^u$, $\beta_{32}^u \equiv \beta_{42}^u$, $\alpha_5^u \equiv \alpha_6^u$, and $\beta_5^u \equiv \beta_6^u$: 8 parameters);
- $\boldsymbol{D}_1 \equiv \boldsymbol{D}_2$, $\boldsymbol{D}_{31} \equiv \boldsymbol{D}_{41}$, $\boldsymbol{D}_{32} \equiv \boldsymbol{D}_{42}$, and $\boldsymbol{D}_5 \equiv \boldsymbol{D}_6$ (i.e. 12 parameters);
- $\boldsymbol{B}_i$ $(\forall i = 1,2,5,6)$ and $\boldsymbol{B}_{ij}$ $(\forall i = 3,4 \text{ and } \forall j = 1,2)$ (i.e. 24 parameters).

For these geometric parameters and for their nominal values given in **§3.4.3.E**, we have investigated the mean and standard deviation of the absolute sensitivity over the desired workspace, DWS, defined in (3.138). The results are depicted in **Fig. 4-8** and **Fig. 4-9** for a representative subset of the aforementioned parameters (particularly the parameters of the simple chain (I) and the complex chain (III))[4]. As it can be clearly noticed from the figures, there are several parameters of negligible influence as compared with the others, particularly: $y_{bi}^{BCD_i}$ $(\forall i = 1,2,5,6)$, $y_{bij}^{BCD_{ij}}$ $(\forall i = 3,4 \text{ and } \forall j = 1,2)$, and the directions of the revolute joints, $\boldsymbol{u}_i$ $(\forall i = 1,2,5,6)$ and $\boldsymbol{u}_{ij}$ $(\forall i = 3,4 \text{ and } \forall j = 1,2)$. These have not only low mean absolute sensitivity, but also a small standard deviation. Hence, we can mainly consider the remaining 68 parameters for the PKM calibration. This number might be even reduced upon performing identifiability study, which is not our concern here.

As we have derived the geometric sensitivity matrix, the upcoming section focuses on the latter's implementation for the purpose of error compensation.

---

[3] Note that we have $\boldsymbol{A}_{ij0} = \begin{pmatrix} x_{aij0} & y_{aij0} & z_{aij0} \end{pmatrix}^{\mathrm{T}} = \boldsymbol{A}_{i0} + \boldsymbol{A}_{ij}^{ba}$. We considered $\boldsymbol{A}_{ij0}$ instead of $\left(\boldsymbol{A}_{i0} + \boldsymbol{A}_{ij}^{ba}\right)$ to avoid obvious redundancy in some geometric parameters.

[4] The results of sensitivity relative to the geometric parameters of the other chains are analogous to those presented in the mentioned figures. This is due to the structural symmetry of the PKM on one hand, and the symmetry of the desired workspace, DWS, with respect to the xy and yz planes on the other hand.

4.4.2- Compensation of Geometric Errors of ARROW PKM

In this part, we focus on the compensation of the geometric errors of the ARROW machine, which is composed of the parallel module, ARROW V2 M2, and the turntable. In **§4.4.1**, we have focused on the parallel module only, as the turntable modeling and calibration study are trivial. Nevertheless, in the scope of precision performance improvement of the whole machine, it is indispensable to put the turntable into the play, the importance of which will become clear by the end of the current section.

In fact, if we consider ARROW V2 M2 separately, we cannot compensate except for four components of $\boldsymbol{\delta x}_c$, specifically those corresponding to the controllable dofs. Similarly, if we consider the treatment of the turntable in isolation from the parallel module, we cannot compensate except for one orientation error. Yet, considering both constituting modules at once, allows for better error compensation where only the insignificant orientation error about the spindle axis is not compensated. This latter technique is what we are going to discuss here.

Fig. 4-10 presents the turntable with its geometric parameters, x_o, y_o, z_o, α_t, β_t, θ_{r1}, and θ_{r2}; these parameters are consolidated in the term $\boldsymbol{\delta\xi}_{TT}$. In nominal conditions, $\boldsymbol{e}_t$ is parallel to $\boldsymbol{e}_x$; i.e. pararllel to the x-axis of the base frame.

Now, we suppose that for $\boldsymbol{\delta\xi}_{TT}$, we have estimated $\delta\theta_t$, the orientation error of the turntable corresponding to the desired orientation, θ_t. Also, we presume that starting from

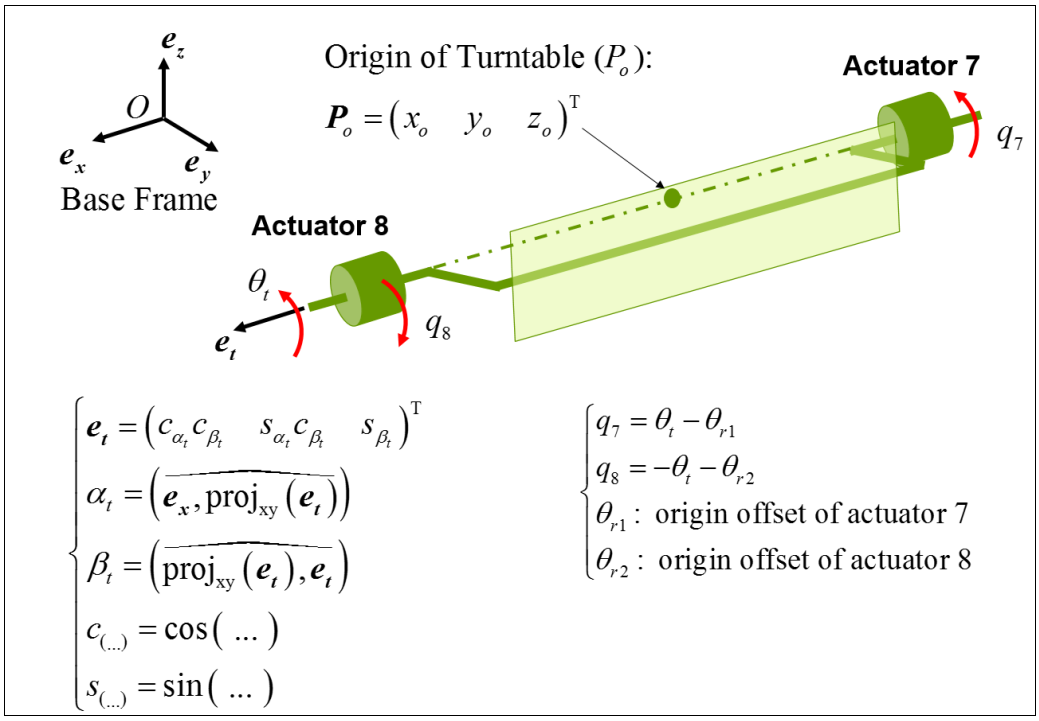

Fig. 4-10: Schematic of the turntable of ARROW machine with notations.

$\boldsymbol{\delta\xi_{PM}}$, we have computed $\boldsymbol{\delta x_c} = \begin{pmatrix}\delta x & \delta y & \delta z & \delta\theta_x & \delta\theta_y & \delta\theta_z\end{pmatrix}^{\mathrm{T}} = \boldsymbol{S_g}\left(\boldsymbol{x_d}\right)\boldsymbol{\delta\xi_{PM}}$, where $\boldsymbol{x_d} = \begin{pmatrix}x_d & y_d & z_d & \theta_{zd}\end{pmatrix}^{\mathrm{T}}$ is the corresponding desired controllable pose of the parallel module.

Based on the above, we have the infinitesimal rotational error vector of the spindle with respect to the base frame given by:

$$\begin{cases} \boldsymbol{e}_{\boldsymbol{PM}}^{\boldsymbol{rot}} = \begin{pmatrix}1\\0\\0\end{pmatrix}\delta\theta_x + \begin{pmatrix}0\\\cos(\theta_x)\\\sin(\theta_x)\end{pmatrix}\delta\theta_y + \begin{pmatrix}\sin(\theta_y)\\-\sin(\theta_x)\cos(\theta_y)\\\cos(\theta_x)\cos(\theta_y)\end{pmatrix}\delta\theta_z = \boldsymbol{\Omega}\,\boldsymbol{\delta\theta}, \text{ with:} \\ \boldsymbol{\Omega} = \begin{bmatrix}1 & 0 & \sin(\theta_y)\\0 & \cos(\theta_x) & -\sin(\theta_x)\cos(\theta_y)\\0 & \sin(\theta_x) & \cos(\theta_x)\cos(\theta_y)\end{bmatrix},\ \boldsymbol{\delta\theta} = \begin{pmatrix}\delta\theta_x\\\delta\theta_y\\\delta\theta_z\end{pmatrix} \end{cases} \tag{4.16}$$

As θ_x and θ_y are practically very small and tend to zero (nominally $\theta_x = \theta_y = 0$), we have $\boldsymbol{\Omega} \cong \mathbf{1}_{3\times3}$. Thus, relation (4.16) becomes:

$$\boldsymbol{e}_{\boldsymbol{PM}}^{\boldsymbol{rot}} = \boldsymbol{\delta\theta} \tag{4.17}$$

Regarding the turntable, we have the infinitesimal rotational error vector given by:

$$\boldsymbol{e}_{\boldsymbol{TT}}^{\boldsymbol{rot}} = \delta\theta_t\,\boldsymbol{e}_t \tag{4.18}$$

Hence, we have the main ingredients that allow us to proceed with error compensation. But before describing this procedure, the reader should keep in mind that our interest is to get rid of the relative errors between the parallel module and the turntable, not the base frame. In fact, to work with the ARROW machine, the trajectory generation should be done in the turntable frame rather than the base one. That is why the relative position and orientation of

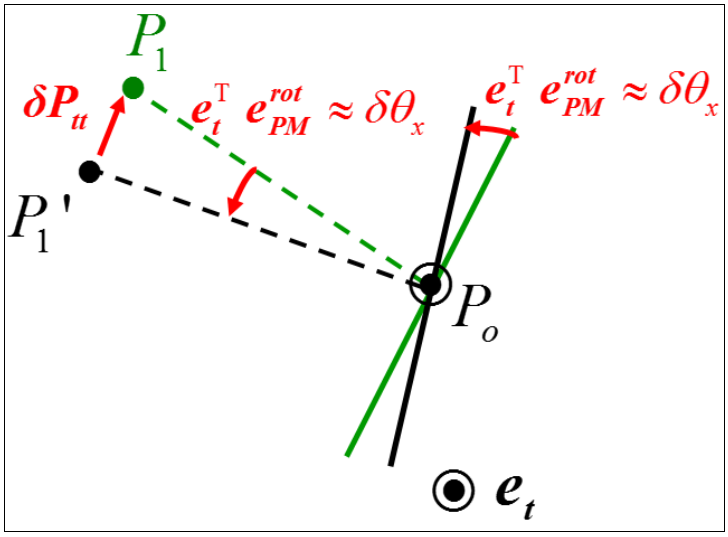

Fig. 4-11: Illustration of the impact of the rotation $\boldsymbol{e}_t^{\mathrm{T}}\,\boldsymbol{e}_{PM}^{rot} \approx \theta_x$ of the turntable.

the spindle with respect to the turntable are the ones to be compensated. This is crucial to understand and make sense of what follows.

We start by considering the rotational errors about $\boldsymbol{e_t}$. The relative rotational error between the spindle and the turntable, $\delta\vartheta_{TT}^{PM}$, is given by[5]:

$$\delta\vartheta_{TT}^{PM} = \boldsymbol{e_t}^{\mathrm{T}}\ \boldsymbol{e_{PM}^{rot}} - \delta\theta_t = \boldsymbol{e_t}^{\mathrm{T}}\ \boldsymbol{\delta\theta} - \delta\theta_t \approx \delta\theta_x - \delta\theta_t \tag{4.19}.$$

Then, we compensate for $\delta\vartheta_{TT}^{PM}$ by commanding the following rotation of the turntable:

$$\theta_{tcomp} = \theta_t + \delta\vartheta_{TT}^{PM} \approx \theta_t + \delta\theta_x - \delta\theta_t \tag{4.20}$$

instead of θ_t.

On the other hand, the relative orientation error between the spindle and the turntable about $\boldsymbol{e_z}$, denoted $\delta\varepsilon_{TT}^{PM}$, is given by:

$$\delta\varepsilon_{TT}^{PM} = \boldsymbol{e_z}^{\mathrm{T}}\ \boldsymbol{e_{PM}^{rot}} - \boldsymbol{e_z}^{\mathrm{T}}\ \boldsymbol{e_{TT}^{rot}} = \delta\theta_z - \left(\boldsymbol{e_z}^{\mathrm{T}}\ \boldsymbol{e_t}\right)\delta\theta_t \approx \delta\theta_z \tag{4.21}$$

Therefore, to compensate for $\delta\varepsilon_{TT}^{PM}$, we need to command the following corrected rotation of the spindle about the z axis:

$$\theta_{zdcomp} = \theta_{zd} - \delta\varepsilon_{TT}^{PM} \approx \theta_{zd} - \delta\theta_z \tag{4.22}.$$

It remains then to consider the compensated position of $P \equiv TCP$, i.e. the tool center point of the spindle. This compensation is divided into parts. The first part accounts for the positional error of the parallel module, $\boldsymbol{\delta P} = \begin{pmatrix}\delta x & \delta y & \delta z\end{pmatrix}^{\mathrm{T}}$, whereas the second considers the positional error, $\boldsymbol{\delta P_{tt}}$, due to the rotation added to compensate $\boldsymbol{e_t}^{\mathrm{T}}\ \boldsymbol{e_{PM}^{rot}} \approx \delta\theta_x$. To clarify this latter point, an illustration is provided in **Fig. 4-11**. In this figure, the point P_o is the center of the turntable, and P_1 is the position of P in the case where no rotation is made to compensate $\boldsymbol{e_t}^{\mathrm{T}}\ \boldsymbol{e_{PM}^{rot}} \approx \delta\theta_x$. When the turntable rotates an additional $\boldsymbol{e_t}^{\mathrm{T}}\ \boldsymbol{e_{PM}^{rot}} \approx \delta\theta_x$ angle, the spindle's TCP remains in its place at P_1. But as we said earlier, we are interested in maintaining the same relative position between the TCP and P_o. This implies the need to move the TCP from P_1 to P_1', where P_1' is obtained via rotating the segment P_oP_1 an angle equal to $\boldsymbol{e_t}^{\mathrm{T}}\ \boldsymbol{e_{PM}^{rot}} \approx \delta\theta_x$. As $\boldsymbol{e_t}^{\mathrm{T}}\ \boldsymbol{e_{PM}^{rot}} \approx \delta\theta_x$ is sufficiently small, we have:

$$\begin{cases}\boldsymbol{\delta P_{tt}} \approx -\delta\theta_x\ \boldsymbol{e_t} \times \boldsymbol{P_oP_d}, \text{ with:} \\ \boldsymbol{P_oP_d} = \begin{pmatrix}x_d - x_o & y_d - y_o & z_d - z_o\end{pmatrix}^{\mathrm{T}}\end{cases} \tag{4.23},$$

[5] Note that we have $\boldsymbol{e_t}^{\mathrm{T}}\ \boldsymbol{\delta\theta} = \cos(\alpha_t)\cos(\beta_t)\,\delta\theta_x + \sin(\alpha_t)\cos(\beta_t)\,\delta\theta_y + \sin(\beta_t)\,\delta\theta_z \approx \delta\theta_x$, where α_t and β_t are supposedly very small (they are nominally equal to zero).

where $\boldsymbol{P_d} = \begin{pmatrix} x_d & y_d & z_d \end{pmatrix}^{\mathrm{T}}$ represents the coordinates of the desired position of $P \equiv TCP$, and $\boldsymbol{P_o} = \begin{pmatrix} x_o & y_o & z_o \end{pmatrix}^{\mathrm{T}}$ corresponds to the coordinates of the turntable center.

As a result, the compensated desired position of the parallel module should be:

$$\boldsymbol{P_{dcomp}} = \begin{pmatrix} x_{dcomp} & y_{dcomp} & z_{dcomp} \end{pmatrix}^{\mathrm{T}} = \boldsymbol{P_d} - \boldsymbol{\delta P} - \boldsymbol{\delta P_{tt}} \tag{4.24}$$

Eventually, the compensated poses of the parallel module and the turntable, which allow maintaining their desired relative configuration, are given by:

$$\begin{cases} \boldsymbol{x_{dcomp}} = \begin{pmatrix} \boldsymbol{P_{dcomp}} \\ \theta_{zdcomp} \end{pmatrix} = \begin{pmatrix} \boldsymbol{P_d} - \boldsymbol{\delta P} - \boldsymbol{\delta P_{tt}} \\ \theta_{zd} - \delta\theta_z \end{pmatrix} \\ \theta_{tcomp} = \theta_t + \delta\theta_x - \delta\theta_t \end{cases} \tag{4.25}$$

As the compensation methodology of geometric errors has been clarified, it remains to stress some essential remarks concerning classical calibration and its execution. This is the subject of the following subsection.

4.4.3- General Remarks on Geometric Calibration

In general, the classical calibration can be carried out with the target of minimizing some cost function related to the pose errors, such as: the root mean square of the different pose errors, the maximal pose error, etc. However, it is important to know that with the current PKM, there are some constraints to be respected due to actuation redundancy.

In particular, one should take into account the minimization of $\left\| \boldsymbol{\delta q} - \boldsymbol{R_m}\, \boldsymbol{\delta q} \right\|$ for all configurations. In fact, having $\left\| \boldsymbol{\delta q} - \boldsymbol{R_m}\, \boldsymbol{\delta q} \right\|$ large implies not only an inconsistency in the geometric parameters, but also a possible increase in deformations. The inclusion of $\left\| \boldsymbol{\delta q} - \boldsymbol{R_m}\, \boldsymbol{\delta q} \right\|$ can be done by means of adding the equality constraint $\left\| \boldsymbol{\delta q} - \boldsymbol{R_m}\, \boldsymbol{\delta q} \right\| = 0$ to the classical optimization, or considering the minimization of $\max\left(\left\| \boldsymbol{\delta q} - \boldsymbol{R_m}\, \boldsymbol{\delta q} \right\| \right)$ as one of the objectives in the optimization problem. In this aspect, we would recommend the former option.

4.5- Compensation of Elastic Deformation

The ARROW machine being well manufactured and having its geometric parameters precisely monitored, we think that geometric calibration will be sufficient to achieve the anticipated precision performance. Nonetheless, if needed, a compensation of the elastic deformations can be done as well. This section summarizes the main guidelines in this aspect.

As we have the joints very stiff, especially after the redesign of the defected ones, their stiffness can be neglected. We can only consider the stiffness of the individual rods under tension/compression forces. These are denoted by K_i $\left(\forall i = 1,2,5,6\right)$ and

K_{ij} $\left(\forall i = 3,4 \text{ and } \forall j = 1,2\right)$; they correspond respectively to the rods of the simple chains (I, II, V, VI), and the complex ones (III, IV). Good estimates of K_i and K_{ij} can be obtained by applying finite element method. It then remains to describe the compensation methodology.

For the compensation of deformation errors, we are going to follow the lead of (DEBLAISE, 2006), but in the general dynamic case instead of the static one. The essence of the aforementioned procedure can be described as follows. First, the forces in the rods are computed. Then, the deformations and the resulting pose error are determined and compensated for in the very same manner as described in **§4.4.2**.

Regarding the determination of the forces, it is straightforward. For the simple arms, it is done by considering the dynamic equations of the corresponding actuators, and knowing their respective actuation forces, thanks to the simplified inverse dynamic model (**§3.4.3.D**). As for the forces in the individual rods of the complex chains (III) and (IV), they are computed by considering the equations of motion of the corresponding actuators in addition to the constraint relations on the platform (i.e. the relation between these forces and the torques about the x and y axes of the base frame). Omitting the details and sticking to the key points, we get the forces' values in these rods, say: F_i $\left(\forall i = 1,2,5,6\right)$ for the simple limbs (I, II, V, and VI), and F_{ij} $\left(\forall i = 3,4 \text{ and } \forall j = 1,2\right)$ for the complex ones (III and IV), with the convention that positive values indicate tension.

The influence of these forces is then translated as variations of the lengths L_i and L_{ij}, which are denoted by δL_i^{def} $\left(\forall i = 1,2,5,6\right)$ and δL_{ij}^{def} $\left(\forall i = 3,4 \text{ and } \forall j = 1,2\right)$, respectively. Their values are simply given by:

$$\begin{cases} \delta L_i^{def} = \dfrac{F_i}{K_i}, \ \forall i = 1,2,5,6 \\ \delta L_{ij}^{def} = \dfrac{F_{ij}}{K_{ij}}, \ \forall i = 3,4 \text{ and } \forall j = 1,2 \end{cases} \tag{4.26}$$

Knowing δL_i^{def} and δL_{ij}^{def}, the compensation of their induced pose error can be achieved through applying the same strategy described in **§4.4.2**. More precisely, it is performed by adding δL_i^{def} and δL_{ij}^{def} to the corresponding geometric errors, δL_i and δL_{ij}.

Hence, we have went an additional step in the precision improvement of the ARROW machine. Perhaps, it is worth mentioning here that although we have considered the rods' deformations only, still we can follow the same technique and include the stiffness matrices of the joints. Nevertheless, the gained accuracy not only might be unworthy compared to the added complexity, but also its online implementation can be infeasible. This is due to the computational time expense.

4.6- Conclusion

In this chapter, several aspects have been discussed. Starting by the exposition of the basic control strategy, some points have been emphasized, specifically concerning the treatment of actuation redundancy. Following that, the preliminary dynamic precision analysis of ARROW V2 M2 prototype has been carried out, founded on the data provided by the proprioceptive sensors. The results have been generally insightful and promising. Actually, they are expected to be better upon the redesign of the defected joints, performing geometric calibration, and applying a more advanced control strategy. In this scope, the geometric calibration and the methodology of compensation have been discussed. Also, the pose sensitivity of the parallel architecture with respect to the different geometric parameters has been presented. It has demonstrated the possibility of considering a reduced list of 68 parameters for ARROW V2 M2 in a first step, which can then be ensued by a further reduction based on identifiability study. Moreover, if geometric error compensation proved to be insufficient for accomplishing the target precision, the possibility of compensating elastic deformation has been highlighted and its main principles have been described.

This was in brief the core of the current chapter and the plan for the performance enhancement of the ARROW machine. Yet, several interesting topics can be investigated in the future. Among these, we mention the possibility of auto-calibration. Having ARROW V2 M2 possessing two extra sensors is a feature worth exploiting via auto-calibration. The purpose behind that should not be bypassing the classical calibration procedure, but rather compensating for very slight parameter modifications during the working phase. These slight modifications could be due to temperature drift, replacement of a damaged component and the alike. Another idea is to exploit auto-calibration as means of signaling when a classical geometric identification is required.

General Conclusions and Perspectives

In this doctoral thesis, we have focused on parallel manipulators (PMs) and their implementation as machine tools. In fact, PMs have been there for more than half a century and attracted a lot of research. Yet, their real exploitation in industry has been shy and limited, not exceeding the research stages at university laboratories and industrial enterprises. This is mainly due to workspace limitations, design complexities, singularities, and lack of good compromise between rapidity and precision. In the attempt to change this harsh reality, we have addressed two main problematics in this field. The first is related to the design itself, in which we have exposed some novel topologies that fulfill the yearned for manufacturability features, while maintaining large workspace, rapidity, and precision. The second problematic that we have focused on is performance assessment regarding precision, kinetostatics, and dynamics. In particular, we have been interested in having the new suggested indices applicable to general manipulators and free of the inherent limitations of the classical measures, regarding redundancy and heterogeneity conflicts. We have considered all of this, while sustaining a physical interpretation and having it directly linked to what the roboticist or end-user look for in such machines. In the light of the above, a new rapid and precise prototype, namely ARROW V2 M2, has been designed. It has been dimensionally synthesized based on the dual criteria of precision and dynamics. The initial performances of this PKM have been quite intriguing, though based on proprioceptive means and not exterioceptive ones.

Actually, we do not claim that the so-far presented work is the perfect approach to acquire rapidity and precision, but perhaps, it is a solid one-step towards the aforementioned goals. In addition, we stress that still the preliminary assessment is not sufficient to verify the acquirement of the preset targets, as a more intensive exterioceptive precision investigation as well as geometric calibration should follow.

In what follows, we emphasize some points that are interesting to research in the future. These fall in the scope of complementary work regarding the suggested performance indices, and the possible enhancements of the implemented PKM.

Possible Advancements Regarding the Suggested Performance Measures

In the currently presented work, we did not deal with two types of manipulators, namely: the task redundant ones, and those with mixed simultaneous kinematic and actuation redundancies (AR and KR, respectively).

The treatment of task redundancy (TR) is rather simple, as long as no AR or KR is involved. Otherwise, its intricacy is similar to the case of mixed-redundancy manipulators (MRMs). For

MRMs, the treatment sophistication is that of obtaining the direct and inverse kinetostatic models. As mentioned earlier, MRMs, especially of rigid type, are not being researched according to our knowledge. Nevertheless, it seems it will not remain the same for cable-driven parallel robots. More precisely, marine robotic designs, based on active cables and thrusters, are currently subject of research at LIRMM. Such designs involve both AR and KR simultaneously. Therefore, it is essential to inspect such situations; especially that one of our targets has been the general applicability of the proposed indices. Assuring that the latter idea holds is important. This is since it aids in evaluating and comparing designs of different types, without invoking any disputes regarding the need for some common basis.

Eventually, as means of promoting the current evaluation methodology, the development of a software package that includes the required functionalities is necessary. This step, in spite of being of technical nature, it is undeniably influential for the sake of popularizing the approach and advancing it, based on the feedback and inspirations supplied by the users.

Possible Improvements Regarding ARROW Machine

With respect to the currently executed ARROW prototype, several possible advancements can be made. These are enumerated below:

1. Geometric or elasto-geometric calibration must be done, at least incorporating the identified geometric errors given in the quality control report. This can be sufficient to effortlessly promote the precision performance further, and reduce the disagreement between the regularized and non-regularized joint errors. In this aspect, it would be also worthy to investigate the possibility of perfoming calibration based on the quality of machined parts, as suggested by (CHANAL, 2006). Such approach is interesting due to having the cost function directly related to the target, which is the agreement between the real machined piece and the desired one.
2. Auto-calibration would be interesting to investigate and exploit for improving the precision performance, via the compensation of some marginal geometric errors (e.g. those arising from temperature drift, component replacement, etc.).
3. In the current thesis, we have done the dimensional synthesis without including the parallel module and turntable inter-collision checks. This has been based on the assumption that it is possible to account for it at the design stage. Yet, it is preferable to consider this point in future optimizations, especially that we have recently developed an advanced collision detection module for this purpose. This module can be used in the optimization procedure on one hand, and for offline collision pre-check in the industrial controller on the other. Nonetheless, it is not recommendable for use in realtime, as it might be time consuming.

These were the main points regarding the current ARROW machine, in its current right-hand left-hand structure. Nevertheless, it is not completely disfavored to consider a hybrid version consisting of ARROW V2 M2 in series with a one-dof (1R) wrist, especially if the application

does not require a massive rotary actuator. At the end, this remains another compromise to make between elevated dynamical capabilities and simple motion planning.

Bibliography

1. ALBUS, J., BOSTELMAN, R. & DAGALAKIS, N., 1993. *The NIST ROBOCRANE.* s.l.:Journal of Robotic Systems, Vol. 10, No. 5, pp. 709-724.

2. ALICI, G. & SHIRINZADEH, B., 2004. *Optimum synthesis of planar parallel manipulators based on kinematic isotropy.* s.l.:Robotica, 22, pp. 97-108.

3. ANCUTA, A. E., 2008. *Machines parallèles 5-axes pour l'usinage aéronautique des pièces minces,* PhD Thesis, Université Montppellier II, December 10.

4. ANGELES, J., 1992. *The design of isotropic manipulator architectures in the presence of redundancies.* s.l.:The International Journal of Robotics Research 11, No. 3 , pp. 196-201.

5. ANGELES, J., 2004. *The qualitative synthesis of parallel manipulators.* s.l.:The qualitative synthesis of parallel manipulators. Journal of Mechanical Design, 126(4), pp. 617-624.

6. ANGELES, J., CARO, S., KHAN, W. & MOROZOV, A., 2006. *The Kinetostatic Design of an Innovative Schönflies Motion Generator.* s.l.:Proceedings of the Institution of Mechanical Engineers, Part C: Journal of Mechanical Engineering Science 220, No. 7, pp. 935-943.

7. ASADA, H., 1983. *A geometrical representation of manipulator dynamics and its application to arm design.* s.l.:H. ASADA, "A geometrical representation of manipulator dynamics and its application to arm design", ASME Journal of Dynamic Systems, Measurement, and Control , Vol. 105 , No. 3, pp. 131-142.

8. ASADA, H., 1984. *Dynamic analysis and design of robot manipulators using inertia ellipsoids.* s.l.:in Proc. of the IEEE International Conference on Robotics and Automation (ICRA 1984), pp. 94-102, Atlanta, USA.

9. BALL, K., 1992. *Ellipsoids of maximal volume in convex bodies.* s.l.:Geom. Dedicata 41 (2): 241–250, DOI: 10.1007/BF00182424, ISSN 0046-5755.

10. BARADAT, C. et al., 2008. *Par2: a Spatial Mechanism for Fast Planar, 2-dof, Pick-and-Place Applications.* in Proc. of the 2nd International Workshop on Fundamental Issues and Future Research Directions for Parallel Mechanisms and Manipulators,pages 261–270, Montpellier, France: s.n.

11. BEN-HORIN, P. & SHOHAM, M., 2009 . *Application of Grassmann–Cayley Algebra to Geometrical Interpretation of Parallel Robot Singularities.* s.l.:The International Journal of Robotics Research 28 (1), pp. 127-141.

12. BEN-HORIN, R., SHOHAM, M. & DJERASSI, S., 1998. *Kinematics, dynamics and construction of a planarly actuated parallel robot.* s.l.:Robotics and Computer-Integrated Manufacturing, Vol. 14, No. 2, pp. 163-172.

13. BONEV, I., 2003. *The true origin of Parallel Robots.* Web review, http//www.parallemic.org/Reviews/Review007.html: s.n.

14. BONEV, I. A., 2002. *Geometric Analysis of Parallel Mechanisms,* PhD Thesis, Université Laval, November.

15. BONEV, I. A., 2008. *Direct kinematics of zero-torsion parallel mechanisms.* s.l.:in Proc. of IEEE International Conference on Robotics and Automation (ICRA 2008), pp. 3851-3856.

16. BONEV, I. & ZLATANOV, D., 2001. *The Mystery of the Singular SNU Translational Parallel Robot.* s.l.:http://www.parallemic.org/Reviews/Review004.html.

17. BOSCHETTI, G., ROSA, R. & TREVISANI, A., 2011. *Parallel Robot Translational Performance Evaluation through Direction-Selective Index (DSI).* s.l.:Journal of Robotics 2011.

18. BOUCHARD, S., GOSSELIN, C. M. & MOORE, B., 2008. *On the Ability of a Cable-Driven Robot to Generate a Prescribed Set of Wrenches.* s.l.:in Proc. of ASME 2008 (IDETC/CIE 2008), Brooklyn, New York, USA, August 3–6.

19. BOWLING, A. & KHATIB, O., 1998. *The motion isotropy hypersurface: a characterization of acceleration capability.* s.l.:in Proc. IEEE/RSJ International Conference on Intelligent Robots and Systems (IROS 1998), Victoria, BC, Vol. 2, pp. 965–971.

20. BOWLING, A. & KHATIB, O., 2000. *Robot acceleration capability: the actuation efficiency measure.* s.l.:in Proc. of IEEE Conference on Robotics and Automation (ICRA 2000), San Francisco, CA, Vol. 4, pp. 3970–3975.

21. BOWLING, A. & KHATIB, O., 2003. *Dynamic loading criteria in actuator selection for desired dynamic performance.* s.l.:Advanced Robotics, Vol. 17, No. 7, pp. 641-656, November.

22. BRETHE, J.-F. & LEFEBVRE, D., 2007. *Granular Space Structure on a Micrometric Scale for Industrial Robots.* s.l.:2007 IEEE International Conference on Robotics and Automation (ICRA 2007),pp. 4931-4936, Roma, Italy, April 10-14.

23. BRIOT, S., ARAKELIAN, V. & GUEGAN, S., 2008. *Design and prototyping of a partially decoupled 4-DOF 3T1R parallel manipulator with high-load carrying capacity.* s.l.:Journal of Mechanical Design 130, No. 12.

24. BRIOT, S. & BONEV, I. A., 2009. *Pantopteron: A New Fully Decoupled 3DOF Translational Parallel Robot for Pick-and-Place Applications.* s.l.:Journal of Mechanisms and Robotics,Vol. 1, Noo. 2, May.

25. BRIOT, S., GLAZUNOV, V. & ARAKELIAN, V., 2013. *Investigation on the Effort Transmission in Planar Parallel Manipulators.* s.l.:Journal of Mechanisms and Robotics, Vol. 5, February.

26. CARDOU, P., BOUCHARD, S. & GOSSELIN, C., 2010. *Kinematic-Sensitivity indices for Dimensionally Nonhomogeneous Jacobian Matrices.* s.l.:IEEE Transactions on Robotics, Vol. 26, No. 1, February.

27. CARRICATO, M., 2005. *Fully Isotropic Four- Degrees-of-Freedom Parallel Mechanisms for Schoenflies Motion.* s.l.:The International Journal of Robotics Research, Vol. 24, No. 5, pp. 397- 414, May.

28. CARRICATO, M. & PARENTI-CASTELLI, V., 2002. *Singularity-Free Fully-Isotropic Translational Parallel Mechanisms.* s.l.:The International Journal of Robotics Research, Vol. 21, No. 2, pp. 161-174, February.

29. CHABLAT, D. & WENGER, P., 2003. *Architecture optimization of a 3-DOF translational parallel mechanism for machining applications, the Orthoglide.* s.l.:IEEE Transactions on Robotics and Automation, Vol. 19, No. 3, pp. 403-410.

30. CHABLAT, D. & WENGER, P., 2003. *Dispositif de déplacement et d'orientation d'un objet dans l'espace et utilisation en usinage rapide,* s.l.: Patent FR2850599.

31. CHANAL, H., 2006. *Etude de l'emploi des machines outils à structure parallèle en usinage,* PhD Thesis, Université Blaise Pascal - Clermont-Ferrand II.

32. CHEMORI, A., SARTORI-NATAL, G. & PIERROT, F., 2013. *Control of Parallel Robots: Towards Very High Accelerations.* in Proc. 10th International Multi-Conference on Systems, Signals & Devices (SSD),Hammamet, Tunisia: s.n.

33. CHEN, C. & ANGELES, J., 2007. *Generalized transmission index and transmission quality for spatial linkages.* s.l.:Mechanism and Machine Theory, Vol. 42, pp. 1225-1237.

34. CLAVEL, R., 1991. *Conception d' un Robot Parallele Rapide à 4 Dégres de Liberté,* Lausanne, Switzerland: s.n.

35. CLAVEL, R., 2002. *HITA-STT: a new 5-dof parallel kinematics for production application,* s.l.: in ISR 2002-International Symposium on Robotics, Stockholm, Sweden, .

36. COMPANY, O., 2000. *Machines-outils rapides à structure parallŁle. MØthodologie de conception, applications et nouveaux concepts,* s.l.: s.n.

37. COMPANY, O. et al., 2011. *Par2: a spatial mechanism for fast planar two-degree-of-freedom pick-and-place applications.* s.l.:Meccanica 46, pp. 239–248.

38. CONCONI, M. & CARRICATO, M., 2009. *A New Assessment of Singularities of Parallel Kinematic Chains.* s.l.: IEEE Transactions on Robotics, Vol. 25, No. 4, pp. 757-770, August .

39. CONKUR, E. S. & BUCKINGHAM, R., 1997. *Clarifying the definition of redundancy as used in robotics.* s.l.:Robotica, Volume 15, Issue 05, pp 583-586, September .

40. CORBEL, D., 2008. *Contribution à l'amélioration de la précision des robots parallèles,* PhD Thesis, Université Montpellier II, December 10.

41. CORBEL, D., GOUTTEFARDE, M., COMPANY, O. & PIERROT, F., 2010. *Towards 100G with PKM. Is actuation redundancy a good solution for pick-and-place?.* in Proc. 2010 IEEE International Conference on Robotics and Automation, pp. 4675-4682, Anchorage, Alaska, USA.

42. COURTEILLE, E., DEBLAISE, D. & MAURINE, P., 2009. *Design Optimization of Robot Manipulators over Global Stiffness Performance Evaluation.* s.l.:in Proc. of 2009 IEEE International Conference on Intelligent Robots and Systems (IROS 2009), Saint-Louis, United States.

43. CUNNINGHAM, D. & H. H. ASADA, 2009. *The Winch-Bot: A Cable-Suspended, Under-Actuated Robot Utilizing Parametric Self-Excitation.* s.l.:2009 IEEE International Conference on Robotics and Automation (IROS 2009), Kobe, Japan, May 12-17.

44. DEBLAISE, D., 2006. *Contribution à la modélisation et à l'étalonnage élasto-géométriques des manipulateurs à structure parallèle,* PhD Thesis, INSA de Rennes, December 5.

45. DONELAN, P. S., 2007. *Singularity-theoretic methods in robot kinematics.* s.l.:in Robotica, Vol. 25, No. 06, pp. 641-659, November.

46. DONG, W., 2002. *Static and dynamic behaviour study of Parallel Kinematics Machine ,* s.l.: www.easy-rob.com/uploads/media/weihuadong_5.pdf, (date 2002-02-14) .

47. EARL, C. & ROONEY, J., 1983. *Some kinematics structures for robot manipulator designs.* s.l.:J. of Mechanisms, Transmissions and Automation in Design, 105(1):15–22, March.

48. FANG, Y. & TSAI, L.-W., 2002. *Structure Synthesis of a Class of 4-DoF and 5-DoF Parallel Manipulators with Identical Limb Structures.* s.l.:The International Journal of Robotics Research, Vol. 21, No. 9, pp. 799-810, September.

49. FIRMANI, F., NOKLEBY, S. B., PODHORODESKI, R. P. & ZIBIL, A., 2008. *Wrench Capabilities of Planar Parallel Manipulators and their Effects Under Redundancy.* s.l.:Parallel Manipulators Towards New Applications, pp. 109-132.

50. FRISOLI, A., CHECCACCI, D., SALSEDO, F. & BERGAMASCO, M., 2000. *Synthesis by screw algebra of translating in-parallel actuated mechanisms.* s.l.:in Lenarˇ c, J., Staniši´ ciˇ c, M.M. (Eds.), Advances in Robot Kinematics. Kluwer Academic Publishers, Dordrecht, pp. 433–440.

51. GAO, F., PENG, B., ZHAO, H. & LI, W., 2006. *A novel 5-DOF fully parallel kinematic machine tool.* s.l.:The International Journal of Advanced Manufacturing Technology 31, pp. 201-207.

52. GAO, F., Weimin LI, X. Z., JIN, Z. & ZHAO, H., 2002. *New kinematic structures for 2-, 3-, 4-, and 5-DOF parallel manipulator designs.* s.l.:Mechanism and Machine Theory 37, pp. 1395–1411.

53. GOGU, G., 2004a. *Structural synthesis of fully-isotropic translational parallel robots via theory of linear transformations.* s.l.:European Journal of Mechanics-A/Solids, 23(6), pp. 1021-1039.

54. GOGU, G., 2004b. *Fully-Isotropic T3R1-Type Parallel Manipulators.* s.l.:On Advances in Robot Kinematics, pp. 265-272. Springer Netherlands.

55. GOGU, G., 2004c. *Structural synthesis of fully-isotropic translational parallel robots via theory of linear transformations.* s.l.:European Journal of Mechanics A/Solids 23, pp. 1021–1039.

56. GOGU, G., 2005a. *Chebychev–Grübler–Kutzbach's criterion for mobility calculation of multi-loop mechanisms revisited via theory of linear transformations.* s.l.:European Journal of Mechanics - A/Solids, Volume 24, Issue 3, May–June 2005, Pages 427–441, February.

57. GOGU, G., 2005b. *Mobility and spatiality of parallel robots revisited via theory of linear transformations.* s.l.:European Journal of Mechanics-A/Solids, 24(4), pp. 690-711.

58. GOGU, G., 2005c. *Singularity-free fully-isotropic parallel manipulators with Schönflies motions.* s.l.:in Proc. of 12th International Conference on Advanced Robotics, Seattle, USA, pp. 194–201.

59. GOGU, G., 2006a. *Fully-Isotropic Parallel Manipulators with Five Degrees of Freedom.* s.l.:in Proc. of 2006 IEEE International Conference on Robotics and Automation, Orlando, USA, pp. 1141–1146..

60. GOGU, G., 2006b. *Fully-Isotropic Redundantly-Actuated Parallel Manipulators with Five Degrees of Freedom.* s.l.:in Proc. of EuCoMeS, the first European Conference on Mechanism Science, Obergurgl, Austria,.

61. GOGU, G., 2006c. *Fully-Isotropic T3R2-Type Parallel Manipulators.* s.l.:in Proc. of IEEE 2006 International Conference on Robotics, Automation and Mecatronics, Bangkok, Thailand, pp. 248–256.

62. GOGU, G., 2007. *Structural synthesis of fully-isotropic parallel robots with Schönflies motions via theory of linear transformations and evolutionary morphology.* s.l.:European Journal of Mechanics A/Solids 26 , pp. 242–269.

63. GOGU, G., 2009. *Structural synthesis of maximally regular T3R2-type parallel robots via theory of linear transformations and evolutionary morphology.* s.l.:Robotica, Vol. 27, pp. 79–101.

64. GOSSELIN, C. & ANGELES, J., 1990. *Singularity Analysis of Closed-Loop Kinematic Chains,* s.l.: IEEE Transactions on Robotics and Automation, Vol. 6 , No. 3, pp. 281-290.

65. GOSSELIN, C. & ANGELES, J., 1991. *A Global Performance Index for the Kinematic Optimization of Robotic Manipulators.* s.l.: Journal of Mechanical Design, Vol. 113, pp. 220-226, September.

66. GOSSELIN, C. M., 1992. *The optimum design of robotic manipulators using dexterity indices.* s.l.:Robotics and Autonomous Systems, Vol. 9, No. 4, pp. 213-226.

67. GOSSELIN, C., ST-PIERRE, E. & GAGNE, M., 1996. *On the development of the agile eye: mechanical design, control issues and experimentation.* s.l.:IEEE Robotics and Automation Society Magazine, Vol. 3, No. 4, pp. 29-37.

68. GOUGH, V. E. & WHITEHALL, S. G., 1962. *Universal tyre testing machine.* in Proceedings of the FISITA 9th International Technical Congress, pp. 117-137: s.n.

69. GRAETTINGER, T. J. & KROGH, B. H., 1988. *The acceleration radius: a global performance measure for robotic manipulators.* s.l.:IEEE J. Robotics Automat. 4 (1), pp. 60–69.

70. GREGORIO, R. D. & PARENTI-CASTELLI, V., 2002. *Mobility Analysis of the 3-UPU Parallel Mechanism Assembled for a Pure Translational Motion.* s.l.:Journal of Mechanical Design , Vol. 124, No. 2, pp. 259-264, June.

71. GUAY, F., CARDOU, P., RUIZ, A. L. C. & CARO, S., 2013. *Measuring How Well a Structure Supports Varying External Wrenches.* s.l.:in Proc. of The Second Conference on Mechanisms, Transmissions and Applications (MeTrApp 2013), Bilbao, Spain, October 2–4.

72. GWINNETT, J. E., 1931. *Amusement devices.* Gwinnett, J.E., "Amusement devices," US Patent No. 1,789,680, January 20,: s.n.

73. HAN, C., KIM, J., KIM, J. & PARK, F. C., 2002. *Kinematic sensitivity analysis of the 3-UPU parallel mechanism.* s.l.:in Mechanism andMachine Theory 37, pp. 787–798.

74. HARIB, K. & SRINIVASAN, K., 2003. *Kinematic and dynamic analysis of Stewart platform-based machine tool structures.* s.l.:Robotica, Vol. 21, No. 5, pp. 541-554.

75. HAYWARD, V., CHOKSI, J., LANVIN, G. & RAMSTEIN, C., 1994. *Design and Multi-Objective Optimization of a Linkage for a Haptic Interface.* s.l.:in Advances in Robot Kinematics, pp. 352-359.

76. HERRERO, A., ZATARAIN, M. & ALMANDOZ, X., 2000. *Development of a Five-drive Parallel Kinematics Machine,* s.l.: Internal Report, Fundacion Tekniker, Avda, Otaola, 20, 20600 Eiber, Spain.

77. HERVE, J., 1995. *Design of parallel manipulators via the displacement group.* s.l.:in Proc. of the 9th World Congress on the Theory of Machines and Mechanisms, pp. 2079–2082, Milan, Italy.

78. HONEGGER, M., CODOUREY, A. & BURDET, E., 1997. *Adaptive Control of the Hexaglide, a 6 dof Parallel Manipulator.* s.l.:in Proc. of 1997 IEEE International Conference on Robotics and Automation ICRA, Vol. 1, pp. 543-548.

79. HUANG, T., MEI, J., ZHAO, X. & LI, Z., 2005. *A Method for Estimating Servomotor Parameters of a Parallel Robot for Rapid Pick-and-Place Operations.* s.l.:ASME Journal of Mechanical Design, Vol. 127, No. 4, pp. 596-601.

80. HUANG, Z. & LI, Q., 2002. *General Methodology for Type Synthesis of Symmetrical Lower-Mobility Parallel Manipulators and Several Novel Manipulators.* s.l.:The International Journal of Robotics Research,Vol. 21, No. 2, pp. 131-145, February.

81. HUANG, Z. & LI, Q. C., 2002. *General Methodology for Type Synthesis of Symmetrical Lower- Mobility Parallel Manipulators and Several Novel Manipulators.* s.l.:The International Journal of Robotics Research, Vol. 21, No. 2, pp. 131-145, February.

82. HUFNAGEL, T. & MULLER, A., 2012. *A Projection Method for the Elimination of Contradicting Decentralized Control Forces in Redundantly Actuated PKM.* s.l.:IEEE Transactions on Robotics, Vol. 28, No. 3, pp. 723-728, June.

83. HUNT, J. A., 2007. *Robot kinematics and the Gantry-Tau parallel machine.* s.l.:Industrial Robot: An International Journal, 34(5), pp. 362-367.

84. HUNT, K. H., 1978. *Kinematic Geometry of Mechanisms.* s.l.:Clarendon Press.

85. HUNT, K. H., 1983. *Structural Kinematics of In-Parallel-Actuated Robot Arms.* s.l.:J. Eng. Mech. Div., 105, pp. 705 – 712. .

86. INSELBERG, A. & DIMSDALE, B., 1990. *Parallel coordinates: a tool for visualizing multi-dimensional geometry.* s.l.:IEEE Conf. on Visualization, pp. 361–378.

87. JIN, Y. et al., 2012. *Optimal Design of a New Parallel Kinematic Machine for Large Volume Machining.* s.l.:In Advances in Reconfigurable Mechanisms and Robots I, pp. 343-354, Springer London.

88. JOSHI, S. A. & TSAI, L.-W., 2002. *Jacobian Analysis of Limited-DOF Parallel Manipulators.* s.l.:Journal of Mechanical Design, 124 (2), pp. 254–258,.

89. KANAAN, D., WENGER, P. & CHABLAT, D., 2009. *Kinematic analysis of a serial–parallel machine tool: The VERNE machine.* s.l.:Mechanism and Machine Theory, Vol. 44, No. 2, pp. 487-498..

90. KARGER, A., 2003. *Architecture singular planar parallel manipulators.* s.l.:in Mechanism and Machine Theory 38, pp. 1149–1164.

91. KAWAMURA, S., CHOE, W., TANAKA, S. & PANADIAN, S., 1995. *Development of an Ultrahigh Speed Robot FALCON using Wire Drive System.* s.l.:in Proc. of 1995 IEEE International Conference on Robotics and Automation (ICRA 1995), pp. 215-220.

92. KAWAMURA, S., KINO, H. & WON, C., 2000. *High-speed manipulation by using parallel wire-driven robots.* s.l.:Robotica, Vol. 18, No. 1, pp. 13-21.

93. KHALIL, W. & GUEGAN, S., 2002. *A Novel Solution for the Dynamic Modeling of Gough-Stewart Manipulators.* s.l.:in Proc. of IEEE International Conference on Robotics and Automation, Washington, DC, pp. 817-822, May.

94. KHATIB, O. & BURDICK, J., 1987. *Optimization of dynamics in manipulator design: the operational space formulation.* s.l.:Int. J. Robotics Automat. 2 (2), pp. 90–98.

95. KIM, H. & TSAI, L.-W., 2002. *Evaluation of Cartesian parallel manipulator.* s.l.:in Advances in Robot Kinematics, Kluwer Academic, pp. 21–28.

96. KIM, S. G. & RYU, J., 2003. *New dimensionally homogeneous Jacobian matrix formulation by three end-effector points for optimal design of parallel manipulators.* s.l.:IEEE Transactions on Robotics and Automation, Vol. 19, No. 4, pp. 731-737.

97. KIM, S. G. & RYU, J., 2004. *Force transmission analyses with dimensionally homogeneous jacobian matrices for parallel manipulators.* s.l.:KSME International Journal, Vol. 18, No. 5, pp. 780–788.

98. KIM, S. M., KIM, W. & YI, B.-J., 2009. *Kinematic Analysis and Optimal Design of a 3T1R Type Parallel Mechanism.* s.l.:in Proc. of 2009 IEEE International Conference on Robotics and Automation (ICRA 2009), Kobe, Japan, May 12-17.

99. KIM, Y. & DESA, S., 1993. *The definition, determination, and characterization of acceleration sets for spatial manipulators.* s.l.:The International Journal of Robotics Research, Vol. 12, No. 6, pp. 572-587, December.

100. KLEIN, C. A. & BLAHO, B. E., 1987. *Dexterity Measures for the Design and Control of Kinematically Redundant Manipulators.* s.l.:The International Journal of Robotics Research, Vol. 6, No. 2, pp. 72-83, June.

101. KLEIN, C. A. & MIKLOS, T. A., 1991. *Spatial Robotic Isotropy.* s.l.: The International Journal of Robotics Research, Vol. 10, No. 4, pp. 426-437, August.

102. KONG, X. & GOSSELIN, C., 2001. *Generation of parallel manipulators with three translational degrees of freedom based on screw theory.* s.l.:in Proc. of CCToMM Symposium on Mechanisms, Machines and Mechatronics, Montreal, Canada.

103. KONG, X. & GOSSELIN, C., 2007. *Type Synthesis of Parallel Mechanisms.* s.l.:Springer Tracts in Advanced Robotics, Volume 33.

104. KONG, X. & GOSSELIN, C. M., 2002. *Kinematics and Singularity Analysis ofaNovelType of 3-CRR 3-DOF Translational Parallel Manipulator.* s.l.:The International Journal of Robotics Research, Vol. 21, No. 9, pp. 791-798, September .

105. KONG, X. & GOSSELIN, C. M., 2004a. *Type Synthesis of 3T1R 4-DOF Parallel Manipulators Based on Screw Theory.* s.l.:IEEE Transactions on Robotics and Automation, Vol. 20, No. 2, April.

106. KREFFT, M. & HESSELBACH, J., 2005. *Elastodynamic Optimization of Parallel Kinematics.* s.l.:in Proc. of the 2005 IEEE International Conference on Automation Science and Engineering, Edmonton, Canada, August 1-2.

107. KRUT, S., 2003. *Contribution à l'étude des robots parallèles légers, 3T-1R et 3T-2R, à forts débattements angulaires,* Université Montpellier 2, November 13.

108. KRUT, S. et al., 2003. *I4: A New Parallel Mechanism for Scara Motions.* s.l.:in Proc. of International Conference on Robotics and Automation (ICRA 2003), pp. 1875-1880, Taipei, Taiwan, September 14-19.

109. KRUT, S., COMPANY, O. & PIERROT, F., 2002. *Velocity Performance Indexes for Parallel Mechanisms with Actuation Redundancy," in Proc. of 2002 Workshop on Fundamental Issues and Future Research Directions for Parallel Mechanisms and Manipulators.* s.l.:in Proc. of 2002 Workshop on Fundamental Issues and Future Research Directions for Parallel Mechanisms and Manipulators, pp. 46-56, Quebec City, Quebec, Canada, October 3-4.

110. KRUT, S., COMPANY, O. & PIERROT, F., 2003. *Eureka: A New 5-Degree-of-Freedom Redundant Parallel Mechanism with High Tilting Capabilities.* s.l.:in Proc. of IROS 2003: International Conference on Intelligent Robots and Systems, pp. 3575-3580, Las Vegas, NV, USA, October 27-31.

111. KRUT, S., COMPANY, O. & PIERROT, F., 2004a. *Force Performance Indexes for Parallel Mechanisms with Actuation Redundancy, especially for Parallel Wire–Driven Manipulators.* s.l.:in Proc. of International Conference on Intelligent Robots and Systems (IROS 2004), pp. 3936-3941, Sendai, Japan, 28th September - 2nd October.

112. KRUT, S., COMPANY, O. & PIERROT, F., 2004b. *Velocity Performance Indexes for Parallel Mechanisms with Actuation Redundancy.* s.l.:International Journal of Robotica (Cambridge University Press), vol. 22(2), pp. 129-139.

113. LAFOURCADE, P. & LLIBRE, M., 2002. *Design of a Parallel Wire-Driven Manipulator for Wind Tunnels.* s.l.:in Proc. of Workshop on Fundamental Issues and Future Research Directions for Parallel Mechanisms and Manipulators, pp. 46-56, Quebec City, Quebec, Canada, October 3-4.

114. LAMAURY, J., 2013. *Contribution à la commande des robots parallèles à câbles à redondance d'actionnement,* PhD Thesis, Université Montpellier II, October 8.

115. LEE, J. H., EOM, K. S., YI, B.-J. & SUH, I. H., 2001. *Design of a New 6-DOF Parallel Haptic Device.* s.l.:in Proc. of the 2001 IEEE International Conference on Robotics and Automation (ICRA 2001), pp. pp. 886-891, Seoul, Korea, May 21-26.

116. LEE, S. S. & LEE, J. M., 2003. *Design of a general purpose 6-DOF haptic interface.* s.l.: Mechatronics, Vol. 13, No. 7, pp. 697-722.

117. LI, M. et al., 2005. *Dynamic formulation and performance comparison of the 3-DOF modules of two reconfigurable PKM : the Tricept and the TriVariant.* s.l.:ASME Journal of Mechanical Design, Vol. 127, No. 6, pp. 1129-1136.

118. LI, Q., HUANG, Z. & HERVE, J. M., 2004. *Type Synthesis of 3R2T 5-DOF Parallel Mechanisms Using the Lie Group of Displacements.* s.l.:IEEE Transactions on Robotics and Automation, Vol. 20, No. 2, April.

119. LIU, G., LOU, Y. & LI, Z., 2003. *Singularities of Parallel Manipulators: A Geometric Treatment.* s.l.:in IEEE Transactions on Robotics and Automation, Vol. 19, No. 4, pp. 579-594, August.

120. LIU, M.-J., LI, C.-X. & LI, C.-N., 2000. *Dynamics Analysis of the Gough–Stewart Platform Manipulator.* s.l.:IEEE Transactions on Robotics and Automation, Vol. 16, No. 1, February.

121. LIU, X.-J. & BONEV, I. A., 2008. *Orientation Capability, Error Analysis, and Dimensional Optimization of Two Articulated Tool Heads With Parallel Kinematics.* s.l.:Journal of Manufacturing Science and Engineering, Vol. 130, No. 1, February.

122. MANSOURI, I. & OUALI, M., 2009. *A new homogeneous manipulability measure of robot manipulators, based on power concept.* s.l.:Mechatronics, Vol. 19, No. 6, pp. 927–944.

123. MANSOURI, I. & OUALI, M., 2011. *The power manipulability—a new homogeneous performance index of robot manipulators.* s.l.:Robotics and Computer-Integrated Manufacturing, Vol. 27, No. 2, pp. 434–449.

124. MA, O. & ANGELES, J., 1990. *The concept of dynamics isotropy and its applications to inverse kinematics and trajectory planning.* s.l.:in Proc. of the IEEE International Conference on Robotics and Automation, pp. 481–486, Cincinnati,USA.

125. MA, O. & ANGELES, J., 1991. *Optimum Architecture Design of Platform Manipulators.* s.l.:Proc. IEEE Int. Conf. Advanced Robotics.

126. MA, O. & ANGELES, J., 1993. *Optimum design of manipulators under dynamic isotropy conditions.* s.l.:in Proc. of the IEEE International Conference on Robotics and Automation, pp. 470–475, Atlanta, USA.

127. MBAREK, T., G.LONIJ & CORVES, B., 2007. *Singularity analysis of a fully parallel manipulator with five-Degrees-of-Freedom based on Grassmann line geometry.* s.l.:in Proc. 12th IFToMM World Congress, Besançon (France), June 18-21.

128. MCGHEE, S., CHAN, T. F., DUBEY, R. V. & KRESS, R. L., 1994. *Probability-Based Weighting of Performance Criteria for a Redundant Manipulator.* s.l.:in Proc. of Scott MCGHEE, Tan F. CHAN, Rajiv V. DUBEY, Reid L. KRESS, Probability-Based Weighin Proc. of 1994 IEEE International Conference on Robotics and Automation (ICRA 1994), pp. 1887-1894.

129. MERLET, J.-P., 2006. *Parallel Robots.* s.l.:Springer.

130. MERLET, J.-P. & DANEY, D., 2005. *Dimensional Synthesis of Parallel Robots with a Guaranteed Given Accuracy over a Specific Workspace.* s.l.:Proceedings of the 2005 IEEE International Conference on Robotics and Automation (ICRA 2005), Barcelona, Spain, April.

131. MERLET, J. P., 2006. *Jacobian, manipulability, condition number, and accuracy of parallel robots.* s.l.:Journal of Mechanical Design, Transactions of the ASME, Vol. 128, No. 1, pp. 199–206.

132. MULLER, A., 2005. *Internal Preload Control of Redundantly Actuated Parallel Manipulators—Its Application to Backlash Avoiding Control.* s.l.:IEEE Transactions on Robotics, Vol. 21, No. 4, August.

133. MULLER, A., 2006. *Stiffness Control of Redundantly Actuated Parallel Manipulators.* s.l.:in Proc. of the 2006 IEEE International Conference on Robotics and Automation, Orlando, Florida, May.

134. MULLER, A., 2013. *On the terminology and geometric aspects of redundant parallel manipulators.* s.l.:Robotica, 31, pp. 137-147.

135. NABAT, V., 2007. *Robots parallèles à nacelle articulée: Du concept à la solution industrielle pour le pick-and-place,* PhD Thesis, Université Montpellier 2, March 2.

136. NABAT, V. et al., 2005. *Par4: very high speed parallel robot for pick-and-place.* s.l.:in Proc. of 2005 IEEE/RSJ International Conference on Intelligent Robots and Systems (IROS 2005), pp. 553-558.

137. NEUMANN, K.-E., 2006. *The key to aerospace automation.* s.l.:SAE Technical Paper.

138. PANG, H. & SHAHINPOOR, M., 1994. *Inverse Dynamics of a Parallel Manipulator.* s.l.:Journal of Robotic Systems, Vol. 11, No. 8, pp. 693-702.

139. PARK, F. C., 1995. *Distance metrics on the rigid-body motions with applications to mechanism design.* s.l.:ASME J. Mechanical Design, Vol. 117, pp. 48-54.

140. PARK, F. C. & KIM, J. W., 1998. *Manipulability of closed kinematic chains.* s.l.: ASME J. Mechanical Design, Vol. 120, No.4.

141. PIERROT, F., 1991. *Robots Pleinement Parallèles Légers: Conception, Modélisation, et Commande,* s.l.: s.n.

142. PIERROT, F. & COMPANY, O., 1999. *H4: a new family of 4-dof parallel robots.* s.l.: in Proc of IEEE/ASME International Conference on Advanced Intelligent Mechatronics, Atlanta, Georgia, USA, pp. 508-513, September 19-22.

143. PIERROT, F., DAUCHEZ, P. & FOURNIER, A., 1991a. *Fast parallel robots.* s.l.:in Journal of Robotic Systems, Vol. 8, No. 6, pp. 829-840.

144. PIERROT, F., DAUCHEZ, P. & FOURNIER, A., 1991b. *HEXA: A fast six-DOF fully-parallel robot.* s.l.:in Proc. of IEEE International Conference on Advanced Robotics (ICAR), pp. 1159-1163, Pise, Italy, June 19-22.

145. PIERROT, F., NABAT, V., COMPANY, O. & KRUT, S., 2008. *From Par4 to Adept Quattro.* in Proc. Robotic Systems for Handling and Assembly - 3rd International Colloquium of the Collaborative Research Center SFB 562, Braunschweig, Germany: s.n.

146. PIERROT, F. & SHIBUKAWA, T., 1999. *From Hexa to HexaM.* s.l.:in Parallel Kinematic Machines, pp. 357-364 , Springer London.

147. POND, G. & CARRETERO, J. A., 2006. *Formulating Jacobian matrices for the dexterity analysis of parallel manipulators.* s.l.:Mechanism and Machine Theory 41, No. 12, pp.1505-1519..

148. REBOULET, C., LAMBERT, C. & NOMBRAIL, N., 1992. *A parallel redundant manipulator:SPEED-R-MAN and its control.* s.l.:In ISRAM, pages 285-291, Santa-Fe, November 11-13.

149. RISOLI, A., PRISCO, G. M., SALSEDO, F. & BERGAMASCO, M., 1999. *A Two Degrees-of-Freedom Planar Haptic Interface with High Kinematic Isotropy.* s.l.:in Proceedings of the 1999 IEEE International Workshop on Robot and Human Interaction, pp. 297-302, Pisa, Italy, September.

150. ROLLAND, L. H., 1999. *THE MANTA AND THE KANUK: NOVEL 4-DOF PARALLEL MECHANISMS FOR INDUSTRIAL HANDLING.* s.l.:in Proc. of 1999 International Mechanical Engineering Congress and Exposition (IMECE 99), Nashville, Tennessee, USA, November 14-19.

151. SALISBURY, J. K. & CRAIG, J. J., 1982. *Articulated hands: force control and kinematic issues.* s.l.: International Journal of Robotics Research, Vol. 1, No. 1, pp. 4-17.

152. SAVOURE, L., Patrick MAURINE, D. C. & KRUT, S., 2006. *An Improved Method for the Geometrical Calibration of Parallelogram-based Parallel Robots.* s.l.:in Proc. of 2006 IEEE International Conference on Robotics and Automation (ICRA 2006), pp. 769-776, Orlando, Florida, May 15-19.

153. SEWARD, N. & BONEV, I. A., 2014. *A new 6-DOF parallel robot with simple kinematic model.* s.l.:2014 IEEE International Conference on Robotics & Automation (ICRA 2014), Hong Kong, China, May 31-June 7.

154. SHAYYA, S. et al., 2013a. *A novel (3T-1R) redundant parallel mechanism with large operational workspace and rotational capability.* s.l.:in Proc. of 2013 IEEE/RSJ International Conference on Intelligent Robots and Systems (IROS 2013), pp. 436-443, Tokyo, Japan, November 3-8.

155. SHAYYA, S. et al., 2013b. *A Novel 4 DoFs (3T-1R) Parallel Manipulator with Actuation Redundancy–Workspace Analysis.* s.l.:in Proc. of MeTrApp 2013: The 2nd Conf. on Mechanisms, Transmissions and Applications, pp. 317-324, Bilbao, Spain, October 2-4.

156. SHAYYA, S. et al., 2014a. *A Novel (3T-2R) Parallel Mechanism with Large Operational Workspace and Rotational Capability.* s.l.:in Proc. of 2014 IEEE International Conference on Robotics and Automation (ICRA 2014), Hong Kong, China, May 31 - June 7.

157. SHAYYA, S. et al., 2014b. *Dimensional Synthesis of 4 DoFs (3T-1R) Actuatedly Redundant Parallel Manipulator Based on Dual Criteria: Dynamics and Precision.* s.l.:in Proc. of 2014 IEEE/RSJ International Conference on Intelligent Robots and Systems (IROS 2014), Chicago, Illinois, September 14–18.

158. SHAYYA, S. et al., 2014c. *Dynamic Analysis of 4 Degrees of Freedom Redundant Parallel Manipulator.* s.l.:in Proc. of Advances in Robot Kinematics (ARK 2014), pp. 545-553, Ljubljana, Slovenia, June 29 - July 3.

159. SHAYYA, S. et al., 2014d. *On the Performance Evaluation and Analysis of General robots with Mixed DoFs.* s.l.:in Proc. of 2014 IEEE/RSJ International Conference on Intelligent Robots and Systems (IROS 2014), Chicago, Illinois, USA, September 14–18.

160. SICILLIANO, B. & KHATIB, O., 2008. *(Editors),Springer Handbook of Robotics.* s.l.:Springer.

161. SOKOLOV, A. & XIROUCHAKIS, P., 2007. *Dynamics analysis of a 3-DOF parallel manipulator with R–P–S joint structure.* s.l.:Mechanism and Machine Theory, Vol. 42, No. 5, pp. 541-557.

162. SPARACINO, F. & HERVE, J. M., 1993. *Synthesis of Parallel Manipulators Using Lie-Groups: Y-Star and H-Robot.* s.l.:Proceedings of the 1993 IEEEnsukuba International Workshop on Advanced Robotics, Tsukuba, Japan, November 8-9.

163. STAFFETTI, E., BRUYNINCKX, H. & SCHUTTER, J. D., 2002. *On the invariance of manipulability indices.* s.l.:in ARK 2002, pp. 57–66, Caldes de Malavalla, June 29- July 2.

164. STEWART, D., 1965. *A Platform with Six Degrees of Freedom.* s.l.:in the Proc. of the IMechE, Vol. 180, No. 15, pp. 371-385.

165. STOCCO, L., SALCUDEAN, S. E. & SASSANI, F., 1998. *Matrix Normalization for Optimal Robot Design.* s.l.:in Proc. of IEEE ICRA, Leuven, Belgium, May 16-21.

166. STOUGHTON, R. & KOKKINIS, T., 1987. *Some properties of a new kinematic structure for robot manipulators.* s.l.:in Proc. of 13th ASME Design Automation Conference, pp. 73-79, Boston, MA.

167. TANG, X., 2014. *An Overview of the Development for Cable-Driven Parallel Manipulator.* s.l.:Advances in Mechanical Engineering, vol. 2014, Article ID 823028, DOI :10.1155/2014/823028.

168. TSAI, L.-W., 1996. *Kinematics of a Three-DOF Platform With Three Extensible.* s.l.:in Recent advances in robot kinematics, pp. 401-410, Springer Netherlands.

169. TYAPIN, I. & HOVLAND, G., 2013. *Kinematic Calibration Method for a 5-DOF Gantry-Tau Parallel Kinematic Machine.* s.l.:2013 IEEE International Conference on Robotics and Automation (ICRA 2013), Karlsruhe, Germany, May 6-10.

170. UNAL, R., KIZILTAS, G. & PATOGLU, V., 2008. *Multi-criteria Design Optimization of Parallel Robots.* s.l.:IEEE Conference on Robotics, Automation and Mechatronics, pp.112-118, September 21-24.

171. UR-REHMAN, R., CARO, S., CHABLAT, D. & WENGER, P., 2010. *Multiobjective Design Optimization of 3–PRR Planar Parallel Manipulators.* s.l.:Global Product Development (2010), pp. 1-10..

172. VOGLEWEDE, P. A. & EBERT-UPHOFF, I., 2005. *Overarching Framework for Measuring Closeness to Singularities of Parallel Manipulators.* s.l.:IEEE Transactions on Robotics, Vol. 21, No. 6, December.

173. WANG, J. & GOSSELIN, C. M., 1998. *A New Approach for the Dynamic Analysis of Parallel Manipulators.* s.l.:Multibody System Dynamics, Vol. 2, No. 3, pp. 317-334.

174. WANG, J., WU, C. & LIU, X.-J., 2010. *Performance evaluation of parallel manipulators: Motion/force transmissibility and its index.* s.l.:Mechanism and Machine Theory, Vol. 45, pp. 1462-1476.

175. WANG, L. T. & RAVANI, B., 1988a. *Dynamic Load Carrying Capacity of Mechanical Manipulators—Part I: Problem Formulation.* s.l.:Journal of Dynamic Systems, Measurement, and Control, Vol. 110, Issue 1, pp. 46–52.

176. WANG, L. T. & RAVANI, B., 1988b. *Dynamic Load Carrying Capacity of Mechanical Manipulators-Part II: Computational Procedure and Applications.* s.l.:Journal of Dynamic Systems, Measurement, and Control, Vol. 110/ 53.

177. WECK, M. & STAIMER, D., 2002. *Parallel kinematic machine tools–current state and future potentials.* s.l.:CIRP Annals-Manufacturing Technology, 51(2), pp. 671-683.

178. WENGER, P. & CHABLAT, D., 2000. *Kinematic Analysis of a New Parallel Machine Tool: The Orthoglide.* s.l.:in Advances in Robot Kinematics, pp. 305-314. Springer Netherlands.

179. WIEGAND, A., HEBSACKER, M. & HONEGGER, M., 1996. *Parallele Kinematik und Linearmotoren: Hexaglide - ein neues, hochdynamisches Werkzeugmaschinenkonzept.* s.l.:Technische Rundschau Transfer Nr. 25.

180. WIJK, V. v. d., KRUT, S., PIERROT, F. & HERDER, J. L., 2013. *Design and experimental evaluation of a dynamically balanced redundant planar 4-RRR parallel manipulator.* s.l.:International Journal of Robotics Research, Vol. 32 , No. 6, pp. 744-759.

181. WOHLHART, K., 1999. *Degrees of shakiness.* s.l.:in Mechanism and Machine Theory 34, pp. 1103-1126.

182. WOLF, A., SHOHAM, M. & PARK, F., 2002. *Investigation of Singularities and Self-Motions of the 3-UPU Robot.* s.l.:in Proc. ARK, Caldes de Malavalla, pp. 165–174,.

183. XIE, F., LIU, X.-J. & WANG, J., 2011. *Performance Evaluation of Redundant Parallel Manipulators Assimilating Motion/Force Transmissibility.* s.l.:International Journal of Advanced Robotic Systems, Vol. 8, No. 5, pp. 113-124.

184. YANG, H., 2012. *Etude d'un système de fabrication agile mobile pour composants de grande taille,* s.l.: s.n.

185. YOSHIKAWA, T., 1985a. *Dynamic manipulability of robot manipulators.* s.l.:in Proc. of IEEE International Conference on Robotics and Automation (ICRA 1985), St Louis, MO, pp. 1033– 1038.

186. YOSHIKAWA, T., 1985b. *Manipulability of robotic mechanisms.* s.l.:International Journal of Robotics Research, Vol. 4, No. 2, pp. 3-9.

187. YOSHIKAWA, T., 1991. *Translational and rotational manipulability of robotic manipulators.* s.l.:in Proc. 1991 IEEE IECON, Kobe, Japan, pp. 1170–1175.

188. ZHAO, Y. & GAO, F., 2009. *Dynamic formulation and performance evaluation of the redundant parallel manipulator.* s.l.:Robotics and Computer-Integrated Manufacturing 2009, 25, pp. 770 – 781.

189. ZHAO, Y. & GAO, F., 2009. *Dynamic formulation and performance evaluation of the redundant parallel manipulator.* s.l.:Robotics and Computer-Integrated Manufacturing 25, pp. 770–781.

190. ZLATANOV, D., BONEV, I. & GOSSELIN, C., 2001. *Constraint Singularities.* s.l.:http://www.parallemic.org/Reviews/Review005.html.

191. ZLATANOV, D., FENTON, R. G. & BENHABIB, B., 1995. *A Unifying Framework for Classification and Interpretation of Mechanism Singularities.* s.l.:Journal of Mechanical Design, Volume 117, Issue 4, pp. 566-572, Decemeber 1.

192. ZLATANOV, D., FENTON, R. G. & BENHABIB, B., 1998. *Identification and Classification of the Singular Configurations of Mechanisms.* s.l.:Mechanism and Machine Theory, Vol. 33, No. 6, pp. 743-760.

Appendices

Appendix A: Precision-Related Performances of Some Rapid Industrial Robots and Prototypes at LIRMM

A.1- Generalities and Definitions

This appendix details the precision evaluation of several prototypes and industrial robots that has been done at LIRMM. This assessment considered accuracy and repeatability not only for static poses, but also in dynamics; i.e. as the robot follows a pre-specified trajectory. Moreover, multi-directional variation of accuracy, in the case of statics, has been investigated as well. The norm adopted for all the aforementioned tests is **[ISO 9283; 1998 (F)]**.

The study considered the following robots: Quattro, Par2, DUAL V, and Veloce (the prototype). However, regarding dynamic performance (path following), not all robots were possible to evaluate due to technical issues and constraints.

In what follows, we clarify all the aforementioned terms, in which we limit ourselves to generic definitions and clarifications. As for the formulae, they are easy to compute based on the provided definitions. Yet, for more insights and details, the reader may refer to **[ISO 9283; 1998 (F)].**

Accuracy

Pose accuracy expresses the deviation between the commanded pose and the mean of the attained ones when approaching the former (i.e. desired/commanded pose) from the same direction. In other words, it is the distance between the mean of the attained poses and the

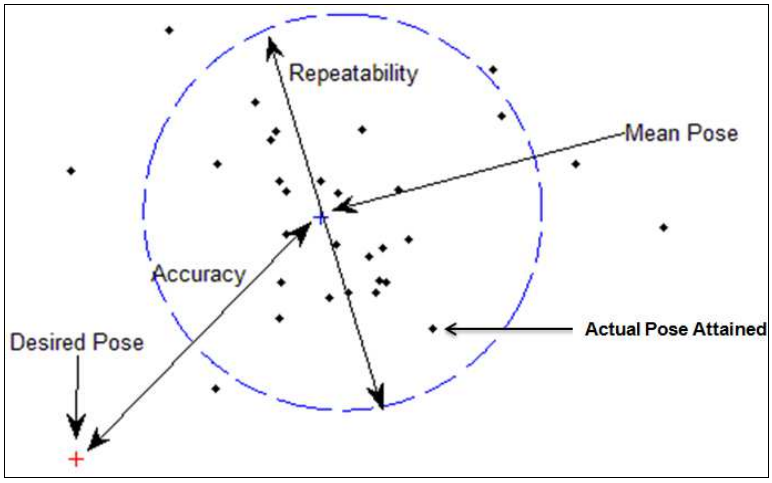

Fig. Ap-1: Static accuracy and repeatability illustration.

desired one. The closer it is to zero the better, indicating an accurate robot. In general, we can distinguish between positional and orientation accuracies.

Repeatability

It expresses the closeness of agreement between the attained poses after n repetitive visits to the same commanded pose, and along the same direction. We speak generally of positional and orientation repeatabilities. This repeatability is also referred to as uni-directional one, as it considers single direction. Geometrically, it is the radius of the sphere centered at the mean pose and embracing all the attained ones.

Assuming that the attained poses are normally distributed about the mean (i.e. Gaussian distribution[1]), the repeatability is $3\widetilde{\sigma}$, with $\widetilde{\sigma}$ being the estimated standard deviation (this is applied for positional and orientation repeatability). The closer the value is to zero the better, indicating a very repeatable robot.

An illustration of the above two terms is depicted in **Fig. Ap-1**. Based on the aforementioned, a robot can be accurate but not repeatable, or vice-versa. In fact, the precision as referred to in several places is more related to repeatability than accuracy. Here, we will use the words “precision” and “precise” to refer globally to all terms such as accuracy, repeatability, and resolution (operational resolution[2]) that has been described in **Chapter 2**. Therefore, when we say a “precise” robot, we mean a one that is both accurate and repeatable.

Multi-Directional Variation of Accuracy

Briefly, this expresses how the pose accuracy (in position and orientation) varies with the change of direction of approach to the desired pose. Mathematically, it is the largest difference between the means of the actual poses obtained for the same commanded pose, but along different directions. An illustration of this term is shown in **Fig. Ap-2**.

Note that in all the aforementioned static precision evaluations, the attained pose is measured after a sufficient settling time.

---

[1] In Gaussian or normal distribution, the region containing the vast majority (99.99%) of the cases are those within a distance of three standard deviations from the mean. Notice that we used the notation $\widetilde{\sigma}$ to denote estimated value of this deviation, σ. For more on this matter, the reader may refer to **[ISO 9283; 1998 (F)]** and any statistical article in this subject (estimators of standard deviations).

[2] Operational resolution is the smallest detectable step the robot can do in the operational space. It is similar to the measurement resolution of a scale (ruler). If the ruler is marked with $1\,\mathrm{mm}$ divisions, it means we cannot use it to measure an object with a length smaller than $1\,\mathrm{mm}$; in fact, any measurement is done with rough $\pm 1\,\mathrm{mm}$ error.

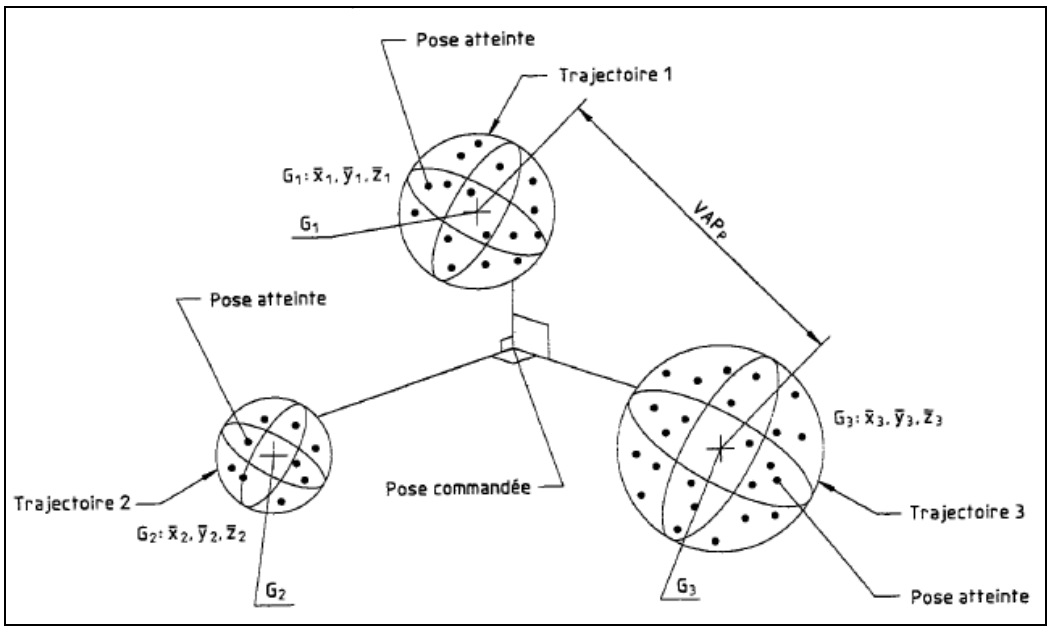

Fig. Ap-2: Illustration of multi-directional variation of accuracy (VAP_p in the figure) [ISO 9283; 1998 (F)].

Also, note that the most important of these measures are repeatability and multi-directional variation of accuracy. This is due to the fact that the reasons behind these mentioned terms are rather of non-deterministic random nature (due for example to backlashes, joint clearances, stick-slip effects, control and sampling time, encoder resolution, disturbances, thermal fluctuations, hysteresis, etc.). As for accuracy, it is due to deterministic sources (such as geometric errors, assembly errors, elasticity, incompleteness of geometric model, etc.). Note also that a part from the non-deterministic influences, specifically their mean, contributes in a secondary part to the accuracy. Theoretically speaking, while accuracy related errors are possible to compensate, repeatability errors are rather impossible to circumvent. That is why having less accurate but repeatable robot is less problematic than the opposite case. Based on **Fig. Ap-1** and **Fig. Ap-2**, it is clear that when repeatability and multi-directional variation of accuracy are both very close to zero, the attained poses for the same commanded destination are tightly clustered, which implies improved multi-directional repeatability as well.

So far, we have defined static precision-related terms. It remains to define the dynamic precision-related measures that quantify the robot performance in trajectory following.

Considering a trajectory that is described several times, then one can define the path accuracy and path repeatability (in position and orientation).

Trajectory or Path Accuracy

Consider the robot moving along a prescribed path several times in the same direction. Then, the trajectory positional accuracy is defined as the maximum distance between the desired path and the barycenters of the different positions attained at different steps of the controlled trajectory. Similar definition is considered regarding orientation accuracy along a desired path. For better understanding, refer to **Fig. Ap-3**.

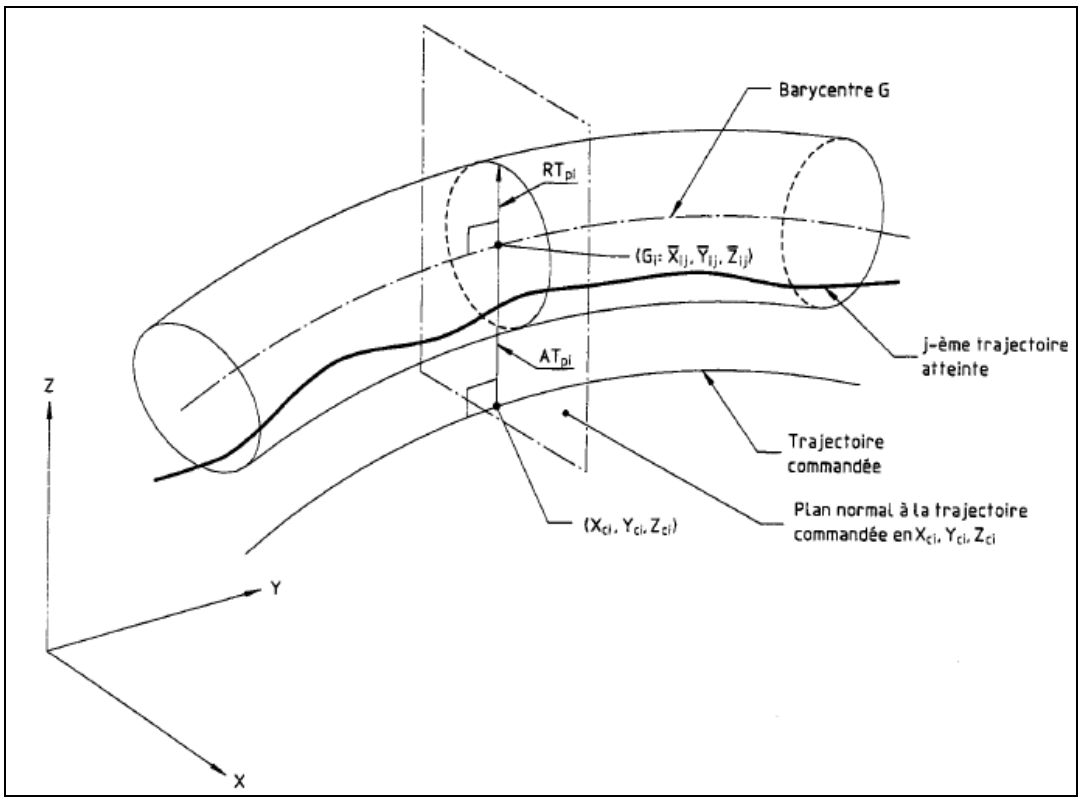

Fig. Ap-3: Illustration of trajectory positional accuracy (AT_p) and trajectory positional repeatability (RT_p) [ISO 9283; 1998 (F)].

Trajectory or Path Repeatability

It expresses the closeness of agreement between the several trajectories traveled for the same commanded path. It also utilizes the six-sigma rule, assuming a Gaussian distribution. For clarification, see **Fig. Ap-3**.

A.2- Briefing on the Procedure and Main Results

Evaluation Procedure in Brief

Having defined the different terms, we can proceed to discuss the evaluation done. First, it is worth mentioning here that the pose of the tested robot has been measured by the use of Metris K600-CMM system (shown in **Fig. Ap-4**). According to its technical specifications, within the first zone of measurement $(1.5 \text{ to } 3\,\text{m})$[3], the uncertainty is $90\,\mu\text{m}+(25\,\mu\text{m}/\,\text{m})\,d_m$, where d_m is the distance between the LEDs and the camera . Yet, it might be slightly different due to the temperature variations, especially that the calibration of the machine is not possible during experimentation. As for the measurement repeatability, we have estimated it by checking several measurements of fixed LEDs (for one second duration), and it was in the vicinity of $10\,\mu\text{m}$.

[3] We have done our measurements in this zone.

Fig. Ap-4: Metris K600 CMM measuring device.

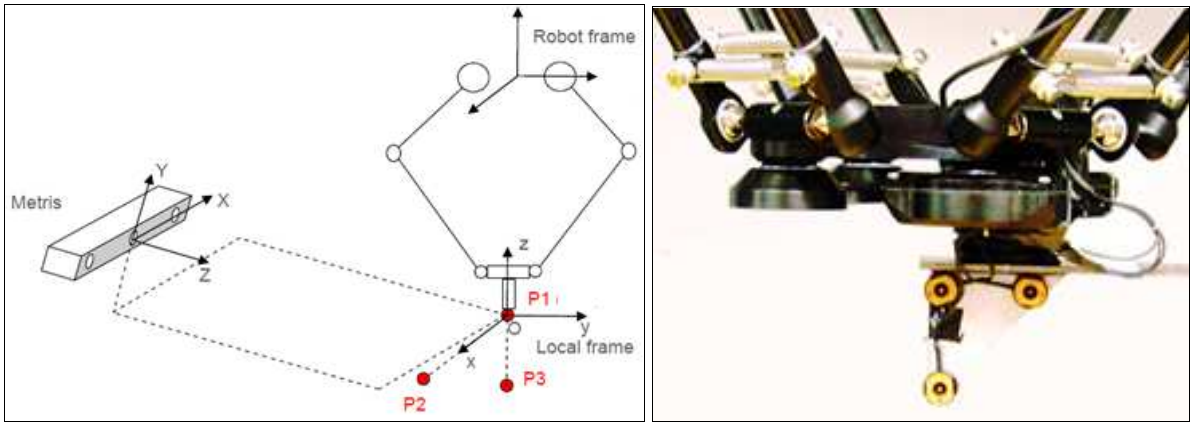

Fig. Ap-5: Experimental setup: an illustrative schematic (left) and a close-up view on the LEDs assembly on the platform (right).

The complete pose of the end-effector is measured by means of fixing three LEDs on the platform as close as possible to the TCP, and some techniques were used to account for the impact of rotational errors on the estimation of the real TCP position –when possible. Also, some estimation technique was used to determine the transformation matrix between the measuring frame and the proper base frame of the tested robot. We will not get further in details into these aspects as being rather technical, but we will highlight later the impact of some of these issues. The reader should keep in mind that the intention behind this evaluation is having insights on the order of magnitude of the precision measures, and not their exact values.

The schematic illustrating the experimentation is depicted in **Fig. Ap-5**. Notice that in this figure, three LEDs are fixed on the moving platform and are measured by the Metris device to estimate the complete end-effector pose. Also, other three LEDs -when possible- are mounted on the fixed base frame as to inspect the vibrational effects and any inconsistencies. When using six LEDs, the measuring frequency is $500\,\mathrm{Hz}$. In the case of using three LEDs, the measuring frequency is $1000\,\mathrm{Hz}$.

Finally, for measurement acquiring, an automatic triggering signal was channeled from the robot controller, allowing for automated procedure -except when it was impossible (due to compatibility issue, as it was the case with DUAL V).

Static Precision Results

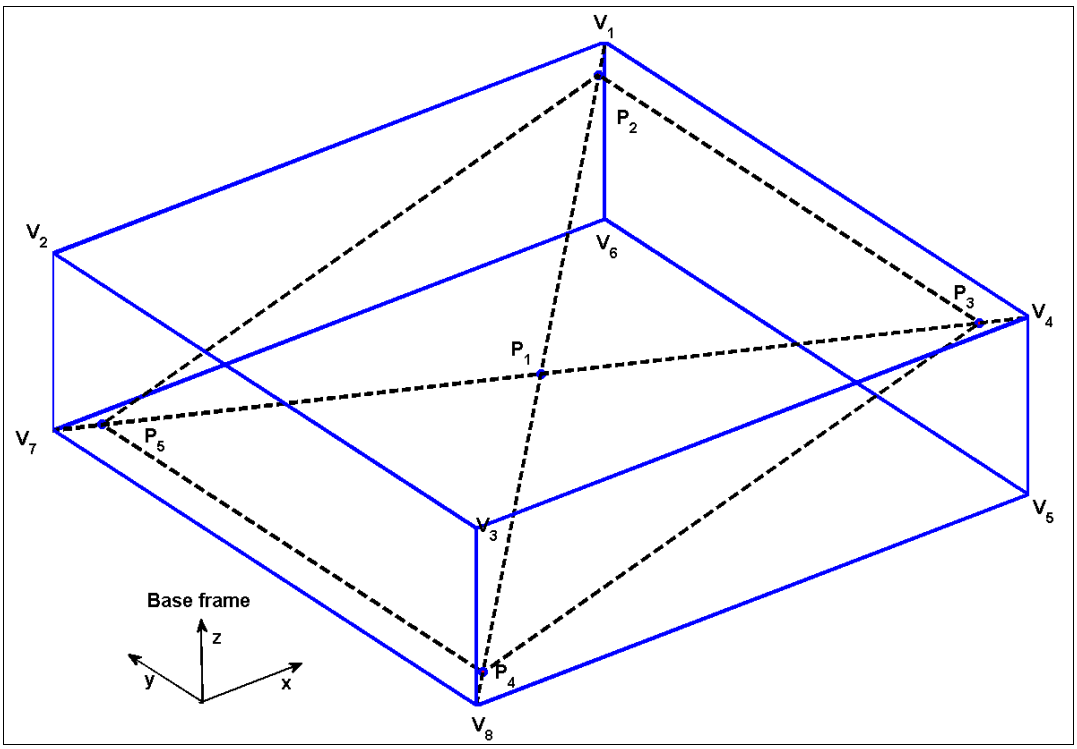

Fig. Ap-6: The largest inscribed cube or rectangular parallelepiped within the accessible workspace, the diagonal plane, and the test points ($P_1 ... P_5$).

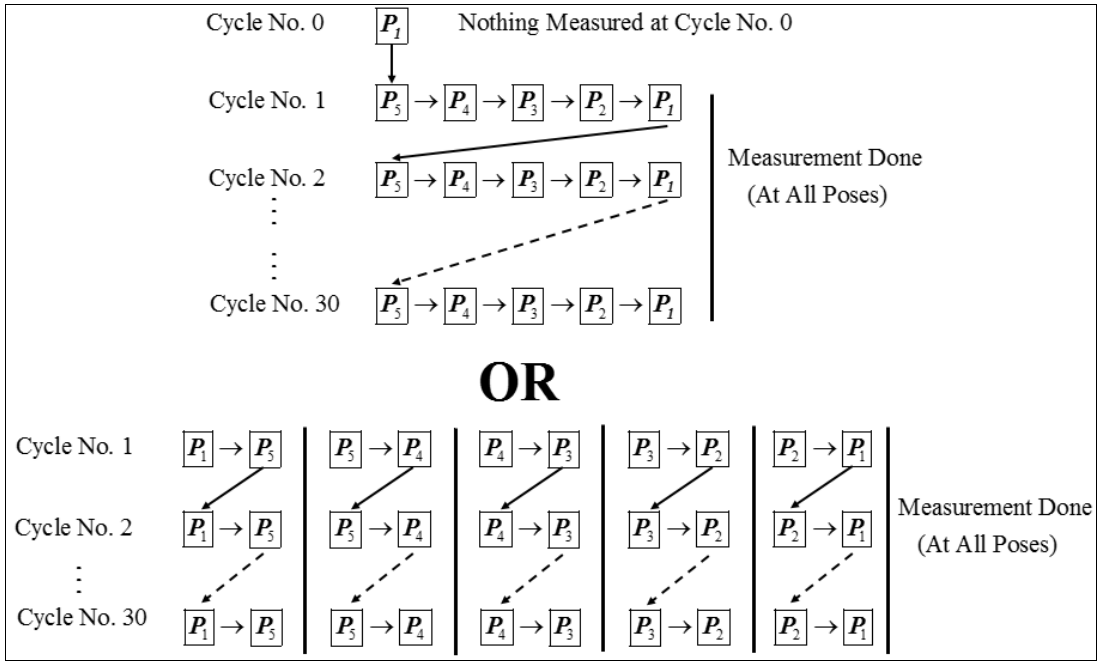

Fig. Ap-7: Illustration of the possible cycle schemes.

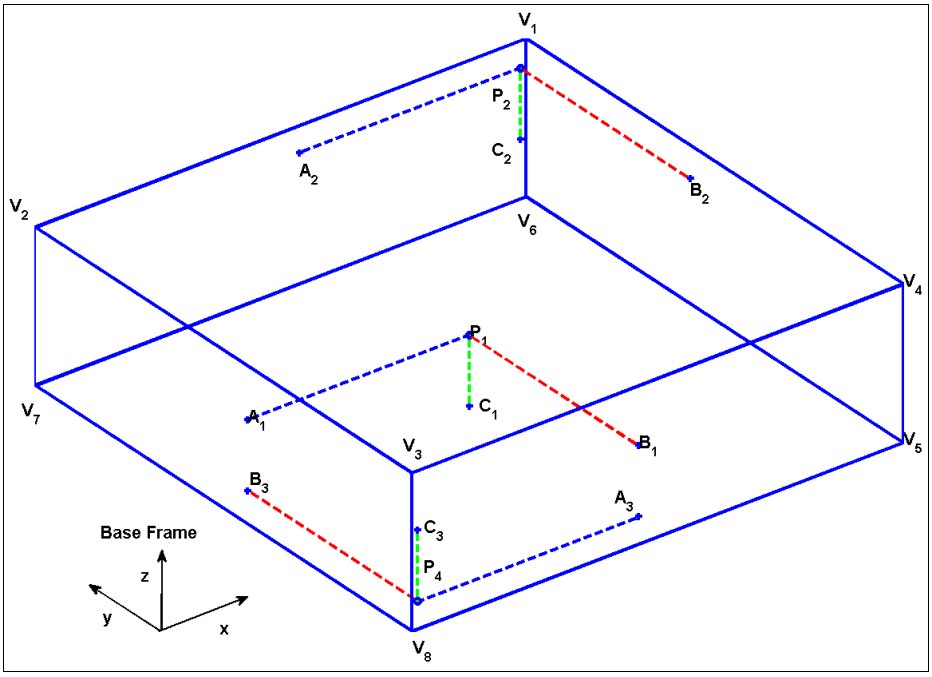

Fig. Ap-8: Multi-directional variation of accuracy: poses (P_1, P_2, and P_4) and the three directions of approach for the pose P_i (A_iP_i, B_iP_i, and C_iP_i, with $i=1,2,4$).

According to **[ISO 9283; 1998 (F)]**, the static tests may be carried by determining the largest cube or rectangular parallelepiped inscribed within the accessible or most frequently utilized workspace. Then, any of the four possible diagonal planes can be used (see **Fig. Ap-6**). Within this plane, five points P_i (with $i=1...5$) are considered being the center, and the points along the diagonals, with the latter ones offset from the vertices a pre-specified distance for safety.

Regarding the way each of the five points (or poses) is approached for static accuracy evaluation, it can be done in one of the two manners depicted in **Fig. Ap-7**. We have chosen the second scheme. As for multi-directional variation of accuracy, the test is only done at P_1, P_2, and P_4, in the way shown in **Fig. Ap-8**. For each of the three poses, P_1, P_2, and P_4, the approach is done along three directions parallel to the axes of the base frame, and each is repeated 30 times.

Having clarified the main points regarding the procedure, we proceed by presenting the static precision results of Quattro (see **Fig. 1-45**), with the articulated platform (four dofs of 3T-1R nature) and the rigid one (three dofs of 3T type) (see **Fig. Ap-9**). Note that in the case of using rigid platform, the robot becomes redundantly actuated with one degree of redundancy. The static accuracies and repeatabilities for position and orientation of Quattro, in its two versions, are presented in **Table Ap-1**, **Table Ap-2, Table Ap-3**, **Table Ap-4**, **Table Ap-5**, and **Table Ap-6**.

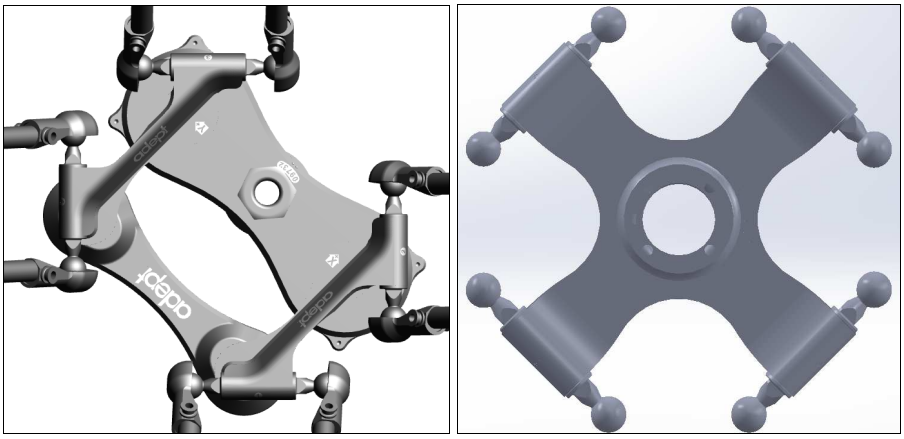

Fig. Ap-9: Adept Quattro platforms: articulated (four dofs 3T-1R on the left) and rigid (three dofs 3T on the right) (http://www.adept.com/products/robots/parallel/quattro-s650h/downloads).

Table Ap-1: Static positional accuracy and repeatability of Adept Quattro (case of articulated platform).

	P_1	P_2	P_3	P_4	P_5
Static Accuracy (mm)	0.0751	1.1729	1.1379	0.7336	0.3378
Static Repeatability (mm)	0.0429	0.0637	0.0724	0.0682	0.0464

Table Ap-2: Static positional accuracy and repeatability of Adept Quattro (case of rigid platform).

	P_1	P_2	P_3	P_4	P_5
Static Accuracy (mm)	0.5281	1.1366	0.6326	0.1799	0.9651
Static Repeatability (mm)	1.0659	1.3096	0.2601	0.1961	0.2366

Table Ap-3: Static orientation accuracy of Adept Quattro (case of articulated platform).

Orientation Accuracy (°)					
Angle\Pose	P_1	P_2	P_3	P_4	P_5
θ_x	-0.0026	-0.0624	-0.2138	-0.1468	0.0095
θ_y	0.0029	-0.2842	0.2440	0.3171	-0.0108
θ_z (controlled)	-0.1218	1.4040	-0.6413	-0.4654	-0.0735

Table Ap-4: Static orientation repeatability of Adept Quattro (case of articulated platform).

Orientation Repeatability (°)					
Angle\Pose	P_1	P_2	P_3	P_4	P_5
θ_x	0.0088	0.0134	0.0108	0.0147	0.0096
θ_y	0.0029	0.0036	0.0027	0.0049	0.0027
θ_z (controlled)	0.0115	0.0221	0.0102	0.0176	0.0194

Table Ap-5: Static orientation accuracy of Adept Quattro (case of rigid platform).

Orientation Accuracy (°)					
Angle\Pose	P_1	P_2	P_3	P_4	P_5
θ_x	-0.0014	0.0744	-0.2785	-0.1257	0.0499
θ_y	-0.0053	-0.1882	-0.0469	0.1339	0.1723
θ_z	-0.0352	-0.0341	-0.0826	-0.1585	-0.1067

Table Ap-6: Static orientation repeatability of Adept Quattro (case of rigid platform).

Orientation Repeatability (°)					
Angle\Pose	P_1	P_2	P_3	P_4	P_5
θ_x	0.0393	0.0413	0.0179	0.0127	0.0134
θ_y	0.0048	0.0064	0.0041	0.0032	0.0028
θ_z	0.0227	0.0333	0.0207	0.0102	0.0103

As for the multi-directional variation of accuracy in position, it is given in **Table Ap-7**. The results show that while Quattro is undeniably rapid, yet its precision performances are still far from the requirements for high-speed and high-precision applications. It is worth mentioning here that the precision evaluation, based on the poses calculated via the feedback sensors, showed a better accuracy (for both versions) and better repeatability (only for rigid platform). In fact, we inferred the problem to be in addition to the use of articulated platforms, to some issues at control level and the implemented direct geometric model (numerical model). However, the control being closed, no further inspection was possible to make at this level. Also, the way in which the parallelograms are executed, by means of ball-socket connections and springs, is an additional contributor to this lack of precision. This is not to mention the geometric errors and calibration related sources. In fact, in another project, called PRADA (executed by Tecnalia France), noticeable improvements on accuracy have been made reaching about $55\,\%$ (thanks to reconsidering the geometric models and performing adequate

Table Ap-7: Multi-directional variation of positional accuracy of Adept Quattro.

Multi-Directional Variation of Accuracy (mm)			
Version\Pose	P_1	P_2	P_4
Quattro (4 dofs, 3T-1R)	0.1007	0.0886	0.2292
Quattro (3 dofs, 3T)	0.0978	0.2253	0.1066

Table Ap-8: Static positional accuracy, repeatability, and multi-directional variation of accuracy of Veloce prototype.

	P_1	P_2	P_3	P_4	P_5
Static Accuracy (mm)	0.1162	3.4294	1.8707	8.3440	5.0229
Static Repeatability (mm)	0.0963	0.0959	0.1053	0.0664	0.1370
Multi-Directional Variation of Accuracy (mm)	0.1207	0.1175	Not Done	0.1772	Not Done

calibration). Nonetheless, the details and precise accuracy values have not been made public so far.

Another four-dof (3T-1R) robot whose static precision has been investigated is Veloce (the prototype). Its static accuracy, repeatability, and multi-directional variation of accuracy are given in **Table Ap-8**, **Table Ap-9**, and **Table Ap-10**. The poor performance regarding Veloce prototype has been expected and it is due to two main reasons. The first is that the robot has never been calibrated, whereas the second is that the rotational errors were large. In fact, the high rotational errors affected the positional accuracy. This is due to the fact that the influence of the offset between the real TCP and the estimated one has not been compensated because of technical issues (note that the rotational errors are sufficiently high to have the influence very noticeable; see the values in **Table Ap-8** and **Table Ap-9** for P_4 and P_5). Regarding repeatability, it is similar somehow to Quattro. Also, the orientation errors, especially for constrained rotations, are rather small and repeatable. These are due to assembly and geometry errors. As a matter of fact, controlled rotation always has more degraded accuracy compared with constrained rotations, but still acceptably repeatable. In Veloce prototype, the main contributor of its diminished accuracy (especially rotational one) is the uncompensated geometrical errors as well as the presence of the screw-nut mechanism, which also has its impact on repeatability.

Table Ap-9: Static orientation accuracy of Veloce prototype.

Orientation Accuracy (°)					
Angle\Pose	P_1	P_2	P_3	P_4	P_5
θ_x	-0.0496	-0.0505	-0.0819	-0.0985	-0.1793
θ_y	-0.0188	-0.0573	0.0090	-0.0044	0.1019
θ_z (controlled)	0.1110	-2.2557	1.9811	9.6003	7.0918

Table Ap-10: Static orientation repeatability of Veloce prototype.

Orientation Repeatability (°)					
Angle\Pose	P_1	P_2	P_3	P_4	P_5
θ_x	0.0121	0.0070	0.0065	0.0062	0.0265
θ_y	0.0089	0.0029	0.0030	0.0024	0.0062
θ_z (controlled)	0.0187	0.0131	0.0422	0.0096	0.0322

It is worth mentioning that the general observations regarding orientation errors are almost the same in all the tested robots. In what follows, we just present the interesting positional accuracy and repeatability of Par2 and DUAL V.

Par2 (see **Fig. Ap-10**) is a two-dof (2T) robot developed for pick-and-place applications. In fact, the coupled two passive chains that characterize this robot help in increasing its transversal stiffness, which constitutes an interesting feature as compared with other planar robots. Moreover, its Delta-like structure allowed it to be the most rapid manipulator with two dofs, having an acceleration capability up to $43\,\mathrm{g}$ and up to $260\,\mathrm{cycle/min}$ capacity (Adept cycle of $700\,\mathrm{mm}$ length and $25\,\mathrm{mm}$ height) (COMPANY, et al., 2011). As for DUAL V (see **Fig. Ap-10**), it is a rapid three-dof (2T-1R) planar motion manipulator characterized by actuation redundancy that not only helps eliminating singularities, but also homogenizing performances. An interesting feature of this robot is the possibility of having it dynamically balanced and thus, reducing the influence of inertial forces and moments. The balanced case has therefore the advantage regarding precision. For more information, refer to (WIJK, et al., 2013). In our experimentation, we considered the unbalanced version and yet we had interesting results.

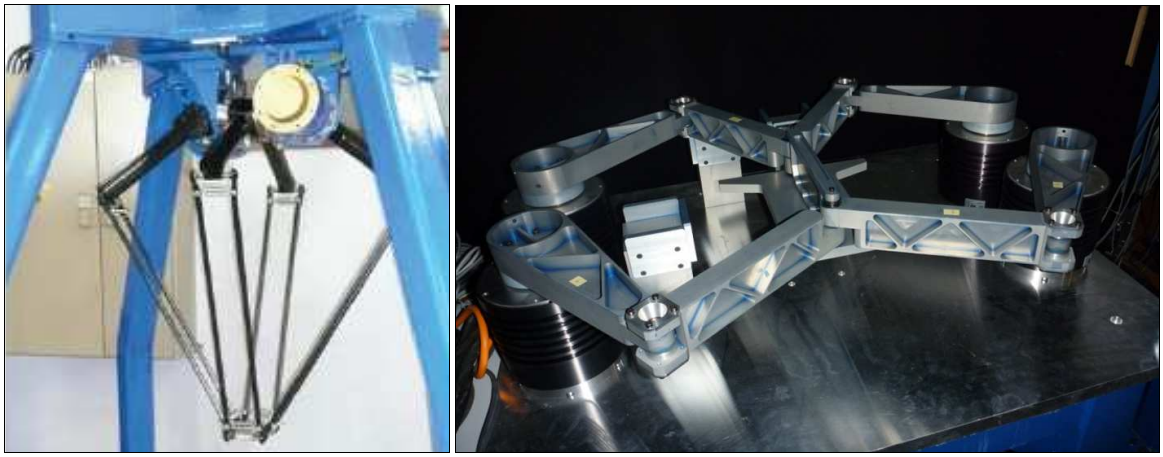

Fig. Ap-10: Par2 (on the left) and DUAL V (on the right) (LIRMM).

Table Ap-11: Static positional accuracy and repeatability of Par2.

	P_1	P_2	P_3	P_4	P_5
Static Accuracy (mm)	0.0330	2.0793	2.1001	1.1723	1.3427
Static Repeatability (mm)	0.0129	0.0128	0.0086	0.0253	0.0252

Table Ap-12: Static accuracy and repeatability of DUAL V.

	P_1	P_2	P_3	P_4	P_5
Static Accuracy (mm)	0.0302	1.0369	0.7291	0.9414	0.3777
Static Repeatability (mm)	0.0244	0.0091	0.0098	0.0103	0.0154

The static accuracy and repeatability of Par2 and DUAL V are given in **Table Ap-11** and **Table Ap-12,** respectively. In fact, though the accuracies are not that better than the previous discussed robots, their repeatabilities are quite interesting being between $10\,\mu m$ and $25\,\mu m$. This is promising, especially that the repeatability of the measurement device is about $10\,\mu m$. Furthermore, we mention that regarding accuracy measurement, there have been several problems that would have highly influenced the results, particularly for these two aforementioned robots (compatibility between Metris K600 and the robots). The latter issue was severely critical in the case of DUAL V and forced us to use manual control for measurement triggering.

An important result concluded from DUAL V experimentation is that actuation redundancy is not a problem, especially if well treated. In fact, based on the results of Quattro with rigid platform, such a conclusion is not possible to make. Also, the use of revolute joints has been an

essential factor in promoting DUAL V precision and particularly its repeatability -as compared with the joint technology used for parallelogram spherical joints (e.g. in Quattro and Veloce). We add to this, the use of direct drive that eliminates the backlash problems coming from the use of gear trains.

So far, we have exposed some static precision results. In the upcoming part, we present some dynamic precision measures concerning trajectory following.

Dynamic Precision Results

For assessing path accuracy and repeatability, **[ISO 9283; 1998 (F)]** suggests several types of trajectories such as straight lines, rectangular paths, and circles. All these trajectories must be inside the chosen diagonal plane. In our case, we have experimented with linear, triangular, and circular paths. However, we only present the main results of two robots, namely Quattro and Par2, for the linear trajectories along P_2P_4 (refer to **Fig. Ap-6**), while focusing solely on positional errors. We emphasize that according to the aforementioned norm, the trajectory is repeated 10 times for $100\,\%$, $50\,\%$, and $10\,\%$ of robot's maximal speed.

The positional path accuracy and repeatability of Quattro and Par2 are presented in **Table**

Table Ap-13: Positional path accuracies and repeatabilities of Quattro and Par 2 (case of linear trajectory P2P4).

		10% Maximum Speed	50% Maximum Speed	100% Maximum Speed
Quattro (4 DoFs, 3T-1R Version)	**Path Positional Accuracy (mm)**	0.2447	0.7820	1.2430
	Path Positional Repeatability (mm)	0.4740	0.7516	1.9674
Quattro (4 DoFs, 3T Version)	**Path Positional Accuracy (mm)**	0.8025	1.0941	1.6241
	Path Positional Repeatability (mm)	1.4066	2.2855	4.1633
Par2 (2 DoFs, 2T)	**Path Positional Accuracy (mm)**	0.2396	0.3222	0.3905
	Path Positional Repeatability (mm)	0.6354	0.6907	0.8588

Ap-13. As it can be noticed and expected, both path accuracy and repeatability are degraded with the increase of speed. This is due in one part to the decreased number of sampled points and in another part to the increase of the other dynamic influences. The values clearly show that rapidity is accompanied by rather poor dynamic precision.

In brief, this section has proven that we are still far from having parallel robots with at least a good compromise between rapidity and precision.

Appendix B: Derivation of Lower Bounds for the Dynamic Specific Isotropic Values in the Case of Rigid Manipulators

B.1- The Derivation Procedure

This appendix details the procedure of obtaining lower bounds for the specific isotropic values in the case of dynamics. For this purpose, we assume the requirements to be: ${}^{d}a_{req}$, ${}^{d}\alpha_{req}$, ${}^{d}v_{req}$, ${}^{d}\omega_{req}$, ${}^{d}f_{ereq}$, and ${}^{d}m_{ereq}$, with their significance being as defined in **§2.3.4**.

We start by considering the following relations:

$$\boldsymbol{K}\,\dot{\boldsymbol{\xi}} + \boldsymbol{h}^{v} + \boldsymbol{h}^{\omega} + \boldsymbol{h}^{v\omega} + \boldsymbol{\tau}_{g} = \boldsymbol{\tau} \qquad \text{(Ap.1)},$$

$$\left|\dot{q}_i\right| \le \dot{q}_i^{\max},\ \forall i = 1...m \qquad \text{(Ap.2)}$$

and

$$\left|\tau_i\right| \le \tau_i^{\max},\ \forall i = 1...m \qquad \text{(Ap.3)}.$$

In addition to the above relations, we recall the inverse kinematic equation that is also necessary for the study. It is given by:

$$\dot{\boldsymbol{q}} = \boldsymbol{J}_{\boldsymbol{m}}\,\boldsymbol{t} \qquad \text{(Ap.4)}.$$

The first step is replacing (Ap.2) and (Ap.4) by deriving their imposed upper bounds on ${}^{d}v_{iso}^{sp}$ and ${}^{d}\omega_{iso}^{sp}$. This is equivalent to getting the specific isotropic linear and angular speeds, ${}^{k}v_{iso}^{sp}$ and ${}^{k}\omega_{iso}^{sp}$, as discussed in **§2.2.3.C**, in which we set $\omega_{req} =^{d} \omega_{req}$ and $v_{req} =^{d} v_{req}$, respectively. Thus, (Ap.2) and (Ap.4) can be replaced by:

$${}^{d}v_{iso}^{sp} \le {}^{k}v_{iso}^{sp} \qquad \text{(Ap.5)}$$

and

$${}^{d}\omega_{iso}^{sp} \le {}^{k}\omega_{iso}^{sp} \qquad \text{(Ap.6)},$$

with:

$$\begin{cases} {}^{k}v_{iso}^{sp} = \min\limits_{i=1...m}\left(A_i\right), \text{ such that:} \\ A_i = \begin{cases} 0\ , \text{ if } \ a_i<0 \\ \dfrac{a_i}{\left\|\boldsymbol{j}_{\boldsymbol{mpr}_i}\right\|}, \text{ if } \ \left\|\boldsymbol{j}_{\boldsymbol{mpr}_i}\right\| \neq 0 \text{ and } a_i \geq 0 \\ \infty\ , \ \text{otherwise} \end{cases} \\ a_i = \dot{q}_i^{\max} - \left\|\boldsymbol{j}_{\boldsymbol{mor}_i}\right\| \omega_{req}^{d} \\ \forall i = 1...m \end{cases} \quad \text{(Ap.7)},$$

and

$$\begin{cases} {}^{k}\omega_{iso}^{sp} = \min\limits_{i=1...m}\left(B_i\right), \text{ such that:} \\ B_i = \begin{cases} 0\ , \text{if } \ b_i < 0 \\ \dfrac{b_i}{\left\|\boldsymbol{j}_{\boldsymbol{mor}_i}\right\|}, \text{ if } \ \left\|\boldsymbol{j}_{\boldsymbol{mor}_i}\right\| \neq 0 \text{ and } b_i \geq 0 \\ \infty\ , \ \text{otherwise} \end{cases} \\ b_i = \dot{q}_i^{\max} - \left\|\boldsymbol{j}_{\boldsymbol{mpr}_i}\right\| v_{req}^{d} \\ \forall i = 1...m \end{cases} \quad \text{(Ap.8)}.$$

If ${}^{k}v_{iso}^{sp} < {}^{d}v_{req}$ (or ${}^{k}\omega_{iso}^{sp} < {}^{d}\omega_{req}$)[4], the robot cannot initially fulfill velocity requirements and consequently, all dynamic specific isotropic values, except those related to velocity, must be set to zero by convention (i.e. ${}^{d}a_{iso}^{sp} = {}^{d}\alpha_{iso}^{sp} = {}^{d}f_{eiso}^{sp} = {}^{d}m_{eiso}^{sp} = 0$). In such a case, one only needs to investigate ${}^{d}v_{iso}^{sp}$ and ${}^{d}\omega_{iso}^{sp}$. Aside from that, we can proceed by deriving the dynamic measures.

However, in what follows, we are going only to elaborate the derivation of two dynamic specific isotropic terms, namely ${}^{d}a_{iso}^{sp}$ and ${}^{d}v_{iso}^{sp}$, being slightly different from each other and as the remaining can be derived in a similar fashion.

For this purpose, we consider (Ap.1) and (Ap.3) that yield the following system of double inequalities:

$$\begin{cases} -\tau_i^{\max} \leq \left(\boldsymbol{k}_{\boldsymbol{r}_i}^{\boldsymbol{a}}\right)^{\mathrm{T}} \boldsymbol{a} + \left(\boldsymbol{k}_{\boldsymbol{r}_i}^{\boldsymbol{\alpha}}\right)^{\mathrm{T}} \boldsymbol{\alpha} + \left(\boldsymbol{k}_{\boldsymbol{r}_i}^{\boldsymbol{f}_e}\right)^{\mathrm{T}} \boldsymbol{f}_{\boldsymbol{e}} + \left(\boldsymbol{k}_{\boldsymbol{r}_i}^{\boldsymbol{m}_e}\right)^{\mathrm{T}} \boldsymbol{m}_{\boldsymbol{e}} + \boldsymbol{v}^{\mathrm{T}} \boldsymbol{H}_i^{\boldsymbol{v}} \boldsymbol{v} + \boldsymbol{\omega}^{\mathrm{T}} \boldsymbol{H}_i^{\boldsymbol{\omega}} \boldsymbol{\omega} \\ \qquad\qquad + 2\,\boldsymbol{v}^{\mathrm{T}} \boldsymbol{H}_i^{\boldsymbol{v\omega}} \boldsymbol{\omega} + \tau_{g_i} \leq +\tau_i^{\max} \\ \forall i = 1...m \end{cases} \quad \text{(Ap.9)},$$

[4] Note that it is enough to do either test of the two, as we have a mutuality influence (meaning: ${}^{k}v_{iso}^{sp} < {}^{d}v_{req} \Leftrightarrow {}^{k}\omega_{iso}^{sp} < {}^{d}\omega_{req}$).

with $\boldsymbol{k}_{r_i}^{a}$ standing for the part of i-th row vector of $\boldsymbol{K}$ corresponding to the acceleration $\boldsymbol{a}$, and similar meaning regarding the others. As for τ_{g_i}, it is the i-th component of $\boldsymbol{\tau}_{\boldsymbol{g}}$. Then, isolating $\left(\boldsymbol{k}_{r_i}^{a}\right)^{\mathrm{T}}\boldsymbol{a}$, we get:

$$\begin{cases} \forall i=1...m: \\ -\tau_i^{\max}-\left(\boldsymbol{k}_{r_i}^{\alpha}\right)^{\mathrm{T}}\boldsymbol{\alpha}-\left(\boldsymbol{k}_{r_i}^{f_e}\right)^{\mathrm{T}}\boldsymbol{f}_e-\left(\boldsymbol{k}_{r_i}^{m_e}\right)^{\mathrm{T}}\boldsymbol{m}_e-\boldsymbol{v}^{\mathrm{T}}\boldsymbol{H}_i^{v}\boldsymbol{v} \\ \qquad\qquad -\boldsymbol{\omega}^{\mathrm{T}}\boldsymbol{H}_i^{\omega}\boldsymbol{\omega}-2\,\boldsymbol{v}^{\mathrm{T}}\boldsymbol{H}_i^{v\omega}\boldsymbol{\omega}-\tau_{g_i}\le\left(\boldsymbol{k}_{r_i}^{a}\right)^{\mathrm{T}}\boldsymbol{a} \end{cases} \quad \text{(Ap.10)}$$

and

$$\begin{cases} \forall i=1...m: \\ \left(\boldsymbol{k}_{r_i}^{a}\right)^{\mathrm{T}}\boldsymbol{a}\le+\tau_i^{\max}-\left(\boldsymbol{k}_{r_i}^{\alpha}\right)^{\mathrm{T}}\boldsymbol{\alpha}-\left(\boldsymbol{k}_{r_i}^{f_e}\right)^{\mathrm{T}}\boldsymbol{f}_e-\left(\boldsymbol{k}_{r_i}^{m_e}\right)^{\mathrm{T}}\boldsymbol{m}_e-\boldsymbol{v}^{\mathrm{T}}\boldsymbol{H}_i^{v}\boldsymbol{v} \\ \qquad\qquad -\boldsymbol{\omega}^{\mathrm{T}}\boldsymbol{H}_i^{\omega}\boldsymbol{\omega}-2\,\boldsymbol{v}^{\mathrm{T}}\boldsymbol{H}_i^{v\omega}\boldsymbol{\omega}-\tau_{g_i} \end{cases} \quad \text{(Ap.11).}$$

Then, let us consider (Ap.10) and the worst case, which can be described as maximizing the left-hand side and minimizing the right-hand one. This worst case is expressed as having:

$$\begin{cases} \forall i=1...m:\ {}^{a}e_i^{-}=-\tau_i^{\max}+\left\|\boldsymbol{k}_{r_i}^{\alpha}\right\|{}^{d}\alpha_{req}+\left\|\boldsymbol{k}_{r_i}^{f_e}\right\|{}^{d}f_{ereq}+\left\|\boldsymbol{k}_{r_i}^{m_e}\right\|{}^{d}m_{ereq} \\ \qquad +\max_{\substack{\|\boldsymbol{v}\|\le{}^{d}v_{req}\\ \|\boldsymbol{\omega}\|\le{}^{d}\omega_{req}}}\left(-\boldsymbol{v}^{\mathrm{T}}\boldsymbol{H}_i^{v}\boldsymbol{v}-\boldsymbol{\omega}^{\mathrm{T}}\boldsymbol{H}_i^{\omega}\boldsymbol{\omega}-2\,\boldsymbol{v}^{\mathrm{T}}\boldsymbol{H}_i^{v\omega}\boldsymbol{\omega}\right)-\tau_{g_i}\le-\left\|\boldsymbol{k}_{r_i}^{a}\right\|a \end{cases} \quad \text{(Ap.12).}$$

In general, obtaining $\max_{\|\boldsymbol{v}\|\le{}^{d}v_{req},\,\|\boldsymbol{\omega}\|\le{}^{d}\omega_{req}}\left(-\boldsymbol{v}^{\mathrm{T}}\boldsymbol{H}_i^{v}\boldsymbol{v}-\boldsymbol{\omega}^{\mathrm{T}}\boldsymbol{H}_i^{\omega}\boldsymbol{\omega}-2\,\boldsymbol{v}^{\mathrm{T}}\boldsymbol{H}_i^{v\omega}\boldsymbol{\omega}\right)$ can be done numerically by classical constrained optimization. However, in the case of homogeneous-dof robot, we can always get the term $\max_{\|\boldsymbol{v}\|\le{}^{d}v_{req}}\left(-\boldsymbol{v}^{\mathrm{T}}\boldsymbol{H}_i\boldsymbol{v}\right)$ or $\max_{\|\boldsymbol{\omega}\|\le{}^{d}\omega_{req}}\left(-\boldsymbol{\omega}^{\mathrm{T}}\boldsymbol{H}_i\boldsymbol{\omega}\right)$ analytically by the use of Lagrange multipliers (see **Appendix B.2**). In this case, we will have the maximum expressed in terms of the eigenvalues of $\boldsymbol{H}_i\equiv\boldsymbol{H}_i^{v}$ or $\boldsymbol{H}_i\equiv\boldsymbol{H}_i^{\omega}$. Also, in the case of having $\boldsymbol{H}_i^{v\omega}=\boldsymbol{0}$ (uncoupled influence of $\boldsymbol{v}$ and $\boldsymbol{\omega}$), we can determine $\max_{\|\boldsymbol{v}\|\le{}^{d}v_{req},\,\|\boldsymbol{\omega}\|\le{}^{d}\omega_{req}}\left(-\boldsymbol{v}^{\mathrm{T}}\boldsymbol{H}_i^{v}\boldsymbol{v}-\boldsymbol{\omega}^{\mathrm{T}}\boldsymbol{H}_i^{\omega}\boldsymbol{\omega}\right)$ analytically, as it reduces to:

$$\max_{\substack{\|\boldsymbol{v}\|\le{}^{d}v_{req}\\ \|\boldsymbol{\omega}\|\le{}^{d}\omega_{req}}}\left(-\boldsymbol{v}^{\mathrm{T}}\boldsymbol{H}_i^{v}\boldsymbol{v}-\boldsymbol{\omega}^{\mathrm{T}}\boldsymbol{H}_i^{\omega}\boldsymbol{\omega}\right)=\max_{\|\boldsymbol{v}\|\le{}^{d}v_{req}}\left(-\boldsymbol{v}^{\mathrm{T}}\boldsymbol{H}_i^{v}\boldsymbol{v}\right)+\max_{\|\boldsymbol{\omega}\|\le{}^{d}\omega_{req}}\left(-\boldsymbol{\omega}^{\mathrm{T}}\boldsymbol{H}_i^{\omega}\boldsymbol{\omega}\right) \quad \text{(Ap.13).}$$

Thus, each term of the right-hand side of (Ap.13) can be expressed in terms of the eigenvalues of $\boldsymbol{H}_i^{v}$ and $\boldsymbol{H}_i^{\omega}$.

So, the only conflict is when $\boldsymbol{H}_i^{v\omega}=\boldsymbol{0},\ \forall i=1...m$. In this case, we either do the optimization, or we avoid its use and its possible time expense by means of utilizing a simple analytical upper bound on $\max_{\|\boldsymbol{v}\|\le{}^{d}v_{req},\,\|\boldsymbol{\omega}\|\le{}^{d}\omega_{req}}\left(-\boldsymbol{v}^{\mathrm{T}}\boldsymbol{H}_i^{v}\boldsymbol{v}-\boldsymbol{\omega}^{\mathrm{T}}\boldsymbol{H}_i^{\omega}\boldsymbol{\omega}-2\,\boldsymbol{v}^{\mathrm{T}}\boldsymbol{H}_i^{v\omega}\boldsymbol{\omega}\right)$. This upper bound is calculated as follows:

$$\begin{cases} \max\limits_{\substack{\|\boldsymbol{v}\|\le {}^{d}v_{req} \\ \|\boldsymbol{\omega}\|\le {}^{d}\omega_{req}}} \left(-\boldsymbol{v}^{\mathrm{T}}\ \boldsymbol{H}_i^{v}\ \boldsymbol{v}-\boldsymbol{\omega}^{\mathrm{T}}\ \boldsymbol{H}_i^{\omega}\ \boldsymbol{\omega}-2\,\boldsymbol{v}^{\mathrm{T}}\ \boldsymbol{H}_i^{v\omega}\ \boldsymbol{\omega}\right) \\ \quad \le \max\limits_{\|\boldsymbol{v}\|\le {}^{d}v_{req}} \left(-\boldsymbol{v}^{\mathrm{T}}\ \boldsymbol{H}_i^{v}\ \boldsymbol{v}\right)+\max\limits_{\|\boldsymbol{\omega}\|\le {}^{d}\omega_{req}} \left(-\boldsymbol{\omega}^{\mathrm{T}}\ \boldsymbol{H}_i^{\omega}\ \boldsymbol{\omega}\right)+\max\limits_{\substack{\|\boldsymbol{v}\|\le {}^{d}v_{req} \\ \|\boldsymbol{\omega}\|\le {}^{d}\omega_{req}}} \left(-2\,\boldsymbol{v}^{\mathrm{T}}\ \boldsymbol{H}_i^{v\omega}\ \boldsymbol{\omega}\right) \end{cases} \quad \text{(Ap.14).}$$

Here, we are going to give the approach for the most general case based on bounding the velocity-dependent terms (the used bounds become exact values in the case of robots with homogeneous dofs or when $\boldsymbol{H}_i^{v\omega}=\boldsymbol{0}, \forall i=1...m$).

Thus, we can rewrite (Ap.12) in the general case as:

$$\begin{cases} \forall i=1...m: \\ \overline{\overline{{}^{a}e_i^{-}}} = -\tau_i^{\max}+\left\|\boldsymbol{k}_{\boldsymbol{r}_i}^{\boldsymbol{\alpha}}\right\|\,{}^{d}\alpha_{req}+\left\|\boldsymbol{k}_{\boldsymbol{r}_i}^{\boldsymbol{f_e}}\right\|\,{}^{d}f_{ereq}+\left\|\boldsymbol{k}_{\boldsymbol{r}_i}^{\boldsymbol{m_e}}\right\|\,{}^{d}m_{ereq} \\ \qquad\qquad -\zeta_{\min_i}^{v}\left({}^{d}v_{req}\right)^2-\zeta_{\min_i}^{\omega}\left({}^{d}\omega_{req}\right)^2+2\,\sigma_{\max_i}^{v\omega}\ {}^{d}v_{req}\ {}^{d}\omega_{req}-\tau_{g_i}\le -\left\|\boldsymbol{k}_{\boldsymbol{r}_i}^{\boldsymbol{a}}\right\|a \end{cases} \quad \text{(Ap.15),}$$

with $\zeta_{\min_i}^{v}=\min\left(\mathrm{eigs}\left(\boldsymbol{H}_i^{v}\right),0\right)$, $\zeta_{\min_i}^{\omega}=\min\left(\mathrm{eigs}\left(\boldsymbol{H}_i^{\omega}\right),0\right)$, and $\sigma_{\max_i}^{v\omega}=\max\left(\mathrm{sing}\left(\boldsymbol{H}_i^{v\omega}\right)\right)$. Note that $\overline{\overline{value}}$ designates an upper bound for the term $value$. Also, notice that ${}^{a}e_i^{-}=\overline{\overline{{}^{a}e_i^{-}}}$ if $\boldsymbol{H}_i^{v\omega}=\boldsymbol{0}$ or $\boldsymbol{H}_i^{v\omega}$ does not exist (meaning pure translational or rotational robot).

A final remark is that as $-\left\|\boldsymbol{k}_{\boldsymbol{r}_i}^{\boldsymbol{a}}\right\|a\le 0$, $\overline{\overline{{}^{a}e_i^{-}}}$ must be less than or equal to zero as well. Otherwise, we cannot assure[5] there exists ${}^{d}a_{iso}^{sp}$.

From (Ap.15), we can write:

$$\begin{cases} a\le \underline{\underline{{}^{a}E_i^{-}}},\ \text{with } (\forall i=1...m): \\ \underline{\underline{{}^{a}E_i^{-}}} = \begin{cases} 0,\ \text{if}\ \ \overline{\overline{{}^{a}e_i^{-}}}>0 \\ -\dfrac{\overline{\overline{{}^{a}e_i^{-}}}}{\left\|\boldsymbol{k}_{\boldsymbol{r}_i}^{\boldsymbol{a}}\right\|},\ \text{if}\ \ \overline{\overline{{}^{a}e_i^{-}}}\le 0 \text{ and } \left\|\boldsymbol{k}_{\boldsymbol{r}_i}^{\boldsymbol{a}}\right\|\ne 0 \\ \infty,\ \text{otherwise} \end{cases} \end{cases} \quad \text{(Ap.16),}$$

where $\underline{\underline{value}}$ indicates a lower bound for $value$.

Similar manner is adopted to deal with (Ap.11), in which we obtain:

$$\begin{cases} \forall i=1...m, \\ \left(\boldsymbol{k}_{\boldsymbol{r}_i}^{\boldsymbol{a}}\right)^{\mathrm{T}}\boldsymbol{a}\le \underline{\underline{{}^{a}e_i^{+}}} = +\tau_i^{\max}-\left\|\boldsymbol{k}_{\boldsymbol{r}_i}^{\boldsymbol{\alpha}}\right\|\,{}^{d}\alpha_{req}-\left\|\boldsymbol{k}_{\boldsymbol{r}_i}^{\boldsymbol{f_e}}\right\|\,{}^{d}f_{ereq}-\left\|\boldsymbol{k}_{\boldsymbol{r}_i}^{\boldsymbol{m_e}}\right\|\,{}^{d}m_{ereq} \\ \qquad\qquad -\zeta_{\max_i}^{v}\left({}^{d}v_{req}\right)^2-\zeta_{\max_i}^{\omega}\left({}^{d}\omega_{req}\right)^2-2\,\sigma_{\max_i}^{v\omega}\ {}^{d}v_{req}\ {}^{d}\omega_{req}-\tau_{g_i} \end{cases} \quad \text{(Ap.17),}$$

[5] We cannot assure that ${}^{d}a_{iso}^{sp}$ exists because we are using an upper bound on ${}^{a}e_i^{-}$ and not its exact value.

with $\zeta^{v}_{\max_i} = \max\left(\text{eigs}\left(\boldsymbol{H}_i^{v}\right),0\right)$ and $\zeta^{\omega}_{\max_i} = \max\left(\text{eigs}\left(\boldsymbol{H}_i^{\omega}\right),0\right)$.

As a result, we get:

$$\begin{cases} a \le \underline{\underline{{}^{a}E_i^{+}}},\ \text{with } (\forall i = 1...m): \\ \underline{\underline{{}^{a}E_i^{+}}} = \begin{cases} 0, \text{ if } \underline{\underline{{}^{a}e_i^{+}}} < 0 \\ \dfrac{\underline{\underline{{}^{a}e_i^{+}}}}{\left\|\boldsymbol{k}_{\boldsymbol{r}_i}^{\boldsymbol{a}}\right\|}, \text{ if } \underline{\underline{{}^{a}e_i^{+}}} \ge 0 \text{ and } \left\|\boldsymbol{k}_{\boldsymbol{r}_i}^{\boldsymbol{a}}\right\| \ne 0 \\ \infty, \text{ otherwise} \end{cases} \end{cases} \quad \begin{cases} a \le \underline{\underline{{}^{a}E_i^{+}}},\ \text{with:} \\ \underline{\underline{{}^{a}E_i^{+}}} = \begin{cases} 0, \text{ if } \underline{\underline{{}^{a}e_i^{+}}} < 0 \\ \dfrac{\underline{\underline{{}^{a}e_i^{+}}}}{\left\|\boldsymbol{k}_{\boldsymbol{r}_i}^{\boldsymbol{a}}\right\|}, \text{ if } \underline{\underline{{}^{a}e_i^{+}}} \ge 0 \text{ and } \left\|\boldsymbol{k}_{\boldsymbol{r}_i}^{\boldsymbol{a}}\right\| \ne 0,\ \forall i = 1...m \\ \infty, \text{ otherwise} \end{cases} \end{cases} \quad \text{(Ap.18).}$$

Merging (Ap.16) and (Ap.18) together with the condition ${}^{k}v_{iso}^{sp} < {}^{d}v_{req}$ (or ${}^{k}\omega_{iso}^{sp} < {}^{d}\omega_{req}$), we obtain:

$$\begin{cases} {}^{d}a_{iso}^{sp} \ge \underline{\underline{{}^{d}a_{iso}^{sp}}} = \min_{i=1...m}\left(K_C, \underline{\underline{{}^{a}E_i^{-}}}, \underline{\underline{{}^{a}E_i^{+}}}\right),\ \text{with:} \\ K_C = \begin{cases} 0, \text{ if } {}^{k}v_{iso}^{sp} < {}^{d}v_{req} \text{ (or } {}^{k}\omega_{iso}^{sp} < {}^{d}\omega_{req}) \\ \infty, \text{ otherwise} \end{cases} \\ \underline{\underline{{}^{a}E_i^{-}}} = \begin{cases} 0, \text{ if } \overline{\overline{{}^{a}e_i^{-}}} > 0 \\ -\dfrac{\overline{\overline{{}^{a}e_i^{-}}}}{\left\|\boldsymbol{k}_{\boldsymbol{r}_i}^{\boldsymbol{a}}\right\|}, \text{ if } \overline{\overline{{}^{a}e_i^{-}}} \le 0 \text{ and } \left\|\boldsymbol{k}_{\boldsymbol{r}_i}^{\boldsymbol{a}}\right\| \ne 0 \\ \infty, \text{ otherwise} \end{cases}, \quad \underline{\underline{{}^{a}E_i^{+}}} = \begin{cases} 0, \text{ if } \underline{\underline{{}^{a}e_i^{+}}} < 0 \\ \dfrac{\underline{\underline{{}^{a}e_i^{+}}}}{\left\|\boldsymbol{k}_{\boldsymbol{r}_i}^{\boldsymbol{a}}\right\|}, \text{ if } \underline{\underline{{}^{a}e_i^{+}}} \ge 0 \text{ and } \left\|\boldsymbol{k}_{\boldsymbol{r}_i}^{\boldsymbol{a}}\right\| \ne 0 \\ \infty, \text{ otherwise} \end{cases} \\ \overline{\overline{{}^{a}e_i^{-}}} = -\tau_i^{\max} + \left\|\boldsymbol{k}_{\boldsymbol{r}_i}^{\boldsymbol{a}}\right\| {}^{d}\alpha_{req} + \left\|\boldsymbol{k}_{\boldsymbol{r}_i}^{\boldsymbol{f_e}}\right\| {}^{d}f_{ereq} + \left\|\boldsymbol{k}_{\boldsymbol{r}_i}^{\boldsymbol{m_e}}\right\| {}^{d}m_{ereq} \\ \qquad - \zeta^{v}_{\min_i}\left({}^{d}v_{req}\right)^2 - \zeta^{\omega}_{\min_i}\left({}^{d}\omega_{req}\right)^2 + 2\,\sigma^{v\omega}_{\max_i}\,{}^{d}v_{req}\,{}^{d}\omega_{req} - \tau_{g_i} \\ \underline{\underline{{}^{a}e_i^{+}}} = +\tau_i^{\max} - \left\|\boldsymbol{k}_{\boldsymbol{r}_i}^{\boldsymbol{a}}\right\| {}^{d}\alpha_{req} - \left\|\boldsymbol{k}_{\boldsymbol{r}_i}^{\boldsymbol{f_e}}\right\| {}^{d}f_{ereq} - \left\|\boldsymbol{k}_{\boldsymbol{r}_i}^{\boldsymbol{m_e}}\right\| {}^{d}m_{ereq} \\ \qquad - \zeta^{v}_{\max_i}\left({}^{d}v_{req}\right)^2 - \zeta^{\omega}_{\max_i}\left({}^{d}\omega_{req}\right)^2 - 2\,\sigma^{v\omega}_{\max_i}\,{}^{d}v_{req}\,{}^{d}\omega_{req} - \tau_{g_i} \\ \forall i = 1...m \end{cases} \quad \text{(Ap.19).}$$

The result in (Ap.19) can be interpreted as follows: the manipulator can achieve an acceleration at least up to $\underline{\underline{{}^{d}a_{iso}^{sp}}}$ in all directions while allowing simultaneously angular acceleration, linear and angular velocities, force, and moment to attain their demanded requirements in all directions. Actually, in (Ap.19) we had established a lower bound for ${}^{d}a_{iso}^{sp}$, which is sufficient as no harm in having ${}^{d}a_{iso}^{sp}$ higher than $\underline{\underline{{}^{d}a_{iso}^{sp}}}$. Nonetheless, if one would like to know an upper bound for ${}^{d}a_{iso}^{sp}$, a similar approach can be used, but this time considering $\underline{\underline{e_i^{-}}}$, and $\overline{\overline{e_i^{+}}}$.

Similarly, we get regarding ${}^{d}\alpha_{iso}^{sp}$, ${}^{d}f_{eiso}^{sp}$, and ${}^{d}m_{eiso}^{sp}$. The corresponding relations are given hereafter:

$$
\begin{cases}
{}^{d}\alpha_{iso}^{sp} \geq \underline{\underline{{}^{d}\alpha_{iso}^{sp}}} = \min\limits_{i=1\ldots m}\left(K_C, \underline{\underline{{}^{\alpha}E_i^-}}, \underline{\underline{{}^{\alpha}E_i^+}}\right), \text{ with:} \\
K_C = \begin{cases} 0, \text{ if } {}^{k}v_{iso}^{sp} < {}^{d}v_{req} \text{ (or } {}^{k}\omega_{iso}^{sp} < {}^{d}\omega_{req}) \\ \infty, \text{ otherwise} \end{cases} \\
\underline{\underline{{}^{\alpha}E_i^-}} = \begin{cases} 0, \text{ if } \overline{\overline{{}^{\alpha}e_i^-}} > 0 \\ -\dfrac{\overline{\overline{{}^{\alpha}e_i^-}}}{\left\|\boldsymbol{k}_{\boldsymbol{r}_i}^{\boldsymbol{\alpha}}\right\|}, \text{ if } \overline{\overline{{}^{\alpha}e_i^-}} \leq 0 \text{ and } \left\|\boldsymbol{k}_{\boldsymbol{r}_i}^{\boldsymbol{\alpha}}\right\| \neq 0 \\ \infty, \text{ otherwise} \end{cases}, \quad \underline{\underline{{}^{\alpha}E_i^+}} = \begin{cases} 0, \text{ if } \underline{\underline{{}^{\alpha}e_i^+}} < 0 \\ \dfrac{\underline{\underline{{}^{\alpha}e_i^+}}}{\left\|\boldsymbol{k}_{\boldsymbol{r}_i}^{\boldsymbol{\alpha}}\right\|}, \text{ if } \underline{\underline{{}^{\alpha}e_i^+}} \geq 0 \text{ and } \left\|\boldsymbol{k}_{\boldsymbol{r}_i}^{\boldsymbol{\alpha}}\right\| \neq 0 \\ \infty, \text{ otherwise} \end{cases} \\
\overline{\overline{{}^{\alpha}e_i^-}} = -\tau_i^{\max} + \left\|\boldsymbol{k}_{\boldsymbol{r}_i}^{\boldsymbol{a}}\right\| {}^{d}a_{req} + \left\|\boldsymbol{k}_{\boldsymbol{r}_i}^{\boldsymbol{f_e}}\right\| {}^{d}f_{ereq} + \left\|\boldsymbol{k}_{\boldsymbol{r}_i}^{\boldsymbol{m_e}}\right\| {}^{d}m_{ereq} - \zeta_{\min_i}^{v}\left({}^{d}v_{req}\right)^2 - \zeta_{\min_i}^{\omega}\left({}^{d}\omega_{req}\right)^2 \\
\qquad + 2\,\sigma_{\max_i}^{v\omega}\,{}^{d}v_{req}\,{}^{d}\omega_{req} - \tau_{g_i} \\
\underline{\underline{{}^{\alpha}e_i^+}} = +\tau_i^{\max} - \left\|\boldsymbol{k}_{\boldsymbol{r}_i}^{\boldsymbol{a}}\right\| {}^{d}a_{req} - \left\|\boldsymbol{k}_{\boldsymbol{r}_i}^{\boldsymbol{f_e}}\right\| {}^{d}f_{ereq} - \left\|\boldsymbol{k}_{\boldsymbol{r}_i}^{\boldsymbol{m_e}}\right\| {}^{d}m_{ereq} - \zeta_{\max_i}^{v}\left({}^{d}v_{req}\right)^2 - \zeta_{\max_i}^{\omega}\left({}^{d}\omega_{req}\right)^2 \\
\qquad - 2\,\sigma_{\max_i}^{v\omega}\,{}^{d}v_{req}\,{}^{d}\omega_{req} - \tau_{g_i} \\
\forall i = 1\ldots m
\end{cases}
\tag{Ap.20},
$$

$$
\begin{cases}
{}^{d}f_{eiso}^{sp} \geq \underline{\underline{{}^{d}f_{eiso}^{sp}}} = \min\limits_{i=1\ldots m}\left(K_C, \underline{\underline{{}^{f_e}E_i^-}}, \underline{\underline{{}^{f_e}E_i^+}}\right), \text{ with:} \\
K_C = \begin{cases} 0, \text{ if } {}^{k}v_{iso}^{sp} < {}^{d}v_{req} \text{ (or } {}^{k}\omega_{iso}^{sp} < {}^{d}\omega_{req}) \\ \infty, \text{ otherwise} \end{cases} \\
\underline{\underline{{}^{f_e}E_i^-}} = \begin{cases} 0, \text{ if } \overline{\overline{{}^{f_e}e_i^-}} > 0 \\ -\dfrac{\overline{\overline{{}^{f_e}e_i^-}}}{\left\|\boldsymbol{k}_{\boldsymbol{r}_i}^{\boldsymbol{f_e}}\right\|}, \text{ if } \overline{\overline{{}^{f_e}e_i^-}} \leq 0 \text{ and } \left\|\boldsymbol{k}_{\boldsymbol{r}_i}^{\boldsymbol{f_e}}\right\| \neq 0 \\ \infty, \text{ otherwise} \end{cases}, \quad \underline{\underline{{}^{f_e}E_i^+}} = \begin{cases} 0, \text{ if } \underline{\underline{{}^{f_e}e_i^+}} < 0 \\ \dfrac{\underline{\underline{{}^{f_e}e_i^+}}}{\left\|\boldsymbol{k}_{\boldsymbol{r}_i}^{\boldsymbol{f_e}}\right\|}, \text{ if } \underline{\underline{{}^{f_e}e_i^+}} \geq 0 \text{ and } \left\|\boldsymbol{k}_{\boldsymbol{r}_i}^{\boldsymbol{f_e}}\right\| \neq 0 \\ \infty, \text{ otherwise} \end{cases} \\
\overline{\overline{{}^{f_e}e_i^-}} = -\tau_i^{\max} + \left\|\boldsymbol{k}_{\boldsymbol{r}_i}^{\boldsymbol{a}}\right\| {}^{d}a_{req} + \left\|\boldsymbol{k}_{\boldsymbol{r}_i}^{\boldsymbol{\alpha}}\right\| {}^{d}\alpha_{req} + \left\|\boldsymbol{k}_{\boldsymbol{r}_i}^{\boldsymbol{m_e}}\right\| {}^{d}m_{ereq} - \zeta_{\min_i}^{v}\left({}^{d}v_{req}\right)^2 - \zeta_{\min_i}^{\omega}\left({}^{d}\omega_{req}\right)^2 \\
\qquad + 2\,\sigma_{\max_i}^{v\omega}\,{}^{d}v_{req}\,{}^{d}\omega_{req} - \tau_{g_i} \\
\underline{\underline{{}^{f_e}e_i^+}} = +\tau_i^{\max} - \left\|\boldsymbol{k}_{\boldsymbol{r}_i}^{\boldsymbol{a}}\right\| {}^{d}a_{req} - \left\|\boldsymbol{k}_{\boldsymbol{r}_i}^{\boldsymbol{\alpha}}\right\| {}^{d}\alpha_{req} - \left\|\boldsymbol{k}_{\boldsymbol{r}_i}^{\boldsymbol{m_e}}\right\| {}^{d}m_{ereq} - \zeta_{\max_i}^{v}\left({}^{d}v_{req}\right)^2 - \zeta_{\max_i}^{\omega}\left({}^{d}\omega_{req}\right)^2 \\
\qquad - 2\,\sigma_{\max_i}^{v\omega}\,{}^{d}v_{req}\,{}^{d}\omega_{req} - \tau_{g_i} \\
\forall i = 1\ldots m
\end{cases}
\tag{Ap.21},
$$

and

$$\begin{cases} {}^{d}m_{eiso}^{sp} \geq \underline{\underline{{}^{d}m_{eiso}^{sp}}} = \min_{i=1...m}\left(K_C, \underline{\underline{{}^{m_e}E_i^-}}, \underline{\underline{{}^{m_e}E_i^+}}\right), \text{ with:} \\ K_C = \begin{cases} 0, \text{ if } {}^{k}v_{iso}^{sp} < {}^{d}v_{req} \text{ (or } {}^{k}\omega_{iso}^{sp} < {}^{d}\omega_{req}) \\ \infty, \text{ otherwise} \end{cases} \\ \underline{\underline{{}^{m_e}E_i^-}} = \begin{cases} 0, \text{ if } \overline{\overline{{}^{m_e}e_i^-}} > 0 \\ -\dfrac{\overline{\overline{{}^{m_e}e_i^-}}}{\left\|\boldsymbol{k}_{\boldsymbol{r}_i}^{\boldsymbol{m_e}}\right\|}, \text{ if } \overline{\overline{{}^{m_e}e_i^-}} \leq 0 \text{ and } \left\|\boldsymbol{k}_{\boldsymbol{r}_i}^{\boldsymbol{m_e}}\right\| \neq 0 \\ \infty, \text{ otherwise} \end{cases}, \quad \underline{\underline{{}^{m_e}E_i^+}} = \begin{cases} 0, \text{ if } \underline{\underline{{}^{m_e}e_i^+}} < 0 \\ \dfrac{\underline{\underline{{}^{m_e}e_i^+}}}{\left\|\boldsymbol{k}_{\boldsymbol{r}_i}^{\boldsymbol{m_e}}\right\|}, \text{ if } \underline{\underline{{}^{m_e}e_i^+}} \geq 0 \text{ and } \left\|\boldsymbol{k}_{\boldsymbol{r}_i}^{\boldsymbol{m_e}}\right\| \neq 0 \\ \infty, \text{ otherwise} \end{cases} \\ \overline{\overline{{}^{m_e}e_i^-}} = -\tau_i^{\max} + \left\|\boldsymbol{k}_{\boldsymbol{r}_i}^{\boldsymbol{a}}\right\| {}^{d}a_{req} + \left\|\boldsymbol{k}_{\boldsymbol{r}_i}^{\boldsymbol{\alpha}}\right\| {}^{d}\alpha_{req} + \left\|\boldsymbol{k}_{\boldsymbol{r}_i}^{\boldsymbol{f_e}}\right\| {}^{d}f_{ereq} - \zeta_{\min_i}^{v}\left({}^{d}v_{req}\right)^2 - \zeta_{\min_i}^{\omega}\left({}^{d}\omega_{req}\right)^2 \\ \qquad + 2\,\sigma_{\max_i}^{v\omega}\,{}^{d}v_{req}\,{}^{d}\omega_{req} - \tau_{g_i} \\ \underline{\underline{{}^{m_e}e_i^+}} = +\tau_i^{\max} - \left\|\boldsymbol{k}_{\boldsymbol{r}_i}^{\boldsymbol{a}}\right\| {}^{d}a_{req} - \left\|\boldsymbol{k}_{\boldsymbol{r}_i}^{\boldsymbol{\alpha}}\right\| {}^{d}\alpha_{req} - \left\|\boldsymbol{k}_{\boldsymbol{r}_i}^{\boldsymbol{f_e}}\right\| {}^{d}f_{ereq} - \zeta_{\max_i}^{v}\left({}^{d}v_{req}\right)^2 - \zeta_{\max_i}^{\omega}\left({}^{d}\omega_{req}\right)^2 \\ \qquad - 2\,\sigma_{\max_i}^{v\omega}\,{}^{d}v_{req}\,{}^{d}\omega_{req} - \tau_{g_i} \\ \forall i = 1...m \end{cases} \quad \text{(Ap.22).}$$

It remains to get $\underline{\underline{{}^{d}v_{iso}^{sp}}}$ and $\underline{\underline{{}^{d}\omega_{iso}^{sp}}}$. We will consider $\underline{\underline{{}^{d}v_{iso}^{sp}}}$ only, as $\underline{\underline{{}^{d}\omega_{iso}^{sp}}}$ can be determined in the same way. For this purpose, we re-examine (Ap.9) that can be rewritten as below, after isolating the velocity terms, $\boldsymbol{v}$ and $\boldsymbol{\omega}$:

$$\begin{cases} \forall i = 1...m: \\ -\tau_i^{\max} - \left(\boldsymbol{k}_{\boldsymbol{r}_i}^{\boldsymbol{a}}\right)^{\mathrm{T}}\boldsymbol{a} - \left(\boldsymbol{k}_{\boldsymbol{r}_i}^{\boldsymbol{\alpha}}\right)^{\mathrm{T}}\boldsymbol{\alpha} - \left(\boldsymbol{k}_{\boldsymbol{r}_i}^{\boldsymbol{f_e}}\right)^{\mathrm{T}}\boldsymbol{f_e} \\ \qquad - \left(\boldsymbol{k}_{\boldsymbol{r}_i}^{\boldsymbol{m_e}}\right)^{\mathrm{T}}\boldsymbol{m_e} - \tau_{g_i} \leq \boldsymbol{v}^{\mathrm{T}}\,\boldsymbol{H}_i^{v}\,\boldsymbol{v} + \boldsymbol{\omega}^{\mathrm{T}}\,\boldsymbol{H}_i^{\omega}\,\boldsymbol{\omega} + 2\,\boldsymbol{v}^{\mathrm{T}}\,\boldsymbol{H}_i^{v\omega}\,\boldsymbol{\omega} \end{cases} \quad \text{(Ap.23),}$$

and

$$\begin{cases} \forall i = 1...m: \\ \boldsymbol{v}^{\mathrm{T}}\,\boldsymbol{H}_i^{v}\,\boldsymbol{v} + \boldsymbol{\omega}^{\mathrm{T}}\,\boldsymbol{H}_i^{\omega}\,\boldsymbol{\omega} + 2\,\boldsymbol{v}^{\mathrm{T}}\,\boldsymbol{H}_i^{v\omega}\,\boldsymbol{\omega} \leq +\tau_i^{\max} - \left(\boldsymbol{k}_{\boldsymbol{r}_i}^{\boldsymbol{a}}\right)^{\mathrm{T}}\boldsymbol{a} - \left(\boldsymbol{k}_{\boldsymbol{r}_i}^{\boldsymbol{\alpha}}\right)^{\mathrm{T}}\boldsymbol{\alpha} \\ \qquad - \left(\boldsymbol{k}_{\boldsymbol{r}_i}^{\boldsymbol{f_e}}\right)^{\mathrm{T}}\boldsymbol{f_e} - \left(\boldsymbol{k}_{\boldsymbol{r}_i}^{\boldsymbol{m_e}}\right)^{\mathrm{T}}\boldsymbol{m_e} - \tau_{g_i} \end{cases} \quad \text{(Ap.24).}$$

Let us study (Ap.23) by considering the worst case to get an upper bound for $v = \|\boldsymbol{v}\|$ attainable in all directions, while all other dynamic requirements are satisfied. This corresponds to maximizing left-hand side of (Ap.23) and minimizing its right-hand one. Thus, we have:

$$\begin{cases} \forall i = 1...m: \\ -\tau_i^{\max} + \left\|\boldsymbol{k}_{\boldsymbol{r}_i}^{\boldsymbol{a}}\right\| {}^{d}a_{req} + \left\|\boldsymbol{k}_{\boldsymbol{r}_i}^{\boldsymbol{\alpha}}\right\| {}^{d}\alpha_{req} + \left\|\boldsymbol{k}_{\boldsymbol{r}_i}^{\boldsymbol{f_e}}\right\| {}^{d}f_{ereq} \\ \qquad + \left\|\boldsymbol{k}_{\boldsymbol{r}_i}^{\boldsymbol{m_e}}\right\| {}^{d}m_{ereq} - \tau_{g_i} \leq \min_{\|\boldsymbol{\omega}\| \leq \omega_{req}} \begin{pmatrix} \boldsymbol{v}^{\mathrm{T}}\,\boldsymbol{H}_i^{v}\,\boldsymbol{v} + \boldsymbol{\omega}^{\mathrm{T}}\,\boldsymbol{H}_i^{\omega}\,\boldsymbol{\omega} \\ + 2\,\boldsymbol{v}^{\mathrm{T}}\,\boldsymbol{H}_i^{v\omega}\,\boldsymbol{\omega} \end{pmatrix} \end{cases} \quad \text{(Ap.25).}$$

Replacing $\min_{\|\boldsymbol{\omega}\| \le {}^{d}\omega_{req}} \left(\boldsymbol{v}^{\mathrm{T}}\, \boldsymbol{H}_i^{v}\, \boldsymbol{v} + \boldsymbol{\omega}^{\mathrm{T}}\, \boldsymbol{H}_i^{\omega}\, \boldsymbol{\omega} + 2\, \boldsymbol{v}^{\mathrm{T}}\, \boldsymbol{H}_i^{v\omega}\, \boldsymbol{\omega} \right)$ by its lower bound, $\zeta^{v}_{\min_i}\, v^2 + \zeta^{\omega}_{\min_i} \left({}^{d}\omega_{req} \right)^2 - 2\, \sigma^{v\omega}_{\max_i}\, {}^{d}\omega_{req}\, v$, yields:

$$\begin{cases} \forall i = 1 \ldots m: \\ -\tau_i^{\max} + \left\| \boldsymbol{k}_{\boldsymbol{r}_i}^{\boldsymbol{a}} \right\| {}^{d}a_{req} + \left\| \boldsymbol{k}_{\boldsymbol{r}_i}^{\boldsymbol{\alpha}} \right\| {}^{d}\alpha_{req} + \left\| \boldsymbol{k}_{\boldsymbol{r}_i}^{\boldsymbol{f_e}} \right\| {}^{d}f_{ereq} + \left\| \boldsymbol{k}_{\boldsymbol{r}_i}^{\boldsymbol{m_e}} \right\| {}^{d}m_{ereq} \\ \qquad\qquad - \zeta^{\omega}_{\min_i} \left({}^{d}\omega_{req} \right)^2 - \tau_{g_i} \le \zeta^{v}_{\min_i}\, v^2 - 2\, \sigma^{v\omega}_{\max_i}\, {}^{d}\omega_{req}\, v \end{cases} \quad \text{(Ap.26).}$$

Note that $\zeta^{v}_{\min_i} \le 0$ and $-2\, \sigma^{v\omega}_{\max_i}\, \omega^{d}_{req} \le 0$ due to having: $\zeta^{v}_{\min_i} = \min\left(\mathrm{eigs}\left(\boldsymbol{H}_i^{v} \right), 0 \right)$, $\sigma^{v\omega}_{\max_i} \ge 0$, and $\omega^{d}_{req} \ge 0$. We can rewrite (Ap.26) as:

$$\begin{cases} \forall i = 1 \ldots m: \\ -\zeta^{v}_{\min_i}\, v^2 + 2\, \sigma^{v\omega}_{\max_i}\, {}^{d}\omega_{req}\, v \le -\overline{\overline{{}^{v}e_i^{-}}}, \text{ with:} \\ \overline{\overline{{}^{v}e_i^{-}}} = -\tau_i^{\max} + \left\| \boldsymbol{k}_{\boldsymbol{r}_i}^{\boldsymbol{a}} \right\| {}^{d}a_{req} + \left\| \boldsymbol{k}_{\boldsymbol{r}_i}^{\boldsymbol{\alpha}} \right\| {}^{d}\alpha_{req} + \left\| \boldsymbol{k}_{\boldsymbol{r}_i}^{\boldsymbol{f_e}} \right\| {}^{d}f_{ereq} \\ \qquad\qquad + \left\| \boldsymbol{k}_{\boldsymbol{r}_i}^{\boldsymbol{m_e}} \right\| {}^{d}m_{ereq} - \zeta^{\omega}_{\min_i} \left({}^{d}\omega_{req} \right)^2 - \tau_{g_i} \end{cases} \quad \text{(Ap.27).}$$

Thus $\overline{\overline{{}^{v}e_i^{-}}}$ must be negative; otherwise, we cannot assure that ${}^{d}v^{sp}_{iso}$ exists and thus, $\underline{\underline{{}^{d}v^{sp}_{iso}}} = 0$ by convention. Since $f(v) = -\zeta^{v}_{\min_i}\, v^2 + 2\, \sigma^{v\omega}_{\max_i}\, {}^{d}\omega_{req}\, v$ is increasing over $[0, +\infty[$, the maximum of $f(v)$ over $[0, v_o[$ occurs at v_o. Therefore, if we have $\overline{\overline{{}^{v}e_i^{-}}} \le 0$, we get an upper bound, v_o, for $\underline{\underline{{}^{d}v^{sp}_{iso}}}$ by solving:

$$-\zeta^{v}_{\min_i}\, v^2 + 2\, \sigma^{v\omega}_{\max_i}\, {}^{d}\omega_{req}\, v + \overline{\overline{{}^{v}e_i^{-}}} = 0, \ \forall i = 1 \ldots m \quad \text{(Ap.28).}$$

In $\zeta^{v}_{\min_i} = 0$, we have:

$$v_o = \begin{cases} \dfrac{-\overline{\overline{{}^{v}e_i^{-}}}}{2\, \sigma^{v\omega}_{\max_i}\, {}^{d}\omega_{req}}, \text{ if } \sigma^{v\omega}_{\max_i}\, {}^{d}\omega_{req} \ne 0 \\ \infty, \text{ if } \sigma^{v\omega}_{\max_i}\, {}^{d}\omega_{req} = 0 \end{cases} \quad \text{(Ap.29).}$$

On the other hand, if $\zeta^{v}_{\min_i} \ne 0$, then (Ap.28) yields:

$$v_o = \begin{cases} \dfrac{-\sigma^{v\omega}_{\max_i}\, \omega^{d}_{req} - \sqrt{\left(\sigma^{v\omega}_{\max_i}\, \omega^{d}_{req} \right)^2 + \zeta^{v}_{\min_i}\, \overline{\overline{{}^{v}e_i^{-}}}}}{-\zeta^{v}_{\min_i}} \le 0 \\ \text{or:} \\ \dfrac{-\sigma^{v\omega}_{\max_i}\, \omega^{d}_{req} + \sqrt{\left(\sigma^{v\omega}_{\max_i}\, \omega^{d}_{req} \right)^2 + \zeta^{v}_{\min_i}\, \overline{\overline{{}^{v}e_i^{-}}}}}{-\zeta^{v}_{\min_i}} \end{cases} \quad \text{(Ap.30).}$$

Yet, as the first solution in (Ap.30) is always negative, it should be rejected and only the second solution must be considered after checking its positiveness. If $\left(-\sigma_{\max_i}^{v\omega}\ \omega_{req}^{d}+\sqrt{\left(\sigma_{\max_i}^{v\omega}\ \omega_{req}^{d}\right)^2+\zeta_{\min_i}^{v}\ \overline{\overline{{}^{v}e_i^-}}}\right)\Big/\left(-\zeta_{\min_i}^{v}\right)<0$, we cannot assure that there exists ${}^{d}v_{iso}^{sp}$ and we set $\underline{\underline{{}^{d}v_{iso}^{sp}}}=0$ by convention. Based on (Ap.29) and (Ap.30), we have:

$$\begin{cases} v\le {}^{v}E_i^- = \begin{cases} v_{oi1}^- = \dfrac{-\overline{\overline{{}^{v}e_i^-}}}{2\,\sigma_{\max_i}^{v\omega}\ {}^{d}\omega_{req}},\ \text{if } \overline{\overline{{}^{v}e_i^-}}\le 0,\ \sigma_{\max_i}^{v\omega}\ {}^{d}\omega_{req}\neq 0,\ \text{and } \zeta_{\min_i}^{v}=0 \\ v_{oi2}^- = \dfrac{\sigma_{\max_i}^{v\omega}\ \omega_{req}^{d}-\sqrt{\left(\sigma_{\max_i}^{v\omega}\ {}^{d}\omega_{req}\right)^2+\zeta_{\min_i}^{v}\ \overline{\overline{{}^{v}e_i^-}}}}{\zeta_{\min_i}^{v}},\ \text{if } \overline{\overline{{}^{v}e_i^-}}\le 0,\ \zeta_{\min_i}^{v}\neq 0,\ \text{and } v_{oi2}^-\ge 0 \\ \infty,\ \text{if } \overline{\overline{{}^{v}e_i^-}}\le 0,\ \sigma_{\max_i}^{v\omega}\ {}^{d}\omega_{req}=0,\ \text{and } \zeta_{\min_i}^{v}=0 \\ 0,\ \text{if } \overline{\overline{{}^{v}e_i^-}}\ge 0 \text{ or } v_{oi2}^-\le 0 \end{cases} \\ \forall i=1...m \end{cases} \quad \text{(Ap.31).}$$

We proceed in the same manner regarding (Ap.24) to get:

$$\begin{cases} v\le {}^{v}E_i^+ = \begin{cases} v_{oi1}^+ = \dfrac{{}^{v}e_i^+}{2\,\sigma_{\max_i}^{v\omega}\ {}^{d}\omega_{req}},\ \text{if } \underline{\underline{{}^{v}e_i^+}}\ge 0,\ \sigma_{\max_i}^{v\omega}\ {}^{d}\omega_{req}\neq 0,\ \text{and } \zeta_{\max_i}^{v}=0 \\ v_{oi2}^+ = \dfrac{-\sigma_{\max_i}^{v\omega}\ \omega_{req}^{d}+\sqrt{\left(\sigma_{\max_i}^{v\omega}\ {}^{d}\omega_{req}\right)^2+\zeta_{\max_i}^{v}\ \underline{\underline{{}^{v}e_i^+}}}}{\zeta_{\min_i}^{v}},\ \text{if } \underline{\underline{{}^{v}e_i^+}}\ge 0,\ \zeta_{\max_i}^{v}\neq 0,\ \text{and } v_{oi2}^+\ge 0 \\ \infty,\ \text{if } \underline{\underline{{}^{v}e_i^+}}\ge 0,\ \sigma_{\max_i}^{v\omega}\ {}^{d}\omega_{req}=0,\ \text{and } \zeta_{\max_i}^{v}=0 \\ 0,\ \text{if } \underline{\underline{{}^{v}e_i^+}}\le 0 \text{ or } v_{oi2}^+\le 0 \end{cases} \\ \text{with:} \\ \underline{\underline{{}^{v}e_i^+}} = \tau_i^{\max}-\left\|\boldsymbol{k}_{\boldsymbol{r}_i}^{\boldsymbol{a}}\right\|{}^{d}a_{req}-\left\|\boldsymbol{k}_{\boldsymbol{r}_i}^{\boldsymbol{\alpha}}\right\|{}^{d}\alpha_{req}-\left\|\boldsymbol{k}_{\boldsymbol{r}_i}^{\boldsymbol{f_e}}\right\|{}^{d}f_{ereq}-\left\|\boldsymbol{k}_{\boldsymbol{r}_i}^{\boldsymbol{m_e}}\right\|{}^{d}m_{ereq}-\zeta_{\max_i}^{\omega}\left({}^{d}\omega_{req}\right)^2-\tau_{g_i} \\ \forall i=1...m \end{cases} \quad \text{(Ap.32).}$$

Thus, we obtain based on (Ap.31), (Ap.32), and the kinematic condition (Ap.5):

$$
\begin{cases}
{}^{d}v_{iso}^{sp} \geq \underline{\underline{{}^{d}v_{iso}^{sp}}} = \min\limits_{i=1\ldots m}\left({}^{k}v_{iso}^{sp}, \underline{\underline{{}^{v}E_i^-}}, \underline{\underline{{}^{v}E_i^+}}\right), \text{ with:} \\
\underline{\underline{{}^{v}E_i^-}} = \begin{cases} v_{oi1}^-, \text{ if } \overline{\overline{{}^{v}e_i^-}} \leq 0,\ \sigma_{\max_i}^{v\omega}\ {}^{d}\omega_{req} \neq 0, \text{ and } \zeta_{\min_i}^{v} = 0 \\ v_{oi2}^-, \text{ if } \overline{\overline{{}^{v}e_i^-}} \leq 0,\ \zeta_{\min_i}^{v} \neq 0, \text{ and } v_{oi2}^- \geq 0 \\ \infty, \text{ if } \overline{\overline{{}^{v}e_i^-}} \leq 0,\ \sigma_{\max_i}^{v\omega}\ {}^{d}\omega_{req} = 0, \text{ and } \zeta_{\min_i}^{v} = 0 \\ 0, \text{ otherwise} \end{cases} \\
\underline{\underline{{}^{v}E_i^+}} = \begin{cases} v_{oi1}^+, \text{ if } \underline{\underline{{}^{v}e_i^+}} \geq 0,\ \sigma_{\max_i}^{v\omega}\ {}^{d}\omega_{req} \neq 0, \text{ and } \zeta_{\max_i}^{v} = 0 \\ v_{oi2}^+, \text{ if } \underline{\underline{{}^{v}e_i^+}} \geq 0,\ \zeta_{\max_i}^{v} \neq 0, \text{ and } v_{oi2}^+ \geq 0 \\ \infty, \text{ if } \underline{\underline{{}^{v}e_i^+}} \geq 0,\ \sigma_{\max_i}^{v\omega}\ {}^{d}\omega_{req} = 0, \text{ and } \zeta_{\max_i}^{v} = 0 \\ 0, \text{ otherwise} \end{cases} \\
v_{oi1}^- = \dfrac{-\overline{\overline{{}^{v}e_i^-}}}{2\,\sigma_{\max_i}^{v\omega}\ {}^{d}\omega_{req}},\ v_{oi2}^- = \dfrac{\sigma_{\max_i}^{v\omega}\ {}^{d}\omega_{req} - \sqrt{\left(\sigma_{\max_i}^{v\omega}\ {}^{d}\omega_{req}\right)^2 + \zeta_{\min_i}^{v}\ \overline{\overline{{}^{v}e_i^-}}}}{\zeta_{\min_i}^{v}} \\
\overline{\overline{{}^{v}e_i^-}} = -\tau_i^{\max} + \left\|\boldsymbol{k}_{\boldsymbol{r}_i}^{\boldsymbol{a}}\right\|\ {}^{d}a_{req} + \left\|\boldsymbol{k}_{\boldsymbol{r}_i}^{\boldsymbol{\alpha}}\right\|\ {}^{d}\alpha_{req} + \left\|\boldsymbol{k}_{\boldsymbol{r}_i}^{\boldsymbol{f_e}}\right\|\ {}^{d}f_{ereq} + \left\|\boldsymbol{k}_{\boldsymbol{r}_i}^{\boldsymbol{m_e}}\right\|\ {}^{d}m_{ereq} - \zeta_{\min_i}^{\omega}\left({}^{d}\omega_{req}\right)^2 - \tau_{g_i} \\
v_{oi1}^+ = \dfrac{\underline{\underline{{}^{v}e_i^+}}}{2\,\sigma_{\max_i}^{v\omega}\ {}^{d}\omega_{req}},\ v_{oi2}^+ = \dfrac{-\sigma_{\max_i}^{v\omega}\ {}^{d}\omega_{req} + \sqrt{\left(\sigma_{\max_i}^{v\omega}\ {}^{d}\omega_{req}\right)^2 + \zeta_{\max_i}^{v}\ \underline{\underline{{}^{v}e_i^+}}}}{\zeta_{\max_i}^{v}} \\
\underline{\underline{{}^{v}e_i^+}} = \tau_i^{\max} - \left\|\boldsymbol{k}_{\boldsymbol{r}_i}^{\boldsymbol{a}}\right\|\ {}^{d}a_{req} - \left\|\boldsymbol{k}_{\boldsymbol{r}_i}^{\boldsymbol{\alpha}}\right\|\ {}^{d}\alpha_{req} - \left\|\boldsymbol{k}_{\boldsymbol{r}_i}^{\boldsymbol{f_e}}\right\|\ {}^{d}f_{ereq} - \left\|\boldsymbol{k}_{\boldsymbol{r}_i}^{\boldsymbol{m_e}}\right\|\ {}^{d}m_{ereq} - \zeta_{\max_i}^{\omega}\left({}^{d}\omega_{req}\right)^2 - \tau_{g_i} \\
\forall i = 1\ldots m
\end{cases}
\quad \text{(Ap.33).}
$$

Likewise, we get a lower bound $\underline{\underline{{}^{d}\omega_{iso}^{sp}}}$ for ${}^{d}\omega_{iso}^{sp}$. The result is given hereafter:

$$
\begin{cases}
{}^{d}\omega_{iso}^{sp} \geq \underline{\underline{{}^{d}\omega_{iso}^{sp}}} = \min\limits_{i=1\ldots m}\left({}^{k}\omega_{iso}^{sp}, \underline{\underline{{}^{\omega}E_i^{-}}}, \underline{\underline{{}^{\omega}E_i^{+}}}\right), \text{ with:} \\
\underline{\underline{{}^{\omega}E_i^{-}}} = \begin{cases} \omega_{oi1}^{-}, \text{ if } \overline{\overline{{}^{\omega}e_i^{-}}} \leq 0,\ \sigma_{\max_i}^{v\omega}\ {}^{d}v_{req} \neq 0, \text{ and } \zeta_{\min_i}^{\omega} = 0 \\ \omega_{oi2}^{-}, \text{ if } \overline{\overline{{}^{\omega}e_i^{-}}} \leq 0,\ \zeta_{\min_i}^{\omega} \neq 0, \text{ and } \omega_{oi2}^{-} \geq 0 \\ \infty, \text{ if } \overline{\overline{{}^{\omega}e_i^{-}}} \leq 0,\ \sigma_{\max_i}^{v\omega}\ {}^{d}v_{req} = 0, \text{ and } \zeta_{\min_i}^{\omega} = 0 \\ 0, \text{ otherwise} \end{cases} \\
\underline{\underline{{}^{\omega}E_i^{+}}} = \begin{cases} \omega_{oi1}^{+}, \text{ if } \underline{\underline{{}^{\omega}e_i^{+}}} \geq 0,\ \sigma_{\max_i}^{v\omega}\ {}^{d}v_{req} \neq 0, \text{ and } \zeta_{\max_i}^{\omega} = 0 \\ \omega_{oi2}^{+}, \text{ if } \underline{\underline{{}^{\omega}e_i^{+}}} \geq 0,\ \zeta_{\max_i}^{\omega} \neq 0, \text{ and } \omega_{oi2}^{+} \geq 0 \\ \infty, \text{ if } \underline{\underline{{}^{\omega}e_i^{+}}} \geq 0,\ \sigma_{\max_i}^{v\omega}\ {}^{d}v_{req} = 0, \text{ and } \zeta_{\max_i}^{\omega} = 0 \\ 0, \text{ otherwise} \end{cases} \\
\omega_{oi1}^{-} = \dfrac{-\overline{\overline{{}^{\omega}e_i^{-}}}}{2\,\sigma_{\max_i}^{v\omega}\ {}^{d}v_{req}},\ \omega_{oi2}^{-} = \dfrac{\sigma_{\max_i}^{v\omega}\ {}^{d}v_{req} - \sqrt{\left(\sigma_{\max_i}^{v\omega}\ {}^{d}v_{req}\right)^2 + \zeta_{\min_i}^{\omega}\ \overline{\overline{{}^{\omega}e_i^{-}}}}}{\zeta_{\min_i}^{\omega}} \\
\overline{\overline{{}^{\omega}e_i^{-}}} = -\tau_i^{\max} + \left\|\boldsymbol{k}_{\boldsymbol{r}_i}^{\boldsymbol{a}}\right\|\ {}^{d}a_{req} + \left\|\boldsymbol{k}_{\boldsymbol{r}_i}^{\boldsymbol{\alpha}}\right\|\ {}^{d}\alpha_{req} + \left\|\boldsymbol{k}_{\boldsymbol{r}_i}^{\boldsymbol{f_e}}\right\|\ {}^{d}f_{ereq} + \left\|\boldsymbol{k}_{\boldsymbol{r}_i}^{\boldsymbol{m_e}}\right\|\ {}^{d}m_{ereq} - \zeta_{\min_i}^{v}\left({}^{d}v_{req}\right)^2 - \tau_{g_i} \\
\omega_{oi1}^{+} = \dfrac{\underline{\underline{{}^{\omega}e_i^{+}}}}{2\,\sigma_{\max_i}^{v\omega}\ {}^{d}v_{req}},\ \omega_{oi2}^{+} = \dfrac{-\sigma_{\max_i}^{v\omega}\ {}^{d}v_{req} + \sqrt{\left(\sigma_{\max_i}^{v\omega}\ {}^{d}v_{req}\right)^2 + \zeta_{\max_i}^{\omega}\ \underline{\underline{{}^{\omega}e_i^{+}}}}}{\zeta_{\max_i}^{\omega}} \\
\underline{\underline{{}^{\omega}e_i^{+}}} = \tau_i^{\max} - \left\|\boldsymbol{k}_{\boldsymbol{r}_i}^{\boldsymbol{a}}\right\|\ {}^{d}a_{req} - \left\|\boldsymbol{k}_{\boldsymbol{r}_i}^{\boldsymbol{\alpha}}\right\|\ {}^{d}\alpha_{req} - \left\|\boldsymbol{k}_{\boldsymbol{r}_i}^{\boldsymbol{f_e}}\right\|\ {}^{d}f_{ereq} - \left\|\boldsymbol{k}_{\boldsymbol{r}_i}^{\boldsymbol{m_e}}\right\|\ {}^{d}m_{ereq} - \zeta_{\max_i}^{v}\left({}^{d}v_{req}\right)^2 - \tau_{g_i} \\
\forall i = 1\ldots m
\end{cases}
\tag{Ap.34}
$$

Hence, we have established lower bounds for specific isotropic values in dynamics. These bounds become the exact values for the corresponding specific isotropic values if we have homogeneous-dof robots, $\boldsymbol{h}^{v\omega} = \boldsymbol{0}$, ${}^{d}v_{req} = 0$, or ${}^{d}\omega_{req} = 0$.

B.2- Optimization Using Lagrange Multipliers

Consider the following optimization problem:

$$
\begin{cases}
\max\limits_{\|\boldsymbol{x}\| \leq b}\left(-\boldsymbol{x}^{\mathrm{T}}\ \boldsymbol{A}\ \boldsymbol{x}\right), \text{ with:} \\
\dim\left(\boldsymbol{A}\right) = n \times n,\ \boldsymbol{x} \in \mathbb{R}^n, \text{ and } b > 0
\end{cases}
\tag{Ap.35}
$$

where $\boldsymbol{A}$ is a real symmetric homogeneous[6] matrix.

Note that as $\boldsymbol{A}$ is a real symmetric matrix, all of its eigenvalues are real. The optimization in (Ap.35) can be written as the following minimization problem:

[6] The meant homogeneity is regarding physical units.

$$\min_{\|\boldsymbol{x}\|\le b}\left(\boldsymbol{x}^{\mathrm{T}}\ \boldsymbol{A}\ \boldsymbol{x}\right) \qquad \text{(Ap.36)}.$$

Several cases exist:

- $\boldsymbol{A}\ge 0$ (positive semi-definite); i.e. for every real $\boldsymbol{x}\ne\boldsymbol{0}$, we have $\boldsymbol{x}^{\mathrm{T}}\ \boldsymbol{A}\ \boldsymbol{x}\ge 0$;
- $\boldsymbol{A}\le 0$ (negative semi-definite); i.e. for every real $\boldsymbol{x}\ne\boldsymbol{0}$, we have $\boldsymbol{x}^{\mathrm{T}}\ \boldsymbol{A}\ \boldsymbol{x}\le 0$;
- $\boldsymbol{A}$ (indefinite); i.e. neither of the above is true.

If we have $\boldsymbol{A}\le 0$, then the function $f\left(\boldsymbol{x}\right)=\boldsymbol{x}^{\mathrm{T}}\ \boldsymbol{A}\ \boldsymbol{x}$ is with upward concavity[7]. Hence, its minimum is at $\boldsymbol{x}_{\boldsymbol{o}}=\boldsymbol{0}$ and $\max_{\|\boldsymbol{x}\|\le b}\left(-\boldsymbol{x}^{\mathrm{T}}\ \boldsymbol{A}\ \boldsymbol{x}\right)=0$.

If we have $\boldsymbol{A}\le 0$, then $f\left(\boldsymbol{x}\right)=\boldsymbol{x}^{\mathrm{T}}\ \boldsymbol{A}\ \boldsymbol{x}$ is with downward concavity, and its minimum is at the boundary of the allowable region of $\boldsymbol{x}$. In our case, the $\boldsymbol{x}$ region is defined by $\|\boldsymbol{x}\|\le b$ and hence, its boundary is the surface of the n-dimensional sphere described by $\|\boldsymbol{x}\|=b$. Therefore, (Ap.36) becomes:

$$\min_{\|\boldsymbol{x}\|=b}\left(\boldsymbol{x}^{\mathrm{T}}\ \boldsymbol{A}\ \boldsymbol{x}\right),\ \text{with}\ \boldsymbol{A}\le 0 \qquad \text{(Ap.37)}.$$

The problem expressed by (Ap.37) can be solved by using Lagrange multipliers as follows:

$$\min_{\boldsymbol{x},\lambda}\left(\boldsymbol{x}^{\mathrm{T}}\ \boldsymbol{A}\ \boldsymbol{x}+\lambda\left(\boldsymbol{x}^{\mathrm{T}}\ \boldsymbol{x}-b^{2}\right)\right) \qquad \text{(Ap.38)},$$

with λ being an arbitrary real number.

The local minimum of $g\left(\boldsymbol{x}\right)=\boldsymbol{x}^{\mathrm{T}}\ \boldsymbol{A}\ \boldsymbol{x}+\lambda\left(\boldsymbol{x}^{\mathrm{T}}\ \boldsymbol{x}-b^{2}\right)$ is at $\left(\boldsymbol{x}_{\boldsymbol{o}},\lambda_{o}\right)$, where:

$$\nabla g\left(\boldsymbol{x}_{\boldsymbol{o}},\lambda_{o}\right)=\begin{pmatrix}\dfrac{\partial g}{\partial \boldsymbol{x}}\left(\boldsymbol{x}_{\boldsymbol{o}},\lambda_{o}\right)\\ \dfrac{\partial g}{\partial \lambda}\left(\boldsymbol{x}_{\boldsymbol{o}},\lambda_{o}\right)\end{pmatrix}=\begin{pmatrix}2\ \boldsymbol{A}\ \boldsymbol{x}_{\boldsymbol{o}}+2\ \lambda_{o}\ \boldsymbol{1}_{n\times n}\ \boldsymbol{x}_{\boldsymbol{o}}\\ \boldsymbol{x}_{\boldsymbol{o}}^{\mathrm{T}}\ \boldsymbol{x}_{\boldsymbol{o}}-b^{2}\end{pmatrix}=\boldsymbol{0} \qquad \text{(Ap.39)}.$$

Based on $2\ \boldsymbol{A}\ \boldsymbol{x}_{\boldsymbol{o}}+2\ \lambda_{o}\ \boldsymbol{1}_{n\times n}\ \boldsymbol{x}_{\boldsymbol{o}}=\boldsymbol{0}$, we get:

$$\left(\boldsymbol{A}+\lambda_{o}\ \boldsymbol{1}_{n\times n}\right)\boldsymbol{x}_{\boldsymbol{o}}=\boldsymbol{0} \qquad \text{(Ap.40)},$$

which is nothing other than the definition of eigenvalues. So, let ξ_{i} (with $i=1\ldots n$) be the n eigenvalues of $\boldsymbol{A}$, which are necessarily negative (since $\boldsymbol{A}\le 0$). Then, $\boldsymbol{x}_{\boldsymbol{o}}$ should be along the direction of the unit eigenvector, $\boldsymbol{e}_{\boldsymbol{min}}$, of the corresponding minimum eigenvalue, $\xi_{\min}=\min_{i=1\ldots n}\left(\xi_{i}\right)\le 0$ and hence, we get:

$$\boldsymbol{x}_{\boldsymbol{o}}=\pm\left\|\boldsymbol{x}_{\boldsymbol{o}}\right\|\boldsymbol{e}_{\boldsymbol{min}} \qquad \text{(Ap.41)}.$$

---

[7] Since the Hessian of f is $2\ \boldsymbol{A}$ where $\boldsymbol{A}\ge 0$.

But we have $\|\boldsymbol{x}_o\| = b$, thus we obtain:

$$\max_{\|\boldsymbol{x}\| \le b} \left(-\boldsymbol{x}^{\mathrm{T}} \ \boldsymbol{A}\ \boldsymbol{x} \right) = \max_{\|\boldsymbol{x}\| = b} \left(-\boldsymbol{x}^{\mathrm{T}} \ \boldsymbol{A}\ \boldsymbol{x} \right) = -\xi_{\min} \ b^2 \qquad \text{(Ap.42)}.$$

Finally, in the case of having $\boldsymbol{A}$ indefinite matrix, we consider its eigenvalues, ξ_i (with $i = 1...n$). These eigenvalues are not all positive. To prove that still (Ap.42) is valid, we consider the optimization:

$$\min_{\|\boldsymbol{e}\| = 1} \left(\boldsymbol{e}^{\mathrm{T}} \ \boldsymbol{A}\ \boldsymbol{e} \right) \qquad \text{(Ap.43)}.$$

The minimization in (Ap.43) can be solved using Lagrange multipliers and yields (similar to (Ap.37)):

$$\boldsymbol{e} = \boldsymbol{e}_{\boldsymbol{min}} \qquad \text{(Ap.44)},$$

where $\boldsymbol{e}_{\boldsymbol{min}}$ is the unit eigenvector corresponding to $\xi_{\min} = \min_{i=1...n} (\boldsymbol{A}) < 0$.

Thus, we have $\forall r > 0$:

$$\max_{\|\boldsymbol{x}\| = r} \left(-\boldsymbol{x}^{\mathrm{T}} \ \boldsymbol{A}\ \boldsymbol{x} \right) = \max_{\|\boldsymbol{x}\| = r} \left(-\boldsymbol{x}^{\mathrm{T}} \ \boldsymbol{A}\ \boldsymbol{x} \right) = -\xi_{\min} \ r^2 \qquad \text{(Ap.45)}.$$

Varying r between zero and b, we get:

$$\max_{\|\boldsymbol{x}\| \le b} \left(-\boldsymbol{x}^{\mathrm{T}} \ \boldsymbol{A}\ \boldsymbol{x} \right) = \max_{0 \le r \le b} \left(-\xi_{\min} \ r^2 \right) = -\xi_{\min} \ b^2 \qquad \text{(Ap.46)}.$$

Thus, we can generalize, for any real symmetric homogeneous square matrix, $\boldsymbol{A}$, the following relations:

$$\begin{cases} \max_{\|\boldsymbol{x}\| \le b} \left(\boldsymbol{x}^{\mathrm{T}} \ \boldsymbol{A}\ \boldsymbol{x} \right) = \vartheta_{\max} \ b^2 \\ \min_{\|\boldsymbol{x}\| \le b} \left(\boldsymbol{x}^{\mathrm{T}} \ \boldsymbol{A}\ \boldsymbol{x} \right) = \vartheta_{\min} \ b^2 \end{cases} \qquad \text{(Ap.47)},$$

with:

$$\begin{cases} \vartheta_{\min} = \min \left(\xi_{\min}, 0 \right) \\ \vartheta_{\max} = \max \left(\xi_{\max}, 0 \right) \\ \xi_{\min} = \min_{i=1...n} \left(\xi_i \right) \\ \xi_{\max} = \max_{i=1...n} \left(\xi_i \right) \\ \xi_i : \text{ i-th egenvalue of } \boldsymbol{A}, \ \forall i = 1...n \end{cases} \qquad \text{(Ap.48)}.$$

B.3-Case Study: DUAL V

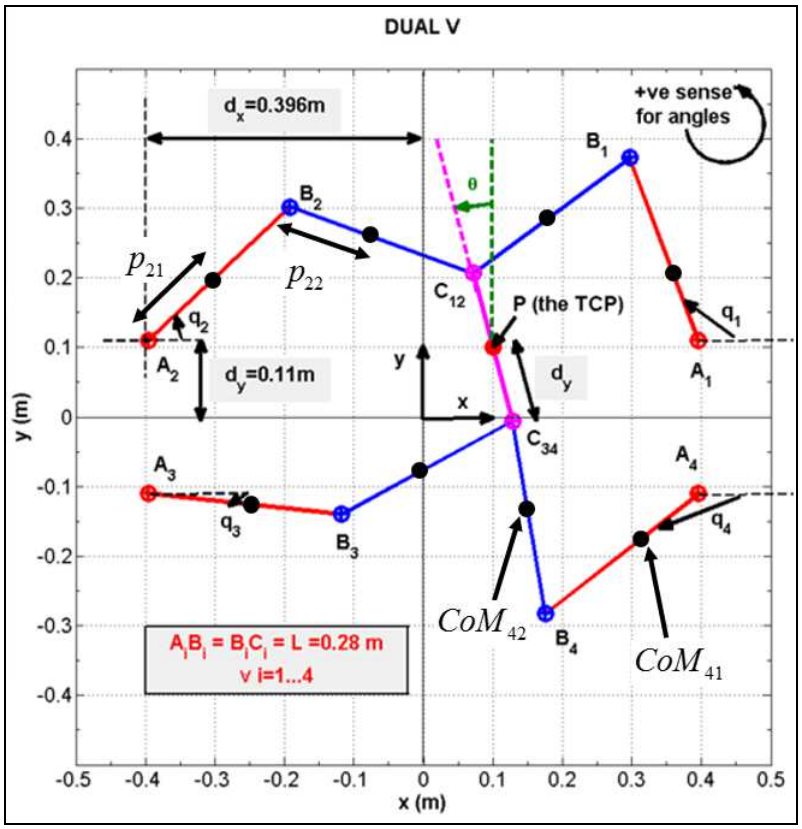

Fig. Ap-11: DUAL V: schematic showing principal geometric parameters and center-of-mass positions of the different parts.

This part presents the dynamic evaluation of DUAL V based on the notion of specific isotropic values. The different required geometric parameters are depicted in **Fig. 2-3** and **Fig. Ap-11**. In the latter figure, the positions of the center of masses of all the parts are illustrated. Additionally, the values of the inertia-related parameters are provided in **Table Ap-14**[8] and the actuators' capabilities, as well as the dynamic performance requirements, are given in **Table Ap-15**.

The DM in the required form can be established as described by (WIJK, et al., 2013). In this aspect, the only difference is that we have assumed the presence of an external force, $\boldsymbol{f_e} = \begin{pmatrix} f_{ex} & f_{ey} \end{pmatrix}^{\mathrm{T}}$, and moment, $\boldsymbol{m_e} = \begin{pmatrix} m_{ez} \end{pmatrix}$, applied on the platform at the TCP. This can be easily introduced into the formulation given in the aforementioned reference.

Based on all the above and applying the concepts of specific isotropic values in the case of dynamics, lower bounds of these latter values have been established over the xy workspace, while fixing $\theta = 0°$. These results are graphed in **Fig. Ap-12**.

[8] The values of these parameters are exactly those given in (WIJK, et al., 2013) for the unbalanced situation.

Table Ap-14: The inertia parameters of DUAL V

Symbol	Value	Symbol	Value
$p_{i1} = \left\| \boldsymbol{A}_i \boldsymbol{CoM}_{i1} \right\|$	0.0737 m	$p_{i2} = \left\| \boldsymbol{B}_i \boldsymbol{CoM}_{i2} \right\|$	0.1279 m
m_{i1}	1.169 kg	m_{i2}	0.606 kg
I_{i1}	0.012967 kg m^2	I_{i2}	0.006417 kg m^2
m_p	0.899 kg	I_{pzz}	0.008168 kg m^2
I_{ma}	0.0041 kg m^2		

CoM_{i1} is the center of mass of the arm A_iB_i, with m_{i1} and I_{i1} being its corresponding mass and moment of inertia relative to the axis passing through CoM_{i1}. Similar significances are to be considered regarding the arm B_iC_i, and its characteristics: CoM_{i2}, m_{i2}, and I_{i2}. The terms m_p and I_{pzz} are the mass and moment of inertia of the platform, with its center of mass being at P. Finally, I_{ma} is the moment of inertia of the individual actuator with respect to its axis of rotation.

Table Ap-15: Actuators' capacities and required dynamic performances for DUAL V

Symbol	Quantity	Value
$\dot{q}^{\max}$	Maximum actuator's speed	100 rpm = 10.47 rad/s
$\tau^{\max}$	Maximum actuator's torque	60 N m
${}^d a_{req}$	Required linear acceleration	30 m/s^2
${}^d \alpha_{req}$	Required angular acceleration	50 rad/s^2
${}^d v_{req}$	Required linear speed	0.25 m/s
${}^d \omega_{req}$	Required angular speed	3 rpm = 0.31 rad/s
${}^d f_{ereq}$	Required force capacity	200 N
${}^d m_{ereq}$	Required moment capacity	15 N m

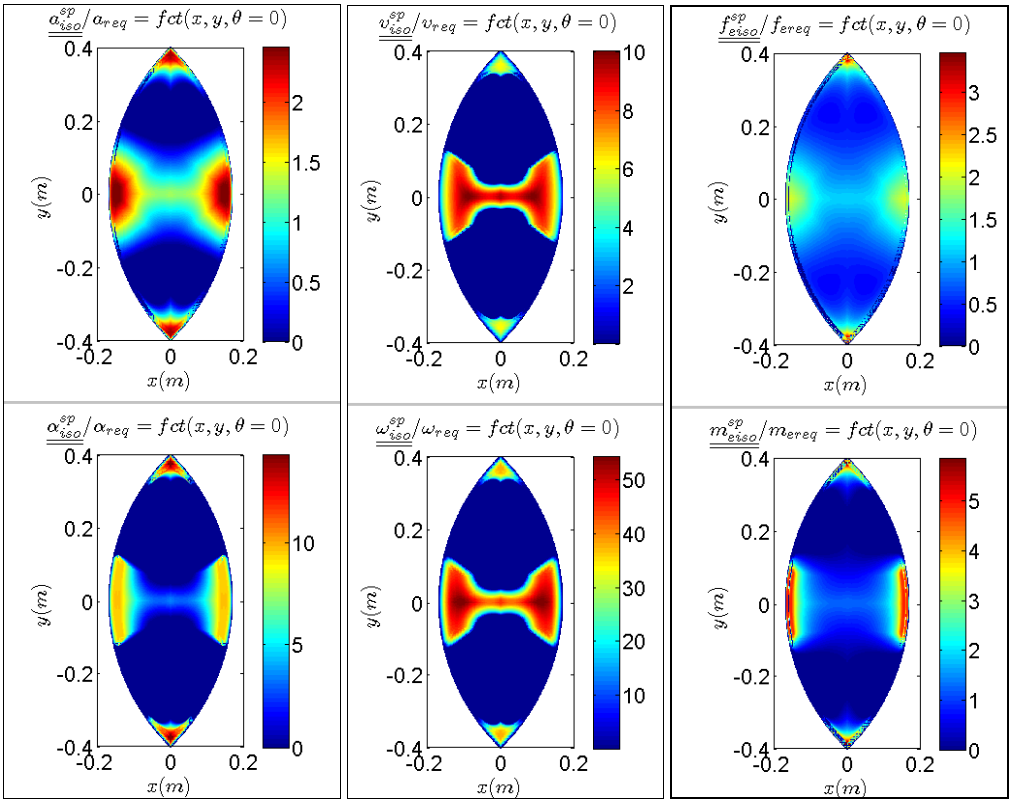

Fig. Ap-12: DUAL V dynamic analysis: ratios of specific isotropic values' lower bounds relative to their corresponding requirements in the case of zero rotation.

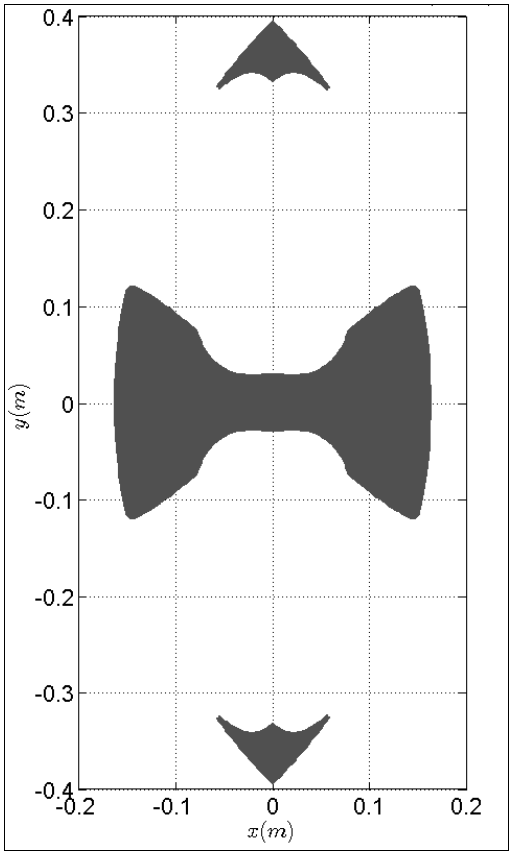

Fig. Ap-13: DUAL V: the regions with specific isotropic values' lower bounds greater or equal to their corresponding requirements in the case of zero rotation.

Moreover, the regions of satisfactory dynamic performances based on the different dynamic indices have been investigated (see **Fig. Ap-13**). These are confounded as it has been expected, based on the property of equivalence in **§2.2.4.B**.

Appendix C: The Establishment of the Operational Wrench Zonotope of Cable-Driven Parallel Robots (CDPRS) in Statics

Consider the following equation that relates the actuators' torques, $\boldsymbol{\tau}$, to the operational wrench, $\boldsymbol{w}$, by:

$$\boldsymbol{w} = \boldsymbol{\Gamma}\ \boldsymbol{\tau} \tag{Ap.49},$$

with $\boldsymbol{\Gamma} = -\boldsymbol{J}_{\boldsymbol{m}}^{\mathrm{T}}$.

Also, assume that we have the following constraints on $\boldsymbol{\tau}$:

$$0 \le \tau_i^{\min} \le \tau_i \le \tau_i^{\max},\ \forall i = 1...m \tag{Ap.50}.$$

Then, to determine the operational wrench zonotope, we follow the methodology of (BOUCHARD, et al., 2008) that is summarized in what follows.

First, we define the following terms:

$$\begin{cases} \boldsymbol{\tau}^{\boldsymbol{min}} = \begin{pmatrix} \tau_1^{\min} & \cdots & \tau_m^{\min} \end{pmatrix}^{\mathrm{T}},\ \boldsymbol{\tau}^{\boldsymbol{max}} = \begin{pmatrix} \tau_1^{\max} & \cdots & \tau_m^{\max} \end{pmatrix}^{\mathrm{T}}, \\ \boldsymbol{\Delta\tau} = \dfrac{1}{2}\left(\boldsymbol{\tau}^{\boldsymbol{max}} - \boldsymbol{\tau}^{\boldsymbol{min}}\right),\ \boldsymbol{N} = \mathrm{diag}\left(\boldsymbol{\Delta\tau}\right), \\ \text{and } \hat{\boldsymbol{\tau}} = \dfrac{1}{2}\left(\boldsymbol{\tau}^{\boldsymbol{min}} + \boldsymbol{\tau}^{\boldsymbol{max}}\right) \end{cases} \tag{Ap.51}.$$

Applying the following change of variables:

$$\begin{cases} \boldsymbol{\tau} = \boldsymbol{N}\ \tilde{\boldsymbol{\tau}} + \hat{\boldsymbol{\tau}},\ \text{with:} \\ -1 \le \tilde{\tau}_i \le +1,\ \forall i = 1...m \\ \tilde{\tau}_i :\ \text{i-th component of } \tilde{\boldsymbol{\tau}} \end{cases} \tag{Ap.52},$$

we get:

$$\begin{cases} \widetilde{\boldsymbol{w}} = \widetilde{\boldsymbol{\Gamma}}\ \tilde{\boldsymbol{\tau}},\ \text{with:} \\ \widetilde{\boldsymbol{\Gamma}} = \boldsymbol{\Gamma}\ \boldsymbol{N},\ \widehat{\boldsymbol{w}} = \boldsymbol{\Gamma}\ \hat{\boldsymbol{\tau}} \\ \text{and } \widetilde{\boldsymbol{w}} = \boldsymbol{w} - \widehat{\boldsymbol{w}} \end{cases} \tag{Ap.53}.$$

Following the lead of (BOUCHARD, et al., 2008), we get the zonotope boundaries of $\widetilde{\boldsymbol{w}}$ by taking all the possible combinations of $d = n-1$ linearly independent column vectors, $\left\{\tilde{\boldsymbol{\gamma}}_{i_1}, \ldots, \tilde{\boldsymbol{\gamma}}_{i_d}\right\}$, of $\widetilde{\boldsymbol{\Gamma}}$, with $i_k \in \{1, \ldots, m\}, \forall k = 1...d$. Then, the unit normal to the boundary is calculated via the cross product defined in the n-dimensional space as follows:

$$\boldsymbol{n} = \frac{\tilde{\boldsymbol{\gamma}}_{i_1} \times \ldots \times \tilde{\boldsymbol{\gamma}}_{i_d}}{\left\| \tilde{\boldsymbol{\gamma}}_{i_1} \times \ldots \times \tilde{\boldsymbol{\gamma}}_{i_d} \right\|} \quad \text{(Ap.54).}$$

In fact, there are two parallel boundaries of the same normal, $\boldsymbol{n}$, but that differ in the points they pass through. These points are determined by the complementary set of vectors defined by:

$$\left\{ \tilde{\boldsymbol{\gamma}}_{j_1}, \ldots, \tilde{\boldsymbol{\gamma}}_{j_t} \right\} = \left\{ \tilde{\boldsymbol{\gamma}}_1, \ldots, \tilde{\boldsymbol{\gamma}}_m \right\} \ominus \left\{ \tilde{\boldsymbol{\gamma}}_{i_1}, \ldots, \tilde{\boldsymbol{\gamma}}_{i_d} \right\} \quad \text{(Ap.55),}$$

with $\ominus$ denoting set subtraction operation[9]. The two aforementioned points are given by:

$$\begin{cases} \widetilde{\boldsymbol{p}^+} = \sum\limits_{k=1\ldots t} \left(\left| \boldsymbol{n}^{\mathrm{T}} \, \tilde{\boldsymbol{\gamma}}_{j_k} \right| \right) \boldsymbol{n} \\ \widetilde{\boldsymbol{p}^-} = \sum\limits_{k=1\ldots t} \left(-\left| \boldsymbol{n}^{\mathrm{T}} \, \tilde{\boldsymbol{\gamma}}_{j_k} \right| \right) \boldsymbol{n} \end{cases} \quad \text{(Ap.56).}$$

Thus, in the $\boldsymbol{w}$ space, the pair of parallel planes is defined using a point and unit outward normal as follows:

$$\begin{cases} \left(pl^+ \right) = \mathrm{plane}\left(\boldsymbol{p}^+, \boldsymbol{n} \right) \\ \left(pl^- \right) = \mathrm{plane}\left(\boldsymbol{p}^-, -\boldsymbol{n} \right) \end{cases} \quad \text{(Ap.57),}$$

in which:

$$\begin{cases} \boldsymbol{p}^+ = \widetilde{\boldsymbol{p}^+} + \widehat{\boldsymbol{w}} \\ \boldsymbol{p}^- = \widetilde{\boldsymbol{p}^-} + \widehat{\boldsymbol{w}} \end{cases} \quad \text{(Ap.58).}$$

Defining n_p as the total number of combinations of d linearly independent d column vectors of $\widetilde{\boldsymbol{\Gamma}}$, we obtain n_p pairs of boundary planes defined as in(Ap.57). The intersection of the latter half-spaces, positioned on the negative side compared to the corresponding outward normal, form the sought zonotope. Note that the number n_p is upper-bounded by C_m^d, which is defined as:

$$C_m^d = \frac{m!}{d!(m-d)!} \quad \text{(Ap.59).}$$

So, the operational-wrench zonotope and its boundary hyperplanes are now known. For the sake of readability, let us say that these hyperplanes are defined each by a point, $\boldsymbol{w}_{0k}$, and outward-unit normal, $\boldsymbol{\eta}_k$, with $k = 1 \ldots 2\, n_p$. Thus, a given wrench, $\boldsymbol{w}$, is feasible if and only if:

$$\boldsymbol{\eta}_k^{\mathrm{T}} \, \boldsymbol{w} \leq \boldsymbol{\eta}_k^{\mathrm{T}} \, \boldsymbol{w}_{0k}, \ \forall k = 1 \ldots 2\, n_p \quad \text{(Ap.60).}$$

[9] $C = A \ominus B = \{ x;\ x \in A \text{ and } x \notin B \}$ with A and B being two sets.

The system of inequalities (Ap.60) is all what we need to compute the specific isotropic force and moment in statics.

Appendix D: Dynamic Performance Evaluation of CDPRs

D.1-Formulation of the Dynamic Model for CDPRs

Neglecting friction, we can write the DM of a CDPR under the following generalized form:

$$\boldsymbol{M}'(\boldsymbol{x})\,\boldsymbol{\rho}+\boldsymbol{C}'(\boldsymbol{x},\boldsymbol{t})\,\boldsymbol{t}-\boldsymbol{w}_{geq}(\boldsymbol{x})-\boldsymbol{w}_{e}=\boldsymbol{J}_{m}^{\mathrm{T}}\,\boldsymbol{\tau} \qquad \text{(Ap.61)},$$

with $\boldsymbol{M}'$, $\boldsymbol{C}'$, $\boldsymbol{w}_{geq}$, and $\boldsymbol{w}_{e}$ corresponding to the generalized inertia matrix, the generalized Coriolis and centrifugal effects matrix, the total gravitational wrench as seen from the platform, and the external non-gravitational wrench acting on the platform, respectively. As for the other symbols, they hold the same meanings as defined earlier[10].

In addition to (Ap.61), we need to consider the relation that allows the computation of cable tensions, $\boldsymbol{f}_{c}$. This can be easily obtained via applying the law of motion on the individual actuators to get:

$$\boldsymbol{I}_{a}\,\ddot{\boldsymbol{q}}-\boldsymbol{w}_{ga}=\boldsymbol{\tau}-\boldsymbol{\Psi}\,\boldsymbol{f}_{c} \qquad \text{(Ap.62)},$$

with $\boldsymbol{I}_{a}$ and $\boldsymbol{w}_{ga}$ corresponding to the $m\times m$ diagonal inertia matrix of the actuators and the gravitational wrenches acting on the actuators due to their proper weight, respectively. As for $\boldsymbol{\Psi}$, it is an $m\times m$ diagonal matrix. Note that: $\boldsymbol{I}_{a}=\boldsymbol{I}_{a}(\boldsymbol{x})$, $\boldsymbol{w}_{ga}=\boldsymbol{w}_{ga}(\boldsymbol{x})$, and $\boldsymbol{\Psi}=\boldsymbol{\Psi}(\boldsymbol{x})$.

In CDPRs with $m\geq n$, we always have the inverse kinematic relation, which is given by:

$$\dot{\boldsymbol{q}}=\boldsymbol{J}_{m}\,\boldsymbol{t} \qquad \text{(Ap.63)}.$$

Differentiating (Ap.63) with respect to time, we get:

$$\ddot{\boldsymbol{q}}=\boldsymbol{J}_{m}\,\boldsymbol{\rho}+\dot{\boldsymbol{J}}_{m}\,\boldsymbol{t} \qquad \text{(Ap.64)}.$$

Substituting (Ap.64) in (Ap.62) yields:

$$\boldsymbol{I}_{a}\,\boldsymbol{J}_{m}\,\boldsymbol{\rho}+\boldsymbol{I}_{a}\,\dot{\boldsymbol{J}}_{m}\,\boldsymbol{t}-\boldsymbol{w}_{ga}=\boldsymbol{\tau}-\boldsymbol{\Psi}\,\boldsymbol{f}_{c} \qquad \text{(Ap.65)}.$$

Merging (Ap.61) and (Ap.65) gives:

[10] Meaning: $\boldsymbol{\rho}=\begin{pmatrix}\boldsymbol{a}^{\mathrm{T}} & \boldsymbol{\alpha}^{\mathrm{T}}\end{pmatrix}^{\mathrm{T}}=\begin{pmatrix}\dot{\boldsymbol{v}}^{\mathrm{T}} & \dot{\boldsymbol{\omega}}^{\mathrm{T}}\end{pmatrix}^{\mathrm{T}}$ (linear and angular operational accelerations), and $\boldsymbol{t}=\begin{pmatrix}\boldsymbol{v}^{\mathrm{T}} & \boldsymbol{\omega}^{\mathrm{T}}\end{pmatrix}^{\mathrm{T}}$ (operational twist: linear and angular velocities).

$$\begin{cases} \boldsymbol{K}\,\boldsymbol{\xi}+\boldsymbol{h}-\boldsymbol{w}_g=\boldsymbol{\Phi}\,\boldsymbol{\gamma}, \text{ with:} \\ \boldsymbol{K}=\begin{bmatrix} \boldsymbol{M}' & -\mathbf{1}_{n\times n} \\ \boldsymbol{I}_a\,\boldsymbol{J}_m & \mathbf{0}_{m\times n} \end{bmatrix},\ \boldsymbol{\xi}=\begin{pmatrix} \boldsymbol{\rho} \\ \boldsymbol{w}_e \end{pmatrix},\ \boldsymbol{h}=\begin{bmatrix} \boldsymbol{C}' \\ \boldsymbol{I}_a\,\dot{\boldsymbol{J}}_m \end{bmatrix}\boldsymbol{t}=\begin{pmatrix} \boldsymbol{t}^{\mathrm{T}}\,\boldsymbol{H}_1(\boldsymbol{x})\,\boldsymbol{t} \\ \vdots \\ \boldsymbol{t}^{\mathrm{T}}\,\boldsymbol{H}_{n+m}(\boldsymbol{x})\,\boldsymbol{t} \end{pmatrix} \\ \boldsymbol{w}_g=\begin{pmatrix} \boldsymbol{w}_{geq} \\ \boldsymbol{w}_{ga} \end{pmatrix},\ \boldsymbol{\Phi}=\begin{bmatrix} \boldsymbol{J}_m^{\mathrm{T}} & \mathbf{0}_{n\times m} \\ \mathbf{1}_{m\times m} & -\boldsymbol{\Psi} \end{bmatrix}, \text{ and } \boldsymbol{\gamma}=\begin{pmatrix} \boldsymbol{\tau} \\ \boldsymbol{f}_c \end{pmatrix} \end{cases} \quad \text{(Ap.66)},$$

where:

$$\begin{cases} \boldsymbol{h}=\boldsymbol{h}(\boldsymbol{x},\boldsymbol{t})=\begin{pmatrix} \boldsymbol{t}^{\mathrm{T}}\,\boldsymbol{H}_1(\boldsymbol{x})\,\boldsymbol{t} & \cdots & \boldsymbol{t}^{\mathrm{T}}\,\boldsymbol{H}_{n+m}(\boldsymbol{x})\,\boldsymbol{t} \end{pmatrix}^{\mathrm{T}} \\ \boldsymbol{H}_i=\boldsymbol{H}_i(\boldsymbol{x})=\begin{bmatrix} \boldsymbol{H}_i^{v}(\boldsymbol{x}) & \boldsymbol{H}_i^{vw}(\boldsymbol{x}) \\ \left(\boldsymbol{H}_i^{vw}(\boldsymbol{x})\right)^{\mathrm{T}} & \boldsymbol{H}_i^{\omega}(\boldsymbol{x}) \end{bmatrix},\ \forall i=1\ldots(n+m) \end{cases} \quad \text{(Ap.67)}.$$

Further reforming of (Ap.67) leads to the favorable form below:

$$\boldsymbol{K}\,\boldsymbol{\xi}+\boldsymbol{h}^{v}+\boldsymbol{h}^{\omega}+\boldsymbol{h}^{v\omega}-\boldsymbol{w}_g=\boldsymbol{\Phi}\,\boldsymbol{\gamma} \quad \text{(Ap.68)},$$

with:

$$\begin{cases} \boldsymbol{h}^{v}=\boldsymbol{h}^{v}(\boldsymbol{x},\boldsymbol{v})=\begin{pmatrix} \boldsymbol{v}^{\mathrm{T}}\,\boldsymbol{H}_1^{v}\,\boldsymbol{v} & \cdots & \boldsymbol{v}^{\mathrm{T}}\,\boldsymbol{H}_{n+m}^{v}\,\boldsymbol{v} \end{pmatrix}^{\mathrm{T}} \\ \boldsymbol{h}^{\omega}=\boldsymbol{h}^{\omega}(\boldsymbol{x},\boldsymbol{\omega})=\begin{pmatrix} \boldsymbol{\omega}^{\mathrm{T}}\,\boldsymbol{H}_1^{\omega}\,\boldsymbol{\omega} & \cdots & \boldsymbol{\omega}^{\mathrm{T}}\,\boldsymbol{H}_{n+m}^{\omega}\,\boldsymbol{\omega} \end{pmatrix}^{\mathrm{T}} \\ \boldsymbol{h}^{v\omega}=\boldsymbol{h}^{v\omega}(\boldsymbol{x},\boldsymbol{t})=\begin{pmatrix} 2\,\boldsymbol{v}^{\mathrm{T}}\,\boldsymbol{H}_1^{v\omega}\,\boldsymbol{\omega} & \cdots & 2\,\boldsymbol{v}^{\mathrm{T}}\,\boldsymbol{H}_{n+m}^{v\omega}\,\boldsymbol{\omega} \end{pmatrix}^{\mathrm{T}} \end{cases} \quad \text{(Ap.69)}.$$

D.2- Case Study: A Fully-Constrained CDPR

This study is carried out on the same CDPR depicted in **Fig. 2-9**. The characteristics of the actuators, the inertia parameters, and the required dynamic performances are those given in **Table Ap-16**. To simplify the dynamic modeling, we neglect the mass of the cables in addition to friction.

The cable tensions are related to the actuators' torques, $\boldsymbol{\tau}$, by:

$$\begin{cases} \boldsymbol{I}_a\,\ddot{\boldsymbol{q}}=\boldsymbol{\tau}-\boldsymbol{\Psi}\ \boldsymbol{f}_c, \text{ with:} \\ \boldsymbol{I}_a=\mathrm{diag}\left(I_{ma},I_{ma},I_{ma},I_{ma}\right) \\ \boldsymbol{\Psi}=\mathrm{diag}\left(r_e,r_e,r_e,r_e\right) \\ f_{c_i}\geq 0,\ \forall i=1\ldots4 \text{ (cables should be under tension)} \end{cases} \quad \text{(Ap.70)}.$$

Regarding the matrices $\boldsymbol{M}'$ and $\boldsymbol{C}'$, they are given by:

Table Ap-16: Actuators' characteristics, inertia parameters, and required dynamic performances for the CDPR in Fig. 2-9.*

Symbol	Quantity	Value
$\dot{q}^{\max}$	Maximum actuator's speed	$100\ \text{rpm} = 10.47\ \text{rad/s}$
$\tau^{\max}$	Maximum actuator's torque	$60\ \text{N m}$
$f_c^{\min}$	Minimum cable tension	$10\ \text{N}$
$f_c^{\max}$	Maximum cable tension	$500\ \text{N}$
${}^d a_{req}$	Required linear acceleration	$30\ \text{m/s}^2$
${}^d \alpha_{req}$	Required angular acceleration	$50\ \text{rad/s}^2$
${}^d v_{req}$	Required linear speed	$0.25\ \text{m/s}$
${}^d \omega_{req}$	Required angular speed	$3\ \text{rpm} = 0.31\ \text{rad/s}$
${}^d f_{ereq}$	Required force capacity	$200\ \text{N}$
${}^d m_{ereq}$	Required moment capacity	$15\ \text{N m}$
I_{ma}	Actuator's Moment of Inertia	$4.92\times10^{-3}\ \text{kg m}^2$
m_p	Platform's mass	$5\ \text{kg}$
I_{pzz}	Platform's Moment of Inertia	$4.3\times10^{-3}\ \text{kg m}^2$

***All actuators are identical. The positive sense of the actuator torque is the same as the positive sense of rotation (which tends to shorten or wind up the cable). The cables are assumed massless.**

$$\begin{cases} \boldsymbol{M}' = \boldsymbol{M}_p + \boldsymbol{J}_m^{\mathrm{T}}\, \boldsymbol{I}_a\, \boldsymbol{J}_m \\ \boldsymbol{M}_p = \mathrm{diag}\left(m_p, m_p, I_{pzz}\right) \\ \boldsymbol{C}' = \boldsymbol{C}_p + \boldsymbol{J}_m^{\mathrm{T}}\, \boldsymbol{I}_a\, \dot{\boldsymbol{J}}_m \\ \boldsymbol{C}_p = \boldsymbol{0}_{3\times3} \end{cases} \quad \text{(Ap.71)},$$

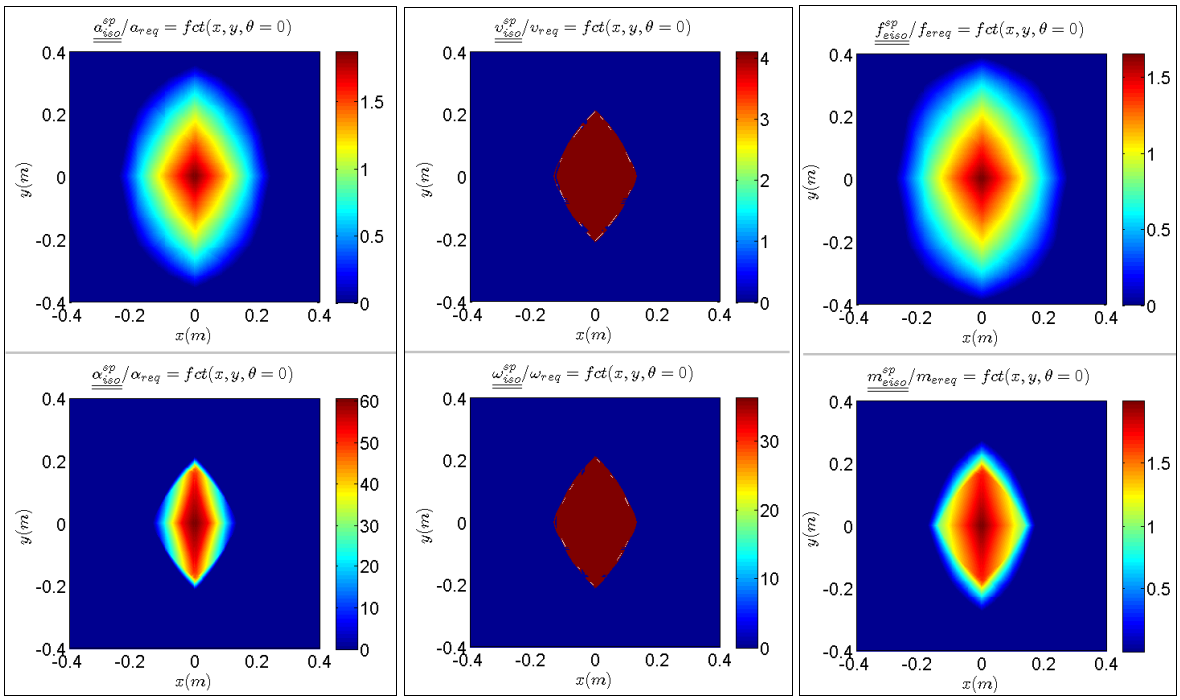

Fig. Ap-14: Ratios of specific isotropic values' lower bounds relative to corresponding requirements for the CDPR presented in Fig. 2-9.

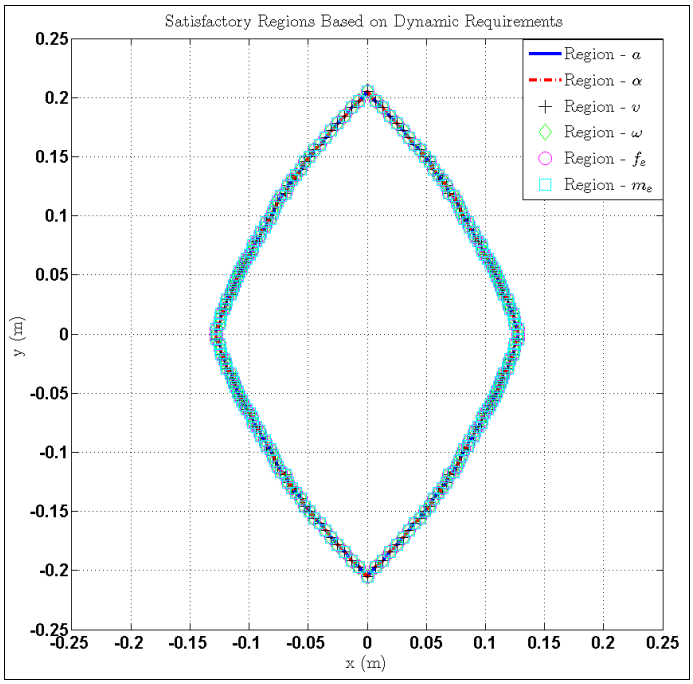

Fig. Ap-15: Satisfactory regions based on lower bounds of specific isotropic dynamic values for the CDPR presented in Fig. 2-9.

with $\boldsymbol{C}_p$ representing the Coriolis and centrifugal effects on the platform[11]. Regarding the external non-gravitational wrench, $\boldsymbol{w}_e$, it is:

[11] Note that the point P (the TCP) is confounded with the center of mass of the platform.

$$\boldsymbol{w}_{\boldsymbol{e}} = \left(\boldsymbol{f}_{\boldsymbol{e}}^{\mathrm{T}} \quad \boldsymbol{m}_{\boldsymbol{e}}^{\mathrm{T}} \right)^{\mathrm{T}} = \left(f_{ex} \quad f_{ey} \quad m_{ez} \right)^{\mathrm{T}} \qquad \text{(Ap.72)}.$$

Utilizing all the aforementioned data, the dynamic evaluation, as described in **§2.3.4**, has been done. The ratios of the dynamic specific isotropic values' lower bounds to their corresponding requirements are shown in **Fig. Ap-14**, for $\theta = 0^{\circ}$. Notice that the lower bounds for the specific isotropic angular acceleration and speed are quite interesting. They are large in comparison with their preset requirements. Finally, the regions of satisfactory dynamic performance are depicted in **Fig. Ap-15**.

Appendix E: Photos of ARROW Machine

In **Fig. Ap-16** and **Fig. Ap-17**, two photos of the implemented ARROW V2 M2 prototype are shown. In **Fig. Ap-18**, a close-up side view of the turntable is depicted. Notice the spring assembly in this latter figure. This is used to counteract the gravitational effect. More precisely, it allows maintaining the static turntable orientation without the need of any actuation torque. This is beneficial regarding energy saving.

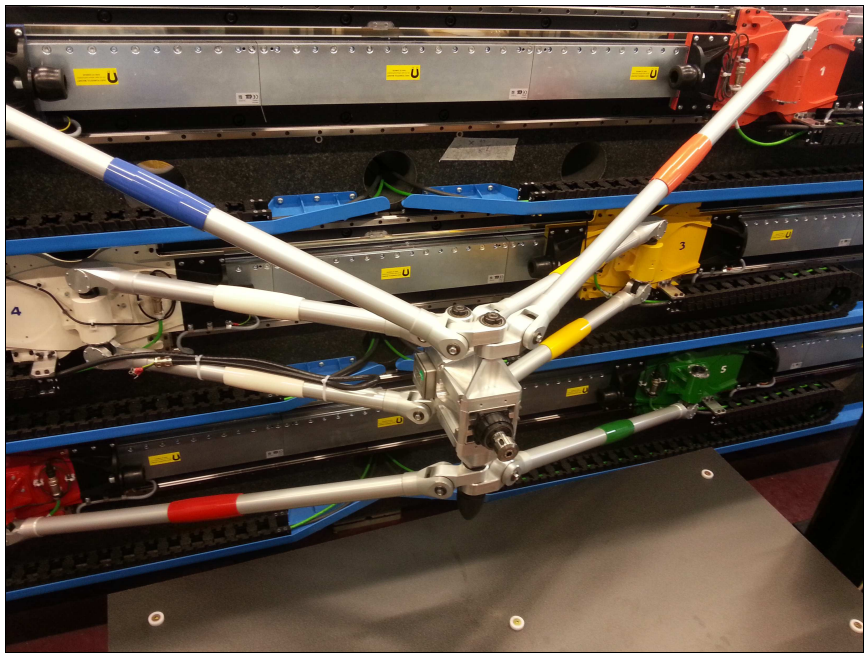

Fig. Ap-16: ARROW V2 M2 prototype.

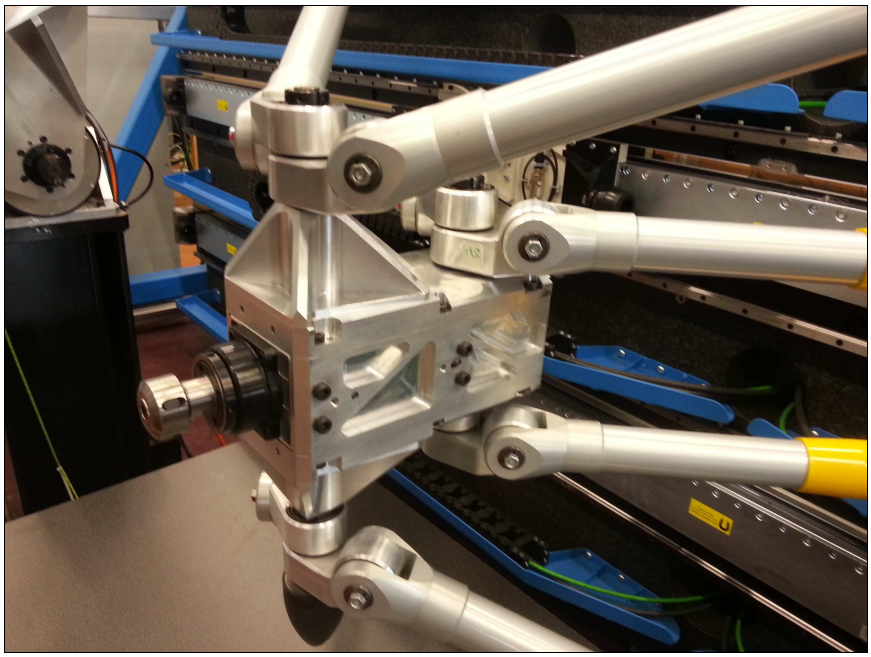

Fig. Ap-17: ARROW V2 M2 prototype: close-up image of the platform.

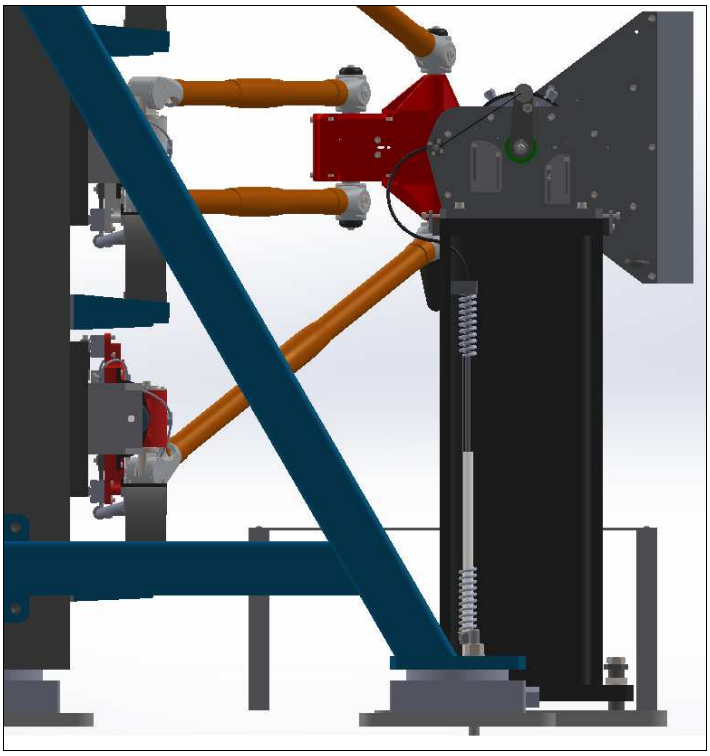

Fig. Ap-18: ARROW machine CAD drawing: close view on the turntable showing the springs used to counteract the gravity effect.

Publications

1. S. SHAYYA, S. KRUT, O. COMPANY, C. BARADAT and F. PIERROT, “A Novel 4 DoFs (3T-1R) Parallel Manipulator with Actuation Redundancy–Workspace Analysis”, in Proc. of MeTrApp 2013: The 2nd Conf. on Mechanisms, Transmissions and Applications, pp. 317-324, Bilbao, Spain, October 2-4, 2013.
2. S. SHAYYA, S. KRUT, O. COMPANY, C. BARADAT and F. PIERROT, “A novel (3T-1R) redundant parallel mechanism with large operational workspace and rotational capability”, in Proc. of 2013 IEEE/RSJ International Conference on Intelligent Robots and Systems (IROS 2013), pp. 436-443, Tokyo, Japan, November 3-8, 2013.
3. S. SHAYYA, S. KRUT, O. COMPANY, C. BARADAT and F. PIERROT, “A Novel (3T-2R) Parallel Mechanism with Large Operational Workspace and Rotational Capability”, in Proc. of 2014 IEEE International Conference on Robotics and Automation (ICRA 2014), Hong Kong, China, May 31 - June 7, 2014.
4. S. SHAYYA, S. KRUT, O. COMPANY, C. BARADAT and F. PIERROT, “Dynamic Analysis of 4 Degrees of Freedom Redundant Parallel Manipulator”, in Proc. of Advances in Robot Kinematics (ARK 2014), pp. 545-553, Ljubljana, Slovenia, June 29 - July 3, 2014.
5. S. SHAYYA, S. KRUT, O. COMPANY, C. BARADAT and F. PIERROT, “Dimensional Synthesis of 4 DoFs (3T-1R) Actuatedly Redundant Parallel Manipulator Based on Dual Criteria: Dynamics and Precision” , in Proc. of 2014 IEEE/RSJ International Conference on Intelligent Robots and Systems (IROS 2014), Chicago, Illinois, September 14–18, 2014.
6. S. SHAYYA, S. KRUT, O. COMPANY, C. BARADAT and F. PIERROT, “On the Performance Evaluation and Analysis of General robots with Mixed DoFs”, in Proc. of 2014 IEEE/RSJ International Conference on Intelligent Robots and Systems (IROS 2014), Chicago, Illinois, USA, September 14–18, 2014.